Technische Universität München

TUM School of Natural Sciences

Novel Minigastrin-derived CCK-2R Targeted Ligands for Radiopharmaceuticals: From Bench to Clinical Translation

Nadine Holzleitner

Vollständiger Abdruck der von der TUM School of Natural Sciences der Technischen Universität München zur Erlangung des akademischen Grades einer

Doktorin der Naturwissenschaften (Dr. rer. nat.)

genehmigten Dissertation.

Vorsitz: Prof. Dr. Job Boekhoven

Prüfer*innen der Dissertation:

1. Prof. Dr. Constantin Lapa
2. Prof. Dr. João D. G. Correia
3. Prof. Dr. Angela Casini

Die Dissertation wurde am 10.10.2023 bei der Technischen Universität München eingereicht und durch die TUM School of Natural Sciences am 17.11.2023 angenommen.

Acknowledgement

First of all, thank you to **Prof. Constantin Lapa** for taking over the supervision of my thesis and the great collaboration. Thank you to **Prof. Hans-Jürgen Wester** for providing me with this interesting PhD project and the supervision of the first part of my thesis. I also want to thank **Prof. Angela Casini**, for the many possibilities she provided me with. I enjoyed being a minion under your watch.

Many thanks to “Uncle Thomas” (**Dr. Thomas Günther**), who was always there for me as a mentor, when I needed him. All in all, we were just a great team. Thank you for all your support over the last years. No Sandro, no party! CC see you.

Thank you to all my co-workers **Franziska Schuderer**, **Sandra Deiser**, **Leon Stopper**, **Marike Drexler**, **Sebastian Fenzl**, **Bernadette Schütz**, **Tanja Pielmeier**, **Veronika Felber**, **Sebastian Fischer**, **Jan-Philipp Kunert** and **Markus Fahnauer** for the many memories we created together. I could always rely on your help. I really enjoyed the many coffee breaks, pasta Mondays and after-work sessions we shared together. Furthermore, I want to thank **Nicole Urtz-Urban** and **Roswitha Beck** for their help with all animal-related studies and **Christine Winkler** for her help with all administrative work.

Thank you to all co-workers of **Prof. Constantin Lapa** at the University Hospital Augsburg, especially **Dr. Ralph A. Bundschuh**, **Georgine Wienand** and **Oliver Viering** for the great collaboration.

Thank you to **Prof. Giuseppe Carlucci** for the possibility to work in his lab at UCLA and for always helping me out, whenever I had questions. I enjoyed my time at your research facilities a lot. Also, many thanks to his co-workers **Meryl Vilangattil**, **Jonathan Godinez**, **Abir Swaidan** and all others for the support with my project and making my stay in Los Angeles more fun. Furthermore, I want to thank the BaCaTec foundation for funding our project Nr. 4 2022-2.

I also want to thank all my research students (**Amira Daoud-Ghadieh**, **Leonard Gareis**, **Denise Dürre** and **Isabel Manyankerikalam**) for working with a lot of motivation and showing great interest in the topic. In addition, I want to thank all the other research students, especially **Max Müller**, **Lena Koller**, **Daniel Werner** and **Viktor König**. All of you made my lab days more fun.

Furthermore, I want to thank **Catalin Alecu**, **Stefanie Schlücking, Christoph Lierse von Gostomski**, **Andreas Cziasto**, **Gerhard Matheis**, **Herbert Größlhuber** and **Alijah Bory** and all

other RCM employees for the great cooperation. I was very happy to receive your help in various situations.

A big thanks goes to my family, especially my parents **Petra** and **Franz Holzleitner**. Without your constant support I wouldn't have made it this far. Thank you for being so understanding and supportive all my life. Many thanks to my sister, **Katrin Holzleitner**, for proofreading all major written works I ever had to submit since high school. I also want to thank all my grandparents for their support along the way.

In addition, thank you to all my friends **Simone Hirmer**, **Fiona Kiefer**, **Nicole Dietl**, **Moritz Ludwig** and **Patrick Gotthardt** for putting up with my stressed-out self and offering me wine whenever I needed it most.

Last but not least, a big thank you to my boyfriend **Dr. Sebastian Schleser**, for always having my back. Thank you for your support, love and patience during the last three years.

List of Publications

1. Journal Contributions

1. **Holzleitner N**, Günther T, Beck R, Lapa C, Wester HJ. Introduction of a SiFA Moiety into the D-Glutamate Chain of DOTA-PP-F11N Results in Radiohybrid-Based CCK-2R-Targeted Compounds with Improved Pharmacokinetics In Vivo. Pharmaceuticals. 2022;15(12):1467.
2. Günther T, **Holzleitner N**, Di Carlo D, Urtz-Urban N, Lapa C, Wester H-J. Development of the First ^{18}F-Labeled Radiohybrid-Based Minigastrin Derivative with High Target Affinity and Tumor Accumulation by Substitution of the Chelating Moiety. Pharmaceutics. 2023; 15(3):826.
3. **Holzleitner N**, Günther T, Daoud-Gadieh A, Lapa C, Wester HJ. Investigation of the structure-activity relationship at the N-terminal part of minigastrin analogs. EJNMMI Research. 2023; 13(65).
4. Koller L, Joksch M, Schwarzenböck S, Kurth J, Heuschkel M, **Holzleitner N**, Beck R, von Amsberg G, Wester HJ, Krause BJ, Günther T. Preclinical Comparison of the ^{64}Cu- and ^{68}Ga-Labeled GRPR-Targeted Compounds RM2 and AMTG, as Well as First-in-Humans [^{68}Ga]Ga-AMTG PET/CT. JNM. 2023; jnumed.123.265771.
5. Viering O, Günther T, **Holzleitner N**, Dierks A, Wienand G, Pfob CH, Bundschuh RA, Wester HJ, Enke JS, Kircher M, Lapa C. CCK2 Receptor-Targeted PET/CT in Medullary Thyroid Cancer Using [^{68}Ga]Ga-DOTA-CCK-66. JNM. 2023; jnumed.123.266380.
6. **Holzleitner N**, Cwojdzinski T, Beck R, Urtz-Urban N, Hillhouse CC, Grundler PV, van der Meulen NP, Talip Z, Ramaekers S, Van de Voorde M, Ponsard B, Casini A, Günther. Preclinical Comparison of the GRPR Antagonists AMTG and RM2 Labeled with Terbium-161 and Lutetium-177. JNM. 2023; jnumed.123.266233.
7. Günther T, **Holzleitner N**, Viering O, Beck R, Wienand G, Dierks A, Pfob CH, Bundschuh RA, Kircher M, Lapa C, Wester HJ. Preclinical Evaluation of Novel Minigastrin Analogs and Proof-of-Concept [^{68}Ga]Ga-DOTA-CCK-66 PET/CT in two Patients With Medullary Thyroid Cancer. JNM. 2023; jnumed.123.266537.

8. **Holzleitner N**, Fischer S, Manyankerikalam I, Beck R, Lapa C, Wester HJ and Günther T. Significant Decrease of Activity Uptake of Radiohybrid-Based Minigastrin Analogs in the Kidneys via Modification of the Charge Distribution Within the Linker Section. EJNMMI Research. 2023; *currently under review.*

2. Conference Contributions

1. **Holzleitner N**, Günther T, Beck R, Lapa C, Wester HJ. Development and preclinical evaluation of novel ^{177}Lu-labelled radiohybrid CCK-2R-targeted ligands based on [^{177}Lu]Lu-DOTA-PP-F11N. 35th Annual Congress of the European Association of Nuclear Medicine. 2022.
2. **Holzleitner N**, Günther T, Beck R, Di Carlo D, Lapa C, Wester HJ. Preclinical Evaluation of [^{18}F]F-[^{nat}Lu]Lu-DOTA-rhCCK-18, the First ^{18}F-Labeled Radiohybrid-Based Minigastrin Derivative with high Target Affinity and Tumor Accumulation. 25th International Symposium on Radiopharmaceutical Sciences. 2023.
3. Günther T, **Holzleitner N**, Wienand G, Urtz-Urban N, Lapa C, Wester HJ. Development and First-in-Man Study of a Novel Tetrapeptidic CCK-2R-Targeted Compound with Improved Metabolic Stability and Pharmacokinetics. 25th International Symposium on Radiopharmaceutical Sciences. 2023.
4. **Holzleitner N**, Günther T, Greifenstein L, Urtz-Urban N, Di Carlo D, Lapa C, Baum RP, Wester HJ. Preclinical Evaluation of [^{18}F]F-[^{nat}Lu]Lu-/[^{19}F]F-[^{177}Lu]Lu-DOTA-rhCCK-18, a Radiohybrid-Based Minigastrin Analog With High Target Affinity and Tumor Accumulation: First Steps Towards Clinical Translation. 36th Annual Congress of the European Association of Nuclear Medicine. 2023.
5. **Holzleitner N**, Günther T, Fischer S, Beck R, Lapa C, Wester HJ. Substantial Reduction of the Activity Retention in the Kidneys of Radiohybrid-Based Minigastrin Analogues by Modifying the Charge Distribution Within the Linker Section. 36th Annual Congress of the European Association of Nuclear Medicine. 2023.
6. Günther T, **Holzleitner N**, Manyiankerikalam I, Greifenstein L, Beck R, Di Carlo D, Baum RP, Wester HJ. Development of [^{18}F]F-[^{nat}Lu]Lu-/[^{19}F]F-[^{177}Lu]Lu-DOTA-rhCCK-84, a Radiohybrid-Based Minigastrin Analogue With High Tumour and low Kidney Accumulation. 36th Annual Congress of the European Association of Nuclear Medicine. 2023.

7. Viering O, Günther T, **Holzleitner N**, Wester HJ, Dierks A, Kircher M, Wienand G, Pfob CH, Bundschuh RA, Lapa C. CCK_2-receptor targeted PET/CT in patients with medullary thyroid cancer using [^{68}Ga]Ga-DOTA-CCK-66 - First clinical experience. 36th Annual Congress of the European Association of Nuclear Medicine. 2023.
8. Günther T, **Holzleitner N**, Cwojdzinski T, Beck R, Urtz-Urban N, Hillhouse CC, Grundler PV, van der Meulen NP, Talip Z, Ramaekers S, Van der Voorde M, Ponsard B, Casini A. Preclinical Comparison of the GRPR Antagonists AMTG and RM2 Labelled With Terbium-161 or Lutetium-177 – A PRISMAP Project. 36th Annual Congress of the European Association of Nuclear Medicine. 2023.

3. Patents

1. Günther T, **Holzleitner N**, Wester HJ, Lapa C. NOVEL MINIGASTRIN-DERIVED CHOLECYSTOKININ 2 RECEPTOR BINDING MOLECULES FOR IMAGING AND TARGETED RADIOTHERAPY. *Patent application pending.* 2022.
2. Wester HJ, Günther T, **Holzleitner N**, Kunert JP, Beck R, Fahnauer M, Fenzl S, Deiser S, Stopper L, Urtz-Urban N, Fischer S. SILICON BASED-FLUORIDE ACCEPTOR GROUPS FOR RADIOPHARMACEUTICALS. *Patent application pending.* 2022.

Abstract

Limited treatment options for patients suffering from progressed medullary thyroid carcinoma (MTC) led to the development of radiolabeled minigastrin analogs targeting the cholecystokinin-2 receptor (CCK-2R), which is overexpressed in over 90% of MTC cases, rendering radioligand therapy (RLT) addressing said target a beneficial clinical tool. In addition, diagnostic applications of CCK-2R targeted peptides could be of value for the localization of tumor lesions, prediction of therapeutic outcome, as well as monitoring of therapeutic efficacy during treatment cycles. Currently, three minigastrin analogs, namely [^{68}Ga]Ga-DOTA-MGS5 ([^{68}Ga]Ga-DOTA-D-Glu-Ala-Tyr-Gly-Trp-(*N*-Me)Nle-Asp-1-Nal-NH_2), [^{177}Lu]Lu-DOTA-PP-F11N ([^{177}Lu]Lu-DOTA-$(D\text{-}Glu)_6$-Ala-Tyr-Gly-Trp-Nle-Asp-Phe-NH_2) and [^{111}In]In-CP04 ([^{111}In]In-DOTA-$(D\text{-}Glu)_6$-Ala-Tyr-Gly-Trp-Met-Asp-Phe-NH_2) are evaluated in clinical trials. However, the lack of ^{18}F-labeling strategies for improved PET imaging as well as limited *in vivo* stability still leave room for further optimizations.

Syntheses of minigastrin analogs were performed according to Fmoc-based solid phase peptide synthesis either manually or automatically (*CEM*, Liberty Blue™ peptide synthesizer, Discover Bio microwave, Liberty Blue application software). ^{177}Lu- as well as ^{64}Cu-labelings were conducted at 90°C for 15 min (1.0 M NaOAc buffer in H_2O, pH=5.5, 0.1 M sodium ascorbate). ^{67}Ga- and ^{68}Ga-labeling procedures were accomplished at 90°C within 15 min (2.5 M HEPES buffer in H_2O). ^{225}Ac-labeling reactions were performed at 90°C for 30 min (10 mg/mL dihydroxybenzoic acid buffer; 1 M NaOAc). ^{18}F-labeling was carried out at 60°C within 5 min (ammonium formiate in DMSO) using previously dried [^{18}F]fluoride with subsequent purification via an ion exchange cartridge. CCK-2R affinity (IC_{50}, *n=3*) was evaluated on AR42J cells (2.0×10^5 cells/mL/well). Lipophilicity (expressed as *n*-octanol/ phosphate buffered saline (PBS) distribution coefficient; log$D_{7.4}$) was determined. Biodistribution (1 to 24 h p.i., *n=4*), µSPECT/CT imaging (1 to 24 h p.i., *n=1*) as well as treatment studies (*n=5* per cohort) were carried out in AR42J tumor-bearing SCID mice.

Completion of a glycine scan as well as evaluation of different tetrapeptidic binding motifs for high affinity CCK-2R targeting, resulted in DOTA-CCK-66 (DOTA-D-*γ*-Glu-$(PEG)_3$-Trp-(*N*-Me)Nle-Asp-1-Nal-NH_2), comprising a D-*γ*-Glu-$(PEG)_3$ linker instead of D-Glu-Ala-Tyr-Gly and the stabilized tetrapeptidic CCK-2R binding sequence, *H*-Trp-(*N*-Me)Nle-Asp-1-Nal-NH_2. When compared to [^{177}Lu]Lu-DOTA-MGS5 (serum: 82.0±0.1%; urine (U): 23.7±9.1%), [^{177}Lu]Lu-DOTA-

CCK-66 (serum: 78.5±3.1%; U: 77.8±2.3%) displayed noticeably enhanced *in vivo* stability, which can be attributed to the modification of the Tyr-Gly and Gly-Trp cleavage sites. In addition, a favorable biodistribution profile of DOTA-CCK-66 at 1 (^{67}Ga; tumor (T): 19.4±3.5%; kidneys (K): 2.5±0.5%) and 24 h (^{177}Lu; T: 8.6±1.1%; K: 1.1±0.1%) after injection was observed. Compassionate use of [^{68}Ga]Ga-DOTA-CCK-66 led to the detection of several lesions in two patients suffering from metastatic MTC. Surgical removal and histological analysis of lesions identified by [^{68}Ga]Ga-DOTA-CCK-66 PET/CT suggests a clinical value of this novel compound. Evaluation of the therapeutic efficacy of [^{225}Ac]Ac-DOTA-CCK-66 exhibited a 4.4-fold increase in mean-survival (54.2±5.7 d *versus* 12.2±2.9 d) of the treatment cohort, when compared to the control group mice, affirming a beneficial therapeutic effect of this radioligand.

Within this thesis we were successfully able to implement the radiohybrid concept to CCK-2R-targeted peptides. Early generation of radiohybrid-based minigastrin analogs displayed superior affinity data for DOTA compared to DOTAGA-comprising compounds. In addition, linker optimization (e.g., change of configuration: D-*α*-Glu to D-*γ*-Glu; reduction of negative charges: substitution of poly-D-*γ*-glutamates by polyethylene glycol (PEG) or poly-hydroxyproline (Hyp) linker chains; evaluation of different SiFA moieties: *p*-SiFA, SiFAlin and SiFA-ipa) of radiohybrid-based minigastrin analogs led to the design of both DOTA-rhCCK-18 (DOTA-D-Dap(*p*-SiFA)-(D-*γ*-Glu)$_8$-Ala-Tyr-Gly-Trp-Nle-Asp-Phe-NH$_2$) and DOTA-rhCCK-84 (DOTA-D-Dap(*p*-SiFA)-D-*γ*-Glu-(Hyp)$_6$-D-*γ*-Glu-(PEG)$_3$-Trp-(*N*-Me)Nle-Asp-1-Nal-NH$_2$). Enhanced tumor-to-kidney ratios (**18**: 0.19±0.01 *versus* **84**: 2.04±0.38) as well as *in vivo* stability (**18**: serum: 64.7±14.6%; U: 15.9±5.6% *v*ersus **84**: serum: 93.5±2.1%; U: 55.4±9.0%) were observed for the latter, which can be attributed to the reduction of negative charges in the linker sequence (substitution of the poly-D-*γ*-glutamates by a poly-Hyp chain) as well as the use of the more stable amino acid sequence, *H*-D-*γ*-Glu-(PEG)$_3$-Trp-(*N*-Me)Nle-Asp-1-Nal-NH$_2$. In comparison, accelerated clearance kinetics of [^{18}F]F-[^{nat}Lu]Lu-DOTA-rhCCK-18 proved to be beneficial for diagnostic applications. Thus, a clinical translation of both compounds was initiated.

In conclusion, we successfully developed three different minigastrin analogs (DOTA-CCK-66, DOTA-rhCCK-18 and DOTA-rhCCK-84), each displaying beneficial preclinical properties, rendering them promising for clinical translation. Among those, [^{68}Ga]Ga-DOTA-CCK-66 has already been applied for PET/CT examinations, which confirmed its diagnostic value for patients suffering from metastatic MTC.

Kurzzusammenfassung

Der Mangel an effizienten Behandlungsmöglichkeiten für Patienten, welche an fortgeschrittenem, medullärem Schilddrüsenkarzinom leiden, führte zur Entwicklung von radioaktiv markierten Minigastrin Analoga, die den CCK-2R, welcher in über 90% der medullären Schildrüsenkarzinome überexprimiert ist und deshalb ein nützliches klinisches Werkzeug für Radioligandtherapie darstellt, adressieren. Darüber hinaus könnten diagnostische Anwendungen CCK-2R-gerichteter Peptide für die Lokalisierung von Metastasen, die Vorhersage des Therapieerfolgs sowie die Überwachung der therapeutischen Wirksamkeit während der Behandlungszyklen von Nutzen sein. Derzeit werden drei Minigastrin-Analoga, [^{68}Ga]Ga-DOTA-MGS5 ([^{68}Ga]Ga-DOTA-D-Glu-Ala-Tyr-Gly-Trp-(*N*-Me)Nle-Asp-1-Nal-NH_2), [^{177}Lu]Lu-DOTA-PP-F11N ([^{177}Lu]Lu-DOTA-$(D\text{-}Glu)_6$-Ala-Tyr-Gly-Trp-Nle-Asp-Phe-NH_2) und [^{111}In]In-CP04 ([^{111}In]In-DOTA-$(D\text{-}Glu)_6$-Ala-Tyr-Gly-Trp-Met-Asp-Phe-NH_2) in klinischen Studien untersucht. Das Fehlen von ^{18}F-Markierungsstrategien sowie die eingeschränkte *in vivo* Stabilität dieser Verbindungen lassen jedoch Raum für weitere Optimierungen.

Die Synthese der Minigastrin-Analoga erfolgte nach der Fmoc-basierten Festphasen-Peptidsynthese entweder manuell oder automatisiert (CEM, Liberty BlueTM Peptidsynthesizer, Discover Bio Mikrowelle, Liberty Blue Anwendungssoftware). Sowohl ^{177}Lu- als auch ^{64}Cu-Markierungen wurden bei 90°C in 15 min durchgeführt (1.0 M NaOAc-Puffer, pH=5.5, 0.1 M Natriumascorbat). ^{67}Ga- und ^{68}Ga-Markierungen wurden bei 90°C in 15 min durchgeführt (2.5 M HEPES-Puffer). ^{225}Ac-Markierungsreaktionen wurden bei 90°C in 30 min durchgeführt (10 mg/mL Dihydroxybenzoesäure; 1 M NaOAc). Die ^{18}F-Markierungen erfolgten bei 60°C in 5 min (Ammoniumformiat in DMSO) unter Verwendung von zuvor getrocknetem [^{18}F]Fluorid mit anschließender Kartuschenaufreinigung. Die CCK-2R-Affinität (IC_{50}, *n=3*) wurde an AR42J Zellen (2.0×10^5 Zellen/mL/Well) untersucht. Die Lipophilie (als *n*-Octanol/PBS-Verteilungskoeffizient; log$D_{7.4}$) wurde bestimmt. Biodistributionsstudien (1 bis 24 h p.i., *n=4*), µSPECT/CT-Bildgebung (1 bis 24 h p.i., *n=1*) sowie Therapiestudien (*n=5* pro Kohorte) wurden an AR42J Tumor-tragenden SCID-Mäusen durchgeführt.

Die Absolvierung eines Glycin-Scans sowie Studien zur Bestimmung des am besten geeigneten tetrapeptidischen Bindemotivs für eine hochaffine CCK-2R Adressierung führten zu DOTA-CCK-66 (DOTA-D-*γ*-Glu-$(PEG)_3$-Trp-(*N*-Me)Nle-Asp-1-Nal-NH_2), bestehend aus einer D-*γ*-Glu-$(PEG)_3$ Linkersequenz anstelle von D-Glu-Ala-Tyr-Gly und der stabilisierten

tetrapeptidischen CCK-2R-Bindesequenz *H*-Trp-(*N*-Me)Nle-Asp-1-Nal-NH_2. Verglichen mit [^{177}Lu]Lu-DOTA-MGS5 (Serum: 82.0±0.1%; Urin: 23.7±9.1%), wies [^{177}Lu]Lu-DOTA-CCK-66 (Serum: 78.5±3.1%; Urin: 77.8±2.3%) eine deutlich höhere *in vivo* Stabilität auf, was auf die Modifizierung der Tyr-Gly- sowie Gly-Trp-Schnittstellen zurückzuführen war. Darüber hinaus wies DOTA-CCK-66 eine vorteilhafte Biodistribution 1 (^{67}Ga; T: 19.4±3.5%; K: 2.5±0.5%) sowie 24 h (^{177}Lu; T: 8.6±1.1%; K: 1.1±0.1%) nach Injektion auf. Eine erste klinische Anwendung von [^{68}Ga]Ga-DOTA-CCK-66 führte zur Entdeckung mehrerer Läsionen bei zwei Patienten mit metastasiertem MTC. Die chirurgische Entfernung und histologische Analyse von Läsion, welche durch [^{68}Ga]Ga-DOTA-CCK-66 PET/CT identifiziert wurden, deutet auf einen klinischen Wert dieser Verbindung hin. Die Bewertung der therapeutischen Wirksamkeit von [^{225}Ac]Ac-DOTA-CCK-66 ergab einen 4.4-fachen Anstieg des mittleren Überlebens (54.2±5.7 d *versus* 12.2±2.9 d) der therapierten Kohorte im Vergleich zu den Mäusen der Kontrollgruppe, was eine positive therapeutische Wirkung dieses Radioliganden bestätigt.

Im Rahmen dieser Arbeit konnten wir das Radiohybrid-Konzept erfolgreich auf CCK-2R-gerichtete Peptide anwenden. Eine erste Generation Radiohybrid-basierter Minigastrin-Analoga zeigte eine verbesserte Affinität der DOTA im Vergleich zu den DOTAGA-basierten Verbindungen. Darüber hinaus wurden Linker-Optimierungen (z. B. Änderung der Konfiguration: D-*α*-Glu zu D-*γ*-Glu; Reduktion negativer Ladungen: Substitution der Poly-D-*γ*-Glutamate durch PEG- oder Poly-Hyp-Linkerketten; Evaluierung verschiedener SiFA-Einheiten: *p*-SiFA, SiFAlin und SiFA-ipa) der Radiohybrid-basierten Minigastrin-Analoga durchgeführt, welche im Design von DOTA-rhCCK-18 (DOTA-D-Dap(*p*-SiFA)-(D-*γ*-Glu)$_8$-Ala-Tyr-Gly-Trp-Nle-Asp-Phe-NH_2) und DOTA-rhCCK-84 (DOTA-D-Dap(*p*-SiFA)-D-*γ*-Glu-(Hyp)$_7$-D-*γ*-Glu-(PEG)$_3$-Trp-(*N*-Me)Nle-Asp-1-Nal-NH_2) resultierten. Verbesserte Tumor-zu-Nieren Verhältnisse (**18**: 0.19±0.01 *versus* **84**: 2.04±0.38) sowie *in vivo* Stabilität (**18**: Serum: 64.7±14.6%; U: 15.9±5.6% *versus* **84**: Serum: 93.5±2.1%; U: 55.4±9.0%) beobachtet für die letztere Verbindung, können der Verringerung der negativen Ladungen in der Linker-Sequenz (Ersatz von Poly-D-*γ*-Glutamaten durch eine poly-Hyp-Kette) sowie der Einführung einer metabolisch stabilisierten Aminosäuresequenz *H*-D-*γ*-Glu-(PEG)$_3$-Trp-(*N*-Me)Nle-Asp-1-Nal-NH_2 zugeschrieben werden. Im Vergleich dazu erwies sich die beschleunigte Ausscheidungskinetik von [^{18}F]F-[^{nat}Lu]Lu-DOTA-rhCCK-18 als vorteilhaft für diagnostische Anwendungen. Daher wurde eine klinische Translation beider Verbindungen initiiert.

Zusammenfassend lässt sich sagen, dass es uns gelungen ist, drei verschiedene Minigastrin-Analoga, DOTA-CCK-66, DOTA-rhCCK-18 und DOTA-rhCCK-84, zu entwickeln, die

vorteilhafte präklinische Eigenschaften für die klinische Umsetzung aufweisen. Von diesen wurde [^{68}Ga]Ga-DOTA-CCK-66 bereits erfolgreich in PET/CT Anwendungen innerhalb von Heilversuchen untersucht, welche den diagnostischen Wert dieser Verbindung für Patienten mit metastasiertem MTC bestätigt haben.

List of Abbreviations

A

ALT	alanine-aminotransferase
AST	aspartate-aminotransferase

B

B	urinary bladder

C

C	colon
CCK	cholecystokinin
CCK-1R	cholecystokinin-1 receptor
CCK-2R	cholecystokinin-2 receptor
CCK-4	*H*-Trp-Asp-Met-Phe-NH_2
CEA	carcinoembryonic antigen
CP04	DOTA-(D-Glu)$_6$-Ala-Tyr-Gly-Trp-Met-Asp-Phe-NH_2
CT	computed tomography
Ctn	calcitonin

D

Demogastrin 2	N_4-Gly-D-Glu-(Glu)$_5$-Ala-Tyr-Gly-Trp-Met-Asp-Phe-NH_2
DOPA	L-3,4-dihydroxyphenylalanin
DOTA	1,4,7,10-tetraazacyclododecan-*N*, *N*', *N*'', *N*'''-tetraacetic acid
DOTA-CCK-62	DOTA-Gly-Trp-(*N*-Me)Nle-Asp-1-Nal-NH_2
DOTA-CCK-63	DOTA-(PEG)$_4$-Trp-(*N*-Me)Nle-Asp-1-Nal-NH_2
DOTA-CCK-64	DOTA-(PEG)$_3$-Trp-(*N*-Me)Nle-Asp-1-Nal-NH_2
DOTA-CCK-66	DOTA-D-*γ*-Glu-(PEG)$_3$-Trp-(*N*-Me)Nle-Asp-1-Nal-NH_2
DOTA-CCK-66.2	DOTA-D-Glu-(PEG)$_3$-Trp-(*N*-Me)Nle-Asp-1-Nal-NH_2
DOTAGA	1,4,7,10-tetraazacyclododecane-*N*-(glutaric acid)-*N*',*N*'',*N*'''-triacetic acid

DOTA-MG0	DOTA-D-Glu-$(Glu)_5$-Ala-Tyr-Gly-Trp-Met-Asp-Phe-NH_2
DOTA-MG11	DOTA-D-Glu-Ala-Tyr-Gly-Trp-Met-Asp-Phe-NH_2
DOTA-MGS5	DOTA-D-Glu-Ala-Tyr-Gly-Trp-(*N*-Me)Nle-Asp-1-Nal-NH_2
DOTA-MGS8	DOTA-D-Glu-Pro-Tyr-Gly-Trp-(*N*-Me)Nle-Asp-1-Nal-NH_2
DOTA-PP-F10	DOTA-$(D\text{-}Gln)_6$-Ala-Tyr-Gly-Trp-Met-Asp-Phe-NH_2
DOTA-PP-F11-L	DOTA-$(L\text{-}Glu)_6$-Ala-Tyr-Gly-Trp-Met-Asp-Phe-NH_2
DOTA-PP-F11N	DOTA-$(D\text{-}Glu)_6$-Ala-Tyr-Gly-Trp-Nle-Asp-Phe-NH_2
DOTA-rhCCK-18	DOTA-D-Dap(*p*-SiFA)-$(D\text{-}\gamma\text{-}Glu)_8$-Ala-Tyr-Gly-Trp-Nle-Asp-Phe-NH_2
DOTA-rhCCK-70	DOTA-D-Dap(*p*-SiFA)-D-γ-Glu-$(PEG)_7$-D-γ-Glu-$(PEG)_3$-Trp-(*N*-Me)Nle-Asp-1-Nal-NH_2
DOTA-rhCCK-84	DOTA-D-Dap(*p*-SiFA)-D-γ-Glu-$(Hyp)_6$-D-γ-Glu-$(PEG)_3$-Trp-(*N*-Me)Nle-Asp-1-Nal-NH_2
DOTA-rhCCK-91	DOTA-D-Dap(SiFAlin)-D-γ-Glu-$(PEG)_4$-D-γ-Glu-$(PEG)_3$-Trp-(*N*-Me)Nle-Asp-1-Nal-NH_2
DTPA	diethylenetriaminepentaacetic acid
DTPA-MG0	DTPA-D-Glu-$(Glu)_5$-Ala-Tyr-Gly-Trp-Met-Asp-Phe-NH_2

E

EBRT	external beam radiation therapy
EDDA	ethylenediamine-*N*,*N*′-diacetic acid
EMA	european medicines agency

F

FDA	food and drug administration
FDG	fluorodeoxyglucose

G

GAS3	DOTAGA-D-Glu-$(PEG)_2$-Z-360
gastrin-17	*H*-pGlu-Gly-Pro-Trp-Leu-$(Glu)_5$-Ala-Tyr-Gly-Trp-Met-Asp-Phe-NH_2
GPCR	G-protein coupled receptor
GRPR	gastrin-releasing peptide receptor

H

HDI	human development index
HSA	human serum albumin
HYNIC	hydrazinonicotinic acid
Hyp	hydroxyproline

K

K	kidneys

M

minigastrin	*H*-Leu-$(Glu)_5$-Ala-Tyr-Gly-Trp-Met-Asp-Phe-NH_2
MTC	medullary thyroid carcinoma

N

N_4	tetraamine chelator (6-(carboxy)-1,4,8,11-tetraazaundecane)
NEP	neutral endopeptidase
NET	neuroendocrine tumor

P

PA	phosphoramidon
PBS	phosphate buffered saline
PEG	polyethylene glycol
PET	positron emission tomography
p.i.	post injection
PRRI	peptide receptor radionuclide imaging
PSMA	prostate-specific membrane antigen

R

(*R*)-DOTAGA-rhCCK-9	(*R*)-DOTAGA-D-Dap(*p*-SiFA)-(D-Glu)$_8$-Ala-Tyr-Gly-Trp-Nle-Asp-Phe-NH_2
(*R*)-DOTAGA-rhCCK-16	(*R*)-DOTAGA-D-Dap(*p*-SiFA)-(D-*γ*-Glu)$_6$-Ala-Tyr-Gly-Trp-Nle-Asp-Phe-NH_2
RET	REarranged during transfection
rh	radiohybrid
RLT	radioligand therapy

S

S	stomach
SG	succinylated gelatin
SiFA	silicon-based fluoride acceptor
p-SiFA	4-(Di-*tert*-butylfluorosilyl)benzoic acid
SiFAlin	*N*-(4-(di-*tert*-butylfluorosilyl)benzyl)-*N*,*N*-dimethylglycine
SiFA-ipa	5-(Di-*tert*-butylfluorosilyl)isophthalic acid
SPECT	single-photon emission computed tomography
SSTR2	somatostatin receptor subtype 2

T

T	tumor
TAT	targeted alpha therapy
TATE	(Tyr^3)-octreotate
^{t}Bu	*tert*-Butyl
TKI	tyrosine kinase inhibitor
TTX	total thyroidectomy

U

U	urine

Table of Contents

I. Theoretical Background

1. A General Perspective on Nuclear Medicine in Oncology

1.1 Cancer: Statistics, Epidemology and Riskfactors

In modern society, cancer represents one of the leading causes of death worldwide. Especially for premature deaths, occurring at the age of 30 to 70 years, cancer is the first or second main cause in 112 out of 183 countries (*1*). According to global cancer statistics, an estimated number of 19.3 million patients were newly diagnosed with cancer and 10 million cancer related deaths occurred in 2020. Out of those, the five most common incidences for newly diagnosed cases were breast (11.7%), lung (11.4%), prostate (7.3%), nonmelanoma of skin (6.2%) and colon (6.0%), whereas five most common leading causes of cancer-related deaths were lung (18%), liver (8.3%), stomach (7.7%), breast (6.9%) and colon (5.8%) tumors (*2*).

Statistical predictions of new cancer cases until 2040 display an increase of 47% globally (**Figure 1**).

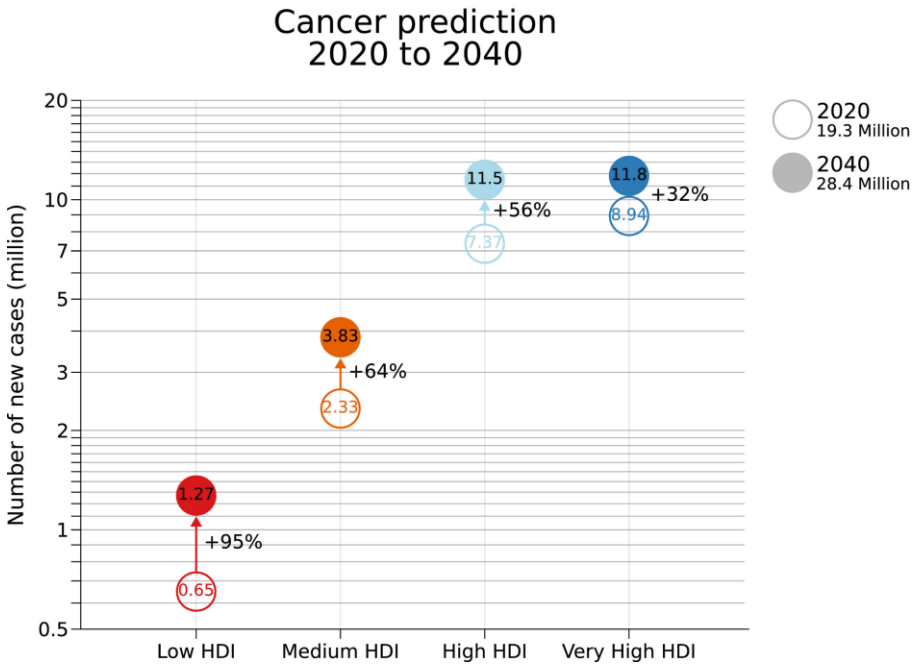

Figure 1. Predicted number of future cancer burden in 2040 in dependence of the 4-Tier Human Development Index (*2*). Copyright © John Wiley and Sons.

Within this extrapolation, only expanding growth as well as aging of the world population is considered, thus, not including the spread of risk factors, which might further aggravate said number (*2*). In literature, a strong correlation between human development and number of cancer cases was reported (*3,4*). Countries with low human development index (HDI), such as Mali, Niger or Sudan, reported the smallest amount of new diagnosed cancer cases. Until 2040, the highest proportional increase of 95% of new cases is predicted to occur in low HDI countries, whereas the highest increase in absolute burden is expected for high HDI countries, such as China, Columbia and Ukraine with a total number of 4.1 million additional new cancer diagnoses (*2*).

Even though Europe only accounts for about 10% of the global population, 23% of all globally diagnosed cancer cases occur in European countries (*2*). Out of those, approximately 40% of all cases are preventable, according to the latest available estimates (*5-7*). Especially life-style related risk factors, such as tobacco and smoking (15-20% of cancer cases), alcohol consumption (10% in men and 3% in women), overweight and obesity (5-7%), poor dietary habits (5-6%) and insufficient physical activity (~1%), account for a major amount of cancer burden. Further known cancer risk factors are environmental factors (e.g., air, water and soil pollution as well as ultraviolet and ionizing radiation), infections by carcinogenic viruses or bacteria, occupational factors (e.g., exposure to asbestos and heavy metals), medical and reproductive factors as well as genetic factors (*6-10*). In 2018, Cancer Prevention Europe has been founded, as a consortium of a number of leading European research institutes, with the purpose of providing an overall strategy for reduction of cancer risk factors (*11*).

1.2 Current Cancer Management: Diagnostic Tools and Treatment Modalities

Despite improving cancer prevention the above-mentioned risk factors continue to pose a substantial health thread, resulting in increasing numbers of new cancer cases each year (*2*). Therefore improving diagnostic as well as therapeutic tools for cancer management are highly necessary (*12*). To date, surgery, external beam radiation therapy (EBRT) as well as chemotherapy are considered the most recommended conventional cancer treatment approaches. Among those, a combinational therapy is often applied (*13*). Whilst surgery is providing the lowest long-term side-effects, its applicability is mainly limited to the handling of primary tumors as well as local metastasis, being most effective at an early stage of diagnosis (*14*). Furthermore, surgical risks (e.g., blood loss, anesthesia, infections and scarring) are often poorly tolerated in patients of high age or poor general health or patients suffering from specific coexisting conditions (*15-18*). In those cases, EBRT is a promising course of treatment. In

addition, EBRT can be applied for treatment of non-surgically accessible solid tumors, local metastatic disease, pain management of regional metastasis as well as follow-up treatment of surgery for prevention of recurrent disease. However, apart from damaging tumor cells, radiation therapy is a burden to healthy tissue, which can result in short-term (e.g., skin irradiation and fatigue), as well as long-term side effects, such as the induction of second cancers (*19-23*). Treatment of metastatic disease is mainly accomplished by chemotherapeutic drugs, for example cisplatin, which has already been approved by the FDA in 1978 (*24*). Even though, chemotherapy can be curative in some cases, major limitations e.g., drug resistance, dosage selection, lack of specificity, rapid drug metabolism, as well as harmful side effects (e.g., fatigue, vomiting, nausea and hair loss) pose a challenge for cancer management (*25,26*).

With increasing numbers of cancer cases and thus, cancer related deaths, research focused on novel approaches for cancer management aiming at personalized treatment. This led to more advanced and innovative modalities, such as stem cell therapy, ablation cancer therapy, gene therapy, immunotherapy and targeted radionuclide therapy, among others (*21,27*). As opposed to EBRT, targeted radionuclide therapy enables the transport of radioisotopes directly to cancer cells, thus harming less healthy tissue independent of tumor size. In addition, multiple tumor sites can be addressed simultaneously, displaying a great advantage for treatment of progressed metastatic disease (*28*). To implement this concept, mainly small molecules, peptides or antibodies in combination with a labeling unit, addressing tumor specific enzymes, receptors, antigens or proteases, respectively, were developed (*29-31*). Radionuclides of choice for therapeutic approaches are β^-- (e.g., ^{177}Lu, ^{90}Y), α- (e.g., ^{225}Ac, ^{212}Pb) or Auger electron-emitting isotopes (e.g., ^{125}I, ^{111}In, ^{161}Tb) (*28,32-34*).

Besides therapeutic applications, one major advantage of targeted radionuclide approaches is their additional applicability for diagnostic evaluations. Dependent on the chelator moiety attached, only the choice of the radionuclide decides whether the compound can be used for diagnostic or therapeutic applications. For single-photon emission computed tomography (SPECT) imaging γ-emitting radionuclides (e.g., ^{99m}Tc) are applied, whereas positron emission tomography (PET) is conducted incorporating positron (β^+)-emitting radioisotopes (e.g., ^{68}Ga, ^{18}F) into the compound (*35-37*). In comparison to more commonly used imaging approaches, such as magnet resonance imaging (MRI) or computed tomography (CT), which both deliver only morphological information, nuclear medicine applications enable the depiction of biochemical processes (*38-40*). To date, SPECT or PET imaging devices are usually complemented with CT or MRI scans, combining the advantages of the different imaging tools (*39,40*).

1.3 Radiohybrid Concept as Novel Theranostic Approach

A common concept for cancer management in the field of nuclear medicine is the use of theranostic compounds, which refers to a compound that allows for both imaging and radioligand therapy (RLT). Besides economic advantages, this combinational approach of ligand design enables the prediction of target expression (and therapy control) by imaging and thus, delivers valuable information on therapy planning (*41,42*). To date, the ^{68}Ga/^{177}Lu as well as ^{68}Ga/^{90}Y pairings for PET imaging (β^+) and RLT (β^-), respectively, are commonly used as theranostic pairs in clinical practice, even though the different radioisotopes applied differ in their chemical properties (*43*). Hence, slightly different characteristics of the compounds labeled with ^{68}Ga as opposed to ^{177}Lu or ^{90}Y can be observed e.g., in case of [^{nat}Ga]Ga- *versus* [^{nat}Y]Y-DOTATATE (IC_{50} = 0.2±0.04 nM *versus* 1.6±0.4 nM; (*44*)) or [^{nat}Ga]Ga- *versus* [^{nat}Lu]Lu- *versus* [^{nat}Y]Y-Pentixafor (IC_{50} = 25±3 nM *versus* 41±12 nM *versus* 40±27 nM; (*45*)), thus influencing the pharmacokinetic properties of the respective drugs.

A different approach to create chemically identical theranostics is the usage of elements providing different radioisotopes with various decay mechanisms e.g., ^{61}Cu (β^+, PET)/^{64}Cu (β^+, PET)/^{67}Cu (β^-, therapy), ^{149}Tb (α, therapy)/^{152}Tb (β^+, PET)/^{155}Tb (γ, SPECT)/^{161}Tb (β^-, therapy), ^{43}Sc (β^+, PET)/^{44}Sc (β^+, PET)/^{47}Sc (β^-, therapy) and ^{123}I (γ, SPECT)/^{124}I (β^+, PET)/^{131}I (β^-, therapy), which can be used for both imaging and RLT (*46-48*). Thereby, these isotopes can create chemically identical compounds, displaying identical *in vitro* parameters and pharmacokinetic properties, only differing in their decay mechanism and thus, nuclear medicine application. Hence, a more precise therapy planning as well as economic advantages, display their superiority to the surrogate pairs (*46,48*). However, this concept is limited by the availability of appropriate theranostic nuclide pairs (copper, scandium, iodine, and terbium nuclides, among others) (*43,48-52*). To circumvent the above mentioned restrictions, Wurzer *et al.* established the radiohybrid (rh) concept, enabling both ^{18}F- (β^+, PET) or ^{177}Lu-labeling (β^-, therapy) while generating a chemically indistinguishable molecule (*53*).

^{177}Lu and ^{18}F are two of the most used radionuclides in clinical practice, because of their beneficial decay characteristics. Providing the possibility to combine them as chemically identical theranostic pairs (RLT: ^{177}Lu/^{19}F; PET: ^{nat}Lu/^{18}F) has the potential to improve patient care. Compared to one of the most common PET isotopes for peptide receptor radionuclide imaging (PRRI), ^{68}Ga, ^{18}F decays with a higher positron decay yield (89% *versus* 97%) in combination with a lower endpoint positron energy emission ($E_{max}(\beta^+)$ = 1899 keV vs 635 keV), which results

in higher image resolution of the latter (*54*). In addition, the longer half-life of ^{18}F as opposed to ^{68}Ga ($t_{1/2}$=109.7 min vs. 67.7 min), allows for an extended window for imaging studies, which can be valuable for tracers with slower distribution kinetics (*55,56*). To date, only the inferior availability of ^{18}F due to the need of a cyclotron production, in comparison to commercially available generator-produced nuclides such as ^{68}Ga, hamper a broad clinical applicability of ^{18}F-labeled tracers (*56,57*).

^{177}Lu is one of the most widespread radionuclides used for cancer treatment. Due to its shorter emission range (1.6 mm *versus* 11 mm) as well as energy ($E_{max}(\beta^-)$ = 0.49 *versus* 2.27 MeV) compared to ^{90}Y, less harm to healthy tissue is caused, whilst high therapeutic efficacies, particularly for small metastases, are maintained (*58*). To date, ^{177}Lu-labeled radiopharmaceuticals, such as [^{177}Lu]Lu-DOTATATE (Luthathera®) and [^{177}Lu]Lu-PSMA-617 (Pluvicto®), have been approved by the FDA for treatment of somatostatin receptor subtype 2-positive gastroenteropancreatic tumor cells and metastatic castration resistant prostate cancer, respectively (*59,60*).

The combination of a silicon-based fluoride acceptor (SiFA) unit, to stably bind [^{18}F]fluoride, and a chelator moiety (e.g., 1,4,7,10-tetraazacyclododecan-*N*, *N*', *N*'', *N*'''-tetraacetic acid, DOTA) within the same compound enables radiofluorination as well as radiometallation (dependent on the intended use) while generating chemically identical molecules (**Figure 2**) (*53*).

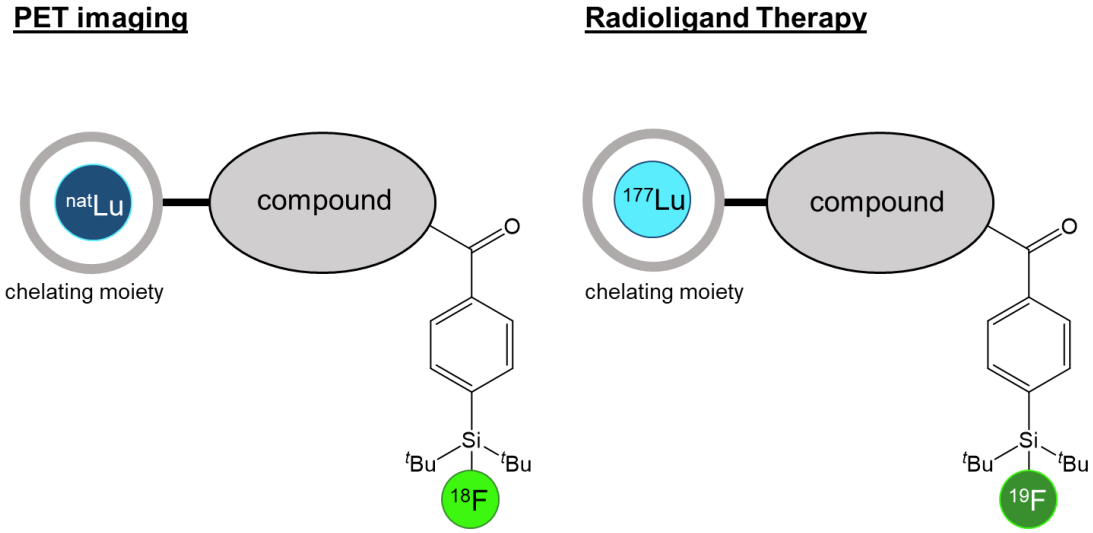

Figure 2. Schematic representation of the radiohybrid concept. Compounds comprising one 4-(di-*tert*-butylfluorosilyl)benzoic acid (*p*-SiFA; ^{18}F-fluorination) as well as one chelator moiety (radiometallation) for radiolabeling. Theranostic pairs always comprise one radioactive as well as one natural isotope for either PET imaging (^{18}F/^{nat}Lu) or RLT (^{19}F/^{177}Lu) (*53*).

Originally introduced by Schirrmacher *et al.* into the field of nuclear medicine, the SiFA methodology using the *p*-SiFA building block is a well-established strategy for ^{18}F-labeling via isotopic exchange, representing good stabilities of the Si-F bond towards hydrolysis due to the steric hindrance by the two *tert*-butyl groups (*61*). Furthermore, mild reaction conditions (low temperature, short reaction times, cartridge purification) of [^{18}F]F-SiFA, as opposed to other established ^{18}F-labeling strategies such as the [^{18}F]AlF_3 labeling approach (high temperature), render this method beneficial (*62*). However, one major limitation of the *p*-SiFA moiety is its high lipophilicity, posing a challenge for ligand design, especially for small molecules or peptides. In general, increased lipophilicity of drugs can result in reduced target availability due to the first pass effect trapping the compound in the liver, as well as a higher unspecific uptake in non-tumor organs (*63,64*). Strategies to compensate the high lipophilicity of the *p*-SiFA building block are mainly accomplished by insertion of hydrophilic groups, such as sugar, polyethylenglycol (PEG) or hydrophilic amino acid, or charged moieties in proximity to the *p*-SiFA unit (*64-66*). Another approach to improve the overall lipophilicity of SiFA-based compounds, is the introduction of less lipophilic SiFA building blocks, such as *N*-(4-(di-*tert*-butylfluorosilyl)benzyl)-*N,N*-dimethylglycine (SiFAlin), comprising a quaternary ammonium cation. Hence, less elaborate linker design is necessary, to enhance the overall lipophilicity of said compounds. This is particularly of advantage for small molecules or peptides, of which linker design in general or insertion of multiple positively or negatively charged building blocks in particular negatively influences target affinity (*65,67*).

To date, the radiohybrid concept has already been successfully applied to prostate-specific membrane antigen (PSMA) targeted compounds. Based on its promising clinical data, [^{18}F]F-[^{nat}Ga]Ga-rhPSMA-7.3 (Posluma®) was approved by the FDA in May 2023. However, the approval of this tracer is limited to the diagnostic pair (^{18}F/^{nat}Ga or ^{19}F/^{68}Ga), lacking the therapeutic option of ^{177}Lu-labeling (*68-72*). Therefore, the chemically similar compound, [^{177}Lu]Lu-[^{19}F]F-rhPSMA-10.1, is currently evaluated in clinical trials for therapeutic applications (NCT05413850) (*73,74*). Due to the great success of the radiohybrid concept for PSMA inhibitors, a transfer to compounds addressing other molecular targets and thus tumor entities could be a promising new strategy for tracer development.

1.4. Radioligand Therapy Using Ac-225: Possibilities and Limitations

Besides β^--emitting radionuclides, such as ^{177}Lu, ^{90}Y and ^{131}I, being routinely employed for RLT, another decay mechanism is emerging into the focus of research. Isotopes emitting *α*-particles during their radioactive decay, provide new possibilities for therapeutic approaches. In comparison to β^--particles, *α*-particles possess a higher particle energy (0.5-2.3 MeV *versus* 5-9 MeV), a lower particle path length (0.05-12 mm *versus* 40-100 µm) as well as a higher linear energy transfer (~0.2 keV/µm *versus* ~80 keV/µm), resulting in enhanced therapeutic efficacies (*75-77*).

To date, research on various *α*-emitters, such as ^{225}Ac, ^{149}Tb, ^{212}Bi, ^{213}Bi, ^{212}Pb, ^{211}At, ^{227}Th, ^{223}Ra or ^{224}Ra, is progressing (*78,79*). Out of these, ^{223}Ra was the first *α*-emitter approved by the FDA in 2013 as [^{223}Ra]$RaCl_2$ (Xofigo®) for the treatment of prostate cancer with metastatic bone lesions (*80*). However, compounds combining *α*-emitting isotopes with tumor-targeting biomolecules yet still remain in a developmental stage, even though various clinical trials have been initiated. One promising radioisotope for targeted alpha therapy (TAT) is ^{225}Ac. On the one hand this is due to its long half-life of 9.9 d, and on the other hand, its decay scheme to the stable ^{209}Bi provides four rapid consecutive *α*-emissions and thus, four *α*-particles per nuclide, each delivering high damage to tumor cells, as well as two *γ*-emissions, which can be used for quantification (**Figure 3**) (*79*).

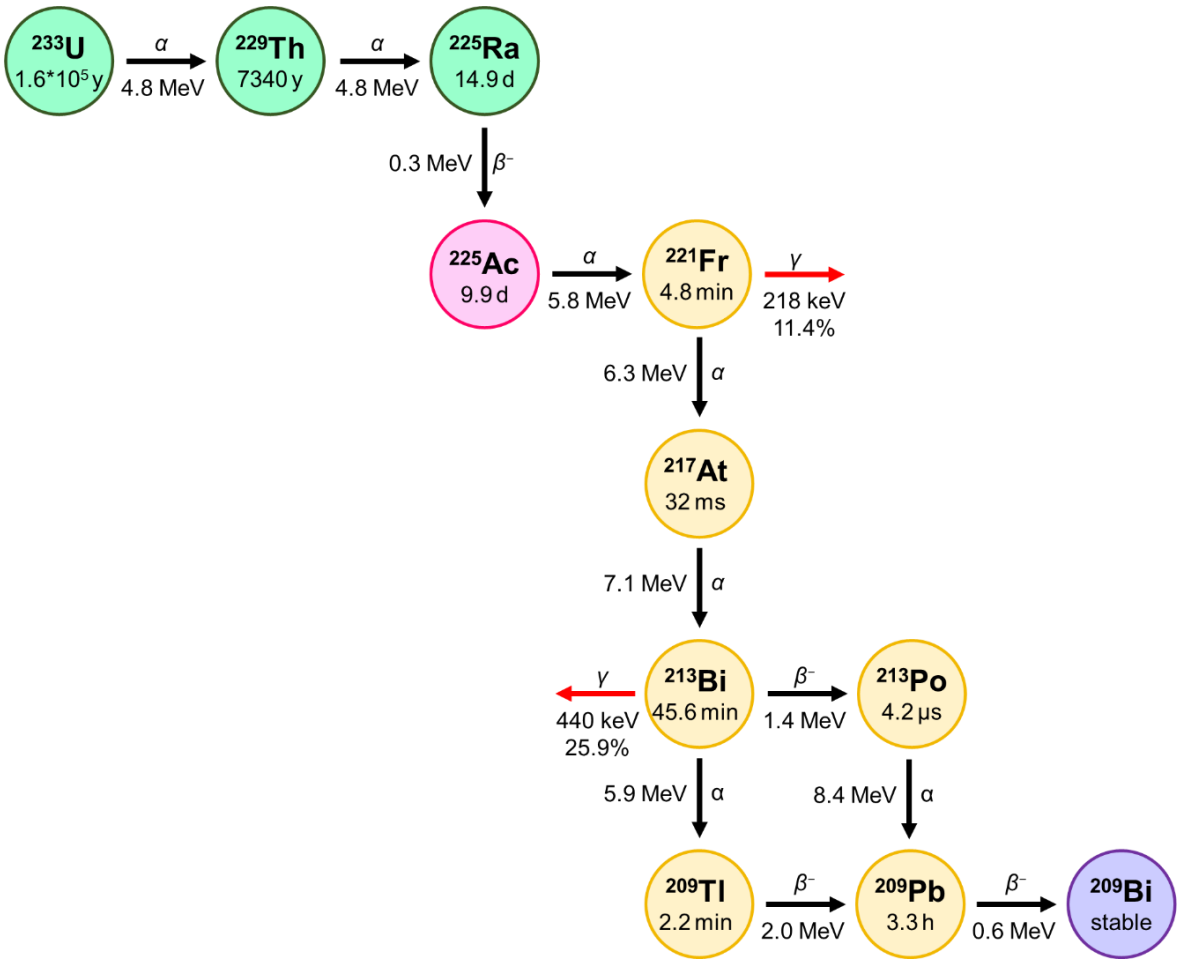

Figure 3. Schematic representation of the production (green) as well as the decay (orange) of ^{225}Ac (pink), resulting in the stable ^{209}Bi (purple). *γ*-emissions used for quantification of ^{225}Ac are depicted in red (*79*).

^{225}Ac is primarily obtained from ^{229}Th/^{225}Ac ($t_{1/2}$=7340 y) generators, which can be eluted every three weeks, thus obtaining ^{225}Ac free of other actinium isotopes (*81*). ^{229}Th itself is a decay product of ^{233}U ($t_{1/2}$=1.6*10^5 y), which was mainly produced between 1954 and 1970 via neutron irradiation of ^{232}Th to be investigated for its use in nuclear weapons and reactors (*82*). ^{229}Th was then extracted from stockpiles of ^{233}U and stored for ^{225}Ac production. However, the non-proliferation act, the long half-lives of ^{233}U and ^{229}Th, as well as the limited number of institutes possessing ^{229}Th sources led to a severe shortage of ^{225}Ac (*78,79,83*). With a global annual availability of only 63 GBq, less than 1000 patients could be provided with a ^{225}Ac-based treatment. Currently, only a small number of clinical trials can be supplied with this isotope, rendering a global implementation into clinical routine impossible (*79,83,84*). Thus, research on novel methods to produce ^{225}Ac, such as irradiation of ^{226}Ra targets using electron (^{226}Ra(*γ*,n)^{225}Ra→^{225}Ac; (*85*)) or low energy proton accelerators (^{226}Ra(p,2n)^{225}Ac; (*86*)), as well

as high energy proton spallation of thorium targets (^{232}Th(p,x)^{225}Ac; (*87*)), is ongoing. In addition, subsequent separation of ^{225}Ac from other metal impurities, especially from ^{227}Ac, occurring during these novel production methods, poses a major challenge for researchers all over the world (*79*).

A chemical limitation of TAT is the recoil effect that occurs during the decay of an *α*-emitter. This so-called recoil energy, which is emitted in parallel to the emission of energetic *α*-particles, is often 1000-times higher than the binding energy of a chemical bond or coordination energy in a complex. Thus, daughter nuclides are ripped out of the chelator moiety attached at the targeting biomolecule. If not internalized into tumor cells, the resulting daughter nuclides can also cause harm to healthy tissue (*88*). To circumvent this issue, research on novel chelator moieties with increased ^{225}Ac-complex stability as well as nanoparticles encapsulating ^{225}Ac is ongoing (*88-90*).

Despite the many obstacles TAT still faces, first clinical studies of [^{225}Ac]Ac-PSMA-617 (NCT04597411), [^{225}Ac]Ac-PSMA-I&T and [^{225}Ac]Ac-DOTATATE revealed impressive results (**Figure 4**) (*91-93*).

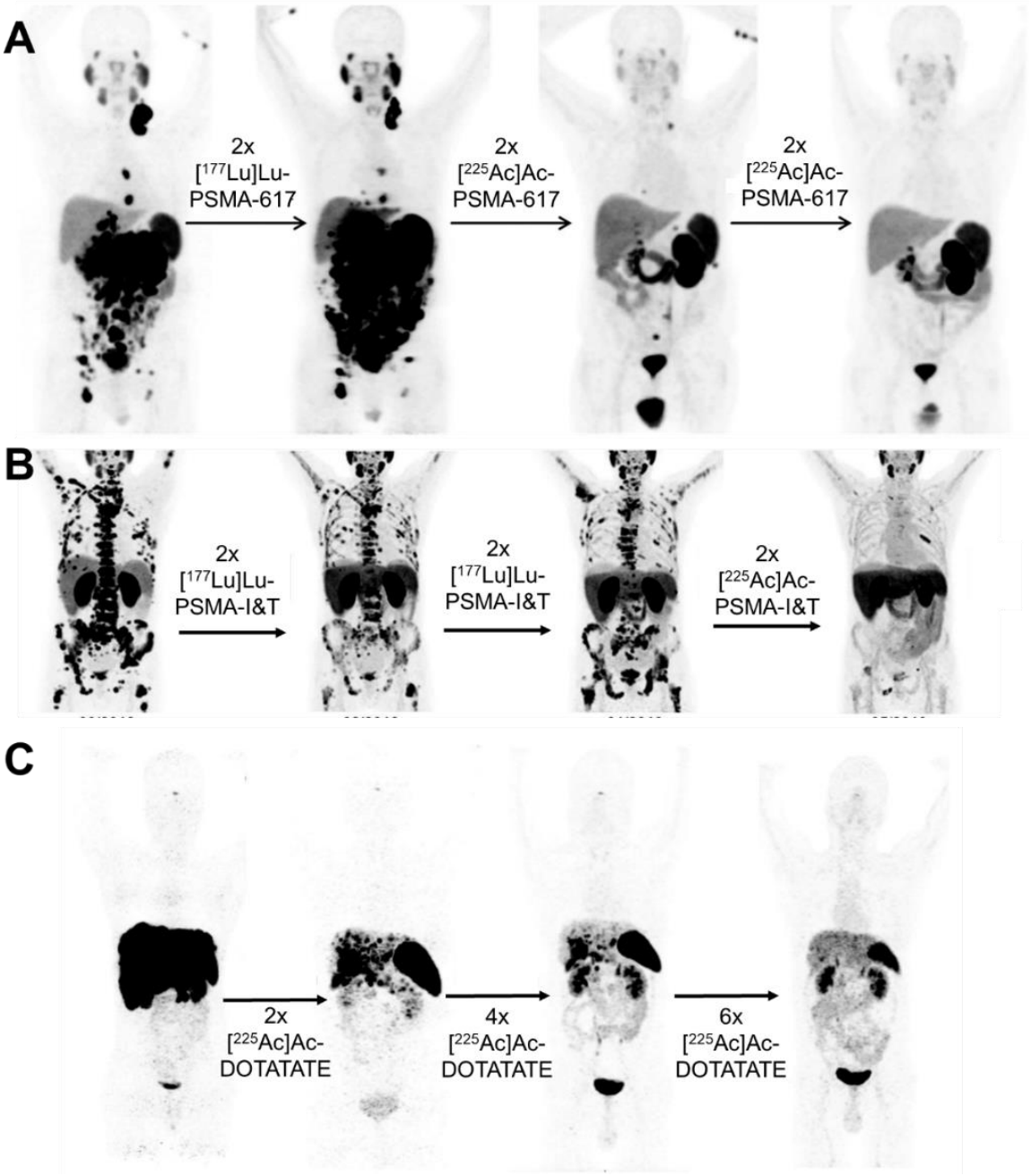

Figure 4. A) [^{68}Ga]Ga-PSMA-11 PET/CT scans of a patient suffering from metastatic castration resistant prostate cancer treated with multiple cycles of [^{177}Lu]Lu-PSMA-617 as well as [^{225}Ac]Ac-PSMA-617. Copyright © 2016 by SNMMI (*93*). B) PSMA PET/CT scans of a patient suffering from metastatic castration resistant prostate cancer treated with multiple cycles of [^{177}Lu]Lu-PSMA-I&T as well as [^{225}Ac]Ac-PSMA-I&T. Copyright © 2021 by SNMMI (*92*). C) [^{68}Ga]Ga-DOTANOC PET/CT scans of a patient suffering from metastatic gastroenteropancreatic neuroendocrine tumor treated with multiple cycles of [^{225}Ac]Ac-DOTATATE. Copyright © 2023 by SNMMI (*91*). All figures depicted were originally published in JNM. Inscription of the arrows was slightly modified.

For example, a study published by Kratochwil *et al.* in 2016 demonstrated a therapeutic effect of [^{225}Ac]Ac-PSMA-617 in a patient refractory to therapy with [^{177}Lu]Lu-PSMA-617 (*93*). Furthermore, Zacherl *et al.* reported a study including 14 patients suffering from metastatic castration-resistant prostate cancer, showing a promising antitumor effect of [^{225}Ac]Ac-PSMA-I&T, comparable to that of [^{225}Ac]Ac-PSMA-617. However, severe side-effects of TAT using [^{225}Ac]Ac-labeled PSMA inhibitors, mainly definitive xerostomia, limit its applicability to late-stage prostate cancer treatment (*92*). In 2023, Ballal *et al.* reported a first clinical experience with [^{225}Ac]Ac-DOTATATE in a cohort of 32 patients suffering from metastatic gastroenteropancreatic neuroendocrine tumors, supporting the observations made for PSMA-targeted compounds. Within this study, a beneficial effect of [^{225}Ac]Ac-based TAT for patients refractory to [^{177}Lu]Lu-based RLT, as well as high response rates, good survival rates (24-month survival probability of 70.8%) and acceptable toxicity profiles of [^{225}Ac]Ac-DOTATATE treatment were observed (*91*). All in all, [^{225}Ac]Ac-based TAT can be considered a valuable tool as complementary treatment option to [^{177}Lu]Lu-based RLT, especially in late-stage cancer management (*91-93*).

2. Medullary Thyroid Carcinoma: Occurrence, Diagnosis and Treatment

The National Cancer Institute estimated 43.720 new thyroid cancer cases in the United States in 2023, which comprises around 2.2% of all patients newly diagnosed with cancer (*94*). With an overall 5-year survival rate of 98.5%, thyroid carcinomas exhibit a noticeably enhanced prognosis compared to that of cancer in general (68.7%) (*94,95*). The four most common types of thyroid cancer are papillary (65-85%, (*96,97*)), follicular (10-14%, (*98*)), medullary (3-5%, MTC, (*99*)) and anaplastic (2-5%, (*100*)) thyroid carcinoma (*98*). Even though MTC represents a rather rare form of thyroid disease, clinical interest in novel treatment approaches is increasing due to limited therapeutic options for patients suffering from metastatic MTC (*101*).

Initial diagnosis of MTC is usually followed by a total thyroidectomy accompanied by dissection of the cervical lymph nodes as a first-line treatment approach, providing the highest survival chances (**Figure 5**) (*102*).

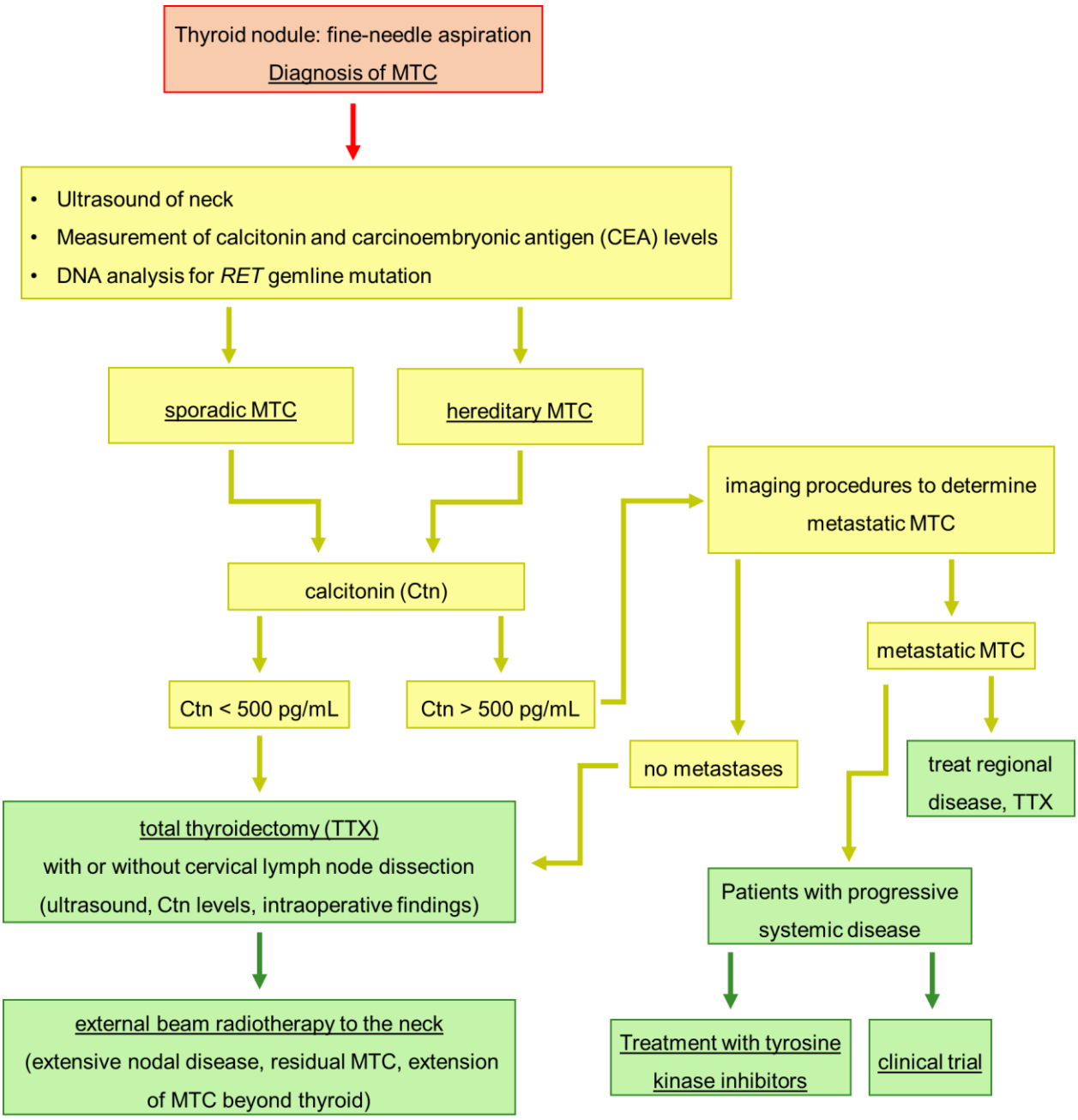

Figure 5. Schematic illustration of MTC patient treatment according to the revised American thyroid association guidelines for management of MTC (*102*). CEA: carcinoembryonic antigen; Ctn: calcitonin; RET: REarranged during Transfection protooncogene; TTX: total thyroidectomy. Depicted in red is the first diagnosis. Diagnostic applications are depicted in yellow. Therapeutic approaches are depicted in green.

In addition, EBRT to the neck is performed for patients at high risk of extensive residual or recurrent disease, despite its controversially discussed survival benefits (*103,104*). Treatment recommendations for patients suffering from recurrent or metastatic disease involve tyrosine kinase inhibitors (TKI), such as vandetanib or carbozantinib, both approved by the FDA in 2011 and 2012, respectively. However, due to their severe adverse effects (e.g., diarrhea, fatigue and nausea) clinical trials evaluating the potential of novel nuclear medicine applications are a second viable option recommended by the American thyroid association guidelines for management of MTC (*101,102,105,106*). As MTC arises from parafollicular calcitonin producing C-cells of neuroendocrine origin, it does not accumulate (radio)iodine unlike other forms of thyroid cancer, excluding radioiodine therapy as possible treatment approach (*107*). To date, 10-year survival of unselected MTC patients is around 75%. However, 10-year survival of patients suffering from recurrent or metastatic disease is noticeably reduced to approximately 40%, displaying the necessity of an early diagnosis (*108,109*).

While the majority of MTC cases occur sporadically (60-80%), 20-40% of patients suffer from hereditary MTC caused by a single germline mutation in the RET proto-oncogene (*110*). Even though hereditary, as opposed to sporadic MTC, often occurs at an earlier age of onset and usually has a more aggressive course of disease, genetic testing of at-risk family members can lead to an early diagnosis followed by a prophylactic total thyroidectomy (*111*). In a study published by Shepet *et al.* in 2013, prophylactic total thyroidectomy before the recommended age of 10 even led to a disease-free survival in 100% of patients (*n=9*) (*112*).

Besides molecular analysis of the DNA for patients at risk of hereditary MTC, fine-needle aspiration biopsy as well as serum calcitonin level testing are used as diagnostic tools, the latter being reported as more accurate (*113-115*). Basal serum calcitonin levels of healthy individuals are usually considered to be below 10 pg/mL. Thus, increasing calcitonin levels can indicate preoperative MTC, postoperative recurrence of MTC or untreated metastatic MTC. In addition, this method allows to differentiate between stable and progressive disease (*116*). To confirm diagnosis in patients with slightly elevated basal serum calcitonin levels and clinically suspected MTC, stimulated serum calcitonin levels are measured using pentagastrin stimulation tests (*114*).

Even though elevated calcitonin levels are a reliable indicator for MTC, localization of the disease is often impossible (*113,117*). Thus, after initial diagnosis, ultrasound, CT as well as nuclear medicine applications, using [^{18}F]fluorodeoxyglucose ([^{18}F]FDG), [^{18}F]fluorodihydroxyphenyl-alanine ([^{18}F]DOPA) and [^{68}Ga]Ga-somatostatin analogs for PET/CT examination, are recommended (*113,118*). As MTC is a tumor of neuroendocrine origin (NET),

increased uptake of [^{18}F]F-DOPA via the large neutral amino acid transporter (LAT1) in combination with increased activity of the amino acid decarboxylase, which transforms [^{18}F]F-DOPA to [^{18}F]fluorodopamin and thus, traps ^{18}F in the malignant cells, leads to the detection of MTC lesions in PET/CT (*119,120*). In addition, well-differentiated NETs often overexpress the somatostatin receptor subtype 2 (SSTR2), enabling targeted imaging approaches using [^{68}Ga]Ga-labeled somatostatin derivatives (*121,122*). In comparison, with a sensitivity of 72% [^{18}F]F-DOPA is outperforming [^{18}F]FDG (17%) and [^{68}Ga]Ga-labeled somatostatin analogs (33%) and is thus currently considered the gold standard for molecular imaging of MTC (*118,123,124*). However, sensitivity of [^{18}F]F-DOPA was only observed to be high for primary tumors (86%), but moderate (57%) to low (6%) for lymph node and distant metastases, respectively (*125,126*). In addition, [^{18}F]F-DOPA is limited to PET imaging applications only, not providing a structurally similar therapeutic equivalent. Thus, there is currently a clinical need for compounds addressing said limitations.

3. CCK-2R Targeting: An Overview

3.1 Characterization of the CCK-2R

Besides using [^{18}F]F-DOPA as PET imaging agent, alternative targeting approaches were conducted addressing the SSTR2, which is possible given MTC's neuroendocrine origin (*127*). However, expression of SSTR2 is only reported in 40% of patients suffering from MTC (*128*). Another potential target overexpressed on MTC cells represents the cholecystokinin-2 receptor (CCK-2R), which was first reported as a viable option in 1996 (*129*). Apart from MTC (92%,(*129*)), a frequent, high-density CCK-2R expression was found on a multitude of malignant tissues such as small cell lung cancer (57%, (*130*)), astrocytomas (65%, (*131*)) and stromal ovarian cancers (100%, (*132*))(*133*). In addition, its physiological expression was reported to be mainly limited to the stomach, and to some extent was observed in the brain, pancreas and gall bladder. CCK-2R expression is assumed to play an important role in the regulation of various physiological functions, such as anxiety, satiety, analgesia and memory in the central nervous system as well as gastric acid secretion, gastrointestinal motility and growth in the gastric mucosa in the gastrointestinal tract (*134-136*).

In general, three different types of cholecystokinin receptors have been identified so far, the cholecystokinin-1 receptor (CCK-1R), the CCK-2R and a splice variant thereof, the CCK-2Ri4sv. In contrast to the CCK-2R, the CCK-1R is only rarely expressed in human healthy (gallbladder and stomach) as well as malignant tissues (e.g., gastroenteropancreatic tumors: 38%, meningiomas: 30%, neuroblastomas: 19%) (*132,137*). The CCK-2Ri4sv was first isolated by Hellmich *et al*. in 2002 in human colorectal cancer and can additionally be found in pancreatic cancer cells. However, due to a low expression density of said receptor on malignant tissue, its use for targeted radiopharmaceutical applications is limited (*138*).

Since all cholecystokinin (CCK) receptors belong to the superfamily of G-protein coupled receptors (GPCR), they comprise their characteristic structure (**Figure 6**). Thus, they consist of seven transmembrane domains, three intracellular and extracellular loops as well as an intracellular and extracellular binding site (*134*). In its inactive state, heterotrimeric G-proteins bind to the GPCRs intracellularly. Upon binding of an agonist to the extracellular binding domain, followed by a conformational change of the receptor, the G-protein is activated and its subunits (G_α, G_β and G_γ) dissociate, inducing a unique intracellular signaling response. After signal transduction, G_α is transformed into its inactive form allowing re-association with G_β and $G_{\gamma.}$ (*139*). In comparison to the human CCK-2R, the human CCK-1R displays an amino acid similarity of 50% (*134*), whereas the human CCK-2Ri4sv comprises 69 additional amino acids in its third intracellular loop domain (*138*).

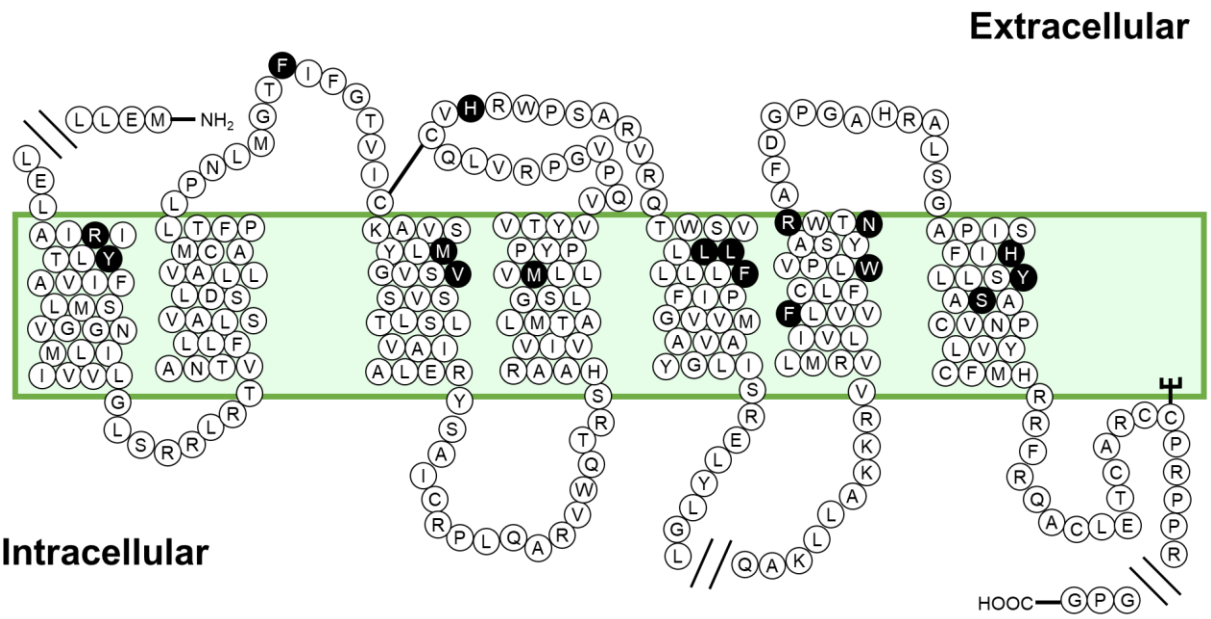

Figure 6. Schematic representation of the human CCK-2R. Main amino acids of the CCK-2R binding site are depicted in black (*140*).

To date, the cDNA encoding the CCK-2R has been isolated in a variety of species, such as mouse, rat, rabbit, cow, dog and human, all displaying a high structural homology of 84% to 93%. However, binding studies have demonstrated a noticeable influence of interspecies polymorphism on the affinity and activity of synthetic ligands. This finding mainly accounts for synthetic non-peptidic antagonists, such as L-365,260 and L-364,718. The endogenous CCK-2R ligands are not affected by this polymorphism-induced alterations, thus binding CCK-2Rs of various species with comparable affinities (*141,142*).

The two main natural ligands identified for cholecystokinin receptors are CCK and gastrin, both comprising an identical *C*-terminal pentapeptidic sequence (*H*-Gly-Trp-Met-Asp-Phe-NH_2) and differing in their sulfation at the sixth (gastrin) and seventh (CCK) tyrosyl residues (**Figure 7**) (*135*).

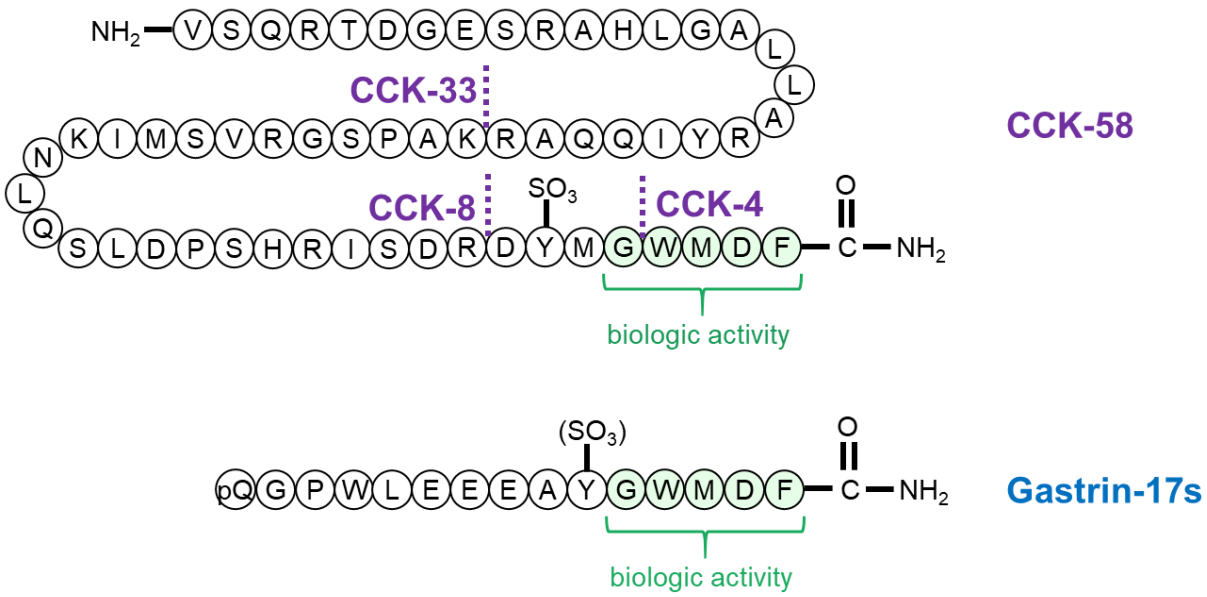

Figure 7. Schematic representation of Gastrin-17s (blue) and CCK analogs (purple). Biologically active sequence is depicted in green (*135*).

Whilst the CCK-2R binds CCK and gastrin with high affinities and does not discriminate between sulfated and non-sulfated peptide analogs, the CCK-1R preferably binds sulfated CCK with a 500- to 1000-fold higher affinity compared to sulfated Gastrin and non-sulfated CCK, respectively (*134*).

3.2 Development of CCK-2R Targeted Compounds: From Discovery to First Clinical Candidates

3.2.1 Development of Minigastrin Analogs With Reduced Activity Uptake in the Kidneys

Even though research focused on the development of both CCK as well as gastrin analogs for CCK-2R targeting in the beginning, to date gastrin derivatives are used preferably. Especially the enhanced hydrophilicity of gastrin analogs in combination with their increased affinity towards the CCK-2R when compared to non-sulfated CCK derivatives, led to enhanced biodistribution profiles of the former (*143*). In addition, sulfated CCK derivatives indeed display a similarly high CCK-2R affinity compared to gastrin, yet accompanied by high CCK-1R affinity and thus, lower CCK-2R specificity (*144,145*).

A first strategy to evaluate the capability as well as feasibility of radiolabeled gastrin for CCK-2R targeting *in vivo*, was the radioiodination of the Tyr moiety in gastrin-17 (*H*-pGlu-Gly-Pro-Trp-Leu-$(Glu)_5$-Ala-Tyr-Gly-Trp-Met-Asp-Phe-NH_2) reported by Behr *et al.* in 1998. Within this study, moderate activity levels for [^{131}I-Tyr^{12}]gastrin-17 (8.9±2.9 %ID/g) were detected in the TT tumor xenograft up to 1 h after injection in nude mice. However, fast washout from the tumor over time (up to 24 h post injection (p.i.)) in combination with high activity levels in non-tumor organs, especially kidneys, stomach, gallbladder, bowel and pancreas, displayed the need for further optimization. Nevertheless, a first proof-of-concept study applying [^{131}I-Tyr^{12}]gastrin-17 in a MTC patient demonstrated promising results, thus confirming gastrin analogs as suitable lead structures for CCK-2R targeting (**Figure 8A**) (*146*).

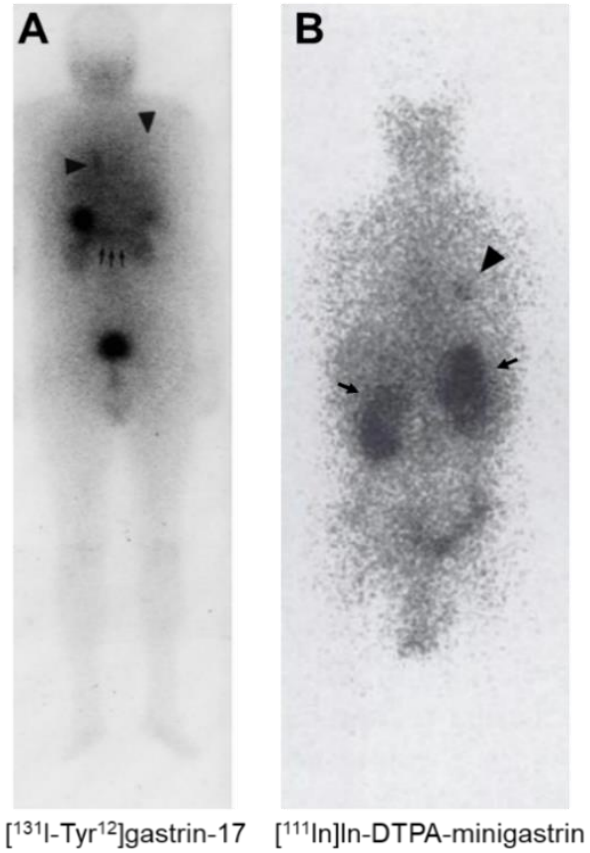

Figure 8. Whole body scan of two patients suffering from MTC injected with A) [^{131}I-Tyr^{12}]gastrin-17 or B) [^{111}In]In-DTPA-minigastrin at 2 and 24 h after injection, respectively. Small arrows: stomach, pancreas and gallbladder; arrowheads: metastasis. Copyright © by SPRINGER INTERNATIONAL (*146*). B) Small arrows: kidneys; arrowhead: metastasis. Copyright © 1999 by SNMMI (*144*).

Further optimization strategies were conducted using minigastrin (*H*-Leu-$(Glu)_5$-Ala-Tyr-Gly-Trp-Met-Asp-Phe-NH_2), which was conjugated to a diethylenetriaminepentaacetic acid (DTPA) chelator *N*-terminally, thus enabling ^{111}In-labeling. Hence, simplified labeling procedures, increased stabilities as well as favorable physical imaging characteristics compared to radioiodinated gastrin analogs were established. Both DTPA-minigastrin and its D-Leu comprising analog, DTPA-[D-Leu^1]minigastrin, were evaluated *in vitro* as well as *in vivo*, displaying similar properties (*117,144*). In comparison to [^{131}I-Tyr^{12}]gastrin-17 decreased activity levels in the tumor were observed, however accompanied by lower activity accumulation in the stomach, gall bladder, bowel and pancreas, which resulted in favorable tumor-to-background ratios *in vivo* (**Figure 8B**) (*145-147*).

As the kinetic stability of DTPA was observed to be sufficient for ^{111}In-labeling only, lacking the option of radiolabeling with therapeutic nuclides such as ^{90}Y, DTPA-MG0 (DTPA-D-Glu-$(Glu)_5$-Ala-Tyr-Gly-Trp-Met-Asp-Phe-NH_2) was developed, which comprised a DTPA-D-Glu chelator moiety. It is assumed that the additional *γ*-carboxylate of D-Glu in proximity to the DTPA chelator has a stabilizing effect on the kinetic stability of the chelator metal complex (*117*). Within a comparative study of DTPA-MG0 and DTPA-minigastrin, evaluated both ^{111}In- as well as ^{88}Y-labeled ($t_{1/2}$=107 d; 1.836 and 898 keV; used for preclinical evaluation of yttrium complexes due to detectable *γ*-emission), a noticeably increased serum half-life of the former was achieved for both nuclide complexes. These results were confirmed by biodistribution studies of [^{88}Y]Y-DTPA-MG0 in TT-tumor-bearing nude mice, displaying significantly reduced activity levels in the liver as well as bone when compared to [^{88}Y]Y-DTPA-minigastrin. It is known that free yttrium as well as indium ions accumulate in the liver and bone. For this reason, a decreased activity accumulation in said organs supports the assumption of an enhanced complex stability. However, even though kinetic stability of [^{88}Y]Y-DTPA was shown to be increased, elevated activity levels in the kidneys limited the therapeutic application of [^{90}Y]Y-DTPA-MG0, which is why further optimization was still required (*147*).

In 2007 Good *et al.* performed a comparative study on minigastrin analogs comprising different glutamate chain lengths (MG0: *n=5*; MG9: *n=2*; MG10: *n=1*; MG11: *n=0*) and macrocyclic chelators (DTPA *versus* DOTA and 1,4,7,10-tetraazacyclododecane-*N*-(glutaric acid)-*N*',*N*'',*N*'''-triacetic acid (DOTAGA)). Exchange of DTPA with DOTA or DOTAGA led to enhanced kinetic stability of the radiometal complexes. In addition, reduction of glutamate moieties in the linker sequence was accompanied by reduced activity accumulation in the kidneys and thus, enhanced tumor-to-kidney ratios. However, a poor *in vitro* stability of the most promising compound

evaluated within this study, [^{111}In]In-DOTA-MG11 ([^{111}In]In-DOTA-D-Glu-Ala-Tyr-Gly-Trp-Met-Asp-Phe-NH_2), led to low activity levels in the tumor (0.34±0.01 %ID/g) at 24 h after injection in AR42J tumor-bearing Lewis rats (*148*).

A novel approach to circumvent high activity levels in the kidneys while maintaining a stabilizing linker sequence was reported by Kolenc-Peitl *et al.* in 2011. Within this study, various polar but uncharged amino acid spacers in different length were evaluated ($(PEG)_4$ to $(PEG)_{12}$; $(D\text{-}Ser)_2$ and $(D\text{-}Ser)_3$; $(D\text{-}Gln)_2$ to $(D\text{-}Gln)_6$). Out of those, especially [^{111}In]In-DOTA-PP-F10 (DOTA-$(D\text{-}Gln)_6$-Ala-Tyr-Gly-Trp-Met-Asp-Phe-NH_2), led to massively improved stability in human serum (495±104 *versus* 75±23 h; expressed as serum half-life time) as well as reduced activity accumulation in the kidneys (0.33±0.05 *versus* 25.5±2.6 %ID/g) at 4 h after injection in AR42J tumor-bearing Lewis rats in comparison to [^{111}In]In-DOTA-PP-F11-L (DOTA-$(L\text{-}Glu)_6$-Ala-Tyr-Gly-Trp-Met-Asp-Phe-NH_2). Therefore, favorable tumor-to-kidney ratios (3.1 *versus* 0.1%) were observed for the former (*149*). Following up on these results, Kolenc-Peitl *et al*. performed a comparative study on amino acid configuration in the spacer sequence, directly comparing DOTA-PP-F11-L and CP04 (DOTA-$(D\text{-}Glu)_6$-Ala-Tyr-Gly-Trp-Met-Asp-Phe-NH_2). The results of this study revealed that not only the charge distribution in the linker sequence but also the configuration of the amino acids and thus, the secondary structure of the peptides have a major influence on their pharmacokinetic properties. Whilst *in vitro* stability ([^{111}In]In-DOTA-PP-F11-L: 75±23 h; [^{111}In]In-CP04: 175±71 h) as well as activity uptake in the kidneys ([^{111}In]In-DOTA-PP-F11-L: 19.4±5.6 %ID/g; [^{111}In]In-CP04: 0.87±0.06 %ID/g; 24 h after injection in AR42J tumor-bearing Lewis rats) benefited from the change from L- to D- hexaglutamate chains, binding affinity ([^{nat}In]In-DOTA-PP-F11-L: 1.5±0.4 nM; [^{nat}In]In-CP04: 2.5±1.4 nM) and internalization kinetics remained similar (*143,150*). The substitution of Met by Nle in CP04, led to DOTA-PP-F11N (DOTA-$(D\text{-}Glu)_6$-Ala-Tyr-Gly-Trp-Nle-Asp-Phe-NH_2), a further stabilized minigastrin analog. Comparable biodistribution profiles with good activity uptake in the tumor ([^{177}Lu]Lu-DOTA-PP-F11N: 6.94±0.82 %ID/g; [^{177}Lu]Lu-CP04: 6.70±0.56 %ID/g) as well as low kidney retention ([^{177}Lu]Lu-DOTA-PP-F11N: 5.75±1.56 %ID/g; [^{177}Lu]Lu-CP04: 4.30±0.56 %ID/g) in A431/CCK-2R tumor-bearing mice at 4 h after injection, in combination with a moderate *in vitro* stability of both ligands, rendered them promising candidates for clinical translation (*151,152*).

3.2.2 Optimization Strategies Towards Enhanced Metabolic Stability

One major limitation of early generations of minigastrin analogs, especially those lacking the pentaglutamate sequence in their linker section (e.g., MG11), was their susceptibility towards enzymatic degradation (*148*). Thus in 2011, Ocak *et al.* performed a comparative study on the *in vivo* stability of different minigastrin analogs to determine their major cleavage sites (**Figure 9**).

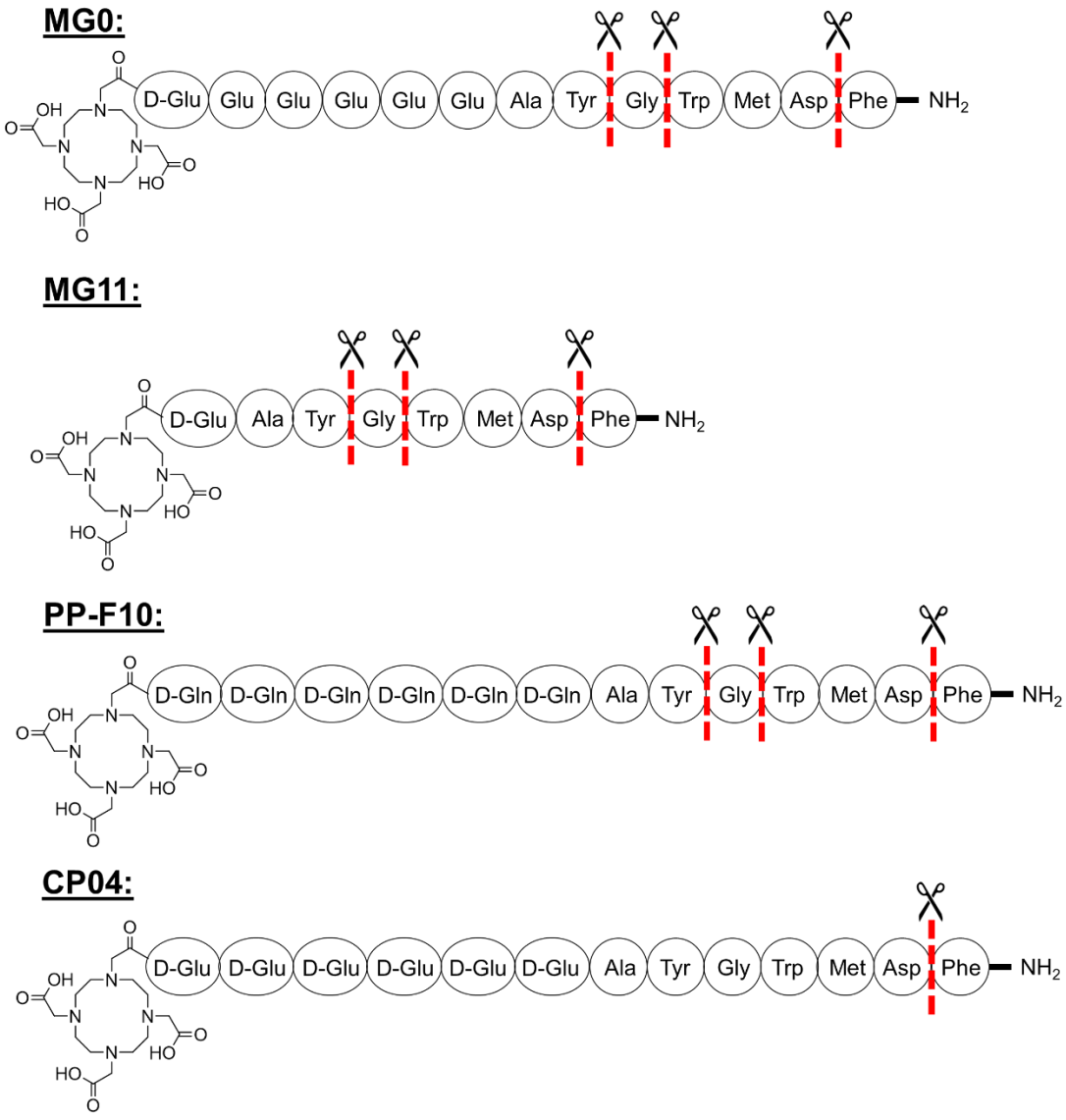

Figure 9. Schematic representation of the main cleavage sites of MG0, MG11, PP-F10 and CP04 *in vitro* as analyzed by MALDI-TOF MS (*152*)**.**

Within this study, the Asp-Phe, Gly-Trp as well as the Tyr-Gly peptide bonds were identified as main instabilities. Furthermore, first stability studies *in vivo* revealed only a poor to moderate stability in serum at 10 min after injection for all compounds evaluated ([^{177}Lu]Lu-DOTA-MG0, [^{177}Lu]Lu-DOTA-MG11, [^{177}Lu]Lu-DOTA-PP-F10 and [^{177}Lu]Lu-CP04). No intact peptide was found in the urine for any of the compounds tested, underlining the need for further stabilization strategies (*152*).

One approach to reduce enzymatic degradation of peptides is their structural optimization via different amino acid modifications (e.g., *N*-methylation, change of configuration from L- to D- or insertion of unnatural amino acids) (*145,150,153*) (**Figure 10**).

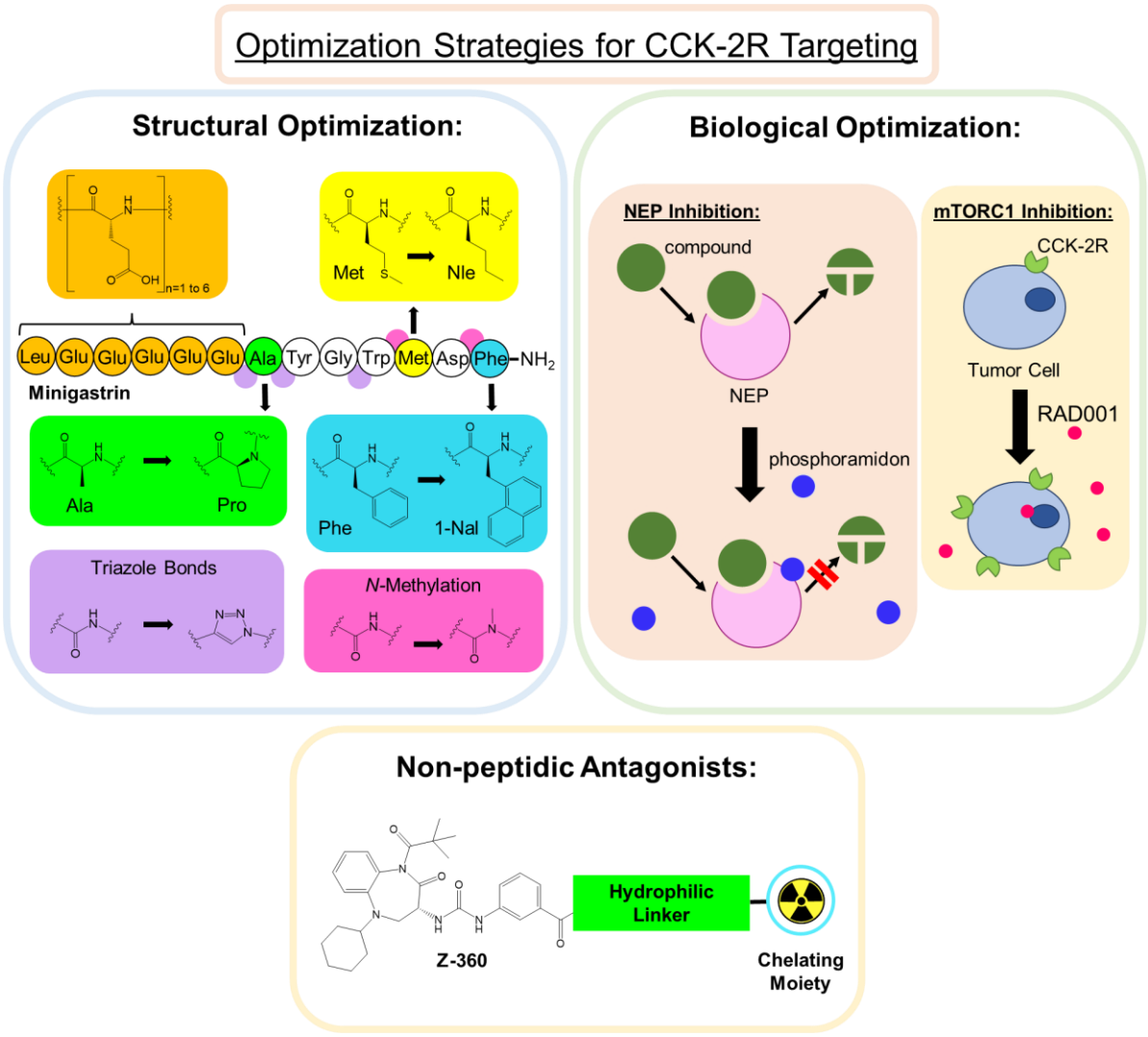

Figure 10. Schematic representation of different optimization strategies for enhanced tumor targeting of compounds addressing the CCK-2R as described in the literature (*30,145,153-167*). NEP = neutral endopeptidase.

However, to perform such structural changes, amino acid sequences crucial for high target affinity need to be identified first. Thus, already in the 1990s, several groups reported about the tetrapeptidic sequence, *H*-Trp-Met-Asp-Phe-NH_2 (CCK-4) having a major influence on high affinity CCK-2R binding (*145,168-170*). Within this tetrapeptide, especially the Met moiety was reported to be very susceptible towards oxidation. Even though, a study performed by Behr e*t al.* demonstrated no influence of oxidized Met on CCK-2R affinity, said stability issue can be easily prevented by substitution of Met with Nle, as successfully demonstrated for various CCK-2R targeted peptides, such as in CP04, which resulted in DOTA-PP-F11N (*144,151,168-170*).

Based on a study reported by Corringer *et al.* already in 1993, Klingler *et al.* evaluated the influence of 1-Nal or (*N*-Me)Phe instead of Phe, as well as (*N*-Me)Nle or Phg instead of Met on the *in vivo* stability as well as CCK-2R affinity of MG11 (*153,170*). Within this study, especially the substitution of Met by (*N*-Me)Nle in position 6 and Phe by 1-Nal in position 8 revealed promising results (*153*). Thus, during a follow-up study published in 2019, DOTA-MGS5 (DOTA-D-Glu-Ala-Tyr-Gly-Trp-(*N*-Me)Nle-Asp-1-Nal-NH_2) was reported, displaying a significantly enhanced *in vivo* stability and thus, biodistribution profile when compared to its predecessor MG11. With a tumor-to-kidney ratio of 4.10±0.16 as well as activity levels in the tumor of 23.3±4.7%ID/g at 1 h after injection in A431-CCK-2R tumor-bearing BALB/c mice, [^{68}Ga]Ga-DOTA-MGS5 is a promising candidate for clinical translation (*159*). However, one drawback was the low number of intact peptide (3.0±1.6% at 10 min after injection) found in the urine of its hydrazinonicotinic acid (HYNIC)-comprising analog (HYNIC-MGS5), which left room for further stabilization (*158*). In 2020, Klingler *et al.* evaluated the influence of increased conformational rigidity on *in vivo* stability, implemented by substitution of either Ala, Tyr or Gly by Pro in DOTA-MGS5, which resulted in highly CCK-2R-affine compounds with enhanced *in vivo* stability (*166,171,172*). Out of those, especially DOTA-MGS8 (DOTA-D-Glu-Pro-Tyr-Gly-Trp-(*N*-Me)Nle-Asp-1-Nal-NH_2) displayed enhanced activity levels in the tumor accompanied by increased tumor-to-kidney ratios compared to its predecessor DOTA-MGS5 (*166*). However, the Tyr-Gly as well as the Gly-Trp cleavage sites were not addressed in this studies. Therefore, the number of intact peptide in the urine (19.4%) at 30 min after injection was reported to be low (*167*).

Another approach to structurally stabilize minigastrin derivatives was published by Grob *et al.* in 2020, which aimed at the gradual substitution of peptide bonds by 1,4-disubstituted 1,2,3-triazoles in DOTA-[Nle]MG11 (DOTA-D-Glu-Ala-Tyr-Gly-Trp-Nle-Asp-Phe-NH_2) and DOTA-PP-F11N. Within this study compounds comprising triazole bonds at the D-Glu-Ala, Tyr-Gly and Gly-Trp position, displayed good IC_{50} values below 20 nM. However, enhanced stability was only

observed for peptides comprising a triazole moiety at the Ala-Tyr, Trp-Nle, Nle-Asp and Asp-Phe position as well as *N*-terminally located triazole moieties, which displayed a noticeably loss in CCK-2R affinity compared to DOTA-[Nle]MG11. Therefore, no beneficial effect on tumor targeting was accomplished (*156,157*). Even though none of the above-mentioned strategies published provided a suitable resolution for structural optimization of the Tyr-Gly or Gly-Trp peptide bond, their findings support the hypothesis of only the *N*-terminal tetrapeptidic sequence being crucial for high affinity CCK-2R binding. Modifications in other parts of the peptide structure were demonstrated to be well tolerated (*157,166*).

Besides structural stabilization of CCK-2R targeted compounds, biological stabilization strategies were evaluated. Already in the late 1980s, it has been demonstrated by Power *et al.*, as well as Deschodt-Lanckman *et al.*, that neutral endopeptidase (NEP) plays a role in degradation of human gastrin-17 (*173,174*). In general, NEP is only rarely found in plasma, however abundantly expressed in most tissues, anchored on the cell surface of the vasculature compartment, as well as in major organs (e.g., kidneys, liver, lungs and gastrointestinal tract) (*175*). Therefore, as a novel approach to increase *in vivo* stability, as well as tumor uptake of minigastrin analogs, such as DOTA-MG11, DOTA-PP-F11N and CP04, co-injection of phosphoramidon (PA), a NEP inhibitor, was evaluated *in vivo* by several groups. Out of these compounds, especially the metabolically unstable DOTA-MG11, benefited from the co-administration of PA. Enhanced numbers of intact peptide in murine serum for [^{177}Lu]Lu-DOTA-MG11, led to a substantially increased activity uptake in the tumor (without PA: 1.45±0.30 %ID/g *versus* with PA: 7.34±1.64 %ID/g) at 4 h after injection in A431-CCK-2R tumor-bearing mice. For [^{177}Lu]Lu-CP04 (without PA: 6.70±0.56 %ID/g *versus* with PA: 9.34±1.11 %ID/g) and [^{177}Lu]Lu-DOTA-PP-F11N (without PA: 6.94±0.82 %ID/g *versus* with PA: 8.53±2.22 %ID/g), co-injection of PA had only a minor influence on activity uptake in the tumor, which can be attributed to the lower susceptibility towards enzymatic degradation than DOTA-MG11 (*151,176,177*). Given these promising preclinical results the authors suggested, that enzyme inhibition might be a valuable alternative to time-consuming and expensive structural optimization approaches. However, when compared to [^{177}Lu]Lu-DOTA-PP-F11N without co-injection of PA, [^{177}Lu]Lu-DOTA-MG11 co-injected with PA displayed similar activity levels in the tumor at 4 h after injection. Besides economical advantages, single-compound applications are favored over co-injections, due to the additional challenges (e.g., optimized inhibitor dose, administration route and time-point of administration) of dual drug administrations (*151,154,176,177*).

A further biological optimization strategy to enhance tumor uptake of minigastrin analogs that does not address the stability of the conjugates evaluated represents the inhibition of mTORC1, reported by Grzmil *et al.* in 2020. Due to the inhibition of the oncogenic AKT/mTOR pathway that supports cancer cell growth and survival, increased CCK-2R expression was observed (*155,178*). Thus, pre-treatment of A431-CCK-2R cells and A431-CCK-2R tumor-bearing mice with the clinically approved mTORC1 inhibitor, RAD001 (everolimus), led to increased internalization values as well as activity levels of [^{177}Lu]Lu-DOTA-PP-F11N in the tumor/cells xenograft (*155,179*). These findings might be a valuable tool for clinical translation with regard to a combination attempt, which might have the potential to improve efficacy of RLT, while reducing the burden to non-tumor tissues (*155*). However, also facing the above-mentioned challenges of dual drug administration.

As a third strategy aimed at optimizing CCK-2R targeting, research on the identification and development of antagonists has progressed (*180,181*). Using radiolabeled receptor antagonists to increase initial tumor uptake, has already been successfully demonstrated for a variety of other GPCRs, such as gastrin-releasing peptide receptor (GRPR) and SST2R, which resulted in first agents evaluated in clinical trials (*133,182-185*). This beneficial effect can be attributed to the assumption that antagonists can target a higher number of binding sites, as they are not limited to active receptors. In addition, antagonists limit the possibility of biological adverse effects upon binding of the receptor, resulting in the reduction of negative side-effects in patients (*133,186*). Novel CCK-2R targeted antagonists mainly comprise the small molecule Z-360 as lead structure, additionally providing enhanced stability towards enzymatic degradation. However, due to the elevated lipophilicity of Z-360, hydrophilic linker structures, such as sugar moieties, charged amino acids or PEG linkers are required (*162-165*). In 2022, the group of Nock *et al.* reported the compound GAS3 (DOTAGA-D-Glu-$(PEG)_2$-Z-360), which displayed favorable preclinical properties when ^{177}Lu-, ^{111}In- or ^{67}Ga-labeled, such as CCK-2R affinity, *in vivo* stability and early biodistribution profiles (1 to 4 h p.i.). However, fast clearance kinetics of [^{177}Lu]Lu-GAS3 (observed at 24 and 72 h p.i.) might be a limiting factor for therapeutic applications. In addition, due to the lack of comparison to a literature-known reference structure, further experiments need to confirm these promising findings (*30*).

3.2.3 Exploring the Palette of Different Radionuclides for CCK-2R Targeting

To date, radionuclides of choice for research as well as clinical translation of CCK-2R-targeted compounds were mainly limited to ^{111}In (SPECT), ^{68}Ga (PET), and ^{177}Lu (RLT) (*161,187,188*), even though a variety of different radionuclides (e.g., ^{18}F, ^{99m}Tc, ^{225}Ac, $^{61/64/67}$Cu, $^{149/152/155/161}$Tb) could offer a wide range of beneficial possibilities for medical applications (*43,78,189-191*). For example, the favorable SPECT imaging properties of ^{99m}Tc ($t_{1/2}$=6.02 h, monoenergetic *γ*-photons of 141 keV) when compared to ^{111}In ($t_{1/2}$=2.83 d, monoenergetic *γ*-photons of 173 and 247 keV), accompanied by the possibility of subsequent radio-guided surgery, render this radioisotope more attractive for diagnostic applications (*192,193*). In addition, availability of ^{99m}Tc is high, as it is mainly obtained via ^{99}Mo/^{99m}Tc generators at low cost (*193*). Thus, already in the early 2000s von Guggenberg *et al.* as well as Nock e*t al.* developed ^{99m}Tc-labeled peptide analogs for CCK-2R targeting (*194,195*). In these studies, [^{99m}Tc]Tc-EDDA/HYNIC-MG11 and [^{99m}Tc]Tc-Demogastrin 2 (N_4-Gly-D-Glu-$(Glu)_5$-Ala-Tyr-Gly-Trp-Met-Asp-Phe-NH_2; N_4-Gly-MG0), demonstrated the most promising results. However, both agents displayed similar limitations as their DOTA-comprising analogs (DOTA-MG0 and DOTA-MG11), such as high activity levels in the kidneys and low metabolic stability. Nevertheless, first patient studies using [^{99m}Tc]Tc-EDDA/HYNIC-MG11 and [^{99m}Tc]Tc-Demogastrin 2 revealed good imaging properties, especially at 4 h after injection (*195-198*). As a follow-up study on the promising preclinical data of DOTA-MGS5, in 2019 Klinger e*t al.* reported about the synthesis and evaluation of its HYNIC-comprising analog, [^{99m}Tc]Tc-HYNIC-MGS5. In this study, high tumor accumulation accompanied by fast clearance from off-target tissue was observed. In addition, *in vivo* stability was demonstrated to be high. Even though a clinical translation of [^{99m}Tc]Tc-HYNIC-MGS5 was recommended, no patient data is available for this compound, yet (*158*).

Another example for a radioisotope beneficial for clinical applications is ^{18}F, as it enables high-resolution PET scans even at later imaging time points (e.g., 6 h), due to its favorable physical properties, as discussed above (*56*). In 2021, Khan *et al.* reported about first studies on ^{18}F-labeled minigastrin analogs based on MG11, attaching different fluorine-containing aromatic (4-fluorobenzoate), heterocyclic (6-fluoronicotinate) and aliphatic (2-fluoropropionate) moieties to the *N*-terminus of said peptide. Even though IC_{50} values of all compounds evaluated were found to be in a low nanomolar range, which suggests a high tolerability of aromatic as well as aliphatic moieties at the *N*-terminal part of MG11 towards CCK-2R affinity, challenges in radiolabeling strategies resulted only in the successful synthesis of one ^{18}F-labeled compound in this study. Said compound comprises a 6-nitronicotinoyl moiety, which can be labeled with [^{18}F]fluoride via

nucleophilic aromatic substitution at 110°C for 5 min. However, a poor chemical stability of the ^{18}F-carbon bond displayed the need for optimized alternatives (*199*). In addition, a low stability of MG11 towards enzymatic degradation hampered its use as a lead structure for development of novel radiopharmaceuticals (*148,176*).

Besides PRRI, research on RLT using β^--emitters, such as ^{177}Lu and ^{90}Y, is well established in the field of CCK-2R targeted compounds. As a complementary approach, TAT could be a valuable tool for patients suffering from late-stage MTC and no longer benefitting from RLT using β^--emitters. Thus, in 2020 Qin *et al.* published an initial preclinical study about the therapeutic efficacy of [^{225}Ac]Ac-DOTA-PP-F11N. Therefore, different doses (30 to 120 kBq) were applied to A431/CCK-2R tumor-bearing nude mice, resulting in an up to 3.4-fold enhanced mean survival of the animals treated with the highest dose (120 kBq, 58 d), when compared to the control group mice (17 d). In addition, no apparent toxicity was observed for all mice treated with [^{225}Ac]Ac-DOTA-PP-F11N. Histological analysis of stomach and kidneys displayed no severe adverse effects after [^{225}Ac]Ac-DOTA-PP-F11N administration. All in all, these promising findings warrant the potential of further preclinical evaluation on the applicability of clinical translation of TAT using minigastrin derivatives (*200*).

3.3 Current Clinical State of the Art

Over the last decades, various CCK-2R targeted compounds have been developed and preclinically evaluated, however only a few were translated into the clinics. To date, clinical interest is focused on mainly three promising minigastrin derivatives: [^{68}Ga]Ga-DOTA-MGS5 and [^{111}In]In-CP04 for diagnostic applications, and [^{177}Lu]Lu-DOTA-PP-F11N for theranostic approaches. Thus, clinical trials of said compounds have been initiated and are currently on-going ([^{177}Lu]Lu-DOTA-PP-F11N: NCT02088645; [^{68}Ga]Ga-DOTA-MGS5: EudraCT:2020-003932-26) or were recently completed ([^{111}In]In-CP04: NCT03246659; [^{177}Lu]Lu-DOTA-PP-F11N: NCT03647657) (*161,187,188*).

In a first phase I clinical trial, [^{111}In]In-CP04 displayed a detection rate of 81%, illustrating lesions in 13 out of 16 patients with elevated calcitonin levels. In addition, [^{111}In]In-CP04 out-performed conventional imaging methods (CT of the neck/thorax, abdomen; [^{18}F]FDG PET/CT) in 6 patients, detecting more lesions or pointing out false-positive lesions (**Figure 11**) (*187*).

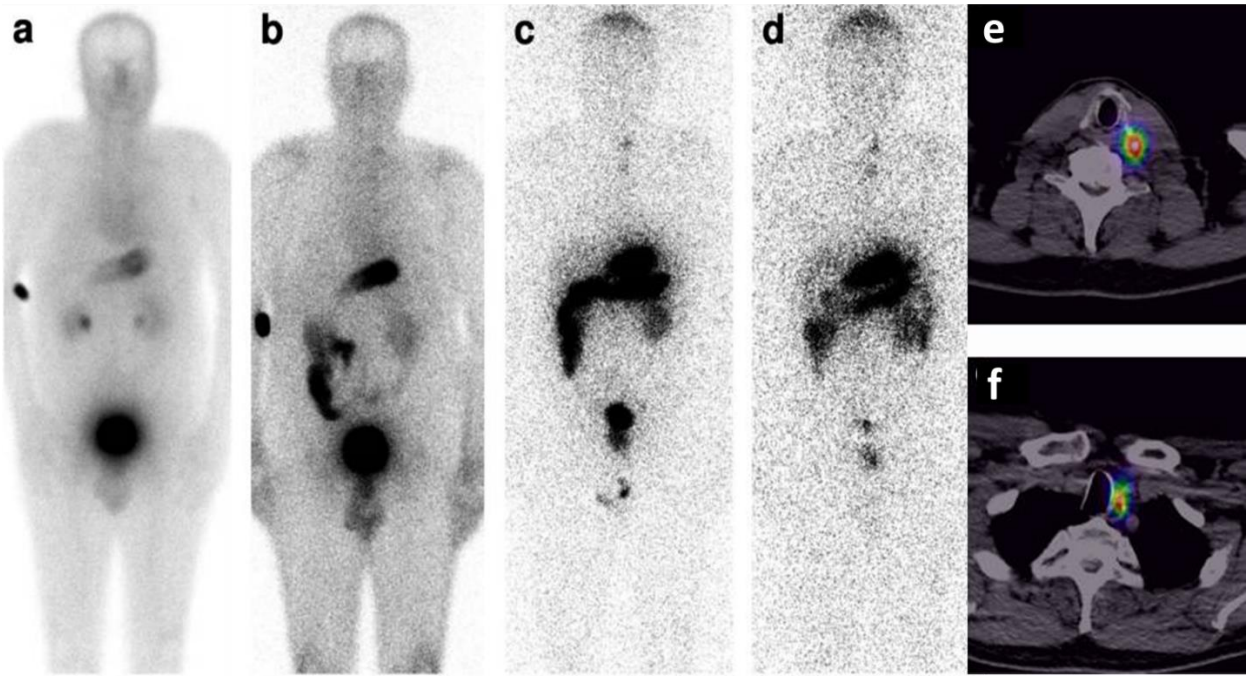

Figure 11. Exemplary whole body dynamic distribution from a clinical GRANT-T-MTC study comprising 16 patients after intravenous administration of [^{111}In]In-CP04 a) immediately after injection, b) at 1 h, c) at 24 h, and d) at 48 h p.i.. e-f) SPECT/CT imaging of two lesions. Copyright © 2022 by Lezaic L, Erba PA, Decristoforo C, Zaletel K, Mikolajczak R, Maecke H, Maina T, Konijnenberg M, Kolenc P, Trofimiuk-Müldner M, Przybylik-Mazurek E, Virgolini I, de Jong M, Fröberg AC, Rangger C, Di Santo G, Skorkiewicz K, Garnuszek P, Solnica B, Nock BA, Fedak D, Gaweda P, Hubalewska-Dydejczyk A (*187*).

Imaging studies of the remaining 10 patients within this study delivered equivalent or complementary results for conventional as well as [^{111}In]In-CP04 SPECT/CT imaging. In addition, a low dose exposition of the non-tumor organs was observed, suggesting the stomach as the sole dose-limiting organ for potential [^{177}Lu]Lu-CP04 RLT, which needs to be verified in further clinical trials (*187*). However, inferior imaging qualities of SPECT *versus* PET, due to a higher resolution, better attenuation correction, less scattering and better contrast of the latter (*201*), as well as fast clearance kinetics of [^{111}In]In-CP04, illustrate the need for further optimized minigastrin analogs.

Not surprisingly, the chemically similar compound [^{177}Lu]Lu-DOTA-PP-F11N, differing only in one amino acid in position 11 (Nle *versus* Met) and the choice of radionuclide used (^{177}Lu *versus* ^{111}In) from [^{111}In]In-CP04, provided comparable biodistribution profiles in a first-in-human clinical trial comprising 6 patients (**Figure 12**) (*161*).

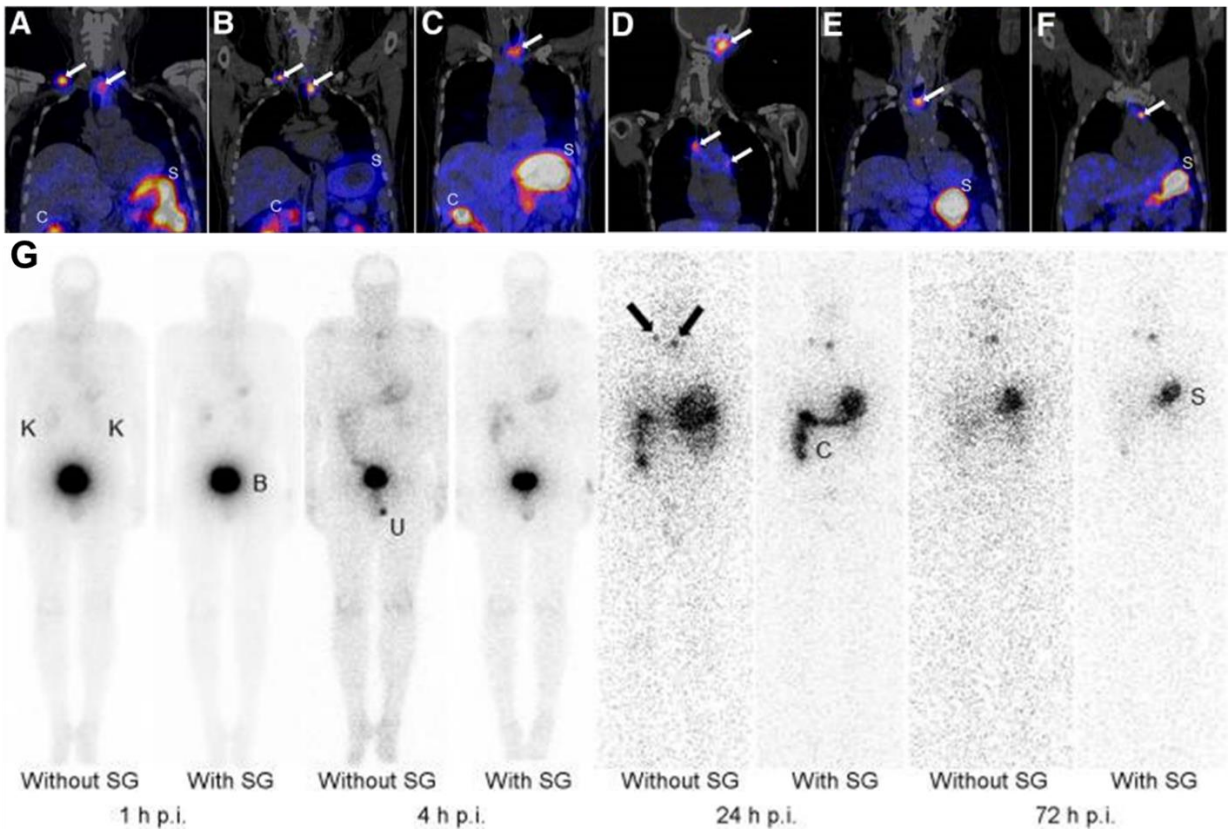

Figure 12. A-F) [^{177}Lu]Lu-DOTA-PP-F11N coronal SPECT/CT scans at 24 h p.i. of 6 different patients G) Exemplary planar scan of one patient injected with either [^{177}Lu]Lu-DOTA-PP-F11N (1 GBq) alone or co-injected with [^{177}Lu]Lu-DOTA-PP-F11N (1 GBq) and succinylated gelatin (SG) at 1 to 72 h p.i. B = urinary bladder; C = colon; K = kidneys; S = stomach; U = urine. Figures have been originally published in JNM and have been combined for this thesis. Copyright © 2020 by SNMMI (*161*).

Within this study, tumor-specific and CCK-2R-mediated accumulation of [^{177}Lu]Lu-DOTA-PP-F11N was confirmed by autoradiography and histologic assessment of one lesion. In addition, low acute toxicity of [^{177}Lu]Lu-DOTA-PP-F11N was reported. Co-administration of succinylated gelatin (SG) did not significantly affect tumor-to-kidney dose ratios. The dose-limiting organ reported in this study represented the stomach (*151,161*). Like [^{111}In]In-CP04, [^{177}Lu]Lu-DOTA-PP-F11N displayed a highly hydrophilic profile, which can be attributed to the hexaglutamate chain in the linker section. Thus, accelerated renal clearance was observed for [^{177}Lu]Lu-DOTA-PP-F11N, leading to a low mean absorbed tumor dose (0.88 Gy/GBq) (*161*), as opposed to clinically established radiopharmaceutical tracers such as: [^{177}Lu]Lu-DOTATATE (3.85±1.74 Gy/GBq, (*202*)) and [^{177}Lu]Lu-PSMA-617 (5.9 –6.1 Gy/GBq, (*203,204*)), which is why alternative options are required.

The third minigastrin analog currently evaluated clinically represents the metabolically more stable compound DOTA-MGS5. So far, first patient data of said compound have been reported (*n=6*) labeled with the PET isotope ^{68}Ga. No adverse effects were detected in any of the patients. In addition, imaging studies at 2 h after injection displayed a superior tumor-to-background ratio in 98.9% of the lesions compared to earlier imaging time points, suggesting a higher accumulation in the tumor lesions, as well as a continuous activity clearance from off-target organs over time (*188*). However, ^{68}Ga imaging is recommended to be performed at 4 h after injection at the latest, due to its rather short half-life, leading to a decreased image resolution for later time points (*203,205,206*). Thus, patient studies including PET isotopes comprising a longer half-life, such as ^{18}F or ^{64}Cu ($t_{1/2}$=12.7 h), would be valuable in order to determine the most suitable imaging time point for minigastrin analogs (*207-211*). A comparative evaluation of [^{68}Ga]Ga-DOTA-MGS5 with the clinical gold standard for MTC imaging, [^{18}F]F-DOPA, displayed complementary results (**Figure 13**) (*212*).

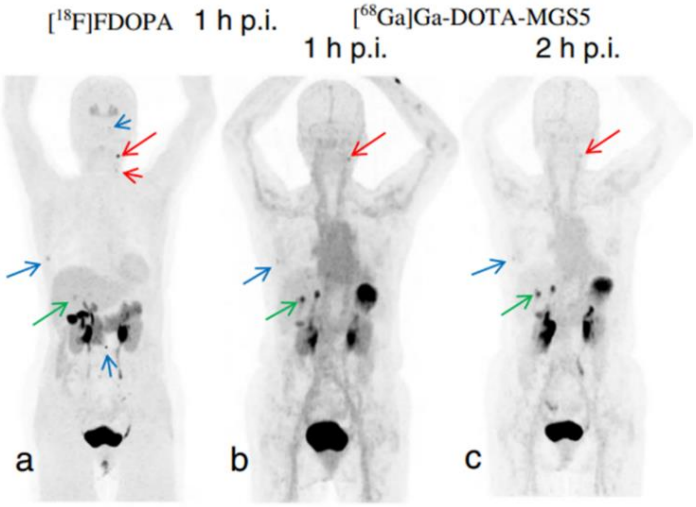

Figure 13. Comparative representation of the maximum intensity projection of a patient suffering from metastatic MTC injected with a) [^{18}F]F-DOPA 1 h after injection and b-c) [^{68}Ga]Ga-DOTA-MGS5 1 and 2 h after injection, respectively. Copyright © 2020, Springer-Verlag GmbH Germany, part of Springer Nature (*212*).

While activity uptake in the lymph nodes and bone lesions was higher for [^{18}F]F-DOPA, activity levels in hepatic lesions were higher for [^{68}Ga]Ga-DOTA-MGS5 (*212*). Therefore, the use of [^{68}Ga]Ga-DOTA-MGS5 might be more attractive than [^{18}F]F-DOPA, given its possible follow-up treatment using [^{177}Lu]Lu-DOTA-MGS5. However, first dosimetry and treatment studies must be performed to confirm this preliminary advantage (*188,212*).

Even though first promising clinical results on PRRI of MTC patients have been reported, small patient cohorts (6 to 16) as well as minor limitations (imaging time point, clearance kinetics, choice of radionuclide) display the need for further evaluation as well as development of alternative minigastrin derivatives. In addition, first clinical trials with therapeutic doses of the ^{177}Lu-labeled peptides (DOTA-MGS5, CP04 and DOTA-PP-F11N) need to be performed to determine their theranostic value. To date, no radiolabeled minigastrin analog has been approved by the FDA or the european medicines agency (EMA).

II. Objectives

In spite of the rare occurrence of MTC, patients diagnosed with metastatic disease are provided with limited therapeutic options, which is why novel treatment modalities are needed to provide sufficient clinical care. Although significant progress in the development and evaluation of novel CCK-2R targeted compounds has been reported over the last years, limitations, such as insufficient *in vivo* stability, high kidney retention, as well as the lack of high quality ^{18}F-labeled CCK-2R-targeted compounds, remain. Therefore, this thesis aimed at addressing these limitations through the development and preclinical evaluation of novel minigastrin analogs from bench to clinical translation.

In order to aim at the design of ^{18}F-labeled minigastrin analogs, we will introduce the radiohybrid concept, which has already been successfully implemented for PSMA-targeted compounds. We thus intend to combine a SiFA building block as well as a chelator unit within the same molecule, which would result in a true theranostic compound (PET Imaging: ^{18}F/^{nat}Lu; RLT: ^{19}F/^{177}Lu) (*53,70,73*). Therefore, we will transfer the radiohybrid concept to minigastrin analogs, and structurally optimize these ligands to balance the advantages and disadvantages of the SiFA methodology.

Our second aim is to address the susceptibility towards enzymatic degradation usually observed for minigastrin derivatives. Based on previous findings, mainly the Tyr-Gly, Gly-Trp as well as Asp-Phe peptide bonds represent major instabilities within the structure. We will try to avoid enzymatic cleavage by substitution of the mentioned peptide bonds by unnatural amino acids or PEG moieties. Therefore, we will carry out a glycine scan within the structure of the reference compound, DOTA-MGS5, to identify suitable sites for substitutions. Furthermore, modifications within the tetrapeptidic binding sequence of minigastrin analogs, *H*-Trp-Nle-Asp-Phe-NH_2, will be evaluated. Promising leads will be also used for the rh-based minigastrin compounds.

As TAT is emerging into the focus of nuclear medicine applications and thus, research, our third aim is to evaluate the potential of ^{225}Ac-labeled minigastrin analogs, using the most favorable compound developed within this work. We particularly aim at investigating a potentially improved therapeutic efficacy over its ^{177}Lu-labeled analog in the course of treatment studies.

III. Results

1. Introduction of a SiFA Moiety into the D-Glutamate Chain of DOTA-PP-F11N Results in Radiohybrid-Based CCK-2R-Targeted Compounds with Improved Pharmacokinetics In Vivo

Holzleitner N[1,*,#], Günther T[1,*,#], Beck R[1], Lapa C[2], Wester HJ[1]

[1] Pharmaceutical Radiochemistry, Technical University of Munich, 85748 Garching, Germany

[2] Nuclear Medicine, Faculty of Medicine, University of Augsburg, 86156 Augsburg, Germany

* Authors to whom correspondence should be addressed.

[#] These authors contributed equally to this work.

Pharmaceuticals **2022**, *15*(12), https://doi.org/10.3390/ph15121467

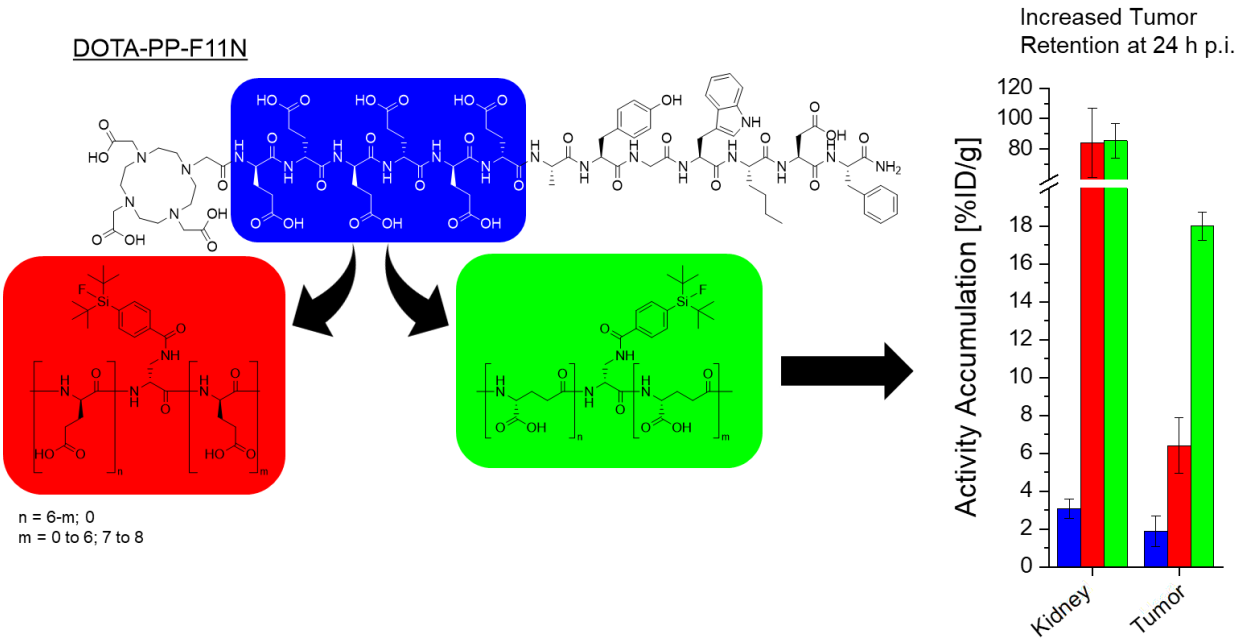

Although several radiolabeled minigastrin analogs targeting the CCK-2R were developed over the years, the availability of ^{18}F-labeled peptides is still limited (*199*). To date, [^{18}F]F-DOPA, a small molecule addressing NETs in general, is considered the gold standard for MTC imaging, even though only moderate sensitivities are accomplished for lymph node as well as distant metastases (*118,213*). Within this study, we wanted to combine the favorable imaging properties

of ^{18}F and PET alongside targeting the CCK-2R. We thus introduced a *p*-SiFA moiety into the various positions within the hexa-D-glutamate linker section of DOTA-PP-F11N, a reference compound currently evaluated in clinical trials. Hence, radiohybrid-based, true theranostic compounds were generated.

One major drawback of DOTA-PP-F11N represents its high hydrophilicity (log$D_{7.4}$=−4.75±0.07), thus leading to accelerated clearance kinetics *in vivo.* By incorporating a lipophilic *p*-SiFA moiety into its peptide structure, we were able to reduce hydrophilicity (log$D_{7.4}$=−2.8 to −1.7). In addition, CCK-2R affinity of the novel compounds was observed to be enhanced with increasing distance between the D-Dap(*p*-SiFA) building block and the binding motif, which resulted in [^{nat}Lu]Lu-(*R*)-DOTAGA-rhCCK-9 ([^{nat}Lu]Lu-(*R*)-DOTAGA-D-Dap(*p*-SiFA)-(D-Glu)$_8$-Ala-Tyr-Gly-Trp-Nle-Asp-Phe-NH_2) and −16 ([^{nat}Lu]Lu-(*R*)-DOTAGA-D-Dap(*p*-SiFA)-(D-*γ*-Glu)$_6$-Ala-Tyr-Gly-Trp-Nle-Asp-Phe-NH_2), each the most affine radiohybrid-based minigastrin analogs comprising either an *α*- or *γ*-linked D-glutamate chain, respectively. Nevertheless, IC_{50} values were found to be 2- (**16**: IC_{50}=20.4±2.7 nM) to 5-fold (**9**: IC_{50}=55.8±7.8 nM) higher compared to [^{nat}Lu]Lu-DOTA-PP-F11N (IC_{50}=12.8±2.8 nM).

However, in comparison with [^{177}Lu]Lu-DOTA-PP-F11N, [^{177}Lu]Lu-(*R*)-DOTAGA-rhCCK-9 and -16 exhibited 3- to 8-fold increased activity levels in the tumor at 24 h p.i (1.9±0.8 %ID/g *versus* 6.4±1.5 %ID/g and 15.7±3.3 %ID/g, respectively), whereas activity accumulation in the kidneys was substantially elevated for both radiohybrid-based compounds (3.1±0.5 %ID/g *versus* 84±23 %ID/g and 86±11 %ID/g). µSPECT/CT imaging at 1, 4 and 24 h p.i. highlighted decelerated clearance of **9** and **16** over time, when compared to DOTA-PP-F11N (all ^{177}Lu-labeled).

In this study we were able to successfully transfer the radiohybrid concept to minigastrin analogs. Furthermore, the insertion of a lipophilic *p*-SiFA moiety into the peptide structure of DOTA-PP-F11N led to a more favorable lipophilicity and thus, decelerated clearance kinetics of our novel compounds, which proved to be beneficial for tumor accumulation and retention despite their lower CCK-2R affinity. However, kidney retention issues need to be addressed in future studies.

Individual Performance Contribution:

Conceptualization, T.G. and H.-J.W.; methodology, **N.H.**, T.G. and R.B.; software, **N.H.** and T.G.; validation, **N.H.** and T.G.; formal analysis, **N.H.** and T.G.; investigation, **N.H.** and T.G.; resources, R.B. and H.-J.W.; data curation, **N.H.** and T.G.; writing—original draft preparation, **N.H.** and T.G.; writing—review and editing, all co-authors; visualization, **N.H.** and T.G.; supervision, H.-J.W. and C.L.; project administration, T.G. and H.-J.W.; funding acquisition, R.B., H.-J.W. and T.G.

2. Development of the First ^{18}F-Labeled Radiohybrid-Based Minigastrin Derivative with High Target Affinity and Tumor Accumulation by Substitution of the Chelating Moiety

Günther T[1,*,#], **Holzleitner N**[1,#], Di Carlo D, Urtz-Urban N[1], Lapa C[2], Wester HJ[1]

[1] Pharmaceutical Radiochemistry, Technical University of Munich, 85748 Garching, Germany

[2] Nuclear Medicine, Faculty of Medicine, University of Augsburg, 86156 Augsburg, Germany

* Author to whom correspondence should be addressed.

[#] These authors contributed equally to this work.

Pharmaceutics **2023**, *15*(3), 826; https://doi.org/10.3390/pharmaceutics15030826

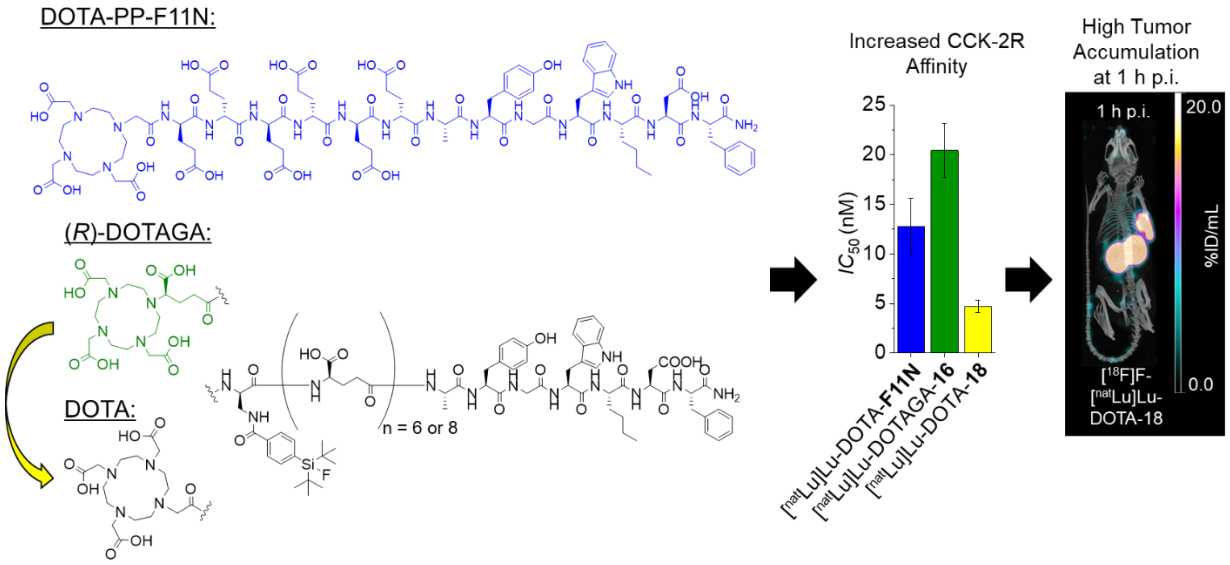

Following our impressive results obtained by the introduction of a D-Dap(*p*-SiFA) moiety into the hexa-D-glutamate chain of DOTA-PP-F11N in a previous study, we wanted to address kidney retention issues of the most promising radiohybrid-based CCK-2R-targeted candidate, [^{177}Lu]Lu-(*R*)-DOTAGA-rhCCK-16, while maintaining its high tumor retention. As we assumed a synergistic effect being responsible for elevated activity levels in the kidneys, in the course of the current study we wanted to reduce negatively charged units in proximity to the *p*-SiFA building block. We thus substituted the (*R*)-DOTAGA by a DOTA moiety, which has previously been demonstrated by Wurzer *et al.* for radiohybrid-based PSMA-targeted compounds, and led to improved tumor-to-kidney ratios (*214*).

Interestingly, substitution of the (*R*)-DOTAGA by a DOTA moiety led to a noticeably improved CCK-2R affinity for all compounds tested (1.3- up to 4-fold decreased IC_{50} values), indicating a negative influence of an additional negative charge at the *C*-terminal end of minigastrin analogs on CCK-2R affinity. The most promising compound evaluated within this study, [^{19}F]F-[^{nat}Lu]Lu-DOTA-rhCCK-18 ([^{19}F]F-[^{nat}Lu]Lu-DOTA-D-Dap(*p*-SiFA)-(D-*γ*-Glu)$_8$-Ala-Tyr-Gly-Trp-Nle-Asp-Phe-NH_2), displayed a 2-fold lower IC_{50} value than DOTA-PP-F11N (4.71±0.62 nM *versus* 12.8±2.8 nM), and was therefore investigated in further biodistribution studies *in vivo.*

Biodistribution of [^{19}F]F-[^{177}Lu]Lu-DOTA-rhCCK-18 at 24 h p.i. in AR42J tumor-bearing CB17-SCID mice showed greatly improved activity levels in the tumor compared to [^{177}Lu]Lu-(*R*)-DOTAGA-rhCCK-16 and [^{177}Lu]Lu-DOTA-PP-F11N (25.4±4.7 %ID/g *versus* 15.7±3.3 %ID/g and 1.9±0.8 %ID/g, respectively). However, kidney retention was observed to be even higher for [^{19}F]F-[^{177}Lu]Lu-DOTA-rhCCK-18 (134±18 %ID/g). Similar observations were made at the 1 h p.i. time point, as high activity uptake could be demonstrated in the tumor (24.1±4.2 %ID/g) and the kidneys (97.2±14.0 %ID/g), whereas overall tumor-to-background ratios were high. μPET/CT imaging studies of the chemically identical [^{18}F]F-[^{nat}Lu]Lu-DOTA-rhCCK-18 at 1 h p.i. further underlined the above-mentioned results.

To conclude, substitution of (*R*)-DOTAGA by a DOTA moiety resulted in a noticeably enhanced CCK-2R affinity, leading to substantially elevated activity levels in the tumor over time for [$^{18/19}$F]F-[$^{nat/177}$Lu]Lu-DOTA-rhCCK-18. However, high activity uptake in the kidneys remained an issue and might limit its clinical use, particularly when ^{177}Lu-labeled. Nevertheless, apart from the kidneys low overall background activity levels were observed. As elevated kidney levels are not considered a limitation for ^{18}F-based PET examinations, clinical translation of [^{18}F]F-[^{nat}Lu]Lu-DOTA-rhCCK-18 has been initiated.

Individual Performance Contribution:

Conceptualization, T.G. and H.-J.W.; methodology, **N.H.**, T.G., N.U.-U. and D.D.C.; software, **N.H.** and T.G.; validation, **N.H.** and T.G.; formal analysis, **N.H.** and T.G.; investigation, **N.H.** and T.G.; resources, N.U.-U. and H.-J.W.; data curation, **N.H.** and T.G.; writing—original draft preparation, **N.H.** and T.G.; writing—review and editing, all co-authors; visualization, **N.H.** and T.G.; supervision, H.-J.W. and C.L.; project administration, T.G. and H.-J.W.; funding acquisition, H.-J.W. and T.G.

3. Investigation of the structure-activity relationship at the *N*-terminal part of minigastrin analogs

Holzleitner N [1,#], Günther T[1,#,*], Daoud-Ghadieh A, Lapa C[2], Wester HJ[1]

[1] Pharmaceutical Radiochemistry, Technical University of Munich, 85748 Garching, Germany

[2] Nuclear Medicine, Faculty of Medicine, University of Augsburg, 86156 Augsburg, Germany

* Author to whom correspondence should be addressed.

[#] These authors contributed equally to this work.

EJNMMI Research **2023**, *13*(65); https://doi.org/10.1186/s13550-023-01016-y

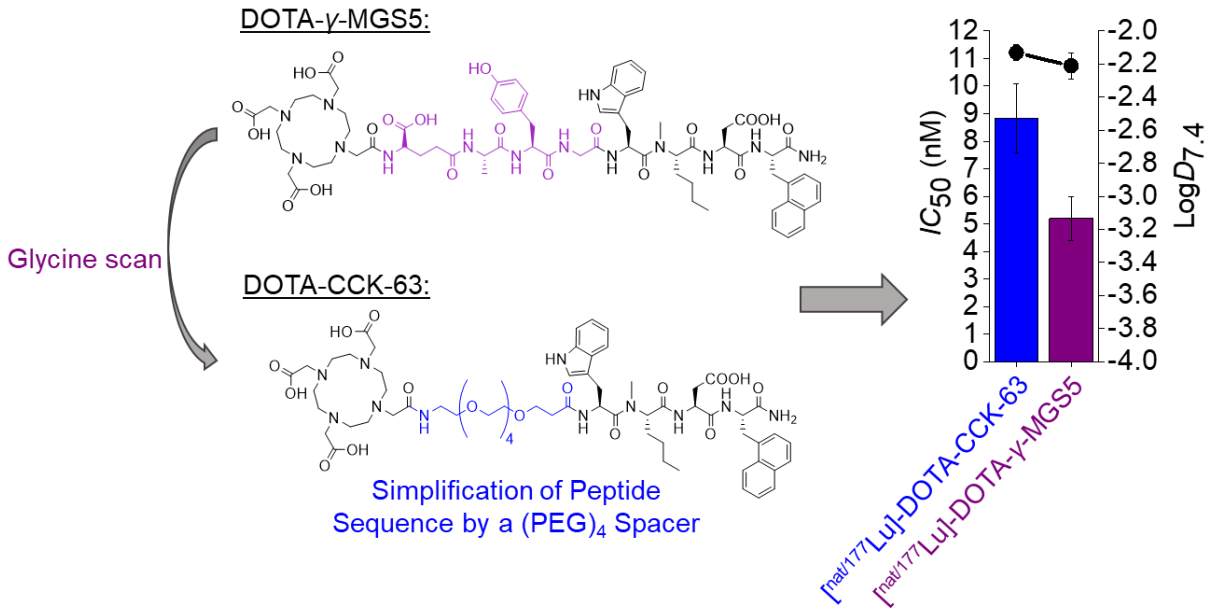

Although different stabilization strategies, such as substitution of peptide by triazole bonds (*157,215*), *N*-methylation (*160,216*) or replacement of alanine by proline (*166,167*), have been carried out over the last years in order to address the limited *in vivo* stability of minigastrin analogs, two major cleavage sites between the Tyr-Gly and Gly-Trp moiety ubiquitously present in minigastrin-based peptides yet remained untouched. By performing a glycine scan at the *N*-terminus of DOTA-MGS5 (DOTA-D-Glu-Ala-Tyr-Gly-Trp-(*N*-Me)Nle-Asp-1-Nal-NH_2), we systemically analyzed the peptide structure to gain further insight into its boundaries towards modifications. In addition, we evaluated the influence of different structural changes within the tetrapeptidic binding motif on CCK-2R affinity.

IC_{50} values of all glycine scan peptides ([^{nat}Lu]Lu-DOTA-CCK-55 to -61) were found to be in a low nanomolar range (4.2-8.5 nM), implying that the amino acids within the D-*γ*-Glu-Ala-Tyr-Gly sequence are not required for high affinity CCK-2R binding. However, a truncated compound lacking said sequence ([^{nat}Lu]Lu-DOTA-CCK-62; [^{nat}Lu]Lu-DOTA-Gly-Trp-(*N*-Me)Nle-Asp-1-Nal-NH_2), displayed a noticeable loss in CCK-2R affinity. Substitution of D-*γ*-Glu-Ala-Tyr-Gly by PEG spacers of different lengths led to a simplification of the peptide structure, while maintaining a high affinity towards the CCK-2R ([^{nat}Lu]Lu-DOTA-CCK-63; [^{nat}Lu]Lu-DOTA-$(PEG)_4$-Trp-(*N*-Me)Nle-Asp-1-Nal-NH_2: IC_{50} = 8.84±1.25 nM, [^{nat}Lu]Lu-DOTA-CCK-64; [^{nat}Lu]Lu-DOTA-$(PEG)_3$-Trp-(*N*-Me)Nle-Asp-1-Nal-NH_2: IC_{50} = 7.64±0.86 nM) and favorable lipophilicity (log$D_{7.4}$ = −2.2 to −2.1). Surprisingly, stability studies in human serum after incubation at 37°C for 24 h revealed only 44-57% intact peptide for the PEG spacer comprising ligands, whereas the reference compound [^{177}Lu]Lu-DOTA-*γ*-MGS5 as well as the glycine scan derivatives [^{177}Lu]Lu-DOTA-CCK-55 and -62 exhibited high metabolic stabilities greater than 90%. Due to the still unclear reason for this observation, this has to be further evaluated in future studies.

Evaluation of different tetrapeptides revealed that the *N*-methyl group at the norleucine moiety is crucial for high affinity CCK-2R binding. Both *H*-Trp-Asp-(*N*-Me)Nle-1-Nal-NH_2 and *H*-Trp-Asp-(*N*-Me)Nle-Phe-NH_2 exhibited IC_{50} values in a low nanomolar range (4.4-5.9 nM), whereas their counterparts lacking the *N*-methyl group displayed a significant loss in CCK-2R affinity (297-468 nM, p<0.0001). Furthermore, substitution of 1-Nal by Tyr had no influence on receptor affinity. In comparison, replacement of 1-Nal by Trp and 2-Nal, respectively, led to 3- to 17-fold higher IC_{50} values.

Even though metabolic stability of [^{nat}Lu]Lu-DOTA-CCK-63 as well as -64, either comprising a $(PEG)_4$ or $(PEG)_3$ spacer, still need to be optimized in the course of future studies, favorable CCK-2R affinity and lipophilicity render this modification promising. In addition, we could confirm that the tetrapeptidic structure *H*-Trp-Asp-(*N*-Me)Nle-1-Nal-NH_2 is sufficient for high affinity CCK-2R binding, yet the presence of an *N*-methyl group at the norleucine moiety is crucial. The combination of the two major findings of this study could affect future design of minigastrin analogs.

Individual Performance Contribution:

N.H. designed the study, carried out the synthesis and evaluation of the peptides and wrote the manuscript. T.G. wrote the manuscript, designed the study, managed the project and acquired funding. A.D-G. carried out the synthesis and evaluation of the peptides. C.L. managed the project and revised the manuscript. H-J.W. designed the study, managed the project and revised the manuscript.

4. Preclinical Evaluation of Novel Minigastrin Analogs and Proof-of-Concept [^{68}Ga]Ga-DOTA-CCK-66 PET/CT in two Patients With Medullary Thyroid Cancer

Günther T[1,#,*], **Holzleitner N**[1,#], Viering O[2], Beck R[1], Wienand G[2], Dierks A[2], Pfob CH[2], Bundschuh RA[2], Kircher M[2], Lapa C[2] and Wester HJ[1]

[1] TUM School of Natural Sciences, Department of Chemistry, Chair of Pharmaceutical Radiochemistry, Technical University of Munich, Garching, Germany

[2] Nuclear Medicine, Faculty of Medicine, University of Augsburg, Augsburg, Germany

* Author to whom correspondence should be addressed.

[#] These authors contributed equally to this work.

JNM **2023**, jnumed.123.266537; https://doi.org/10.2967/jnumed.123.266537

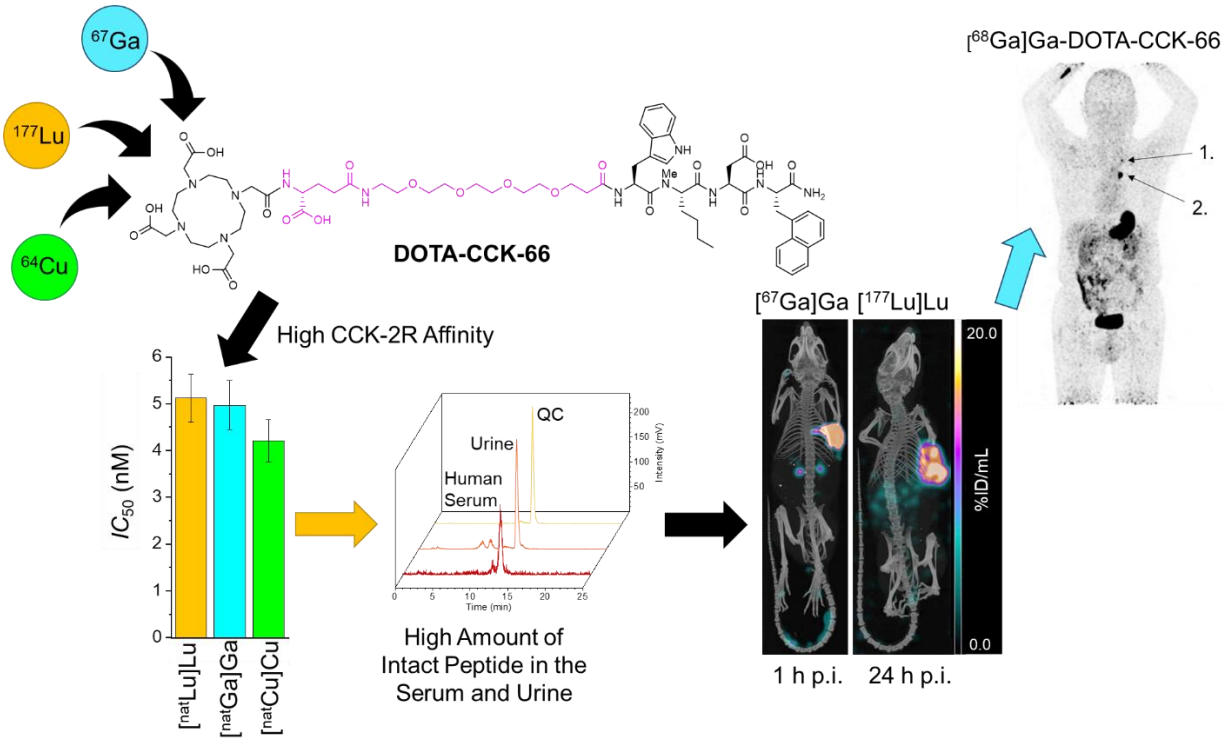

We recently demonstrated, that substitution of the D-Glu-Ala-Tyr-Gly sequence in DOTA-MGS5 by $(PEG)_3$ and $(PEG)_4$ led to comparable IC_{50} values to the reference, [^{nat}Lu]Lu-DOTA-MGS5. However, a surprisingly lower serum stability was observed (*217*). Thus, within this study we wanted to further enhance the metabolic stability of linear minigastrin analogs by substitution

of D-Glu-Ala-Tyr-Gly with D-γ-Glu-$(PEG)_3$ (DOTA-CCK-66) and D-Glu-$(PEG)_3$ (DOTA-CCK-66.2). Hence, we performed a comparative preclinical evaluation of DOTA-CCK-66, DOTA-CCK-66.2 and DOTA-MGS5 labeled with either $^{nat/64}$Cu, $^{nat/67}$Ga or $^{nat/177}$Lu.

Within these studies, a high CCK-2R affinity (IC_{50}: 3.6-6.0 nM) was observed for all compounds evaluated, regardless of the metal ion (copper, gallium or lutetium) used. In addition, favorable log$D_{7.4}$ values (log$D_{7.4}$: −3.0 to −2.2) were observed for all compounds (DOTA-CCK-66, DOTA-CCK-66.2 and DOTA-MGS5) and radionuclides (^{64}Cu, ^{67}Ga and ^{177}Lu) tested. HSA (human serum albumin) binding was decreased for the novel compounds ([^{nat}Lu]Lu-, [^{nat}Ga]Ga- and [^{nat}Cu]Cu-DOTA-CCK-66 as well as [^{nat}Lu]Lu-, [^{nat}Ga]Ga- and [^{nat}Cu]Cu-DOTA-CCK-66.2), when compared to [^{nat}Lu]Lu-, [^{nat}Ga]Ga- and [^{nat}Cu]Cu-DOTA-MGS5. Furthermore, stability in human serum was high for all ^{177}Lu-labeled compounds evaluated (>89%).

Due to its slightly more favorable characteristics *in vitro*, DOTA-CCK-66 was further evaluated *in vivo.* In comparison, [^{177}Lu]Lu-DOTA-CCK-66 (78.5±3.1%) displayed a similarly high *in vivo* stability in murine serum at 30 min after injection as [^{177}Lu]Lu-DOTA-MGS5 (82.0±0.1%). However, the amount of intact peptide in the urine was observed to be substantially increased for the former (77.8±2.3% versus 23.7±9.2%), confirming a positive impact of modifications of the Tyr-Gly and Gly-Trp bond on metabolic stability. Furthermore, high activity levels in the tumor accompanied by low uptake in non-tumor organs for [^{67}Ga]Ga-DOTA-CCK-66 at 1 h p.i. (19.4±3.5 %ID/g) led to favorable tumor-to-background ratios of said compound. When compared to [^{177}Lu]Lu-DOTA-MGS5, [^{177}Lu]Lu-DOTA-CCK-66 exhibited slightly decreased activity levels in the tumor (11.0±1.2 %ID/g *versus* 8.6±1.1 %ID/g) at 24 h after injection. Nevertheless, due to the lower activity uptake of the latter in non-target tissues, similar tumor-to-background ratios were achieved.

These promising preclinical results led to further evaluation of [^{68}Ga]Ga-DOTA-CCK-66 in a first clinical proof-of-concept study. PET/CT imaging at 120 min after injection in two patients suffering from metastatic MTC displayed a favorable biodistribution pattern with high uptake in tumor lesions. In accordance with the biodistribution studies in mice, elevated activity uptake was only observed for the stomach physiologically expressing CCK-2R, while activity uptake in non-target tissues was low. Furthermore, lymph nodes of one patient identified by [^{68}Ga]Ga-DOTA-CCK-66 PET/CT were surgically removed and histologically confirmed as lymph node metastases of MTC.

In conclusion, we were able to demonstrate a beneficial effect of substitution of D-Glu-Ala-Tyr-Gly by D-γ-Glu-$(PEG)_3$ in DOTA-MGS5 on metabolic stability of the compound, DOTA-CCK-66. In addition, a first clinical proof-of-concept PET/CT study using [^{68}Ga]Ga-DOTA-CCK-66 in two patients suffering from metastatic MTC, displayed favorable biodistribution patterns resulting in the detection of several tumor lesions. In the course of future studies, these results need to be confirmed in larger patient cohorts. In addition, first therapy studies using [^{177}Lu]Lu-DOTA-CCK-66 are warranted in order to confirm the theranostic value of this novel compound.

Individual Performance Contribution:

T.G. acquired funding, designed the study, helped with the animal experiments and wrote the manuscript. **N.H.** designed the study, carried out the synthesis and evaluation of the peptides and analysed the preclinical data. R.B. supervised all animal experiments. G.W. established and carried out GMP production of the compound for clinical use. V.O., A.D., C.H.P., R.A.B., M.K., carried out the clinical trials and analysed the clinical data. C.L. supervised all clinical trials. H.J.W managed the project and acquired funding. All co-authors revised the manuscript.

5. Significant Decrease of Activity Uptake of Radiohybrid-Based Minigastrin Analogs in the Kidneys via Modification of the Charge Distribution Within the Linker Section

Holzleitner N[1], Fischer S[2], Manyankerikalam I[1], Beck R[1], Lapa C[2], Wester HJ[1] and Günther T[1]

[1] TUM School of Natural Sciences, Department of Chemistry, Chair of Pharmaceutical Radiochemistry, Technical University of Munich, Garching, Germany

[2] Nuclear Medicine, Faculty of Medicine, University of Augsburg, Augsburg, Germany

EJNMMI Research **2023**, *currently under review.*

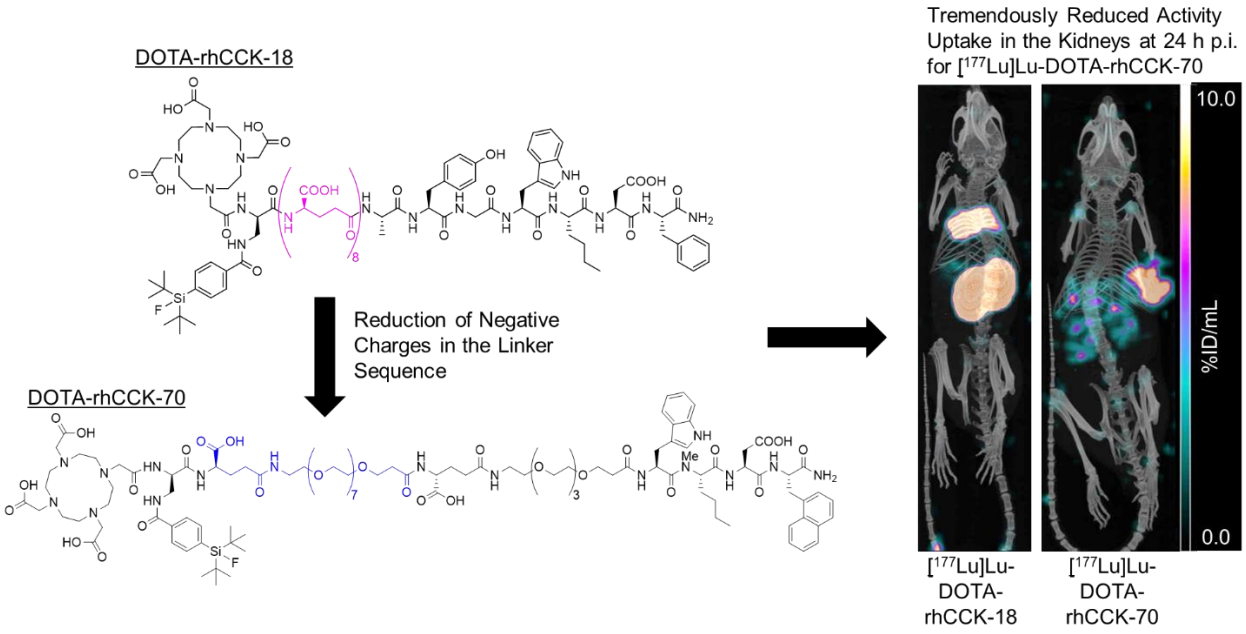

In this study, we aimed to address kidney retention issues of previous radiohybrid-based minigastrin analogs via a reduction of negatively charged moieties in proximity to the *p*-SiFA group, namely reducing poly-D-*γ*-glutamate moieties, and introduce the stabilized binding motif discovered in the previous study. We thus substituted the poly-D-*γ*-glutamate chain of [^{177}Lu]Lu-DOTA-rhCCK-18, which displayed the highest activity levels in the tumor at 24 h after injection among all radiohybrid-based compounds, by PEG linkers of various length (4 to 11 PEG units). We further evaluated the influence of negatively charged (SiFA-ipa), uncharged (*p*-SiFA) as well as positively charged (SiFAlin) silicon-based fluoride acceptor moieties on CCK-2R affinity and lipophilicity. Moreover, we replaced the binding motif of DOTA-rhCCK-18, which was derived from

DOTA-PP-F11N, with the optimized binding motif established for DOTA-CCK-66, our most favorable non-radiohybrid compound, which is currently under clinical evaluation.

Compared to [^{nat}Lu]Lu-DOTA-rhCCK-18 (IC_{50}=4.7±0.6 nM) and [^{nat}Lu]Lu-DOTA-PP-F11N (IC_{50}=12.8±2.8 nM), respectively, slightly increased or comparable IC_{50} values were found for most of the novel compounds (8-20 nM). Radiohybrid-based derivatives containing a SiFA-ipa moiety displayed noticeably lower CCK-2R affinity (43-52 nM), which were thus not further evaluated. While the SiFA-ipa moiety had a positive impact on overall hydrophilicity of the peptides, compounds containing the positively charged SiFAlin unit displayed similar or slightly higher log$D_{7.4}$ values compared to their *p*-SiFA comprising equivalents. However, as we prioritized high affinity (over low lipophilicity), and to further evaluate the influence of charge reduction on activity levels in the kidneys, the two compounds displaying the most promising *in vitro* data among all derivatives investigated, [$^{177/nat}$Lu]Lu-DOTA-rhCCK-70 (DOTA-D-Dap(*p*-SiFA)-D-*γ*-Glu-$(PEG)_7$-D-*γ*-Glu-$(PEG)_3$-Trp-(*N*-Me)Nle-Asp-1-Nal-NH_2; IC_{50}: 12.6±2.0 nM; log$D_{7.4}$: −1.67±0.08) and [$^{177/nat}$Lu]Lu-DOTA-rhCCK-91 (DOTA-D-Dap(SiFAlin)-D-*γ*-Glu-$(PEG)_4$-D-*γ*-Glu-$(PEG)_3$-Trp-(*N*-Me)Nle-Asp-1-Nal-NH_2; IC_{50}: 8.6±0.7 nM; log$D_{7.4}$: −1.66±0.07) were further investigated in biodistribution as well as µSPECT/CT imaging studies at 24 h after injection in AR42J tumor-bearing mice.

Not surprisingly, the charge reduction in the linker sequence and thus, in close neighborhood to the respective SiFA moiety led to substantially decreased activity levels in the kidneys for both [^{177}Lu]Lu-DOTA-rhCCK-70 and [^{177}Lu]Lu-DOTA-rhCCK-91, when compared to [^{177}Lu]Lu-DOTA-rhCCK-18 (8.4±0.8 and 6.6±0.5 %ID/g *versus* 134±18 %ID/g). Consequently, favorable tumor-to-kidney ratios were determined (1.45±0.12 and 1.13±0.12 *versus* 0.62±0.30). However, lower tumor-to-background ratios in all other organs were observed, which can be attributed to their noticeably decreased tumor uptake (12.0±0.8 and 7.5±1.0 *versus* 25.4±4.7 %ID/g), thus displaying the need for further optimization.

Nevertheless, we could accomplish our goal in this study to successfully reduce activity levels in the kidneys by a reduction of negatively charged residues within the linker section of radiohybrid-based minigastrin analogs. This project further assisted in planning the next developmental steps to improve lipophilicity but also CCK-2R affinity and thus, activity levels in the tumor, which will be addressed in future studies.

Individual Performance Contribution:

N.H. designed the study, carried out the synthesis and evaluation of the peptides and wrote the manuscript. S.F. developed the novel SiFA-ipa building block. I.M. carried out the synthesis and evaluation of the peptides. R.B. acquired funding, revised the manuscript and supervised the animal experiments. C.L. managed the project and revised the manuscript. H.-J.W. managed the project and acquired funding. T.G. wrote the manuscript, designed the study, managed the project and acquired funding. All authors have approved the final version of the manuscript.

6. Development of [^{18}F]F-[^{nat}Lu]Lu-/[^{19}F]F-[^{177}Lu]Lu-DOTA-rhCCK-84, a Radiohybrid-Based Minigastrin Analogue With High Tumour and low Kidney Accumulation

Günther T[1], **Holzleitner N**[1], Manyankerikalam I[1], Greifenstein L[2], Beck R[1], Di Carlo D[1], Baum RP[2] and Wester HJ[1]

[1] Pharmaceutical Radiochemistry, Technical University of Munich, Germany

[2] Curanosticum, DKD HELIOS Klinik Wiesbaden, Wiesbaden, Germany

36th Annual Congress of the European Association of Nuclear Medicine **2023**, Oral Presentation.

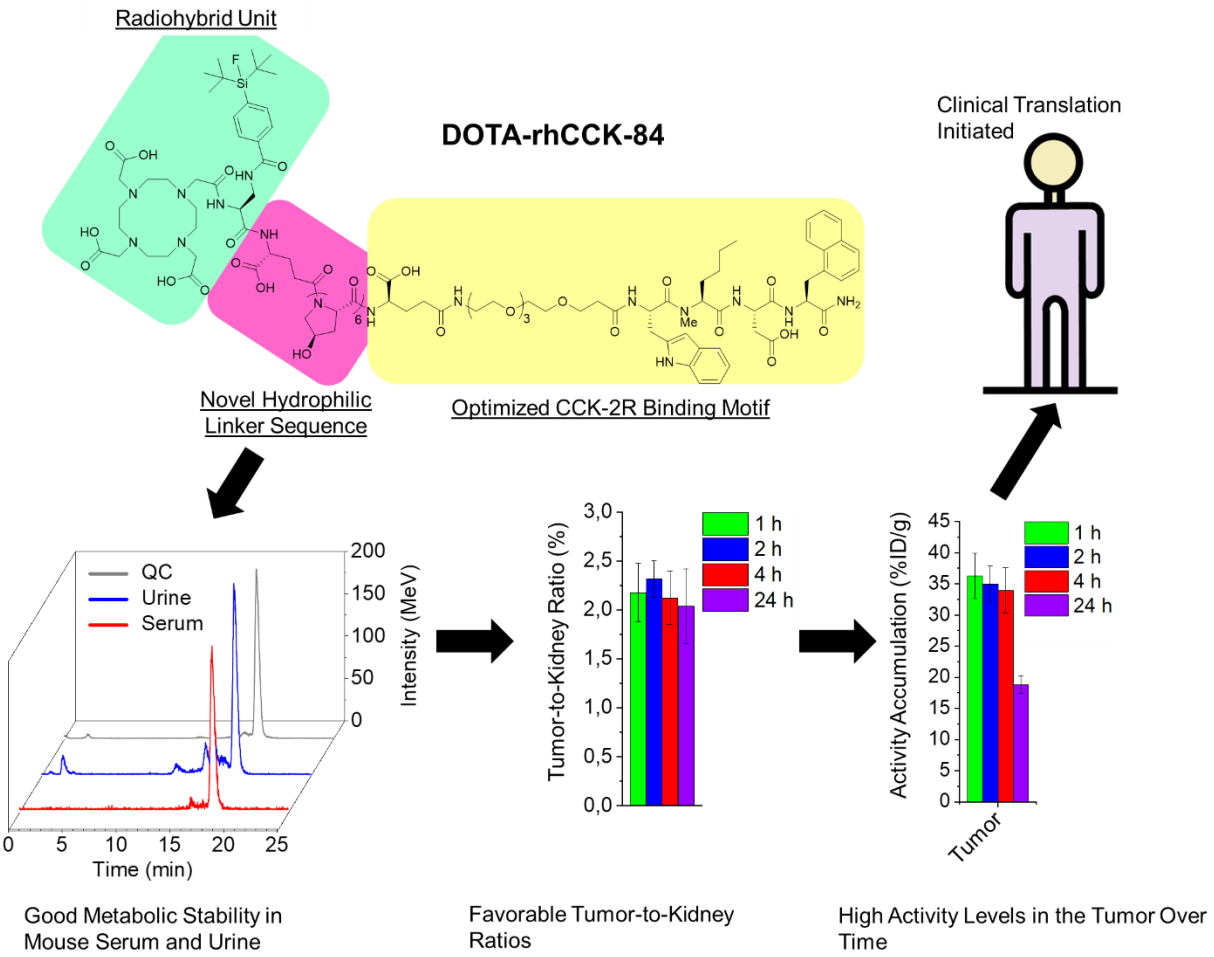

Based on our previous results, which revealed a noticeably reduced activity retention in the kidneys for a radiohybrid-based minigastrin analog that contains a D-*γ*-Glu-$(PEG)_7$ ([^{18}F]F-[^{nat}Lu]Lu-/[^{19}F]F-[^{177}Lu]Lu-DOTA-rhCCK-70) instead of a poly-D-*γ*-glutamate chain ([^{18}F]F-[^{nat}Lu]Lu-/[^{19}F]F-[^{177}Lu]Lu-DOTA-rhCCK-18), we aimed to increase CCK-2R affinity, lipophilicity, and thus, tumor uptake and retention in this study. Therefore, we evaluated the influence of novel hydrophilic, uncharged linker sequences (83: $(Hyp)_3$, 84: $(Hyp)_6$, 85: $(D\text{-}Cit)_3$-$(Hyp)_3$, 86: $(Hyp)_8$) on *in vitro* and *in vivo* properties of these radiohybrid-based minigastrin analogs (**Figure 14**).

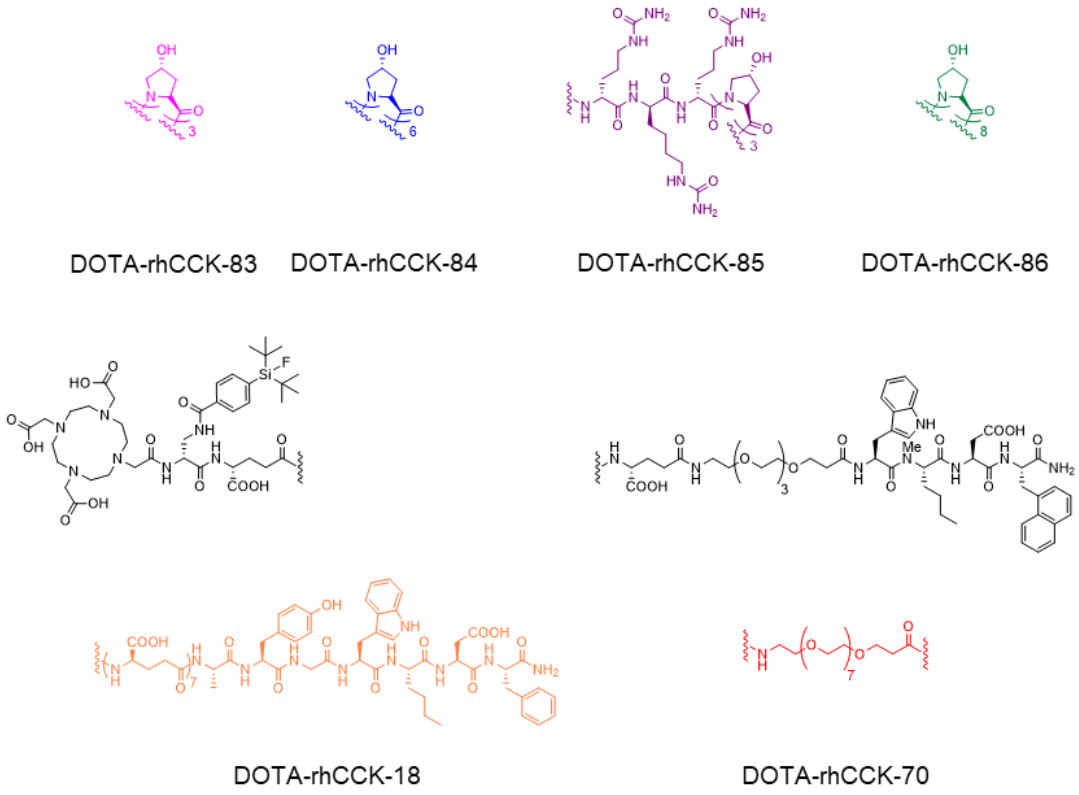

Figure 14. Chemical structures of novel rhCCK derivatives evaluated in comparison to the reference compounds, DOTA-rhCCK-18 and -70. Novel compounds (DOTA-rhCCK-83 to -86) and DOTA-rhCCK-70 comprising identical *N*-terminal sequences (D-*γ*-Glu-$(PEG)_3$-Trp-(*N*-Me)Nle-Asp-1-Nal-NH_2), whereas DOTA-rhCCK-18 consists of a different binding unit (Ala-Tyr-Gly-Trp-Nle-Asp-Phe-NH_2). *C*-terminal sections (DOTA-D-Dap(SiFA)-D-*γ*-Glu) of all minigastrin analogs are structurally identical. All peptides differ in their linker unit. Synthesis of all compounds was accomplished via Fmoc-based solid phase peptide synthesis using an *H*-Rink Amide ChemMatrix resin.

All experimental procedures (peptide synthesis, IC_{50}- and log$D_{7.4}$-determinations, stability studies *in vivo* as well as biodistribution studies) conducted within this study, were performed in analogy to previously published protocols (*217*, *218*, *219*, 220).

All peptides evaluated displayed IC_{50} values of 7.9-12.9 nM, which were similar or slightly increased compared to that of [^{nat}Lu]Lu-DOTA-rhCCK-70 (IC_{50} = 12.6±2.0 nM) and [^{177}Lu]Lu-DOTA-rhCCK-18 (IC_{50} = 4.7±0.6 nM), respectively (**Figure 15**).

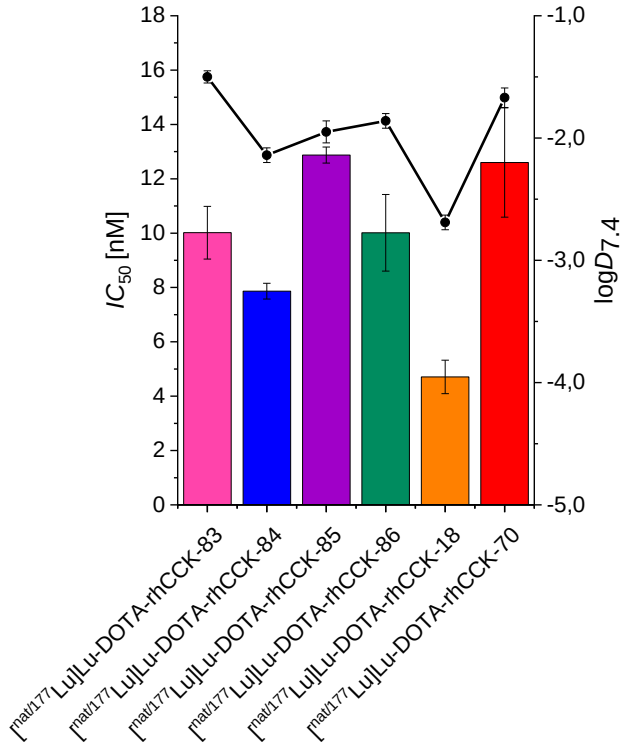

Figure 15. IC_{50} and log$D_{7.4}$ values of the novel radiohybrid based minigastrin analogs, [$^{nat/177}$Lu]Lu-DOTA-rhCCK-83 (pink), [$^{nat/177}$Lu]Lu-DOTA-rhCCK-84 (blue), [$^{nat/177}$Lu]Lu-DOTA-rhCCK-85 (purple), [$^{nat/177}$Lu]Lu-DOTA-rhCCK-86 (green), as well as the reference ligands [$^{nat/177}$Lu]Lu-DOTA-rhCCK-18 (orange) and [$^{nat/177}$Lu]Lu-DOTA-rhCCK-70 (red). Data are expressed as mean ± SD. IC_{50} values were determined using AR42J cells (2.0 × 10^5 cells per well) and [^{177}Lu]Lu-DOTA-PP-F11N (0.3 pmol/well) as the radiolabeled reference (3 h, 37°C, RPMI 1640, 5 mM L-Gln, 5 mL non-essential amino acids (100×), 10% fetal calf serum (FCS) + 5% bovine serum albumin (BSA) (v/v)).

In addition, lipophilicity of [^{177}Lu]Lu-DOTA-rhCCK-84 (DOTA-D-Dap(*p*-SiFA)-D-*γ*-Glu-$(Hyp)_6$-D-*γ*-Glu-$(PEG)_3$-Trp-(*N*-Me)Nle-Asp-1-Nal-NH_2), comprising a D-*γ*-Glu-$(Hyp)_6$ linker sequence, was observed to be lower compared to that of [^{177}Lu]Lu-DOTA-rhCCK-70 (log$D_{7.4}$: −2.14±0.07 *versus* −1.67±0.08) and all other novel compounds tested (log$D_{7.4}$: −1.95 to −1.50). As it displayed the most favorable *in vitro* properties among all new compounds of this study, [^{18}F]F-[^{nat}Lu]Lu-/[^{19}F]F-[^{177}Lu]Lu-DOTA-rhCCK-84 was further evaluated *in vivo.*

Apart from a noticeably enhanced *in vivo* stability at 30 min after injection of [^{19}F]F-[^{177}Lu]Lu-DOTA-rhCCK-84, when compared to [^{19}F]F-[^{177}Lu]Lu-DOTA-rhCCK-18 (94±2% *versus* 65±15% intact tracer in serum, 55±9% *versus* 16±6% intact tracer in urine) (**Figure 16**), substantially increased tumor-to-kidney ratios were observed for the former (2.04±0.38 *versus* 0.19±0.01) (**Figure 17C**).

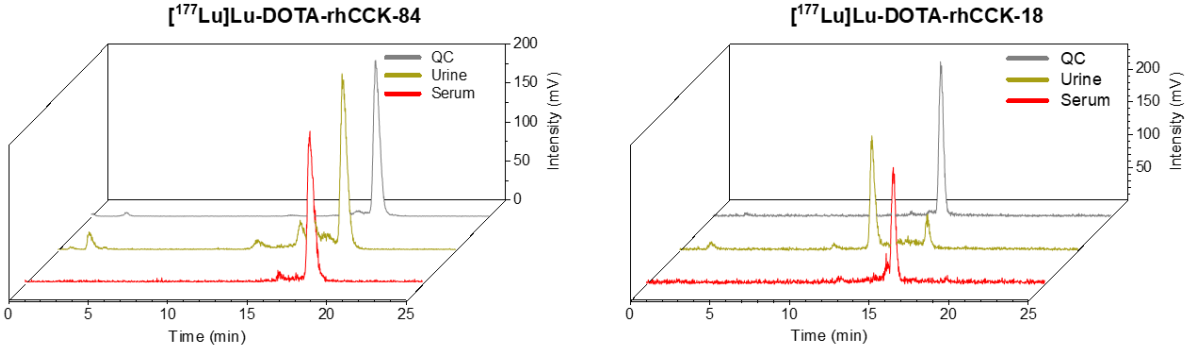

Figure 16. *In vivo* stability of CCK-2R ligands: amount of intact compound at 30 min after injection into the tail vein of healthy CB17-SCID mice (3 each) in murine serum (red) and urine (yellow) for [^{177}Lu]Lu-DOTA-rhCCK-84 and [^{177}Lu]Lu-DOTA-rhCCK-18. Quality control is depicted in grey.

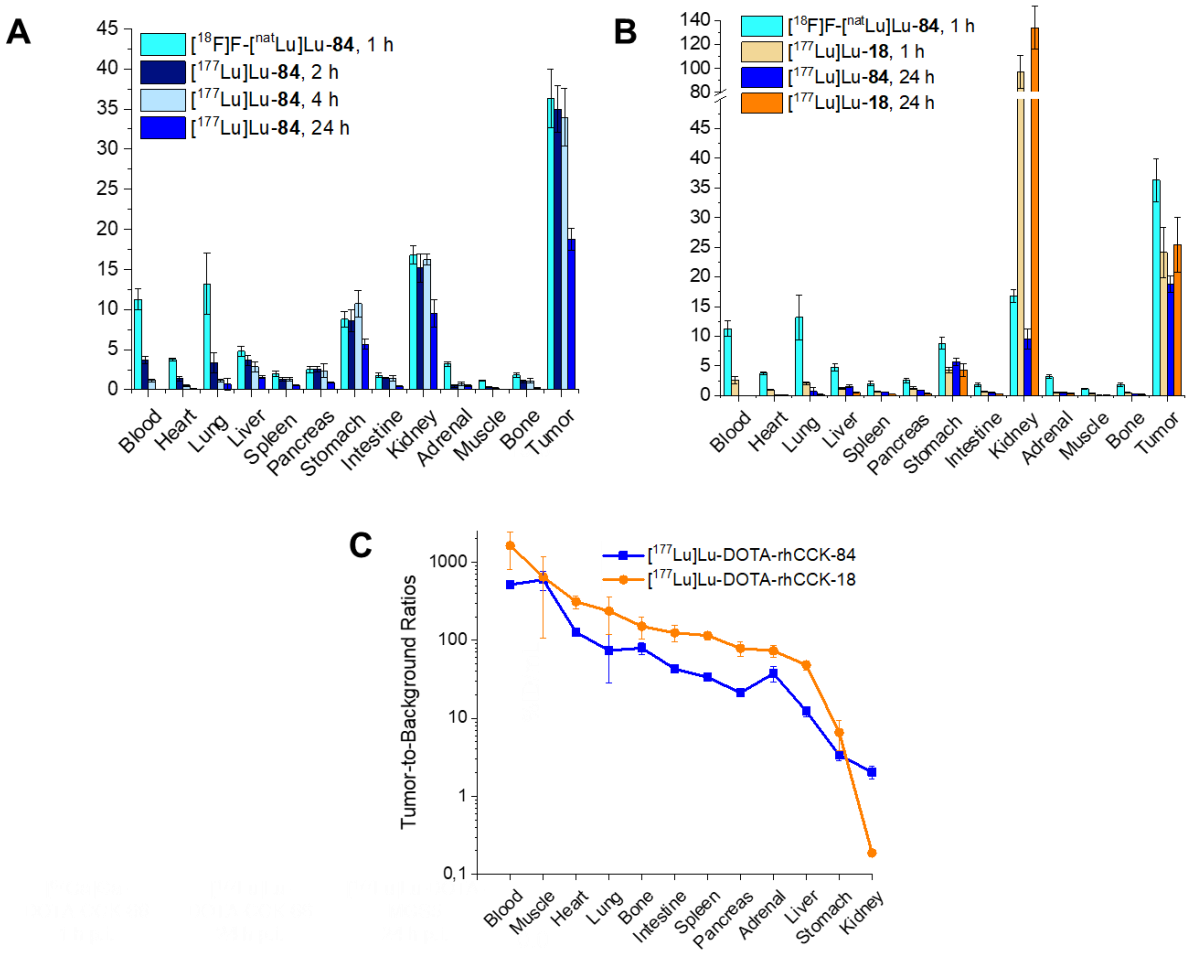

Figure 17. Biodistribution of (A) [18/natF]-[177/natLu]-DOTA-rhCCK-84 (orange) at 1, 2, 4 and 24 h after injection and (B) [18/natF]-[177/natLu]-DOTA-rhCCK-84 in comparison to [natF]-[177Lu]-DOTA-rhCCK-18 (blue) at 1 and 24 h after injection into the tail vein of AR42J tumor-bearing CB17-SCID mice (*n*=4 each). (C) Tumor-to-background ratios of the two compounds at 24 h after injection. Data are expressed as mean ± SD.

At 1 h after injection, [18F]F-[natLu]Lu-DOTA-rhCCK-84 revealed increased activity levels in the tumor (36.3±3.7 *versus* 24.1±4.2 %ID/g), accompanied by distinctly lower activity accumulation in the kidneys (16.8±1.1 *versus* 97.2±14.0 %ID/g) than [19F]F-[177Lu]Lu-DOTA-rhCCK-18 (**Figure 17A and B**). In addition, we could demonstrate that at 24 h after injection activity levels in the tumor were only slightly lower for [19F]F-[177Lu]Lu-DOTA-rhCCK-84 compared to [19F]F-[177Lu]Lu-DOTA-rhCCK-18 (18.8±1.4 *versus* 25.4±4.7 %ID/g), while activity levels in the kidneys were distinctly lower (9.5±1.7 *versus* 134±18 %ID/g). Activity uptake in other non-target tissue was low for [18F]F-[natLu]Lu-/[19F]F-[177Lu]Lu-DOTA-rhCCK-84. However, decelerated clearance kinetics were observed for [18F]F-[natLu]Lu-/[19F]F-[177Lu]Lu-DOTA-rhCCK-84 compared

to [^{18}F]F-[^{nat}Lu]Lu-/[^{19}F]F-[^{177}Lu]Lu-DOTA-rhCCK-18, thus resulting in elevated activity levels in the blood at 1 h after injection (11.3±1.3 *versus* 2.6±0.6 %ID/g). Hence, we carried out additional biodistribution studies at 2 and 4 h after injection, which exhibited a good activity clearance from the blood for [^{19}F]F-[^{177}Lu]Lu-DOTA-rhCCK-84 (2 h: 3.7±0.5 %ID/g, 4 h: 1.1±0.2 %ID/g). Based on these encouraging results, a clinical translation of DOTA-rhCCK-84 for ^{18}F-PET imaging as well as ^{177}Lu-based RLT has been initiated.

In conclusion, [^{18}F]F-[^{nat}Lu]Lu-/[^{19}F]F-[^{177}Lu]Lu-DOTA-rhCCK-84 developed in this study exhibited reduced activity levels in the kidneys, while maintaining high activity accumulation and retention in the tumor, which is in contrast to previously published radiohybrid-based minigastrin analogs, and renders this compound promising for further clinical evaluation. Combining the possibility of ^{18}F- (PET) as well as ^{177}Lu-labeling (RLT) generating chemically identical compounds, DOTA-rhCCK-84 might be a useful tool for imaging and treatment of MTC patients.

Individual Performance Contribution:

Conceptualization, **N.H.** and T.G.; methodology, **N.H.**, T.G., I.M., L.G. and D.D.C.; software, **N.H.** and T.G.; validation, **N.H.** and T.G.; formal analysis, **N.H.** and T.G.; investigation, **N.H.** and T.G.; resources, R.B. and H.-J.W.; data curation, **N.H.** and T.G.; writing—original draft preparation, T.G.; writing—review and editing, all co-authors; visualization, **N.H.** and T.G.; supervision, R.P.B., H.-J.W. and T.G.; project administration, T.G. and H.-J.W.; funding acquisition, H.-J.W. and T.G.

7. Unpublished Results: Preliminary Data of a First Proof-of-Concept Therapy Study Using [^{225}Ac]Ac-DOTA-CCK-66

Nadine Holzleitner[1], Meryl Vilangattil[2], Marco Taddio[2], Pauline Jean-Jean[2], Christine Mona[2], Constantin Lapa[3], Angela Casini[1], Thomas Günther[4] and Giuseppe Carlucci[2]

[1] TUM School of Natural Sciences, Department of Chemistry, Chair of Pharmaceutical Radiochemistry, Technical University of Munich, Garching, Germany

[2] Department of Molecular and Medical Pharmacology, University of California, Los Angeles (UCLA), Los Angeles, USA

[3] Nuclear Medicine, University Hospital Augsburg, Augsburg, Germany

[4] Molecular Imaging Program at Stanford, Department of Radiology, Stanford University, Palo Alto, USA

Manuscript in preparation.

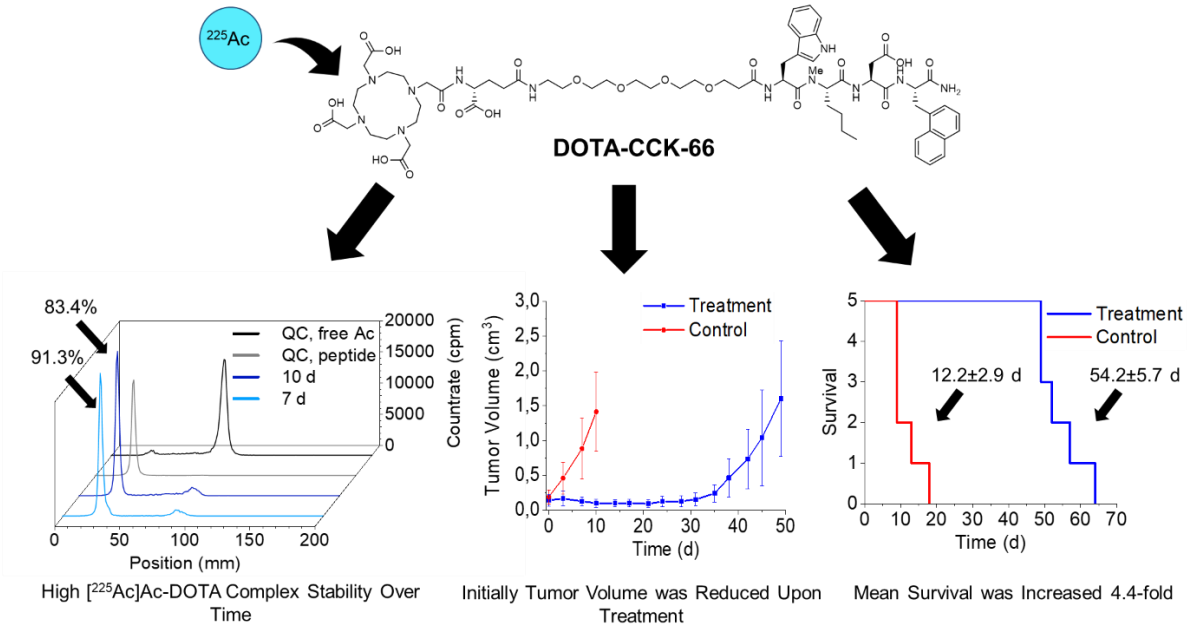

Due to the high linear energy transfer, short tissue penetration range and high particle energy provided by *α*-emitters, which results in enhanced therapeutic efficacy when compared to *β*$^-$-emitting isotopes, research on these radionuclides (e.g., ^{225}Ac, ^{149}Tb, ^{212}Pb) has been expanding in recent years. Especially in the field of PSMA- and SST2R-targeted radioligands, first clinical trials of ^{225}Ac-labeled compounds demonstrated promising results (*91-93*). Within this study, we wanted to set everything up for targeted *α*-therapy using a previously designed

minigastrin analog (*220*). Therefore, we completed a treatment study in AR42J tumor-bearing CB17-SCID mice to evaluate the therapeutic efficacy of [^{225}Ac]Ac-DOTA-CCK-66.

Manual ^{225}Ac-labeling of the peptide precursor DOTA-CCK-66 at 90°C for 30 min proceeded quantitatively and resulted in high radiochemical purities (>95%) and molar activities (A_m=208 MBq/µmol), which was used without further purification steps. Stability studies in human serum over time (1-10 d, 37°C) as determined by radio-thin layer chromatography, displayed a comparable *in vitro* stability of [^{225}Ac]Ac-DOTA-CCK-66 (91.3±0.32%) to its previously published [^{177}Lu]Lu-DOTA-CCK-66 analog (94.6±1.2%) (**Figure 18**).

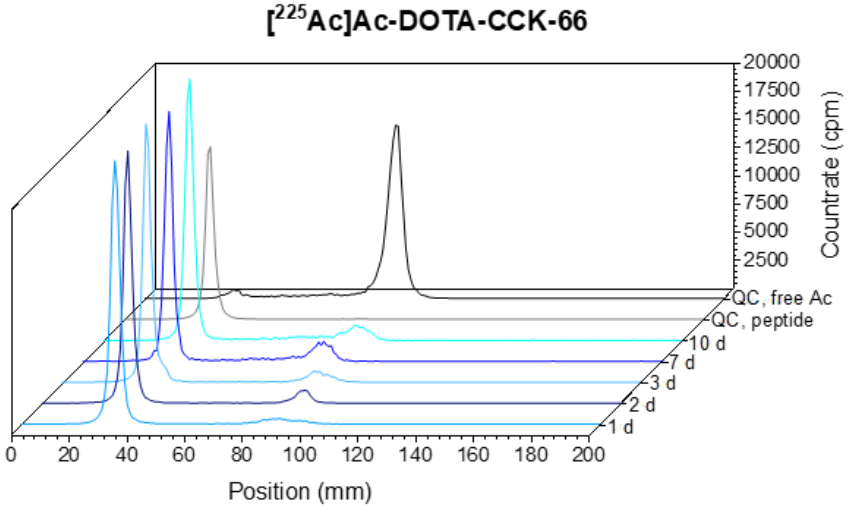

Figure 18. *In vitro* characterization of [^{225}Ac]Ac-DOTA-CCK-66 (depicted in green). (A) Stability in human serum after incubation at 37°C for 1 to 10 days (*n*=3). Quality control chromatograms of the peptide (light grey) and free ^{225}Ac (dark grey) are added in comparison. Data expressed as mean ± SD.

In addition, serum stability after incubation at 37°C for 10 d was observed to be high (83.4±10.3%), indicating a good stability of the [^{225}Ac]Ac-DOTA chelate.

For ^{225}Ac-treatment studies, a group of five AR42J tumor-bearing mice (394-NOD SCID, female) per cohort (tumor volume: 0.03 to 0.27 mm^3) were injected with either [^{225}Ac]Ac-DOTA-CCK-66 (37 kBq, treatment group) or [^{68}Ga]Ga-DOTA-CCK-66 (1.1 MBq, control group) 14 days after tumor cell inoculation. Animals were sacrificed after reaching one of the termination criteria, namely weight loss of more than 20%, a tumor size of more than 2,000 mm^3 (caliper measurements), ulceration of the tumor, respiratory distress or change of behavior. In comparison to the control cohort, tumor growth in mice treated with [^{225}Ac]Ac-DOTA-CCK-66 was observed to be significantly decelerated (**Figure 19A**).

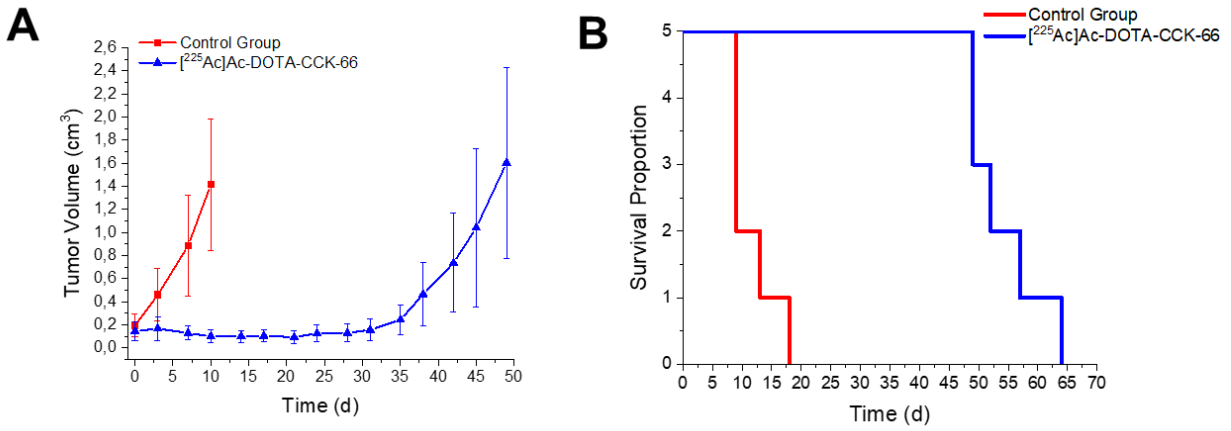

Figure 19. (A) Tumor growth inhibition and (B) prolonged life span (depicted as Kaplan-Meyer curve) of [^{225}Ac]Ac-DOTA-CCK-66 (37 kBq, *n*=5, blue) treated AR42J tumor-bearing 394-NOD SCID mice. Control group mice were injected with [^{68}Ga]Ga-DOTA-CCK-66 for PET/CT imaging (30 µCi, *n*=5, red) on day zero of the experiment. Data expressed as mean ± SD.

In addition, mean tumor volume, determined twice a week by caliper measurements, was observed to decrease until day 21 and only slowly grow until day 31 after treatment. When looking at Kaplan-Meier plots, mean survival of treatment cohort was increased by 4.4-fold (54.2±5.7 *versus* 12.2±2.9 d), when compared to the control cohort, demonstrating a tremendous effect upon ^{225}Ac-treatment (**Figure 19B**).

Furthermore, blood samples of all animals reaching one of the pre-defined end-points were collected and evaluated (VetScan VS2, Abaxis). No measurable burden of [^{225}Ac]Ac-DOTA-CCK-66 treatment on the kidneys was displayed (**Figure 20A**).

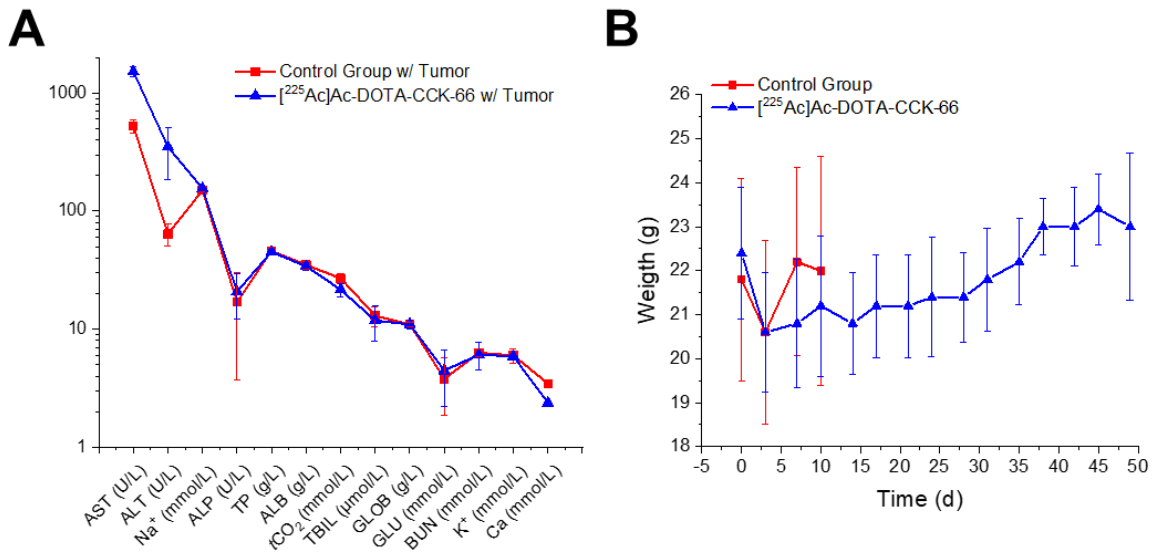

Figure 20. (A) Blood analysis data and (B) body weight of control group ([^{68}Ga]Ga-DOTA-CCK-66: 1.1 MBq, *n*=5, red) *versus* treatment group ([^{225}Ac]Ac-DOTA-CCK-66: 37 MBq, *n*=5, blue) AR42J tumor bearing 394-NOD SCID mice.

However, alanine-aminotransferase (ALT; 350±166 U/L *versus* 79±13 U/L) and aspartate-aminotransferase (AST; 1713±264 U/L *versus* 516±68 U/L) values of ^{225}Ac-treated mice were noticeably elevated compared to the control cohort, which indicates liver toxicity. Thus, further studies on [^{225}Ac]Ac-DOTA-CCK-66 treatment of healthy mice need to be conducted, to be able to better assess whether liver toxicity originates from tumor burden or ^{225}Ac decay. In addition, body weight of the mice was monitored twice a week to evaluate the effect of TAT on the CCK-2R expressing stomach (**Figure 20B**). After an initial weight loss upon treatment, which can be attributed to the stress the animals were put under, mean weight of the mice was slowly increasing, indicating no negative effects of [^{225}Ac]Ac-based RLT on the stomach.

In conclusion, we were able to successfully demonstrate the therapeutic efficacy of [^{225}Ac]Ac-DOTA-CCK-66, namely a 4.4-fold increase in mean survival of animals assigned to the treatment cohort. However, a small animal cohort of only 5 animals per group as well as elevated ALT as well as AST values in ^{225}Ac-treated mice indicate the need for further evaluation. Moreover, treatment studies will also be carried out using [^{177}Lu]Lu-DOTA-CCK-66 in order to elucidate a beneficial effect of α- towards β^--emitters.

Individual Performance Contribution:

N.H. designed the study, carried out the synthesis and evaluation of the peptide and acquired funding. M.V. helped with the labeling experiments and performed the animal studies. M.T. helped with the cell culture and the animal experiments. P.J.-J. helped with the animal experiments. C.M. supervised the study. C.L. supervised the study. A.C. acquired funding. T.G. helped with the study design and data analysis. G.C. acquired funding and managed the project.

IV. Summary and Outlook

To date, preclinical as well as preliminary clinical data of only three minigastrin analogs looked promising for future clinical use for imaging or treatment of MTC, namely CP04, DOTA-PP-F11N, and DOTA-MGS5. However, all those compounds still suffered from low tumor accumulation, unfavorable clearance kinetics or no option for ^{18}F-labeling to apply ^{18}F-based PET imaging. We thus aimed at the development of novel CCK-2R-targeted compounds that have the potential to improve diagnostic as well as therapeutic applications in patients suffering from MTC. Looking at the different structural units of our peptide-based CCK-2R-targeted compounds, we stepwise optimized the targeting vector, the linker units and the chelator moiety (**Figure 18**).

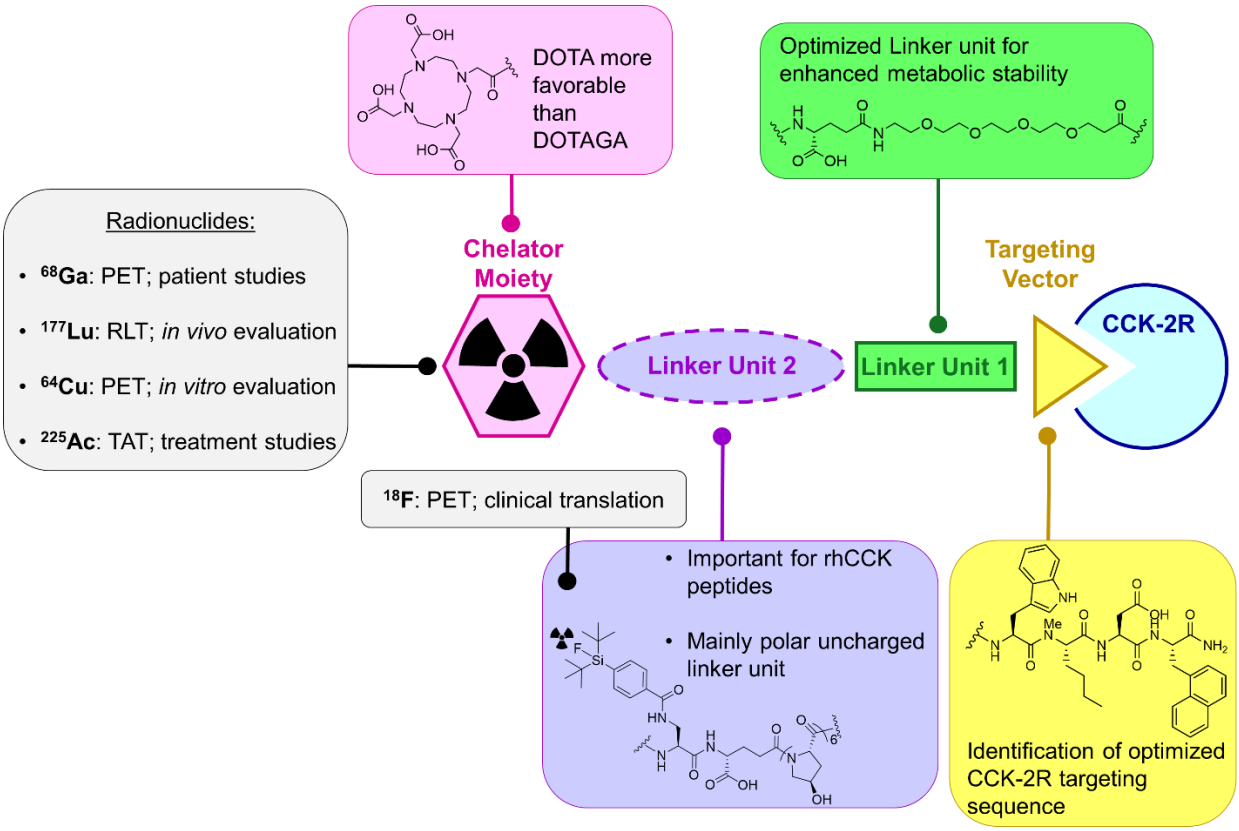

Figure 21. Schematic overview of the structural optimization strategies as well as radionuclides evaluated within this thesis. Linker Unit 2 is depicted in dashed lines as it is only necessary for radiohybrid-based peptides. Structural sequences are highlighted with different color coding.

In the course of a comparative *in vitro* analysis of various tetrapeptidic sequences, we were able to define the most suitable CCK-2R targeting vector *H*-Trp-(*N*-Me)Nle-Asp-1-Nal-NH_2, which is derived from DOTA-MGS5. However, we discovered that substitution of the D-Glu-Ala-Tyr-Gly sequence by D-*γ*-Glu-$(PEG)_3$ led to stabilized compounds, as two major cleavage sites ubiquitously present in minigastrin analogs, namely the Tyr-Gly and the Gly-Trp site, are circumvented by this modification, while CCK-2R affinity and lipophilicity are not impacted significantly. A comparative study on the influence of different chelating units on CCK-2R affinity demonstrated beneficial IC_{50} values for DOTA-comprising peptides.

Combining all these findings in one compound, DOTA-CCK-66 (DOTA-D-*γ*-Glu-$(PEG)_3$-Trp-(*N*-Me)Nle-Asp-1-Nal-NH_2) exhibited an improved *in vivo* stability compared to DOTA-MGS5 and DOTA-PP-F11N. In addition, a high CCK-2R affinity, favorable log$D_{7.4}$ values, as well as beneficial biodistribution profiles at 1 h (^{67}Ga-labeled) and 24 h (^{177}Lu-labeled) after injection were observed. A first proof-of-concept investigation using [^{68}Ga]Ga-DOTA-CCK-66 PET/CT for two patients with metastatic MTC displayed promising results. Further clinical evaluation in larger patient cohorts is ongoing, paving the way for initial therapeutic applications using [^{177}Lu]Lu-DOTA-CCK-66.

In the course of a collaborative project with the University of California, Los Angeles (UCLA), [^{225}Ac]Ac-DOTA-CCK-66 was evaluated for therapeutic efficacy in animals. With a 4.4-fold increase in mean survival of the treatment cohort in comparison to the control group animals, high therapeutic efficacy of [^{225}Ac]Ac-DOTA-CCK-66 could be determined. Collection of further data on blood toxicity, therapeutic efficacy of [^{177}Lu]Lu-DOTA-CCK-66 as well as treatment of larger animal cohorts is recommended to confirm these promising preliminary results. Furthermore, development and preclinical evaluation of DOTA-CCK-66 labeled with alternative, rare radioisotopes emerging into the focus of research due to their favorable decay characteristics (e.g., terbium, scandium or copper isotopes), might be an interesting option with distinct clinical potential in the near future.

A second major project of this work was the transfer of the radiohybrid concept to minigastrin analogs. After various optimization strategies, such as configuration of glutamate units (*α*- to *γ*-linked D-Glu), reduction of negative charges in the linker sequence (PEG or poly-Hyp units), evaluation of different SiFA moieties (*p*-SiFA, SiFAlin, SiFA-ipa), [$^{18/19}$F]F-[$^{177/nat}$Lu]Lu-DOTA-rhCCK-18 and [$^{18/19}$F]F-[$^{177/nat}$Lu]Lu-DOTA-rhCCK-84 represent the most promising compounds of this thesis. When compared to DOTA-rhCCK-18, DOTA-rhCCK-84 displayed a higher *in vivo* stability, as it comprises the more stable *H*-D-*γ*-Glu-$(PEG)_3$-Trp-(*N*-Me)Nle-Asp-1-

Nal-NH_2 unit integrated into the peptide sequence. In addition, at 24 h after injection [^{19}F]F-[^{177}Lu]Lu-DOTA-rhCCK-84 displayed tremendously reduced activity levels in the kidneys, resulting in enhanced tumor-to-kidney ratios. Thus, DOTA-rhCCK-84 might be the more favorable radiohybrid compound in a therapeutic setting. However, biodistribution data at 1 h p.i. were in favor of [^{18}F]F-[^{nat}Lu]Lu-DOTA-rhCCK-18, rendering this compound promising for imaging applications. In the course of future work, further experiments on therapeutic efficacy, toxicity, as well as dosimetry might be beneficial to further exploit the possibilities and limitations of both these compounds. In addition, a clinical evaluation of both is initiated to define the most promising clinical candidate for PET/CT imaging and RLT.

Concluded, within this thesis we reported about three novel minigastrin analogs, namely [^{68}Ga]Ga-/[^{177}Lu]Lu/[^{225}Ac]Ac-DOTA-CCK-66, [^{18}F]F-[^{nat}Lu]Lu-DOTA-rhCCK-18 and [^{18}F]F-[^{nat}Lu]Lu-/[^{19}F]F-[^{177}Lu]Lu-DOTA-rhCCK-84, with high potential for clinical translation in the fields of [^{18}F]F-PET, [^{68}Ga]Ga-PET, [^{177}Lu]Lu-RLT, as well as [^{225}Ac]Ac-TAT, four important applications of nuclear medicine in oncology. In addition, first clinical proof-of-concept PET/CT imaging studies of [^{68}Ga]Ga-DOTA-CCK-66 already confirmed its diagnostic value. Hence, in the course of future work, further studies on PET/CT imaging, therapeutic efficacy, dosimetry and toxicity in a preclinical, as well as clinical setting are recommended, to confirm the theranostic value of our novel compounds.

V. References

1. Bray F, Laversanne M, Weiderpass E, Soerjomataram I. The ever-increasing importance of cancer as a leading cause of premature death worldwide. *Cancer.* 2021;127:3029-3030.

2. Sung H, Ferlay J, Siegel RL, et al. Global Cancer Statistics 2020: GLOBOCAN Estimates of Incidence and Mortality Worldwide for 36 Cancers in 185 Countries. *CA: Cancer J Clin.* 2021;71:209-249.

3. Bray F, Jemal A, Grey N, Ferlay J, Forman D. Global cancer transitions according to the Human Development Index (2008;2013;2030): a population-based study. *The Lancet Oncology.* 2012;13:790-801.

4. Fidler MM, Soerjomataram I, Bray F. A global view on cancer incidence and national levels of the human development index. *International Journal of Cancer.* 2016;139:2436-2446.

5. Islami F, Goding Sauer A, Miller KD, et al. Proportion and number of cancer cases and deaths attributable to potentially modifiable risk factors in the United States. *CA Cancer J Clin.* 2018;68:31-54.

6. Brown KF, Rumgay H, Dunlop C, et al. The fraction of cancer attributable to modifiable risk factors in England, Wales, Scotland, Northern Ireland, and the United Kingdom in 2015. *Br J Cancer.* 2018;118:1130-1141.

7. IARC. Les cancers attribuables au mode de vie et à l'environnement en France métropolitaine. Lyon: International Agency for Research on Cancer. Accès https://gco.iarc.fr/projects/paf-france-fr. Accessed 05.09.2023, 2023.

8. Scoccianti C, Cecchini M, Anderson AS, et al. European Code against Cancer 4th Edition: Alcohol drinking and cancer. *Cancer Epidemiol.* 2016;45:181-188.

9. Stein CJ, Colditz GA. Modifiable risk factors for cancer. *British Journal of Cancer.* 2004;90:299-303.

10. Couspel N, Price R. Strengthening Europe in the fight against cancer - Going further, faster. Policy Department for Economic, Scientific and Quality of Life Policies; 2020.

11. Forman D, Bauld L, Bonanni B, et al. Time for a European initiative for research to prevent cancer: A manifesto for Cancer Prevention Europe (CPE). *Journal of Cancer Policy.* 2018;17:15-23.

12. Wild CP, Espina C, Bauld L, et al. Cancer Prevention Europe. *Molecular Oncology.* 2019;13:528-534.

13. Debela DT, Muzazu SG, Heraro KD, et al. New approaches and procedures for cancer treatment: Current perspectives. *SAGE Open Med.* 2021;9:20503121211034366.

14. Wyld L, Audisio RA, Poston GJ. The evolution of cancer surgery and future perspectives. *Nature Reviews Clinical Oncology.* 2015;12:115-124.

15. Dharap SB, Barbaniya P, Navgale S. Incidence and Risk Factors of Postoperative Complications in General Surgery Patients. *Cureus.* 2022;14:e30975.

16. Dindo D, Demartines N, Clavien PA. Classification of surgical complications: a new proposal with evaluation in a cohort of 6336 patients and results of a survey. *Ann Surg.* 2004;240:205-213.

17. Schmidt AP, Stefani LC. How to identify a high-risk surgical patient? *Braz J Anesthesiol.* 2022;72:313-315.

18. Turrentine FE, Wang H, Simpson VB, Jones RS. Surgical risk factors, morbidity, and mortality in elderly patients. *J Am Coll Surg.* 2006;203:865-877.

19. Dietrich A, Koi L, Zöphel K, et al. Improving external beam radiotherapy by combination with internal irradiation. *The British Journal of Radiology.* 2015;88:20150042.

20. Brown LC, Mutter RW, Halyard MY. Benefits, risks, and safety of external beam radiation therapy for breast cancer. *International Journal of Women's Health.* 2015;7:449-458.

21. Zaigham A, Sakina R. An Overview of Cancer Treatment Modalities. In: Hafiz Naveed S, ed. *Neoplasm*. Rijeka: IntechOpen; 2018:Ch. 6.

22. Schnur JB, Ouellette SC, Bovbjerg DH, Montgomery GH. Breast Cancer Patients' Experience of External-Beam Radiotherapy. *Qualitative Health Research.* 2009;19:668-676.

23. Swift PS, Larson S, Clark OH, Ruan D. 34 - Cancer of the Thyroid. In: Hoppe RT, Phillips TL, Roach M, eds. *Leibel and Phillips Textbook of Radiation Oncology (Third Edition)*. Philadelphia: W.B. Saunders; 2010:726-736.

24. Arnesano F, Natile G. Mechanistic insight into the cellular uptake and processing of cisplatin 30 years after its approval by FDA. *Coordination Chemistry Reviews.* 2009;253:2070-2081.

25. Mondal J, Panigrahi A, Khuda-Bukhsh A. Conventional Chemotherapy: Problems and Scope for Combined Therapies with Certain Herbal Products and Dietary Supplements. 2014:1-10.

26. Neugut AI, Prigerson HG. Curative, Life-Extending, and Palliative Chemotherapy: New Outcomes Need New Names. *Oncologist.* 2017;22:883-885.

27. Gudkov SV, Shilyagina NY, Vodeneev VA, Zvyagin AV. Targeted Radionuclide Therapy of Human Tumors. *International Journal of Molecular Sciences.* 2016;17:33.

28. Sgouros G, Bodei L, McDevitt MR, Nedrow JR. Radiopharmaceutical therapy in cancer: clinical advances and challenges. *Nature Reviews Drug Discovery.* 2020;19:589-608.

29. Kręcisz P, Czarnecka K, Królicki L, Mikiciuk-Olasik E, Szymański P. Radiolabeled Peptides and Antibodies in Medicine. *Bioconjugate Chemistry.* 2021;32:25-42.

30. Nock BA, Kanellopoulos P, Chepurny OG, et al. Nonpeptidic Z360-Analogs Tagged with Trivalent Radiometals as Anti-CCK(2)R Cancer Theranostic Agents: A Preclinical Study. *Pharmaceutics.* 2022;14.

31. Liu Y, Watabe T, Kaneda-Nakashima K, et al. Fibroblast activation protein targeted therapy using [(177)Lu]FAPI-46 compared with [(225)Ac]FAPI-46 in a pancreatic cancer model. *Eur J Nucl Med Mol Imaging.* 2022;49:871-880.

32. Ward JF. DNA Damage Produced by Ionizing Radiation in Mammalian Cells: Identities, Mechanisms of Formation, and Reparability. In: Cohn WE, Moldave K, eds. *Progress in Nucleic Acid Research and Molecular Biology.* Vol 35: Academic Press; 1988:95-125.

33. Behr TM, Sgouros G, Vougioukas V, et al. Therapeutic efficacy and dose-limiting toxicity of auger-electron vs. beta emitters in radioimmunotherapy with internalizing antibodies: Evaluation of 125I- vs. 131I-labeled CO17-1A in a human colorectal cancer model. *International Journal of Cancer.* 1998;76:738-748.

34. Lehenberger S, Barkhausen C, Cohrs S, et al. The low-energy β− and electron emitter 161Tb as an alternative to 177Lu for targeted radionuclide therapy. *Nuclear Medicine and Biology.* 2011;38:917-924.

35. Conti M, Eriksson L. Physics of pure and non-pure positron emitters for PET: a review and a discussion. *EJNMMI Physics.* 2016;3:8.

36. Rangacharyulu C, Roh CK. Isotopes for combined PET/SPECT imaging. *Journal of Radioanalytical and Nuclear Chemistry.* 2015;305:87-92.

37. Crișan G, Moldovean-Cioroianu NS, Timaru DG, Andrieș G, Căinap C, Chiș V. Radiopharmaceuticals for PET and SPECT Imaging: A Literature Review over the Last Decade. *Int J Mol Sci.* 2022;23.

38. Pietrzyk U, Herholz K, Schuster A, Stockhausen H-Mv, Lucht H, Heiss W-D. Clinical applications of registration and fusion of multimodality brain images from PET, SPECT, CT, and MRI. *European Journal of Radiology.* 1996;21:174-182.

39. Bernsen MR, Vaissier PEB, Van Holen R, Booij J, Beekman FJ, de Jong M. The role of preclinical SPECT in oncological and neurological research in combination with either CT or MRI. *Eur J Nucl Med Mol Imaging.* 2014;41:36-49.

40. Griffeth LK. Use of PET/CT scanning in cancer patients: technical and practical considerations. *Proc (Bayl Univ Med Cent).* 2005;18:321-330.

41. Gomes Marin JF, Nunes RF, Coutinho AM, et al. Theranostics in Nuclear Medicine: Emerging and Re-emerging Integrated Imaging and Therapies in the Era of Precision Oncology. *RadioGraphics.* 2020;40:1715-1740.

42. Könik A, O'Donoghue JA, Wahl RL, Graham MM, Van den Abbeele AD. Theranostics: The Role of Quantitative Nuclear Medicine Imaging. *Seminars in Radiation Oncology.* 2021;31:28-36.

43. Müller C, Domnanich KA, Umbricht CA, van der Meulen NP. Scandium and terbium radionuclides for radiotheranostics: current state of development towards clinical application. *Br J Radiol.* 2018;91:20180074.

44. Reubi JC, Schär J-C, Waser B, et al. Affinity profiles for human somatostatin receptor subtypes SST1–SST5 of somatostatin radiotracers selected for scintigraphic and radiotherapeutic use. *European Journal of Nuclear Medicine.* 2000;27:273-282.

45. Osl T, Schmidt A, Schwaiger M, Schottelius M, Wester HJ. A new class of PentixaFor- and PentixaTher-based theranostic agents with enhanced CXCR4-targeting efficiency. *Theranostics.* 2020;10:8264-8280.

46. Yordanova A, Eppard E, Kürpig S, et al. Theranostics in nuclear medicine practice. *Onco Targets Ther.* 2017;10:4821-4828.

47. Rowshanfarzad P, Sabet M, Reza Jalilian A, Kamalidehghan M. An overview of copper radionuclides and production of 61Cu by proton irradiation of natZn at a medical cyclotron. *Applied Radiation and Isotopes.* 2006;64:1563-1573.

48. Mikolajczak R, Huclier-Markai S, Alliot C, et al. Production of scandium radionuclides for theranostic applications: towards standardization of quality requirements. *EJNMMI Radiopharmacy and Chemistry.* 2021;6:19.

49. Szymański P, Frączek T, Markowicz M, Mikiciuk-Olasik E. Development of copper based drugs, radiopharmaceuticals and medical materials. *BioMetals.* 2012;25:1089-1112.

50. Kusić Z, Becker DV, Saenger EL, et al. Comparison of Technetium-99m and Iodine 123 Imaging of Thyroid Nodules: Correlation with Pathologic Findings. *J Nucl Med.* 1990;31:393-399.

51. Silberstein EB. Radioiodine: The Classic Theranostic Agent. *Seminars in Nuclear Medicine.* 2012;42:164-170.

52. Drude N, Tienken L, Mottaghy FM. Theranostic and nanotheranostic probes in nuclear medicine. *Methods.* 2017;130:14-22.

53. Wurzer A, DiCarlo D, Schmidt A, et al. Radiohybrid ligands: a novel tracer concept exemplified by 18F- or 68Ga-labeled rhPSMA-inhibitors. *J Nucl Med.* 2019.

54. Sanchez-Crespo A. Comparison of Gallium-68 and Fluorine-18 imaging characteristics in positron emission tomography. *Applied Radiation and Isotopes.* 2013;76:55-62.

55. Zimmerman BE, Cessna JT, Fitzgerald R. Standardization of (68)Ge/(68)Ga Using Three Liquid Scintillation Counting Based Methods. *J Res Natl Inst Stand Technol.* 2008;113:265-280.

56. Jacobson O, Kiesewetter DO, Chen X. Fluorine-18 radiochemistry, labeling strategies and synthetic routes. *Bioconjug Chem.* 2015;26:1-18.

57. The Current Status of the Production and Supply of Gallium-68. *Cancer Biotherapy and Radiopharmaceuticals.* 2020;35:163-166.

58. Kim K, Kim SJ. Lu-177-Based Peptide Receptor Radionuclide Therapy for Advanced Neuroendocrine Tumors. *Nucl Med Mol Imaging.* 2018;52:208-215.

59. Hennrich U, Kopka K. Lutathera(®): The First FDA- and EMA-Approved Radiopharmaceutical for Peptide Receptor Radionuclide Therapy. *Pharmaceuticals (Basel).* 2019;12.

60. Hennrich U, Eder M. [(177)Lu]Lu-PSMA-617 (Pluvicto(TM)): The First FDA-Approved Radiotherapeutical for Treatment of Prostate Cancer. *Pharmaceuticals (Basel).* 2022;15.

61. Schirrmacher R, Bradtmöller G, Schirrmacher E, et al. 18F-Labeling of Peptides by means of an Organosilicon-Based Fluoride Acceptor. *Angewandte Chemie International Edition.* 2006;45:6047-6050.

62. Wängler C, Niedermoser S, Chin J, et al. One-step 18F-labeling of peptides for positron emission tomography imaging using the SiFA methodology. *Nature Protocols.* 2012;7:1946-1955.

63. Arnott JA, Planey SL. The influence of lipophilicity in drug discovery and design. *Expert Opinion on Drug Discovery.* 2012;7:863-875.

64. Wängler C, Kostikov A, Zhu J, Chin J, Wängler B, Schirrmacher R. Silicon-[18F]Fluorine Radiochemistry: Basics, Applications and Challenges. *Applied Sciences.* 2012;2:277-302.

65. Litau S, Niedermoser S, Vogler N, et al. Next Generation of SiFAlin-Based TATE Derivatives for PET Imaging of SSTR-Positive Tumors: Influence of Molecular Design on In Vitro SSTR Binding and In Vivo Pharmacokinetics. *Bioconjugate Chemistry.* 2015;26:2350-2359.

66. Wängler C, Waser B, Alke A, et al. One-step **[18]**F-labeling of carbohydrate-conjugated octreotate-derivatives containing a silicon-fluoride-acceptor (SiFA): in vitro and in vivo evaluation as tumor imaging agents for positron emission tomography (PET). *Bioconjug Chem.* 2010;21:2289-2296.

67. Kostikov AP, Iovkova L, Chin J, et al. N-(4-(di-tert-butyl[18F]fluorosilyl)benzyl)-2-hydroxy-N,N-dimethylethylammonium bromide ([18F]SiFAN+Br−): A novel lead compound for the development of hydrophilic SiFA-based prosthetic groups for 18F-labeling. *Journal of Fluorine Chemistry.* 2011;132:27-34.

68. Eiber M, Kroenke M, Wurzer A, et al. (18)F-rhPSMA-7 PET for the Detection of Biochemical Recurrence of Prostate Cancer After Radical Prostatectomy. *J Nucl Med.* 2020;61:696-701.

69. Langbein T, Wang H, Rauscher I, et al. Utility of (18)F-rhPSMA-7.3 PET for Imaging of Primary Prostate Cancer and Preoperative Efficacy in N-Staging of Unfavorable Intermediate- to Very High-Risk Patients Validated by Histopathology. *J Nucl Med.* 2022;63:1334-1342.

70. Wurzer A, Parzinger M, Konrad M, et al. Preclinical comparison of four [(18)F, (nat)Ga]rhPSMA-7 isomers: influence of the stereoconfiguration on pharmacokinetics. *EJNMMI Res.* 2020;10:149.

71. Jani AB, Ravizzini GC, Gartrell BA, et al. Diagnostic Performance and Safety of (18)F-rhPSMA-7.3 Positron Emission Tomography in Men With Suspected Prostate Cancer Recurrence: Results From a Phase 3, Prospective, Multicenter Study (SPOTLIGHT). *J Urol.* 2023;210:299-311.

72. Lowentritt B. Impact of Clinical Factors on ^{18}F-rhPSMA-7.3 Detection Rates in Men with Recurrent Prostate Cancer: Findings from the Phase 3 SPOTLIGHT Study. *International Journal of Radiation Oncology, Biology, Physics.* 2022;114:S130-S131.

73. Wurzer A, Kunert J-P, Fischer S, et al. Synthesis and Preclinical Evaluation of ^{177}Lu-labeled Radiohybrid PSMA Ligands (rhPSMAs) for Endoradiotherapy of Prostate Cancer. *J Nucl Med.* 2022:jnumed.121.263371.

74. Bundschuh RA, Pfob CH, Wienand G, Dierks A, Kircher M, Lapa C. 177 Lu-rhPSMA-10.1 Induces Tumor Response in a Patient With mCRPC After PSMA-Directed Radioligand Therapy With 177 Lu-PSMA-I&T. *Clin Nucl Med.* 2023;48:337-338.

75. Marcu L, Bezak E, Allen BJ. Global comparison of targeted alpha vs targeted beta therapy for cancer: In vitro, in vivo and clinical trials. *Critical Reviews in Oncology/Hematology.* 2018;123:7-20.

76. Navalkissoor S, Grossman A. Targeted Alpha Particle Therapy for Neuroendocrine Tumours: The Next Generation of Peptide Receptor Radionuclide Therapy. *Neuroendocrinology.* 2018;108:256-264.

77. Sgouros G. Alpha-particles for targeted therapy. *Advanced Drug Delivery Reviews.* 2008;60:1402-1406.

78. Makvandi M, Dupis E, Engle JW, et al. Alpha-Emitters and Targeted Alpha Therapy in Oncology: from Basic Science to Clinical Investigations. *Targeted Oncology.* 2018;13:189-203.

79. Robertson AKH, Ramogida CF, Schaffer P, Radchenko V. Development of (225)Ac Radiopharmaceuticals: TRIUMF Perspectives and Experiences. *Curr Radiopharm.* 2018;11:156-172.

80. Kluetz PG, Pierce W, Maher VE, et al. Radium Ra 223 dichloride injection: U.S. Food and Drug Administration drug approval summary. *Clin Cancer Res.* 2014;20:9-14.

81. Boll RA, Malkemus D, Mirzadeh S. Production of actinium-225 for alpha particle mediated radioimmunotherapy. *Applied Radiation and Isotopes.* 2005;62:667-679.

82. Alvarez R. Managing the Uranium-233 Stockpile of the United States. *Science & Global Security.* 2013;21:53-69.

83. Morgenstern A, Bruchertseifer F, Apostolidis C. Bismuth-213 and actinium-225 -- generator performance and evolving therapeutic applications of two generator-derived alpha-emitting radioisotopes. *Curr Radiopharm.* 2012;5:221-227.

84. Zhuikov BL. Successes and problems in the development of medical radioisotope production in Russia. *Physics-Uspekhi.* 2016;59:481.

85. Melville G, Meriarty H, Metcalfe P, Knittel T, Allen BJ. Production of Ac-225 for cancer therapy by photon-induced transmutation of Ra-226. *Applied Radiation and Isotopes.* 2007;65:1014-1022.

86. Apostolidis C, Molinet R, McGinley J, Abbas K, Möllenbeck J, Morgenstern A. Cyclotron production of Ac-225 for targeted alpha therapy11Dedicated to Prof. Dr. Franz Baumgärtner on the occasion of his 75th birthday. *Applied Radiation and Isotopes.* 2005;62:383-387.

87. Griswold JR, Medvedev DG, Engle JW, et al. Large scale accelerator production of (225)Ac: Effective cross sections for 78-192MeV protons incident on (232)Th targets. *Appl Radiat Isot.* 2016;118:366-374.

88. De Kruijff RM, Wolterbeek HT, Denkova AG. A Critical Review of Alpha Radionuclide Therapy—How to Deal with Recoiling Daughters? *Pharmaceuticals.* Vol 8; 2015:321-336.

89. Hu A, Simms ME, Kertesz V, Wilson JJ, Thiele NA. Chelating Rare-Earth Metals (Ln(3+)) and (225)Ac(3+) with the Dual-Size-Selective Macrocyclic Ligand Py(2)-Macrodipa. *Inorg Chem.* 2022;61:12847-12855.

90. Mdanda S, Ngema LM, Mdlophane A, Sathekge MM, Zeevaart JR. Recent Innovations and Nano-Delivery of Actinium-225: A Narrative Review. *Pharmaceutics.* 2023;15.

91. Ballal S, Yadav MP, Tripathi M, Sahoo RK, Bal C. Survival Outcomes in Metastatic Gastroenteropancreatic Neuroendocrine Tumor Patients Receiving Concomitant ^{225}Ac-DOTATATE–Targeted α-Therapy and Capecitabine: A Real-World-Scenario Management-Based Long-Term Outcome Study. *J Nucl Med.* 2023;64:211-218.

92. Zacherl MJ, Gildehaus FJ, Mittlmeier L, et al. First Clinical Results for PSMA-Targeted α-Therapy Using (225)Ac-PSMA-I&T in Advanced-mCRPC Patients. *J Nucl Med.* 2021;62:669-674.

93. Kratochwil C, Bruchertseifer F, Giesel FL, et al. ^{225}Ac-PSMA-617 for PSMA-Targeted α-Radiation Therapy of Metastatic Castration-Resistant Prostate Cancer. *J Nucl Med.* 2016;57:1941-1944.

94. Cancer Stat Facts: Thyroid Cancer. https://seer.cancer.gov/statfacts/html/thyro.html. Accessed 07.07.2023, 2023.

95. Cancer Stat Facts: Cancer of Any Site. https://seer.cancer.gov/statfacts/html/all.html. Accessed 07.07.2023, 2023.

96. Oertel J, Oertel Y. Papillary Carcinoma. In: Wartofsky L, ed. *Thyroid Cancer: A Comprehensive Guide to Clinical Management*. Totowa, NJ: Humana Press; 2000:193-208.

97. Wartofsky L. Papillary Carcinoma. In: Wartofsky L, Van Nostrand D, eds. *Thyroid Cancer: A Comprehensive Guide to Clinical Management*. Totowa, NJ: Humana Press; 2006:253-260.

98. Nguyen QT, Lee EJ, Huang MG, Park YI, Khullar A, Plodkowski RA. Diagnosis and treatment of patients with thyroid cancer. *Am Health Drug Benefits.* 2015;8:30-40.

99. Ball DW. Clinical Aspects of Medullary Thyroid Carcinoma. In: Wartofsky L, Van Nostrand D, eds. *Thyroid Cancer: A Comprehensive Guide to Clinical Management*. Totowa, NJ: Humana Press; 2006:581-589.

100. Sherman SI. Anaplastic Carcinoma. In: Wartofsky L, Van Nostrand D, eds. *Thyroid Cancer: A Comprehensive Guide to Clinical Management*. Totowa, NJ: Humana Press; 2006:629-632.

101. Araque KA, Gubbi S, Klubo-Gwiezdzinska J. Updates on the Management of Thyroid Cancer. *Horm Metab Res.* 2020;52:562-577.

102. Wells SA, Jr., Asa SL, Dralle H, et al. Revised American Thyroid Association guidelines for the management of medullary thyroid carcinoma. *Thyroid.* 2015;25:567-610.

103. Jin M, Megwalu UC, Noel JE. External Beam Radiotherapy for Medullary Thyroid Cancer Following Total or Near-Total Thyroidectomy. *Otolaryngol Head Neck Surg.* 2021;164:97-103.

104. Terezakis SA, Lee NY. The role of radiation therapy in the treatment of medullary thyroid cancer. *J Natl Compr Canc Netw.* 2010;8:532-540; quiz 541.

105. Wells SA, Jr., Robinson BG, Gagel RF, et al. Vandetanib in patients with locally advanced or metastatic medullary thyroid cancer: a randomized, double-blind phase III trial. *J Clin Oncol.* 2012;30:134-141.

106. Elisei R, Schlumberger MJ, Müller SP, et al. Cabozantinib in progressive medullary thyroid cancer. *J Clin Oncol.* 2013;31:3639-3646.

107. Bhattacharyya N. A population-based analysis of survival factors in differentiated and medullary thyroid carcinoma. *Otolaryngol Head Neck Surg.* 2003;128:115-123.

108. Roman S, Lin R, Sosa JA. Prognosis of medullary thyroid carcinoma. *Cancer.* 2006;107:2134-2142.

109. Hundahl SA, Fleming ID, Fremgen AM, Menck HR. A National Cancer Data Base report on 53,856 cases of thyroid carcinoma treated in the U.S., 1985-1995 [see commetns]. *Cancer.* 1998;83:2638-2648.

110. O'Riordain DS, O'Brien T, Weaver AL, et al. Medullary thyroid carcinoma in multiple endocrine neoplasia types 2A and 2B. *Surgery.* 1994;116:1017-1023.

111. Sippel RS, Kunnimalaiyaan M, Chen H. Current management of medullary thyroid cancer. *Oncologist.* 2008;13:539-547.

112. Shepet K, Alhefdhi A, Lai N, Mazeh H, Sippel R, Chen H. Hereditary medullary thyroid cancer: age-appropriate thyroidectomy improves disease-free survival. *Ann Surg Oncol.* 2013;20:1451-1455.

113. Kaliszewski K, Ludwig M, Ludwig B, Mikuła A, Greniuk M, Rudnicki J. Update on the Diagnosis and Management of Medullary Thyroid Cancer: What Has Changed in Recent Years? *Cancers (Basel).* 2022;14.

114. Bae YJ, Schaab M, Kratzsch J. Calcitonin as Biomarker for the Medullary Thyroid Carcinoma. *Recent Results Cancer Res.* 2015;204:117-137.

115. Thomas CM, Asa SL, Ezzat S, Sawka AM, Goldstein D. Diagnosis and pathologic characteristics of medullary thyroid carcinoma-review of current guidelines. *Curr Oncol.* 2019;26:338-344.

116. Laure Giraudet A, Al Ghulzan A, Aupérin A, et al. Progression of medullary thyroid carcinoma: assessment with calcitonin and carcinoembryonic antigen doubling times. *European Journal of Endocrinology.* 2008;158:239-246.

117. Béhé M, Behr TM. Cholecystokinin-B (CCK-B)/gastrin receptor targeting peptides for staging and therapy of medullary thyroid cancer and other CCK-B receptor expressing malignancies. *Peptide Science.* 2002;66:399-418.

118. Giovanella L, Treglia G, Iakovou I, Mihailovic J, Verburg FA, Luster M. EANM practice guideline for PET/CT imaging in medullary thyroid carcinoma. *Eur J Nucl Med Mol Imaging.* 2020;47:61-77.

119. Koopmans KP, Neels ON, Kema IP, et al. Molecular imaging in neuroendocrine tumors: molecular uptake mechanisms and clinical results. *Crit Rev Oncol Hematol.* 2009;71:199-213.

120. Minn H, Kauhanen S, Seppänen M, Nuutila P. ^{18}F-FDOPA: A Multiple-Target Molecule. *J Nucl Med.* 2009;50:1915-1918.

121. Kvols LK, Reubi JC, Horisberger U, Moertel CG, Rubin J, Charboneau JW. The presence of somatostatin receptors in malignant neuroendocrine tumor tissue predicts responsiveness to octreotide. *Yale J Biol Med.* 1992;65:505-518; discussion 531-506.

122. Hofland LJ, Lamberts SWJ. The Pathophysiological Consequences of Somatostatin Receptor Internalization and Resistance. *Endocrine Reviews.* 2003;24:28-47.

123. Treglia G, Castaldi P, Villani MF, et al. Comparison of Different Positron Emission Tomography Tracers in Patients with Recurrent Medullary Thyroid Carcinoma: Our Experience and a Review of the Literature, 2013; Berlin, Heidelberg.

124. Romero-Lluch AR, Cuenca-Cuenca JI, Guerrero-Vázquez R, et al. Diagnostic utility of PET/CT with 18F-DOPA and 18F-FDG in persistent or recurrent medullary thyroid carcinoma: the importance of calcitonin and carcinoembryonic antigen cutoff. *Eur J Nucl Med Mol Imaging.* 2017;44:2004-2013.

125. Brammen L, Niederle MB, Riss P, et al. Medullary Thyroid Carcinoma: Do Ultrasonography and F-DOPA-PET-CT Influence the Initial Surgical Strategy? *Ann Surg Oncol.* 2018;25:3919-3927.

126. Asa S, Sonmezoglu K, Uslu-Besli L, et al. Evaluation of F-18 DOPA PET/CT in the detection of recurrent or metastatic medullary thyroid carcinoma: comparison with GA-68 DOTA-TATE PET/CT. *Annals of Nuclear Medicine.* 2021;35:900-915.

127. Tisell LE, Ahlman H, Wängberg B, et al. Somatostatin receptor scintigraphy in medullary thyroid carcinoma. *BJS (British Journal of Surgery).* 1997;84:543-547.

128. Gotthardt M, Béhé MP, Beuter D, et al. Improved tumour detection by gastrin receptor scintigraphy in patients with metastasised medullary thyroid carcinoma. *Eur J Nucl Med Mol Imaging.* 2006;33:1273-1279.

129. Reubi JC, Waser B. Unexpected high incidence of cholecystokinin-B/gastrin receptors in human medullary thyroid carcinomas. *Int J Cancer.* 1996;67:644-647.

130. Matsumori Y, Katakami N, Ito M, et al. Cholecystokinin-B/gastrin receptor: a novel molecular probe for human small cell lung cancer. *Cancer Res.* 1995;55:276-279.

131. Camby I, Salmon I, Danguy A, et al. Influence of gastrin on human astrocytic tumor cell proliferation. *J Natl Cancer Inst.* 1996;88:594-600.

132. Reubi JC, Schaer JC, Waser B. Cholecystokinin(CCK)-A and CCK-B/gastrin receptors in human tumors. *Cancer Res.* 1997;57:1377-1386.

133. Nock BA, Kanellopoulos P, Joosten L, Mansi R, Maina T. Peptide Radioligands in Cancer Theranostics: Agonists and Antagonists. *Pharmaceuticals.* 2023;16:674.

134. Noble F, Roques BP. CCK-B receptor: chemistry, molecular biology, biochemistry and pharmacology. *Progress in Neurobiology.* 1999;58:349-379.

135. Wank SA. Cholecystokinin receptors. *American Journal of Physiology-Gastrointestinal and Liver Physiology.* 1995;269:G628-G646.

136. Wank SA. I. CCK receptors: an exemplary family. *American Journal of Physiology-Gastrointestinal and Liver Physiology.* 1998;274:G607-G613.

137. Roosenburg S, Laverman P, van Delft FL, Boerman OC. Radiolabeled CCK/gastrin peptides for imaging and therapy of CCK2 receptor-expressing tumors. *Amino Acids.* 2011;41:1049-1058.

138. Hellmich MR, Rui X-L, Hellmich HL, Fleming RYD, Evers BM, Townsend CM, Jr. Human Colorectal Cancers Express a Constitutively Active Cholecystokinin-B/Gastrin Receptor That Stimulates Cell Growth *. *Journal of Biological Chemistry.* 2000;275:32122-32128.

139. Tuteja N. Signaling through G protein coupled receptors. *Plant Signal Behav.* 2009;4:942-947.

140. Marco E, Foucaud M, Langer I, Escrieut C, Tikhonova IG, Fourmy D. Mechanism of Activation of a G Protein-coupled Receptor, the Human Cholecystokinin-2 Receptor*. *Journal of Biological Chemistry.* 2007;282:28779-28790.

141. Langer I, Tikhonova IG, Travers M-A, et al. Evidence That Interspecies Polymorphism in the Human and Rat Cholecystokinin Receptor-2 Affects Structure of the Binding Site for the Endogenous Agonist Cholecystokinin*. *Journal of Biological Chemistry.* 2005;280:22198-22204.

142. Kopin AS, McBride EW, Schaffer K, Beinborn M. CCK receptor polymorphisms: an illustration of emerging themes in pharmacogenomics. *Trends Pharmacol Sci.* 2000;21:346-353.

143. Laverman P, Joosten L, Eek A, et al. Comparative biodistribution of 12 ^{111}In-labelled gastrin/CCK2 receptor-targeting peptides. *Eur J Nucl Med Mol Imaging.* 2011;38:1410-1416.

144. Behr TM, Jenner N, Béhé M, et al. Radiolabeled Peptides for Targeting Cholecystokinin-B/Gastrin Receptor-Expressing Tumors. *J Nucl Med.* 1999;40:1029-1044.

145. Behr TM, Béhé M, Angerstein C, et al. Cholecystokinin-B/gastrin receptor binding peptides: preclinical development and evaluation of their diagnostic and therapeutic potential. *Clin Cancer Res.* 1999;5:3124s-3138s.

146. Behr TM, Jenner N, Radetzky S, et al. Targeting of cholecystokinin-B/gastrin receptors in vivo: preclinical and initial clinical evaluation of the diagnostic and therapeutic potential of radiolabelled gastrin. *Eur J Nucl Med.* 1998;25:424-430.

147. Béhé M, Becker W, Gotthardt M, Angerstein C, Behr TM. Improved kinetic stability of DTPA-dGlu as compared with conventional monofunctional DTPA in chelating indium and yttrium: preclinical and initial clinical evaluation of radiometal labelled minigastrin derivatives. *Eur J Nucl Med Mol Imaging.* 2003;30:1140-1146.

148. Good S, Walter MA, Waser B, et al. Macrocyclic chelator-coupled gastrin-based radiopharmaceuticals for targeting of gastrin receptor-expressing tumours. *Eur J Nucl Med Mol Imaging.* 2008;35:1868-1877.

149. Kolenc-Peitl P, Mansi R, Tamma M, et al. Highly Improved Metabolic Stability and Pharmacokinetics of Indium-111-DOTA-Gastrin Conjugates for Targeting of the Gastrin Receptor. *J Med Chem.* 2011;54:2602-2609.

150. Kolenc Peitl P, Tamma M, Kroselj M, et al. Stereochemistry of Amino Acid Spacers Determines the Pharmacokinetics of 111In–DOTA–Minigastrin Analogues for Targeting the CCK2/Gastrin Receptor. *Bioconjugate Chemistry.* 2015;26:1113-1119.

151. Sauter AW, Mansi R, Hassiepen U, et al. Targeting of the Cholecystokinin-2 Receptor with the Minigastrin Analog ^{177}Lu-DOTA-PP-F11N: Does the Use of Protease Inhibitors Further Improve In Vivo Distribution? *J Nucl Med.* 2019;60:393-399.

152. Ocak M, Helbok A, Rangger C, et al. Comparison of biological stability and metabolism of CCK2 receptor targeting peptides, a collaborative project under COST BM0607. *Eur J Nucl Med Mol Imaging.* 2011;38:1426-1435.

153. Klingler M, Decristoforo C, Rangger C, et al. Site-specific stabilization of minigastrin analogs against enzymatic degradation for enhanced cholecystokinin-2 receptor targeting. *Theranostics.* 2018;8:2896-2908.

154. von Guggenberg E, Kolenc P, Rottenburger C, Mikołajczak R, Hubalewska-Dydejczyk A. Update on Preclinical Development and Clinical Translation of Cholecystokinin-2 Receptor Targeting Radiopharmaceuticals. *Cancers (Basel).* 2021;13.

155. Grzmil M, Qin Y, Schleuniger C, et al. Pharmacological inhibition of mTORC1 increases CCKBR-specific tumor uptake of radiolabeled minigastrin analogue [^{177}Lu]Lu-PP-F11N. *Theranostics.* 2020;10:10861-10873.

156. Grob NM, Schibli R, Béhé M, Mindt TL. Improved Tumor-Targeting with Peptidomimetic Analogs of Minigastrin (177)Lu-PP-F11N. *Cancers (Basel).* 2021;13.

157. Grob NM, Häussinger D, Deupi X, Schibli R, Behe M, Mindt TL. Triazolo-Peptidomimetics: Novel Radiolabeled Minigastrin Analogs for Improved Tumor Targeting. *J Med Chem.* 2020;63:4484-4495.

158. Klingler M, Rangger C, Summer D, Kaeopookum P, Decristoforo C, von Guggenberg E. Cholecystokinin-2 Receptor Targeting with Novel C-terminally Stabilized HYNIC-Minigastrin Analogs Radiolabeled with Technetium-99m. *Pharmaceuticals (Basel).* 2019;12.

159. Klingler M, Summer D, Rangger C, et al. DOTA-MGS5, a New Cholecystokinin-2 Receptor-Targeting Peptide Analog with an Optimized Targeting Profile for Theranostic Use. *J Nucl Med.* 2019;60:1010-1016.

160. Hörmann AA, Klingler M, Rangger C, et al. Effect of N-Terminal Peptide Modifications on In Vitro and In Vivo Properties of 177Lu-Labeled Peptide Analogs Targeting CCK2R. *Pharmaceutics.* 2023;15:796.

161. Rottenburger C, Nicolas GP, McDougall L, et al. Cholecystokinin 2 Receptor Agonist (177)Lu-PP-F11N for Radionuclide Therapy of Medullary Thyroid Carcinoma: Results of the Lumed Phase 0a Study. *J Nucl Med.* 2020;61:520-526.

162. Kaloudi A, Kanellopoulos P, Radolf T, et al. [99mTc]Tc-DGA1, a Promising CCK2R-Antagonist-Based Tracer for Tumor Diagnosis with Single-Photon Emission Computed Tomography. *Molecular Pharmaceutics.* 2020;17:3116-3128.

163. Novak D, Tomašič T, Krošelj M, et al. Radiolabelled CCK2R Antagonists Containing PEG Linkers: Design, Synthesis and Evaluation. *ChemMedChem.* 2021;16:155-163.

164. Wayua C, Low P. Evaluation of a Nonpeptidic Ligand for Imaging of Cholecystokinin 2 Receptor-Expressing Cancers. *Journal of Nuclear Medicine : official publication, Society of Nuclear Medicine.* 2014;56.

165. Verona M, Rubagotti S, Croci S, et al. Preliminary Study of a 1,5-Benzodiazepine-Derivative Labelled with Indium-111 for CCK-2 Receptor Targeting. *Molecules.* 2021;26:918.

166. Klingler M, Hörmann AA, Rangger C, et al. Stabilization Strategies for Linear Minigastrin Analogues: Further Improvements via the Inclusion of Proline into the Peptide Sequence. *J Med Chem.* 2020;63:14668-14679.

167. Hörmann AA, Klingler M, Rezaeianpour M, et al. Initial In Vitro and In Vivo Evaluation of a Novel CCK2R Targeting Peptide Analog Labeled with Lutetium-177. *Molecules.* 2020;25.

168. Silvente-Poirot S, Escrieut C, Galès C, et al. Evidence for a direct interaction between the penultimate aspartic acid of cholecystokinin and histidine 207, located in the second extracellular loop of the cholecystokinin B receptor. *The Journal of biological chemistry.* 1999;274:23191-23197.

169. Bellier B, Million ME, DaNascimento S, et al. Replacement of glycine with dicarbonyl and related moieties in analogues of the C-terminal pentapeptide of cholecystokinin: CCK(2) agonists displaying a novel binding mode. *J Med Chem.* 2000;43:3614-3623.

170. Corringer PJ, Weng JH, Ducos B, et al. CCK-B agonist or antagonist activities of structurally hindered and peptidase-resistant Boc-CCK4 derivatives. *J Med Chem.* 1993;36:166-172.

171. Krieger F, Möglich A, Kiefhaber T. Effect of Proline and Glycine Residues on Dynamics and Barriers of Loop Formation in Polypeptide Chains. *Journal of the American Chemical Society.* 2005;127:3346-3352.

172. Krieger F, Fierz B, Bieri O, Drewello M, Kiefhaber T. Dynamics of Unfolded Polypeptide Chains as Model for the Earliest Steps in Protein Folding. *Journal of Molecular Biology.* 2003;332:265-274.

173. Power DM, Bunnett N, Turner AJ, Dimaline R. Degradation of endogenous heptadecapeptide gastrin by endopeptidase 24.11 in the pig. *American Journal of Physiology-Gastrointestinal and Liver Physiology.* 1987;253:G33-G39.

174. Deschodt-Lanckman M, Pauwels S, Najdovski T, Dimaline R, Dockray GJ. In vitro and in vivo degradation of human gastrin by endopeptidase 24.11. *Gastroenterology.* 1988;94:712-721.

175. Roques BP, Noble F, Daugé V, Fournié-Zaluski MC, Beaumont A. Neutral endopeptidase 24.11: structure, inhibition, and experimental and clinical pharmacology. *Pharmacological Reviews.* 1993;45:87-146.

176. Nock BA, Maina T, Krenning EP, de Jong M. "To serve and protect": enzyme inhibitors as radiopeptide escorts promote tumor targeting. *J Nucl Med.* 2014;55:121-127.

177. Kaloudi A, Nock BA, Lymperis E, et al. Impact of clinically tested NEP/ACE inhibitors on tumor uptake of [(111)In-DOTA]MG11-first estimates for clinical translation. *EJNMMI Res.* 2016;6:15.

178. Chen Y, Li WW, Peng P, et al. mTORC1 inhibitor RAD001 (everolimus) enhances non-small cell lung cancer cell radiosensitivity in vitro via suppressing epithelial-mesenchymal transition. *Acta Pharmacol Sin.* 2019;40:1085-1094.

179. Hasskarl J. Everolimus. *Recent Results Cancer Res.* 2018;211:101-123.

180. Kopin AS, McBride EW, Chen C, et al. Identification of a series of CCK-2 receptor nonpeptide agonists: Sensitivity to stereochemistry and a receptor point mutation. *Proceedings of the National Academy of Sciences.* 2003;100:5525-5530.

181. Novak D, Anderluh M, Kolenc Peitl P. CCK2R antagonists: from SAR to clinical trials. *Drug Discovery Today.* 2020;25:1322-1336.

182. Ginj M, Zhang H, Waser B, et al. Radiolabeled somatostatin receptor antagonists are preferable to agonists for *in vivo* peptide receptor targeting of tumors. *Proceedings of the National Academy of Sciences.* 2006;103:16436-16441.

183. Koller L, Joksch M, Schwarzenböck S, et al. Preclinical Comparison of the ^{64}Cu- and ^{68}Ga-Labeled GRPR-Targeted Compounds RM2 and AMTG, as Well as First-in-Humans [^{68}Ga]Ga-AMTG PET/CT. *J Nucl Med.* 2023:jnumed.123.265771.

184. Beheshti M, Taimen P, Kemppainen J, et al. Value of (68)Ga-labeled bombesin antagonist (RM2) in the detection of primary prostate cancer comparing with [(18)F]fluoromethylcholine PET-CT and multiparametric MRI-a phase I/II study. *Eur Radiol.* 2023;33:472-482.

185. Baum RP, Zhang J, Schuchardt C, Müller D, Mäcke H. First-in-Humans Study of the SSTR Antagonist ^{177}Lu-DOTA-LM3 for Peptide Receptor Radionuclide Therapy in Patients with Metastatic Neuroendocrine Neoplasms: Dosimetry, Safety, and Efficacy. *J Nucl Med.* 2021;62:1571-1581.

186. Ubl P, Gincu T, Keilani M, et al. Comparison of side effects of pentagastrin test and calcium stimulation test in patients with increased basal calcitonin concentration: the gender-specific differences. *Endocrine.* 2014;46:549-553.

187. Lezaic L, Erba PA, Decristoforo C, et al. [(111)In]In-CP04 as a novel cholecystokinin-2 receptor ligand with theranostic potential in patients with progressive or metastatic medullary thyroid cancer: final results of a GRAN-T-MTC Phase I clinical trial. *Eur J Nucl Med Mol Imaging.* 2022.

188. Guggenberg Ev, Uprimny C, Klingler M, et al. Preliminary clinical experience of cholecystokinin-2 receptor PET/CT imaging using the ^{68}Ga-labeled minigastrin analog DOTA-MGS5 in patients with medullary thyroid cancer. *J Nucl Med.* 2023:jnumed.122.264977.

189. Wang Y, Lin Q, Shi H, Cheng D. Fluorine-18: Radiochemistry and Target-Specific PET Molecular Probes Design. *Frontiers in Chemistry.* 2022;10.

190. Niccoli Asabella A, Cascini GL, Altini C, Paparella D, Notaristefano A, Rubini G. The copper radioisotopes: a systematic review with special interest to 64Cu. *Biomed Res Int.* 2014;2014:786463.

191. Duatti A. Review on (99m)Tc radiopharmaceuticals with emphasis on new advancements. *Nucl Med Biol.* 2021;92:202-216.

192. Davey RJ, AuBuchon JP. Chapter 33 - Post-Transfusion Red Blood Cell and Platelet Survival and Kinetics: Basic Principles and Practical Aspects. In: Hillyer CD, Silberstein LE, Ness PM, Anderson KC, Roback JD, eds. *Blood Banking and Transfusion Medicine (Second Edition)*. Philadelphia: Churchill Livingstone; 2007:455-466.

193. Liu S, Edwards DS. 99mTc-Labeled Small Peptides as Diagnostic Radiopharmaceuticals. *Chemical Reviews.* 1999;99:2235-2268.

194. von Guggenberg E, Behe M, Behr TM, Saurer M, Seppi T, Decristoforo C. 99mTc-Labeling and in Vitro and in Vivo Evaluation of HYNIC- and (Nα-His)Acetic Acid-Modified [d-Glu1]-Minigastrin. *Bioconjugate Chemistry.* 2004;15:864-871.

195. Nock BA, Maina T, Béhé M, et al. CCK-2/Gastrin Receptor–Targeted Tumor Imaging with ^{99m}Tc-Labeled Minigastrin Analogs. *J Nucl Med.* 2005;46:1727-1736.

196. Kosowicz J, Mikołajczak R, Czepczyński R, Ziemnicka K, Gryczyńska M, Sowiński J. Two Peptide Receptor Ligands 99mTc-EDDA/HYNIC-Tyr3-Octreotide and 99mTc-EDDA/HYNIC-DGlu-Octagastrin for Scintigraphy of Medullary Thyroid Carcinoma. *Cancer Biotherapy and Radiopharmaceuticals.* 2007;22:613-628.

197. Fröberg AC, de Jong M, Nock BA, et al. Comparison of three radiolabelled peptide analogues for CCK-2 receptor scintigraphy in medullary thyroid carcinoma. *Eur J Nucl Med Mol Imaging.* 2009;36:1265-1272.

198. Fröberg A, Herder Wd, Burger J, et al. The use of ^{99m}Tc-Demogastrin 2 in staging of medullary thyroid carcinoma. *J NuclMed.* 2012;53:2049-2049.

199. Khan N-U-H, Corlett A, Hutton CA, Haskali MB. Investigation of Fluorine-18 Labelled Peptides for Binding to Cholecystokinin-2 Receptors with High Affinity. *International Journal of Peptide Research and Therapeutics.* 2021;28:6.

200. Qin Y, Imobersteg S, Blanc A, et al. Evaluation of Actinium-225 Labeled Minigastrin Analogue [(225)Ac]Ac-DOTA-PP-F11N for Targeted Alpha Particle Therapy. *Pharmaceutics.* 2020;12.

201. Bateman TM. Advantages and disadvantages of PET and SPECT in a busy clinical practice. *Journal of Nuclear Cardiology.* 2012;19:3-11.

202. Thakral P, Sen I, Pant V, et al. Dosimetric analysis of patients with gastro entero pancreatic neuroendocrine tumors (NETs) treated with PRCRT (peptide receptor chemo radionuclide therapy) using Lu-177 DOTATATE and capecitabine/temozolomide (CAP/TEM). *The British Journal of Radiology.* 2018;91:20170172.

203. Fendler WP, Reinhardt S, Ilhan H, et al. Preliminary experience with dosimetry, response and patient reported outcome after 177Lu-PSMA-617 therapy for metastatic castration-resistant prostate cancer. *Oncotarget.* 2017;8:3581-3590.

204. Schuchardt C, Zhang J, Kulkarni HR, Chen X, Müller D, Baum RP. Prostate-Specific Membrane Antigen Radioligand Therapy Using (177)Lu-PSMA I&T and (177)Lu-PSMA-617 in Patients with Metastatic Castration-Resistant Prostate Cancer: Comparison of Safety, Biodistribution, and Dosimetry. *J Nucl Med.* 2022;63:1199-1207.

205. Meyer C, Dahlbom M, Lindner T, et al. Radiation Dosimetry and Biodistribution of ^{68}Ga-FAPI-46 PET Imaging in Cancer Patients. *J Nucl Med.* 2020;61:1171-1177.

206. Virgolini I, Ambrosini V, Bomanji JB, et al. Procedure guidelines for PET/CT tumour imaging with 68Ga-DOTA-conjugated peptides: 68Ga-DOTA-TOC, 68Ga-DOTA-NOC, 68Ga-DOTA-TATE. *Eur J Nucl Med Mol Imaging.* 2010;37:2004-2010.

207. Guedj E, Varrone A, Boellaard R, et al. EANM procedure guidelines for brain PET imaging using [(18)F]FDG, version 3. *Eur J Nucl Med Mol Imaging.* 2022;49:632-651.

208. Prieto E, Martí-Climent JM, Domínguez-Prado I, et al. Voxel-Based Analysis of Dual-Time-Point ^{18}F-FDG PET Images for Brain Tumor Identification and Delineation. *J Nucl Med.* 2011;52:865-872.

209. Lodge MA, Lucas JD, Marsden PK, Cronin BF, O'Doherty MJ, Smith MA. A PET study of 18FDG uptake in soft tissue masses. *Eur J Nucl Med.* 1999;26:22-30.

210. Laforest R, Ghai A, Fraum TJ, et al. First-in-Humans Evaluation of Safety and Dosimetry of ^{64}Cu-LLP2A for PET Imaging. *J Nucl Med.* 2023;64:320-328.

211. Anderson CJ, Ferdani R. Copper-64 radiopharmaceuticals for PET imaging of cancer: advances in preclinical and clinical research. *Cancer Biother Radiopharm.* 2009;24:379-393.

212. Uprimny C, von Guggenberg E, Svirydenka A, Mikołajczak R, Hubalewska-Dydejczyk A, Virgolini IJ. Comparison of PET/CT imaging with [18F]FDOPA and cholecystokinin-2 receptor targeting [68Ga]Ga-DOTA-MGS5 in a patient with advanced medullary thyroid carcinoma. *Eur J Nucl Med Mol Imaging.* 2021;48:935-936.

213. Koopmans KP, de Groot JWB, Plukker JTM, et al. 18F-Dihydroxyphenylalanine PET in Patients with Biochemical Evidence of Medullary Thyroid Cancer: Relation to Tumor Differentiation. *J Nucl Med.* 2008;49:524-531.

214. Wurzer A, Kunert J-P, Fischer S, et al. Synthesis and Preclinical Evaluation of ^{177}Lu-Labeled Radiohybrid PSMA Ligands for Endoradiotherapy of Prostate Cancer. *J Nucl Med.* 2022;63:1489-1495.

215. Grob NM, Schibli R, Béhé M, Valverde IE, Mindt TL. 1,5-Disubstituted 1,2,3-Triazoles as Amide Bond Isosteres Yield Novel Tumor-Targeting Minigastrin Analogs. *ACS Med Chem Lett.* 2021;12:585-592.

216. Klingler M, Rangger C, Summer D, Kaeopookum P, Decristoforo C, von Guggenberg E. Cholecystokinin-2 Receptor Targeting with Novel C-terminally Stabilized HYNIC-Minigastrin Analogs Radiolabeled with Technetium-99m. *Pharmaceuticals.* 2019;12:13.

217. Holzleitner N, Günther T, Daoud-Gadieh A, Lapa C, Wester H-J. Investigation of the structure-activity relationship at the *N*-terminal part of minigastrin analogs. *EJNMMI Research.* 2023;13:65.

218. Holzleitner N, Günther T, Beck R, Lapa C, Wester H-J. Introduction of a SiFA Moiety into the D-Glutamate Chain of DOTA-PP-F11N Results in Radiohybrid-Based CCK-2R-Targeted Compounds with Improved Pharmacokinetics In Vivo. *Pharmaceuticals*. 2022; *15*(12): 1467.

219. Günther T, Holzleitner N, Di Carlo D, Urtz-Urban N, Lapa C, Wester H-J. Development of the First ^{18}F-Labeled Radiohybrid-Based Minigastrin Derivative with High Target Affinity and Tumor Accumulation by Substitution of the Chelating Moiety. *Pharmaceutics*. 2023; 15(3): 826.

220. Günther T, Holzleitner N, Viering O, Beck R, Wienand G, Dierks A, Pfob CH, Bundschuh RA, Kircher M, Lapa C, Wester H-J. Preclinical Evaluation of Minigastrin Analogs and Proof-of-Concept [^{68}Ga]Ga-DOTA-CCK-66 PET/CT in 2 Patients with Medullary Thyroid Cancer. *Journal of Nuclear Medicine.* 2023; jnumed.123.266537.

VI. Appendix

1. List of Figures

2. Reprints of Original Publications

2.1 Introduction of a SiFA Moiety into the D-Glutamate Chain of DOTA-PP-F11N Results in Radiohybrid-Based CCK-2R-Targeted Compounds with Improved Pharmacokinetics In Vivo

pharmaceuticals

MDPI

Article

Introduction of a SiFA Moiety into the D-Glutamate Chain of DOTA-PP-F11N Results in Radiohybrid-Based CCK-2R-Targeted Compounds with Improved Pharmacokinetics In Vivo

Nadine Holzleitner [1,*,†], Thomas Günther [1,*,†], Roswitha Beck [1], Constantin Lapa [2] and Hans-Jürgen Wester [1]

[1] Pharmaceutical Radiochemistry, Technical University of Munich, 85748 Garching, Germany
[2] Nuclear Medicine, Faculty of Medicine, University of Augsburg, 86156 Augsburg, Germany
* Correspondence: nadine.holzleitner@tum.de (N.H.); thomas.guenther@tum.de (T.G.)
† These authors contributed equally to this work.

Abstract: In order to enable ^{18}F- and ^{177}Lu-labelling within the same molecule, we introduced a silicon-based fluoride acceptor (SiFA) into the hexa-D-glutamate chain of DOTA-PP-F11N. In addition, minigastrin analogues with a prolonged as well as γ-linked D-glutamate chain were synthesised and evaluated. CCK-2R affinity (IC_{50}, AR42J cells) and lipophilicity ($\log D_{7.4}$) were determined. Biodistribution studies at 24 h post-injection (p.i.) and μSPECT/CT imaging at 1, 4 and 24 h p.i. were carried out in AR42J tumour-bearing CB17-SCID mice. CCK-2R affinity of (*R*)-DOTAGA-rhCCK-1 to 18 was enhanced with increasing distance between the SiFA building block and the binding motif. Lipophilicity of [^{177}Lu]Lu-(*R*)-DOTAGA-rhCCK-1 to 18 was higher compared to that of [^{177}Lu]Lu-DOTA-PP-F11N and [^{177}Lu]Lu-CP04. The respective α- and γ-linked rhCCK derivatives revealing the highest CCK-2R affinity were further evaluated in vivo. In comparison with [^{177}Lu]Lu-DOTA-PP-F11N, [^{177}Lu-]Lu-(*R*)-DOTAGA-rhCCK-9 and -16 exhibited three- to eight-fold increased activity levels in the tumour at 24 h p.i. However, activity levels in the kidneys were elevated as well. We could show that the introduction of a lipophilic SiFA moiety into the hydrophilic backbone of [^{177}Lu]Lu-DOTA-PP-F11N led to a decelerated blood clearance and thus improved tumour retention. However, elevated kidney retention has to be addressed in future studies.

Keywords: cholecystokinin-2 receptor (CCK-2R); cholecystokinin-B receptor (CCK-BR); medullary thyroid cancer (MTC); minigastrin analogues; radiohybrid; rhCCK

Citation: Holzleitner, N.; Günther, T.; Beck, R.; Lapa, C.; Wester, H.-J. Introduction of a SiFA Moiety into the D-Glutamate Chain of DOTA-PP-F11N Results in Radiohybrid-Based CCK-2R-Targeted Compounds with Improved Pharmacokinetics In Vivo. *Pharmaceuticals* **2022**, *15*, 1467. https://doi.org/10.3390/ph15121467

Academic Editors: Petra Kolenc, Rosalba Mansi and Marko Krošelj

Received: 7 November 2022
Accepted: 24 November 2022
Published: 25 November 2022

1. Introduction

Medullary thyroid carcinoma (MTC) constitutes for only 2–3% of all thyroid cancer cases and is therefore rather rare, but treatment options are limited: neither external beam radiation, nor conventional chemotherapy, nor radioiodine therapy are recommended, as all three concepts have not shown curative effects [1–4]. Tyrosine kinase inhibitors such as selpercatinib, vandetanib or cabozantinib are usually applied for systematic treatment but these agents are associated with distinct side effects such as renal toxicity, myelosuppression, arterial thromboembolism, hepatotoxicity, and muscle wasting [3,5].

Since Reubi et al. discovered that approximately 92% of all MTCs overexpress the cholecystokinin-2 receptor (CCK-2R), designing small compounds that address this target became attractive in combination with peptide receptor radionuclide imaging (PRRI) and therapy (PRRT) [6]. While first compounds were based on the structure of cholecystokinin, nowadays minigastrin-based ligands are clearly favoured because of their increased hydrophilicity [7]. However, early radiolabelled minigastrin analogues suffered from elevated activity levels in the kidneys, which hampered a potential therapeutic use [8,9].

An important step for the applicability of these minigastrin derivatives was the modification within the linker section, namely the substitution of the hexa-L-glutamate by a

hexa-D-glutamate chain, which resulted in compounds such as CP04 and DOTA-PP-F11N, amongst others. The latter consists of a stabilised binding motif of seven amino acid with high CCK-2R affinity (*H*-Ala-Tyr-Gly-Trp-Nle-Asp-Phe-NH_2), a hexa-D-glutamate linker and DOTA (1,4,7,10-tetraazacyclododecane-1,4,7,10- tetraacetic acid) as a chelator [10,11]. Nevertheless, due to the high hydrophilicity of [^{177}Lu]Lu-DOTA-PP-F11N, first patient studies revealed a very rapid renal clearance already at 1 h post-injection (p.i.), which resulted in a median (interquartile range) absorbed tumour dose of only 0.88 Gy/GBq [12]. Moreover, none of the currently available CCK-2R-targeted compounds for clinical application bears an option for ^{18}F-labelling.

Recently, radiohybrid (rh)-based prostate-specific membrane antigen (PSMA)-targeted compounds were developed by our group, implementing a new class of theranostic compounds. These compounds comprise a silicon-based fluoride acceptor (SiFA) moiety for rapid and facile ^{18}F-fluorination via a ^{18}F/^{19}F isotopic exchange reaction and additionally contains a chelator for radiometallation (with ^{68}Ga or ^{177}Lu, amongst others). This concept results in a chemically identical pair of compounds (either ^{18}F/non-radioactive metal or ^{19}F/radiometal), which thus exhibits identical pharmacokinetics and can be used for either diagnostic or therapeutic applications [13,14].

Given the promising clinical data of the rhPSMA derivatives [15–18], the aim of this study was to transfer the concept of rh-based compounds to minigastrin analogues. For this reason, we introduced a SiFA group into the highly hydrophilic hexa-D-glutamate chain of DOTA-PP-F11N via conjugation through a D-2,3-diaminopropionic acid (dap) moiety to generate a possibility for ^{18}F-labelling and compensate for the high lipophilicity of the SiFA group. Moreover, DOTA was replaced by the more hydrophilic (*R*)-DOTAGA (2-(4,7,10-tris(carboxymethyl)-1,4,7,10-tetraazacyclododecan-1-6yl)pentanedioic acid) in all of our rhCCK derivatives. Besides the usually present α-linked poly-D-glutamate chain the rhCCK ligands were designed with a γ-linked poly-D-glutamate chain (Figure 1) as well and evaluated in state-of-the-art experiments.

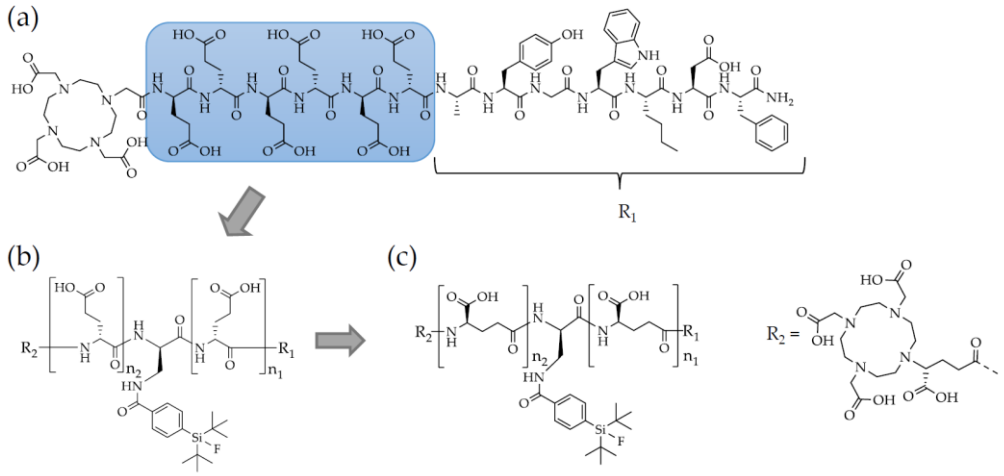

Figure 1. Structure of (**a**) DOTA-PP-F11N. (**b**) Structure of the rhCCK derivatives ((*R*)-DOTAGA-rhCCK-1-9) comprising a modified linker section generated via the introduction of a dap(SiFA) moiety into the D-glutamate chain ((*R*)-DOTAGA-rhCCK-1-7: n_1 = 0 to 6 and n_2 = 6 − n_1; (*R*)-DOTAGA-rhCCK-8: n_1 = 7 and n_2 = 0; (*R*)-DOTAGA-rhCCK-9: n_1 = 8 and n_2 = 0) of DOTA-PP-F11N. (**c**) Structure of the rhCCK derivatives ((*R*)-DOTAGA-rhCCK-10-18) generated analogous to B but containing a γ-instead of an α-linked D-glutamate chain ((*R*)-DOTAGA-rhCCK-10-16: n_1 = 0 to 6 and n_2 = 6 − n_1; (*R*)-DOTAGA-rhCCK-17: n_1 = 7 and n_2 = 0; (*R*)-DOTAGA-rhCCK-18: n_1 = 8 and n_2 = 0).

2. Results

2.1. Synthesis and Radiolabelling

The uncomplexed ligands were synthesised via standard Fmoc-based SPPS, yielding 5–20% RP-HPLC purified precursors (chemical purity > 95%, determined by RP-HPLC at

λ = 220 nm). Non-radioactive labelling proceeded quantitatively using a 2.5-fold excess of [^{nat}Lu]LuCl$_3$. No purification prior to affinity studies was performed, as the remaining free Lu^{3+} was shown to not affect affinity data [19]. ^{177}Lu-labelling of all compounds was carried out manually resulting in quantitative radiochemical yields and purities of >95% as well as molar activities of 30 ± 10 GBq/μmol. After radiolabelling all peptides were used without further purification. Confirmation of peptide integrity and quality controls are depicted in the Supplementary Materials (Figures S1–S3).

2.2. In Vitro Characterisation

The affinity and lipophilicity data of all compounds are summarised in Figure 2 and Table S1.

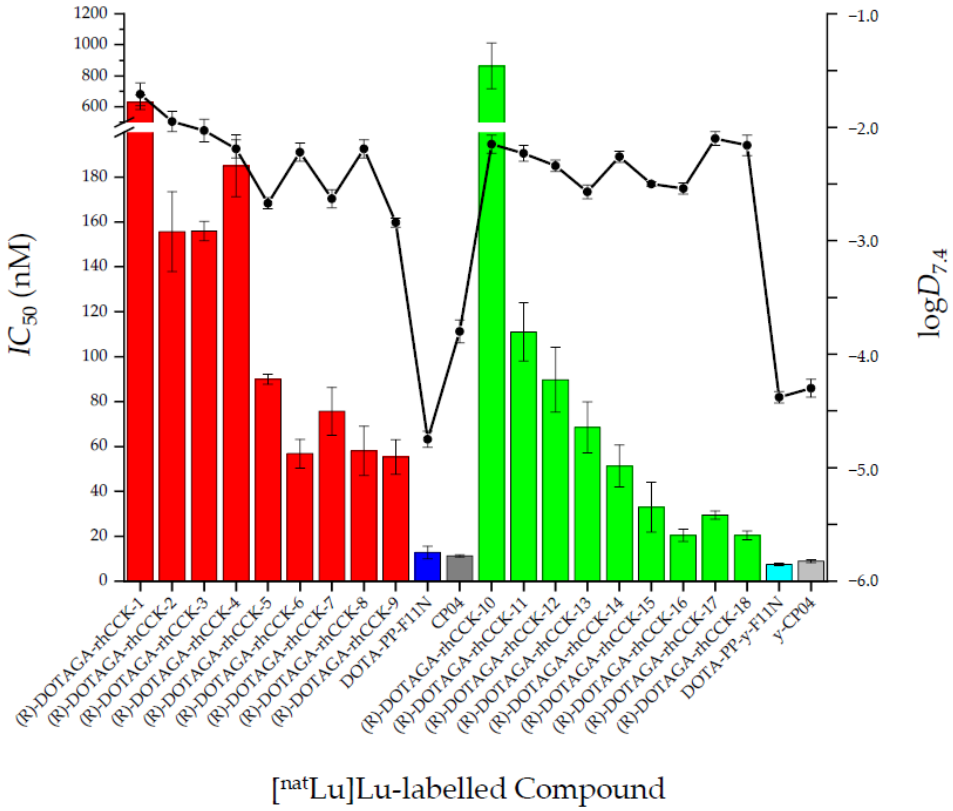

Figure 2. Affinity (IC_{50}) and lipophilicity (log$D_{7.4}$) data of the ^{nat}Lu-labelled references DOTA-PP-F11N (dark blue) and CP04 (dark grey) compared to their γ-linked analogues DOTA-PP-γ-F11N (light blue) and γ-CP04 (light grey), the ^{nat}Lu-labelled rhCCK derivatives comprising an α-linked D-glutamate chain ([^{nat}Lu]Lu-(*R*)-DOTAGA-rhCCK-1-9, red) and the ^{nat}Lu-labelled rhCCK derivatives containing a γ-linked D-glutamate chain ([^{nat}Lu]Lu-(*R*)-DOTAGA-rhCCK-10-18, green). IC_{50} values were determined using AR42J cells (2.0 × 10^5 cells per well) and [^{177}Lu]Lu-DOTA-PP-F11N (0.3 pmol/well) as radiolabelled reference (3 h, 37 °C, RPMI 1640, 5 mM L-Gln, 5 mL non-essential amino acids (100×), 10% fetal calf serum (FCS) + 5% bovine serum albumin (BSA) (*v*/*v*)).

In general, all ligands containing a γ-linked D-glutamate chain revealed a higher affinity towards CCK-2R compared to their α-linked counterparts, except for [^{nat}Lu]Lu-**10**. Furthermore, a trend could be observed that with increasing distance of the dap(SiFA) moiety to the binding motif IC_{50} values decreased, irrespective whether the compounds are α- or γ-linked. Overall, [^{nat}Lu]Lu-(*R*)-DOTAGA-rhCCK-16 and [^{nat}Lu]Lu-(*R*)-DOTAGA-rhCCK-18 displayed the highest CCK-2R affinity among all SiFA-containing compounds. Nevertheless, all four reference ligands showed lower IC_{50} values, suggesting a negative impact of the SiFA unit irrespective of its position within the molecule.

All four reference ligands revealed a high hydrophilicity, exhibiting distribution coefficients ($\log D_{7.4}$) in a range of −4.8 and −3.8. Not surprisingly, the rhCCK derivatives comprising the lipophilic SiFA moiety displayed a distinctly higher lipophilicity ($\log D_{7.4}$ = −2.9 to −1.7).

Internalisation values at different time points were determined for the respective most affine α- and γ-linked rhCCK derivative ([^{177}Lu]Lu-(*R*)-DOTAGA-rhCCK-9 and -16) compared to the references. The amount of internalised activity (%) on AR42J cells increased over time for all compounds tested from 2–8% (1 h) to 13–32% (6 h) (Figure 3, Table S2). Most of the cell-associated activity was internalized, while cell membrane-bound activity was ≤1.1% (Tables S2 and S3).

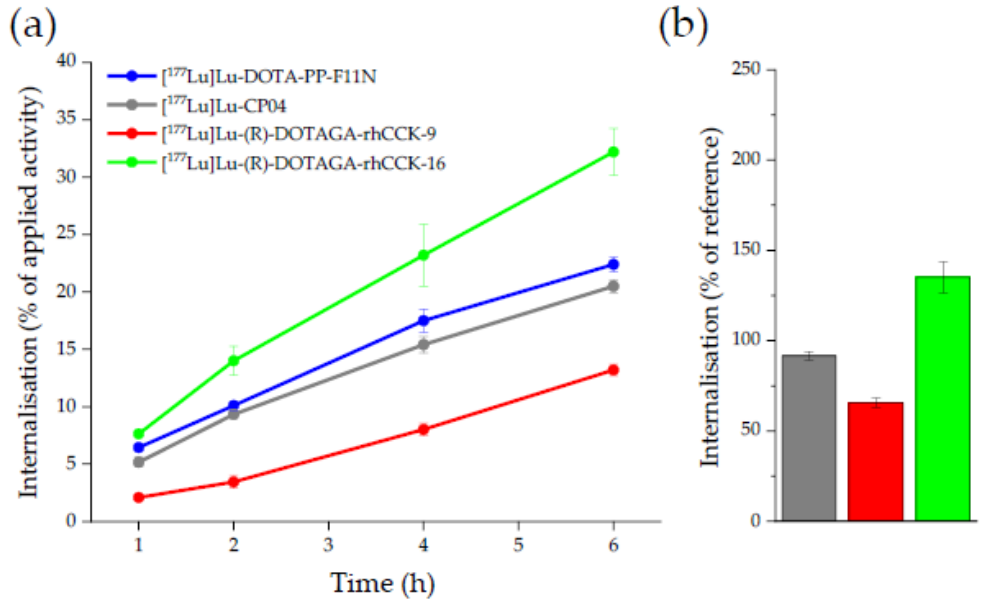

Figure 3. (**a**) CCK-2R-mediated internalisation (0.25 pmol/well) on AR42J cells as percent (%) of the applied activity (incubation at 37 °C for 1, 2, 4 and 6 h, RPMI 1640, 5 mM L-Gln, 5 mL non-essential amino acids (100×), 10% FCS + 5% BSA (*v*/*v*), 3.0 × 10^5 cells/mL/well). (**b**) CCK-2R mediated internalisation (% of the reference [^{177}Lu]Lu-DOTA-PP-F11N) of [^{177}Lu]Lu-CP04 (grey), [^{177}Lu]Lu-(*R*)-DOTAGA-rhCCK-9 (red) and [^{177}Lu]Lu-(*R*)-DOTAGA-rhCCK-16 (green) after incubation for 6 h.

The ^{177}Lu-labelled rhCCK derivative [^{177}Lu]Lu-(*R*)-DOTAGA-rhCCK-16 exhibited distinctly higher internalisation values than the reference compounds, [^{177}Lu]Lu-DOTA-PP-F11N and [^{177}Lu]Lu-CP04. In comparison, the internalisation kinetics of [^{177}Lu]Lu-(*R*)-DOTAGA-rhCCK-9 were found to be lower.

2.3. In Vivo Characterisation

The most affine α-linked([^{177}Lu]Lu-(*R*)-DOTAGA-rhCCK-9) and γ-linked ([^{177}Lu]Lu-(*R*)-DOTAGA-rhCCK-16) rhCCK derivatives were evaluated in vivo in comparison to the reference [^{177}Lu]Lu-DOTA-PP-F11N, which is already being applied in clinical trials (Figure 4, Table S4).

In vivo, the rhCCK derivatives showed 3- (6.40 ± 1.48 %ID/g, [^{177}Lu]Lu-(*R*)-DOTAGA-rhCCK-9) to 8-fold (15.7 ± 3.3 %ID/g, [^{177}Lu]Lu-(*R*)-DOTAGA-rhCCK-16) higher activity levels in the tumour and 5- to 10-fold higher levels in the CCK-2R-positive stomach than the reference ligand, which was statistically significant in groups of four mice ($p < 0.02$). Activity levels in the liver were not significantly increased for both rhCCK derivatives compared to the reference compound at 24 h p.i. despite their increased lipophilicity ($p > 0.15$). Blood levels of both rhCCK derivatives were 10- to 11-fold increased to [^{177}Lu]Lu-DOTA-PP-F11N ($p < 0.001$) but still favourably low at 24 h p.i. (~0.015 %ID/g) despite their decelerated clearance kinetics. However, activity levels in the kidneys were almost 30-fold higher for

the rhCCK derivatives compared to [^{177}Lu]Lu-DOTA-PP-F11N at 24 h p.i. (84.4 ± 22.7 and 85.5 ± 11.3 vs. 3.08 ± 0.51 %ID/g, respectively, $p < 0.001$). [^{177}Lu]Lu-DOTA-PP-F11N revealed lower activity levels in most organs at 24 h p.i., indicating a more rapid clearance.

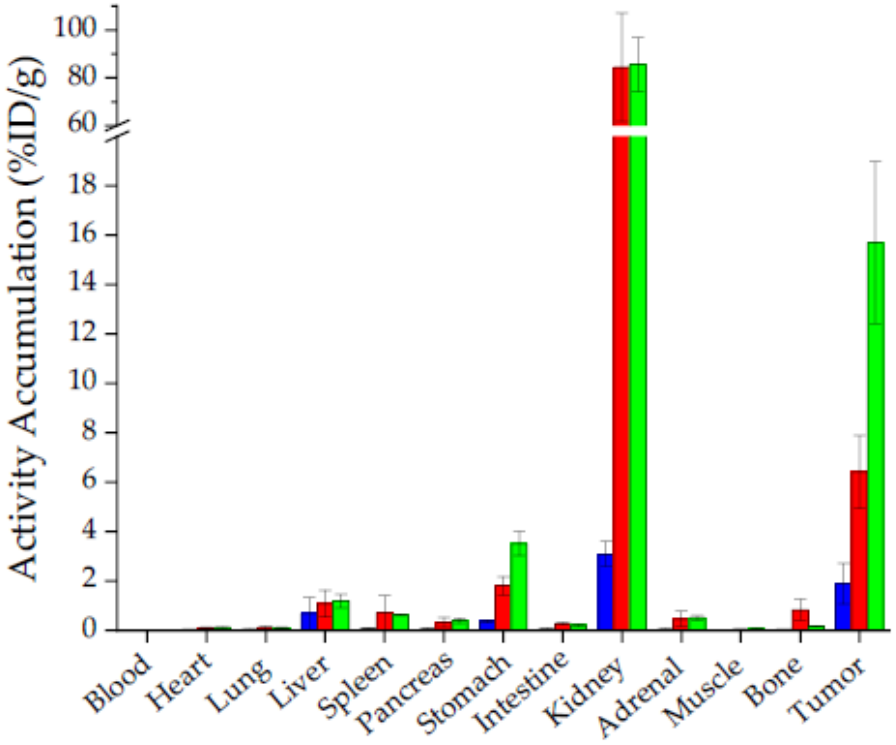

Figure 4. Biodistribution of the reference compound, [^{177}Lu]Lu-DOTA-PP-F11N (blue), the α-linked [^{177}Lu]Lu-(*R*)-DOTAGA-rhCCK-9 (red) and the γ-linked [^{177}Lu]Lu-(*R*)-DOTAGA-rhCCK-16 (green) in selected organs (%ID/g) at 24 h p.i. in AR42J tumour-bearing CB17-SCID mice (100 pmol each, $n = 4$). Data is expressed as mean ± SD.

μSPECT/CT studies of mice ($n = 1$) injected with [^{177}Lu]Lu-(*R*)-DOTAGA-rhCCK-9, [^{177}Lu]Lu-(*R*)-DOTAGA-rhCCK-16 and [^{177}Lu]Lu-DOTA-PP-F11N at 1, 4 and 24 h p.i. revealed a low overall background activity for all three compounds at each time point, except for a high kidney accumulation and retention for the latter two (Figure 5). Activity levels in the tumour were highest for [^{177}Lu]Lu-(*R*)-DOTAGA-rhCCK-16 (15.7 ± 3.3 %ID/g) and lowest for the reference ligand (1.8 ± 0.8 %ID/g).

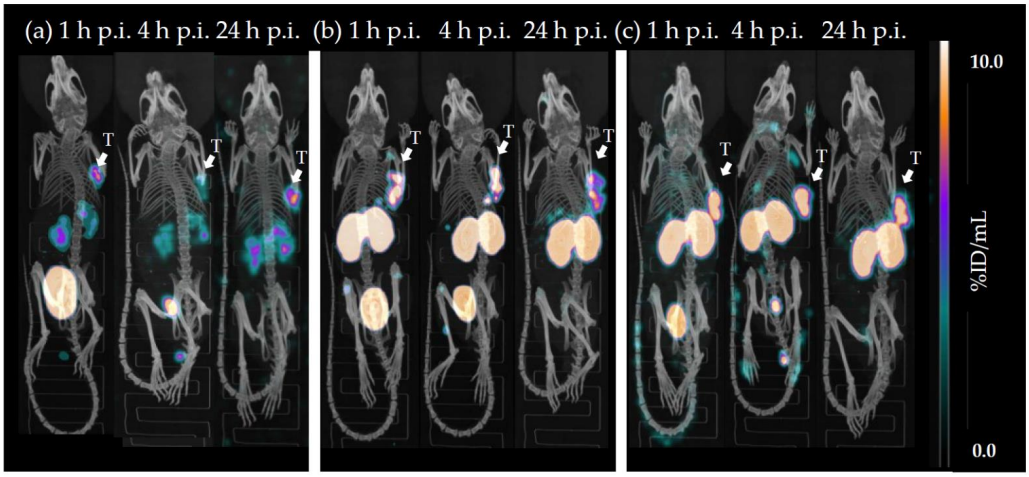

Figure 5. Representative μSPECT/CT images of (**a**) [^{177}Lu]Lu-DOTA-PP-F11N, (**b**) [^{177}Lu]Lu-*(R)*-DOTAGA-rhCCK-9 and (**c**) [^{177}Lu]Lu-*(R)*-DOTAGA-rhCCK-16 at 1, 4 and 24 h p.i. in AR42J tumour-bearing CB17- SCID mice (100 pmol each). Tumours (T) are indicated by white arrows.

CCK-2R specificity of [^{177}Lu]Lu-(*R*)-DOTAGA-rhCCK-16 was evaluated via co-injection of an excess of the CCK2R-targeted compound, [^{nat}Lu]Lu-DOTA-MGS5, which resulted in activity levels in the tumour < 1%. Activity levels in the stomach, which endogenously expresses the CCK-2R, were found to be <0.3% (Figure S4, Table S4).

3. Discussion

Among the currently most promising minigastrin-derived peptides for clinical application (DOTA-MGS5, DOTA-PP-F11N and CP04), there is no option available for facile ^{18}F-labelling [20–23]. Particularly a ^{18}F-labelled minigastrin analogue would be beneficial for the detection of small MTC-derived metastases due to the low tissue penetration and thus high resolution of fluorine-18, consequently to its low positron energy ($E_{\beta,max}$ = 635 keV), compared to gallium-68, for example [24]. Furthermore, up to now there is no CCK-2R-targeted ligand that enables both ^{18}F- and ^{177}Lu-labelling. This radiohybrid-based concept has been successfully implemented for PSMA inhibitors and resulted in impressive results over the last three years, which is why the compounds rhPSMA-7.3 and rhPSMA-10.1 are evaluated in clinical studies [13,25–32]. With the aim to develop a ^{177}Lu-labelled minigastrin analogue, which can also be labelled with fluorine-18, we introduced the lipophilic SiFA moiety into different sites within the highly hydrophilic, *N*-terminal D-glutamate chain of DOTA-PP-F11N and compared these novel compounds to the reference compounds, [^{177}Lu]Lu-DOTA-PP-F11N and [^{177}Lu]Lu-CP04.

The SiFA moiety was introduced into different sites within both an α-linked poly-D-glutamate chain (= (*R*)-DOTAGA-rhCCK-1 to -9) and a γ-linked poly-D-glutamate chain (= (*R*)-DOTAGA-rhCCK-10 to -18), while the binding sequence of DOTA-PP-F11N was maintained. In general, for both linker concepts it could be observed that with increasing distance of the SiFA moiety to the binding motif, CCK-2R affinity was enhanced, which indicates that the bulky SiFA building block does not fit into the binding pocket of the receptor. However, at a farther distance the SiFA group seems to be located outside of the binding pocket and thus CCK-2R affinity increases. In direct comparison of these series of minigastrin derivatives (α- or γ-linked D-glutamate chain) that each exhibit the same site for the SiFA moiety, it is evident that those ligands containing a γ-linked D-glutamate chain generally show a higher CCK-2R affinity. Similar results were observed for the respective γ-linked analogues of the references, [^{nat}Lu]Lu-DOTA-PP-γ-F11N and [^{nat}Lu]Lu-γ-CP04, pointing to a beneficial effect of a prolonged linker section and thus the use of γ-linked D-glutamate residues. Nevertheless, IC_{50} values of the most affine compounds were still approximately fivefold (α-linked poly-D-glutamate linker) and twofold (γ-linked poly-D-glutamate linker) higher compared to [^{nat}Lu]Lu-DOTA-PP-F11N and [^{nat}Lu]Lu-CP04 (IC_{50} of 11–13 nM). Hence, it is assumed that the lower CCK-2R affinity of the novel rhCCK derivatives is due either to the addition of the sterically demanding SiFA moiety or the (*R*)-DOTAGA chelator, which comprises one negative charge more than the DOTA chelator present in the reference compounds when labelled with [$^{nat/177}$Lu]lutetium.

The addition of the SiFA moiety was also accompanied by an enhanced lipophilicity (log$D_{7.4}$: −2.9 to −1.7), which is one to three magnitudes higher compared to [^{177}Lu]Lu-DOTA-PP-F11N and [^{177}Lu]Lu-CP04. However, this was desired since for tumour targeting we consider a log$D_{7.4}$ value of about −4 or lower unfavourable because we assume that high tumour uptake is prevented by a too rapid clearance rate. Indeed, first patient studies with [^{177}Lu]Lu-DOTA-PP-F11N showed low activity levels in the tumour but high levels in the bladder at 1 h p.i., most likely due to an accelerated clearance [12]. Based on previous experiences in our group, a range of −3 to −2 seems to be ideal for tumour targeting.

We thus selected the most promising α- and γ-linked compound with regard to CCK-2R affinity (IC_{50}) and lipophilicity (log$D_{7.4}$), (*R*)-DOTAGA-rhCCK-9 and -16 (Figure 6), respectively, for in vivo studies.

Interestingly, both SiFA-containing compounds revealed noticeably higher activity levels in the tumour at all time points than [^{177}Lu]Lu-DOTA-PP-F11N despite their distinctly lower CCK-2R affinity. [^{177}Lu]Lu-(*R*)-DOTAGA-rhCCK-16 revealed a higher CCK-2R-

mediated internalisation than [^{177}Lu]Lu-DOTA-PP-F11N, which points to an enhanced uptake by the tumour cells. [^{177}Lu]Lu-(*R*)-DOTAGA-rhCCK-9 revealed low internalisation values, which is in accordance with its low CCK-2R affinity but contradicting to the higher tumour uptake found compared to the reference. It has to be added that tumour values for [^{177}Lu]Lu-DOTA-PP-F11N were low despite its high CCK-2R affinity, which is, however, in accordance to the patient data and most likely caused its high hydrophilicity and thus rapid clearance [12]. Although further studies have to be carried out to elucidate the beneficial effects observed in this study, we proved that the introduction of the SiFA group not only generated a possibility for ^{18}F-labelling but also improved overall bioavailability in vivo. Besides the decreased hydrophilicity, we further suspect an elevated albumin binding potential of the SiFA group, which decelerates the activity clearance, increases circulation time of the compounds in the blood and thus enhances activity uptake and retention in the tumour. Similar observations were made for PSMA-targeted compounds [14,33].

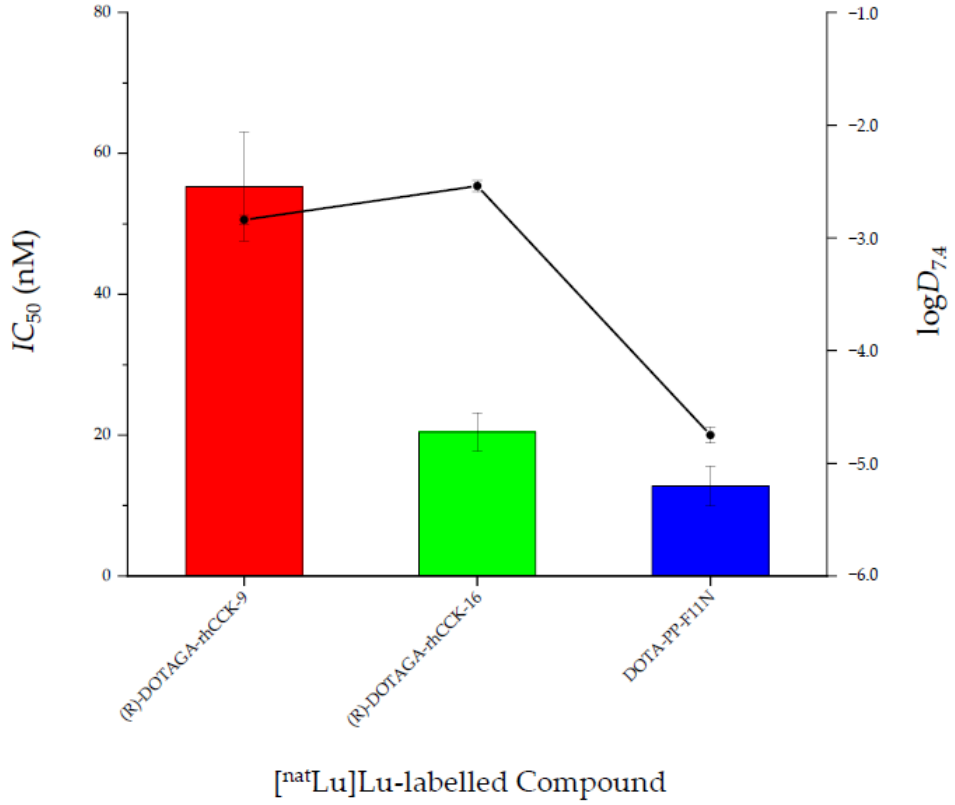

Figure 6. Affinity (IC_{50}) and lipophilicity (log$D_{7.4}$) data of $^{nat/177}$Lu-labelled rhCCK ligands, (*R*)-DOTAGA-rhCCK-9 and -16, as well as DOTA-PP-F11N.

Hence, [^{177}Lu]Lu-(*R*)-DOTAGA-rhCCK-9 and -16 showed 3- and 8-fold higher activity levels in the tumour, respectively, than the reference ligand at 24 h p.i. Similar observations were made for stomach levels due to the endogenous CCK-2R expression in this organ. Competition studies using an excess of the CCK-2R-specific ligand, [^{nat}Lu]Lu-DOTA-MGS5 [34], confirmed CCK-2R specificity. Despite their enhanced lipophilicity, liver levels were not significantly increased compared to [^{177}Lu]Lu-DOTA-PP-F11N at 24 h p.i. Blood levels of both rhCCK derivatives were significantly higher than those of [^{177}Lu]Lu-DOTA-PP-F11N but still in a comparable range to compounds addressing other tumour targets in nuclear medicine, such as PSMA-, gastrin releasing peptide receptor-, chemokine receptor CXCR4- and somatostatin-2 receptor-targeted probes [14,19,35–37].

Despite these respectable results, our current rhCCK derivatives suffer from elevated activity levels in the kidneys (30-fold higher compared to the reference). We assume a synergistic effect of the negative charges in proximity of the SiFA moiety within the linker section, as [^{177}Lu]Lu-DOTA-PP-F11N did not show comparable kidney values although it

comprises a similar amount of negative charges in its linker. These kidney issues have to be addressed in future studies to enable a clinical translation of this rh-based concept for minigastrin analogues. One possible strategy to decrease kidney accumulation and retention might be a reduction of the albumin binding of the rhCCK derivatives, as beneficial effects were observed for PSMA inhibitors when negative charges in direct proximity to the SiFA-building block were depleted [14]. Furthermore, co-injection of lysine or gelofusine could also be a valuable tool. Tumour values were noticeably higher at 1 and 4 h p.i. compared to the reference in μSPECT/CT imaging (n = 1). However, further studies at 1 and 4 h p.i. have to be conducted to statistically confirm these observations and, furthermore, elucidate the imaging potential of the respective ^{18}F-labeled rhCCK analogues.

In summary, we could successfully introduce a SiFA building block into the minigastrin analogue DOTA-PP-F11N, which not only generated a possibility for ^{18}F-labelling but also considerably improved pharmacokinetics. We further could show that the rh-based concept successfully applied for PSMA-targeted compounds can be applied for CCK-2R-targeted ligands as well, which enables both ^{18}F- and ^{177}Lu-labelling for a theranostic use. Nevertheless, elevated activity levels in the kidneys are of concern, which has to be optimised in future studies. Moreover, CCK-2R affinity might possibly be further improved, either by varying the position of the SiFA building block or a DOTA-for-(*R*)-DOTAGA substitution. However, a beneficial effect of a γ- instead of an α-linked D-glutamate chain in minigastrin derivatives was found, which might be applicable for other peptides and their linker as well.

4. Materials and Methods

Characterisation of all CCK-2R-targeted compounds is provided in the Supplementary Materials (Figures S1–S4). Electrospray ionisation-mass spectra for characterisation of the substances were acquired on an expression^{L} CMS mass spectrometer (Advion Ltd., Harlow, UK).

4.1. Chemical Synthesis and Labelling Procedures

All compounds were synthesised via standard Fmoc-based solid phase peptide synthesis (SPPS) using a H-Rink Amide ChemMatrix® resin (35–100 mesh particle size, 0.4–0.6 mmol/g loading, Merck KGaA, Darmstadt, Germany). Final purification of the peptides was performed by reversed phase high performance liquid chromatography (RP-HPLC).

^{177}Lu- and ^{nat}Lu-complexation of the peptides was performed according to a previously published procedure [14].

4.2. In Vitro Experiments

Detailed description of all cell-based experiments is provided in the Supplementary Materials. In brief, competitive binding studies were conducted on AR42J cells (2.0×10^5 cells per 1 mL/well) via incubation at 37 °C for 3 h using [^{177}Lu]Lu-DOTA-PP-F11N (0.3 pmol) as a radiolabelled reference (n = 3).

Internalisation studies of the ^{177}Lu-labelled conjugates (0.3 pmol) were performed on AR42J cells (3.0×10^5 cells per 1 mL/well) at 37 °C for 1, 2, 4 and 6 h (n = 3). Data were corrected for non-specific binding (competition by 10^{-4} M [^{nat}Lu]Lu-DOTA-PP-F11N).

Lipophilicity (depicted as octanol-phosphate-buffered saline solution (PBS, pH = 7.4) distribution coefficient, log$D_{7.4}$) was determined via dissolving the ^{177}Lu-labelled peptide (approx. 1 MBq) in a mixture (1/1, v/v) of n-octanol and PBS. The suspension was vortexed in a reaction vial (1.5 mL) for 3 min at RT and the vial was centrifuged at 9000× g rpm for 5 min (Biofuge 15, Heraus Sepatech GmbH, Osterode, Germany). 200 µL aliquots of both layers were measured separately in a γ-counter (Perkin Elmer, Waltham, MA, USA). The experiment was repeated at least five times.

4.3. In Vivo Experiments

All animal experiments were conducted in accordance with general animal welfare regulations in Germany (German animal protection act, in the edition of the announcement, dated 18 May 2006, as amended by Article 280 of 19 June 2020, approval no. ROB-55.2-1-2532.Vet_02-18-109 by the General Administration of Upper Bavaria) and the institutional guidelines for the care and use of animals. CB17-SCID mice of both genders and aged 2–12 months (Charles River Laboratories International Inc., Sulzfeld, Germany) were allowed to acclimate at the in-house animal facility for at least one week prior to tumour cell inoculation was performed. Tumour xenografts were generated using AR42J cells (5.0×10^6 cells per 200 µL) suspended in a 1/1 mixture (*v*/*v*) of RPMI 1640 medium and Cultrex® Basement Membrane Matrix Type 3 (Trevigen, Gaithersburg, MD, USA). This suspension was inoculated subcutaneously onto the right shoulder and animals were used when tumour volume was >100 mm^3 (1–2 week after inoculation). Exclusion criteria for animals from an experiment were either weight loss higher than 20%, a tumour size above 1500 mm^3, an ulceration of the tumour, respiratory distress or a change of behaviour. None of these criteria applied to any animal from the experiment. Neither randomisation nor blinding was applied in the allocation of the experiments. Health status is SPF according to FELASA.

For biodistribution studies, the ^{177}Lu-labelled compound (approx. 2–3 MBq, 100 pmol) was injected into a lateral tail vein (n = 4) of anesthetised (2% isoflurane) AR42J tumour-bearing CB-17-SCID mice. At 24 h post-injection (p.i.), the mice were euthanised. Thereafter, the pertinent organs were removed, weighed and measured using a γ-counter.

Imaging studies were carried out according to a recently published protocol [19]. Static images were recorded at t = 1, 4 and 24 h p.i. (anesthesia by 2% isoflurane, n = 1) with an acquisition time of t + (45–60 min) using a high-energy general-purpose rat and mouse collimator via MILabs acquisition software v11.00 and v12.26 from MILabs (Utrecht, The Netherlands).

For all competition studies, 2.90 mg/kg (40 nmol) of [^{nat}Lu]Lu-DOTA-MGS5 (10^{-3} M in phosphate-buffered saline) were co-administered.

Acquired data were statistically analysed by performing a Student's t-test via Excel (Microsoft Corporation, Redmond, WA, USA) and OriginPro software (version 9.7) from OriginLab Corporation (Northampton, MA, USA). Acquired p values of <0.05 were considered statistically significant.

5. Conclusions

We could demonstrate that the radiohybrid-based concept could easily be transferred to minigastrin derivatives, whose hydrophilic linker section compensates for the high lipophilicity of the introduced SiFA moiety. This offers not only the possibility of ^{18}F- and ^{177}Lu-labelling with the same molecule but also had a beneficial impact on overall pharmacokinetics, as clearance kinetics were decelerated. Thereby, activity retention in the tumour could be increased by approximately eightfold compared to the clinically applied [^{177}Lu]Lu-DOTA-PP-F11N. However, these compounds also suffer from a noticeably enhanced kidney retention. This will be addressed in further studies.

Supplementary Materials: The following supporting information can be downloaded at: https://www.mdpi.com/article/10.3390/ph15121467/s1, general information and characterisation of all CCK2R-targeted compounds, detailed description of cell-based experiments. Figure S1: Confirmation of peptide identity and integrity for (**a**) [^{nat}Lu]Lu-DOTA-PP-F11N and (**b**) [^{177}Lu]Lu-DOTA-PP-F11N as analysed by analytical (radio-)RP-HPLC (MultoKrom 100-5 C18, 5 µm, 125 × 4.6 mm, CS Chromatographie GmbH, Langerwehe, Germany; 10→90% MeCN in H_2O + 0.1% TFA in 15 min). (**c**) Mass spectrum of [^{nat}Lu]Lu-DOTA-PP-F11N; Figure S2: Confirmation of peptide identity and integrity for (**a**) [^{nat}Lu]Lu-(*R*)-DOTAGA-rhCCK-9 and (**b**) [^{177}Lu]Lu-(*R*)-DOTAGA-rhCCK-9 as analysed by analytical (radio-)RP-HPLC (MultoKrom 100-5 C18, 5 µm, 125 × 4.6 mm, CS Chromatographie GmbH, Langerwehe, Germany; 10→90% MeCN in H_2O + 0.1% TFA in 15 min). (**c**) Mass spectrum of [^{nat}Lu]Lu-(*R*)-DOTAGA-rhCCK-9; Figure S3: Confirmation of peptide identity and integrity for

(**a**) [^{nat}Lu]Lu-(*R*)-DOTAGA-rhCCK-16 and (**b**) [^{177}Lu]Lu-(*R*)-DOTAGA-rhCCK-16 as analysed by analytical (radio-)RP-HPLC (MultoKrom 100-5 C18, 5 µm, 125 × 4.6 mm, CS Chromatographie GmbH, Langerwehe, Germany; 10→90% MeCN in H_2O + 0.1% TFA in 15 min). (**c**) Mass spectrum of [^{nat}Lu]Lu-(*R*)-DOTAGA-rhCCK-16; Figure S4: (**a**) Biodistribution of [^{177}Lu]Lu-DOTA-rhCCK-16 (100 pmol) co-injected with [^{nat}Lu]Lu-DOTA-MGS5 (40 nmol) in selected organs (%ID/g) at 24 h p.i. in AR42J tumour-bearing CB17-SCID mice. Data is expressed as mean ± SD (n = 2). (**b**) Representative μSPECT/CT images of [^{177}Lu]Lu-DOTA-rhCCK-16 co-injected with [^{nat}Lu]Lu-DOTA-MGS5 (40 nmol) at 24 h p.i. in AR42J tumour-bearing CB17- SCID mice; Table S1: Affinity and lipophilicity data of the compounds evaluated. Affinity data were determined on AR42J cells (2.0 × 10^5 cells/well) and [^{177}Lu]Lu-DOTA-PP-F11N (0.3 pmol/well) as radiolabelled reference (3 h, 37 °C, RPMI 1640, 5 mM L-Gln, 5 mL non-essential amino acids (100×), 10% FCS + 5% BSA (v/v)); Table S2: Receptor-mediated internalisation values (37 °C, RPMI 1640, 5 mM L-Gln, 5 mL non-essential amino acids (100×), 10% FCS, 0.25 pmol/well) determined as percent (%) of the applied activity of [^{177}Lu]Lu-(*R*)-DOTAGA-rhCCK-16 and the references [^{177}Lu]Lu-DOTA-PP-F11N and [^{177}Lu]Lu-CP04 using AR42J cells (3.0 × 10^5 cells/well) at different time points (1, 2, 4 and 6 h). Data are corrected for non-specific binding (10 µmol/well, [^{nat}Lu]Lu-DOTA-PP-F11N); Table S3: Total cell uptake (37 °C, RPMI 1640, 5 mM L-Gln, 5 mL non-essential amino acids (100×), 10% FCS, 0.25 pmol/well) determined as percent (%) of the applied activity of [^{177}Lu]Lu-(*R*)-DOTAGA-rhCCK-9 and -16 as well as the references [^{177}Lu]Lu-DOTA-PP-F11N and [^{177}Lu]Lu-CP04 using AR42J cells (3.0 × 10^5 cells/well) at different time points (1, 2, 4 and 6 h). Data are corrected for non-specific binding (10 µmol/well, [^{nat}Lu]Lu-DOTA-PP-F11N); Table S4: Biodistribution data of [^{177}Lu]Lu-DOTA-PP-F11N, [^{177}Lu]Lu-(*R*)-DOTAGA-rhCCK-9 and [^{177}Lu]Lu-(*R*)-DOTAGA-rhCCK-16 in selected organs at 24 h p.i. in AR42J tumour-bearing CB17-SCID mice (100 pmol each). Data are expressed as %ID/g, mean ± SD.

Author Contributions: Conceptualisation, T.G. and H.-J.W.; methodology, N.H., T.G. and R.B.; software, N.H. and T.G.; validation, N.H. and T.G.; formal analysis, N.H. and T.G.; investigation, N.H. and T.G.; resources, R.B. and H.-J.W.; data curation, N.H. and T.G.; writing—original draft preparation, N.H. and T.G.; writing—review and editing, all co-authors; visualisation, N.H. and T.G.; supervision, H.-J.W. and C.L.; project administration, T.G. and H.-J.W.; funding acquisition, R.B., H.-J.W. and T.G. All authors have read and agreed to the published version of the manuscript.

Funding: This study has been funded by Deutsche Forschungsgemeinschaft (DFG, German Research Foundation—391523415 and 461577150).

Institutional Review Board Statement: All animal experiments were conducted in accordance with general animal welfare regulations in Germany (German animal protection act, in the edition of the announcement, dated 18 May 2006, as amended by Article 280 of 19 June 2020, approval no. ROB-55.2-1-2532.Vet_02-18-109 by the General Administration of Upper Bavaria) and the institutional guidelines for the care and use of animals. The study was carried out in compliance with the ARRIVE guidelines. This article does not contain any studies with human participants.

Informed Consent Statement: Not applicable.

Data Availability Statement: Data is contained within the article and Supplementary Materials.

Acknowledgments: We thank Sebastian Fischer for providing us with the SiFA building block for synthesis.

Conflicts of Interest: H.J.-W. is founder and shareholder of *Scintomics GmbH*, Munich, Germany. No other potential conflicts of interest relevant to this article exist.

References

1. Stamatakos, M.; Paraskeva, P.; Stefanaki, C.; Katsaronis, P.; Lazaris, A.; Safioleas, K.; Kontzoglou, K. Medullary thyroid carcinoma: The third most common thyroid cancer reviewed. *Oncol. Lett.* **2011**, *2*, 49–53. [CrossRef] [PubMed]
2. Wells, S.A., Jr.; Asa, S.L.; Dralle, H.; Elisei, R.; Evans, D.B.; Gagel, R.F.; Lee, N.; Machens, A.; Moley, J.F.; Pacini, F.; et al. Revised American Thyroid Association guidelines for the management of medullary thyroid carcinoma. *Thyroid* **2015**, *25*, 567–610. [CrossRef]
3. Hadoux, J.; Schlumberger, M. Chemotherapy and tyrosine-kinase inhibitors for medullary thyroid cancer. *Best Pract. Res. Clin. Endocrinol. Metab.* **2017**, *31*, 335–347. [CrossRef]
4. Hazard, J.B. The C cells (parafollicular cells) of the thyroid gland and medullary thyroid carcinoma. A review. *Am. J. Pathol.* **1977**, *88*, 213–250.

5. Resteghini, C.; Cavalieri, S.; Galbiati, D.; Granata, R.; Alfieri, S.; Bergamini, C.; Bossi, P.; Licitra, L.; Locati, L.D. Management of tyrosine kinase inhibitors (TKI) side effects in differentiated and medullary thyroid cancer patients. *Best Pract. Res. Clin. Endocrinol. Metab.* **2017**, *31*, 349–361. [CrossRef] [PubMed]
6. Reubi, J.C.; Waser, B. Unexpected high incidence of cholecystokinin-B/gastrin receptors in human medullary thyroid carcinomas. *Int. J. Cancer* **1996**, *67*, 644–647. [CrossRef]
7. Behr, T.M.; Jenner, N.; Béhé, M.; Angerstein, C.; Gratz, S.; Raue, F.; Becker, W. Radiolabeled Peptides for Targeting Cholecystokinin-B/Gastrin Receptor-Expressing Tumors. *J. Nucl. Med.* **1999**, *40*, 1029–1044.
8. Behe, M.; Becker, W.; Gotthardt, M.; Angerstein, C.; Behr, T.M. Improved kinetic stability of DTPA-dGlu as compared with conventional monofunctional DTPA in chelating indium and yttrium: Preclinical and initial clinical evaluation of radiometal labelled minigastrin derivatives. *Eur. J. Nucl. Med. Mol. Imaging* **2003**, *30*, 1140–1146. [CrossRef] [PubMed]
9. Laverman, P.; Joosten, L.; Eek, A.; Roosenburg, S.; Peitl, P.K.; Maina, T.; Macke, H.; Aloj, L.; von Guggenberg, E.; Sosabowski, J.K.; et al. Comparative biodistribution of 12 (1)(1)(1)In-labelled gastrin/CCK2 receptor-targeting peptides. *Eur. J. Nucl. Med. Mol. Imaging* **2011**, *38*, 1410–1416. [CrossRef]
10. Sauter, A.W.; Mansi, R.; Hassiepen, U.; Muller, L.; Panigada, T.; Wiehr, S.; Wild, A.M.; Geistlich, S.; Béhé, M.; Rottenburger, C.; et al. Targeting of the Cholecystokinin-2 Receptor with the Minigastrin Analog (177)Lu-DOTA-PP-F11N: Does the Use of Protease Inhibitors Further Improve In Vivo Distribution? *J. Nucl. Med.* **2019**, *60*, 393–399. [CrossRef] [PubMed]
11. Martin, B.; Schibli, R. Mini-Gastrin Analogue, in Particular for Use in CCK2 Receptor Positive Tumour Diagnosis and/or Treatment. U.S. Patent 10,130,724, 20 November 2018.
12. Rottenburger, C.; Nicolas, G.P.; McDougall, L.; Kaul, F.; Cachovan, M.; Vija, A.H.; Schibli, R.; Geistlich, S.; Schumann, A.; Rau, T.; et al. Cholecystokinin 2 Receptor Agonist (177)Lu-PP-F11N for Radionuclide Therapy of Medullary Thyroid Carcinoma: Results of the Lumed Phase 0a Study. *J. Nucl. Med.* **2020**, *61*, 520–526. [CrossRef] [PubMed]
13. Wurzer, A.; Di Carlo, D.; Schmidt, A.; Beck, R.; Eiber, M.; Schwaiger, M.; Wester, H.-J. Radiohybrid Ligands: A Novel Tracer Concept Exemplified by 18F- or 68Ga-Labeled rhPSMA Inhibitors. *J. Nucl. Med.* **2020**, *61*, 735–742. [CrossRef] [PubMed]
14. Wurzer, A.; Kunert, J.P.; Fischer, S.; Felber, V.; Beck, R.; Rose, F.; D'Alessandria, C.; Weber, W.; Wester, H.J. Synthesis and Preclinical Evaluation of (177)Lu-Labeled Radiohybrid PSMA Ligands for Endoradiotherapy of Prostate Cancer. *J. Nucl. Med.* **2022**, *63*, 1489–1495. [CrossRef] [PubMed]
15. Eiber, M.; Kronke, M.; Wurzer, A.; Ulbrich, L.; Jooss, L.; Maurer, T.; Horn, T.; Schiller, K.; Langbein, T.; Buschner, G.; et al. (18)F-rhPSMA-7 positron emission tomography for the detection of biochemical recurrence of prostate cancer following radical prostatectomy. *J. Nucl. Med.* **2020**, *61*, 696–701. [CrossRef]
16. Kronke, M.; Wurzer, A.; Schwamborn, K.; Ulbrich, L.; Jooss, L.; Maurer, T.; Horn, T.; Rauscher, I.; Haller, B.; Herz, M.; et al. Histologically-confirmed diagnostic efficacy of (18)F-rhPSMA-7 positron emission tomography for N-staging of patients with primary high risk prostate cancer. *J. Nucl. Med.* **2020**, *61*, 710–715. [CrossRef]
17. Oh, S.W.; Wurzer, A.; Teoh, E.J.; Oh, S.; Langbein, T.; Kronke, M.; Herz, M.; Kropf, S.; Wester, H.J.; Weber, W.A.; et al. Quantitative and Qualitative Analyses of Biodistribution and PET Image Quality of Novel Radiohybrid PSMA, (18)F-rhPSMA-7, in Patients with Prostate Cancer. *J. Nucl. Med.* **2020**, *61*, 702–709. [CrossRef]
18. Kroenke, M.; Mirzoyan, L.; Horn, T.; Peeken, J.C.; Wurzer, A.; Wester, H.J.; Makowski, M.; Weber, W.A.; Eiber, M.; Rauscher, I. Matched-Pair Comparison of (68)Ga-PSMA-11 and (18)F-rhPSMA-7 PET/CT in Patients with Primary and Biochemical Recurrence of Prostate Cancer: Frequency of Non-Tumor-Related Uptake and Tumor Positivity. *J. Nucl. Med.* **2021**, *62*, 1082–1088. [CrossRef]
19. Guenther, T.; Deiser, S.; Felber, V.; Beck, R.; Wester, H.J. Substitution of L-Tryptophan by a-Methyl-L-Tryptophan in 177Lu-RM2 Results in 177Lu-AMTG, a High-Affinity Gastrin-Releasing Peptide Receptor Ligand with Improved In Vivo Stability. *J. Nucl. Med.* **2022**, *63*, 1364–1370. [CrossRef] [PubMed]
20. Uprimny, C.; von Guggenberg, E.; Svirydenka, A.; Mikolajczak, R.; Hubalewska-Dydejczyk, A.; Virgolini, I.J. Comparison of PET/CT imaging with [(18)F]FDOPA and cholecystokinin-2 receptor targeting [(68)Ga]Ga-DOTA-MGS5 in a patient with advanced medullary thyroid carcinoma. *Eur. J. Nucl. Med. Mol. Imaging* **2020**, *48*, 935–936. [CrossRef]
21. Hörmann, A.A.; Klingler, M.; Rangger, C.; Mair, C.; Decristoforo, C.; Uprimny, C.; Virgolini, I.J.; von Guggenberg, E. Radiopharmaceutical Formulation and Preclinical Testing of 68Ga-Labeled DOTA-MGS5 for the Regulatory Approval of a First Exploratory Clinical Trial. *Pharmaceuticals* **2021**, *14*, 575. [CrossRef] [PubMed]
22. 177Lu-PP-F11N for Receptor Targeted Therapy and Imaging of Metastatic Thyroid Cancer. Available online: https://ClinicalTrials.gov/show/NCT02088645 (accessed on 23 July 2022).
23. Radiolabelled CCK-2/Gastrin Receptor Analogue for Personalized Theranostic Strategy in Advanced MTC. Available online: https://ClinicalTrials.gov/show/NCT03246659 (accessed on 23 July 2022).
24. Bernard-Gauthier, V.; Wangler, C.; Schirrmacher, E.; Kostikov, A.; Jurkschat, K.; Wangler, B.; Schirrmacher, R. (1)(8)F-labeled silicon-based fluoride acceptors: Potential opportunities for novel positron emitting radiopharmaceuticals. *Biomed. Res. Int.* **2014**, *2014*, 454503. [CrossRef] [PubMed]
25. Malaspina, S.; Taimen, P.; Kallajoki, M.; Oikonen, V.; Kuisma, A.; Ettala, O.; Mattila, K.; Boström, P.J.; Minn, H.; Kalliokoski, K.; et al. Uptake of (18)F-rhPSMA-7.3 in Positron Emission Tomography Imaging of Prostate Cancer: A Phase 1 Proof-of-Concept Study. *Cancer Biother. Radiopharm.* **2022**, *37*, 205–213. [CrossRef]

26. Feuerecker, B.; Chantadisai, M.; Allmann, A.; Tauber, R.; Allmann, J.; Steinhelfer, L.; Rauscher, I.; Wurzer, A.; Wester, H.J.; Weber, W.A.; et al. Pre-therapeutic comparative dosimetry of (177)Lu-rhPSMA-7.3 and (177)Lu-PSMAI&T in patients with metastatic castration resistant prostate cancer (mCRPC). *J. Nucl. Med.* **2021**, *63*, 833–839. [CrossRef] [PubMed]
27. Yusufi, N.; Wurzer, A.; Herz, M.; D'Alessandria, C.; Feuerecker, B.; Weber, W.; Wester, H.J.; Nekolla, S.; Eiber, M. Comparative Preclinical Biodistribution, Dosimetry, and Endoradiotherapy in Metastatic Castration-Resistant Prostate Cancer Using (19)F/(177)Lu-rhPSMA-7.3 and (177)Lu-PSMA I&T. *J. Nucl. Med.* **2021**, *62*, 1106–1111. [CrossRef] [PubMed]
28. Imaging Study to Investigate the Safety and Diagnostic Performance of rhPSMA 7.3 (18F) in Newly Diagnosed Prostate Cancer (LIGHTHOUSE). Available online: https://ClinicalTrials.gov/show/NCT04186819 (accessed on 2 November 2022).
29. Imaging Study to Investigate Safety and Diagnostic Performance of rhPSMA 7.3 (18F) PET Ligand in Suspected Prostate Cancer Recurrence (SPOTLIGHT). Available online: https://ClinicalTrials.gov/show/NCT04186845 (accessed on 2 November 2022).
30. Anti-tumour Activity of (177Lu) rhPSMA-10.1 Injection. Available online: https://ClinicalTrials.gov/show/NCT05413850 (accessed on 2 November 2022).
31. Assessing Radio-hybrid Prostate Specific Membrane Antigen (rhPSMA-7.3) (18F) in Healthy Volunteers and Subjects with Prostate Cancer. Available online: https://ClinicalTrials.gov/show/NCT03995888 (accessed on 2 November 2022).
32. An Investigational Scan (rh PSMA 7.3 PET/MRI) for the Detection of Recurrent Disease and Aid in Radiotherapy Planning in Biochemically Recurrent Prostate Cancer. Available online: https://ClinicalTrials.gov/show/NCT04978675 (accessed on 2 November 2022).
33. Kunert, J.P.; Fischer, S.; Wurzer, A.; Wester, H.J. Albumin-Mediated Size Exclusion Chromatography: The Apparent Molecular Weight of PSMA Radioligands as Novel Parameter to Estimate Their Blood Clearance Kinetics. *Pharmaceuticals* **2022**, *15*, 1161. [CrossRef] [PubMed]
34. Klingler, M.; Summer, D.; Rangger, C.; Haubner, R.; Foster, J.; Sosabowski, J.; Decristoforo, C.; Virgolini, I.; von Guggenberg, E. DOTA-MGS5, a New Cholecystokinin-2 Receptor-Targeting Peptide Analog with an Optimized Targeting Profile for Theranostic Use. *J. Nucl. Med.* **2019**, *60*, 1010–1016. [CrossRef] [PubMed]
35. Schottelius, M.; Osl, T.; Poschenrieder, A.; Hoffmann, F.; Beykan, S.; Hänscheid, H.; Schirbel, A.; Buck, A.K.; Kropf, S.; Schwaiger, M.; et al. [(177)Lu]pentixather: Comprehensive Preclinical Characterization of a First CXCR4-directed Endoradiotherapeutic Agent. *Theranostics* **2017**, *7*, 2350–2362. [CrossRef] [PubMed]
36. Dalm, S.U.; Nonnekens, J.; Doeswijk, G.N.; de Blois, E.; van Gent, D.C.; Konijnenberg, M.W.; de Jong, M. Comparison of the Therapeutic Response to Treatment with a 177Lu-Labeled Somatostatin Receptor Agonist and Antagonist in Preclinical Models. *J. Nucl. Med.* **2016**, *57*, 260–265. [CrossRef]
37. Nicolas, G.P.; Mansi, R.; McDougall, L.; Kaufmann, J.; Bouterfa, H.; Wild, D.; Fani, M. Biodistribution, Pharmacokinetics, and Dosimetry of (177)Lu-, (90)Y-, and (111)In-Labeled Somatostatin Receptor Antagonist OPS201 in Comparison to the Agonist (177)Lu-DOTATATE: The Mass Effect. *J. Nucl. Med.* **2017**, *58*, 1435–1441. [CrossRef]

Introduction of a SiFA Moiety into the D-Glutamate Chain of DOTA-PP-F11N Results in Radiohybrid-Based CCK-2R-Targeted Compounds with Improved Pharmacokinetics *in vivo*

- Supplementary Materials -

Nadine Holzleitner[1,#,*] Thomas Günther[1,#], Roswitha Beck[1], Constantin Lapa[2] and Hans-Jürgen Wester[1]

[1]Chair of Pharmaceutical Radiochemistry, Department of Chemistry, Technical University of Munich, Garching, Germany

[2]Clinic for Nuclear Medicine, University Hospital Augsburg, Augsburg, Germany

Corresponding co-authors:

Nadine Holzleitner and Thomas Günther

Phone: +49.89.289.12203

Technical University of Munich,

Chair of Pharmaceutical Radiochemistry,

Walther-Meissner-Str. 3

85748 Garching

GERMANY

Fax: +49.89.289.12204

E-Mail: nadine.holzleitner@tum.de and thomas.guenther@tum.de

ORCID: https://orcid.org/0000-0001-8258-3526 (NH) and https://orcid.org/0000-0002-7412-0297 (TG)

Analytical data of $^{nat/177}$Lu-labeled minigastrin analogues

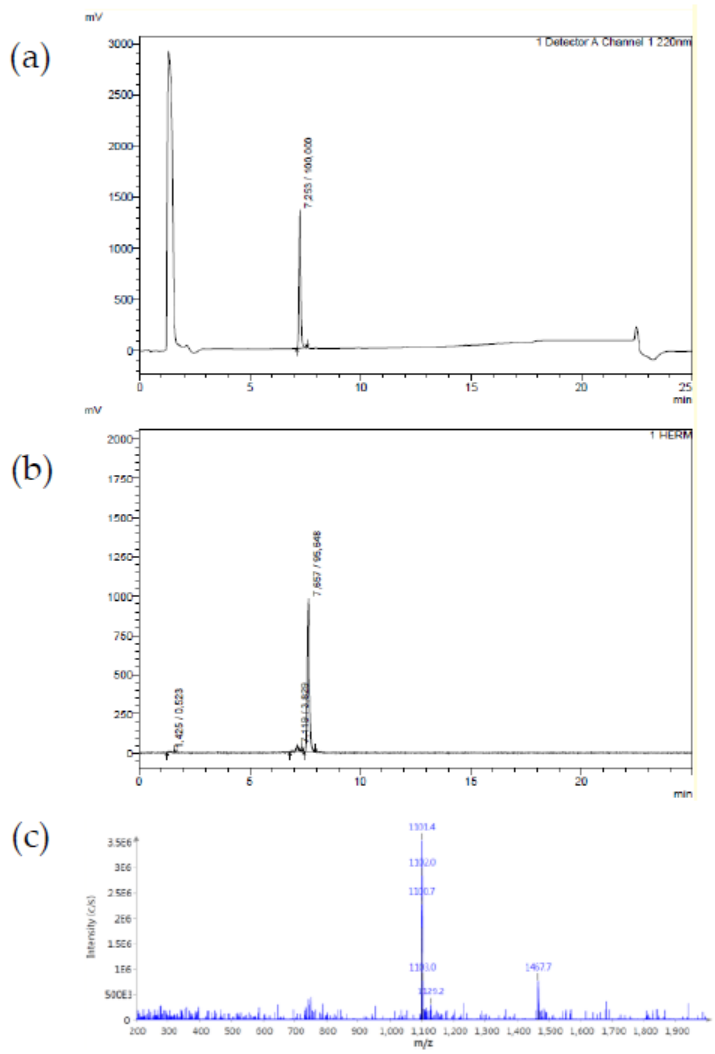

Figure S1. Confirmation of peptide identity and integrity for (**a**) [^{nat}Lu]Lu-DOTA-PP-F11N and (**b**) [^{177}Lu]Lu-DOTA-PP-F11N as analysed by analytical (radio-)RP-HPLC (MultoKrom 100-5 C18, 5 µm, 125 × 4.6 mm, CS Chromatographie GmbH, Langerwehe, Germany; 10→90% MeCN in H_2O + 0.1% TFA in 15 min). (**c**) Mass spectrum of [^{nat}Lu]Lu-DOTA-PP-F11N.

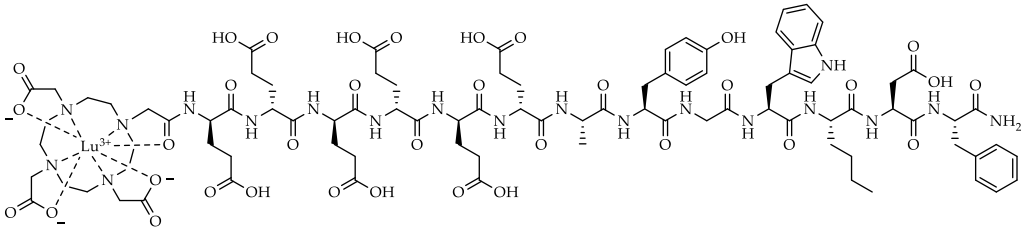

[^{nat}Lu]Lu-DOTA-PP-F11N: RP-HPLC (10→90% MeCN in H_2O with 0.1% TFA, 15 min, λ = 220 nm): t_R = 7.55 min, K′ = 3.48; MS (ESI, positive): m/z calculated for $C_{90}H_{120}LuN_{19}O_{35}$: 2203.0, found: m/z = 1101.4 $[M+2H]^{2+}$.

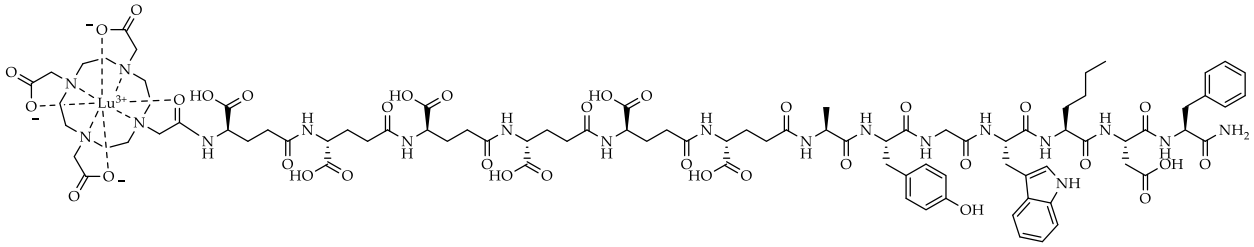

[^{nat}Lu]Lu-DOTA-PP-γ-F11N: RP-HPLC (10→90% MeCN in H_2O with 0.1% TFA, 15 min, λ = 220 nm): t_R = 7.41 min, K′ = 3.39; MS (ESI, positive): m/z calculated for $C_{90}H_{120}LuN_{19}O_{35}$: 2203.0, found: m/z = 1101.9 $[M+2H]^{2+}$.

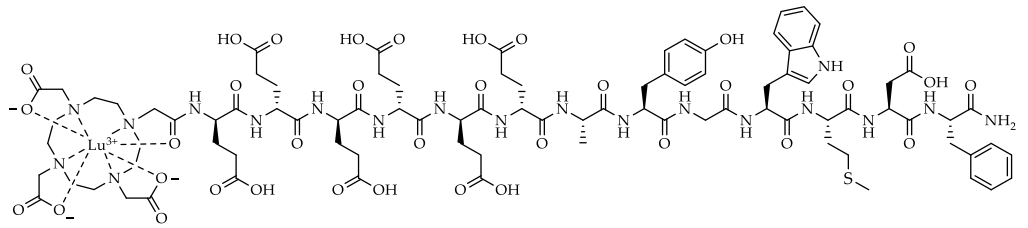

[^{nat}Lu]Lu-CP04: RP-HPLC (10→90% MeCN in H_2O with 0.1% TFA, 15 min, λ = 220 nm): t_R = 7.60 min, K′ = 3.51; MS (ESI, positive): m/z calculated for $C_{89}H_{118}LuN_{19}O_{35}S$: 2219.7, found: m/z = 1110.3 $[M+2H]^{2+}$.

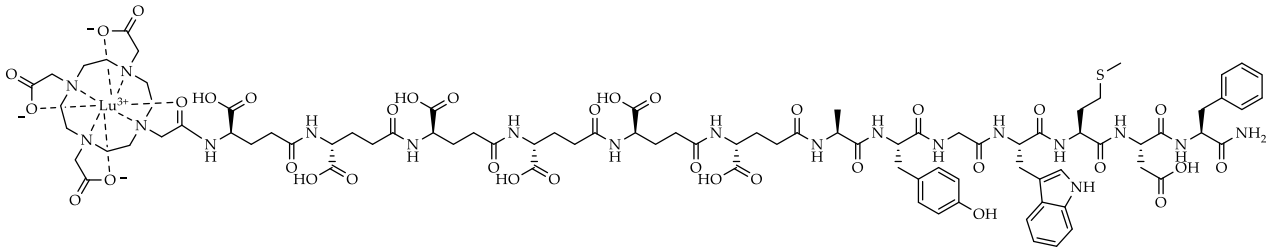

[^{nat}Lu]Lu-γ-CP04: RP-HPLC (10→90% MeCN in H_2O with 0.1% TFA, 15 min, λ = 220 nm): t_R = 7.40 min, K′ = 3.39; MS (ESI, positive): m/z calculated for $C_{89}H_{118}LuN_{19}O_{35}S$: 2219.7, found: m/z = 1110.8 $[M+2H]^{2+}$.

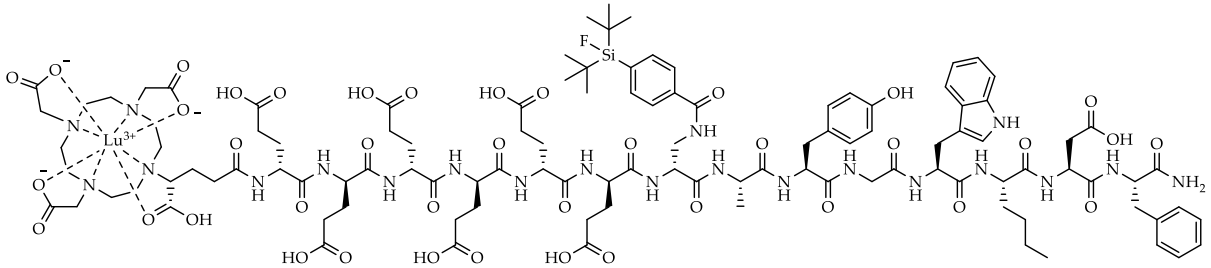

[^{nat}Lu]Lu-(R)-DOTAGA-rhCCK-1: RP-HPLC (10→90% MeCN in H_2O with 0.1% TFA, 15 min, λ = 220 nm): t_R = 10.1 min, K′ = 4.99; MS (ESI, positive): m/z calculated for $C_{111}H_{151}FLuN_{21}O_{39}Si$: 2625.6, found: m/z = 1312.8 $[M+2H]^{2+}$.

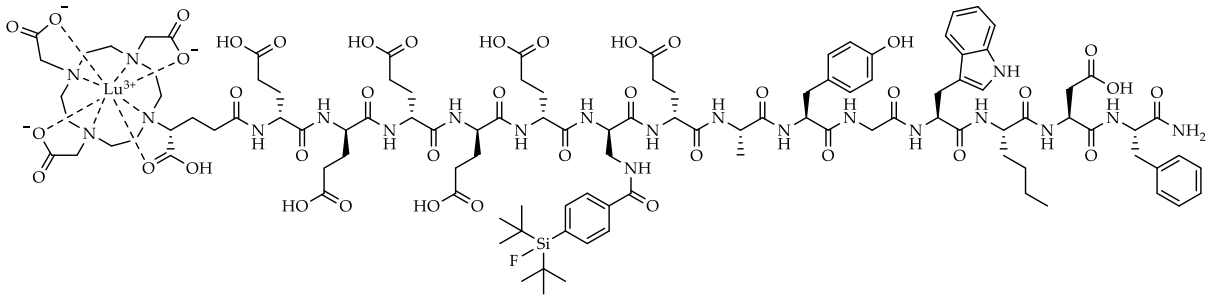

[^{nat}Lu]Lu-(R)-DOTAGA-rhCCK-2: RP-HPLC (10→90% MeCN in H_2O with 0.1% TFA, 15 min, λ = 220 nm): t_R = 9.84 min, K′ = 4.83; MS (ESI, positive): m/z calculated for $C_{111}H_{151}FLuN_{21}O_{39}Si$: 2625.6, found: m/z = 1312.7 $[M+2H]^{2+}$.

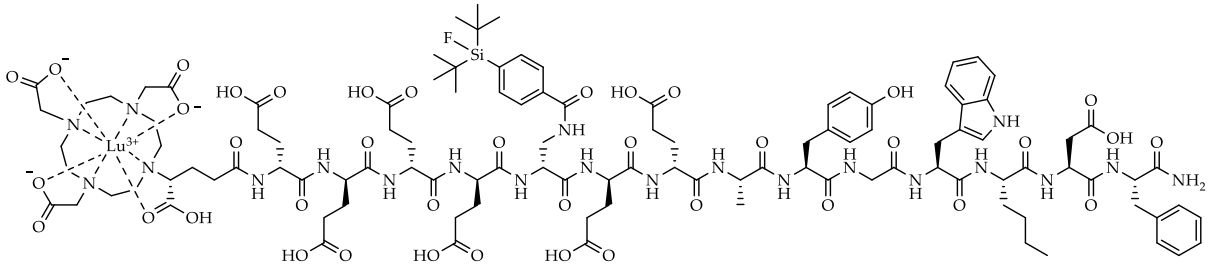

[^{nat}Lu]Lu-(R)-DOTAGA-rhCCK-3: RP-HPLC (10→90% MeCN in H_2O with 0.1% TFA, 15 min, λ = 220 nm): t_R = 9.85 min, K′ = 4.84; MS (ESI, positive): m/z calculated for $C_{111}H_{151}FLuN_{21}O_{39}Si$: 2625.6, found: m/z = 1312.3 $[M+2H]^{2+}$.

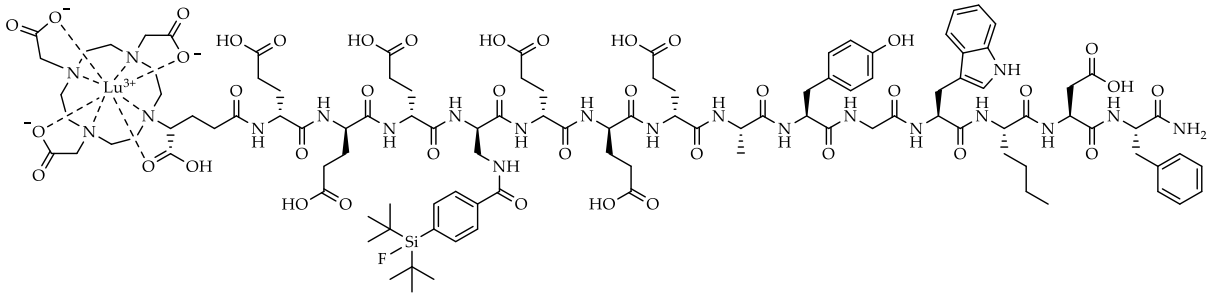

[^{nat}Lu]Lu-(R)-DOTAGA-rhCCK-4: RP-HPLC (10→70% MeCN in H_2O with 0.1% TFA, 15 min, λ = 220 nm): t_R = 11.9 min, K′ = 6.05; MS (ESI, positive): m/z calculated for $C_{111}H_{151}FLuN_{21}O_{39}Si$: 2625.6, found: m/z = 1313.0 $[M+2H]^{2+}$.

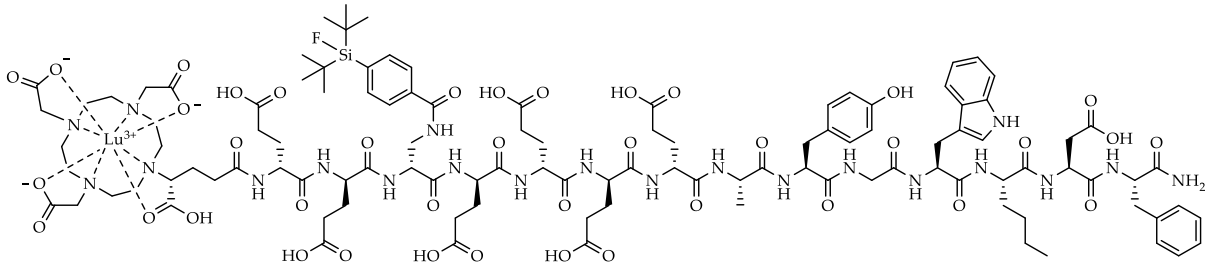

[^{nat}Lu]Lu-(R)-DOTAGA-rhCCK-5: RP-HPLC (10→90% MeCN in H_2O with 0.1% TFA, 15 min, λ = 220 nm): t_R = 9.67 min, K′ = 4.73; MS (ESI, positive): m/z calculated for $C_{111}H_{151}FLuN_{21}O_{39}Si$: 2625.6, found: m/z = 1313.3 $[M+2H]^{2+}$.

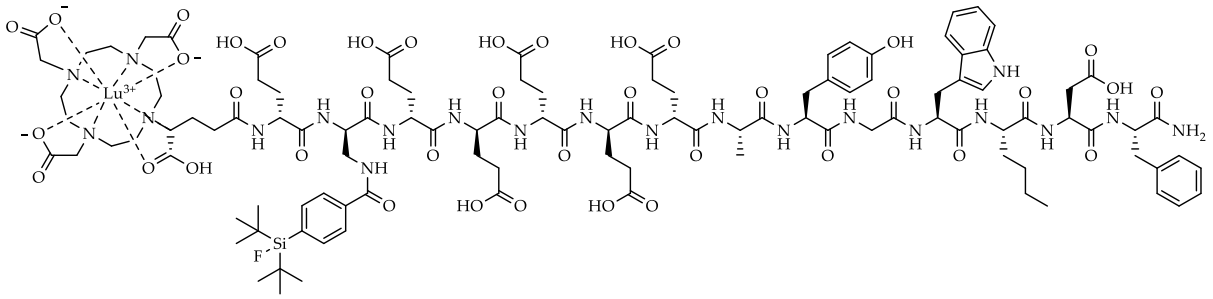

[^{nat}Lu]Lu-(R)-DOTAGA-rhCCK-6: RP-HPLC (10→90% MeCN in H_2O with 0.1% TFA, 15 min, λ = 220 nm): t_R = 9.71 min, K′ = 4.76; MS (ESI, positive): m/z calculated for $C_{111}H_{151}FLuN_{21}O_{39}Si$: 2625.6, found: m/z = 1312.9 $[M+2H]^{2+}$.

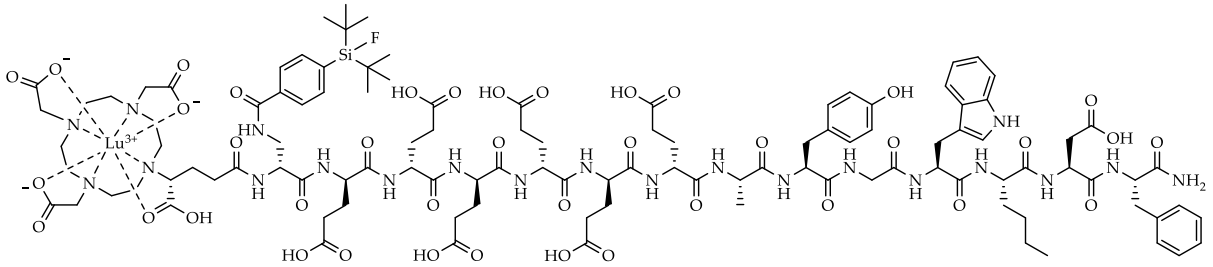

[^{nat}Lu]Lu-(R)-DOTAGA-rhCCK-7: RP-HPLC (10→90% MeCN in H_2O with 0.1% TFA, 15 min, λ = 220 nm): t_R = 9.62 min, K′ = 4.70; MS (ESI, positive): m/z calculated for $C_{111}H_{151}FLuN_{21}O_{39}Si$: 2625.6, found: m/z = 1313.0 $[M+2H]^{2+}$.

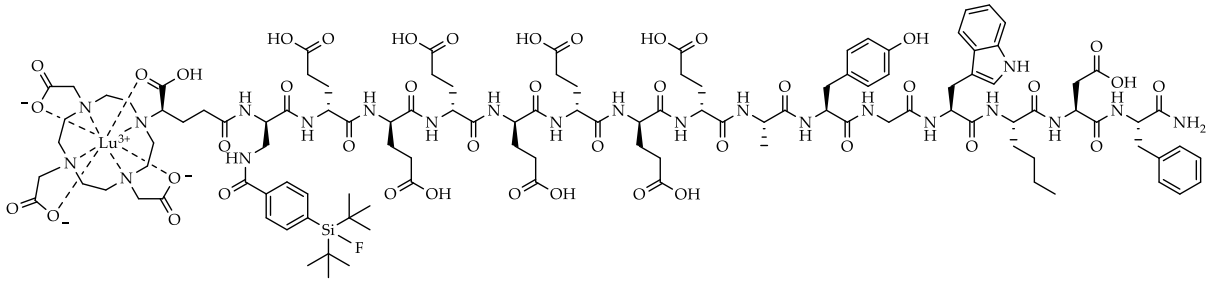

[^{nat}Lu]Lu-(R)-DOTAGA-rhCCK-8: RP-HPLC (10→90% MeCN in H_2O with 0.1% TFA, 15 min, λ = 220 nm): t_R = 9.77 min, K′ = 4.79; MS (ESI, positive): m/z calculated for $C_{116}H_{158}FLuN_{22}O_{42}Si$: 2754.7, found: m/z = 1378.2 $[M+2H]^{2+}$.

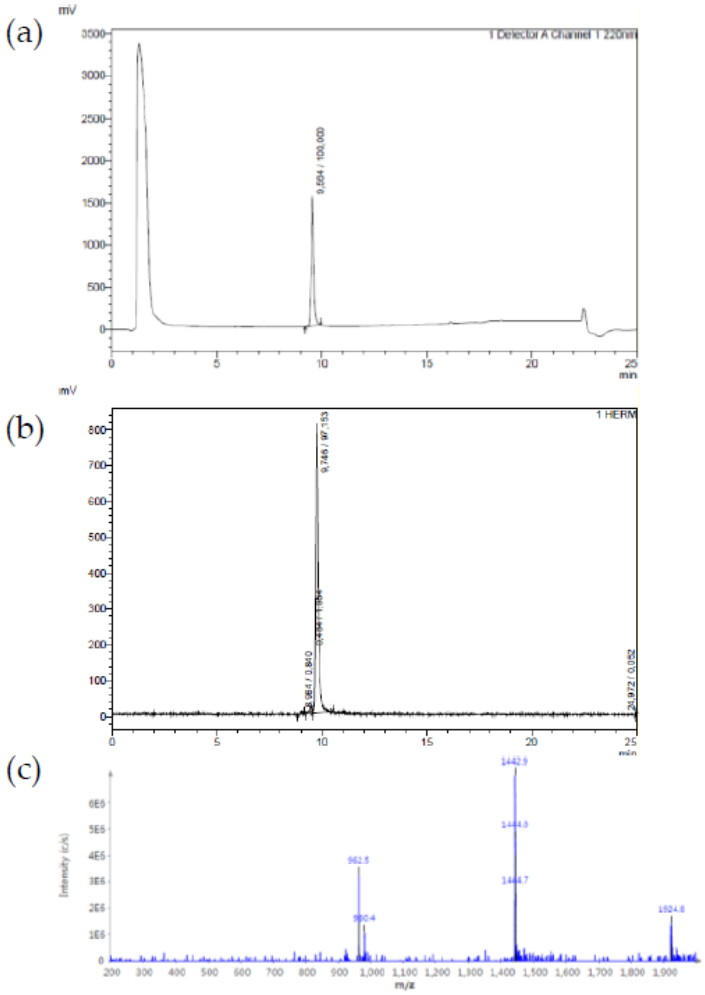

Figure S2. Confirmation of peptide identity and integrity for (**a**) [^{nat}Lu]Lu-(*R*)-DOTAGA-rhCCK-9 and (**b**) [^{177}Lu]Lu-(*R*)-DOTAGA-rhCCK-9 as analysed by analytical (radio-)RP-HPLC (MultoKrom 100-5 C18, 5 µm, 125 × 4.6 mm, CS Chromatographie GmbH, Langerwehe, Germany; 10→90% MeCN in H_2O + 0.1% TFA in 15 min). (**c**) Mass spectrum of [^{nat}Lu]Lu-(*R*)-DOTAGA-rhCCK-9.

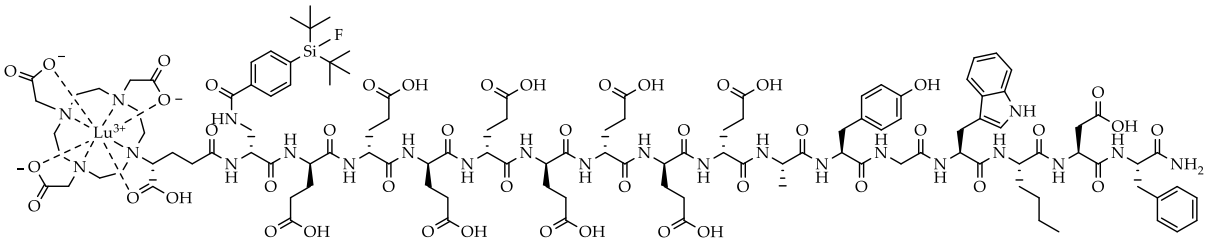

[^{nat}Lu]Lu-(R)-DOTAGA-rhCCK-9: RP-HPLC (10→90% MeCN in H_2O with 0.1% TFA, 15 min, λ = 220 nm): t_R = 9.56 min, K′ = 4.67; MS (ESI, positive): m/z calculated for $C_{121}H_{165}FLuN_{23}O_{45}Si$: 2883.8, found: m/z = 1441.5 $[M+2H]^{2+}$.

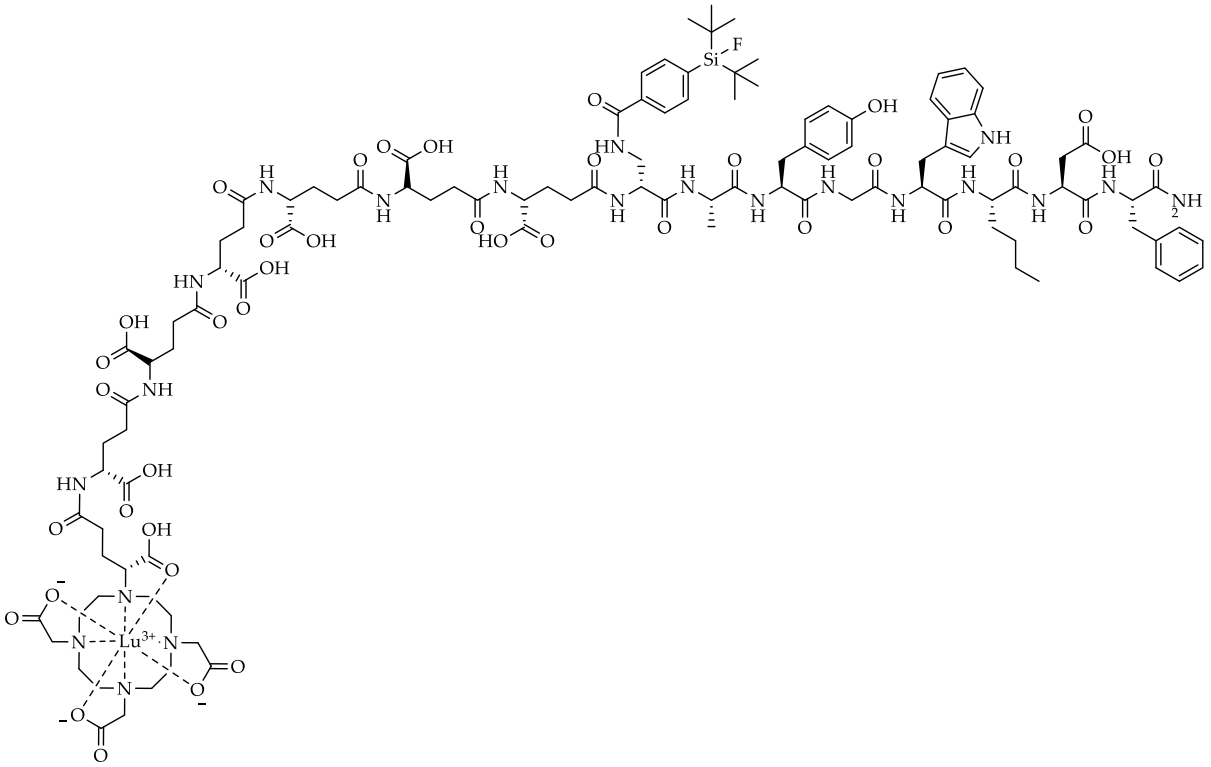

[^{nat}Lu]Lu-(R)-DOTAGA-rhCCK-10: RP-HPLC (10→90% MeCN in H_2O with 0.1% TFA, 15 min, λ = 220 nm): t_R = 10.2 min, K′ = 5.05; MS (ESI, positive): m/z calculated for $C_{111}H_{151}FLuN_{21}O_{39}Si$: 2625.6, found: m/z = 1313.6 $[M+2H]^{2+}$.

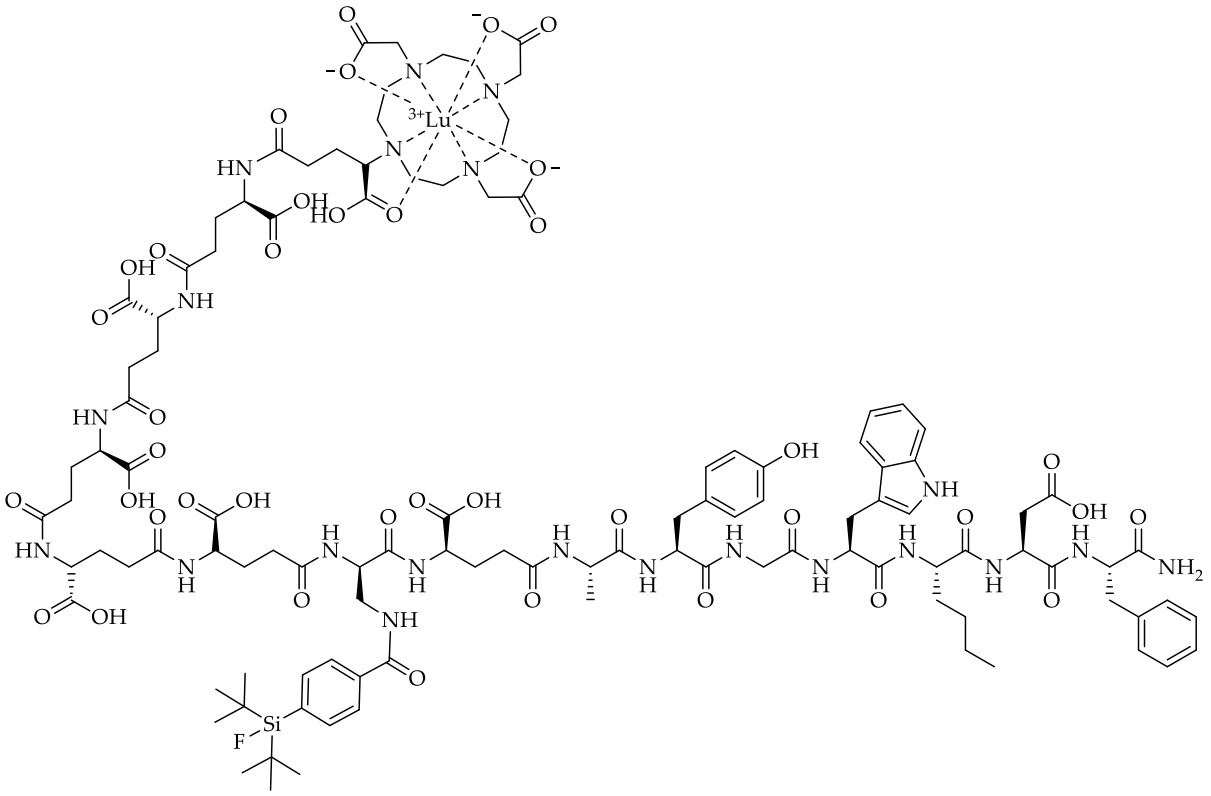

[^{nat}Lu]Lu-(R)-DOTAGA-rhCCK-11: RP-HPLC (10→90% MeCN in H_2O with 0.1% TFA, 15 min, λ = 220 nm): t_R = 9.72 min, K′ = 4.76; MS (ESI, positive): m/z calculated for $C_{111}H_{151}FLuN_{21}O_{39}Si$: 2625.6, found: m/z = 1313.0 $[M+2H]^{2+}$.

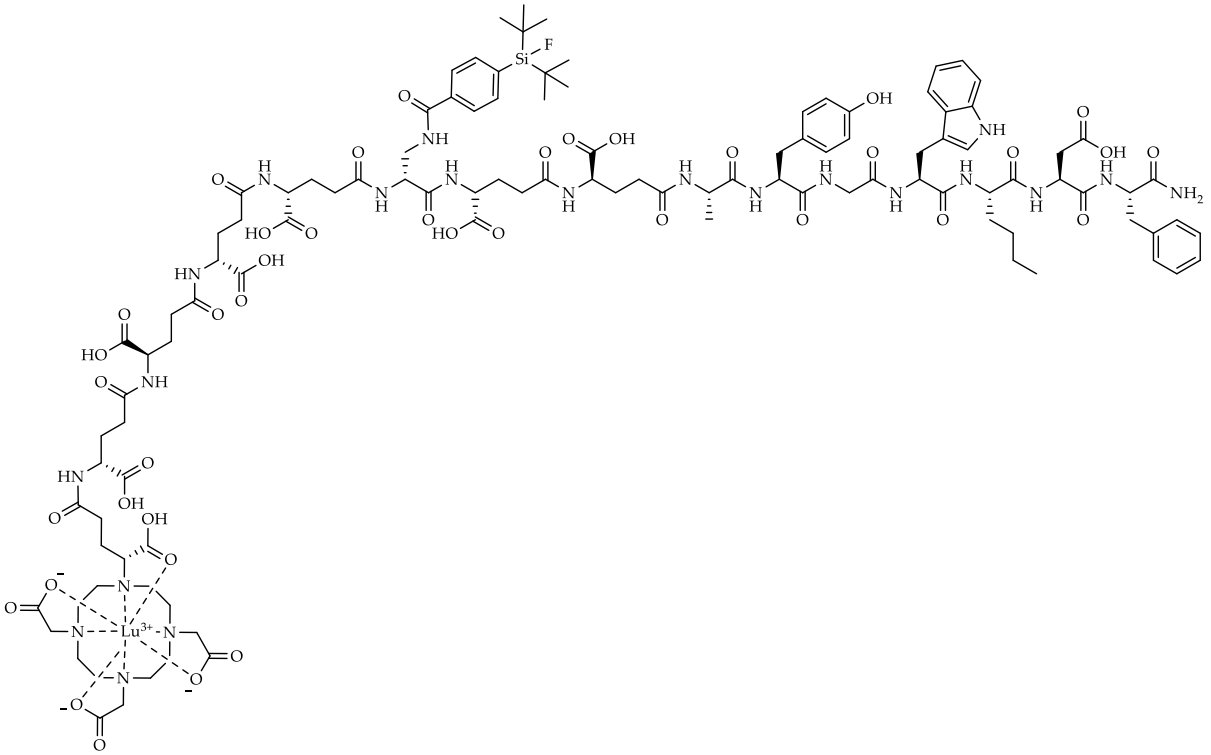

[^{nat}Lu]Lu-(R)-DOTAGA-rhCCK-12: RP-HPLC (10→90% MeCN in H_2O with 0.1% TFA, 15 min, λ = 220 nm): t_R = 9.87 min, K′ = 4.85; MS (ESI, positive): m/z calculated for $C_{111}H_{151}FLuN_{21}O_{39}Si$: 2625.6, found: m/z = 1312.9 $[M+2H]^{2+}$.

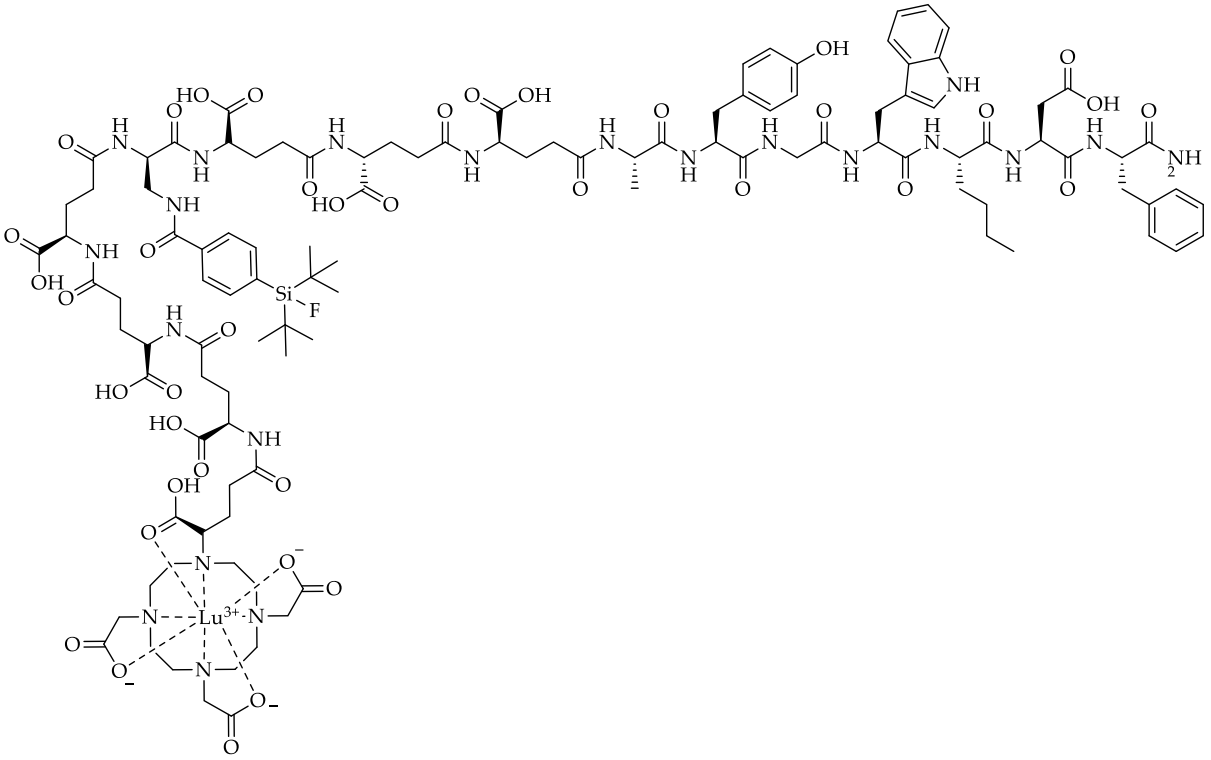

[natLu]Lu-(R)-DOTAGA-rhCCK-13: RP-HPLC (10→90% MeCN in H_2O with 0.1% TFA, 15 min, λ = 220 nm): t_R = 9.61 min, K′ = 4.70; MS (ESI, positive): m/z calculated for $C_{111}H_{151}FLuN_{21}O_{39}Si$: 2625.6, found: m/z = 1313.2 $[M+2H]^{2+}$.

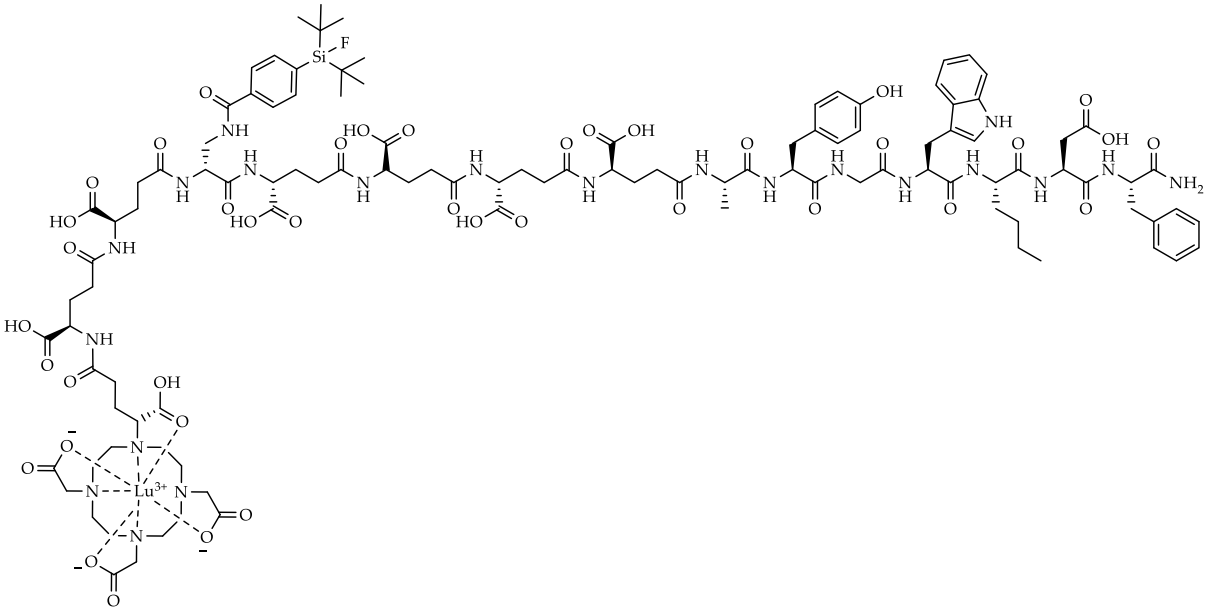

[natLu]Lu-(R)-DOTAGA-rhCCK-14: RP-HPLC (10→90% MeCN in H_2O with 0.1% TFA, 15 min, λ = 220 nm): t_R = 9.60 min, K′ = 4.69; MS (ESI, positive): m/z calculated for $C_{111}H_{151}FLuN_{21}O_{39}Si$: 2625.6, found: m/z = 1313.9 $[M+2H]^{2+}$.

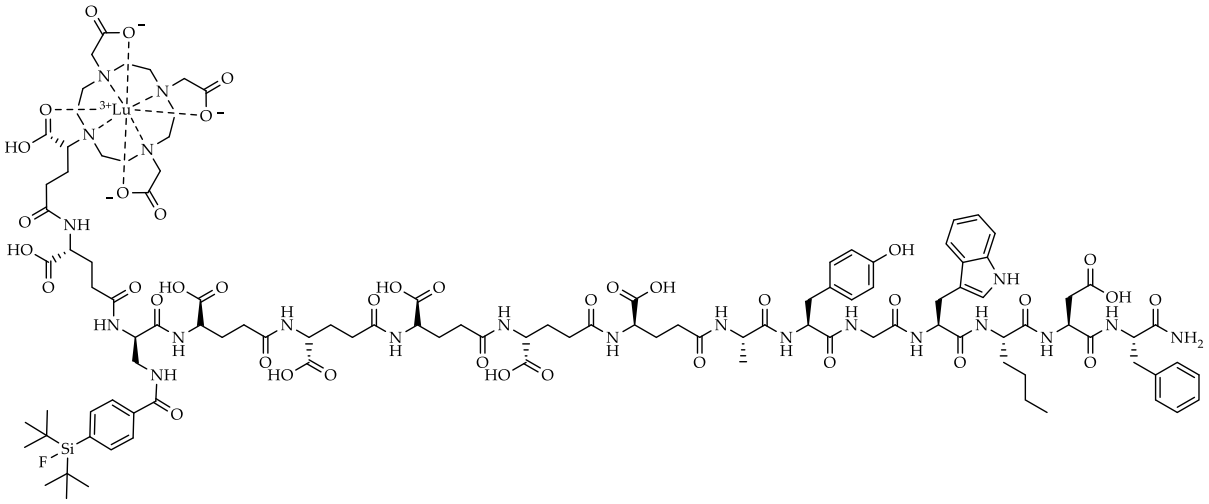

[natLu]Lu-(R)-DOTAGA-rhCCK-15: RP-HPLC (10→90% MeCN in H_2O with 0.1% TFA, 15 min, λ = 220 nm): t_R = 9.62 min, K′ = 4.70; MS (ESI, positive): m/z calculated for $C_{111}H_{151}FLuN_{21}O_{39}Si$: 2625.6, found: m/z = 1313.3 $[M+2H]^{2+}$.

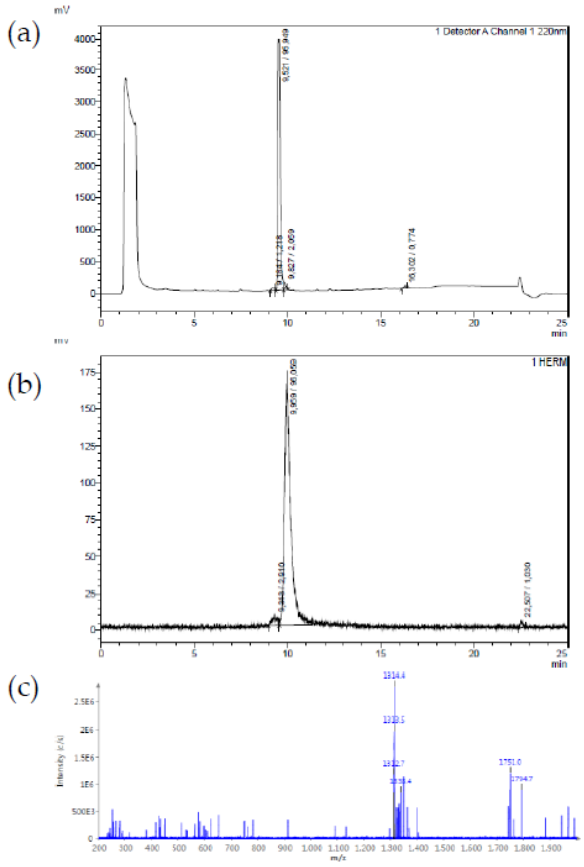

Figure S3. Confirmation of peptide identity and integrity for (**a**) [natLu]Lu-(*R*)-DOTAGA-rhCCK-16 and (**b**) [177Lu]Lu-(*R*)-DOTAGA-rhCCK-16 as analysed by analytical (radio-)RP-HPLC (MultoKrom 100-5 C18, 5 µm, 125 × 4.6 mm, CS Chromatographie GmbH, Langerwehe, Germany; 10→90% MeCN in H_2O + 0.1% TFA in 15 min). (**c**) Mass spectrum of [natLu]Lu-(*R*)-DOTAGA-rhCCK-16.

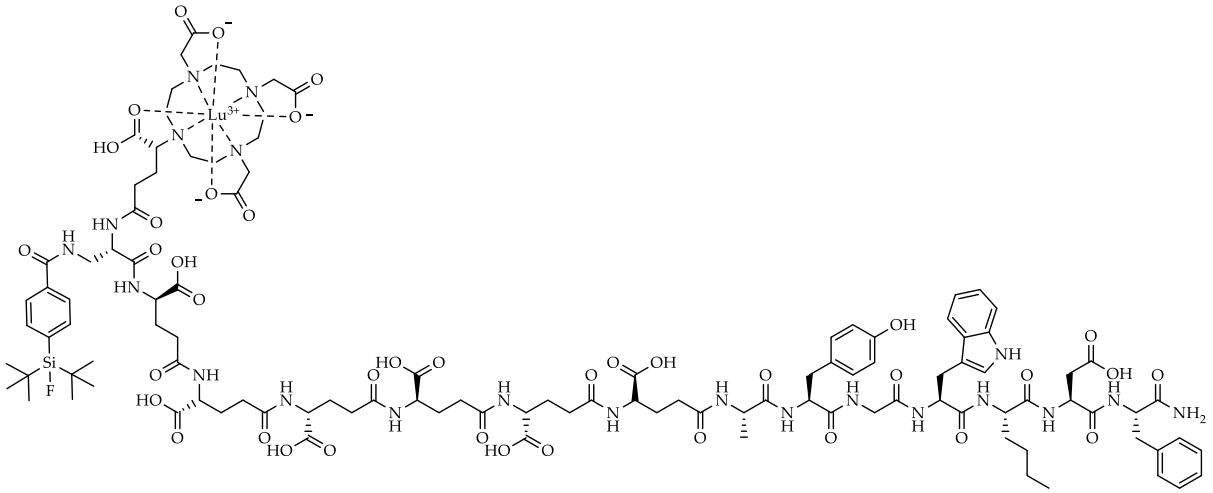

[^{nat}Lu]Lu-(R)-DOTAGA-rhCCK-16: RP-HPLC (10→90% MeCN in H_2O with 0.1% TFA, 15 min, λ = 220 nm): t_R = 9.52 min, K′ = 4.64; MS (ESI, positive): m/z calculated for $C_{111}H_{151}FLuN_{21}O_{39}Si$: 2625.6, found: m/z = 1314.4 $[M+2H]^{2+}$.

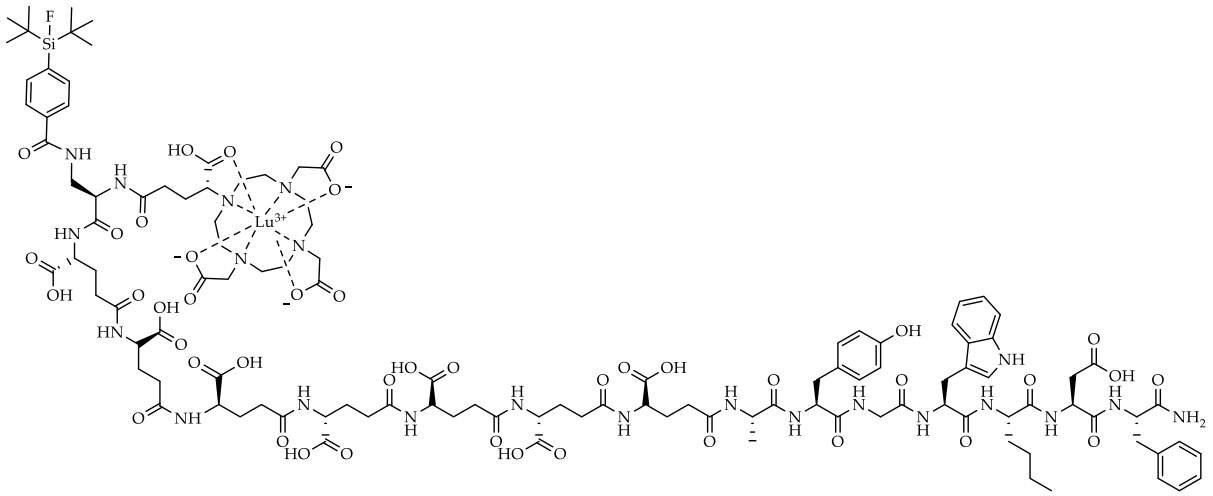

[^{nat}Lu]Lu-(R)-DOTAGA-rhCCK-17: RP-HPLC (10→90% MeCN in H_2O with 0.1% TFA, 15 min, λ = 220 nm): t_R = 9.48 min, K′ = 4.62; MS (ESI, positive): m/z calculated for $C_{116}H_{158}FLuN_{22}O_{42}Si$: 2754.7, found: m/z = 1377.7 $[M+2H]^{2+}$.

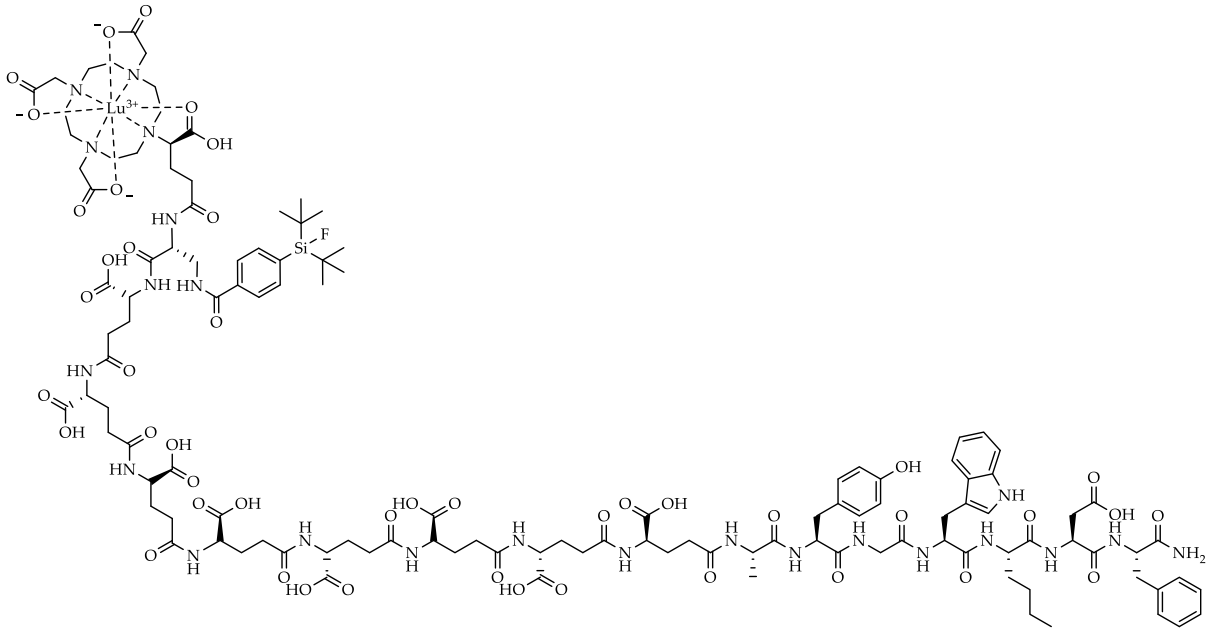

[^{nat}Lu]Lu-(R)-DOTAGA-rhCCK-18: RP-HPLC (10→90% MeCN in H_2O with 0.1% TFA, 15 min, λ = 220 nm): t_R = 9.50 min, K' = 4.63; MS (ESI, positive): m/z calculated for $C_{121}H_{165}FLuN_{23}O_{45}Si$: 2883.8, found: m/z = 1443.1 $[M+2H]^{2+}$.

^{177}Lu-labelling

For ^{177}Lu-labelling experiments, [^{177}Lu]$LuCl_3$ dissolved in hydrochloric acid (0.04 M, 40 GBq/mL) was acquired from *ITM Isotope Technologies Munich SE* (Garching, Germany). Radiolabelling of the peptide precursor (1 nmol) was performed at 90 °C for 15 min in a NaOAc-buffered (1 M, pH = 5.5) hydrochloric acid (0.04 M) solution. After radiolabelling, a radiolysis quencher (sodium ascorbate, 1 M in H_2O) was added and radiochemical purity was determined via radio-RP-HPLC and radio-TLC (instant thin layer chromatography paper impregnated with silica gel (iTLC-SG, *Agilent Technologies Inc.*, Folsom, United States); sodium citrate*1.5 H_2O (0.1 M)).

***In Vitro* Experiments**

Cell Culture. CCK-2R expressing rat pancreatic cancer cells AR42J (*CLS GmbH,* Eppelheim, Germany) were cultivated in monolayers in CELLSTAR® cell culture flasks acquired from *Greiner Bio-One GmbH* (Frickenhausen, Germany) at 37 °C in a humidified atmosphere (5% CO_2) using a HERAcell 150i-Incubator (*Thermo Fisher Scientific Inc.*, Waltham, United States). As nutrient medium RPMI 1640 medium, supplemented with 5 mM L-Gln 5 mL non-essential amino acids (100×) and 10% FCS, was used. Furthermore, a Dulbecco's PBS solution with 0.1% EDTA (*v*/*v*) was applied to detach the cells for cell passaging. The detached cells were counted using a Neubauer hemocytometer (*Paul Marienfeld*, Lauda-Königshofen, Germany). In addition, all operations under sterile conditions were accomplished using a MSC-Advantage safety workbench (*Thermo Fisher Scientific Inc*., Waltham, United States).

Determination of IC_{50}. AR42J cells (2.0×10^5 cells/well) were seeded into 24-well plates 24 ± 2 h prior to testing, using 1 mL of nutrient medium (RPMI 1640, 5 mM L-Gln, 5 mL non-essential amino acids (100×), 10% FCS). Cells were incubated at 37 °C in a humidified atmosphere (5% CO_2).
After removal of the medium, each well was washed with 500 µL PBS. For the cell-based assay, 200 µL of nutrient medium (+5% BSA), [^{177}Lu]Lu-DOTA-PP-F11N (25 µL, 0.3 pmol) as a radiolabeled reference and 25 µL of the peptide of interest in increasing concentrations (10^{-10} to 10^{-4} M) in triplicate were added to the cells. Thereafter, the assay was incubated for 3 h at 37 °C and thereafter, the supernatant was collected. The cells were washed with 300 µL PBS and the collected supernatant fractions were unified. After lysis of the cells with NaOH (300 µL, 1 N) for 15 min, the respective wells were washed with NaOH (300 µL, 1 N) and both fractions were unified. The radioactivity of both, the supernatant and the lysed fractions was quantified using a γ-counter (*PerkinElmer Inc.,* Waltham, United States). The obtained data were evaluated *via* the GraphPad PRISM software (*GraphPad Software Inc*., La Jolla, United States), which calculates the halfmaximal inhibitory concentration (IC_{50}) of the peptides.

Internalisation Studies. For the determination of the internalisation kinetics of the various peptides, AR42J cells (3.0×10^5 cells/well) were seeded into polylysine coated 24-well plates adding 1 mL of nutrient medium. Afterwards, the cells were incubated for 24 ± 2 h at 37 °C in a humidified atmosphere (5% CO_2).
On the day of the experiment, the medium was removed, and each well was washed with nutrient medium (300 µL). Afterwards 200 µL of nutrient medium, 25 µL of the ^{177}Lu-labeled peptide (0.3 pmol, $n = 6$) and either 25 µL of nutrient medium for internalisation studies ($n = 3$) or 25 µL of [^{nat}Lu]Lu-DOTA-PP-F11N (10 µmol) for competition studies ($n = 3$) were added. Thereafter, the assay was incubated for various time points (1, 2, 4and 6 h) at 37 °C in a humidified atmosphere (5% CO_2). After incubation, the cells were put on ice for at least 1 min to stop internalisation kinetics and the supernatant was collected. Then, the cells were washed with an ice-cold nutrient medium (300 µL) and both fractions were unified. For the acid wash, 300 µL of an ice-cold glycine buffer (1 M, p1 M, pAfter lysis of the cells with NaOH (300 µL, 1 N) for 15 min, the respective wells were washed with NaOH (300 µL, 1 N) and both fractions were unified. The radioactivity of the supernatant, the acid wash and the lysed fractions were quantified using a γ-counter.

Table S1. Affinity and lipophilicity data of the compounds evaluated. Affinity data were determined on AR42J cells (2.0×10^5 cells/well) and [^{177}Lu]Lu-DOTA-PP-F11N (0.3 pmol/well) as radiolabeled reference (3 h, 37 °C, RPMI 1640, 5 mM L-Gln, 5 mL non-essential amino acids (100×), 10% FCS + 5% BSA (*v*/*v*)).

peptide	IC_{50} [nM]	log$D_{7.4}$
[$^{nat/177}$Lu]Lu-DOTA-PP-F11N	12.8 ± 2.8	−4.75 ± 0.07
[$^{nat/177}$Lu]Lu-DOTA-PP-γ-F11N	7.55 ± 0.48	−4.38 ± 0.05
[$^{nat/177}$Lu]Lu-CP04	11.2 ± 0.2	−3.80 ± 0.10
[$^{nat/177}$Lu]Lu-γ-CP04	8.88 ± 0.67	−4.30 ± 0.08
[$^{nat/177}$Lu]Lu-(*R*)-DOTAGA-rhCCK-1	629 ± 48	−1.71 ± 0.10
[$^{nat/177}$Lu]Lu-(*R*)-DOTAGA-rhCCK-2	156 ± 18	−1.95 ± 0.09
[$^{nat/177}$Lu]Lu-(*R*)-DOTAGA-rhCCK-3	156 ± 4	−2.03 ± 0.10
[$^{nat/177}$Lu]Lu-(*R*)-DOTAGA-rhCCK-4	185 ± 14	−2.19 ± 0.08
[$^{nat/177}$Lu]Lu-(*R*)-DOTAGA-rhCCK-5	90.0 ± 2.3	−2.67 ± 0.05
[$^{nat/177}$Lu]Lu-(*R*)-DOTAGA-rhCCK-6	56.8 ± 6.4	−2.22 ± 0.08
[$^{nat/177}$Lu]Lu-(*R*)-DOTAGA-rhCCK-7	75.7 ± 10.7	−2.63 ± 0.08
[$^{nat/177}$Lu]Lu-(*R*)-DOTAGA-rhCCK-8	58.0 ± 11.0	−2.19 ± 0.08
[$^{nat/177}$Lu]Lu-(*R*)-DOTAGA-rhCCK-9	55.3 ± 7.8	−2.84 ± 0.04
[$^{nat/177}$Lu]Lu-(*R*)-DOTAGA-rhCCK-10	863 ± 148	−2.15 ± 0.08
[$^{nat/177}$Lu]Lu-(*R*)-DOTAGA-rhCCK-11	111 ± 13	−2.23 ± 0.07
[$^{nat/177}$Lu]Lu-(*R*)-DOTAGA-rhCCK-12	89.7 ± 14.5	−2.34 ± 0.05
[$^{nat/177}$Lu]Lu-(*R*)-DOTAGA-rhCCK-13	68.5 ± 11.4	−2.57 ± 0.06
[$^{nat/177}$Lu]Lu-(*R*)-DOTAGA-rhCCK-14	51.3 ± 9.3	−2.26 ± 0.05
[$^{nat/177}$Lu]Lu-(*R*)-DOTAGA-rhCCK-15	33.0 ± 11.1	−2.50 ± 0.02
[$^{nat/177}$Lu]Lu-(*R*)-DOTAGA-rhCCK-16	20.4 ± 2.7	−2.54 ± 0.05
[$^{nat/177}$Lu]Lu-(*R*)-DOTAGA-rhCCK-17	29.5 ± 1.9	−2.10 ± 0.06
[$^{nat/177}$Lu]Lu-(*R*)-DOTAGA-rhCCK-18	20.4 ± 2.0	−2.16 ± 0.09

Table S2. Receptor-mediated internalisation values (37 °C, RPMI 1640, 5 mM L-Gln, 5 mL non-essential amino acids (100×), 10% FCS, 0.25 pmol/well) determined as percent (%) of the applied activity of [^{177}Lu]Lu-(*R*)-DOTAGA-rhCCK-9 and -16 as well as the references [^{177}Lu]Lu-DOTA-PP-F11N and [^{177}Lu]Lu-CP04 using AR42J cells (3.0×10^5 cells/well) at different time points (1, 2, 4 and 6 h). Data are corrected for non-specific binding (10 µmol/well, [^{nat}Lu]Lu-DOTA-PP-F11N).

Peptide	Internalisation Values (%)				Internalisation Values* (% of reference)
	1 h	2 h	4 h	6 h	6 h
[^{177}Lu]Lu-DOTA-PP-F11N	6.44 ± 0.32	10.1 ± 0.4	17.5 ± 1.0	22.4 ± 0.6	-
[^{177}Lu]Lu-CP04	5.16 ± 0.44	9.33 ± 0.36	15.4 ± 0.7	20.5 ± 0.5	91.6 ± 2.4
[^{177}Lu]Lu-(*R*)-DOTAGA-rhCCK-9	2.08 ± 0.12	3.44 ± 0.55	8.01 ± 0.53	13.2 ± 0.5	65.7 ± 2.5
[^{177}Lu]Lu-(*R*)-DOTAGA-rhCCK-16	7.63 ± 0.13	14.0 ± 1.3	23.2 ± 2.7	32.2 ± 2.1	135 ± 9

* Internalisation values are depicted as % of the reference [^{177}Lu]Lu-DOTA-PP-F11N

Table S3. Total cell uptake (37 °C, RPMI 1640, 5 mM L-Gln, 5 mL non-essential amino acids (100×), 10% FCS, 0.25 pmol/well) determined as percent (%) of the applied activity of [^{177}Lu]Lu-(*R*)-DOTAGA-rhCCK-9 and -16 as well as the references [^{177}Lu]Lu-DOTA-PP-F11N and [^{177}Lu]Lu-CP04 using AR42J cells (3.0×10^5 cells/well) at different time points (1, 2, 4 and 6 h). Data are corrected for non-specific binding (10 μmol/well, [^{nat}Lu]Lu-DOTA-PP-F11N).

Peptide	**Total cell uptake** (%)			
	1 h	**2 h**	**4 h**	**6 h**
[^{177}Lu]Lu-DOTA-PP-F11N	7.03 ± 1.45	10.6 ± 1.5	18.5 ± 2.5	23.5 ± 1.4
[^{177}Lu]Lu-CP04	6.00 ± 0.42	10.0 ± 0.4	16.5 ± 0.9	20.4 ± 1.7
[^{177}Lu]Lu-(*R*)-DOTAGA-rhCCK-9	2.25 ± 0.23	3.46 ± 0.56	8.31 ± 0.59	13.4 ± 0.7
[^{177}Lu]Lu-(*R*)-DOTAGA-rhCCK-16	8.37 ± 0.07	14.4 ± 1.3	23.6 ± 2.8	32.8 ± 2.3

Table S4. Biodistribution data of [^{177}Lu]Lu-DOTA-PP-F11N, [^{177}Lu]Lu-(*R*)-DOTAGA-rhCCK-9 and [^{177}Lu]Lu-(*R*)-DOTAGA-rhCCK-16 in selected organs at 24 h p.i. in AR42J tumour-bearing CB17-SCID mice (100 pmol each). Data are expressed as %ID/g, mean ± SD.

Organ	**[^{177}Lu]Lu-DOTA-PP-F11N** *(n = 4)*	**[^{177}Lu]Lu-(*R*)-DOTAGA-rhCCK-9** *(n = 4)*	**[^{177}Lu]Lu-(*R*)-DOTAGA-rhCCK-16** *(n = 4)*	**[^{177}Lu]Lu-(*R*)-DOTAGA-rhCCK-16 competition studies** *(n = 2)*
Blood	0.00 ± 0.00	0.02 ± 0.00	0.01 ± 0.00	0.05 ± 0.00
Heart	0.02 ± 0.01	0.09 ± 0.03	0.11 ± 0.01	0.13 ± 0.01
Lung	0.03 ± 0.02	0.10 ± 0.05	0.09 ± 0.02	2.59 ± 1.27
Liver	0.67 ± 0.64	1.07 ± 0.54	1.18 ± 0.27	2.31 ± 0.66
Spleen	0.07 ± 0.03	0.70 ± 0.69	0.62 ± 0.03	1.73 ± 0.01
Pancreas	0.05 ± 0.01	0.31 ± 0.20	0.39 ± 0.12	0.20 ± 0.01
Stomach	0.36 ± 0.05	1.80 ± 0.37	3.51 ± 0.50	0.15 ± 0.04
Intestine	0.04 ± 0.02	0.26 ± 0.04	0.20 ± 0.04	0.16 ± 0.03
Kidney	3.08 ± 0.51	84.4 ± 22.7	85.5 ± 11.3	105 ± 21
Adrenal	0.03 ± 0.03	0.45 ± 0.30	1.49 ± 1.50	0.40 ± 0.11
Muscle	0.00 ± 0.00	0.03 ± 0.01	0.05 ± 0.01	0.06 ± 0.04
Bone	0.03 ± 0.01	0.82 ± 0.42	0.17 ± 0.02	0.24 ± 0.04
Tumour	1.88 ± 0.82	6.40 ± 1.48	15.70 ± 3.27	0.91 ± 0.04

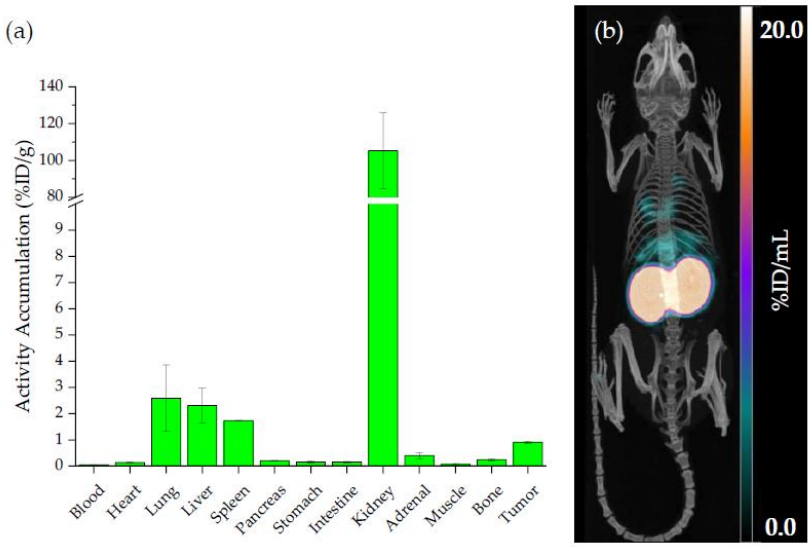

Figure S4. (**a**) Biodistribution of [^{177}Lu]Lu-DOTA-rhCCK-16 (100 pmol) co-injected with [^{nat}Lu]Lu-DOTA-MGS5 (40 nmol) in selected organs (%ID/g) at 24 h p.i. in AR42J tumour-bearing CB17-SCID mice. Data is expressed as mean ± SD ($n = 2$). (**b**) Representative μSPECT/CT images of [^{177}Lu]Lu-DOTA-rhCCK-16 co-injected with [^{nat}Lu]Lu-DOTA-MGS5 (40 nmol) at 24 h p.i. in AR42J tumour-bearing CB17- SCID mice.

2.2 Development of the First ^{18}F-Labeled Radiohybrid-Based Minigastrin Derivative with High Target Affinity and Tumor Accumulation by Substitution of the Chelating Moiety

Reprint Permission:

pharmaceutics

MDPI

Article

Development of the First ^{18}F-Labeled Radiohybrid-Based Minigastrin Derivative with High Target Affinity and Tumor Accumulation by Substitution of the Chelating Moiety

Thomas Günther [1,*,†], Nadine Holzleitner [1,†], Daniel Di Carlo [1], Nicole Urtz-Urban [1], Constantin Lapa [2] and Hans-Jürgen Wester [1]

[1] Pharmaceutical Radiochemistry, Technical University of Munich, 85748 Garching, Germany
[2] Nuclear Medicine, Faculty of Medicine, University of Augsburg, 86156 Augsburg, Germany
* Correspondence: thomas.guenther@tum.de
† These authors contributed equally to this work.

Abstract: In order to optimize elevated kidney retention of previously reported minigastrin derivatives, we substituted (*R*)-DOTAGA by DOTA in (*R*)-DOTAGA-rhCCK-16/-18. CCK-2R-mediated internalization and affinity of the new compounds were determined using AR42J cells. Biodistribution and μSPECT/CT imaging studies at 1 and 24 h p.i. were carried out in AR42J tumor-bearing CB17-SCID mice. Both DOTA-containing minigastrin analogs exhibited 3- to 5-fold better IC_{50} values than their (*R*)-DOTAGA-counterparts. ^{nat}Lu-labeled peptides revealed higher CCK-2R affinity than their ^{nat}Ga-labeled analogs. In vivo, tumor uptake at 24 h p.i. of the most affine compound, [^{19}F]F-[^{177}Lu]Lu-DOTA-rhCCK-18, was 1.5- and 13-fold higher compared to its (*R*)-DOTAGA derivative and the reference compound, [^{177}Lu]Lu-DOTA-PP-F11N, respectively. However, activity levels in the kidneys were elevated as well. At 1 h p.i., tumor and kidney accumulation of [^{19}F]F-[^{177}Lu]Lu-DOTA-rhCCK-18 and [^{18}F]F-[^{nat}Lu]Lu-DOTA-rhCCK-18 was high. We could demonstrate that the choice of chelators and radiometals has a significant impact on CCK-2R affinity and thus tumor uptake of minigastrin analogs. While elevated kidney retention of [^{19}F]F-[^{177}Lu]Lu-DOTA-rhCCK-18 has to be further addressed with regard to radioligand therapy, its radiohybrid analog, [^{18}F]F-[^{nat}Lu]Lu-DOTA-rhCCK-18, might be ideal for positron emission tomography (PET) imaging due to its high tumor accumulation at 1 h p.i. and the attractive physical properties of fluorine-18.

Keywords: cholecystokinin-2 receptor (CCK-2R); cholecystokinin-B receptor (CCK-BR); MTC; ^{18}F-labeled minigastrin analogs; radiohybrid; rhCCK

Citation: Günther, T.; Holzleitner, N.; Di Carlo, D.; Urtz-Urban, N.; Lapa, C.; Wester, H.-J. Development of the First ^{18}F-Labeled Radiohybrid-Based Minigastrin Derivative with High Target Affinity and Tumor Accumulation by Substitution of the Chelating Moiety. *Pharmaceutics* **2023**, *15*, 826. https://doi.org/10.3390/pharmaceutics15030826

Academic Editor: Leonard I. Wiebe

Received: 13 January 2023
Revised: 25 February 2023
Accepted: 28 February 2023
Published: 3 March 2023

1. Introduction

In 2022, an estimated number of 43,800 new thyroid cancer cases will occur in the United States [1]. Out of these, medullary thyroid carcinoma (MTC) comprises only 2–3% and thus rarely occurs. However, due to comparably late tumor detection in advanced stages and limited treatment options of this disease, the 5- and 10-year survival of MTC (65–89% and 71–87%, respectively) is lower compared to that of the more common types of differentiated thyroid cancer [2,3]. The 10-year survival rate for patients developing metastatic MTC is only 10%, which underlines the importance of an early diagnosis as well as novel therapeutic options [4].

In contrast to conventional diagnostic methodologies, nuclear medicine provides an opportunity to exhibit biochemical information through non-invasive molecular imaging applications. Amongst other uses, this allows for the localization of tumor lesions and metastases because most malignant cells overexpress certain target structures that can be addressed by radiopharmaceutical drugs. In the case of MTC, over 90% of tumors overexpress the cholecystokinin-2 receptor (CCK-2R) in high density [5]. In spite of this characteristic, the gold standard for MTC imaging is ^{18}F-based positron emission tomography (PET) using

[^{18}F]F-DOPA (3,4-dihydroxy-6-[^{18}F]fluoro-L-phenylalanine) instead of a CCK-2R-targeted compound [6]. This can be attributed to the lack of an efficient ^{18}F-labeled CCK-2R-targeted compound, which could combine the favorable properties of fluorine-18 and PET alongside targeting the CCK-2R, as well as the fact that [^{18}F]F-DOPA is already clinically established for neuroimaging [7–9]. Because [^{18}F]F-DOPA is trapped in neuroendocrine tumor cells such as MTC due to the availability of an excess of aromatic L-amino acid decarboxylase (AADC) in these cells [7,10,11], a sensitivity of 86% was observed for primary MTC [12]. However, only moderate sensitivity was determined for [^{18}F]F-DOPA-PET in both lymph node metastases and distant metastases [10,13].

In 2021, Khan et al. reported the first attempts to introduce scaffolds into the peptide structure of the CCK-2R-targeting minigastrin analog MG11 (glu-Ala-Tyr-Gly-Trp-Met-Asp-Phe-NH_2) that enables direct radiofluorination via a nucleophilic aromatic substitution of a nitro group by [^{18}F]fluoride (K_2CO_3, kryptofix 2.2.2, azeotropic drying). However, rapid de-fluorination due to the poor chemical stability of these compounds was observed, which illustrates the need for optimized alternatives [14]. In addition, the earlier studies of Good et al. demonstrated a poor metabolic stability for MG11 in vivo [15,16], aggravating the use of this basic structure as a scaffold for radiopharmaceuticals, which is why alternative strategies are desired.

In a previous study, we addressed this topic by introducing a silicon-based fluoride acceptor (SiFA) moiety into the peptide structure of DOTA-PP-F11N, a minigastrin analog that is currently in clinical trials. However, one of the biggest limitations of [^{177}Lu]Lu-DOTA-PP-F11N represents its high hydrophilicity and thus fast clearance kinetics [17]. In contrast, the introduction of the SiFA building block enables facile ^{18}F-labeling via an isotopic exchange reaction, which is chemically stable [18]. Conversly, the highly lipophilic SiFA moiety compensates for the high hydrophilic character of the peptide. The presence of a SiFA and a chelator moiety within the same molecule allows for either ^{18}F- or ^{177}Lu-labeling generating chemically identical agents, which are called radiohybrids (rh). Previous rhCCK derivatives, [^{19}F]F-[^{177}Lu-]Lu-(*R*)-DOTAGA-rhCCK-9 and -16, revealed 3- to 8-fold increased activity levels in the tumor compared to [^{177}Lu]Lu-DOTA-PP-F11N at 24 h p.i., respectively, despite a noticeably lower CCK-2R affinity. Nevertheless, activity uptake and retention in the kidneys was substantially elevated, which was likely due to the numerous negative charges in proximity to the SiFA moiety [19].

Hence, in this study, we wanted to maintain high activity levels in the tumor while reducing elevated kidney retention. Because we aimed to retain the peptide structure (*H*-(γ-glu)$_{6–8}$-Ala-Tyr-Gly-Trp-Nle-Asp-Phe-NH_2), we only substituted (*R*)-DOTAGA (2-(4,7,10-tris(carboxymethyl)-1,4,7,10-tetraazacyclododecan-1-6yl)pentanedioic acid) by the DOTA (1,4,7,10-tetraazacyclododecane-1,4,7,10- tetraacetic acid) chelator to reduce the negative charge distribution in the direct neighborhood to the SiFA moiety. The resulting analogs (Figure 1) were evaluated by state-of-the-art experiments (IC_{50}, log$D_{7.4}$, receptor-mediated internalization, biodistribution and imaging studies).

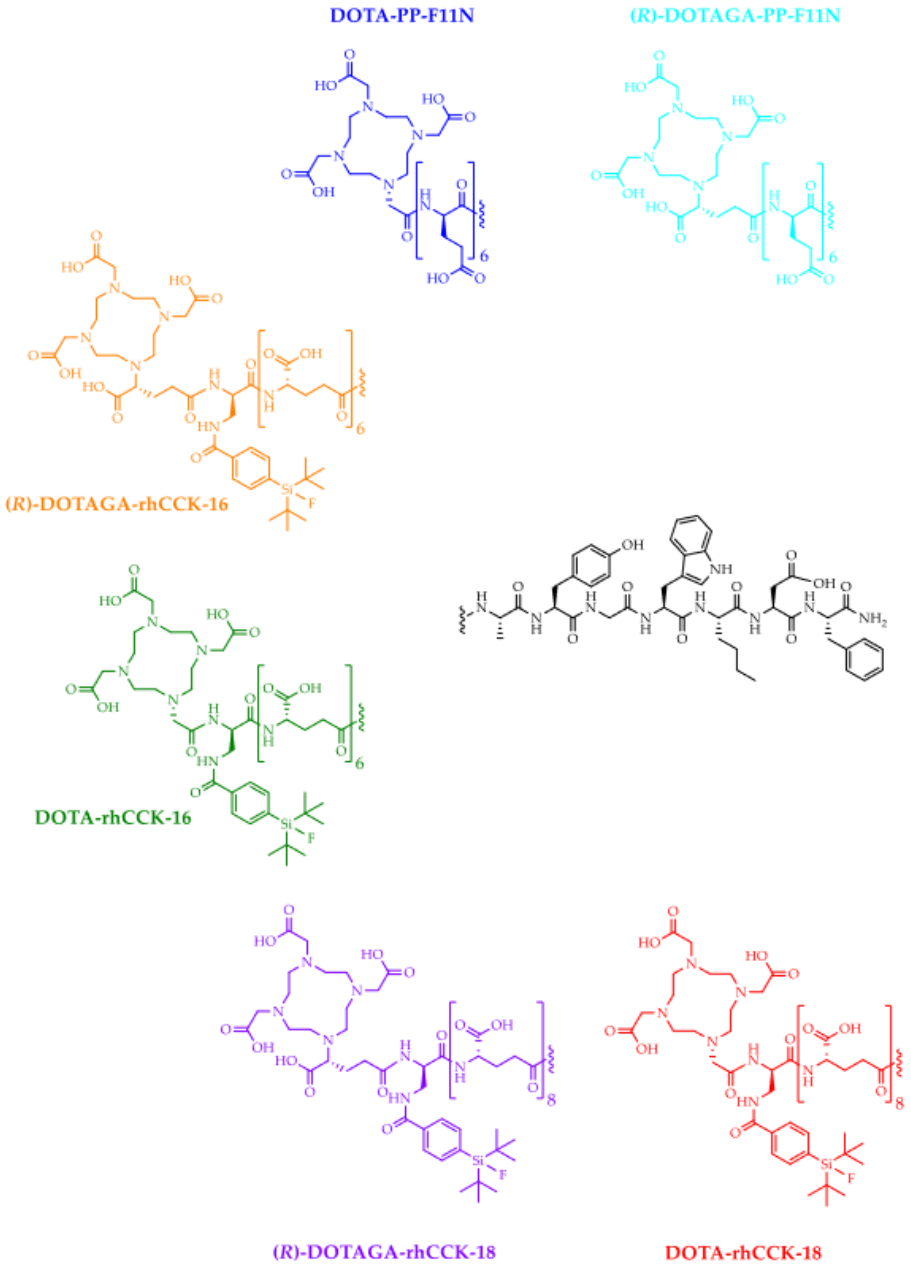

Figure 1. Chemical structures of the (*R*)-DOTAGA- and DOTA-comprising minigastrin analogs evaluated in this study.

2. Materials and Methods

Characterization of all CCK-2R-targeted compounds is provided in the Supplementary Materials (Figures S1–S17). Electrospray ionization mass spectrometry for characterization of the substances were acquired on an expression^{L} CMS mass spectrometer (Advion Ltd., Harlow, UK).

2.1. Chemical Synthesis and Labeling Procedures

Synthesis of all compounds was conducted via standard Fmoc-based solid phase peptide synthesis (SPPS) on a *H*-Rink Amide ChemMatrix® resin (35–100 mesh particle size, 0.4–0.6 mmol/g loading, Merck KGaA, Darmstadt, Germany) either manually or with a Liberty Blue peptide synthesizer (*H*-Rink Amide ProTide resin, 100–200 mesh particle size, 0.6–0.8 mmol/g loading, CEM GmbH, Stuttgart, Germany). Purification of the peptide precursors was carried out by reversed-phase high-performance liquid chromatog-

raphy (RP-HPLC). Labeling with [$^{nat/177}$Lu]lutetium or [^{nat}Ga]gallium was performed as previously published [20,21]. A detailed description of ^{18}F-labeling is provided in the Supplementary Materials. Briefly, ^{18}F-fluorination of [^{nat}Lu]Lu-DOTA-rhCCK-18 (1 nmol) was conducted via an isotopic exchange reaction at the SiFA building block at 60°C for 5 min using previously dried [^{18}F]fluoride (approx. 400 MBq). Afterwards, the ^{18}F-labeled peptide was purified via an Oasis® HLB (30 mg) Light Cartridge (Waters GmbH, Eschborn, Germany).

2.2. In Vitro Experiments

Cell-based experiments and determination of lipophilicity (log$D_{7.4}$) were performed as previously published [19]. A detailed description of the in vitro experiments is provided in the Supplementary Materials.

Human serum albumin (HSA) binding was determined in analogy to a previously published ultracentrifugation method [22]. Therefore, the peptides of interest were incubated in a solution of HSA (700 µM in phosphate-buffered saline) at 37 °C for 30 min (n = 6). All values were corrected for unspecific binding.

In vitro stability studies in human serum after incubation at 37 °C for 24 h were performed as described in the Supplemental Material.

2.3. In Vivo Experiments

All animal experiments were conducted in accordance with general animal welfare regulations in Germany (German animal protection act, in the edition of the announcement, dated 18 May 2006, as amended by Article 280 of 19 June 2020, approval no. ROB-55.2-1-2532.Vet_02-18-109 by the General Administration of Upper Bavaria) and the institutional guidelines for the care and use of animals. CB17-SCID mice of both genders and aged 2–12 months (Charles River Laboratories International Inc., Sulzfeld, Germany) were allowed to acclimate at the in-house animal facility for at least one week before inoculation was performed. Tumor xenografts were established as previously reported [19]. Exclusion criteria for animals from an experiment were either weight loss higher than 20%, a tumor size above 1500 mm^3, an ulceration of the tumor, respiratory distress or a change of behavior. None of these criteria applied to any animal from the experiment. Neither randomization nor blinding was applied in the allocation of the experiments. Health status is SPF according to FELASA recommendation.

Biodistribution studies (n = 4) and μSPECT/CT as well as μPET/CT imaging (using a MILabs VECTor^4 small-animal SPECT/PET/OI/CT device, MILabs, Utrecht, The Netherlands) at 1 and 24 h p.i. were carried out as previously published [19,23]. For all ^{177}Lu-labeled compounds, approximately 2–3 MBq (100 pmol)—and for the ^{18}F-labeled analog, approximately 7 MBq (100 pmol)—were administered. For all competition studies, 2.90 mg/kg (40 nmol) of [^{nat}Lu]Lu-DOTA-MGS5 (10^{-3} M in phosphate-buffered saline) were co-administered.

Acquired data were statistically analyzed by performing a Student's t-test via Excel (Microsoft Corporation, Redmond, WA, USA) and OriginPro software (version 9.7) from OriginLab Corporation (Northampton, MA, USA). Acquired p values of <0.05 were considered statistically significant.

3. Results

3.1. Synthesis and Radiolabeling

The precursors were synthesized via standard Fmoc-based SPPS with subsequent RP-HPLC purification in yields of 5–20% (chemical purity >95%, determined by RP-HPLC at λ = 220 nm). Labeling with [^{nat}Lu]lutetium as well as [^{nat}Ga]gallium was achieved in quantitative yields using a 2.5-fold excess of $LuCl_3$ and $Ga(NO_3)_3$, respectively. No purification step was performed because an excess of free ions was not shown to have any impact on overall affinity data [23]. All compounds were labeled manually with lutetium-177, resulting in quantitative radiochemical yields and purities (RCYs, RCPs) and molar activities (A_m) of 10–50 GBq/µmol. After radiolabeling, no further purification steps

were conducted. ^{18}F-Labeling of [^{nat}Lu]Lu-DOTA-rhCCK-18 was performed manually at 60°C for 5 min. After purification of the ^{18}F-labeled peptide via an Oasis® HLB (30 mg) Light Cartridge, RCYs (without further optimization) of 10–30% and molar activities of A_m ~85 GBq/μmol and RCPs > 95% were achieved.

3.2. In Vitro Characterization

The affinity data of all compounds evaluated are outlined in Figure 2 and Table S1.

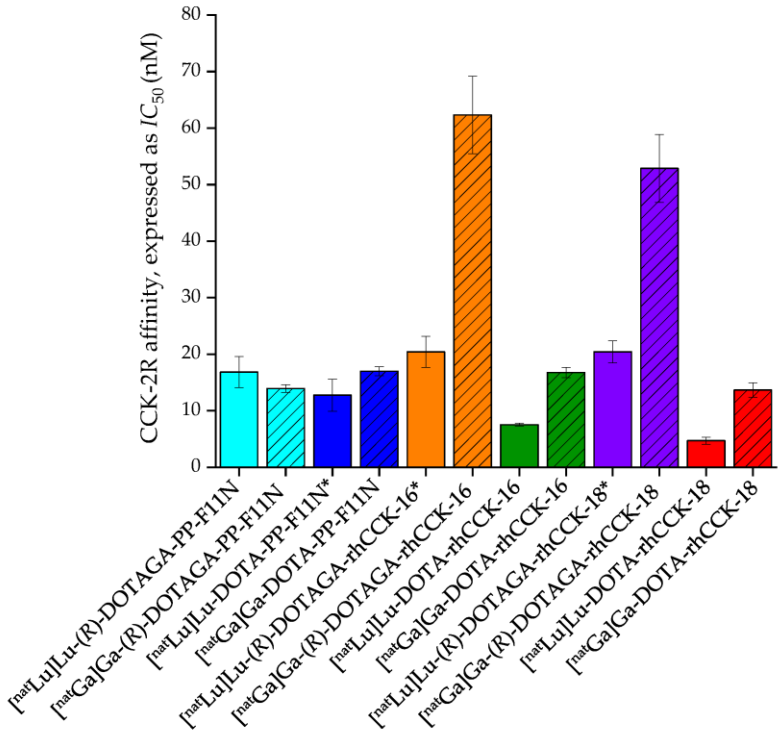

Figure 2. CCK-2R affinity (expressed as IC_{50}) of the reference compound DOTA-PP-F11N in comparison to rhCCK-16 and -18 containing either a DOTA or (*R*)-DOTAGA moiety labeled either with [^{nat}Ga]gallium (hatched bars) or [^{nat}Lu]lutetium. IC_{50} values were determined using AR42J cells (2.0×10^5 cells per well) and [^{177}Lu]Lu-DOTA-PP-F11N (0.3 pmol/well) as the radiolabeled reference (3 h, 37°C, RPMI 1640, 5 mM L-Gln, 5 mL non-essential amino acids (100×), 10% fetal calf serum (FCS) + 5% bovine serum albumin (BSA) (*v*/*v*)). * data taken from Holzleitner et al. [19]. These data have been determined in our lab under identical conditions.

In comparison to their (*R*)-DOTAGA-comprising counterparts, all DOTA-containing ligands revealed lower IC_{50} values, except for [^{nat}Ga]Ga-(*R*)-DOTAGA-PP-F11N. Furthermore, the ^{nat}Lu-labeled compounds exhibited higher CCK-2R affinity than their ^{nat}Ga-labeled derivatives, except for [^{nat}Ga]Ga-(*R*)-DOTAGA-PP-F11N. Overall, [^{nat}Lu]Lu-DOTA-rhCCK-18 exhibited the highest CCK-2R affinity among all compounds, and its IC_{50} value was 2-fold lower compared to the reference, [^{nat}Lu]Lu-DOTA-PP-F11N.

Lipophilicity (log$D_{7.4}$) and human serum albumin (HSA) binding data are summarized in Table 1.

In general, all compounds containing a (*R*)-DOTAGA chelator revealed a significantly higher lipophilicity than their DOTA-comprising counterparts ($p < 0.002$). Furthermore, all rhCCK derivatives that comprise a SiFA moiety displayed a distinctly higher lipophilicity (log$D_{7.4} > -2.7$) compared to the reference, [^{177}Lu]Lu-DOTA-PP-F11N, and its (*R*)-DOTAGA-containing analog (log$D_{7.4} < -4.0$, $p < 0.001$). Similar log$D_{7.4}$ values were found for the chemically identical compounds [^{19}F]F-[^{177}Lu]Lu-DOTA-rhCCK-18 and [^{18}F]F-[^{nat}Lu]Lu-DOTA-rhCCK-18 ($p > 0.22$). In addition, HSA binding was observed to be increased for [^{177}Lu]Lu-DOTA-rhCCK-16 (89.1%) compared to [^{177}Lu]Lu-DOTA-rhCCK-18 (62.6%).

Table 1. Lipophilicity (log$D_{7.4}$) and HSA binding data of the ^{177}Lu-labeled peptides.

Compound	Log$d_{7.4}$	HSA Binding (%)
[^{177}Lu]Lu-DOTA-PP-F11N	−4.75 ± 0.07	n.d.
[^{177}Lu]Lu-(*R*)-DOTAGA-PP-F11N	−3.95 ± 0.06	n.d.
[^{177}Lu]Lu-DOTA-rhCCK-16	−2.70 ± 0.09	89.1%
[^{177}Lu]Lu-(*R*)-DOTAGA-rhCCK-16 *	−2.54 ± 0.05	n.d.
[^{19}F]F-[^{177}Lu]Lu-DOTA-rhCCK-18	−2.69 ± 0.06	62.6%
[^{18}F]F-[^{nat}Lu]Lu-DOTA-rhCCK-18	−2.71 ± 0.04	n.d.
[^{177}Lu]Lu-(*R*)-DOTAGA-rhCCK-18 *	−2.16 ± 0.09	n.d.

* data taken from Holzleitner et al. [19]. These data have been determined in our lab under identical conditions, n.d.: not determined.

For the ^{177}Lu-labeled compounds rhCCK-16 and -18 containing either DOTA or (*R*)-DOTAGA as chelator, internalization studies were performed at different time points and compared to [^{177}Lu]Lu-DOTA-PP-F11N (Figure 3, Table S2).

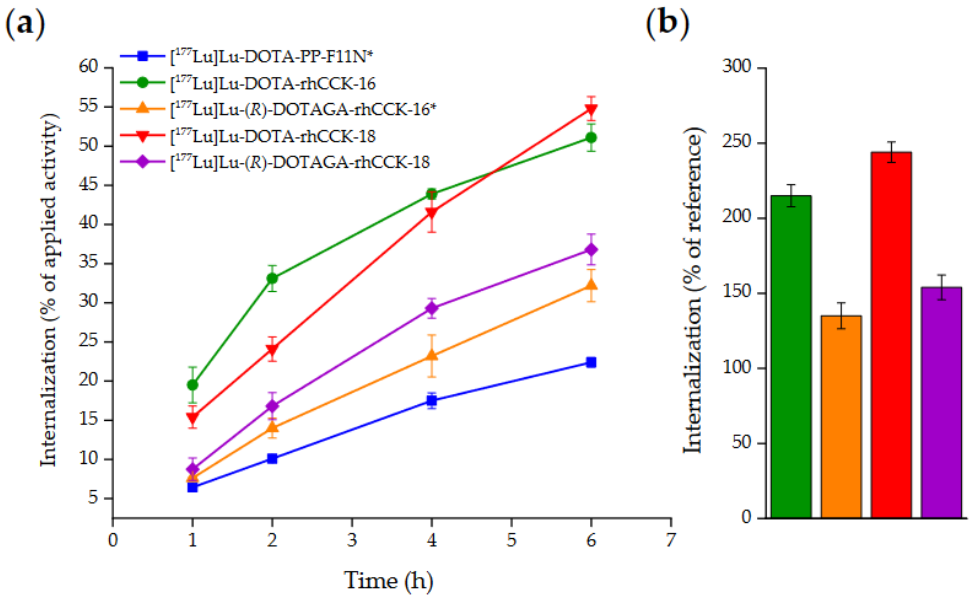

Figure 3. (**a**) CCK-2R-mediated internalization (0.25 pmol/well) measured on AR42J cells as percent (%) of applied activity (incubation at 37 °C for 1, 2, 4 and 6 h, RPMI 1640, 5 mm L-Gln, 5 mL non-essential amino acids (100×), 10% FCS + 5% BSA (*v*/*v*), 3.0 × 10^5 cells/mL/well). (**b**) CCK-2R-mediated internalization of [^{177}Lu]Lu-DOTA-rhCCK-16 (green), [^{177}Lu]Lu-(*R*)-DOTAGA-rhCCK-16 (orange), [^{177}Lu]Lu-DOTA-rhCCK-18 (red) and [^{177}Lu]Lu-DOTA-rhCCK-16 (violet) after incubation at 37 °C for 6 h as percent of reference (% of [^{177}Lu]Lu-DOTA-PP-F11N). * data taken from Holzleitner et al. [19]. These data have been determined in our lab under identical conditions.

In general, all compounds demonstrated increasing internalization values on AR42J cells over time, while [^{177}Lu]Lu-DOTA-rhCCK-16 and -18 exhibited a significantly higher internalization than their (*R*)-DOTAGA analogs and [^{177}Lu]Lu-DOTA-PP-F11N at all time points ($p < 0.001$).

Stability studies on [^{67}Ga]Ga-DOTA-rhCCK-16 and -18 as well as [^{177}Lu]Lu-DOTA-rhCCK-16 and -18 in human serum (incubation at 37 °C for 24 h) revealed two major signals (Δt_R ~ 2 min) for each derivative (Figure S18, Table S3). While the latter signal displays the amount of the respective intact compound (21–44%), the former was attributed to their analogs comprising a hydrolyzed SiFA moiety (SiOH-containing analog, 54–69%). The number of metabolites was <7% for all four derivatives.

3.3. In Vivo Characterization

Due to its favorable in vitro data (highest CCK-2R affinity and internalization, excellent lipophilicity, preferable *HSA binding*), [^{19}F]F-[^{177}Lu]Lu-DOTA-rhCCK-18 was selected for further in vivo studies at 1 and 24 h p.i. (Figure 4, Table S4).

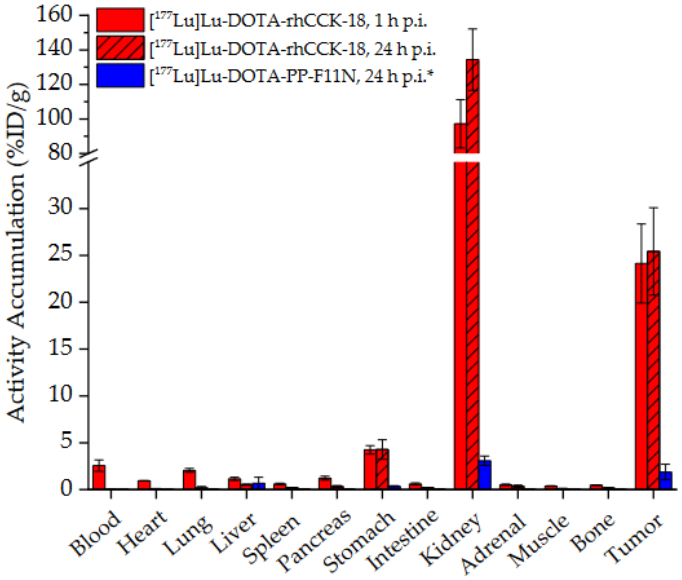

Figure 4. Biodistribution of [^{177}Lu]Lu-DOTA-rhCCK-18 in selected organs (%ID/g) at 1 and 24 h p.i. in comparison to [^{177}Lu]Lu-DOTA-PP-F11N at 24 h p.i. in AR42J tumor-bearing CB17-SCID mice (100 pmol each). Data is expressed as mean ± SD (n = 4). * data taken from Holzleitner et al. [19]. These data have been determined in our lab under identical conditions.

At 1 h p.i., activity levels of 24.1 ± 4.2 %ID/g were found for [^{177}Lu]Lu-DOTA-rhCCK-18 in the AR42J tumor, which remained high over time, and levels of 25.4 ± 4.7 %ID/g were determined at 24 h p.i. ($p > 0.35$). Blood, heart and lung levels were slightly elevated at 1 h p.i. (0.9–2.6 %ID/g), while low levels (<0.2 %ID/g) were observed at 24 h p.i. in these organs ($p < 0.01$). Moreover, increased activity levels were found in the stomach at 1 and 24 h p.i., which was expected due to the endogenous CCK-2R expression in this organ. High kidney uptake was observed at 1 h p.i. for [^{177}Lu]Lu-DOTA-rhCCK-18, which increased over time ($p < 0.03$). In comparison to the reference, [^{177}Lu]Lu-DOTA-PP-F11N, [^{177}Lu]Lu-DOTA-rhCCK-18 exhibited 13-fold increased tumor values at 24 h p.i. ($p = 0.0001$), while kidney values were also 40-fold enhanced ($p < 0.0001$).

μSPECT/CT studies with [^{177}Lu]Lu-DOTA-rhCCK-18 at 1 and 24 h p.i. revealed a low overall background activity at both time points, except for elevated tumor and kidney values (Figure 5, left). Moreover, the chemically identical compound, [^{18}F]F-[^{nat}Lu]Lu-DOTA-rhCCK-18, was evaluated via μPET/CT in a AR42J tumor-bearing mouse (n = 1), which confirmed high tumor and kidney uptake at 1 h p.i. and low overall off-target accumulation (Figure 5, right).

The specificity of the uptake of [^{177}Lu]Lu-DOTA-rhCCK-18 was confirmed via co-injection of excess (2.90 mg/kg, 40 nmol) of [^{nat}Lu]Lu-DOTA-MGS5 (Figure S19).

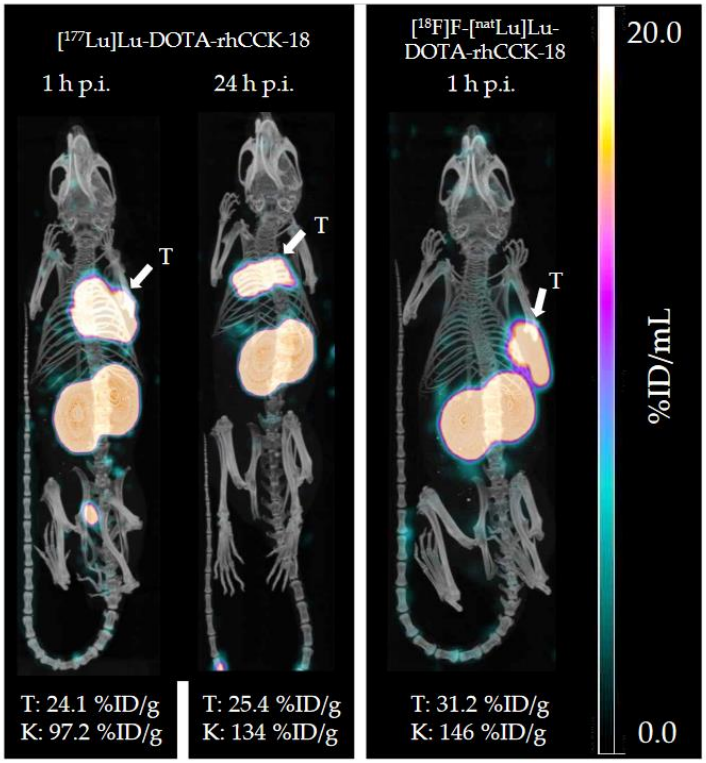

Figure 5. Representative μSPECT/CT images of [^{177}Lu]Lu-DOTA-rhCCK-18 at 1 and 24 h p.i. (**left**) and μPET/CT image of [^{18}F]F-[^{nat}Lu]Lu-DOTA-rhCCK-18 at 1 h p.i. (**right**) in AR42J tumor-bearing CB17- SCID mice (100 pmol each). Tumors (T) are indicated by white arrows. Kidney (K) and tumor (T) values are depicted at the bottom.

4. Discussion

Due to its effective trapping via decarboxylation by the aromatic L-amino acid decarboxylase (AADC), [^{18}F]F-DOPA is a clinically established neuroimaging agent, but can also be used for the detection of neuroendocrine tumors such as medullary thyroid carcinoma (MTC). Although high sensitivities are only observed for the detection of primary MTC lesions, [^{18}F]F-DOPA is still considered the gold standard for MTC imaging in clinical practice [10,24], most likely as a consequence of the favorable properties of ^{18}F-based positron emission tomography (PET) and the lack of reliable alternatives. Notwithstanding that the majority of MTC cells overexpress the cholecystokinin-2 receptor (CCK-2R) in high density, there is currently no CCK-2R-targeted compound available that shows promising pharmacokinetics and bears the possibility of ^{18}F-labeling.

In recent studies, we thus introduced a silicon-based fluoride acceptor (SiFA) moiety into the D-glutamate chain of DOTA-PP-F11N. The resulting radiohybrid (rh)-based compounds enable labeling with both fluorine-18 and radiometals such as lutetium-177 due to the presence of a chelator and a SiFA moiety. We could show that these rhCCK ligands, for example [$^{nat/177}$Lu]Lu-(*R*)-DOTAGA-rhCCK-16, revealed up to 8-fold increased activity levels in the tumor but also approximately 30-fold higher levels in the kidney when compared to [$^{nat/177}$Lu]Lu-DOTA-PP-F11N, despite its distinctly lower CCK-2R affinity [19]. While we assume that the elevated tumor uptake and retention is due to a decelerated clearance of the compound, the charge distribution within the linker section and thus in proximity to the SiFA moiety likely causes the increased kidney values. Hence, the aim of this study was to retain favorable tumor values while reducing the activity levels in the kidneys. Therefore, (*R*)-DOTAGA was substituted by a DOTA chelator in two rhCCK derivatives to reduce the negative charges within the linker section and maintain the peptide sequence to retain high CCK-2R affinity.

Interestingly, substitution of (*R*)-DOTAGA by DOTA in the most affine rhCCK derivatives from previous studies, [^{nat}Lu]Lu-(*R*)-DOTAGA-rhCCK-16 and -18, resulted in 3- to 4-fold lower IC_{50} values for the DOTA-comprising analogs, surpassing even the highly affine reference compound, [^{nat}Lu]Lu-DOTA-PP-F11N (Figure 2). It is thus anticipated that the additional free carboxylic group of the (*R*)-DOTAGA chelator at the respective site has a negative impact on the overall CCK-2R affinity. Similar observations were made for the ^{nat}Ga-labeled rhCCK ligands because the additional free carboxylic group at the Ga-(*R*)-DOTAGA chelate compared to the respective Ga-DOTA chelate as well as the additional free carboxylic group of the Ga-DOTA compared to the respective Lu-DOTA chelate [25–27] led to a decreased overall CCK-2R affinity (Figure 2). Stability studies in human serum did not reveal a lower stability for the [^{67}Ga]Ga-DOTA-rhCCK-16 or -18 as compared to their ^{177}Lu-labeled analogs, which can be thus excluded as a potential reason for the decreased CCK-2R affinity of the ^{nat}Ga-labeled compounds. Interestingly, the stability studies in human serum showed the formation of a slightly more hydrophilic analog (Δt_R ~ 2 min) for all four compounds tested (Figure S18). This was attributed to their corresponding SiOH-containing derivatives, and we suggest that the SiFA building block is hydrolyzed over time under these conditions. In order to confirm this assumption, we performed RP-HPLC analysis of the ^{nat}Ga/^{nat}Lu-labeled SiOH-containing analogs, which were generated by treatment with sodium hydroxide. All four SiOH-containing analogs (peptide identity confirmed by ESI-MS) revealed the same retention time as their respective ^{67}Ga/^{177}Lu-labeled derivative, which was observed after incubation in human serum. Because the SiFA- and their respective SiOH-containing ligands only differ by the atom/group bound to the silicon atom, but the remaining compound is identical, we do not consider this a metabolite but rather an intact compound. Further studies have to be conducted to elucidate whether the SiFA moiety is also hydrolyzed in vivo.

In addition to a lower CCK-2R affinity, all ^{177}Lu-labeled (*R*)-DOTAGA-comprising compounds showed higher log$D_{7.4}$ values than their DOTA-containing analogs (Table 1). Because it was assumed that the negatively charged ^{177}Lu-(*R*)-DOTAGA chelates should be more hydrophilic than the neutral ^{177}Lu-DOTA chelates, further investigations are necessary to understand this dedicated structure–activity relationship. Furthermore, the increased CCK-2R affinity was paralleled by an improved receptor-mediated internalization because both [^{177}Lu]Lu-DOTA-rhCCK-16 and -18 exhibited the highest internalization values at all time points. While the slope of the internalization curves of most compounds decreases after the first hours (Figure 3a), the curve of [^{177}Lu]Lu-DOTA-rhCCK-18 seems to rise with an almost unaffected slope up to the end of the experiment at 6 h. Thus, although this compound initially shows a decelerated internalization rate, its continuous cellular uptake might result in a noticeably higher overall uptake at later time points when compared with the other ligands of this series. Worth mentioning, both [^{177}Lu]Lu-(*R*)-DOTAGA-rhCCK-16 and -18 showed significantly higher internalization values at all time points than [^{177}Lu]Lu-DOTA-PP-F11N despite their significantly lower CCK-2R affinity, which points to a beneficial impact of the SiFA moiety on internalization kinetics.

In vivo, [$^{nat/177}$Lu]Lu-DOTA-rhCCK-18 revealed a 1.5 and 13-fold increased activity uptake in the tumor (25.4 ± 4.7 %ID/g, Figure 4) at 24 h p.i., as compared to the previously published compound, [^{177}Lu]Lu-(*R*)-DOTAGA-rhCCK-16 (15.7 ± 3.3 %ID/g), and the parent peptide, [^{177}Lu]Lu-DOTA-PP-F11N (1.9 ± 0.8 %ID/g), respectively, which can be attributed to its significantly higher CCK-2R affinity and internalization [19]. Consequently, tumor-to-background ratios were higher for [^{177}Lu]Lu-DOTA-rhCCK-18 compared to the previously published compounds (Table S5). Tumor specificity was demonstrated by competition studies using excess of the CCK-2R-specific compound, [^{nat}Lu]Lu-DOTA-MGS5 [28], which led to tumor and stomach values <2 %ID/g. Moreover, the high tumor values obtained for [^{177}Lu]Lu-DOTA-rhCCK-18 demonstrated that the low tumor values for [^{177}Lu]Lu-DOTA-PP-F11N were not caused by an excessive amount of substance (100 pmol per animal) for such a high-affinity ligand.

Similar to previously published rhCCK derivatives [19], tumor and kidney uptake for [^{177}Lu]Lu-DOTA-rhCCK-18 was high at 1 h p.i. and remained high at 24 h p.i. Elevated tumor and stomach retention can be attributed to the decelerated clearance kinetics (higher log$D_{7.4}$ and albumin binding) of the rhCCK ligands and their prolonged bioavailability, the increased kidney retention is likely caused by a synergistic effect of the negatively charged side chains in proximity of the SiFA building block. This assumption is supported by the fact that [^{177}Lu]Lu-DOTA-PP-F11N contains a similar number of negative charges but no SiFA moiety and does not show an enhanced kidney retention. Recent reports demonstrated that SiFA-comprising PSMA inhibitors show a higher albumin binding and thus decelerated clearance kinetics, which results in increased tumor uptake, but also increased kidney retention [21,29], which correlated well with our observations because [^{177}Lu]Lu-DOTA-rhCCK-18 also exhibited an elevated albumin binding in vitro. Furthermore, it was shown that negative charges in the direct neighborhood to the SiFA moiety cause a higher albumin binding and stronger kidney retention, which could explain our results because the rhCCK derivatives contain several negative charges in proximity to the SiFA group. As the substitution of a (*R*)-DOTAGA by a DOTA moiety did not result in lower kidney retention, it is assumed that most of the negatively charged γ-D-glutamic acid moieties have to be removed in future studies to prevent an elevated kidney uptake and retention. In addition, it will be interesting to see whether the impact of these negative charges of radiohybrid and other CCK-2R ligands on the kidney retention will be confirmed by the first comparative studies in humans.

Nevertheless, even in the case that such behavior would be confirmed in human studies, unfavorable kidney uptake of [^{19}F]F-[^{177}Lu]Lu-DOTA-rhCCK-18 does not necessarily prevent its use for PET imaging with the corresponding ^{18}F-radiohybrid. When ^{18}F-labeled, and taking into account the short half-life of fluorine-18, an elevated kidney accumulation will not result in an unacceptable dosimetry. Similar kidney uptake is, for example, also observed for commonly applied PSMA inhibitors [30–33]. Despite this minor disadvantage, [^{18}F]F-[^{nat}Lu]Lu-DOTA-rhCCK-18 seems to have great potential for the detection of even small and distant metastases in MTC patients due to the unique properties of ^{18}F-PET and the high overexpression of the CCK-2R on these cancer cells.

In order to confirm the expected favorable pharmacokinetics of the chemically identical [^{18}F]F-[^{nat}Lu]Lu-DOTA-rhCCK-18, we carried out a μPET/CT image (n = 1, Figure 5), which revealed similarly high activity levels in the tumor and kidneys compared to [^{19}F]F-[^{177}Lu]Lu-DOTA-rhCCK-18. Moreover, bone uptake was observed to be low (1.69 %ID/g) for [^{18}F]F-[^{nat}Lu]Lu-DOTA-rhCCK-18, underlining the high metabolic stability of the Si-^{18}F bond. Therefore, the formation of the SiOH-containing analog observed in stability studies in human serum does not seem to occur in vivo, at least not within the first hours after injection, and should therefore not be of concern for PET imaging using this compound. However, stability of this compound (particularly of the Si-F bond) in men must be investigated to confirm this assumption. Due to these results, particularly its high tumor accumulation at 1 h p.i., [^{18}F]F-[^{nat}Lu]Lu-DOTA-rhCCK-18 could surpass the detection rate of currently applied CCK-2R-targeted compounds such as [^{111}In]In-CP04 or [^{68}Ga]Ga-DOTA-MGS5 [9,28,34,35] and might even compete with the current gold standard for MTC imaging, [^{18}F]F-DOPA, i.e., for the detection of distant metastases.

^{18}F-labeling was carried out via an isotopic exchange reaction by a novel labeling strategy, which led to molar activities of ~85 GBq/µmol in a total synthesis time of ~30 min. Unlike the Munich Method [36], this strategy includes the use of ammonium formiate (in anhydrous DMSO) instead of [$K^+\subset$2.2.2]OH^- (in anhydrous MeCN) for the elution of dry [^{18}F]fluoride from a SEP-Pak® Light (46 mg) Accell Plus QMA cartridge (Waters GmbH, Eschborn, Germany), which enables a less time-consuming preparation and more cost efficient ^{18}F-fluorination method. In comparison to conventional radiofluorination techniques [37], no azeotropic drying steps must be conducted. Furthermore, anhydrous DMSO is used as the reaction solvent, which is beneficial for the ^{18}F-labeling of CCK-2R-targeting peptides.

In summary, we could demonstrate a significantly higher CCK-2R affinity and thus enhanced tumor accumulation by exchanging the chelator moiety in previously published rhCCK derivatives from (*R*)-DOTAGA to DOTA. Nevertheless, elevated kidney retention of rhCCK derivatives could not be reduced in this study, which must be addressed in future studies by extinguishing most of the negatively charged residues within the SiFA-containing linker section. Despite increased kidney uptake, [^{18}F]F-[^{nat}Lu]Lu-DOTA-rhCCK-18 holds great promise as an imaging agent and is expected to be highly competitive to currently applied radiotracers for PET imaging of medullary thyroid carcinoma.

5. Conclusions

While a simple substitution of (*R*)-DOTAGA by DOTA in previously reported rhCCK derivatives led to a noticeably increased CCK-2R affinity and thus high activity levels in the tumor for [^{19}F]F-[^{177}Lu]Lu-DOTA-rhCCK-18 at 24 h p.i., kidney retention was also high. Nevertheless, due to its very high tumor accumulation at already 1 h p.i., the chemically identical [^{18}F]F-[^{nat}Lu]Lu-DOTA-rhCCK-18 might compete with or even surpass the detection rate of currently applied imaging agents for MTC such as ^{68}Ga- or ^{111}In-labeled CCK-2R or SSTR2-targeted compounds and [^{18}F]F-DOPA, which is why a clinical translation of this compound for MTC imaging is recommended.

Supplementary Materials: The following supporting information can be downloaded at: https://www.mdpi.com/article/10.3390/pharmaceutics15030826/s1, general information and characterization of all CCK2R-targeted compounds, detailed description of cell-based experiments. Figure S1: (a) Confirmation of peptide identity and integrity for [^{nat}Lu]Lu-DOTA-PP-F11N, as analyzed by analytical RP-HPLC (10→90% MeCN in H_2O + 0.1% TFA in 15 min). (b) Mass spectrum of [^{nat}Lu]Lu-DOTA-PP-F11N. (c) Confirmation of peptide identity and integrity for [^{177}Lu]Lu-DOTA-PP-F11N, as analyzed by analytical (radio-)RP-HPLC (10→90% MeCN in H_2O + 0.1% TFA in 15 min); Figure S2: (a) Confirmation of peptide identity and integrity for [^{nat}Lu]Lu-(*R*)-DOTAGA-PP-F11N, as analyzed by analytical RP-HPLC (10→90% MeCN in H_2O + 0.1% TFA in 15 min). (b) Mass spectrum of [^{nat}Lu]Lu-(*R*)-DOTAGA-PP-F11N. (c) Confirmation of peptide identity and integrity for [^{177}Lu]Lu-(*R*)-DOTAGA-PP-F11N, as analyzed by analytical (radio-)RP-HPLC (10→90% MeCN in H_2O + 0.1% TFA in 15 min); Figure S3: (a) Confirmation of peptide identity and integrity for [^{nat}Lu]Lu-DOTA-rhCCK-16, as analyzed by analytical RP-HPLC (10→90% MeCN in H_2O + 0.1% TFA in 15 min). (b) Mass spectrum of [^{nat}Lu]Lu-DOTA-rhCCK-16. (c) Confirmation of peptide identity and integrity for [^{177}Lu]Lu-DOTA-rhCCK-16, as analyzed by analytical (radio-)RP-HPLC (10→90% MeCN in H_2O + 0.1% TFA in 15 min); Figure S4: (a) Confirmation of peptide identity and integrity for [^{177}Lu]Lu-DOTA-rhCCK-16.2, as analyzed by analytical RP-HPLC (10→30% MeCN in H_2O + 0.1% TFA in 5 min, 30→60% MeCN in H_2O + 0.1% TFA in 15 min). (b) Mass spectrum of [^{nat}Lu]Lu-DOTA-rhCCK-16.2; Figure S5: (a) Confirmation of peptide identity and integrity for [^{nat}Lu]Lu-(*R*)-DOTAGA-rhCCK-16, as analyzed by analytical RP-HPLC (10→90% MeCN in H_2O + 0.1% TFA in 15 min). (b) Mass spectrum of [^{nat}Lu]Lu-(*R*)-DOTAGA-rhCCK-16. (c) Confirmation of peptide identity and integrity for [^{177}Lu]Lu-(*R*)-DOTAGA-rhCCK-16, as analyzed by analytical (radio-)RP-HPLC (10→90% MeCN in H_2O + 0.1% TFA in 15 min); Figure S6: (a) Confirmation of peptide identity and integrity for [^{nat}Lu]Lu-DOTA-rhCCK-18, as analyzed by analytical RP-HPLC (10→90% MeCN in H_2O + 0.1% TFA in 15 min). (b) Mass spectrum of [^{nat}Lu]Lu-DOTA-rhCCK-18. (c) Confirmation of peptide identity and integrity for [^{177}Lu]Lu-DOTA-rhCCK-18, as analyzed by analytical (radio-)RP-HPLC (10→90% MeCN in H_2O + 0.1% TFA in 15 min); Figure S7: Confirmation of peptide identity and integrity for [^{18}F]F-[^{nat}Lu]Lu-DOTA-rhCCK-18, as analyzed by analytical radio-RP-HPLC (10→70% MeCN in H_2O + 0.1% TFA in 15 min); Figure S8: (a) Confirmation of peptide identity and integrity for [^{177}Lu]Lu-DOTA-rhCCK-18.2, as analyzed by analytical RP-HPLC (10→30% MeCN in H_2O + 0.1% TFA in 5 min, 30→60% MeCN in H_2O + 0.1% TFA in 15 min). (b) Mass spectrum of [^{nat}Lu]Lu-DOTA-rhCCK-18.2; Figure S9: (a) Confirmation of peptide identity and integrity for [^{nat}Lu]Lu-(*R*)-DOTAGA-rhCCK-18, as analyzed by analytical RP-HPLC (10→90% MeCN in H_2O + 0.1% TFA in 15 min). (b) Mass spectrum of [^{nat}Lu]Lu-(*R*)-DOTAGA-rhCCK-18. (c) Confirmation of peptide identity and integrity for [^{177}Lu]Lu-(*R*)-DOTAGA-rhCCK-18, as analyzed by analytical (radio-)RP-HPLC (10→90% MeCN in H_2O + 0.1% TFA in 15 min); Figure S10: (a) Confirmation of peptide identity and integrity for [^{nat}Ga]Ga-(*R*)-DOTAGA-PP-F11N, as analyzed

by analytical RP-HPLC (10→90% MeCN in H_2O + 0.1% TFA in 15 min). (b) Mass spectrum of [^{nat}Ga]Ga-(*R*)-DOTAGA-PP-F11N; Figure S11: (a) Confirmation of peptide identity and integrity for [^{nat}Ga]Ga-DOTA-PP-F11N, as analyzed by analytical RP-HPLC (10→90% MeCN in H_2O + 0.1% TFA in 15 min). (b) Mass spectrum of [^{nat}Ga]Ga-DOTA-PP-F11N; Figure S12: (a) Confirmation of peptide identity and integrity for [^{nat}Ga]Ga-DOTA-rhCCK-16, as analyzed by analytical RP-HPLC (10→90% MeCN in H_2O + 0.1% TFA in 15 min). (b) Mass spectrum of [^{nat}Ga]Ga-DOTA-rhCCK-16; Figure S13: (a) Confirmation of peptide identity and integrity for [^{67}Ga]Ga-DOTA-rhCCK-16.2, as analyzed by analytical RP-HPLC (10→30% MeCN in H_2O + 0.1% TFA in 5 min, 30→60% MeCN in H_2O + 0.1% TFA in 15 min). (b) Mass spectrum of [^{nat}Ga]Ga-DOTA-rhCCK-16.2; Figure S14: (a) Confirmation of peptide identity and integrity for [^{nat}Ga]Ga-(*R*)-DOTAGA-rhCCK-16, as analyzed by analytical RP-HPLC (10→90% MeCN in H_2O + 0.1% TFA in 15 min). (b) Mass spectrum of [^{nat}Ga]Ga-(*R*)-DOTAGA-rhCCK-16; Figure S15: (a) Confirmation of peptide identity and integrity for [^{nat}Ga]Ga-DOTA-rhCCK-18, as analyzed by analytical RP-HPLC (10→90% MeCN in H_2O + 0.1% TFA in 15 min). (b) Mass spectrum of [^{nat}Ga]Ga-DOTA-rhCCK-18; Figure S16: (a) Confirmation of peptide identity and integrity for [^{67}Ga]Ga-DOTA-rhCCK-18.2, as analyzed by analytical RP-HPLC (10→30% MeCN in H_2O + 0.1% TFA in 5 min, 30→60% MeCN in H_2O + 0.1% TFA in 5 min). (b) Mass spectrum of [^{nat}Ga]Ga-DOTA-rhCCK-18.2; Figure S17: (a) Confirmation of peptide identity and integrity for [^{nat}Ga]Ga-(*R*)-DOTAGA-rhCCK-18, as analyzed by analytical RP-HPLC (10→90% MeCN in H_2O + 0.1% TFA in 15 min). (b) Mass spectrum of [^{nat}Ga]Ga-(*R*)-DOTAGA-rhCCK-18; Figure S18: Stability studies of (a) [^{177}Lu]Lu-DOTA-rhCCK-16, (b) [^{177}Lu]Lu-DOTA-rhCCK-18, (c) [^{67}Ga]Ga-DOTA-rhCCK-16, and (d) [^{67}Ga]Ga-DOTA-rhCCK-18 in human serum (37 °C, 24 h), as analyzed by analytical RP-HPLC (10→30% MeCN in H_2O + 0.1% TFA in 5 min, 30→60% MeCN in H_2O + 0.1% TFA in 5 min). The chromatograms of the respective compounds after incubation in human serum (37 °C, 24 h) are depicted in red. Quality controls of the intact compounds comprising a SiFA moiety are depicted in gray and quality controls of the SiOH-comprising analogs ("hydrolyzed SiFA moiety") are depicted in blue; Figure S19: (a) Biodistribution and (b) a representative μSPECT/CT image of [^{177}Lu]Lu-DOTA-rhCCK-18 (100 pmol) co-injected with [^{nat}Lu]Lu-DOTA-MGS5 (40 nmol) in selected organs (%ID/g) at 24 h p.i. in AR42J tumor-bearing CB17-SCID mice. Data is expressed as mean ± SD (n = 2); Table S1: Affinity data (n = 3) of the compounds evaluated, determined on AR42J cells (2.0×10^5 cells/well) with [^{177}Lu]Lu-DOTA-PP-F11N (0.3 pmol/well) as radiolabeled reference (3 h, 37 °C, RPMI 1640, 5 mM L-Gln, 5 mL non-essential amino acids (100×), 10% FCS + 5% BSA (v/v)); Table S2: Receptor-mediated internalization values (37 °C, RPMI 1640, 5 mM L-Gln, 5 mL non-essential amino acids (100×), 10% FCS, 0.25 pmol/well) determined as percentages (%) of the applied activity of [^{177}Lu]Lu-(*R*)-DOTAGA-rhCCK-18 as well as [^{177}Lu]Lu-DOTA-rhCCK-16 and -18 using AR42J cells (3.0×10^5 cells/well) at different time points (1, 2, 4 and 6 h). Data are corrected for non-specific binding (10 µmol, [^{nat}Lu]Lu-DOTA-PP-F11N); Table S3: Amounts of intact peptides and their analogs containing a hydrolyzed SiFA (=SiOH) moiety (n = 3) of the compounds evaluated, determined in human serum after incubation at 37 °C for 24 h; Table S4: Biodistribution data of [^{177}Lu]Lu-DOTA-rhCCK-18 in selected organs at 1 and 24 h p.i. in AR42J tumor-bearing CB17-SCID mice (100 pmol each). Data are expressed as %ID/g, mean ± SD (n = 4). Biodistribution data of [^{177}Lu]Lu-DOTA-rhCCK-18 (100 pmol) co-injected with [^{177}Lu]Lu-DOTA-MGS5 in selected organs at 24 h p.i. in AR42J tumor-bearing CB17-SCID mice. Data are expressed as %ID/g, mean ± SD (n = 2); Table S5: Tumor-to-background ratios of [^{177}Lu]Lu-DOTA-rhCCK-18, [^{177}Lu]Lu-(*R*)-DOTAGA-rhCCK-16 and [^{177}Lu]Lu-(*R*)-DOTAGA-rhCCK-9 for the selected organs of AR42J tumor-bearing CB17-SCID mice at 24 h p.i. (100 pmol each). Data are expressed as mean ± SD (n = 4).

Author Contributions: Conceptualization, T.G. and H.-J.W.; methodology, N.H., T.G., N.U.-U. and D.D.C.; software, N.H. and T.G.; validation, N.H. and T.G.; formal analysis, N.H. and T.G.; investigation, N.H. and T.G.; resources, N.U.-U. and H.-J.W.; data curation, N.H. and T.G.; writing—original draft preparation, N.H. and T.G.; writing—review and editing, all co-authors; visualization, N.H. and T.G.; supervision, H.-J.W. and C.L.; project administration, T.G. and H.-J.W.; funding acquisition, H.-J.W. and T.G. All authors have read and agreed to the published version of the manuscript.

Funding: This study has been funded by Deutsche Forschungsgemeinschaft (DFG, German Research Foundation—391523415 and 461577150.

Institutional Review Board Statement: All animal experiments were conducted in accordance with general animal welfare regulations in Germany (German animal protection act, in the edition of

the announcement, dated 18 May 2006, as amended by Article 280 of 19 June 2020, approval no. ROB-55.2-1-2532.Vet_02-18-109 by the General Administration of Upper Bavaria) and the institutional guidelines for the care and use of animals. The study was carried out in compliance with the ARRIVE guidelines. This article does not contain any studies with human participants.

Informed Consent Statement: Not applicable.

Data Availability Statement: Data is contained within the article and Supplementary Materials.

Acknowledgments: We thank Sebastian Fischer for providing the SiFA building block used for synthesis. Furthermore, we thank Franziska Schuderer for her help with ^{18}F-labeling experiments. In addition, we thank Daniel Werner for his help with the graphics.

Conflicts of Interest: H.-J.W. is founder and shareholder of Scintomics GmbH, Munich, Germany. No other potential conflict of interest relevant to this article exist.

References

1. Siegel, R.L.; Miller, K.D.; Fuchs, H.E.; Jemal, A. Cancer statistics, 2022. *CA Cancer J. Clin.* **2022**, *72*, 7–33. [CrossRef] [PubMed]
2. Stamatakos, M.; Paraskeva, P.; Stefanaki, C.; Katsaronis, P.; Lazaris, A.; Safioleas, K.; Kontzoglou, K. Medullary thyroid carcinoma: The third most common thyroid cancer reviewed. *Oncol. Lett.* **2011**, *2*, 49–53. [CrossRef] [PubMed]
3. Wells, S.A., Jr.; Asa, S.L.; Dralle, H.; Elisei, R.; Evans, D.B.; Gagel, R.F.; Lee, N.; Machens, A.; Moley, J.F.; Pacini, F.; et al. Revised American Thyroid Association guidelines for the management of medullary thyroid carcinoma. *Thyroid* **2015**, *25*, 567–610. [CrossRef] [PubMed]
4. Schlumberger, M.; Carlomagno, F.; Baudin, E.; Bidart, J.M.; Santoro, M. New therapeutic approaches to treat medullary thyroid carcinoma. *Nat. Clin. Pract. Endocrinol. Metab.* **2008**, *4*, 22–32. [CrossRef]
5. Reubi, J.C.; Schaer, J.C.; Waser, B. Cholecystokinin(CCK)-A and CCK-B/gastrin receptors in human tumors. *Cancer Res.* **1997**, *57*, 1377–1386.
6. Giovanella, L.; Treglia, G.; Iakovou, I.; Mihailovic, J.; Verburg, F.A.; Luster, M. EANM practice guideline for PET/CT imaging in medullary thyroid carcinoma. *Eur. J. Nucl. Med. Mol. Imaging* **2020**, *47*, 61–77. [CrossRef]
7. Pretze, M.; Wängler, C.; Wängler, B. 6-[^{18}F]fluoro-L-DOPA: A well-established neurotracer with expanding application spectrum and strongly improved radiosyntheses. *BioMed Res. Int.* **2014**, *2014*, 674063. [CrossRef]
8. Nanni, C.; Fanti, S.; Rubello, D. ^{18}F-DOPA PET and PET/CT. *J. Nucl. Med.* **2007**, *48*, 1577–1579. [CrossRef]
9. Uprimny, C.; von Guggenberg, E.; Svirydenka, A.; Mikołajczak, R.; Hubalewska-Dydejczyk, A.; Virgolini, I.J. Comparison of PET/CT imaging with [^{18}F]FDOPA and cholecystokinin-2 receptor targeting [^{68}Ga]Ga-DOTA-MGS5 in a patient with advanced medullary thyroid carcinoma. *Eur. J. Nucl. Med. Mol. Imaging* **2021**, *48*, 935–936. [CrossRef]
10. Koopmans, K.P.; de Groot, J.W.; Plukker, J.T.; de Vries, E.G.; Kema, I.P.; Sluiter, W.J.; Jager, P.L.; Links, T.P. ^{18}F-dihydroxyphenylalanine PET in patients with biochemical evidence of medullary thyroid cancer: Relation to tumor differentiation. *J. Nucl. Med.* **2008**, *49*, 524–531. [CrossRef]
11. Jager, P.L.; Chirakal, R.; Marriott, C.J.; Brouwers, A.H.; Koopmans, K.P.; Gulenchyn, K.Y. 6-L-^{18}F-fluorodihydroxyphenylalanine PET in neuroendocrine tumors: Basic aspects and emerging clinical applications. *J. Nucl. Med.* **2008**, *49*, 573–586. [CrossRef]
12. Brammen, L.; Niederle, M.B.; Riss, P.; Scheuba, C.; Selberherr, A.; Karanikas, G.; Bodner, G.; Koperek, O.; Niederle, B. Medullary Thyroid Carcinoma: Do Ultrasonography and F-DOPA-PET-CT Influence the Initial Surgical Strategy? *Ann. Surg. Oncol.* **2018**, *25*, 3919–3927. [CrossRef]
13. Verbeek, H.H.G.; Plukker, J.T.M.; Koopmans, K.P.; de Groot, J.W.B.; Hofstra, R.M.W.; Muller Kobold, A.C.; van der Horst-Schrivers, A.N.A.; Brouwers, A.H.; Links, T.P. Clinical Relevance of ^{18}F-FDG PET and ^{18}F-DOPA PET in Recurrent Medullary Thyroid Carcinoma. *J. Nucl. Med.* **2012**, *53*, 1863–1871. [CrossRef]
14. Khan, N.-U.-H.; Corlett, A.; Hutton, C.A.; Haskali, M.B. Investigation of Fluorine-18 Labelled Peptides for Binding to Cholecystokinin-2 Receptors with High Affinity. *Int. J. Pept. Res. Ther.* **2021**, *28*, 6. [CrossRef]
15. Good, S.; Walter, M.A.; Waser, B.; Wang, X.; Müller-Brand, J.; Béhé, M.P.; Reubi, J.C.; Maecke, H.R. Macrocyclic chelator-coupled gastrin-based radiopharmaceuticals for targeting of gastrin receptor-expressing tumours. *Eur. J. Nucl. Med. Mol. Imaging* **2008**, *35*, 1868–1877. [CrossRef]
16. Nock, B.A.; Maina, T.; Krenning, E.P.; de Jong, M. "To serve and protect": Enzyme inhibitors as radiopeptide escorts promote tumor targeting. *J. Nucl. Med.* **2014**, *55*, 121–127. [CrossRef]
17. Rottenburger, C.; Nicolas, G.P.; McDougall, L.; Kaul, F.; Cachovan, M.; Vija, A.H.; Schibli, R.; Geistlich, S.; Schumann, A.; Rau, T.; et al. Cholecystokinin 2 Receptor Agonist (177) Lu-PP-F11N for Radionuclide Therapy of Medullary Thyroid Carcinoma: Results of the Lumed Phase 0a Study. *J. Nucl. Med.* **2020**, *61*, 520–526. [CrossRef]
18. Bernard-Gauthier, V.; Wängler, C.; Schirrmacher, E.; Kostikov, A.; Jurkschat, K.; Wängler, B.; Schirrmacher, R. ^{18}F-Labeled Silicon-Based Fluoride Acceptors: Potential Opportunities for Novel Positron Emitting Radiopharmaceuticals. *BioMed Res. Int.* **2014**, *2014*, 454503. [CrossRef]

19. Holzleitner, N.; Günther, T.; Beck, R.; Lapa, C.; Wester, H.-J. Introduction of a SiFA Moiety into the D-Glutamate Chain of DOTA-PP-F11N Results in Radiohybrid-Based CCK-2R-Targeted Compounds with Improved Pharmacokinetics In Vivo. *Pharmaceuticals* **2022**, *15*, 1467. [CrossRef]
20. Wurzer, A.; Di Carlo, D.; Schmidt, A.; Beck, R.; Eiber, M.; Schwaiger, M.; Wester, H.-J. Radiohybrid Ligands: A Novel Tracer Concept Exemplified by ^{18}F- or ^{68}Ga-Labeled rhPSMA Inhibitors. *J. Nucl. Med.* **2020**, *61*, 735–742. [CrossRef]
21. Wurzer, A.; Kunert, J.-P.; Fischer, S.; Felber, V.; Beck, R.; De Rose, F.; D′Alessandria, C.; Weber, W.A.; Wester, H.-J. Synthesis and Preclinical Evaluation of ^{177}Lu-labeled Radiohybrid PSMA Ligands (rhPSMAs) for Endoradiotherapy of Prostate Cancer. *J. Nucl. Med.* **2022**, *121*, 263371. [CrossRef]
22. Kunert, J.P.; Müller, M.; Günther, T.; Stopper, L.; Urtz-Urban, N.; Beck, R.; Wester, H.J. Synthesis and preclinical evaluation of novel (99m)Tc-labeled PSMA ligands for radioguided surgery of prostate cancer. *EJNMMI Res.* **2023**, *13*, 2. [CrossRef] [PubMed]
23. Guenther, T.; Deiser, S.; Felber, V.; Beck, R.; Wester, H.J. Substitution of L-Tryptophan by a-Methyl-L-Tryptophan in 177Lu-RM2 Results in 177Lu-AMTG, a High-Affinity Gastrin-Releasing Peptide Receptor Ligand with Improved In Vivo Stability. *J. Nucl. Med.* **2022**, *63*, 1364–1370. [CrossRef] [PubMed]
24. Giovanella, L.; Deandreis, D.; Vrachimis, A.; Campenni, A.; Petranovic Ovcaricek, P. Molecular Imaging and Theragnostics of Thyroid Cancers. *Cancers* **2022**, *14*, 1272. [CrossRef] [PubMed]
25. Wadas, T.J.; Wong, E.H.; Weisman, G.R.; Anderson, C.J. Coordinating radiometals of copper, gallium, indium, yttrium, and zirconium for PET and SPECT imaging of disease. *Chem. Rev.* **2010**, *110*, 2858–2902. [CrossRef] [PubMed]
26. Aime, S.; Barge, A.; Botta, M.; Fasano, M.; Ayala, J.D.; Bombieri, G. Crystal structure and solution dynamics of the lutetium(III) chelate of DOTA. *Inorg. Chim. Acta* **1996**, *246*, 423–429. [CrossRef]
27. Baranyai, Z.; Tircsó, G.; Rösch, F. The Use of the Macrocyclic Chelator DOTA in Radiochemical Separations. *Eur. J. Inorg. Chem.* **2020**, *2020*, 36–56. [CrossRef]
28. Klingler, M.; Summer, D.; Rangger, C.; Haubner, R.; Foster, J.; Sosabowski, J.; Decristoforo, C.; Virgolini, I.; von Guggenberg, E. DOTA-MGS5, a New Cholecystokinin-2 Receptor-Targeting Peptide Analog with an Optimized Targeting Profile for Theranostic Use. *J. Nucl. Med.* **2019**, *60*, 1010–1016. [CrossRef]
29. Kunert, J.P.; Fischer, S.; Wurzer, A.; Wester, H.J. Albumin-Mediated Size Exclusion Chromatography: The Apparent Molecular Weight of PSMA Radioligands as Novel Parameter to Estimate Their Blood Clearance Kinetics. *Pharmaceuticals* **2022**, *15*, 1161. [CrossRef]
30. Umbricht, C.A.; Benešová, M.; Schmid, R.M.; Türler, A.; Schibli, R.; van der Meulen, N.P.; Müller, C. 44Sc-PSMA-617 for radiotheragnostics in tandem with 177Lu-PSMA-617—Preclinical investigations in comparison with ^{68}Ga-PSMA-11 and ^{68}Ga-PSMA-617. *EJNMMI Res.* **2017**, *7*, 9. [CrossRef]
31. Weineisen, M.; Schottelius, M.; Simecek, J.; Baum, R.P.; Yildiz, A.; Beykan, S.; Kulkarni, H.R.; Lassmann, M.; Klette, I.; Eiber, M.; et al. ^{68}Ga- and 177Lu-Labeled PSMA I&T: Optimization of a PSMA-Targeted Theranostic Concept and First Proof-of-Concept Human Studies. *J. Nucl. Med.* **2015**, *56*, 1169–1176. [CrossRef]
32. Cardinale, J.; Schäfer, M.; Benešová, M.; Bauder-Wüst, U.; Leotta, K.; Eder, M.; Neels, O.C.; Haberkorn, U.; Giesel, F.L.; Kopka, K. Preclinical Evaluation of (18)F-PSMA-1007, a New Prostate-Specific Membrane Antigen Ligand for Prostate Cancer Imaging. *J. Nucl. Med.* **2017**, *58*, 425–431. [CrossRef]
33. Robu, S.; Schmidt, A.; Eiber, M.; Schottelius, M.; Günther, T.; Hooshyar Yousefi, B.; Schwaiger, M.; Wester, H.-J. Synthesis and preclinical evaluation of novel ^{18}F-labeled Glu-urea-Glu-based PSMA inhibitors for prostate cancer imaging: A comparison with ^{18}F-DCFPyl and ^{18}F-PSMA-1007. *EJNMMI Res.* **2018**, *8*, 30. [CrossRef]
34. Maina, T.; Konijnenberg, M.W.; KolencPeitl, P.; Garnuszek, P.; Nock, B.A.; Kaloudi, A.; Kroselj, M.; Zaletel, K.; Maecke, H.; Mansi, R.; et al. Preclinical pharmacokinetics, biodistribution, radiation dosimetry and toxicity studies required for regulatory approval of a phase I clinical trial with 111In-CP04 in medullary thyroid carcinoma patients. *Eur. J. Pharm. Sci.* **2016**, *91*, 236–242. [CrossRef]
35. Lezaic, L.; Kolenc, P.; Zaletel, K.; Erba, P.; Decristoforo, C.; Mikolajczak, R.; Garnuszek, P.; Virgolini, I.; Rangger, C.; Di Santo, G.; et al. Final results of a GRAN-T-MTC phase I clinical trial using a novel CCK2 receptor-localising radiolabelled peptide probe for personalized diagnosis and therapy of patients with metastatic medullary thyroid cancer. *Eur. J. Nucl. Med. Mol. Imaging* **2022**, *49*, 1–751. [CrossRef]
36. Wessmann, S.H.; Henriksen, G.; Wester, H.J. Cryptate mediated nucleophilic ^{18}F-fluorination without azeotropic drying. *Nuklearmedizin* **2012**, *51*, 1–8. [CrossRef]
37. Jacobson, O.; Kiesewetter, D.O.; Chen, X. Fluorine-18 radiochemistry, labeling strategies and synthetic routes. *Bioconjug. Chem.* **2015**, *26*, 1–18. [CrossRef]

Development of the First ^{18}F-Labeled Radiohybrid-Based Minigastrin Derivative with High Target Affinity and Tumor Accumulation by Substitution of the Chelating Moiety

- Supplementary Materials -

Thomas Günther [1,*,†], Nadine Holzleitner [1,†], Daniel Di Carlo [1], Roswitha Beck [1], Constantin Lapa [2] and Hans-Jürgen Wester [1]

General information

Analytical and preparative reversed-phase high performance liquid chromatography (RP-HPLC) were performed using Shimadzu gradient systems (Shimadzu Deutschland GmbH, Neufahrn, Germany), each equipped with an SPD-20A UV/Vis detector (220 nm, 254 nm). Different gradients of MeCN (0.1% TFA, 2 or 5% H_2O for analytical or preparative applications, respectively) in H_2O (0.1% TFA) were used as eluents for all RP-HPLC operations.

For analytical measurements, a MultoKrom 100-5 C18 (150 mm x 4.6 mm) column (CS Chromatographie Service GmbH, Langerwehe, Germany) was used at a flow rate of 1 mL/min. Both specific gradients and the corresponding retention times t_R as well as the capacity factor K' are cited in the text.

Preparative RP-HPLC purification was performed using a MultoKrom 100-5 C18 (250 mm x 20 mm) column (CS Chromatographie GmbH, Langerwehe, Germany) at a constant flow rate of 10 mL/min.

Lyophilization was accomplished using an Alpha 1-2 LDplus lyophilizer (Martin Christ Gefriertrocknungsanlagen GmbH, Osterode am Harz, Deutschland) combined with a RZ-2 vacuum pump (Vacuubrand GmbH & Co KG, Olching, Germany).

Analytical and preparative radio RP-HPLC was performed using a MultoKrom 100-5 C18 (5 µm, 125 × 4.6 mm) column (CS Chromatographie GmbH, Langerwehe, Germany). A HERM LB 500 NaI scintillation detector (Berthold Technologies, Bad Wildbad, Germany) was connected to the outlet of the UV photometer for the detection of radioactivity.

Radioactive samples were measured by a WIZARD$^{2®}$ 2480 Automatic γ-Counter (Perkin Elmer Inc., Waltham, MA, USA).

Analytical data of $^{nat/177}$Lu-labeled minigastrin analogs

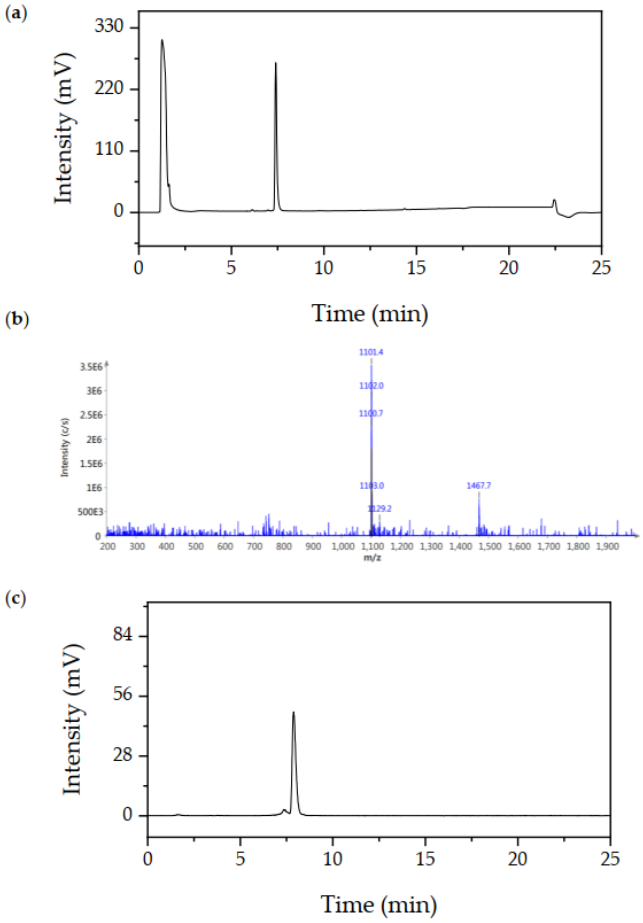

Figure S1. (**a**) Confirmation of peptide identity and integrity for [^{nat}Lu]Lu-DOTA-PP-F11N, as analyzed by analytical RP-HPLC (10→90% MeCN in H_2O + 0.1% TFA in 15 min). (**b**) Mass spectrum of [^{nat}Lu]Lu-DOTA-PP-F11N. (**c**) Confirmation of peptide identity and integrity for [^{177}Lu]Lu-DOTA-PP-F11N, as analyzed by analytical (radio-)RP-HPLC (10→90% MeCN in H_2O + 0.1% TFA in 15 min).

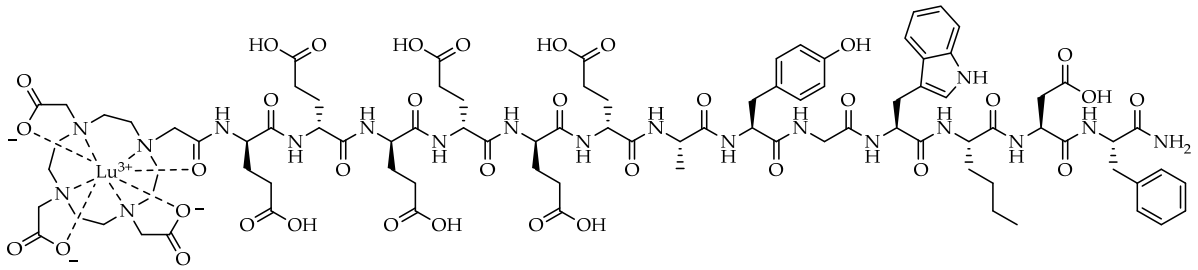

[^{nat}Lu]Lu-DOTA-PP-F11N: RP-HPLC (10→90% MeCN in H_2O with 0.1% TFA, 15 min, λ = 220 nm): t_R = 7.55 min, K′ = 3.48; MS (ESI, positive): m/z calculated for $C_{90}H_{120}LuN_{19}O_{35}$: 2203.0, found: m/z = 1101.4 $[M+2H]^{2+}$.

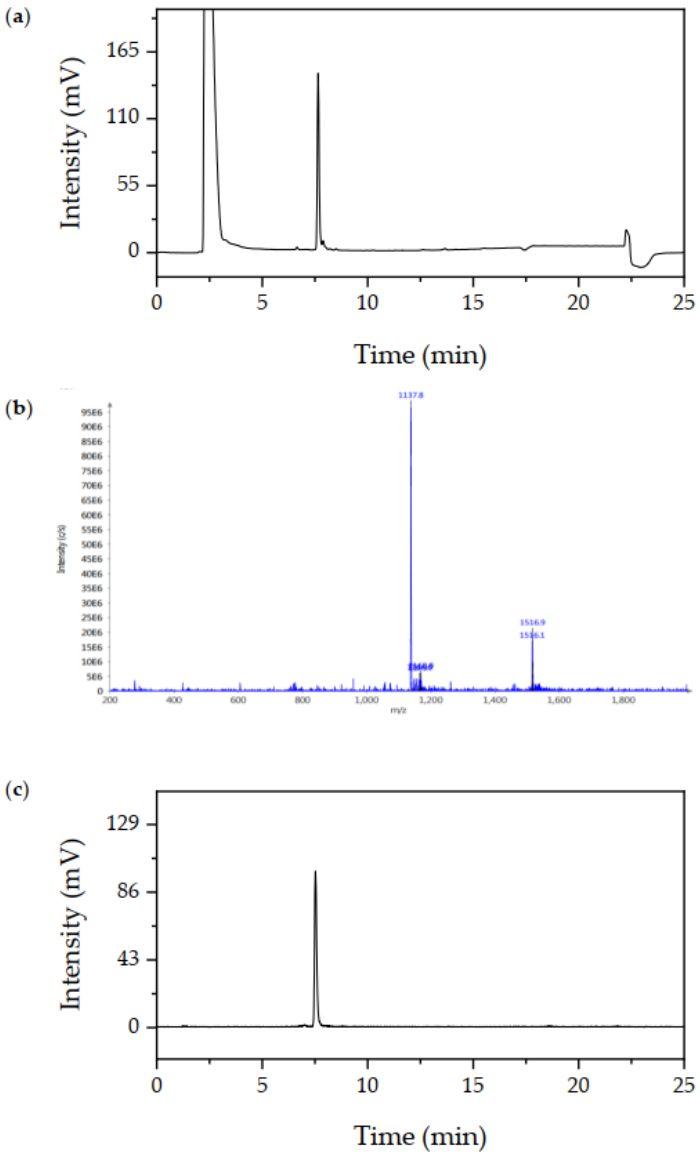

Figure S2. (**a**) Confirmation of peptide identity and integrity for [^{nat}Lu]Lu-(*R*)-DOTAGA-PP-F11N, as analyzed by analytical RP-HPLC (10→90% MeCN in H_2O + 0.1% TFA in 15 min). (**b**) Mass spectrum of [^{nat}Lu]Lu-(*R*)-DOTAGA-PP-F11N. (**c**) Confirmation of peptide identity and integrity for [^{177}Lu]Lu-(*R*)-DOTAGA-PP-F11N, as analyzed by analytical (radio-)RP-HPLC (10→90% MeCN in H_2O + 0.1% TFA in 15 min).

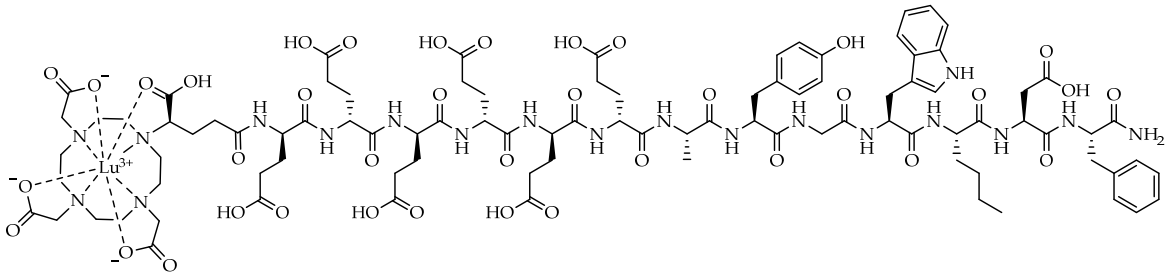

[^{nat}Lu]Lu-(R)-DOTAGA-PP-F11N: RP-HPLC (10→90% MeCN in H_2O with 0.1% TFA, 15 min, λ = 220 nm): t_R = 7.8 min, K' = 3.88; MS (ESI, positive): m/z calculated for $C_{93}H_{124}LuN_{19}O_{37}$: 2273.8, found: m/z = 1137.8 $[M+2H]^{2+}$.

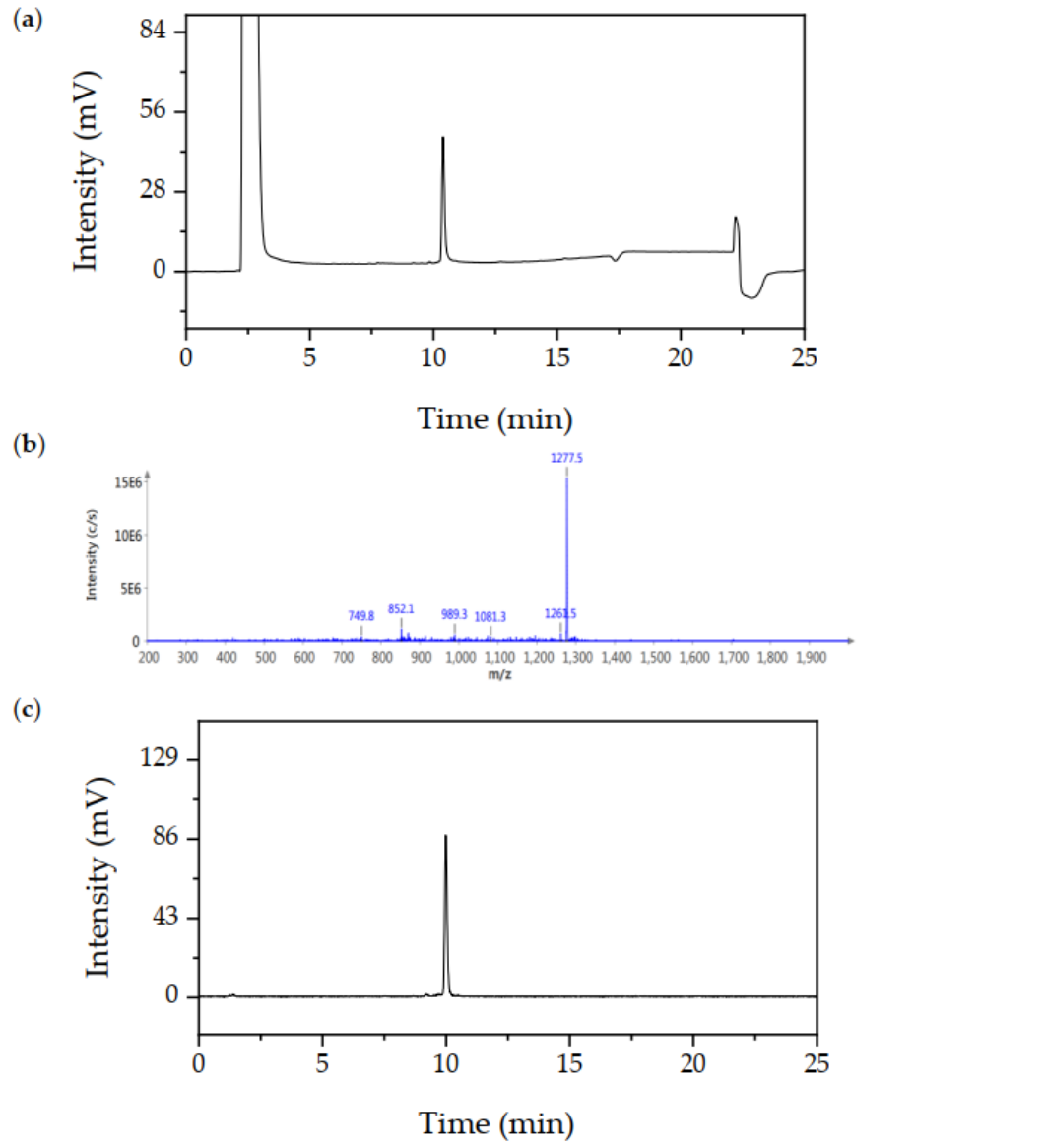

Figure S3. (**a**) Confirmation of peptide identity and integrity for [^{nat}Lu]Lu-DOTA-rhCCK-16, as analyzed by analytical RP-HPLC (10→90% MeCN in H_2O + 0.1% TFA in 15 min). (**b**) Mass spectrum of [^{nat}Lu]Lu-DOTA-rhCCK-16. (**c**) Confirmation of peptide identity and integrity for [^{177}Lu]Lu-DOTA-rhCCK-16, as analyzed by analytical (radio-)RP-HPLC (10→90% MeCN in H_2O + 0.1% TFA in 15 min).

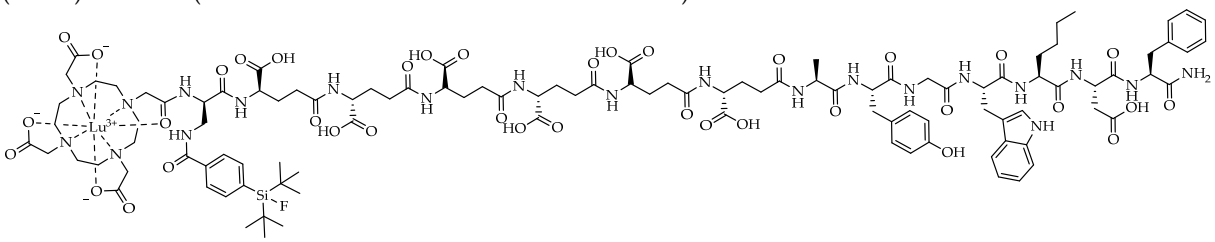

[^{nat}Lu]Lu-DOTA-rhCCK-16: RP-HPLC (10→90% MeCN in H_2O with 0.1% TFA, 15 min, λ = 220 nm): t_R = 10.4 min, K′ = 5.16; MS (ESI, positive): m/z calculated for $C_{108}H_{147}FLuN_{21}O_{37}Si$: 2553.5, found: m/z = 1277.5 $[M+2H]^{2+}$.

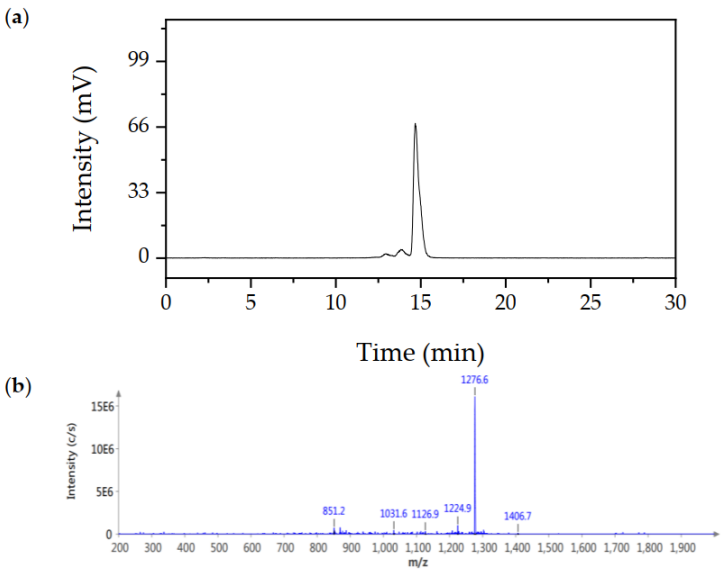

Figure S4. (**a**) Confirmation of peptide identity and integrity for [^{177}Lu]Lu-DOTA-rhCCK-16.2, as analyzed by analytical RP-HPLC (10→30% MeCN in H_2O + 0.1% TFA in 5 min, 30→60% MeCN in H_2O + 0.1% TFA in 15 min). (**b**) Mass spectrum of [^{nat}Lu]Lu-DOTA-rhCCK-16.2.

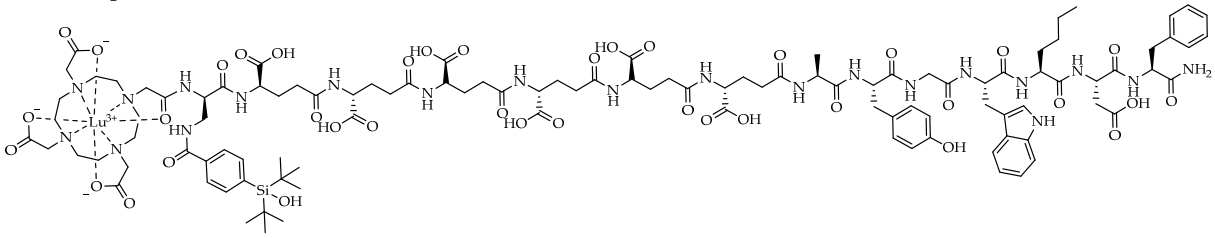

[$^{nat/177}$Lu]Lu-DOTA-rhCCK-16.2: RP-HPLC (10→30% MeCN in H_2O with 0.1% TFA, 5 min, 30→60% MeCN in H_2O with 0.1% TFA, 15 min, λ = 220 nm): t_R = 14.7 min, K′ = 6.35; MS (ESI, positive): m/z calculated for $C_{108}H_{148}LuN_{21}O_{38}Si$: 2551.5, found: m/z = 1276.6 $[M+2H]^{2+}$.

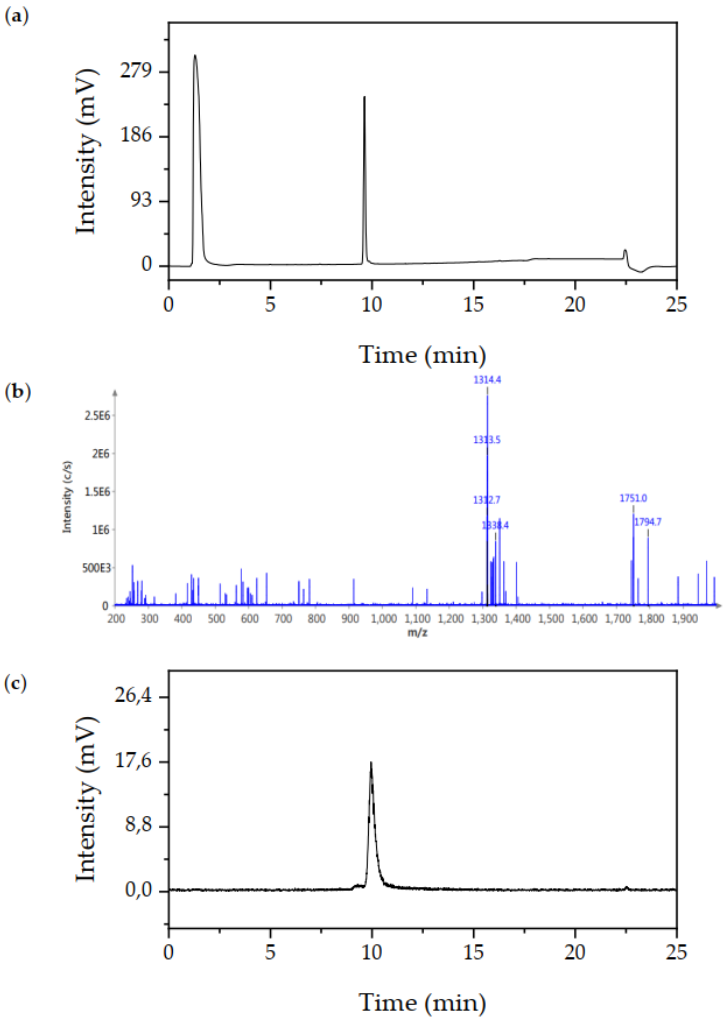

Figure S5. (**a**) Confirmation of peptide identity and integrity for [^{nat}Lu]Lu-(*R*)-DOTAGA-rhCCK-16, as analyzed by analytical RP-HPLC (10→90% MeCN in H_2O + 0.1% TFA in 15 min). (**b**) Mass spectrum of [^{nat}Lu]Lu-(*R*)-DOTAGA -rhCCK-16. (**c**) Confirmation of peptide identity and integrity for [^{177}Lu]Lu-(*R*)-DOTAGA-rhCCK-16, as analyzed by analytical (radio-)RP-HPLC (10→90% MeCN in H_2O + 0.1% TFA in 15 min).

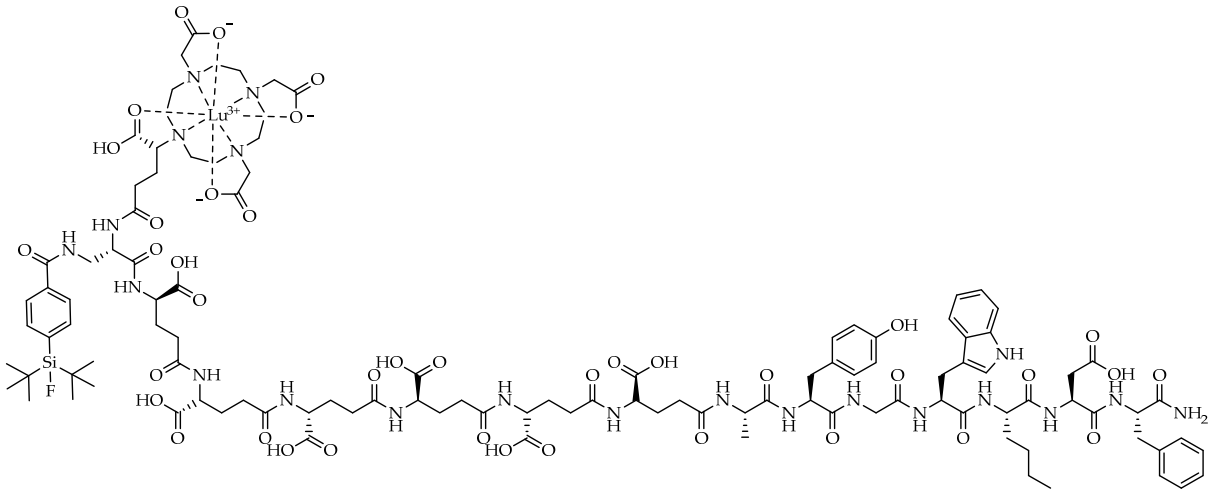

[^{nat}Lu]Lu-(R)-DOTAGA-rhCCK-16: RP-HPLC (10 → 90% MeCN in H_2O with 0.1% TFA, 15 min, λ = 220 nm): t_R = 9.52 min, K′ = 4.64; MS (ESI, positive): m/z calculated for $C_{111}H_{151}FLuN_{21}O_{39}Si$: 2625.6, found: m/z = 1314.4 $[M+2H]^{2+}$.

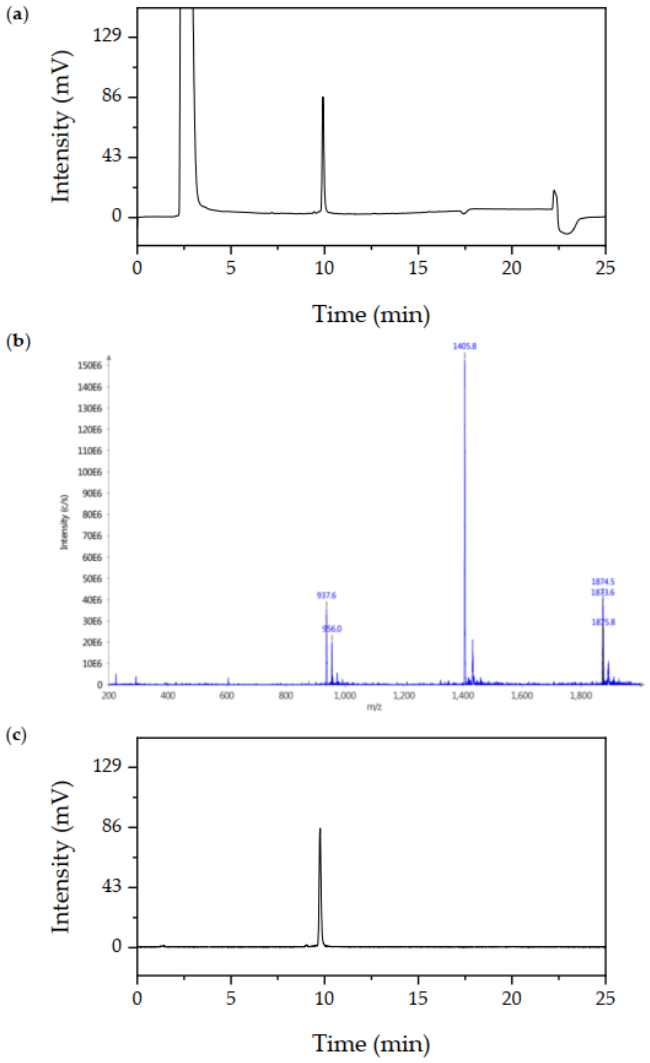

Figure S6. (**a**) Confirmation of peptide identity and integrity for [^{nat}Lu]Lu-DOTA-rhCCK-18, as analyzed by analytical RP-HPLC (10→90% MeCN in H_2O + 0.1% TFA in 15 min). (**b**) Mass spectrum of [^{nat}Lu]Lu-DOTA-rhCCK-18. (**c**) Confirmation of peptide identity and integrity for [^{177}Lu]Lu-DOTA-rhCCK-18, as analyzed by analytical (radio-)RP-HPLC (10→90% MeCN in H_2O + 0.1% TFA in 15 min).

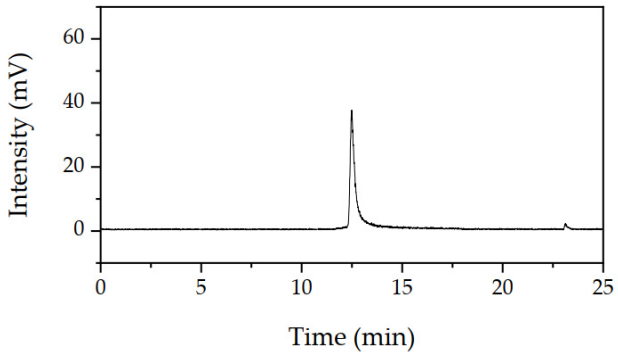

Figure S7. Confirmation of peptide identity and integrity for [^{18}F]F-[^{nat}Lu]Lu-DOTA-rhCCK-18, as analyzed by analytical radio-RP-HPLC (10→70% MeCN in H_2O + 0.1% TFA in 15 min).

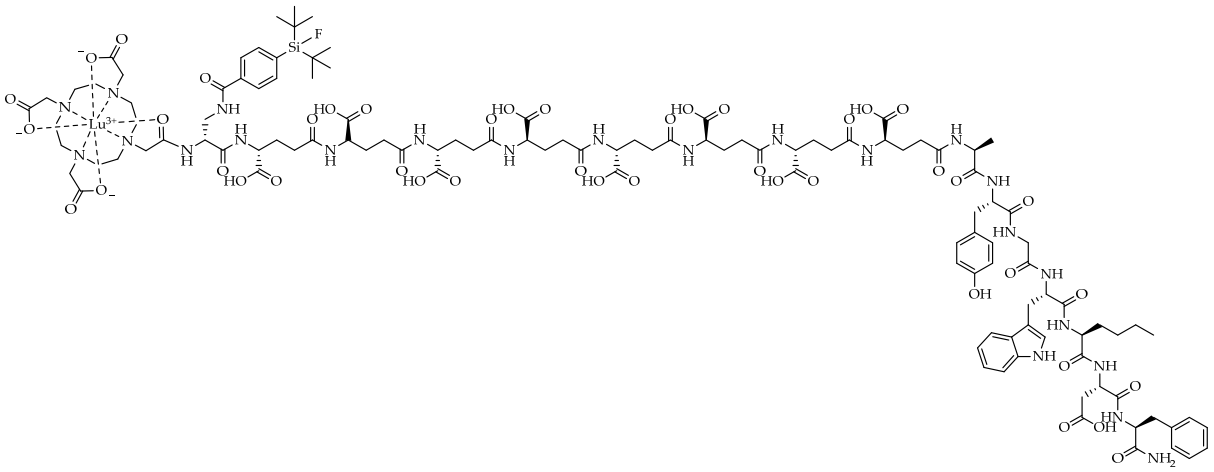

[^{nat}Lu]Lu-DOTA-rhCCK-18: RP-HPLC (10→90% MeCN in H_2O with 0.1% TFA, 15 min, λ = 220 nm): t_R = 9.92 min, K′ = 4.88; MS (ESI, positive): m/z calculated for $C_{116}H_{161}FLuN_{23}O_{43}Si$: 2811.8, found: m/z = 1405.8 $[M+2H]^{2+}$, 937.6 $[M+3H]^{3+}$.

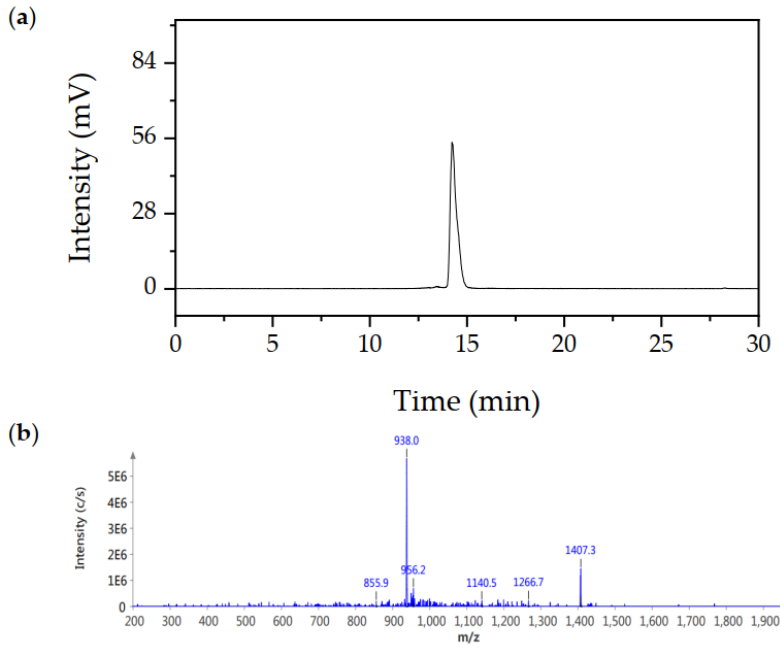

Figure S8. (**a**) Confirmation of peptide identity and integrity for [^{177}Lu]Lu-DOTA-rhCCK-18.2, as analyzed by analytical RP-HPLC (10→30% MeCN in H_2O + 0.1% TFA in 5 min, 30→60% MeCN in H_2O + 0.1% TFA in 15 min). (**b**) Mass spectrum of [^{nat}Lu]Lu-DOTA-rhCCK-18.2.

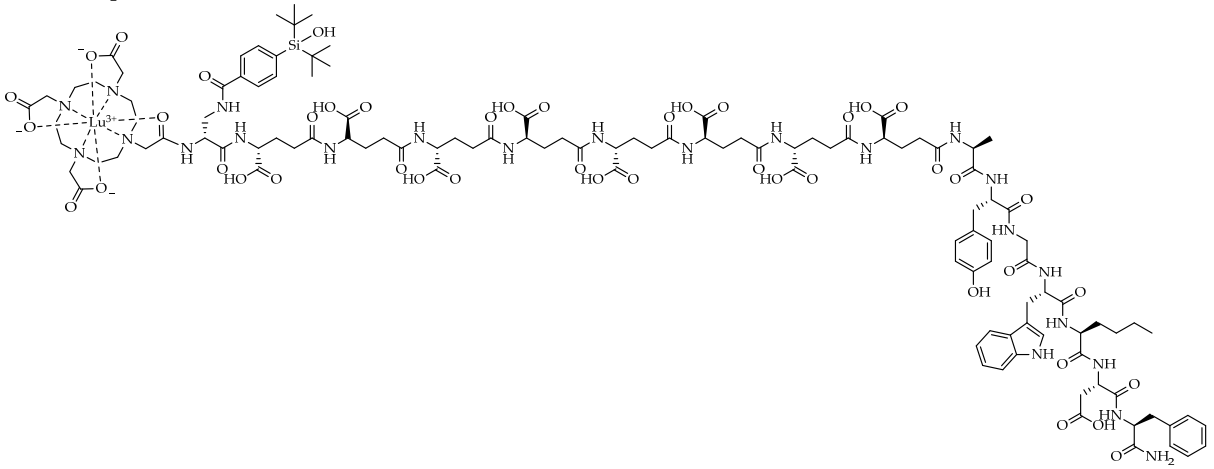

[$^{nat/177}$Lu]Lu-DOTA-rhCCK-18.2: RP-HPLC (10→30% MeCN in H_2O with 0.1% TFA, 5 min, 30→60% MeCN in H_2O with 0.1% TFA, 15 min, λ = 220 nm): t_R = 14.3 min, K' = 6.15; MS (ESI, positive): m/z calculated for $C_{116}H_{162}LuN_{23}O_{44}Si$: 2809.7, found: m/z = 1407.3 $[M+2H]^{2+}$, 938.0 $[M+3H]^{3+}$.

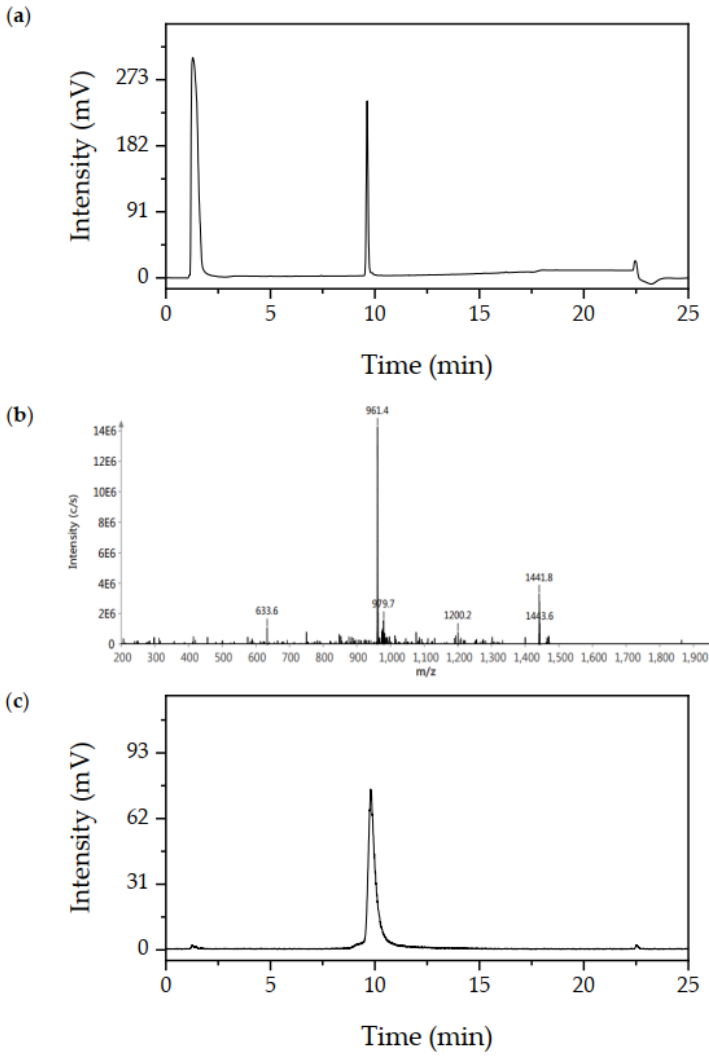

Figure S9. (**a**) Confirmation of peptide identity and integrity for [^{nat}Lu]Lu-(*R*)-DOTAGA-rhCCK-18, as analyzed by analytical RP-HPLC (10→90% MeCN in H_2O + 0.1% TFA in 15 min). (**b**) Mass spectrum of [^{nat}Lu]Lu-(*R*)-DOTAGA-rhCCK-18. (**c**) Confirmation of peptide identity and integrity for [^{177}Lu]Lu-(*R*)-DOTAGA-rhCCK-18, as analyzed by analytical (radio-)RP-HPLC (10→90% MeCN in H_2O + 0.1% TFA in 15 min).

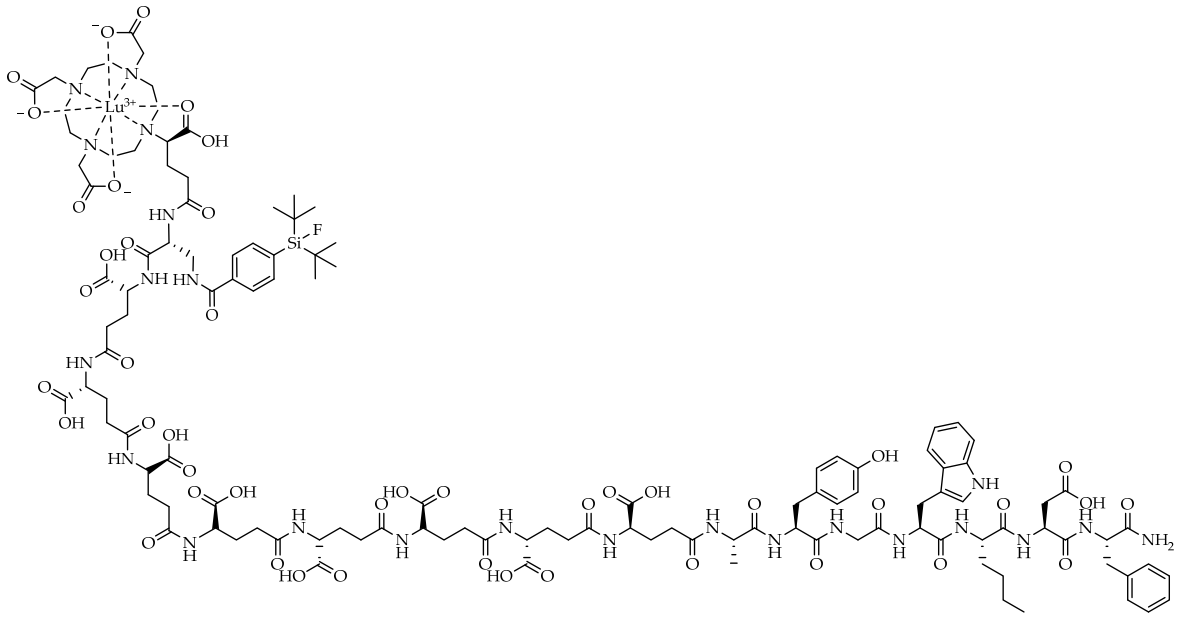

[^{nat}Lu]Lu-(R)-DOTAGA-rhCCK-18: RP-HPLC (10 → 90% MeCN in H_2O with 0.1% TFA, 15 min, λ = 220 nm): t_R = 9.50 min, K' = 4.63; MS (ESI, positive): m/z calculated for $C_{121}H_{165}FLuN_{23}O_{45}Si$: 2883.8, found: m/z = 1441.8 $[M+2H]^{2+}$, 961.4 $[M+3H]^{3+}$.

Analytical data of ^{nat}Ga-labeled minigastrin analogs

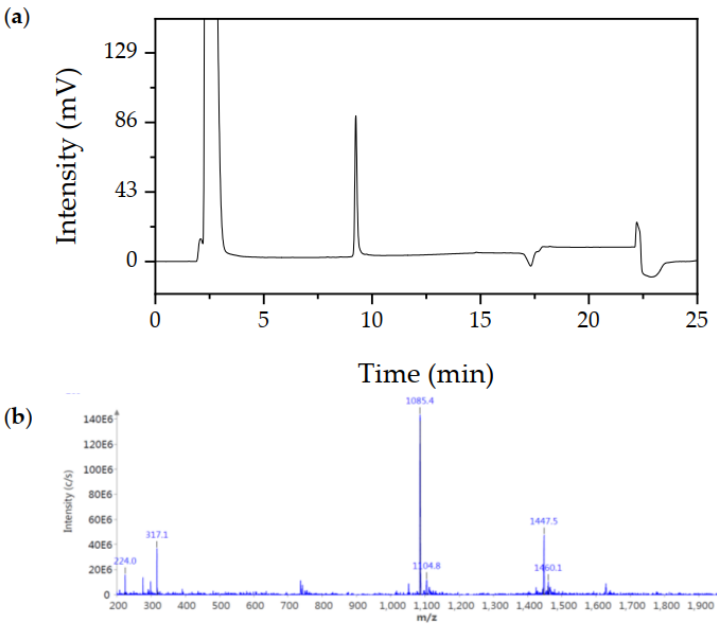

Figure S10. (**a**) Confirmation of peptide identity and integrity for [^{nat}Ga]Ga-(*R*)-DOTAGA-PP-F11N, as analyzed by analytical RP-HPLC (10→90% MeCN in H_2O + 0.1% TFA in 15 min). (**b**) Mass spectrum of [^{nat}Ga]Ga-(*R*)-DOTAGA-PP-F11N.

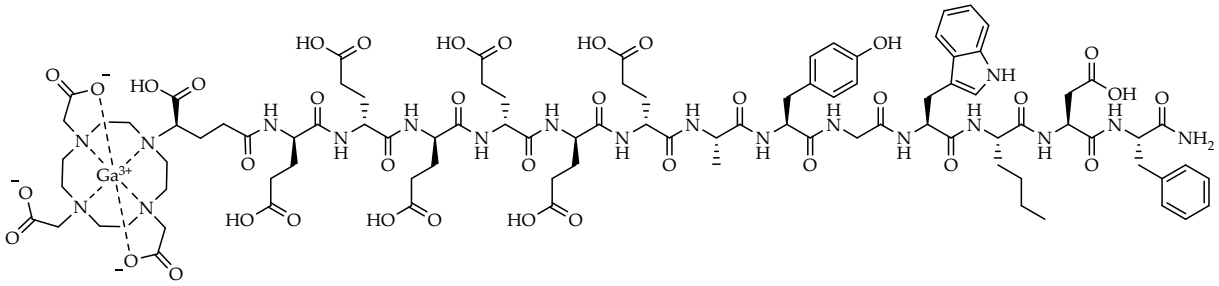

[^{nat}Ga]Ga-(R)-DOTAGA-PP-F11N: RP-HPLC (10→70% MeCN in H_2O with 0.1% TFA, 15 min, λ = 220 nm): t_R = 9.3 min, K′ = 5.51; MS (ESI, positive): m/z calculated for $C_{93}H_{124}GaN_{19}O_{37}$: 2169.8, found: m/z = 1085.4 $[M+2H]^{2+}$.

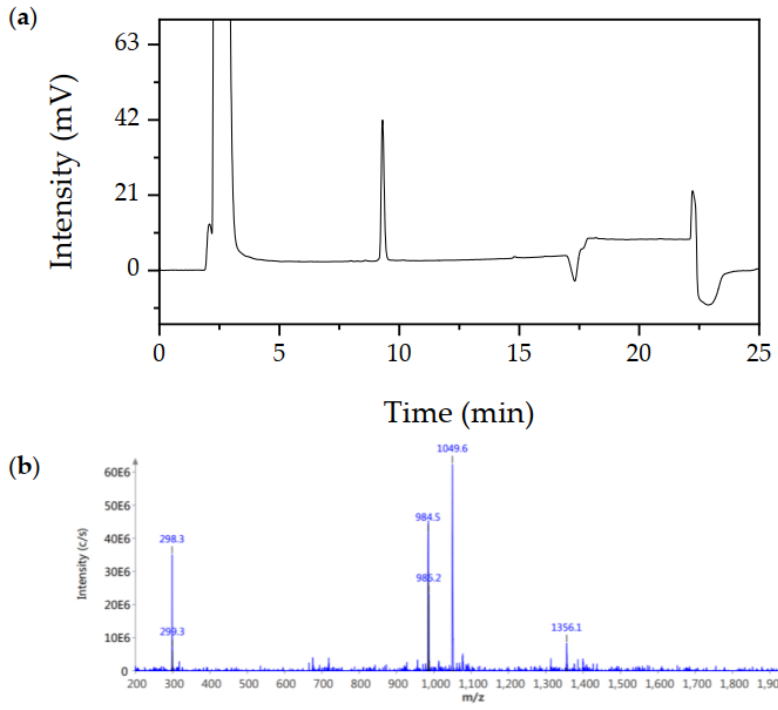

Figure S11. (**a**) Confirmation of peptide identity and integrity for [^{nat}Ga]Ga-DOTA-PP-F11N, as analyzed by analytical RP-HPLC (10→90% MeCN in H_2O + 0.1% TFA in 15 min). (**b**) Mass spectrum of [^{nat}Ga]Ga-DOTA-PP-F11N.

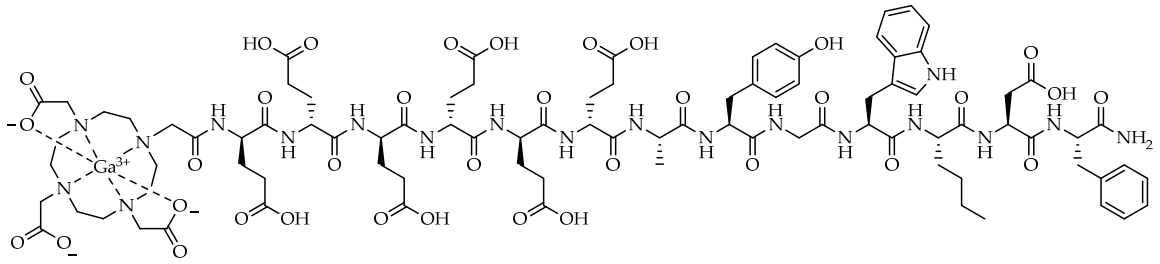

[^{nat}Ga]Ga-DOTA-PP-F11N: RP-HPLC (10→70% MeCN in H_2O with 0.1% TFA, 15 min, λ = 220 nm): t_R = 9.3 min, K′ = 5.51; MS (ESI, positive): m/z calculated for $C_{90}H_{120}GaN_{19}O_{35}$: 2097.8, found: m/z = 1049.6 $[M+2H]^{2+}$.

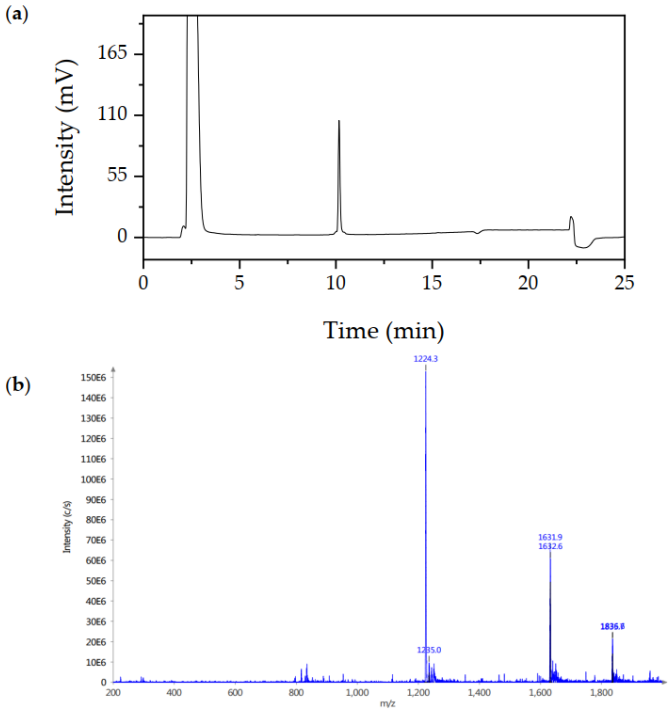

Figure S12. (**a**) Confirmation of peptide identity and integrity for [^{nat}Ga]Ga-DOTA-rhCCK-16, as analyzed by analytical RP-HPLC (10→90% MeCN in H_2O + 0.1% TFA in 15 min). (**b**) Mass spectrum of [^{nat}Ga]Ga-DOTA-rhCCK-16.

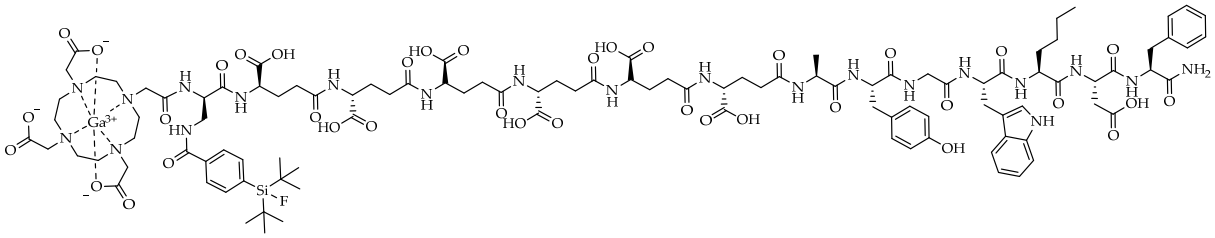

[^{nat}Ga]Ga-DOTA-rhCCK-16: RP-HPLC (10→90% MeCN in H_2O with 0.1% TFA, 15 min, λ = 220 nm): t_R = 10.2 min, K′ = 5.05; MS (ESI, positive): m/z calculated for $C_{108}H_{147}FGaN_{21}O_{37}Si$: 2448.3, found: m/z = 1224.3 $[M+2H]^{2+}$.

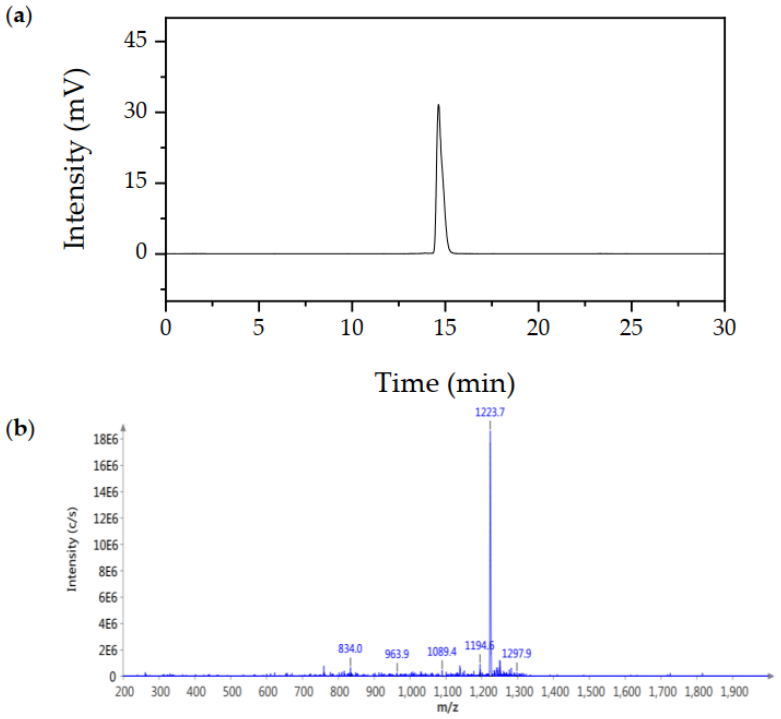

Figure S13. (**a**) Confirmation of peptide identity and integrity for [^{67}Ga]Ga-DOTA-rhCCK-16.2, as analyzed by analytical RP-HPLC (10→30% MeCN in H_2O + 0.1% TFA in 5 min, 30→60% MeCN in H_2O + 0.1% TFA in 15 min). (**b**) Mass spectrum of [^{nat}Ga]Ga-DOTA-rhCCK-16.2.

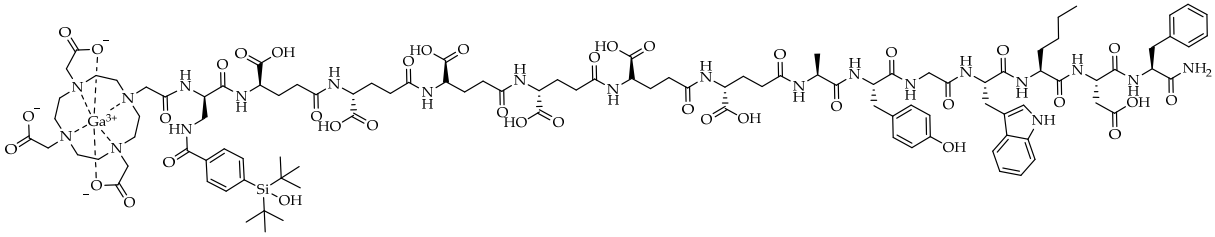

[$^{nat/67}$Ga]Ga-DOTA-rhCCK-16.2: RP-HPLC (10→30% MeCN in H_2O with 0.1% TFA, 5 min, 30→60% MeCN in H_2O with 0.1% TFA, 15 min λ = 220 nm): t_R = 14.6 min, K′ = 6.30; MS (ESI, positive): m/z calculated for $C_{108}H_{148}GaN_{21}O_{38}Si$: 2446.3, found: m/z = 1223.7 $[M+2H]^{2+}$.

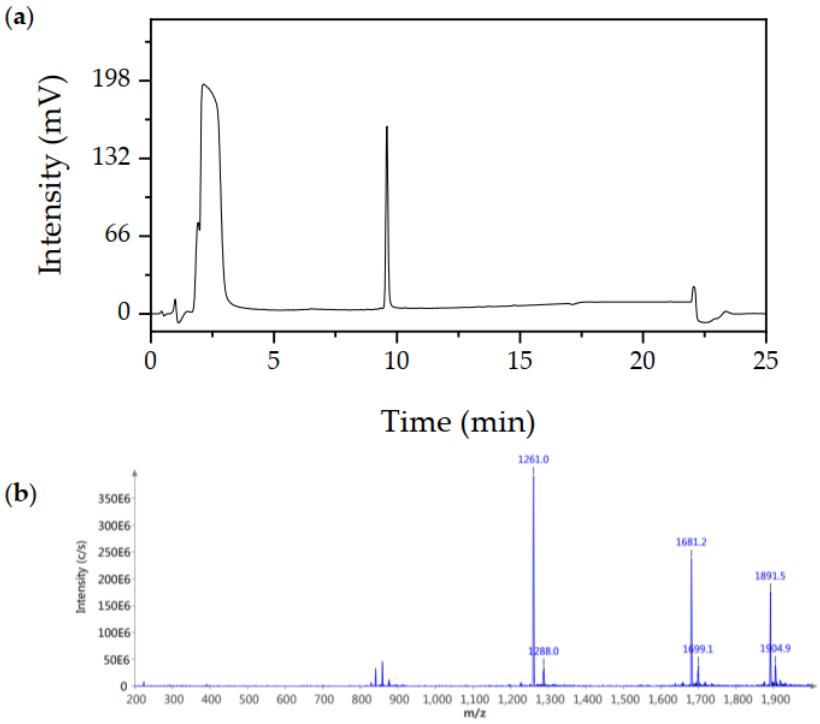

Figure S14. (**a**) Confirmation of peptide identity and integrity for [^{nat}Ga]Ga-(*R*)-DOTAGA-rhCCK-16, as analyzed by analytical RP-HPLC (10→90% MeCN in H_2O + 0.1% TFA in 15 min). (**b**) Mass spectrum of [^{nat}Ga]Ga-(*R*)-DOTAGA-rhCCK-16.

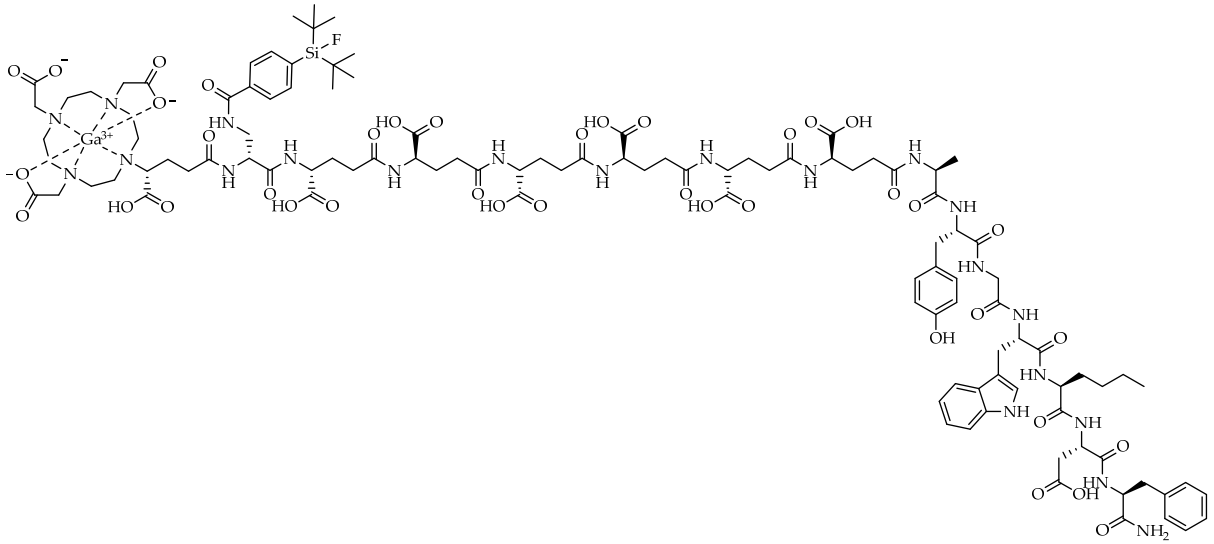

[^{nat}Ga]Ga-(R)-DOTAGA-rhCCK-16: RP-HPLC (10→70% MeCN in H_2O with 0.1% TFA, 15 min, λ = 220 nm): t_R = 9.73 min, K′ = 5.08; MS (ESI, positive): m/z calculated for $C_{111}H_{151}FGaN_{21}O_{39}Si$: 2520.3, found: m/z = 1261.0 $[M+2H]^{2+}$.

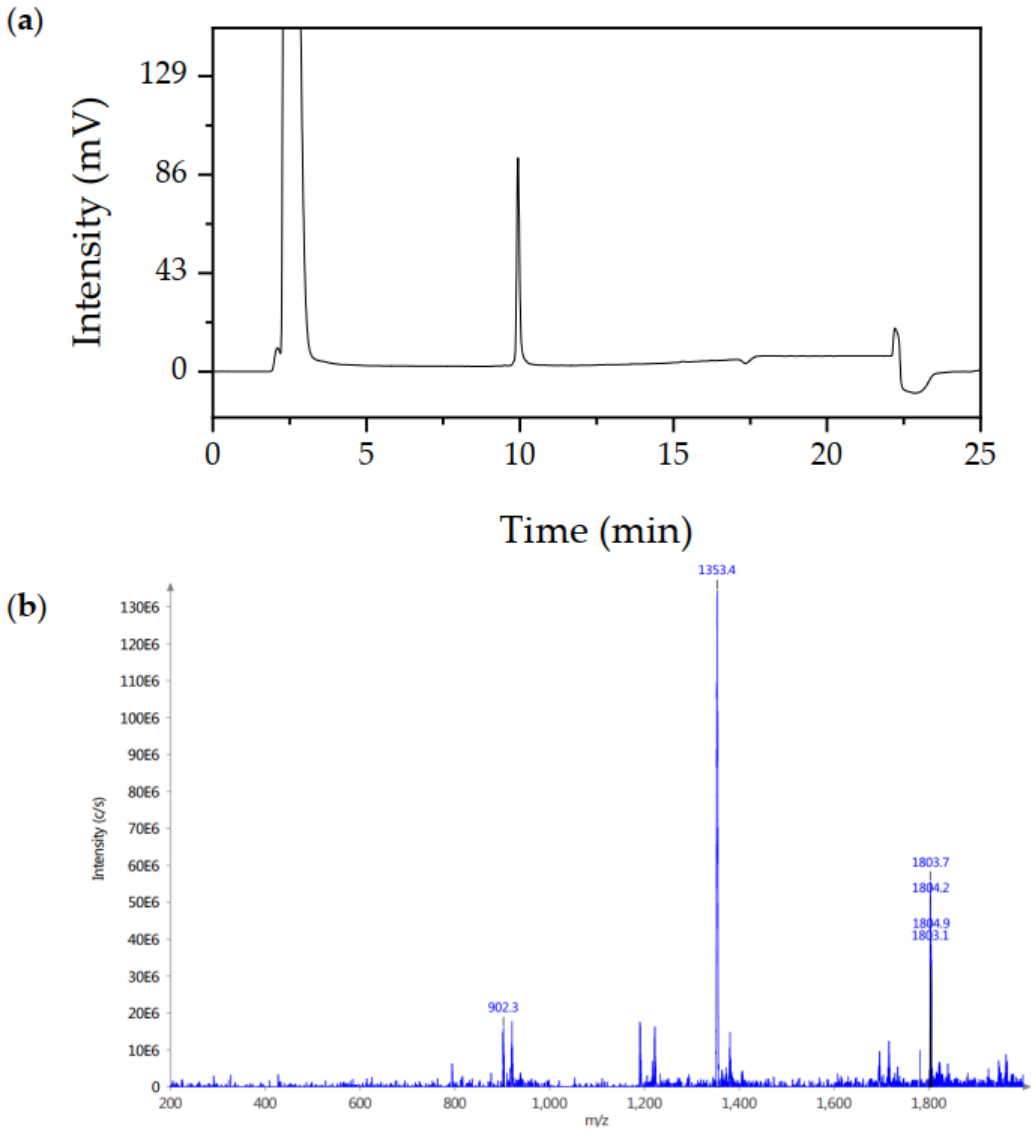

Figure S15. (**a**) Confirmation of peptide identity and integrity for [^{nat}Ga]Ga-DOTA-rhCCK-18, as analyzed by analytical RP-HPLC (10→90% MeCN in H_2O + 0.1% TFA in 15 min). (**b**) Mass spectrum of [^{nat}Ga]Ga-DOTA-rhCCK-18.

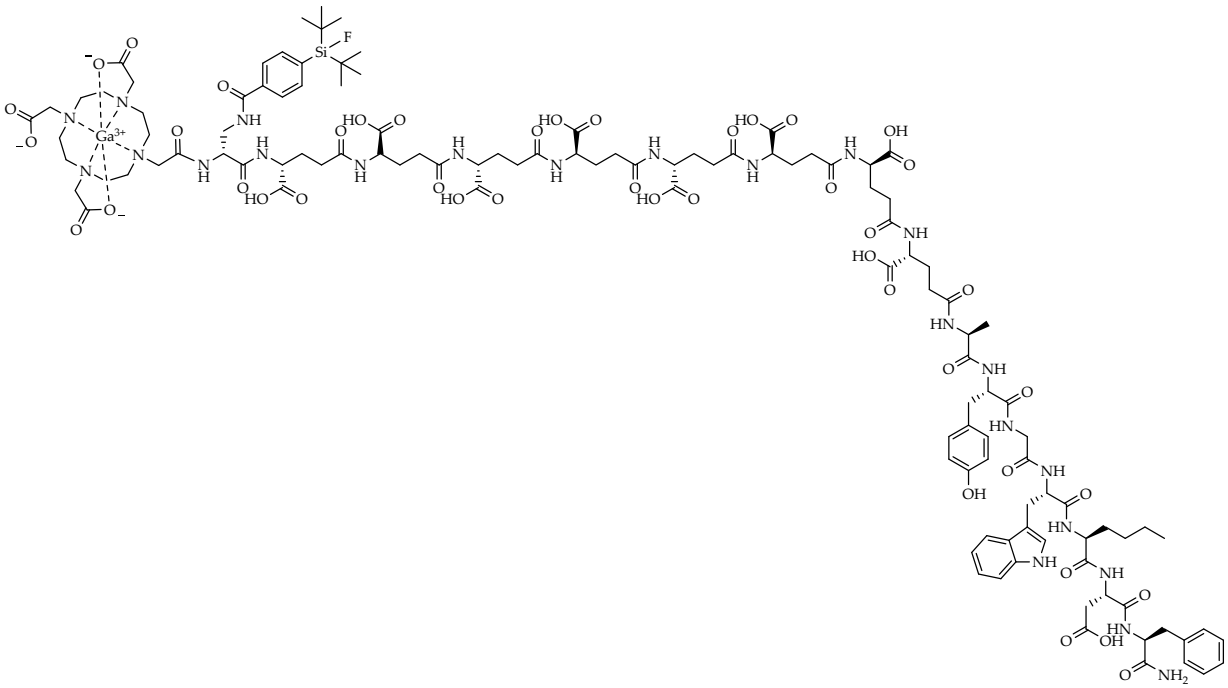

[^{nat}Ga]Ga-DOTA-rhCCK-18: RP-HPLC (10→90% MeCN in H_2O with 0.1% TFA, 15 min, λ = 220 nm): t_R = 9.90 min, K′ = 4.87; MS (ESI, positive): m/z calculated for $C_{118}H_{161}FGaN_{23}O_{43}Si$: 2706.5, found: m/z = 1353.4 $[M+2H]^{2+}$.

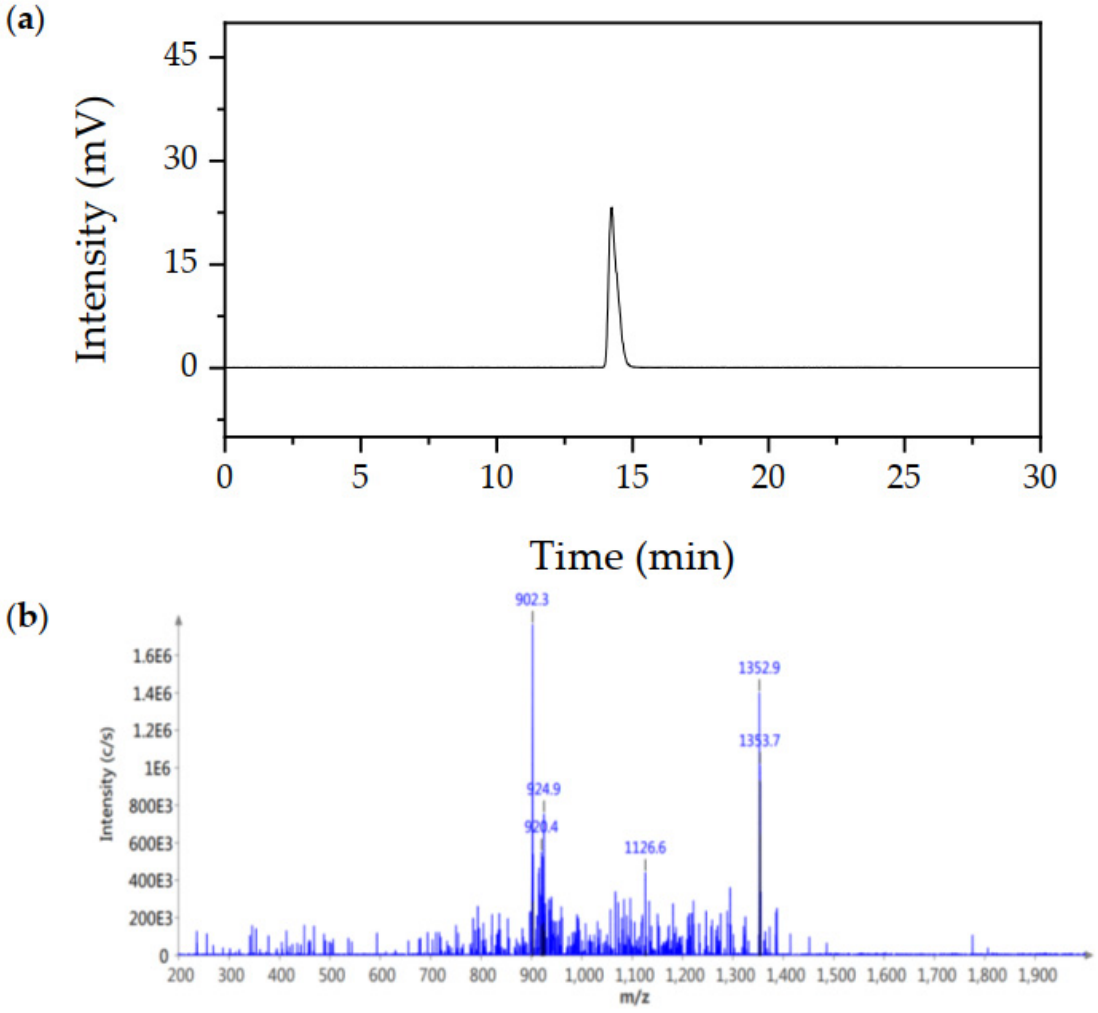

Figure S16. (**a**) Confirmation of peptide identity and integrity for [^{67}Ga]Ga-DOTA-rhCCK-18.2, as analyzed by analytical RP-HPLC (10→30% MeCN in H_2O + 0.1% TFA in 5 min, 30→60% MeCN in H_2O + 0.1% TFA in 5 min). (**b**) Mass spectrum of [^{nat}Ga]Ga-DOTA-rhCCK-18.2.

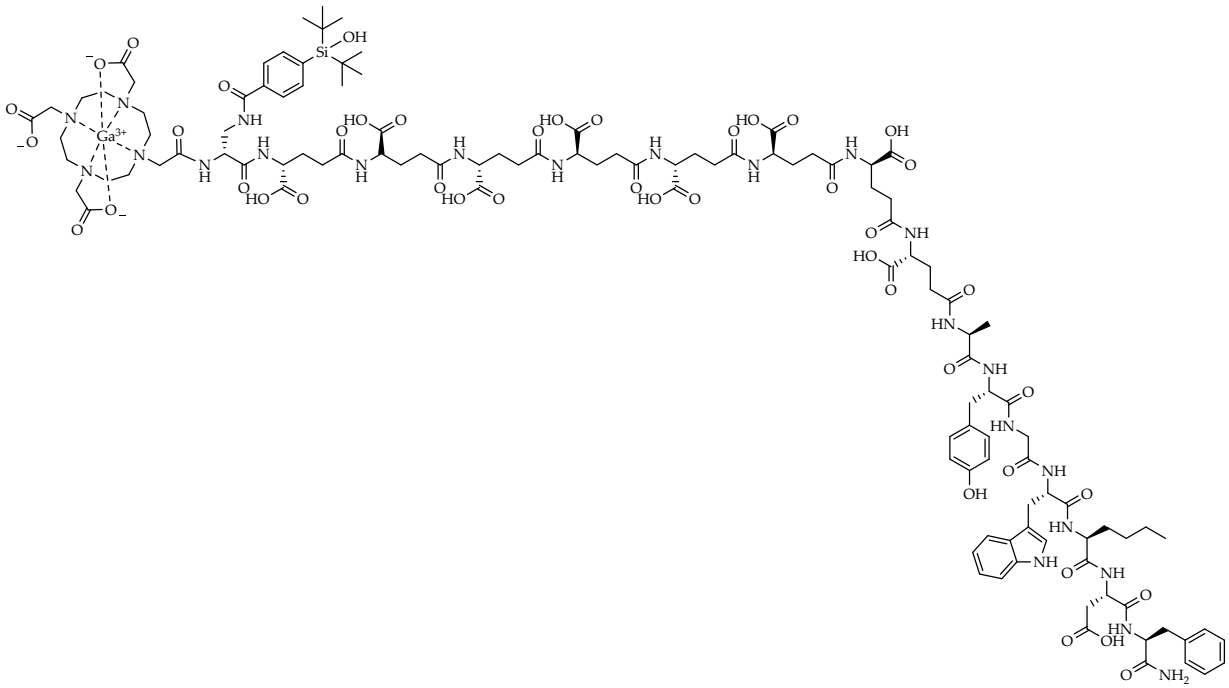

[nat/67Ga]Ga-DOTA-rhCCK-18.2: RP-HPLC (10→30% MeCN in H_2O with 0.1% TFA, 5 min, 30→60% MeCN in H_2O with 0.1% TFA, 15 min $\lambda = 220$ nm): $t_R = 14.2$ min, K′ = 6.10; MS (ESI, positive): m/z calculated for $C_{118}H_{162}GaN_{23}O_{44}Si$: 2704.5, found: m/z = 1352.9 $[M+2H]^{2+}$, 902.3 $[M+3H]^{3+}$.

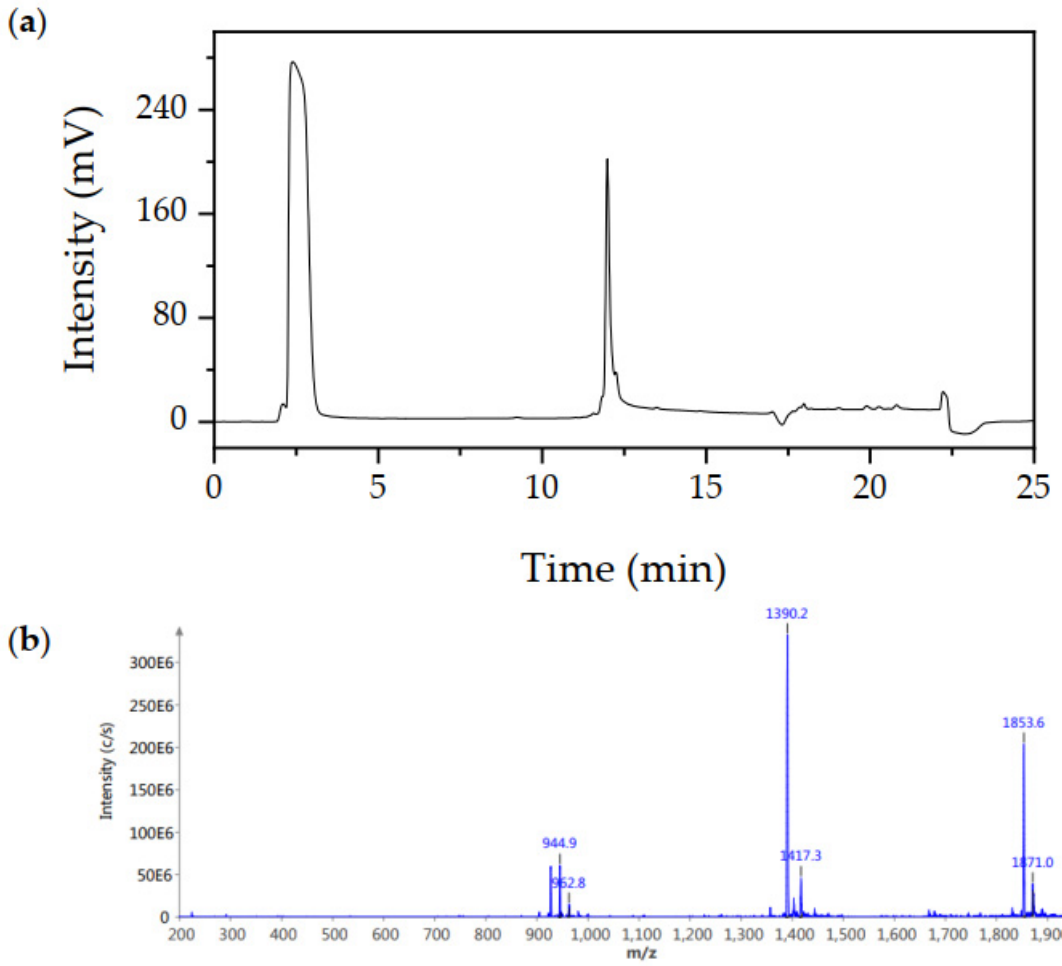

Figure S17. (**a**) Confirmation of peptide identity and integrity for [^{nat}Ga]Ga-(*R*)-DOTAGA-rhCCK-18, as analyzed by analytical RP-HPLC (10→90% MeCN in H_2O + 0.1% TFA in 15 min). (**b**) Mass spectrum of [^{nat}Ga]Ga-(*R*)-DOTAGA-rhCCK-18.

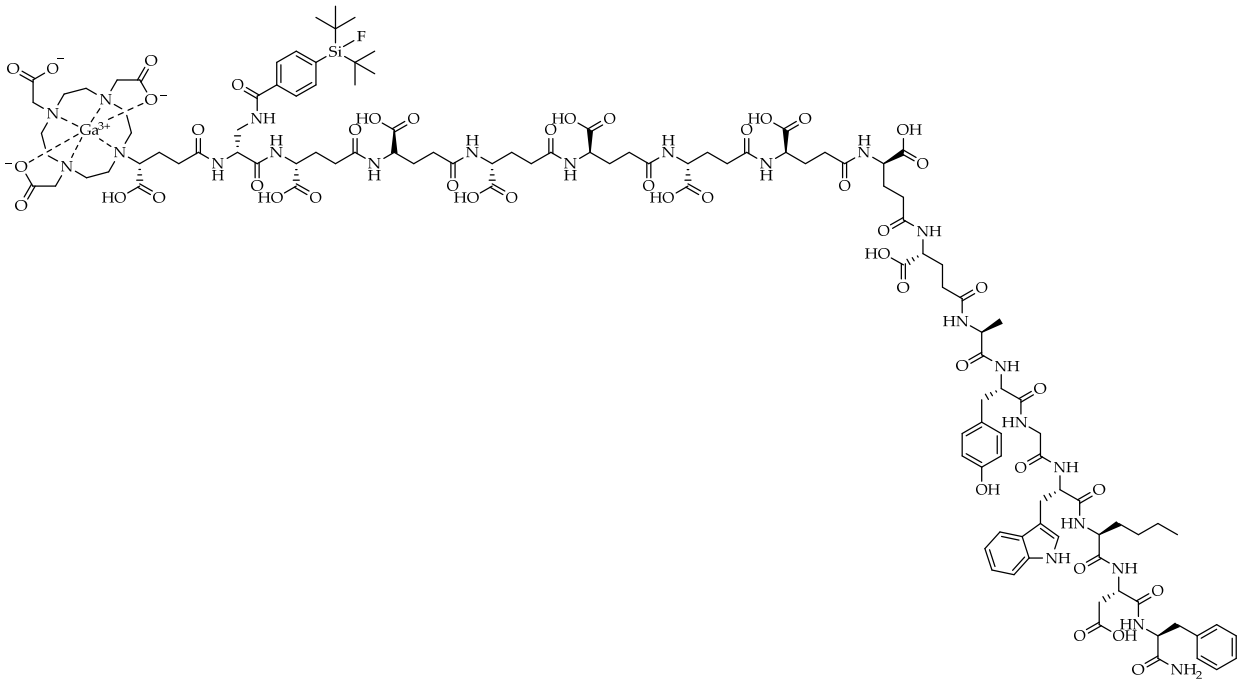

[^{nat}Ga]Ga-(R)-DOTAGA-rhCCK-18: RP-HPLC (10→70% MeCN in H_2O with 0.1% TFA, 15 min, λ = 220 nm): t_R = 12.0 min, K' = 6.11; MS (ESI, positive): m/z calculated for $C_{121}H_{165}FGaN_{25}O_{45}Si$: 2520.3, found: m/z = 1390.2 $[M+2H]^{2+}$.

SiFA hydrolysis

In order to hydrolyze the SiFA building block of the peptide precursors DOTA-rhCCK-16 and -18 to generate their SiOH-comprising analogs, DOTA-rhCCK-16.2 and 18.2, 1 eq. of each compound was treated with NaOH (15 eq., 12.5 mM), and the resulting solution was left at room temperature overnight. To terminate the reaction, HCl (15 eq., 25 mM) was added. Afterwards, the product was purified via RP-HPLC.

Labeling Procedures

^{18}F-Labeling

[^{18}F]fluoride (approx. 2-3 GBq) dissolved in H_2O was loaded onto a SEP-Pak® Light (46 mg) AccellTM Plus QMA cartridge (Waters GmbH, Eschborn, Germany) preconditioned with H_2O (10 mL). Afterwards, [^{18}F]fluoride was dried using 8 mL of anhydrous DMSO and inversely eluted from the cartridge with ammonium formate (250 µL, 50 mg NH_4HCOO dissolved in 500 µL anhydrous DMSO). Peptide precursor (1 nmol) was added to 50 µL eluate and the reaction mixture was heated to 60°C for 5 min. Afterwards, the reaction mixture was dissolved in PBS (10 mL, pH = 3) and the ^{18}F-labeled peptide was loaded onto an Oasis® HLB (30 mg) Light Cartridge (Waters GmbH, Eschborn, Germany) preconditioned with 10 mL EtOH and 10 mL H_2O. After washing the crude product with PBS (10 mL, pH = 7.4), the peptide was inversely eluted from the cartridge with 200 µL EtOH/H_2O (7/3). Radiochemical purity was determined using radio RP-HPLC and radio TLC (MeCN/PBS (pH = 7.4), 6/4 (*v*/*v*), +10% sodium acetate (2 M) + 1% TFA).

^{177}Lu-Labeling

For ^{177}Lu-labeling experiments, [^{177}Lu]$LuCl_3$ dissolved in hydrochloric acid (0.04 M, 40 GBq/mL) was acquired from ITM Isotope Technologies Munich SE (Garching, Germany). Radiolabeling of the peptide precursor (1 nmol) was performed at 90°C for 15 min in a NaOAc-buffered (1 M, pH = 5.5) hydrochloric acid (0.04 M) solution. After radiolabeling, a radiolysis quencher (sodium ascorbate, 1 M in H_2O) was added and radiochemical purity was determined via radio-RP-HPLC and radio-TLC (instant thin layer chromatography paper impregnated with silica gel (iTLC-SG, Agilent Technologies Inc., Folsom, United States); sodium citrate*1.5 H_2O (0.1 M)).

^{nat}Lu-Labeling

Quantitative ^{nat}Lu-labeling was conducted by stirring a solution of [^{nat}Lu]$LuCl_3$ (2.5 eq., 20 mM), peptide precursor (1 eq., 1 mM in DMSO) and Tracepur® H_2O at 90°C for 15 min. Confirmation of peptide integrity was performed via RP-HPLC and ESI-MS.

^{67}Ga-Labeling

^{67}Ga-Labeling experiments were conducted using 10-40 MBq of [^{67}Ga]$GaCl_3$ (Curium™ (Berlin, Germany), 4-(2-hydroxyethyl)-1-piperazineethanesulfonic acid-buffer (7 µL, 2.5 M, HEPES) and peptide precursor (1 nmol). The reaction mixture was stirred at 80 °C for 20 min. After radiolabeling, sodium ascorbate (1 M in H_2O) was added to prevent radiolysis, and radiochemical purity was determined via radio RP-HPLC and radio TLC (sodium citrate*1.5 H_2O (0.1 M)).

^{nat}Ga-Labeling

^{nat}Ga-Complexation of the CCK-2R ligands was accomplished by stirring a solution of [^{nat}Ga]$Ga(NO_3)_3$ (2.5 eq., 10 mM), peptide precursor (1 eq., 1 mM) and Tracepur® H_2O at 70 °C for 30 min. Confirmation of peptide integrity was performed via RP-HPLC and ESI-MS.

In Vitro Experiments

Cell Culture. CCK-2R-expressing rat pancreatic cancer cells AR42J (CLS GmbH, Eppelheim, Germany) were cultivated in monolayers in CELLSTAR® cell culture flasks acquired from Greiner Bio-One GmbH (Frickenhausen, Germany) at 37°C in a humidified atmosphere (5% CO_2) using a HERAcell 150i-Incubator (Thermo Fisher Scientific Inc., Waltham, United States). The nutrient medium RPMI 1640 medium, supplemented with 5 mM L-Gln 5 mL non-essential amino acids (100×) and 10% FCS, was used. Furthermore, a Dulbecco's PBS solution with 0.1% EDTA (*v*/*v*) was applied to detach the cells for cell passaging. The detached cells were counted using a Neubauer hemocytometer (Paul Marienfeld, Lauda-Königshofen, Germany). In addition, all operations under sterile conditions were accomplished using a MSC-Advantage safety workbench (Thermo Fisher Scientific Inc., Waltham, United States).

Determination of IC_{50}. AR42J cells (2.0×10^5 cells/well) were seeded into 24-well plates 24 ± 2 h prior to testing using 1 mL of nutrient medium (RPMI 1640, 5 mM L-Gln, 5 mL non-essential amino acids (100×), 10% FCS). Cells were incubated at 37°C in a humidified atmosphere (5% CO_2).
After the removal of the medium, each well was washed with 500 µL PBS. For the cell-based assay, 200 µL of the nutrient medium (+5% BSA), [^{177}Lu]Lu-DOTA-PP-F11N (25 µL, 0.3 pmol) as a radiolabeled reference and 25 µL of the peptide of interest in increasing concentrations (10^{-10} to 10^{-4} M) were added to the cells in triplicate. Thereafter, the assay was incubated for 3 h at 37°C and the supernatant was collected. The cells were washed with 300 µL PBS and the collected supernatant fractions were unified. After lysis of the cells with NaOH (300 µL, 1 N) for 15 min, the respective wells were washed with NaOH (300 µL, 1 N) and both fractions were unified. The radioactivity of both the supernatant and the lysed fractions were quantified using a γ-counter (PerkinElmer Inc., Waltham, United States). The obtained data were evaluated via the GraphPad PRISM software (GraphPad Software Inc., La Jolla, United States), which calculates the half-maximal inhibitory concentration (IC_{50}) of the peptides.

Internalization Studies. For the determination of the internalization kinetics of the various peptides, AR42J cells (3.0×10^5 cells/well) were seeded into polylysine-coated 24-well plates, adding 1 mL of nutrient medium. Afterwards, the cells were incubated for 24 ± 2 h at 37°C in a humidified atmosphere (5% CO_2).

On the day of the experiment, the medium was removed, and each well was washed with nutrient medium (300 µL). Afterwards 200 µL of nutrient medium, 25 µL of the ^{177}Lu-labeled peptide (0.3 pmol, $n = 6$) and either 25 µL of nutrient medium for internalization studies ($n = 3$) or 25 µL of [^{nat}Lu]Lu-DOTA-PP-F11N (10 µmol) for competition studies ($n = 3$) were added. Thereafter, the assay was incubated for various time points (1, 2, 4 and 6 h) at 37°C in a humidified atmosphere (5% CO_2). After incubation, the cells were put on ice for at least 1 min to stop internalization kinetics and the supernatant was collected. Then, the cells were washed with an ice-cold nutrient medium (300 µL) and both fractions were unified. In order to displace the peptides from the cell membrane, 300 µL of an ice-cold glycine buffer (1 M, pH = 2.2) were added and the cells were incubated on ice for 15 min. Afterwards, the supernatant was collected, and the cells were washed with an ice-cold glycine buffer (300 µL, 1 M, pH = 2.2) while both fractions were unified. After lysis of the cells with NaOH (300 µL, 1 N) for 15 min, the respective wells were washed with NaOH (300 µL, 1 N) and both fractions were unified. The radioactivity of the supernatant, the acid wash and the lysed fractions were quantified using a γ-counter.

Lipophilicity Studies. Lipophilicity (depicted as octanol-phosphate-buffered saline solution (PBS, pH = 7.4) distribution coefficient, log$D_{7.4}$) was determined by dissolving the ^{177}Lu-labelled peptide (approx. 1 MBq) in a mixture (1/1, *v*/*v*) of n-octanol and PBS. The suspension was vortexed in a reaction vial (1.5 mL) for 3 min at room temperature and the vial was centrifuged at 9000 rpm for 5 min (Biofuge 15, Heraus Sepatech GmbH, Osterode, Germany). Amounts of 200 µL aliquots of both layers were measured separately in a γ-counter (Perkin Elmer, Waltham, MA, USA). The experiment was repeated at least five times.

Stability Studies in Human Serum. The ^{177}Lu- as well as ^{67}Ga-labeled CCK-2R ligands (1 nmol, approx. 5 MBq) were incubated for 24 h in human serum (200 µL) at 37 °C. After incubation, ice-cold EtOH (125 µL) and MeCN (375 µL) were added and the suspension was centrifuged for 5 min at 5000 rpm. Then, the supernatant was transferred into new vials and centrifuged for another 5 min at 5000 rpm. After separating the precipitate from the solution, the stability of the ligands was determined via RP-HPLC chromatography (10→30% MeCN in H_2O + 0.1% TFA in 5 min, 30→60% MeCN in H_2O + 0.1% TFA in 15 min).

Table S1. Affinity data (n = 3) of the compounds evaluated, determined on AR42J cells (2.0 x 10^5 cells/well) with [^{177}Lu]Lu-DOTA-PP-F11N (0.3 pmol/well) as radiolabeled reference (3 h, 37°C, RPMI 1640, 5 mM L-Gln, 5 mL non-essential amino acids (100x), 10% FCS + 5% BSA (*v*/*v*)).

peptide	IC_{50} (nM) ^{nat}Lu-labeled	IC_{50} (nM) ^{nat}Ga-labeled
DOTA-PP-F11N	12.8 ± 2.8	17.0 ± 0.8
(*R*)-DOTAGA-PP-F11N	16.8 ± 2.8	13.9 ± 0.7
(*R*)-DOTAGA-rhCCK-16	20.4 ± 2.7	62.3 ± 6.9
DOTA-rhCCK-16	7.54 ± 0.26	16.8 ± 0.9
(*R*)-DOTAGA-rhCCK-18	20.4 ± 2.0	52.9 ± 6.0
DOTA-rhCCK-18	4.71 ± 0.62	13.7 ± 1.3

Table S2. Receptor-mediated internalization values (37 °C, RPMI 1640, 5 mM L-Gln, 5 mL non-essential amino acids (100x), 10% FCS, 0.25 pmol/well) determined as percentages (%) of the applied activity of [^{177}Lu]Lu-(*R*)-DOTAGA-rhCCK-18 as well as [^{177}Lu]Lu-DOTA-rhCCK-16 and -18 using AR42J cells (3.0 x 10^5 cells/well) at different time points (1, 2, 4 and 6 h). Data are corrected for non-specific binding (10 µmol, [^{nat}Lu]Lu-DOTA-PP-F11N).

Peptide	**Internalization Values** (%)				**Internalization Values*** (%F11N)
	1 h	**2 h**	**4 h**	**6 h**	**6 h**
[^{177}Lu]Lu-DOTA-PP-F11N	6.44 ± 0.32	10.1 ± 0.4	17.5 ± 1.0	22.4 ± 0.6	-
[$^{nat/177}$Lu]Lu-DOTA-rhCCK-16	19.5 ± 2.3	33.1 ± 1.7	43.9 ± 0.7	51.1 ± 1.7	215 ± 7
[$^{nat/177}$Lu]Lu-DOTA-rhCCK-18	15.4 ± 1.4	24.1 ± 1.6	41.6 ± 2.6	54.8 ± 1.5	244 ± 7
[^{177}Lu]Lu-(*R*)-DOTAGA-rhCCK-16	7.63 ± 0.13	14.0 ± 1.3	23.2 ± 2.7	32.2 ± 2.1	135 ± 9
[$^{nat/177}$Lu]Lu-(*R*)-DOTAGA-rhCCK-18	8.75 ± 1.43	16.8 ± 1.7	29.3 ± 1.3	36.8 ± 2.0	154 ± 8

* Internalization values are listed relative to the reference DOTA-PP-F11N

Table S3. Amounts of intact peptides and their analogs containing a hydrolyzed SiFA (=SiOH) moiety (n = 3) of the compounds evaluated, determined in human serum after incubation at 37°C for 24 h.

Peptide	Intact peptide (%)	SiOH-containing analog (%)
[^{67}Ga]Ga-DOTA-rhCCK-16	39.6 ± 7.9	56.5 ± 8.0
[^{177}Lu]Lu-DOTA-rhCCK-16	21.8 ± 0.8	69.1 ± 1.0
[^{67}Ga]Ga-DOTA-rhCCK-18	43.7 ± 6.9	53.6 ± 6.6
[^{177}Lu]Lu-DOTA-rhCCK-18	25.3 ± 3.1	67.7 ± 3.1

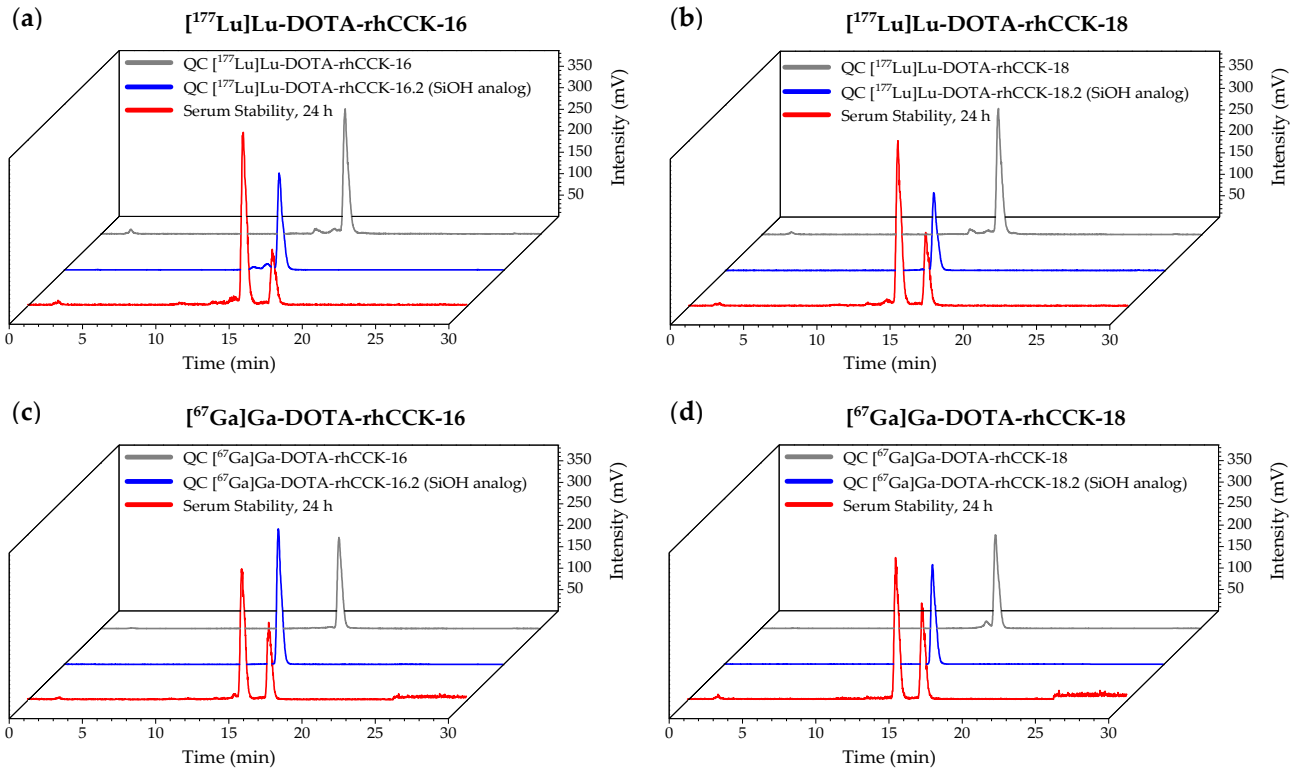

Figure S18. Stability studies of (a) [^{177}Lu]Lu-DOTA-rhCCK-16, (b) [^{177}Lu]Lu-DOTA-rhCCK-18, (c) [^{67}Ga]Ga-DOTA-rhCCK-16, and (d) [^{67}Ga]Ga-DOTA-rhCCK-18 in human serum (37°C, 24 h), as analyzed by analytical RP-HPLC (10→30% MeCN in H_2O + 0.1% TFA in 5 min, 30→60% MeCN in H_2O + 0.1% TFA in 5 min). The chromatograms of the respective compounds after incubation in human serum (37°C, 24 h) are depicted in red. Quality controls of the intact compounds comprising a SiFA moiety are depicted in gray and quality controls of the SiOH-comprising analogs ("hydrolyzed SiFA moiety") are depicted in blue.

Table S4. Biodistribution data of [^{177}Lu]Lu-DOTA-rhCCK-18 in selected organs at 1 and 24 h p.i. in AR42J tumor-bearing CB17-SCID mice (100 pmol each). Data are expressed as %ID/g, mean ± SD (n = 4). Biodistribution data of [^{177}Lu]Lu-DOTA-rhCCK-18 (100 pmol) co-injected with [^{177}Lu]Lu-DOTA-MGS5 in selected organs at 24 h p.i. in AR42J tumor-bearing CB17-SCID mice. Data are expressed as %ID/g, mean ± SD (n = 2).

Organ	[^{177}Lu]Lu-DOTA-rhCCK-18 (1 h p.i.)	[^{177}Lu]Lu-DOTA-rhCCK-18 (24 h p.i.)	[^{177}Lu]Lu-DOTA-rhCCK-18 (24 h p.i.) competition studies
Blood	2.56 ± 0.60	0.02 ± 0.01	0.02 ± 0.00
Heart	0.94 ± 0.02	0.08 ± 0.02	0.08 ± 0.01
Lung	2.05 ± 0.20	0.18 ± 0.15	0.76 ± 0.17
Liver	1.15 ± 0.18	0.53 ± 0.07	1.51 ± 0.02
Spleen	0.60 ± 0.08	0.22 ± 0.02	0.95 ± 0.14
Pancreas	1.22 ± 0.21	0.34 ± 0.09	0.22 ± 0.02
Stomach	4.25 ± 0.45	4.28 ± 1.05	0.18 ± 0.02
Intestine	0.61 ± 0.11	0.21 ± 0.02	0.17 ± 0.06
Kidney	97.2 ± 14.0	134 ± 18	193 ± 15
Adrenal	0.52 ± 0.07	0.37 ± 0.12	5.02 ± 4.64
Muscle	0.38 ± 0.03	0.08 ± 0.06	0.07 ± 0.04
Bone	0.48 ± 0.02	0.18 ± 0.03	0.22 ± 0.06
Tumor	24.1 ± 4.2	25.4 ± 4.7	1.75 ± 0.26

Table S5. Tumor-to-background ratios of [^{177}Lu]Lu-DOTA-rhCCK-18, [^{177}Lu]Lu-(*R*)-DOTAGA-rhCCK-16 and [^{177}Lu]Lu-(*R*)-DOTAGA-rhCCK-9 for the selected organs of AR42J tumor-bearing CB17-SCID mice at 24 h p.i. (100 pmol each). Data are expressed as mean ± SD (n = 4).

Organ	[^{177}Lu]Lu-DOTA-rhCCK-18	[^{177}Lu]Lu-(*R*)-DOTAGA-rhCCK-16	[^{177}Lu]Lu-(*R*)-DOTAGA-rhCCK-18
Blood	1630 ± 823	1067 ± 112	421 ± 152
Heart	312 ± 58	144 ± 35	72.4 ± 4.0
Lung	236 ± 118	176 ± 59	79.9 ± 29.9
Liver	48.1 ± 6.7	14.5 ± 5.1	7.24 ± 2.54
Spleen	115 ± 15	25.3 ± 5.9	19.8 ± 11.7
Pancreas	78.8 ± 17.5	46.2 ± 19.6	27.6 ± 14.0
Stomach	6.58 ± 2.77	4.59 ± 1.37	3.64 ± 0.99
Intestine	124 ± 30	81.9 ± 20.9	25.3 ± 8.3
Kidney	0.19 ± 0.01	0.18 ± 0.04	0.08 ± 0.01
Adrenal	73.3 ± 13.4	28.9 ± 18.5	26.8 ± 20.3
Muscle	650 ± 542	321 ± 77	307 ± 149
Bone	151 ± 48	96.8 ± 28.6	9.57 ± 4.67

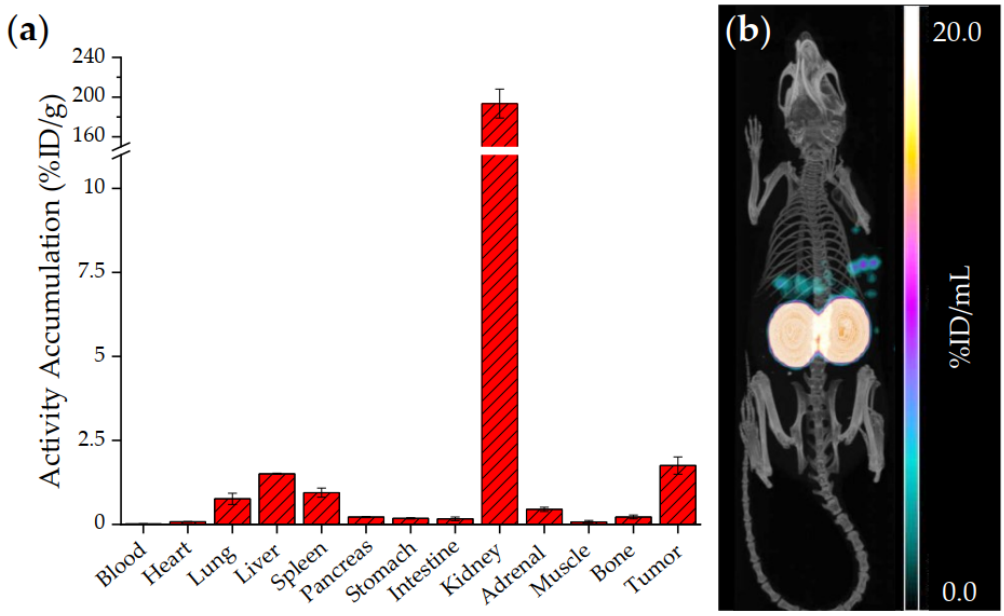

Figure S19. (**a**) Biodistribution and (**b**) a representative μSPECT/CT image of [^{177}Lu]Lu-DOTA-rhCCK-18 (100 pmol) co-injected with [^{nat}Lu]Lu-DOTA-MGS5 (40 nmol) in selected organs (%ID/g) at 24 h p.i. in AR42J tumor-bearing CB17-SCID mice. Data is expressed as mean ± SD (n = 2).

2.3 Investigation of the structure-activity relationship at the N-terminal part of minigastrin analogs

Reprint Permission:

EJNMMI RESEARCH

ORIGINAL RESEARCH

Open Access

Investigation of the structure-activity relationship at the *N*-terminal part of minigastrin analogs

Nadine Holzleitner[1†], Thomas Günther[1*†], Amira Daoud-Gadieh[1], Constantin Lapa[2] and Hans-Jürgen Wester[1]

Abstract

Background Over the last years, several strategies have been reported to improve the metabolic stability of minigastrin analogs. However, currently applied compounds still reveal limited in vitro and in vivo stability. We thus performed a glycine scan at the *N*-terminus of DOTA-MGS5 (DOTA-D-Glu-Ala-Tyr-Gly-Trp-(*N*-Me)Nle-Asp-1-Nal) to systematically analyze the peptide structure. We substituted *N*-terminal amino acids by simple PEG spacers and investigated in vitro stability in human serum. Furthermore, we evaluated different modifications on its tetrapeptide binding sequence (*H*-Trp-(*N*-Me)Nle-Asp-1-Nal-NH_2).

Results Affinity data of all glycine scan peptides were found to be in a low nanomolar range (4.2–8.5 nM). However, a truncated compound lacking the D-γ-Glu-Ala-Tyr sequence revealed a significant loss in CCK-2R affinity. Substitution of the D-γ-Glu-Ala-Tyr-Gly sequence of DOTA-γ-MGS5 (DOTA- D-γ-Glu-Ala-Tyr-Gly-Trp-(*N*-Me)Nle-Asp-1-Nal-NH_2) by polyethylene glycol (PEG) spacers of different length exhibited only a minor influence on CCK-2R affinity and lipophilicity. However, in vitro stability of the PEG-containing compounds was significantly decreased. In addition, we confirmed that the tetrapeptide sequence *H*-Trp-Asp-(*N*-Me)Nle-1-Nal-NH_2 is indeed sufficient for high CCK-2R affinity.

Conclusion We could demonstrate that a substitution of D-γ-Glu-Ala-Tyr-Gly by PEG spacers simplified the peptide structure of DOTA-MGS5 while high CCK-2R affinity and favorable lipophilicity were maintained. Nevertheless, further optimization with regard to metabolic stability must be carried out for these minigastrin analogs.

Keywords Cholecystokinin-2 receptor (CCK-2R), Cholecystokinin-B receptor (CCK-BR), Medullary thyroid carcinoma (MTC), Minigastrin, Tetrapeptide

Introduction

In 1999, Behr et al. reported first studies on the human peptide hormone minigastrin (*H*-Leu-$(Glu)_5$-Ala-Tyr-Gly-Trp-Met-Asp-Phe-NH_2) and its diethylenetriaminepentaacetic acid (DTPA)-conjugated analog targeting the cholecystokinin-2 receptor (CCK-2R) [1], which is overexpressed in a high percentage on several human tumor types such as medullary thyroid carcinoma (MTC, 92%), small cell lung cancer (57%), stromal ovarian cancer (100%) and astrocytoma (65%) [2, 3]. Over the years, many modifications have been published, improving the pharmacokinetic properties of radiolabeled minigastrin derivatives. For example, the substitution of Leu by D-Glu led to an improved complex stability of [^{111}In]In- and [^{88}Y]Y-DTPA-MG0 (DTPA-D-Glu-$(Glu)_5$-Ala-Tyr-Gly-Trp-Met-Asp Phe-NH_2) [4]. Due to an observed elevated kidney accumulation, approaches to decrease this uptake by a reduction of the *N*-terminal D-glutamate chain as for MG11 (*H*-D-Glu-Ala-Tyr-Gly-Trp-Met-Asp-Phe-NH_2)

†Nadine Holzleitner and Thomas Günther contributed equally to this work.

*Correspondence:
Thomas Günther
thomas.guenther@tum.de
[1] Department of Chemistry, Technical University of Munich, 85748 Garching, Germany
[2] Nuclear Medicine, University Hospital Augsburg, 86156 Augsburg, Germany

[5, 6], or the substitution of the six L- by six D-glutamate moieties as for CP04 (DOTA-(D-Glu)$_6$-Ala-Tyr-Gly-Trp-Met-Asp-Phe-NH$_2$) [7, 8] were performed.

However, one major drawback of minigastrin analogs with regard to a clinical use was their low in vivo stability. Therefore, Ocak et al. performed comparative stability studies in vitro as well as in vivo of various CCK-2R-targeted peptides, including MG11 and CP04. In the course of these experiments, the Asp-Phe, Gly-Trp and Tyr-Gly sequences were identified as the major cleavage sites of minigastrin analogs [8, 9].

In 2018, Klingler et al. reported that the substitution of Phe by 1-Nal and Met by (*N*-Me)Nle (Nle: norleucine) in MG11 led to an increased metabolic stability of the resulting compound (DOTA-MGS5) while high CCK-2R affinity was maintained [10]. Furthermore, [^{68} Ga]Ga-DOTA-MGS5 revealed high activity levels in the tumor (23.3 ± 4.7%ID/g), while displaying low activity uptake in the kidneys (5.7 ± 1.4%ID/g) at 1 h p.i. in A431-CCK-2R tumor-bearing nude mice [11, 12]. Further studies on substituting either Ala, Tyr or Gly in DOTA-MGS5 by Pro residues resulted in highly CCK-2R-affine peptides with improved metabolic stability. Especially DOTA-MGS8 (DOTA-D-Glu-Pro-Tyr-Gly-Trp-(*N*-Me)Nle-Asp-1-Nal-NH$_2$) led to improved activity levels in the tumor and thus, tumor/background ratios as compared to DOTA-MGS5 [13–15].

Another strategy to stabilize CCK-2R-targeted compounds was attempted by a systematic substitution of peptide bonds by 1,4-disubstituted 1,2,3-triazoles in DOTA-[Nle^{15}]MG11 (DOTA-D-Glu-Ala-Tyr-Gly-Trp-Nle-Asp-Phe-NH$_2$) and DOTA-PP-F11N (DOTA-(D-Glu)$_6$-Ala-Tyr-Gly-Trp-Nle-Asp-Phe-NH$_2$). Only a minor impact on CCK-2R affinity was observed for peptides comprising a triazole bond between the D-Glu-Pro, Pro-Tyr, Tyr-Gly and Gly-Trp sequence. However, increased metabolic stability was only observed for compounds that comprise triazole bonds between Trp-Nle, Nle-Asp or Asp-Phe, which led to a loss in CCK-2R affinity, though. Therefore, no noticeable benefit on tumor accumulation was observed [16, 17].

Considering the above-mentioned studies, a high tolerance toward modifications within minigastrin analogs with regard to CCK-2R affinity was observed, especially when the *N*-terminal sequence (D-Glu-Ala-Tyr-Gly) was addressed [10, 13, 16, 17]. Indeed, substitution of α- by γ-linked D-glutamate moieties within DOTA-PP-F11N had a beneficial impact on CCK-2R affinity [18]. Due to this high tolerability toward modifications at the *N*-terminus, one aim of this study was to provide a better insight on the structure–activity relationship of minigastrin analogs at this part. Therefore, we carried out a glycine scan to elucidate the influence of the D-γ-Glu-Ala-Tyr-Gly sequence in DOTA-γ-MGS5 (DOTA-D-γ-Glu-Ala-Tyr-Gly-Trp-(*N*-Me)Nle-Asp-1-Nal-NH$_2$) on CCK-2R affinity and if a simple polyethylene glycol (PEG) spacer can retain high CCK-2R affinity and concurrently improve metabolic stability (Fig. 1). Furthermore, it was investigated whether the *C*-terminal tetrapeptide is sufficient for high CCK-2R affinity and which impact small modifications within this tetrapeptide unit have on affinity.

Materials and methods

Characterization of all CCK-2R-targeted compounds is provided in the Additional file 1: (Fig. S1–S17). Electrospray ionization-mass spectra for characterization of the substances were acquired on an expression^L CMS mass spectrometer (Advion Ltd., Harlow, UK).

Chemical synthesis and labeling procedures

Synthesis of the peptide precursors was conducted via solid-phase peptide synthesis (SPPS) using an *H*-Rink amide ChemMatrix® resin (35–100 mesh particle size, 0.4–0.6 mmol/g loading, Merck KGaA, Darmstadt, Germany). After resin cleavage with concomitant cleavage of acid-labile protecting groups, final purification was performed by reversed phase high performance liquid chromatography (RP-HPLC). ^{nat}Lu- and ^{177}Lu-labeling was conducted according to previously published procedures [19].

In vitro *experiments*

IC_{50} values of all compounds were determined according to a previously published procedure [18]. In brief, competitive binding studies were performed via co-incubation of increasing concentrations of the peptide of interest (10^{-10} to 10^{-4} M, in triplicate) together with the reference compound [^{177}Lu]Lu-DOTA-PP-F11N (0.3 pmol/well) on AR42J cells (2×10^5 cells per 1 mL/well) at 37 °C for 3 h.

Lipophilicity (depicted as *n*-octanol-phosphate-buffered saline solution (PBS, $pH=7.4$) distribution coefficient, log$D_{7.4}$) of ^{177}Lu-labeled minigastrin analogs was evaluated as previously published [18].

In vitro stability of the ^{177}Lu-labeled peptides (1 nmol, ~ 5 MBq) was analyzed via radio-RP-HPLC after incubation at 37 °C for 24 h in human serum of a healthy donor via an established protocol [20].

Statistics

Acquired data were statistically analyzed by performing a Student's *t*-test via Excel (Microsoft Corporation, Redmond, WA, USA) and OriginPro software (version 9.7) from OriginLab Corporation (Northampton, MA, USA). Acquired *p* values of <0.05 were considered statistically significant.

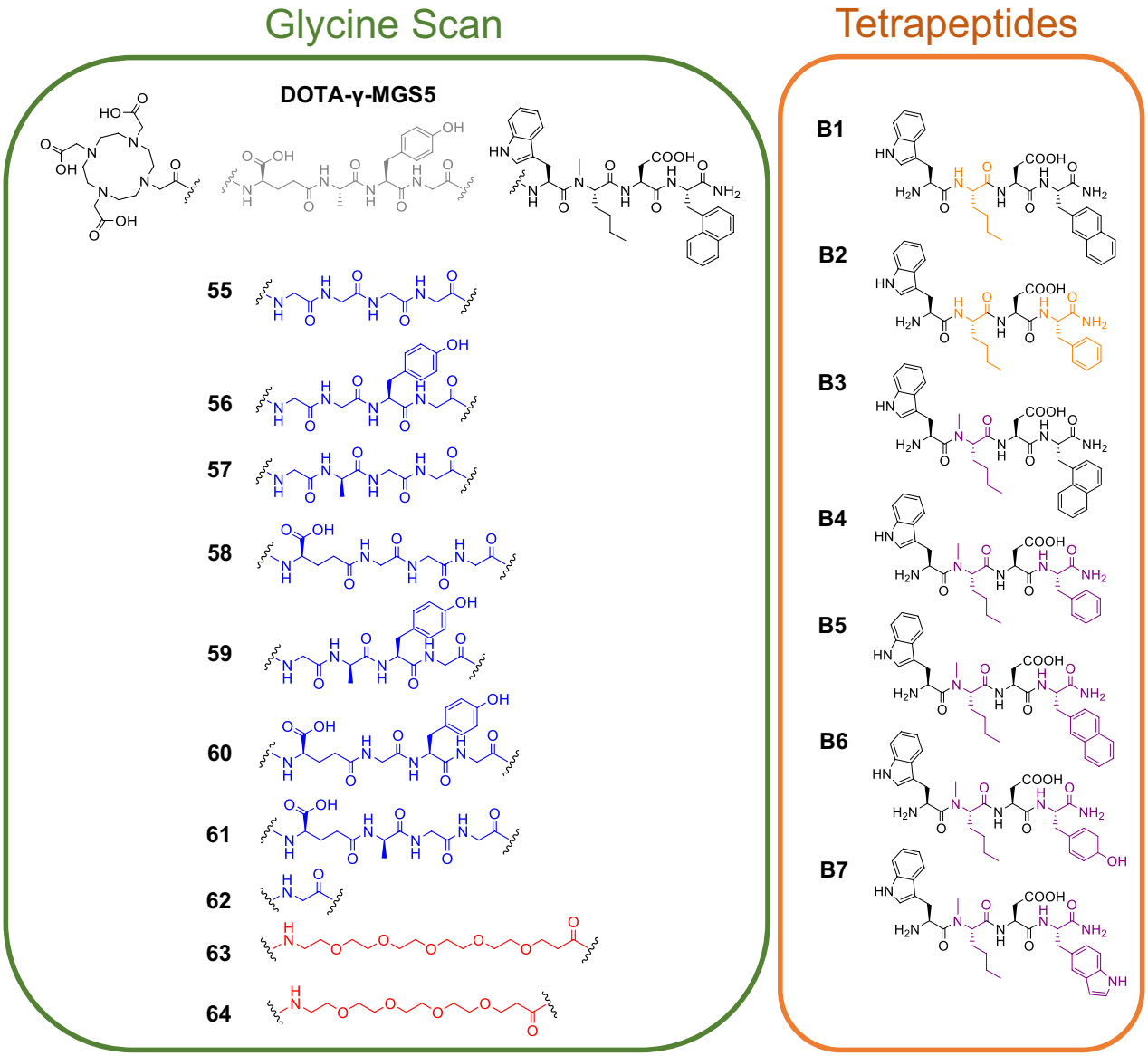

Fig. 1 Chemical structures of the glycine scan derivatives (blue), the PEG-linked compounds (red), the tetrapeptides lacking an *N*-methyl group at the norleucine (Nle) moiety (orange) and the tetrapeptides comprising an *N*-methyl group at the Nle moiety (purple)

Results

Chemical synthesis and radiolabeling

Synthesis via SPPS and subsequent RP-HPLC purification yielded 4–8% off-white solid (chemical purity > 95%, determined by RP-HPLC at $\lambda = 220$ nm). Quantitative ^{nat}Lu-labeling of the peptides was accomplished by adding a 2.5-fold excess of [^{nat}Lu]$LuCl_3$ to the DOTA-comprising peptides and heating the solution to 90 °C for 15 min. As unbound Lu^{3+} did not reveal any influence on affinity experiments, no further purification steps were conducted prior to usage [21]. ^{177}Lu-labeling proceeded in radiochemical yields and purities of > 95% and molar activities of 10–50 GBq/µmol.

In vitro evaluation

Affinity and lipophilicity data of the glycine scan derivatives are summarized in Fig. 2.

In general, [^{nat}Lu]Lu-DOTA-CCK-55 to -61 revealed IC_{50} values (4.2–9.7 nM, Additional file 1: Table S1) in a low nanomolar range, comparable to those of the reference compounds [^{nat}Lu]Lu-DOTA-MGS5 (5.2 ± 0.8 nM) and [^{nat}Lu]Lu-DOTA-γ-MGS5 (4.9 ± 0.8 nM), while [^{nat}Lu]Lu-DOTA-CCK-62, a compound completely lacking the amino acid sequence D-γ-Glu-Ala-Tyr, exhibited a significant loss in CCK-2R affinity ($IC_{50} = 98.9 \pm 8.4$ nM, $p < 0.0001$). Substitution of the amino acid sequence Dγ-Glu-Ala-Tyr-Gly by a $(PEG)_4$ or $(PEG)_3$ linker ([^{nat}Lu]

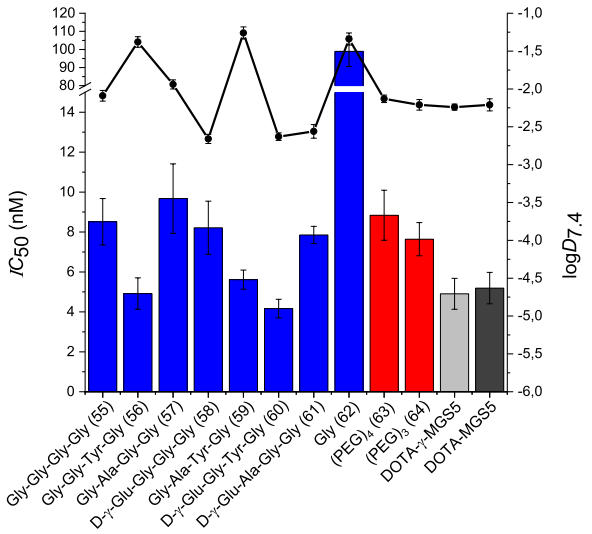

Fig. 2 IC_{50} and log$D_{7.4}$ values of the glycine scan derivatives ([$^{nat/177}$Lu]Lu-DOTA-CCK-55 to – 62, depicted in blue) and peptides containing a PEG spacer unit (depicted in red, [$^{nat/177}$Lu] Lu-DOTA-CCK-63 and -64), as well as the reference ligands [$^{nat/177}$Lu]Lu-DOTA-MGS5 (depicted in light gray) and [$^{nat/177}$Lu] Lu-DOTA-γ-MGS5 (depicted in dark gray)

Lu-DOTA-CCK-63 and -64, respectively) had only a minor impact on CCK-2R affinity (IC_{50}: 8.8 ± 1.3 and 7.6 ± 0.9 nM).

Log$D_{7.4}$ values of [^{177}Lu]Lu-DOTA-CCK-55, -58, -60, -61, -63, and -64 were observed to be in a range of –2.7 to –2.1, similar to the references [^{177}Lu]Lu-DOTA-MGS5 (log$D_{7.4}$ = − 2.21 ± 0.08) and [^{177}Lu]Lu-DOTA-γ-MGS5 (log$D_{7.4}$ = − 2.24 ± 0.04). In contrast, [^{177}Lu]Lu-DOTA-CCK-56, − 57, − 59 and − 62 were found to be more lipophilic (log$D_{7.4}$ = − 1.9 to − 1.2).

Stability studies revealed high in vitro stability in human serum (incubation for 24 h at 37 °C, Fig. 3, Additional file 1: Table S2) for both [^{177}Lu]Lu-DOTA-γ-MGS5 (96.8 ± 2.8%) as well as [^{177}Lu]Lu-DOTA-CCK-55 (87.5 ± 1.9%) and − 62 (97.9 ± 1.8%), which comprised a $(Gly)_4$ and Gly, respectively, instead of a D-γ-Glu-Ala-Tyr-Gly linker (as in [^{177}Lu]Lu-DOTA-γ-MGS5). In contrast, [^{177}Lu]Lu-DOTA-CCK-63 (57.4 ± 3.7%) and − 64 (43.8 ± 2.3%) that contain a $(PEG)_4$ and $(PEG)_3$ moiety, respectively, instead of a D-γ-Glu-Ala-Tyr-Gly linker, displayed distinctly lower in vitro stability than the other compounds.

In order to evaluate whether a *C*-terminal tetrapeptide is sufficient for high CCK-2R affinity, we determined the IC_{50} values of various tetrapeptides (Fig. 4, Additional file 1: Table S1).

B3, B4 and B6, which contain an *N*-methyl group at the L-Nle moiety revealed IC_{50} values in a low nanomolar range (4.5–5.9 nM), whereas B1 and B2, which did not comprise an *N*-methylated Nle residue, exhibited a significant loss in CCK-2R affinity ($p < 0.0001$). However, B5 and B7, comprising either an L-2-naphtylalanine or L-tryptophan moiety at the *N*-terminus of the tetrapeptide sequence demonstrated 3.5- to 19-fold elevated IC_{50} values compared to B3, B4 and B6, despite carrying an *N*-methylated L-Nle.

Discussion

Over the years, the effect of various modifications in minigastrin analogs on CCK-2R affinity and in vivo stability was investigated. Especially the *N*-terminal amino acids D-Glu, Ala, Tyr and Gly were substituted by different building blocks, such as proline moieties (Klingler et al.) or triazole bonds (Grob et al.), which did not result in a major loss in CCK-2R affinity [13, 16, 17]. As we wanted to examine whether the presence of all of these four amino acids (D-Glu, Ala, Tyr and Gly) is crucial for high CCK-2R affinity, one aim of this study was to systematically substitute said amino acids by glycine to elucidate the structure–activity relationship of these amino acids within minigastrin analogs. As recently published data by our group suggested a beneficial impact of γ- instead of α-linked D-glutamate moieties on CCK-2R affinity [18], we carried out our studies on the peptide DOTA-γ-MGS5 (DOTA- D-γ-Glu-Ala-Tyr-Gly-Trp-(*N*-Me)Nle-Asp-1-Nal-NH_2). Furthermore, we wanted to investigate whether the *C*-terminal tetrapeptide (*H*-Trp-(*N*-Me)Nle-Asp-1-Nal-NH_2) might be sufficient for high CCK-2R affinity.

The glycine scan revealed that D-γ-Glu, Ala and Tyr each can be substituted by a Gly, without causing a major loss in CCK-2R affinity (IC_{50} = 4.2–9.7 nM), in comparison to the references [^{nat}Lu]Lu-DOTA-MGS5 (IC_{50} = 5.2 ± 0.8 nM) and [^{nat}Lu]Lu-DOTA-γ-MGS5 (IC_{50} = 4.9 ± 0.8 nM). Therefore, it can be concluded that these three amino acids are not necessary for high CCK-2R affinity, as each could be easily replaced by a glycine residue. Similar observations were made by Silvente-Poirot et al. when successively substituting each amino acid in CCK2–9 (*H*-Asp-Tyr-Met-Gly-Trp-Met-Asp-Phe-NH_2) by an alanine residue, which exhibited only slight loss of CCK-2R affinity for the substitution of the *N*-terminal amino acids, while substitution of the four *C*-terminal amino acids resulted in low CCK-2R affinity [22]. These data accompany previously reported data on modifications at the *N*-terminal part of minigastrin analogs, as it could be demonstrated that the tolerability toward substitutions is high [14, 17, 18]. However, it could be shown that the presence of these amino acids is required with regard to the distance of the DOTA chelator to the pharmacophore, as [^{nat}Lu]Lu-DOTA-CCK-62 (DOTA-Gly-Trp-(*N*-Me)Nle-Asp-1-Nal-NH_2, IC_{50} = 98.9 ± 8.4 nM) revealed a significant loss in CCK-2R affinity ($p < 0.0001$).

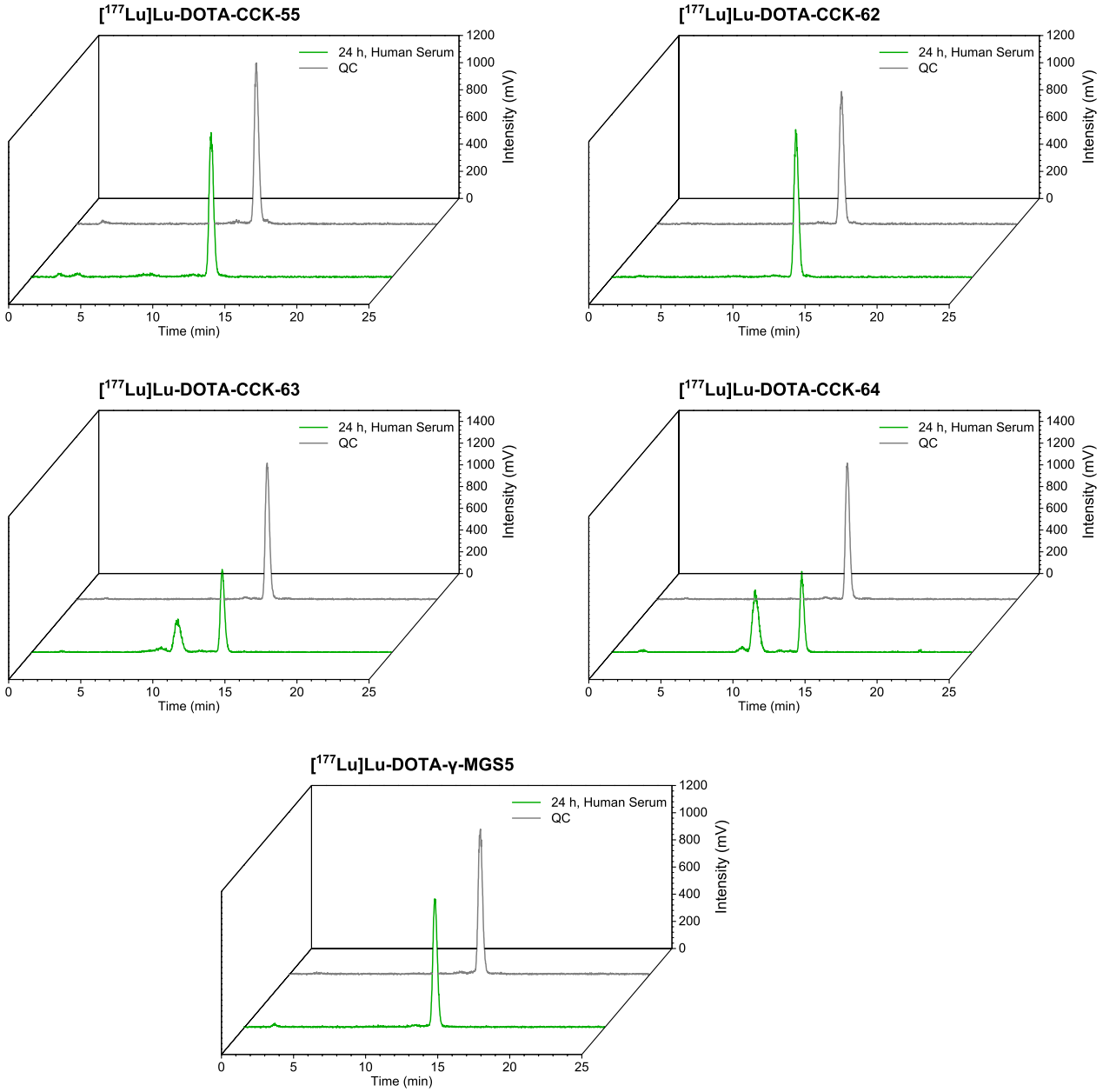

Fig. 3 In vitro stability studies in human serum (24 h, 37 °C) as analyzed by analytical RP-HPLC (10 → 30% MeCN in H_2O + 0.1% TFA in 5 min, 30 → 60% MeCN in H_2O + 0.1% TFA in 5 min)

Hence, a spacer unit between the binding motif and the chelator moiety is necessary, in order to retain high CCK-2R binding. Nevertheless, it is legitimate to question whether the pharmacophore consists of only four instead of seven amino acids, as the three *N*-terminal amino acids could be replaced by glycine residues, which are usually not linked to a pharmacological effect. This is supported by Silvente-Poirot et al. who showed high CCK-2R affinity for the *H*-Trp-Met-Asp-Phe-NH_2 fragment [22].

In order to further examine this assumption, we substituted D-γ-Glu-Ala-Tyr-Gly in DOTA-γ-MGS5 by a $(PEG)_4$ as well as a $(PEG)_3$ spacer, which resulted in slightly less (compared to the references) yet still highly CCK-2R-affine minigastrin analogs ([^{nat}Lu]Lu-DOTA-CCK-63: $IC_{50} = 8.8 \pm 1.3$ nM, [^{nat}Lu]Lu-DOTA-CCK-64: $IC_{50} = 7.6 \pm 0.9$ nM). The loss of affinity can be attributed to the lack of negative charges within the linker section, as it was shown that the CCK-2R comprises a high

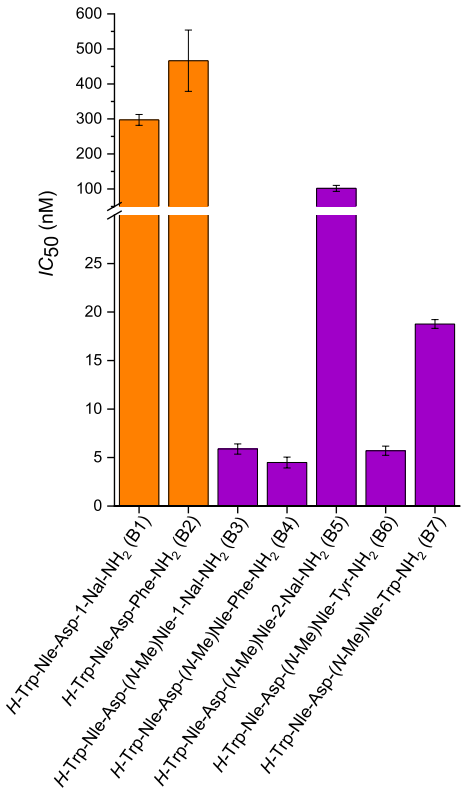

Fig. 4 IC_{50} values of various tetrapeptide CCK-2R binding sequences

number of positively charged residues in the region that interacts with the linker section of its ligands, which is why negatively charged moieties at the *N*-terminus usually lead to increased CCK-2R affinity [23]. Supported by our results, we strongly suggest that the pharmacophore of minigastrin analogs indeed consists of only four amino acids, while the remaining *N*-terminal amino acids such as D-γ-Glu or D-Glu, Ala, Tyr and Gly can be mainly considered a spacer for the (DOTA) chelator.

With the replacement of four *N*-terminal amino acids (of which three are L-amino acids) by an unnatural PEG chain, we aimed to improve metabolic stability of minigastrin analogs, as this should hamper their enzymatic cleavage at two major cleavage sites reported in the literature (Tyr-Gly and Gly-Trp) [8]. However, while high in vitro stability was observed in human serum for the reference, [^{177}Lu]Lu-DOTA-γ-MGS5, as well as [^{177}Lu]Lu-DOTA-CCK-55 (-$(Gly)_3$-) and -62 (-Gly-), a distinctly lower stability was determined for [^{177}Lu]Lu-DOTA-CCK-63 (-$(PEG)_4$-) and -64 (-$(PEG)_3$-), which was surprising, given the robustness of a PEG chain and its usually positive impact on stability [24–27] and the susceptibility of L-amino acids toward in vitro and in vivo degradation. An experimental error can be excluded, as all compounds were incubated (in separate vials) at the same time using the same batch of human serum. The respective metabolites observed for the two PEG-comprising compounds could not be identified, which is why further studies have to be carried out to elucidate the reason for this unexpected observation and to find a strategy to increase metabolic stability of such PEG-containing minigastrin derivatives.

Nevertheless, to further prove that a tetrapeptide motif is sufficient for high CCK-2R affinity, we determined the IC_{50} values of various tetrapeptides based on the *C*-terminus of DOTA-(γ-)MGS5, which confirmed our assumption, as the peptides B3 (*H*-Trp-(*N*-Me)Nle-Asp-1-Nal-NH_2), B4 (*H*-Trp-(*N*-Me)Nle-Asp-Phe-NH_2) and B6 (*H*-Trp-(*N*-Me)Nle-Asp-Tyr-NH_2) exhibited CCK-2R affinities in the low nanomolar range. Moreover, it could be demonstrated that the *C*-terminal position tolerates various aromatic residues, such as phenylalanine, L-1-naphtylalanine and tyrosine but not L-2-naphtylalanine or tryptophan. This observation confirmed that there is some tolerability at the *C*-terminus despite options for modifications within the pharmacophore are usually scarce, as even small changes can cause a distinct loss of affinity. Interestingly, when we extended our tetrapeptide analysis to DOTA-PP-F11N, a minigastrin analog currently tested in clinical trials [28], we found that the respective tetrapeptide (*H*-Trp-Nle-Asp-Phe-NH_2) revealed a noticeably decreased CCK-2R affinity, while this sequence in combination with a linker sequence, such as $(D\text{-Glu})_6$-Ala-Tyr-Gly showed high affinity [18, 29]. This was surprising, as Silvente-Poirot et al. reported high CCK-2R affinity for the tetrapeptide *H*-Trp-Met-Asp-Phe-NH_2 [22].

As the tetrapeptide B1 (*H*-Trp-Nle-Asp-1-Nal-NH_2) also displayed low CCK-2R affinity, we suspected that *N*-methylation at the Nle moiety is crucial for high CCK-2R affinity of Nle-comprising tetrapeptides. In fact, B1 containing a Nle moiety displayed a 50-fold higher IC_{50} value than B3 comprising an *N*-methylated Nle moiety, while the remaining sequence was identical. We thus conclude that a tetrapeptide motif at the *C*-terminus of minigastrin derivatives can be sufficient when containing a Nle moiety but seems to require an *N*-methylated peptide backbone at the Nle site, which is the most substantial finding of this work. We are aware that Silvente-Poirot et al. showed high CCK-2R affinity for the tetrapeptide *H*-Trp-Met-Asp-Phe-NH_2, which does not contain any *N*-methylation [22]. However, as Met is usually replaced by a Nle moiety due to its susceptibility toward in vivo oxidation and thus in vivo degradation, we

believe that our results could affect the future design of CCK-2R-targeted compounds.

Not surprisingly, log$D_{7.4}$ values confirmed the positive impact of a negatively charged D-γ-Glu moiety on lipophilicity. [^{177}Lu]Lu-DOTA-CCK-63 and -64, comprising either a $(PEG)_4$ or $(PEG)_3$ spacer instead of D-γ-Glu-Ala-Tyr-Gly, still revealed comparable log$D_{7.4}$ values to those of the references [^{177}Lu]Lu-DOTA-MGS5 and [^{177}Lu]Lu-DOTA-γ-MGS5 (-2.13 ± 0.05 and -2.21 ± 0.07 *versus* -2.21 ± 0.08 and -2.24 ± 0.04, respectively), which suggests a positive impact of the PEG spacer on lipophilicity.

Conclusion

We could confirm that the amino acid sequence D-γ-Glu-Ala-Tyr-Gly of minigastrin analogs is not required for high CCK-2R affinity but can be rather considered a spacer. Hence, substitution by PEG spacers simplified the peptide structure while maintaining high CCK-2R affinity and sufficient lipophilicity. In addition, we could confirm that only the tetrapeptide amino acid sequence *H*-Trp-(*N*-Me)Nle-Asp-1-Nal-NH_2 in DOTA-MGS5 is required for high CCK-2R affinity, yet the presence of a tiny *N*-methyl group at the peptide backbone of the Nle moiety is crucial, which could affect future design of CCK-2R-targeted compounds. However, our initial rationale that substitution of the *N*-terminal L-amino acids Ala-Tyr-Gly by unnatural PEG chains would increase metabolic stability could not be confirmed. This unexpected finding has to be further investigated in future studies, particularly whether the introduction of additional moieties in these PEG-containing minigastrin analogs could improve metabolic stability while maintaining the beneficial aspects of PEGylation observed in this study.

Abbreviations

CCK-2R	Cholecystokinin-2 receptor
CP04	DOTA-(D-Glu)6-Ala-Tyr-Gly-Trp-Met-Asp-Phe-NH_2
DOTA	1,4,7,10-Tetraazacyclododecan-1,4,7,10-tetracetic acid
DOTA-MGS5	DOTA-D-Glu-Ala-Tyr-Gly-Trp-(N-Me)Nle-Asp-1-Nal-NH_2
DOTA-MGS8	DOTA- D-Glu-Pro-Tyr-Gly-Trp-(N-Me)Nle-Asp-1-Nal-NH_2
DOTA-[Nle^{15}]MG11	DOTA- D-Glu-Ala-Tyr-Gly-Trp-Nle-Asp-Phe-NH_2
DOTA-PP-F11N	DOTA-$(D\text{-Glu})_6$-Ala-Tyr-Gly-Trp-Nle-Asp-Phe-NH_2
DTPA	Diethylenetriaminepentaacetic acid
DTPA-MG0	DTPA- D-Glu-$(Glu)_5$-Ala-Tyr-Gly-Trp-Met-Asp-Phe-NH_2
ESI–MS	Electro-spray ionization mass spectrometry
Fmoc	9-Fluorenylmethoxycarbonyl
MG11	H-D-Glu-Ala-Tyr-Gly-Trp-Met-Asp-Phe-NH_2
MTC	Medullary thyroid carcinoma
PEG	Polyethylene glycol
radio-TLC	Radio-thin layer chromatography
RCP	Radiochemical purity
RCY	Radiochemical yield
RP-HPLC	Reversed-phase high performance liquid chromatography
SPPS	Solid-phase peptide synthesis

Supplementary Information

The online version contains supplementary material available at https://doi.org/10.1186/s13550-023-01016-y.

Additional file 1. Characterization of all CCK-2R-targeted compounds (Figure S1-S17) evaluated in this work, as well as additional information on CCK-2R affinity, lipophilicity (Table S1) and stability in human serum (Table S2).

Acknowledgements

We thank Susanne Kossatz for providing the AR42J cells used for this study.

Author contributions

N.H. designed the study, carried out the synthesis and evaluation of the peptides and wrote the manuscript. T.G. wrote the manuscript, designed the study, managed the project and acquired funding. A.D.-G. carried out the synthesis and evaluation of the peptides. C.L. managed the project and revised the manuscript. H.-J.W. designed the study, managed the project and revised the manuscript. All authors have approved the final manuscript.

Funding

Open Access funding enabled and organized by Projekt DEAL. This study has been funded by Deutsche Forschungsgemeinschaft (DFG, German Research Foundation – 68647618 and 461577150).

Availability of data and materials

Data are contained within the article and Additional file 1.

Declarations

Ethics approval and consent to participate

Not applicable.

Consent for publication

Not applicable.

Competing interests

H.-J.W. is founder and shareholder of Scintomics GmbH, Munich, Germany. No other potential conflicts of interest relevant to this article exist. A patent application on CCK-2R-targeted compounds has been filed (T.G., N.H., H.-J.W., C.L.).

Received: 18 April 2023 Accepted: 29 June 2023
Published online: 08 July 2023

References

1. Behr TM, Jenner N, Béhé M, Angerstein C, Gratz S, Raue F, et al. Radiolabeled peptides for targeting cholecystokinin-B/gastrin receptor-expressing tumors. J Nucl Med. 1999;40(6):1029–44.
2. Reubi JC, Schaer JC, Waser B. Cholecystokinin(CCK)-A and CCK-B/gastrin receptors in human tumors. Cancer Res. 1997;57(7):1377–86.
3. Reubi JC, Waser B. Unexpected high incidence of cholecystokinin-B/gastrin receptors in human medullary thyroid carcinomas. Int J Cancer. 1996;67(5):644–7.
4. Béhé M, Becker W, Gotthardt M, Angerstein C, Behr TM. Improved kinetic stability of DTPA-dGlu as compared with conventional monofunctional DTPA in chelating indium and yttrium: preclinical and initial clinical evaluation of radiometal labelled minigastrin derivatives. Eur J Nucl Med Mol Imaging. 2003;30(8):1140–6.
5. Good S, Walter MA, Waser B, Wang X, Müller-Brand J, Béhé MP, et al. Macrocyclic chelator-coupled gastrin-based radiopharmaceuticals for targeting of gastrin receptor-expressing tumours. Eur J Nucl Med Mol Imaging. 2008;35(10):1868–77.
6. von Guggenberg E, Dietrich H, Skvortsova I, Gabriel M, Virgolini IJ, Decristoforo C. 99mTc-labelled HYNIC-minigastrin with reduced kidney uptake

for targeting of CCK-2 receptor-positive tumours. Eur J Nucl Med Mol Imaging. 2007;34(8):1209–18.
7. Kolenc Peitl P, Tamma M, Kroselj M, Braun F, Waser B, Reubi JC, et al. Stereochemistry of amino acid spacers determines the pharmacokinetics of 111In–DOTA–minigastrin analogues for targeting the CCK2/gastrin receptor. Bioconjug Chem. 2015;26(6):1113–9.
8. Ocak M, Helbok A, Rangger C, Peitl PK, Nock BA, Morelli G, et al. Comparison of biological stability and metabolism of CCK2 receptor targeting peptides, a collaborative project under COST BM0607. Eur J Nucl Med Mol Imaging. 2011;38(8):1426–35.
9. Pauwels S, Najdovski T, Dimaline R, Lee CM, Deschodt-Lanckman M. Degradation of human gastrin and CCK by endopeptides 2411: differential behaviour of the sulphated and unsulphated peptides. Biochim Biophys Acta (BBA)— Protein Struct Mol Enzymol. 1989;996(1–2):82–8.
10. Klingler M, Decristoforo C, Rangger C, Summer D, Foster J, Sosabowski JK, et al. Site-specific stabilization of minigastrin analogs against enzymatic degradation for enhanced cholecystokinin-2 receptor targeting. Theranostics. 2018;8(11):2896–908.
11. Klingler M, Summer D, Rangger C, Haubner R, Foster J, Sosabowski J, et al. DOTA-MGS5, a new cholecystokinin-2 receptor-targeting peptide analog with an optimized targeting profile for theranostic use. J Nucl Med. 2019;60(7):1010–6.
12. Hörmann AA, Klingler M, Rangger C, Mair C, Decristoforo C, Uprimny C, et al. Radiopharmaceutical formulation and preclinical testing of (68) Ga-labeled DOTA-MGS5 for the regulatory approval of a first exploratory clinical trial. Pharm. 2021;14(6):575.
13. Klingler M, Hormann AA, Rangger C, Desrues L, Castel H, Gandolfo P, et al. Stabilization strategies for linear minigastrin analogues: further improvements via the inclusion of proline into the peptide sequence. J Med Chem. 2020;63(23):14668–79.
14. Hormann AA, Klingler M, Rezaeianpour M, Hormann N, Gust R, Shahhosseini S, et al. Initial in vitro and in vivo evaluation of a novel CCK2R targeting peptide analog labeled with Lutetium-177. Molecules. 2020;25(19):4585.
15. Hormann AA, Plhak E, Klingler M, Rangger C, Pfister J, Schwach G, et al. Automated synthesis of (68)Ga-labeled DOTA-MGS8 and preclinical characterization of cholecystokinin-2 receptor targeting. Molecules. 2022;27(6):2034.
16. Grob NM, Schibli R, Behe M, Mindt TL. Improved tumor-targeting with peptidomimetic analogs of minigastrin (177)Lu-PP-F11N. Cancers. 2021;13(11):2629.
17. Grob NM, Haussinger D, Deupi X, Schibli R, Behe M, Mindt TL. Triazolopeptidomimetics: novel radiolabeled minigastrin analogs for improved tumor targeting. J Med Chem. 2020;63(9):4484–95.
18. Holzleitner N, Günther T, Beck R, Lapa C, Wester H-J. Introduction of a SiFA moiety into the D-glutamate chain of DOTA-PP-F11N results in radiohybrid-based CCK-2R-targeted compounds with improved pharmacokinetics in vivo. Pharmaceuticals. 2022;15(12):1467.
19. Wurzer A, Kunert JP, Fischer S, Felber V, Beck R, De Rose F, D'Alessandria C, Weber W, Wester HJ. Synthesis and preclinical evaluation of 177Lu-labeled radiohybrid PSMA ligands for endoradiotherapy of prostate cancer. J Nucl Med. 2022;63(10):1489–95.
20. Günther T, Holzleitner N, Di Carlo D, Urtz-Urban N, Lapa C, Wester H-J. Development of the first 18F-labeled radiohybrid-based minigastrin derivative with high target affinity and tumor accumulation by substitution of the chelating moiety. Pharmaceutics. 2023;15(3):826.
21. Guenther T, Deiser S, Felber V, Beck R, Wester H-J. Substitution of L-Trp by α-methyl-L-Trp in ¹⁷⁷Lu-RM2 results in ¹⁷⁷Lu-AMTG, a high affinity GRPR ligand with improved in vivo stability. Journal of Nuclear Medicine. 2022; jnumed.121.263323.
22. Silvente-Poirot S, Escrieut C, Galès C, Fehrentz JA, Escherich A, Wank SA, et al. Evidence for a direct interaction between the penultimate aspartic acid of cholecystokinin and histidine 207, located in the second extracellular loop of the cholecystokinin B receptor. J Biol Chem. 1999;274(33):23191–7.
23. Ritler A, Shoshan MS, Deupi X, Wilhelm P, Schibli R, Wennemers H, et al. Elucidating the structure-activity relationship of the pentaglutamic acid sequence of minigastrin with cholecystokinin receptor subtype 2. Bioconjug Chem. 2019;30(3):657–66.
24. Däpp S, Müller C, Garayoa EG, Bläuenstein P, Maes V, Brans L, et al. PEGylation, increasing specific activity and multiple dosing as strategies to improve the risk-benefit profile of targeted radionuclide therapy with 177Lu-DOTA-bombesin analogues. EJNMMI Res. 2012;2(1):24.
25. Sharma AK, Sharma R, Vats K, Sarma HD, Mukherjee A, Das T, et al. Synthesis and comparative evaluation of (177)Lu-labeled PEG and non-PEG variant peptides as HER2-targeting probes. Sci Rep. 2022;12(1):15720.
26. Hausner SH, Abbey CK, Bold RJ, Gagnon MK, Marik J, Marshall JF, et al. Targeted in vivo imaging of integrin alphavbeta6 with an improved radiotracer and its relevance in a pancreatic tumor model. Cancer Res. 2009;69(14):5843–50.
27. Harris JM, Chess RB. Effect of pegylation on pharmaceuticals. Nat Rev Drug Discov. 2003;2(3):214–21.
28. Rottenburger C, Nicolas GP, McDougall L, Kaul F, Cachovan M, Vija AH, et al. Cholecystokinin 2 receptor agonist (177)Lu-PP-F11N for radionuclide therapy of medullary thyroid carcinoma: results of the lumed phase 0a study. J Nucl Med. 2020;61(4):520–6.
29. Sauter AW, Mansi R, Hassiepen U, Muller L, Panigada T, Wiehr S, et al. Targeting of the cholecystokinin-2 receptor with the minigastrin analog (177)Lu-DOTA-PP-F11N: does the use of protease inhibitors further improve in vivo distribution? J Nucl Med. 2019;60(3):393–9.

Publisher's Note

Investigation of the Structure-Activity Relationship at the *N*-terminal part of Minigastrin Analogs

- Supplementary Materials -

Nadine Holzleitner[1,#,*], Thomas Günther[1,#,*], Amira Daoud-Gadieh[1], Constantin Lapa[2] and Hans-Jürgen Wester[1]

[1] Technical University of Munich, Department of Chemistry, 85748 Garching, Germany

[2] University Hospital Augsburg, Nuclear Medicine, 86156 Augsburg, Germany

[#] both authors contributed equally

* Corresponding author: Thomas Günther, thomas.guenther@tum.de, Technical University of Munich, Department of Chemistry, Garching, Germany

Nadine Holzleitner, nadine.holzleitner@tum.de, Technical University of Munich, Department of Chemistry, Garching, Germany

Corresponding authors:

Thomas Günther and Nadine Holzleitner

Phone: +49.89.289.12203

Technical University of Munich,

Chair of Pharmaceutical Radiochemistry,

Walther-Meissner-Str. 3

85748 Garching

GERMANY

Fax: +49.89.289.12204

E-Mail: thomas.guenther@tum.de and nadine.holzleitner@tum.de

ORCID: https://orcid.org/0000-0002-7412-0297 (TG) and https://orcid.org/0000-0001-8258-3526 (NH)

Analytical data of $^{nat/177}$Lu-labeled minigastrin analogs

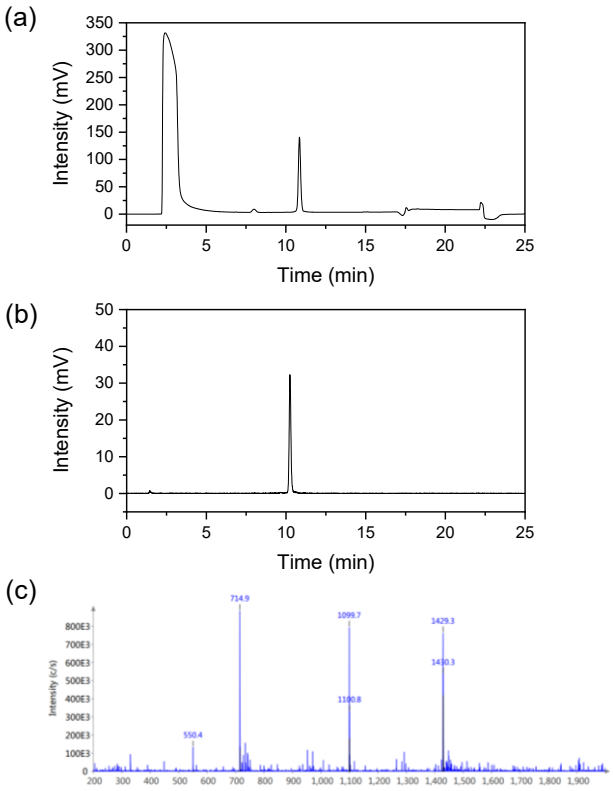

Figure S1. Confirmation of peptide identity and integrity for (**a**) [^{nat}Lu]Lu-DOTA-CCK-55 and (**b**) [^{177}Lu]Lu-DOTA-CCK-55 as analyzed by analytical (radio-)RP-HPLC (MultoKrom 100-5 C18, 5 µm, 125 × 4.6 mm, CS Chromatographie GmbH, Langerwehe, Germany; 10→70% MeCN in H_2O + 0.1% TFA in 15 min). (**c**) Mass spectrum of [^{nat}Lu]Lu-DOTA-CCK-55.

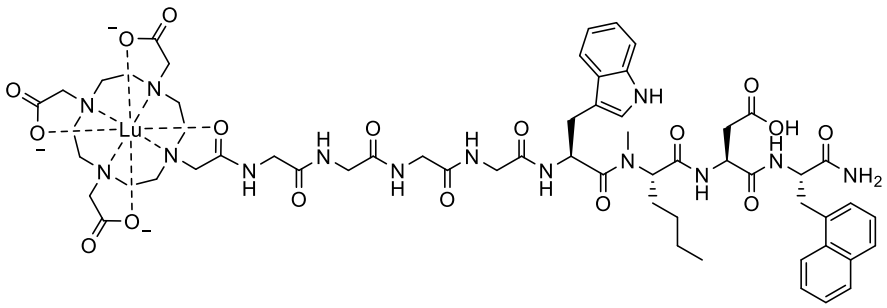

[^{nat}Lu]Lu-DOTA-CCK-55: RP-HPLC (10→70% MeCN in H_2O with 0.1% TFA, 15 min, λ = 220 nm): t_R = 10.9 min, K' = 5.46; MS (ESI, positive): m/z calculated for $C_{59}H_{77}LuN_{14}O_{17}$: 1429.3, found: m/z = 1429.3 $[M+H]^+$, 714.9 $[M+2H]^{2+}$.

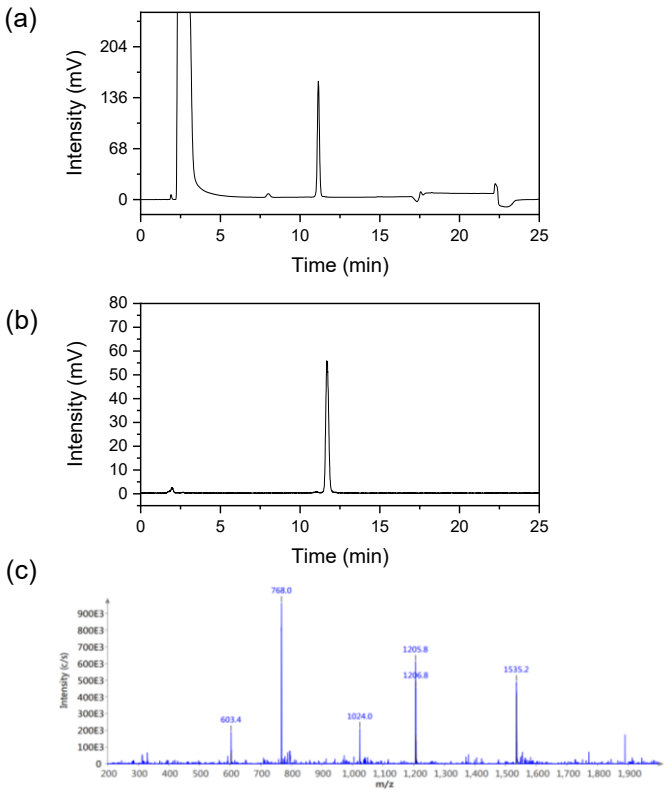

Figure S2. Confirmation of peptide identity and integrity for (**a**) [^{nat}Lu]Lu-DOTA-CCK-56 and (**b**) [^{177}Lu]Lu-DOTA-CCK-56 as analyzed by analytical (radio-)RP-HPLC (MultoKrom 100-5 C18, 5 µm, 125 × 4.6 mm, CS Chromatographie GmbH, Langerwehe, Germany; 10→70% MeCN in H_2O + 0.1% TFA in 15 min). (**c**) Mass spectrum of [^{nat}Lu]Lu-DOTA-CCK-56.

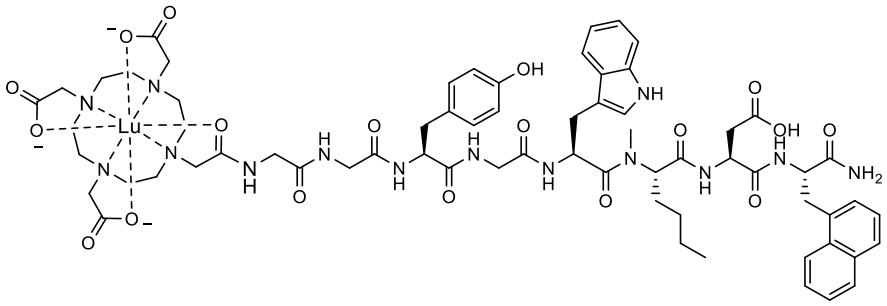

[^{nat}Lu]Lu-DOTA-CCK-56: RP-HPLC (10→70% MeCN in H_2O with 0.1% TFA, 15 min, λ = 220 nm): t_R = 11.1 min, K' = 5.58; MS (ESI, positive): m/z calculated for $C_{56}H_{83}LuN_{14}O_{18}$: 1535.4, found: m/z = 1535.2 $[M+H]^+$, 768.0 $[M+2H]^{2+}$.

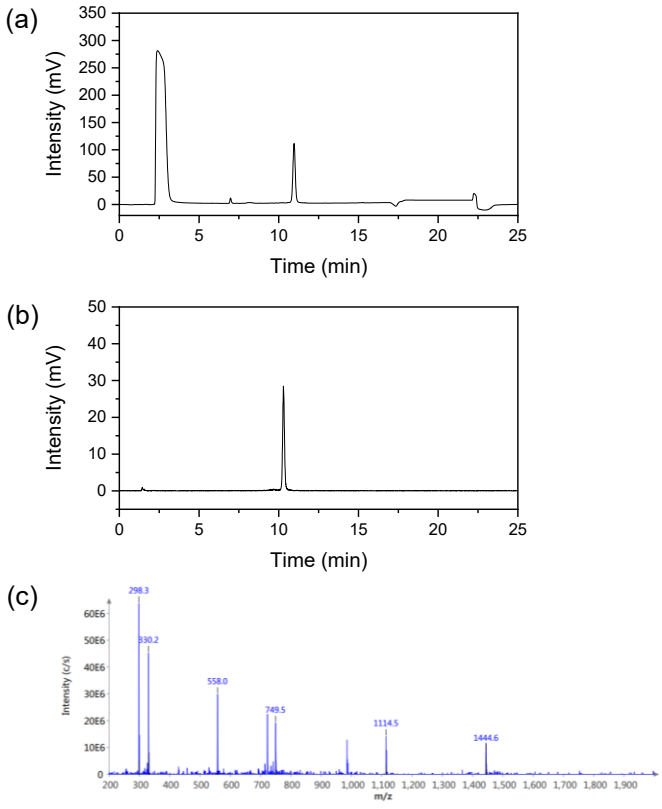

Figure S3. Confirmation of peptide identity and integrity for (**a**) [^{nat}Lu]Lu-DOTA-CCK-57 and (**b**) [^{177}Lu]Lu-DOTA-CCK-57 as analyzed by analytical (radio-)RP-HPLC (MultoKrom 100-5 C18, 5 µm, 125 × 4.6 mm, CS Chromatographie GmbH, Langerwehe, Germany; 10→70% MeCN in H_2O + 0.1% TFA in 15 min). (**c**) Mass spectrum of [^{nat}Lu]Lu-DOTA-CCK-57.

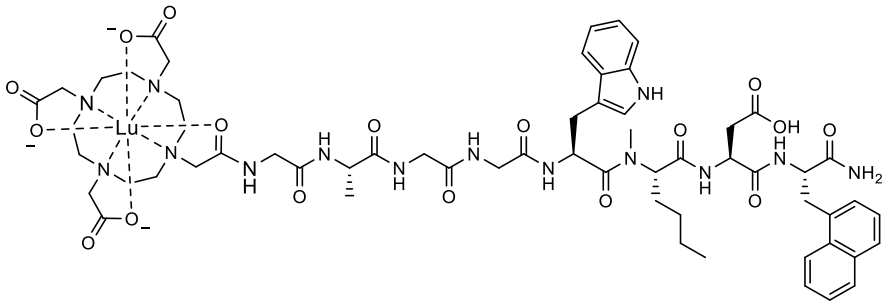

[^{nat}Lu]Lu-DOTA-CCK-57: RP-HPLC (10→70% MeCN in H_2O with 0.1% TFA, 15 min, λ = 220 nm): t_R = 11.0 min, K' = 5.52; MS (ESI, positive): m/z calculated for $C_{60}H_{79}LuN_{14}O_{17}$: 1443.3, found: m/z = 1444.6 $[M+H]^+$.

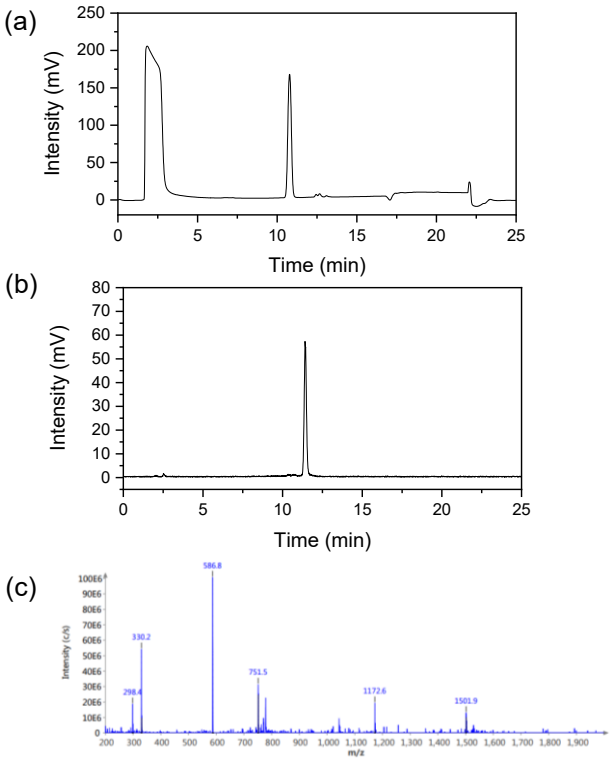

Figure S4. Confirmation of peptide identity and integrity for (**a**) [^{nat}Lu]Lu-DOTA-CCK-58 and (**b**) [^{177}Lu]Lu-DOTA-CCK-58 as analyzed by analytical (radio-)RP-HPLC (MultoKrom 100-5 C18, 5 µm, 125 × 4.6 mm, CS Chromatographie GmbH, Langerwehe, Germany; 10→70% MeCN in H_2O + 0.1% TFA in 15 min). (**c**) Mass spectrum of [^{nat}Lu]Lu-DOTA-CCK-58.

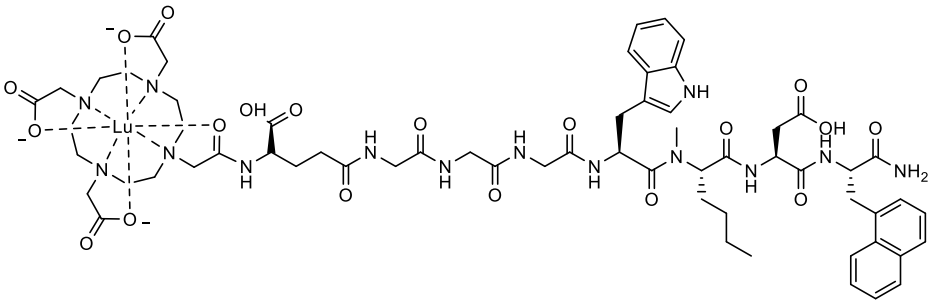

[^{nat}Lu]Lu-DOTA-CCK-58: RP-HPLC (10→70% MeCN in H_2O with 0.1% TFA, 15 min, λ = 220 nm): t_R = 10.8 min, K' = 5.40; MS (ESI, positive): m/z calculated for $C_{62}H_{81}LuN_{14}O_{19}$: 1501.4, found: m/z = 1501.9 $[M+H]^+$, 751.5 $[M+2H]^{2+}$.

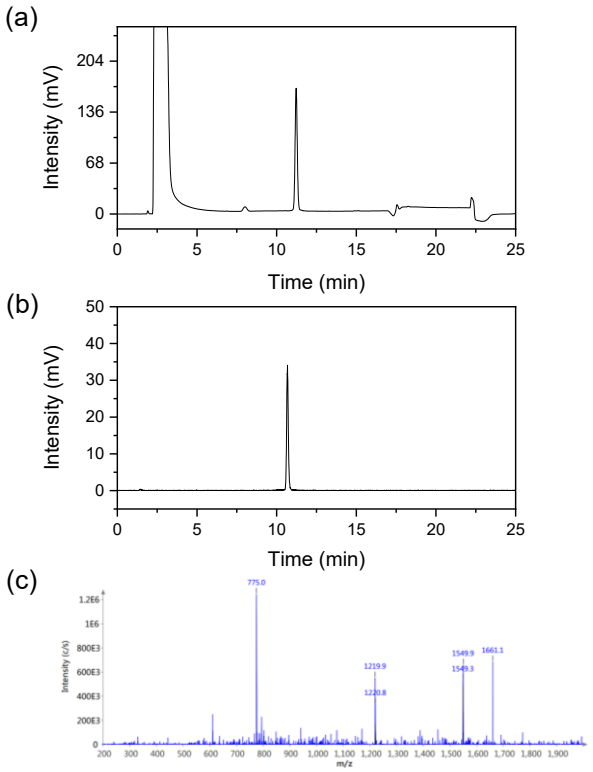

Figure S5. Confirmation of peptide identity and integrity for (**a**) [^{nat}Lu]Lu-DOTA-CCK-59 and (**b**) [^{177}Lu]Lu-DOTA-CCK-59 as analyzed by analytical (radio-)RP-HPLC (MultoKrom 100-5 C18, 5 µm, 125 × 4.6 mm, CS Chromatographie GmbH, Langerwehe, Germany; 10→70% MeCN in H_2O + 0.1% TFA in 15 min). (**c**) Mass spectrum of [^{nat}Lu]Lu-DOTA-CCK-59.

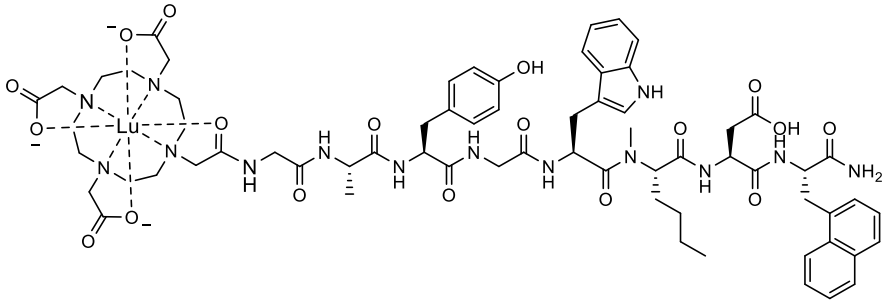

[^{nat}Lu]Lu-DOTA-CCK-59: RP-HPLC (10→70% MeCN in H_2O with 0.1% TFA, 15 min, λ = 220 nm): t_R = 11.2 min, K' = 5.64; MS (ESI, positive): m/z calculated for $C_{67}H_{85}LuN_{14}O_{18}$: 1549.5, found: m/z = 1549.9 $[M+H]^+$, 775.0 $[M+2H]^{2+}$.

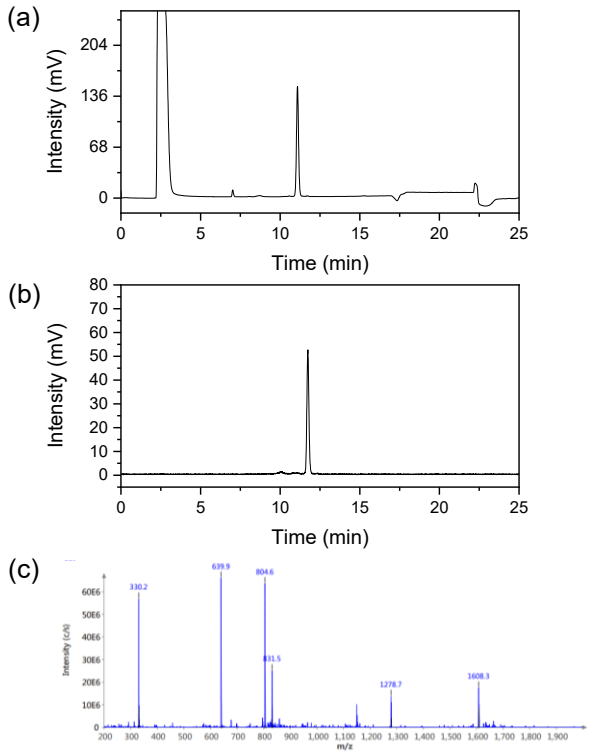

Figure S6. Confirmation of peptide identity and integrity for (**a**) [^{nat}Lu]Lu-DOTA-CCK-60 and (**b**) [^{177}Lu]Lu-DOTA-CCK-60 as analyzed by analytical (radio-)RP-HPLC (MultoKrom 100-5 C18, 5 µm, 125 × 4.6 mm, CS Chromatographie GmbH, Langerwehe, Germany; 10→70% MeCN in H_2O + 0.1% TFA in 15 min). (**c**) Mass spectrum of [^{nat}Lu]Lu-DOTA-CCK-60.

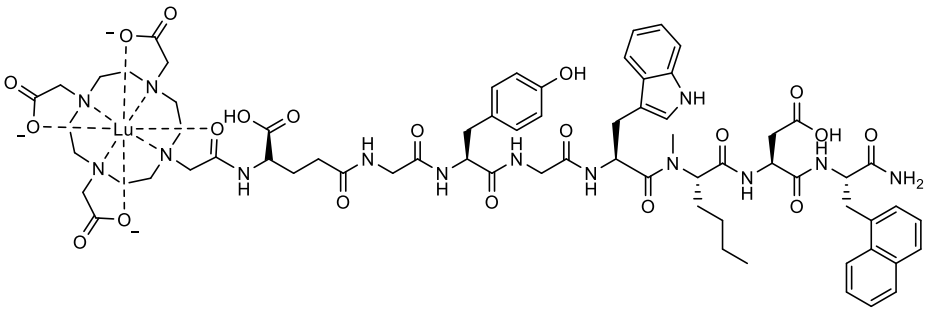

[^{nat}Lu]Lu-DOTA-CCK-60: RP-HPLC (10→70% MeCN in H_2O with 0.1% TFA, 15 min, λ = 220 nm): t_R = 11.1 min, K' = 5.58; MS (ESI, positive): m/z calculated for $C_{69}H_{87}LuN_{14}O_{20}$: 1607.5, found: m/z = 1608.3 $[M+H]^+$, 804.6 $[M+2H]^{2+}$.

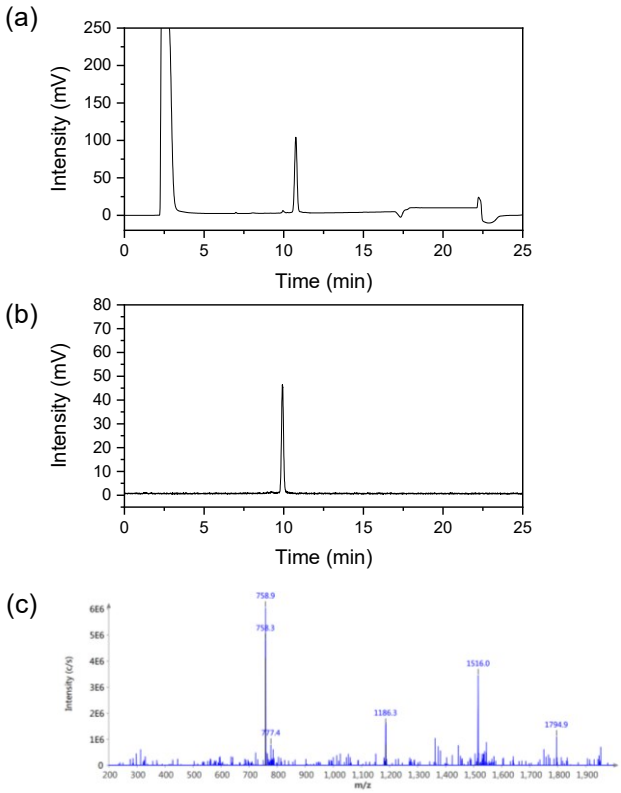

Figure S7. Confirmation of peptide identity and integrity for (**a**) [^{nat}Lu]Lu-DOTA-CCK-61 and (**b**) [^{177}Lu]Lu-DOTA-CCK-61 as analyzed by analytical (radio-)RP-HPLC (MultoKrom 100-5 C18, 5 µm, 125 × 4.6 mm, CS Chromatographie GmbH, Langerwehe, Germany; 10→70% MeCN in H_2O + 0.1% TFA in 15 min). (**c**) Mass spectrum of [^{nat}Lu]Lu-DOTA-CCK-61.

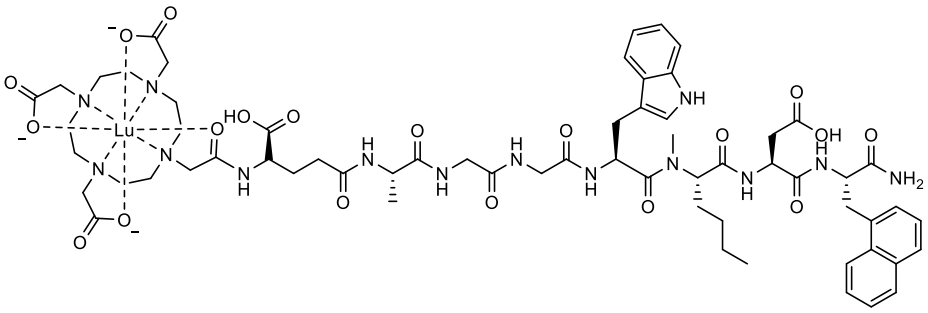

[^{nat}Lu]Lu-DOTA-CCK-61: RP-HPLC (10→70% MeCN in H_2O with 0.1% TFA, 15 min, λ = 220 nm): t_R = 10.8 min, K' = 5.40; MS (ESI, positive): m/z calculated for $C_{63}H_{83}LuN_{14}O_{19}$: 1515.4, found: m/z = 1516.0 $[M+H]^+$, 758.9 $[M+2H]^{2+}$.

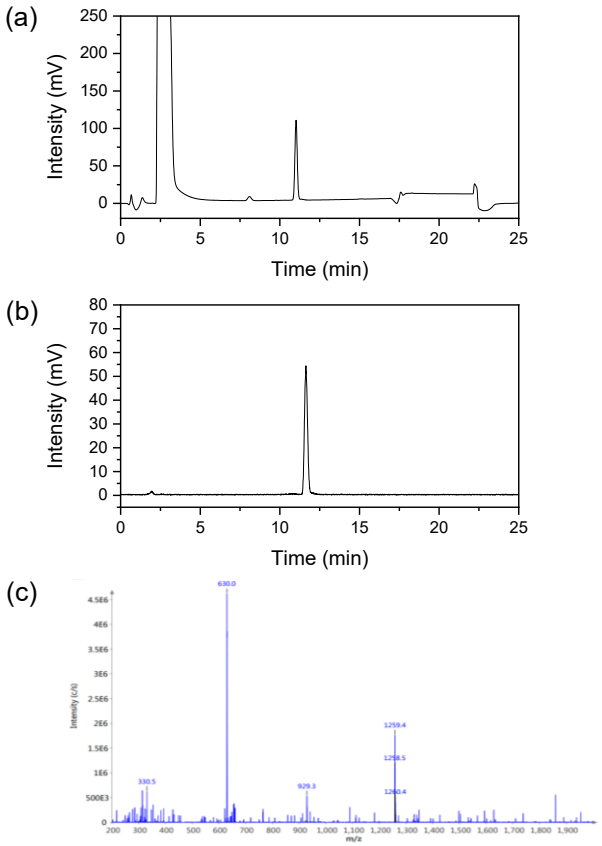

Figure S8. Confirmation of peptide identity and integrity for (**a**) [^{nat}Lu]Lu-DOTA-CCK-62 and (**b**) [^{177}Lu]Lu-DOTA-CCK-62 as analyzed by analytical (radio-)RP-HPLC (MultoKrom 100-5 C18, 5 µm, 125 × 4.6 mm, CS Chromatographie GmbH, Langerwehe, Germany; 10→70% MeCN in H_2O + 0.1% TFA in 15 min). (**c**) Mass spectrum of [^{nat}Lu]Lu-DOTA-CCK-62.

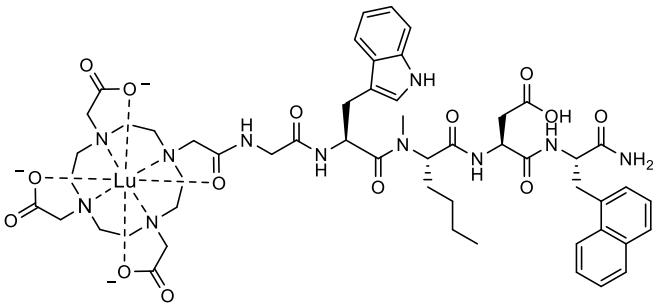

[^{nat}Lu]Lu-DOTA-CCK-62: RP-HPLC (10→70% MeCN in H_2O with 0.1% TFA, 15 min, λ = 220 nm): t_R = 11.0 min, K' = 5.52; MS (ESI, positive): m/z calculated for $C_{53}H_{68}LuN_{11}O_{14}$: 1258.2, found: m/z = 1259.4 $[M+H]^+$, 630.0 $[M+2H]^{2+}$.

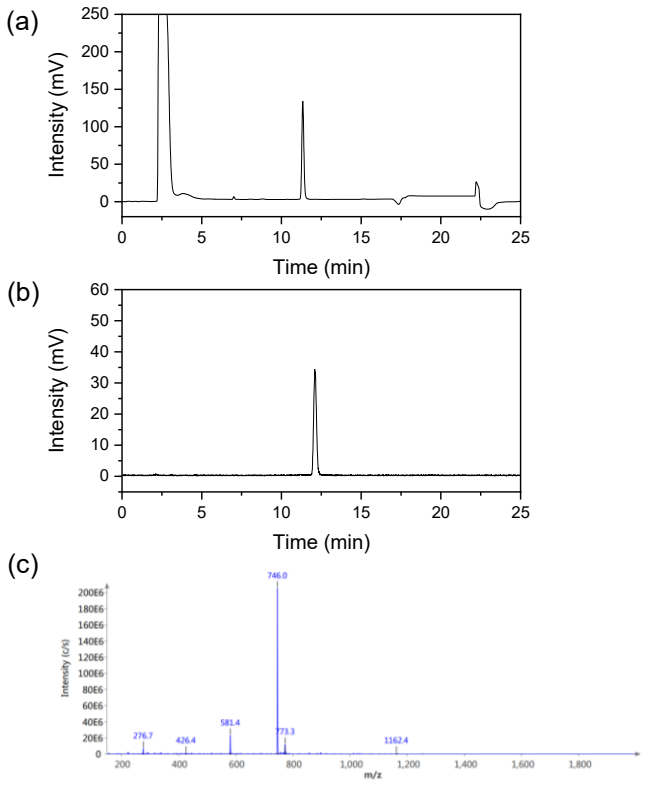

Figure S9. Confirmation of peptide identity and integrity for (**a**) [^{nat}Lu]Lu-DOTA-CCK-63 and (**b**) [^{177}Lu]Lu-DOTA-CCK-63 as analyzed by analytical (radio-)RP-HPLC (MultoKrom 100-5 C18, 5 µm, 125 × 4.6 mm, CS Chromatographie GmbH, Langerwehe, Germany; 10→70% MeCN in H_2O + 0.1% TFA in 15 min). (**c**) Mass spectrum of [^{nat}Lu]Lu-DOTA-CCK-63.

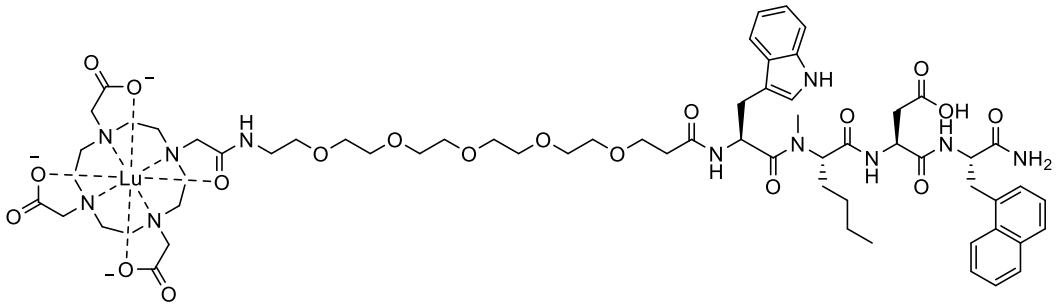

[^{nat}Lu]Lu-DOTA-CCK-63: RP-HPLC (10→70% MeCN in H_2O with 0.1% TFA, 15 min, λ = 220 nm): t_R = 11.3 min, K' = 5.70; MS (ESI, positive): m/z calculated for $C_{64}H_{90}LuN_{11}O_{19}$: 1491.6, found: m/z = 746.0 $[M+2H]^{2+}$.

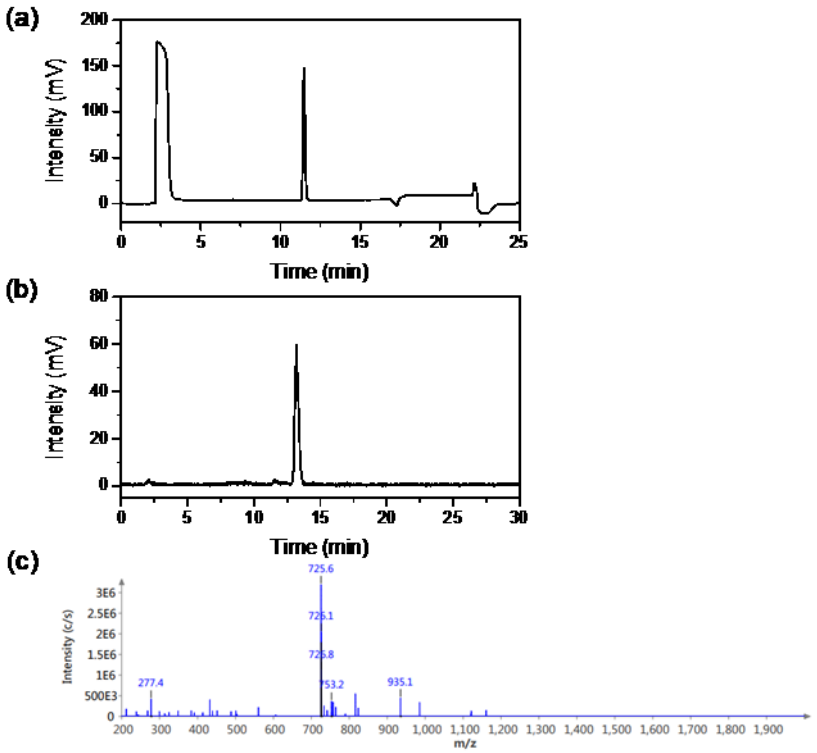

Figure S10. Confirmation of peptide identity and integrity for (**a**) [^{nat}Lu]Lu-DOTA-CCK-64 as analyzed by analytical RP-HPLC (MultoKrom 100-5 C18, 5 µm, 125 × 4.6 mm, CS Chromatographie GmbH, Langerwehe, Germany; 10→70% MeCN in H_2O + 0.1% TFA in 15 min) and (**b**) [^{177}Lu]Lu-DOTA-CCK-64 as analyzed by analytical radio-RP-HPLC (10→30% MeCN in H_2O + 0.1% TFA in 5 min; 30→60% MeCN in H_2O + 0.1% TFA in 15 min). (**c**) Mass spectrum of [^{nat}Lu]Lu-DOTA-CCK-64.

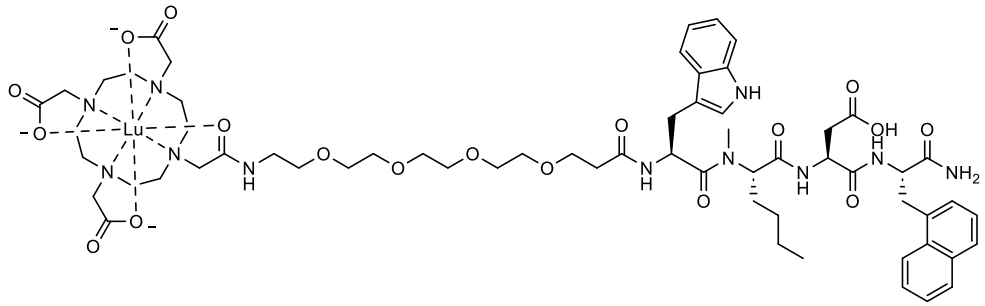

[^{nat}Lu]Lu-DOTA-CCK-64: RP-HPLC (10→70% MeCN in H_2O with 0.1% TFA, 15 min, λ = 220 nm): t_R = 11.5 min, K' = 5.80; MS (ESI, positive): m/z calculated for $C_{62}H_{86}LuN_{11}O_{18}$: 1448.4, found: m/z = 725.6 $[M+2H]^{2+}$.

Analytical data of tetrapeptidic sequences

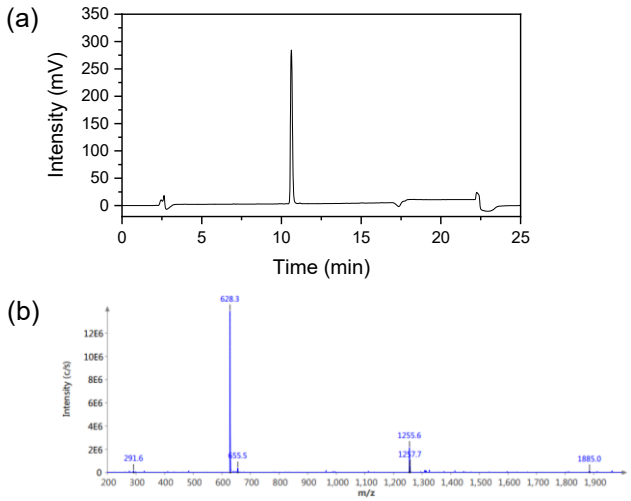

Figure S11. Confirmation of peptide identity and integrity for (**a**) *H*-Trp-Nle-Asp-1-Nal-NH_2 as analyzed by analytical RP-HPLC (MultoKrom 100-5 C18, 5 µm, 125 × 4.6 mm, CS Chromatographie GmbH, Langerwehe, Germany; 10→70% MeCN in H_2O + 0.1% TFA in 15 min). (**b**) Mass spectrum of *H*-Trp-Nle-Asp-1-Nal-NH_2.

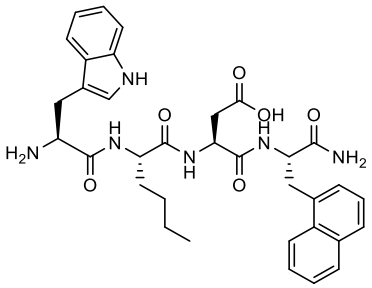

***H*-Trp-Nle-Asp-1-Nal-NH_2 (B1):** RP-HPLC (10→70% MeCN in H_2O with 0.1% TFA, 15 min, λ = 220 nm): t_R = 10.6 min, K' = 5.28; MS (ESI, positive): m/z calculated for $C_{34}H_{40}N_6O_6$: 628.3, found: m/z = 1255.6 $[2M+H]^+$, 628.3 $[M+H]^+$.

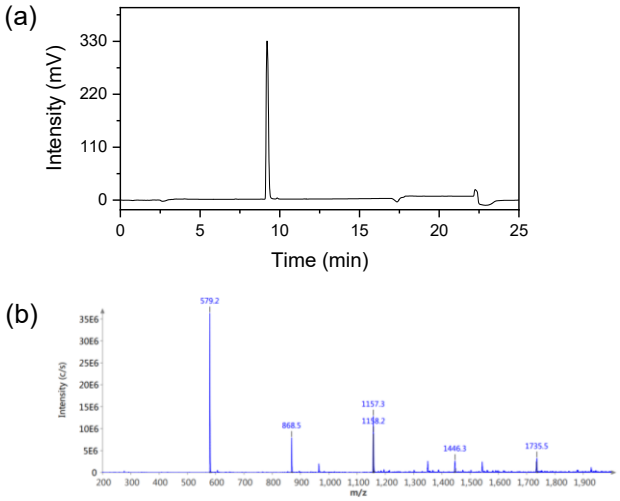

Figure S12. Confirmation of peptide identity and integrity for (**a**) *H*-Trp-Nle-Asp-Phe-NH_2 as analyzed by analytical RP-HPLC (MultoKrom 100-5 C18, 5 µm, 125 × 4.6 mm, CS Chromatographie GmbH, Langerwehe, Germany; 10→70% MeCN in H_2O + 0.1% TFA in 15 min). (**b**) Mass spectrum of *H*-Trp-Nle-Asp-Phe-NH_2.

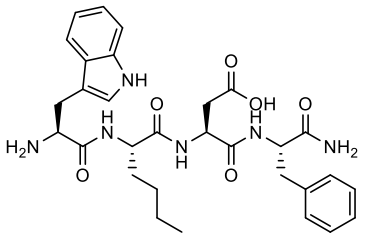

***H*-Trp-Nle-Asp-Phe-NH_2 (B2):** RP-HPLC (10→70% MeCN in H_2O with 0.1% TFA, 15 min, λ = 220 nm): t_R = 9.2 min, K' = 4.45; MS (ESI, positive): m/z calculated for $C_{30}H_{38}N_6O_6$: 578.3, found: m/z = 1157.3 $[2M+H]^+$, 579.2 $[M+H]^+$.

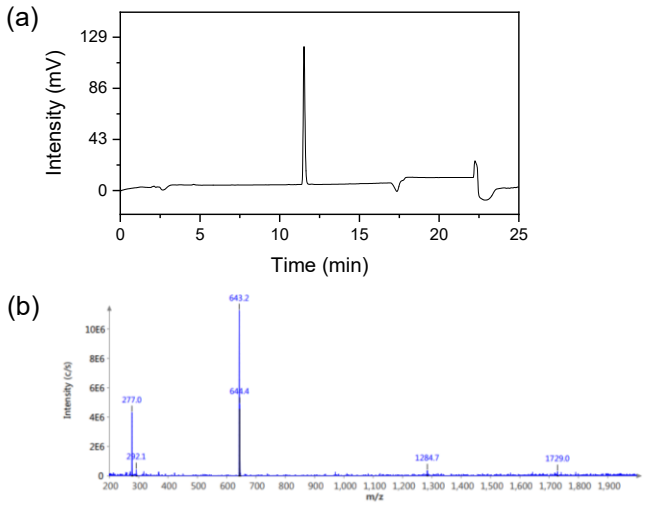

Figure S13. Confirmation of peptide identity and integrity for (**a**) *H*-Trp-(*N*-Me)Nle-Asp-1-Nal-NH_2 as analyzed by analytical RP-HPLC (MultoKrom 100-5 C18, 5 µm, 125 × 4.6 mm, CS Chromatographie GmbH, Langerwehe, Germany; 10→70% MeCN in H_2O + 0.1% TFA in 15 min). (**b**) Mass spectrum of *H*-Trp-(*N*-Me)Nle-Asp-1-Nal-NH_2.

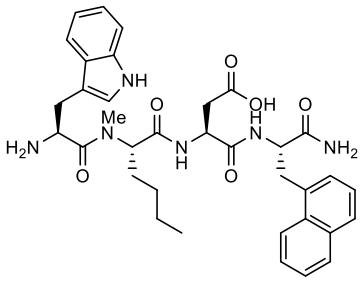

***H*-Trp-(*N*-Me)Nle-Asp-1-Nal-NH_2 (B3):** RP-HPLC (10→70% MeCN in H_2O with 0.1% TFA, 15 min, λ = 220 nm): t_R = 11.5 min, K' = 5.82; MS (ESI, positive): m/z calculated for $C_{35}H_{42}N_6O_6$: 642.3, found: m/z = 1284.7 $[2M+H]^+$, 643.2 $[M+H]^+$.

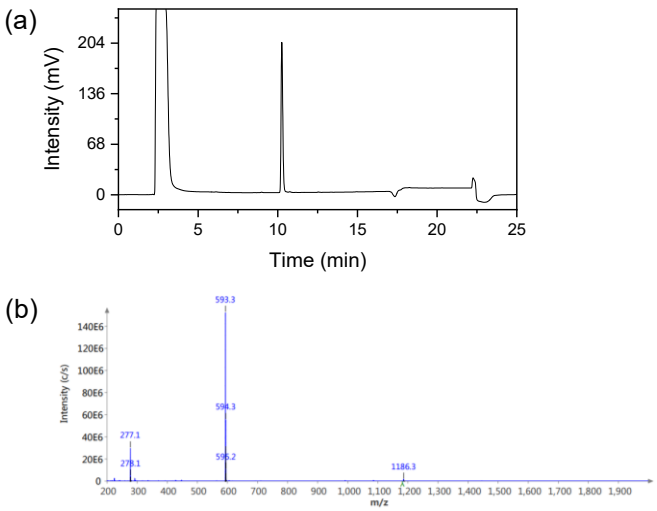

Figure S14. Confirmation of peptide identity and integrity for (**a**) *H*-Trp-(*N*-Me)Nle-Asp-Phe-NH_2 as analyzed by analytical RP-HPLC (MultoKrom 100-5 C18, 5 µm, 125 × 4.6 mm, CS Chromatographie GmbH, Langerwehe, Germany; 10→70% MeCN in H_2O + 0.1% TFA in 15 min). (**b**) Mass spectrum of *H*-Trp-(*N*-Me)Nle-Asp-Phe-NH_2.

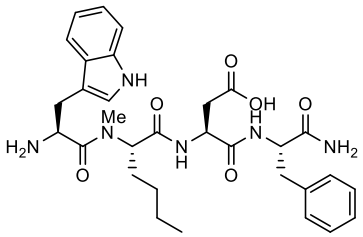

***H*-Trp-(*N*-Me)Nle-Asp-Phe-NH_2 (B4):** RP-HPLC (10→70% MeCN in H_2O with 0.1% TFA, 15 min, λ = 220 nm): t_R = 10.3 min, K' = 5.11; MS (ESI, positive): m/z calculated for $C_{31}H_{40}N_6O_6$: 592.3, found: m/z = 1186.3 $[2M+H]^+$, 593.3 $[M+H]^+$.

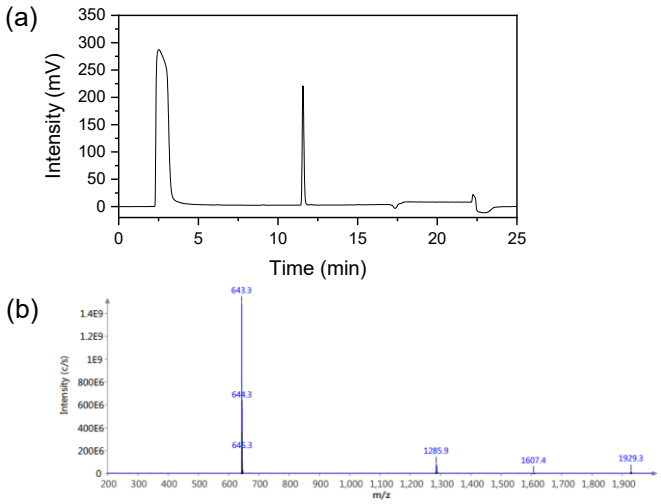

Figure S15. Confirmation of peptide identity and integrity for (**a**) *H*-Trp-(*N*-Me)Nle-Asp-2-Nal-NH_2 as analyzed by analytical RP-HPLC (MultoKrom 100-5 C18, 5 µm, 125 × 4.6 mm, CS Chromatographie GmbH, Langerwehe, Germany; 10→70% MeCN in H_2O + 0.1% TFA in 15 min). (**b**) Mass spectrum of *H*-Trp-(*N*-Me)Nle-Asp-2-Nal-NH_2.

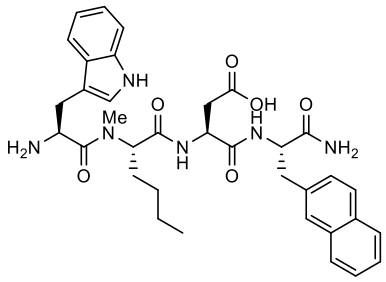

***H*-Trp-(*N*-Me)Nle-Asp-2-Nal-NH_2 (B5):** RP-HPLC (10→70% MeCN in H_2O with 0.1% TFA, 15 min, λ = 220 nm): t_R = 11.6 min, K' = 5.88; MS (ESI, positive): m/z calculated for $C_{35}H_{42}N_6O_6$: 642.3, found: m/z = 1285.9 $[2M+H]^+$, 643.3 $[M+H]^+$.

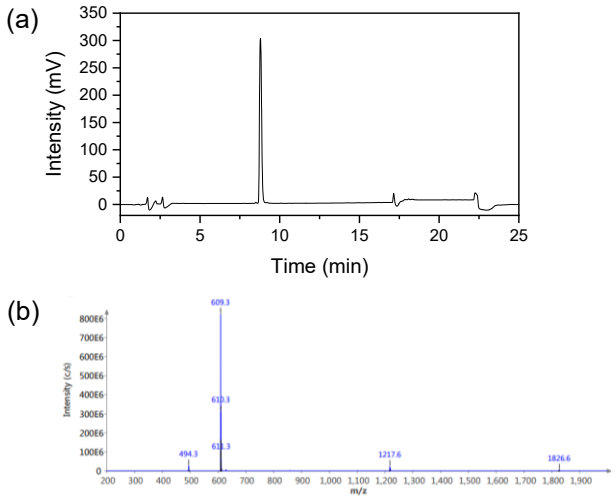

Figure S16. Confirmation of peptide identity and integrity for (**a**) *H*-Trp-(*N*-Me)Nle-Asp-1-Tyr-NH_2 as analyzed by analytical RP-HPLC (MultoKrom 100-5 C18, 5 µm, 125 × 4.6 mm, CS Chromatographie GmbH, Langerwehe, Germany; 10→70% MeCN in H_2O + 0.1% TFA in 15 min). (**b**) Mass spectrum of *H*-Trp-(*N*-Me)Nle-Asp-1-Tyr-NH_2.

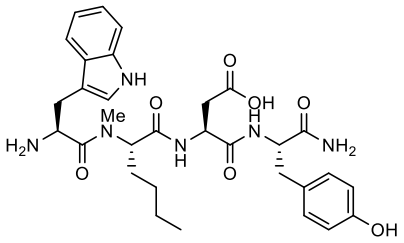

***H*-Trp-(*N*-Me)Nle-Asp-1-Tyr-NH_2 (B6):** RP-HPLC (10→70% MeCN in H_2O with 0.1% TFA, 15 min, λ = 220 nm): t_R = 8.8 min, K' = 4.21; MS (ESI, positive): m/z calculated for $C_{31}H_{40}N_6O_7$: 608.3, found: m/z = 1217.6 $[2M+H]^+$, 609.3 $[M+H]^+$.

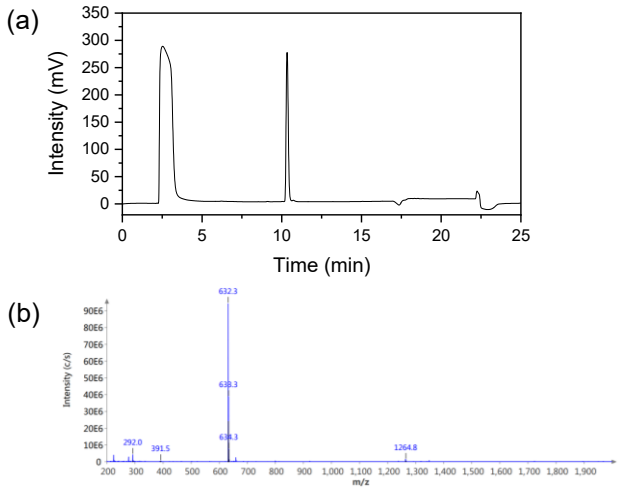

Figure S17. Confirmation of peptide identity and integrity for (**a**) *H*-Trp-(*N*-Me)Nle-Asp-Trp-NH_2 as analyzed by analytical RP-HPLC (MultoKrom 100-5 C18, 5 µm, 125 × 4.6 mm, CS Chromatographie GmbH, Langerwehe, Germany; 10→70% MeCN in H_2O + 0.1% TFA in 15 min). (**b**) Mass spectrum of *H*-Trp-(*N*-Me)Nle-Asp-Trp-NH_2.

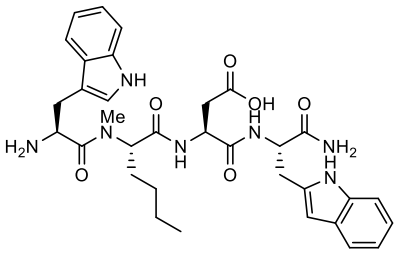

***H*-Trp-(*N*-Me)Nle-Asp-Trp-NH_2 (B7):** RP-HPLC (10→70% MeCN in H_2O with 0.1% TFA, 15 min, λ = 220 nm): t_R = 10.3 min, K' = 5.11; MS (ESI, positive): m/z calculated for $C_{33}H_{41}N_7O_6$: 631.3, found: m/z = 1264.8 $[2M+H]^+$, 632.3 $[M+H]^+$.

^{177}Lu-Labeling

For ^{177}Lu-labeling experiments, [^{177}Lu]$LuCl_3$ dissolved in hydrochloric acid (0.04 M, 40 GBq/mL) was acquired from ITM Isotope Technologies Munich SE (Garching, Germany). Radiolabeling of the peptide precursor (1 nmol) was performed at 90°C for 15 min in a NaOAc-buffered (1 M, pH = 5.5) hydrochloric acid (0.04 M) solution. After radiolabeling, a sodium ascorbate (1 M in H_2O) was added to prevent radiolysis and radiochemical purity was determined via radio-RP-HPLC and radio-TLC (instant thin layer chromatography paper impregnated with silica gel (iTLC-SG, Agilent Technologies Inc., Folsom, CA, United States); sodium citrate × 1.5 H_2O (0.1 M)).

Table S1. CCK-2R affinity and lipophilicity data of the compounds evaluated. Affinity data were determined on AR42J cells (2.0 x 10^5 cells/well/mL) and [^{177}Lu]Lu-DOTA-PP-F11N (0.3 pmol/well) as radiolabeled reference (3 h, 37°C, RPMI 1640, 5 mM L-Gln, 5 mL non-essential amino acids (100x), 10% FCS + 5% BSA (*v*/*v*)).

Peptide	IC_{50} [nM]	log$D_{7.4}$
[$^{nat/177}$Lu]Lu-DOTA-CCK-55	8.51 ± 1.16	−2.09 ± 0.07
[$^{nat/177}$Lu]Lu-DOTA-CCK-56	4.92 ± 0.79	−1.38 ± 0.07
[$^{nat/177}$Lu]Lu-DOTA-CCK-57	9.67 ± 1.74	−1.94 ± 0.06
[$^{nat/177}$Lu]Lu-DOTA-CCK-58	8.21 ± 1.33	−2.66 ± 0.06
[$^{nat/177}$Lu]Lu-DOTA-CCK-59	5.61 ± 0.48	−1.26 ± 0.08
[$^{nat/177}$Lu]Lu-DOTA-CCK-60	4.16 ± 0.47	−2.63 ± 0.05
[$^{nat/177}$Lu]Lu-DOTA-CCK-61	7.85 ± 0.43	−2.56 ± 0.09
[$^{nat/177}$Lu]Lu-DOTA-CCK-62	98.9 ± 8.4	−1.34 ± 0.08
[$^{nat/177}$Lu]Lu-DOTA-CCK-63	8.84 ± 1.25	−2.13 ± 0.05
[$^{nat/177}$Lu]Lu-DOTA-CCK-64	7.64 ± 0.86	−2.21 ± 0.07
[$^{nat/177}$Lu]Lu-DOTA-γ-MGS5	4.90 ± 0.78	−2.24 ± 0.04
H-Trp-Nle-Asp-1-Nal-NH_2 (B1)	297 ± 15	not determined (n.d.)
H-Trp-Nle-Asp-Phe-NH_2 (B2)	466 ± 88	n.d.
H-Trp-(*N*-Me)Nle-Asp-1-Nal-NH_2 (B3)	5.88 ± 0.52	n.d.
H-Trp-(*N*-Me)Nle-Asp-Phe-NH_2 (B4)	4.49 ± 0.56	n.d.
H-Trp-(*N*-Me)Nle-Asp-2-Nal-NH_2 (B5)	102 ± 9	n.d.
H-Trp-(*N*-Me)Nle-Asp-Tyr-NH_2 (B6)	5.70 ± 0.48	n.d.
H-Trp-(*N*-Me)Nle-Asp-Trp-NH_2 (B7)	18.8 ± 0.5	n.d.

Table S2. *In vitro* stability of [^{177}Lu]Lu-DOTA-CCK-55, [^{177}Lu]Lu-DOTA-CCK-62, [^{177}Lu]Lu-DOTA-CCK-63 and [^{177}Lu]Lu-DOTA-γ-MGS5 after incubation for 24 h at 37°C in human serum. Values are depicted in percent of intact peptide as analyzed by radio-RP-HPLC (MultoKrom 100-5 C18, 5 µm, 125 × 4.6 mm, CS Chromatographie GmbH, Langerwehe, Germany; 10→30% MeCN in H_2O + 0.1% TFA in 5 min; 30→60% MeCN in H_2O + 0.1% TFA in 5 min).

Compound	Intact Peptide (%)
[^{177}Lu]Lu-DOTA-CCK-55	87.5 ± 1.9
[^{177}Lu]Lu-DOTA-CCK-62	97.9 ± 1.8
[^{177}Lu]Lu-DOTA-CCK-63	57.4 ± 3.7
[^{177}Lu]Lu-DOTA-CCK-64	43.8 ± 2.3
[^{177}Lu]Lu-DOTA-γ-MGS5	96.8 ± 2.8

2.4 Preclinical Evaluation of Novel Minigastrin Analogs and Proof-of-Concept [^{68}Ga]Ga-DOTA-CCK-66 PET/CT in two Patients With Medullary Thyroid Cancer

Journal of Nuclear Medicine, published on November 9, 2023 as doi:10.2967/jnumed.123.266537

Preclinical Evaluation of Minigastrin Analogs and Proof-of-Concept [^{68}Ga]Ga-DOTA-CCK-66 PET/CT in 2 Patients with Medullary Thyroid Cancer

Thomas Günther*[1], Nadine Holzleitner*[1], Oliver Viering[2], Roswitha Beck[1], Georgine Wienand[2], Alexander Dierks[2], Christian H. Pfob[2], Ralph A. Bundschuh[2], Malte Kircher[2], Constantin Lapa[2], and Hans-Jürgen Wester[1]

[1]*Department of Chemistry, Chair of Pharmaceutical Radiochemistry, TUM School of Natural Sciences, Technical University of Munich, Garching, Germany; and* [2]*Nuclear Medicine, Faculty of Medicine, University of Augsburg, Augsburg, Germany*

Because of the need for radiolabeled theranostics for the detection and treatment of medullary thyroid cancer (MTC), and the yet unresolved stability issues of minigastrin analogs targeting the cholecystokinin-2 receptor (CCK-2R), our aim was to address in vivo stability, our motivation being to develop and evaluate DOTA-CCK-66 (DOTA-γ-glu-PEG_3-Trp-(*N*-Me)Nle-Asp-1-Nal-NH_2, PEG: polyethylene glycol) and DOTA-CCK-66.2 (DOTA-glu-PEG_3-Trp-(*N*-Me)Nle-Asp-1-Nal-NH_2), both derived from DOTA-MGS5 (DOTA-glu-Ala-Tyr-Gly-Trp-(*N*-Me)Nle-Asp-1-Nal-NH_2), and clinically translate [^{68}Ga]Ga-DOTA-CCK-66. **Methods:** ^{64}Cu and ^{67}Ga labeling of DOTA-CCK-66, DOTA-CCK-66.2, and DOTA-MGS5 was performed at 90°C within 15 min (1.0 M NaOAc buffer, pH 5.5, and 2.5 M 4-(2-hydroxyethyl)-1-piperazineethanesulfonic acid buffer, respectively). ^{177}Lu labeling of these 3 compounds was performed at 90°C within 15 min (1.0 M NaOAc buffer, pH 5.5, 0.1 M sodium ascorbate). CCK-2R affinity of ^{nat}Ga/^{nat}Cu/^{nat}Lu-labeled DOTA-CCK-66, DOTA-CCK-66.2, and DOTA-MGS5 was examined on AR42J cells. The in vivo stability of ^{177}Lu-labeled DOTA-CCK-66 and DOTA-MGS5 was examined at 30 min after injection in CB17-SCID mice. Biodistribution studies at 1 h ([^{67}Ga]Ga-DOTA-CCK-66) and 24 h ([^{177}Lu]Lu-DOTA-CCK-66/DOTA-MGS5) after injection were performed on AR42J tumor–bearing CB17-SCID mice. In a translation to the human setting, [^{68}Ga]Ga-DOTA-CCK-66 was administered and whole-body PET/CT was acquired at 120 min after injection in 2 MTC patients. **Results:** Irrespective of the metal or radiometal used (copper, gallium, lutetium), high CCK-2R affinity (half-maximal inhibitory concentration, 3.6–6.0 nM) and favorable lipophilicity were determined. In vivo, increased numbers of intact peptide were found for [^{177}Lu]Lu-DOTA-CCK-66 compared with [^{177}Lu]Lu-DOTA-MGS5 in murine urine (23.7% ± 9.2% vs. 77.8% ± 2.3%). Overall tumor-to-background ratios were similar for both ^{177}Lu-labeled analogs. [^{67}Ga]Ga-DOTA-CCK-66 exhibited accumulation (percentage injected dose per gram) that was high in tumor (19.4 ± 3.5) and low in off-target areas (blood, 0.61 ± 0.07; liver, 0.31 ± 0.02; pancreas, 0.23 ± 0.07; stomach, 1.81 ± 0.19; kidney, 2.51 ± 0.49) at 1 h after injection. PET/CT examination in 2 MTC patients applying [^{68}Ga]Ga-DOTA-CCK-66 confirmed multiple metastases. **Conclusion:** Because of the high in vivo stability and favorable overall preclinical performance of [$^{nat/67}$Ga]Ga-/[$^{nat/177}$Lu]Lu-DOTA-CCK-66, a proof-of-concept clinical investigation of [^{68}Ga]Ga-DOTA-CCK-66 was completed. As several lesions could be identified and excellent biodistribution patterns were observed, further patient studies applying [^{68}Ga]Ga- and [^{177}Lu]Lu-DOTA-CCK-66 are warranted.

Received Aug. 11, 2023; revision accepted Oct. 19, 2023.

For correspondence or reprints, contact Thomas Günther (thomas.guenther@tum.de).

*Contributed equally to this work.

Published online Nov. 9, 2023.

Key Words: DOTA-CCK-66; clinical translation; CCK-2R; medullary thyroid cancer

J Nucl Med 2024; 00:1–7
DOI: 10.2967/jnumed.123.266537

Despite progress in cancer treatment, metastasis still accounts for more than 90% and remains the primary cause of cancer death (*1*). For medullary thyroid cancer (MTC), which accounts for less than 3% of all thyroid cancers, the 10-y survival rate for patients who already had distant metastases at initial diagnosis was only 40% (*2,3*). Because of the limited role of conventional therapies in metastatic MTC not amenable to local treatment (*4,5*), and given the fact that tyrosine kinase inhibitors including antiangiogenic as well as selective RET (rearranged during transfection) inhibitors—though effective—can cause significant toxicity or induce resistance (*6,7*), alternative treatment options for early detection of MTC are needed. Elevated basal calcitonin plasma levels are common in MTC patients and can be measured after calcium or pentagastrin stimulation testing (*8,9*). Patients with confirmed elevated calcitonin levels usually undergo PET imaging using, for example, 3,4-dihydroxy-6-[^{18}F]fluoro-L-phenylalanine ([^{18}F]F-DOPA), given the neuroendocrine origin of MTC cells (*10*). Despite good detection rates using [^{18}F]F-DOPA PET/CT for primary and metastatic MTC, an even improved sensitivity at lower calcitonin levels would be desirable (*11–13*). Moreover, even if metastases are accurately identified by [^{18}F]F-DOPA PET/CT, there is no therapeutic analog available for this compound for subsequent radioligand therapy.

The cholecystokinin-2 receptor (CCK-2R) has been shown to be overexpressed on most MTC cells, thus promoting the development of several different compounds addressing this target over the last few years (*14–18*). CCK-2R ligands carrying a DOTA chelator can be used for imaging (^{68}Ga-labeled) or radioligand therapy (^{177}Lu-labeled)—an advantage over [^{18}F]F-3,4-dihydroxyphenylalanine (DOPA). Apart from ^{68}Ga, ^{64}Cu could be an interesting alternative for PET imaging because of its favorable half-life (12.7 h) and positron energy (653 keV), enabling later imaging time points and high spatial resolution (*19*). However, the low metabolic stability of minigastrin derivatives targeting CCK-2R is still a problem that affects therapeutic efficacy. Several cleavage sites were reported for minigastrin analogs (Tyr-Gly, Gly-Trp, and Asp-Phe) (*20*), of which some were chemically addressed in DOTA-MGS5 (DOTA-glu-Ala-Tyr-Gly-Trp-(*N*-Me)Nle-Asp-1-Nal-NH_2, Fig. 1) (*21*). In vivo

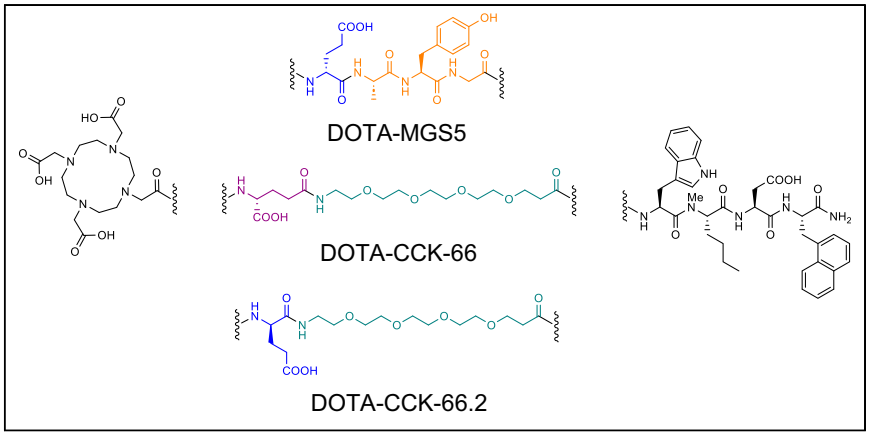

FIGURE 1. Chemical structures of compounds evaluated. All comprise same C-terminal tetrapeptide binding motif and N-terminal DOTA chelator but differ in linker section. Orange = Ala-Tyr-Gly sequence; green = PEG_3 moiety; blue = α-bridged D-glutamic acid moiety; violet = γ-bridged D-glutamic acid moiety.

properties in animals and first patient data thus looked promising for [^{68}Ga]Ga-DOTA-MGS5 (*21,22*).

However, particularly the cleavage sites Tyr-Gly and Gly-Trp are still not addressed in this compound. Therefore, we recently reported on a series of CCK-2R ligands in which we substituted the N-terminal L-amino acids in DOTA-MGS5 (*H*-glu-Ala-Tyr-Gly) by simple polyethylene glycol (PEG) linkers. Interestingly, we observed a lower in vitro stability in human serum (*23*), although the introduction of PEG linkers usually increases stability (*24*). Because negative charges at the N-terminus of minigastrin analogs seem to increase metabolic stability (*25*), we introduced either a γ-D-glutamic acid (γ-glu) or a α-D-glutamic acid (glu) moiety between the DOTA chelator and the PEG_3 linker of DOTA-CCK-64 (DOTA-PEG_3-Trp-(*N*-Me)Nle-Asp-1-Nal-NH_2), which resulted in DOTA-CCK-66 (DOTA-γ-glu-PEG_3-Trp-(N-Me)Nle-Asp-1-Nal-NH_2) and DOTA-CCK-66.2 (DOTA-glu-PEG_3-Trp-(*N*-Me)Nle-Asp-1-Nal-NH_2) (Fig. 1). Furthermore, this study aimed to elucidate whether this simple modification could tackle the stability issues observed in previous studies. Hence, a comparative preclinical evaluation of DOTA-CCK-66, DOTA-CCK-66.2, and DOTA-MGS5, each labeled with [$^{nat/64}$Cu]copper, [$^{nat/67}$Ga]gallium, or [$^{nat/177}$Lu]lutetium, encompassed the determination of CCK-2R affinity (half-maximal inhibitory concentration [IC_{50}]) on AR42J cells, lipophilicity (expressed as n-octanol/phosphate-buffered saline distribution coefficient [log$D_{7.4}$]), human serum albumin binding, in vivo stability, and biodistribution studies on AR42J tumor–bearing mice. Moreover, we selected [^{68}Ga]Ga-DOTA-CCK-66 for proof-of-concept PET/CT examinations in 2 MTC patients.

MATERIALS AND METHODS

Synthesis and Labeling Procedures

Precursor synthesis was conducted via solid-phase peptide synthesis using an *H*-Rink Amide ChemMatrix resin (loading, 0.55 mmol/g; Sigma-Aldrich Chemie GmbH). Characterization of all compounds is provided in Supplemental Figures 1–9 (supplemental materials are available at http://jnm.snmjournals.org). Purification was accomplished via reversed-phase high-performance liquid chromatography (RP-HPLC).

^{64}Cu- and ^{177}Lu-labeling of DOTA-CCK-66, DOTA-CCK-66.2, and DOTA-MGS5 was completed using an established protocol (*26*). ^{67}Ga-labeling of these 3 compounds was performed analogously using 4-(2-hydroxyethyl)-1-piperazineethanesulfonic acid (2.5 M in H_2O) buffer. Detailed descriptions of all labeling procedures ($^{nat/68}$Ga, $^{nat/64}$Cu, $^{nat/177}$Lu) are provided in the supplemental materials. [^{64}Cu]$CuCl_2$ was purchased from DSD-Pharma GmbH. [^{67}Ga]$GaCl_3$ was acquired from Curium. [^{177}Lu]$LuCl_3$ was purchased from ITM Isotope Technologies Munich SE.

The synthesis of [^{68}Ga]Ga-DOTA-CCK-66 for human PET/CT studies was completed in agreement with good manufacturing practices using a good-radiopharmaceutical-practice module (Scintomics GmbH) equipped with an SC-01 gallium peptide labeling kit (ABX). [^{68}Ga]$GaCl_3$ was obtained from a ^{68}Ge/^{68}Ga-generator (GalliAD; IRE Elit Radiopharma). A 900 ± 300 MBq activity of the ^{68}Ga-eluate was combined with a solution of the DOTA-CCK-66 precursor (50 μg) and NaOAc buffer in the reactor and heated. Afterward, the solution was transferred onto a Sep-Pak C18 Light cartridge (Waters) for purification. The cartridge was washed with water and eluted with ethanol, and the solution was diluted with phosphate-buffered saline. Subsequently, sterile filtration was completed using a Millex-GV filter (Merck KGaA). Quality control was conducted using thin-layer chromatography (NH_4OAc/MeOH; Agilent) and HPLC measurement against the corresponding reference compound, [^{nat}Ga]Ga-DOTA-CCK-66. Furthermore, a sterile filter integrity test, a limulus amebocyte lysate, and a postapplication sterility test were performed.

In Vitro Experiments

The CCK-2R affinity (by means of IC_{50}) of ^{nat}Ga/^{nat}Cu/^{nat}Lu-labeled DOTA-CCK-66, DOTA-CCK-66.2, and DOTA-MGS5 and the log$D_{7.4}$ of ^{67}Ga/^{64}Cu/^{177}Lu-labeled DOTA-CCK-66, DOTA-CCK-66.2, and DOTA-MGS5 were determined according to a published procedure (*27*). Human serum albumin binding of ^{nat}Ga/^{nat}Cu/^{nat}Lu-labeled DOTA-CCK-66, DOTA-CCK-66.2, and DOTA-MGS5 was determined by high-performance affinity chromatography (Supplemental Fig. 10), as previously reported (*28,29*). In vitro stability studies of ^{177}Lu-labeled DOTA-CCK-66, DOTA-CCK-66.2, and DOTA-MGS5 in human serum were completed in analogy to a published procedure (*30*). A detailed description of in vitro experiments is provided in the supplemental materials.

In Vivo Experiments

Animal Experiments. All animal experiments were approved by the General Administration of Upper Bavaria (ROB-55.2-1-2532.Vet_02-18-109) and completed using a previously published protocol (*26*). All animal studies were in compliance with the ARRIVE (Animal Research: Reporting of In Vivo Experiments) guidelines (supplemental materials).

In vivo stability studies at 30 min after intravenous injection (n = 3) were completed according to a published procedure using about 30–40 MBq (1 nmol) of [^{177}Lu]Lu-DOTA-CCK-66 and [^{177}Lu]Lu-DOTA-MGS5, respectively, for each animal (*26*).

For biodistribution studies, approximately 2–4 MBq (100 pmol, 150 μL) of [^{67}Ga]Ga-DOTA-CCK-66, [^{177}Lu]Lu-DOTA-CCK-66, or [^{177}Lu]Lu-DOTA-MGS5 were injected into the tail vein of anesthetized (2% isoflurane) 2- to 3-mo-old female AR42J tumor–bearing CB17-SCID mice (n = 4). Organs were removed and weighed, and the accumulated radioactivity was measured in a γ-counter (Perkin Elmer) after euthanasia at 1 h (^{67}Ga-labeled) and 24 h (^{177}Lu-labeled) after injection.

Imaging studies using [^{67}Ga]Ga-DOTA-CCK-66, [^{177}Lu]Lu-DOTA-CCK-66, or [^{177}Lu]Lu-DOTA-MGS5 were performed according to a

published protocol (*26*). Static images were recorded at t = 1 and 24 h after injection (anesthesia by 2% isoflurane, n = 1) with an acquisition time of t + (45–60 min) using a high-energy general-purpose rat and mouse collimator via MILabs acquisition software versions 11.00 and 12.26 from MILabs.

For competition studies (n = 2), a 3.03 mg/kg concentration (40 nmol) of [^{nat}Ga]Ga-DOTA-MGS5 (10^{-3} M in phosphate-buffered saline) was coinjected with [^{67}Ga]Ga-DOTA-CCK-66 (100 pmol), or a 3.25 mg/kg concentration (40 nmol) of [^{nat}Lu]Lu-DOTA-MGS5 (10^{-3} M in phosphate-buffered saline) was coadministered with [^{177}Lu]Lu-DOTA-CCK-66 (100 pmol).

Acquired data were statistically analyzed using the Student t-test via Excel (Microsoft Corp.) and OriginPro software (version 9.7; OriginLab Corp.). Acquired P values of less than 0.05 were considered statistically significant.

Clinical PET/CT. [^{68}Ga]Ga-DOTA-CCK-66 was applied for restaging purposes in 2 MTC patients (male, aged 64 y, and female, aged 46 y). Both patients presented with rising calcitonin levels and calcitonin doubling times shorter than 24 mo at the time of PET/CT imaging, indicating tumor progression. Before CCK-2R–directed imaging, [^{18}F]F-DOPA PET/CT had been negative in both subjects, prompting further diagnostic work-up. The application is allowed by the German Medical Act (§13 2b Arzneimittelgesetz), which waives the need for institutional review board approval. Both patients gave written informed consent after receiving comprehensive medical information from a board-certified nuclear medicine physician. All procedures were completed in accordance with the Declaration of Helsinki and its later amendments and the legal considerations of clinical guidelines. The ethical compliance of this approach was confirmed by the local Ethics Committee of Ludwig-Maximilians-Universität München (approval 23-0627).

A detailed description of the patients' histories is provided in the supplemental materials. Both patients underwent [^{68}Ga]Ga-DOTA-CCK-66 whole-body imaging using a PET/CT scanner (Biograph mCT 40; Siemens Healthineers) at 120 min after injection of 151 and 193 MBq of [^{68}Ga]Ga-DOTA-CCK-66 (~18 μg each), respectively. Whole-body CT imaging was performed as auxiliary CT (120 kVp, 40 mAs). PET datasets were reconstructed using a standard protocol provided by the manufacturer (2 iterations, 21 subsets), corrected for randoms, scatter, decay, and attenuation (using whole-body auxiliary CT).

RESULTS

Synthesis and Radiolabeling

The synthesized precursors were obtained in yields of 3%–7% (chemical purity > 95%) after RP-HPLC purification. Labeling using a 2.5-fold excess of [^{nat}Ga]Ga(NO_3)$_3$, [^{nat}Lu]LuCl_3, or [^{nat}Cu]Cu(OAc)$_2$ resulted in quantitative yields. No purification step was conducted before in vitro experiments, as no effects of free metal ions on overall affinity data was observed in previous experiments (*26*). ^{177}Lu, ^{67}Ga, and ^{64}Cu labeling of DOTA-CCK-66, DOTA-CCK-66.2, and DOTA-MGS5 was performed manually, each resulting in radiochemical yields and purities of more than 95% and molar activities of 10–50 GBq/μmol (non–decay-corrected). All compounds were used without further purification.

The synthesized batches of [^{68}Ga]Ga-DOTA-CCK-66 used for proof-of-concept studies in 2 MTC patients yielded 150 ± 50 MBq (~56% non–decay-corrected). All specifications were fulfilled. The pH of the 16-mL solution was 7.5. Both the ^{nat}Ga-labeled reference compound and the ^{68}Ga-labeled product showed the same retention times using RP-HPLC. The radiochemical purity determined by

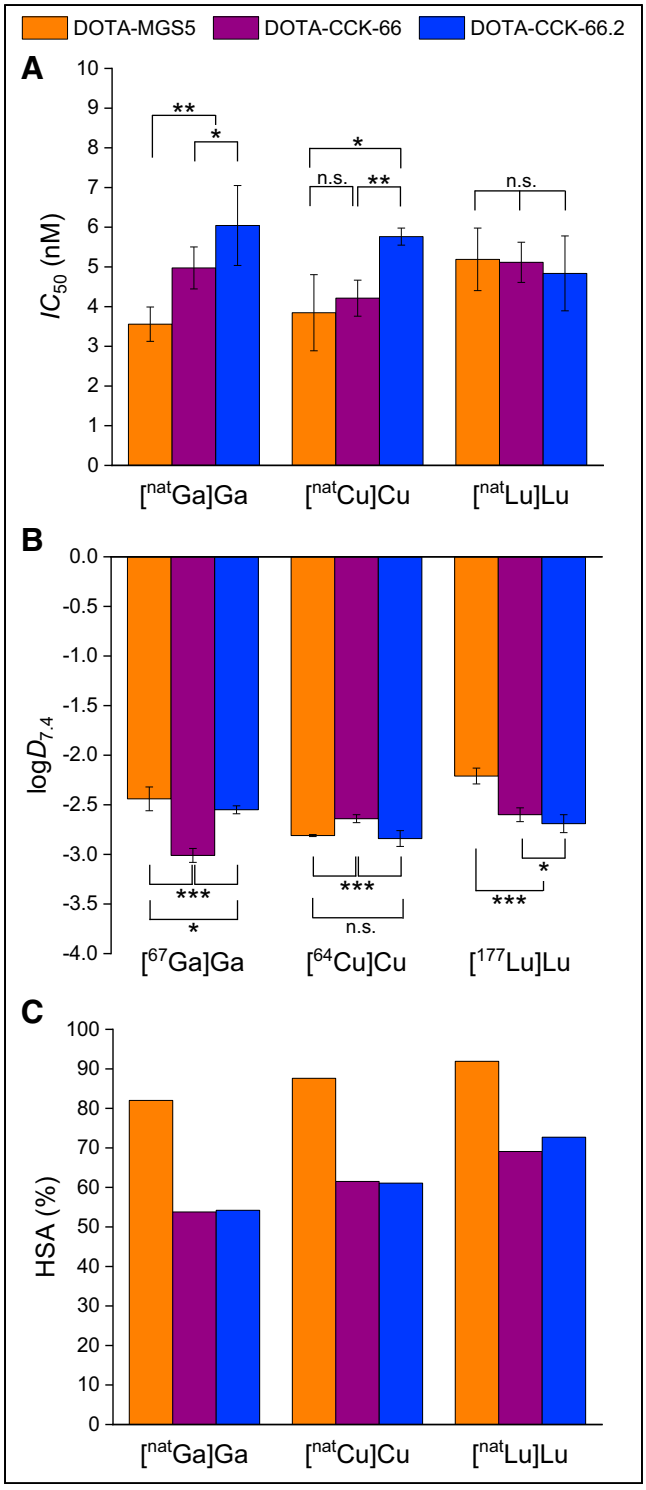

FIGURE 2. In vitro data of $^{nat/64}$Cu-, $^{nat/67}$Ga-, and $^{nat/177}$Lu-labeled CCK-2R ligands. Data are expressed as mean ± SD. (A) Affinity data (n = 3) on AR42J cells (2.0 × 10^5 cells per well) using [^{177}Lu]Lu-DOTA-PP-F11N (0.3 pmol/well) as radiolabeled reference (3 h, 37°C, RPMI 1640, 5 mM L-Gln, 5 mL nonessential amino acids [×100], 10% fetal calf serum + 5% bovine serum albumin [*v/v*]). (B) log$D_{7.4}$ (n = 6). (C) Human serum albumin binding as determined by high-performance affinity chromatography. n.s. = not significant. *P < 0.05. **P < 0.01. ***P < 0.0001.

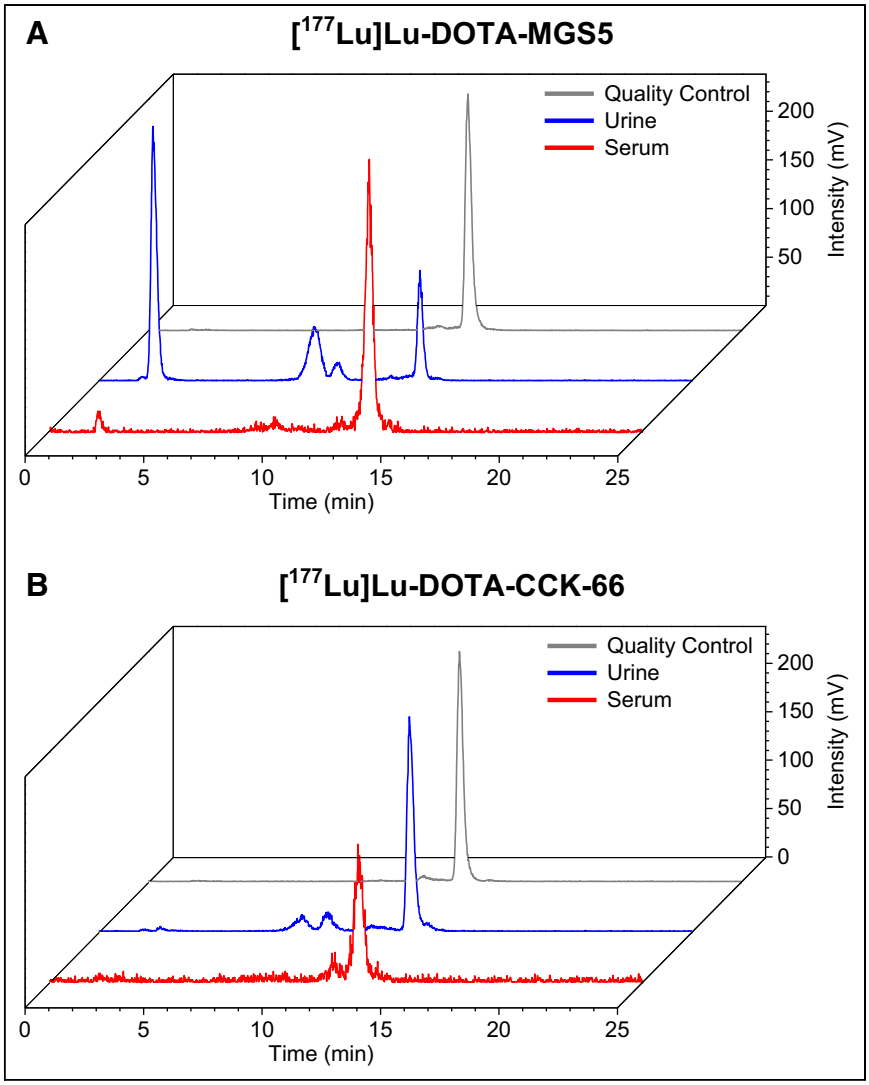

FIGURE 3. In vivo stability of CCK-2R ligands: amount of intact compound at 30 min after injection (3 each) in murine serum (red) and urine (blue) for [^{177}Lu]Lu-DOTA-MGS5 (A) and [^{177}Lu]Lu-DOTA-CCK-66 (B) (quality control in gray).

RP-HPLC was higher than 95%, and the content of unbound [^{68}Ga]Ga species was less than 0.8%. Thin-layer chromatography measurement also revealed less than 0.8% of unbound [^{68}Ga]Ga^{3+}.

In Vitro Characterization

All 3 compounds exhibited high CCK-2R affinity on AR42J cells (IC_{50}, 3.6–6.0 nM, irrespective of whether ^{nat}Ga-, ^{nat}Cu-, or ^{nat}Lu-labeled; Fig. 2A; Supplemental Table 1). [^{nat}Ga]Ga-DOTA-MGS5 revealed significantly lower IC_{50} values than [^{nat}Ga]Ga-DOTA-CCK-66 and -66.2 ($P < 0.004$), and [^{nat}Cu]Cu-DOTA-CCK-66.2 displayed significantly higher IC_{50} values than [^{nat}Cu]Cu-DOTA-MGS5 and [^{nat}Cu]Cu-DOTA-CCK-66 ($P < 0.03$). Distribution coefficients ($\log D_{7.4}$) were in the range of −3.0 to −2.2 for all 3 ligands, independent of whether ^{67}Ga-, ^{64}Cu-, or ^{177}Lu-labeled (Fig. 2B, Supplemental Table 1). [^{67}Ga]Ga-DOTA-CCK-66 revealed significantly lower $\log D_{7.4}$ values than [^{67}Ga]Ga-DOTA-MGS5 and [^{67}Ga]Ga-DOTA-CCK-66.2 ($P < 0.0001$), [^{64}Cu]Cu-DOTA-CCK-66 exhibited significantly higher $\log D_{7.4}$ values than [^{64}Cu]Cu-DOTA-MGS5 and [^{64}Cu]Cu-DOTA-CCK-66.2 ($P < 0.0001$), and [^{177}Lu]Lu-DOTA-MGS5 displayed significantly higher $\log D_{7.4}$ values than [^{177}Lu]Lu-DOTA-CCK-66 and -66.2 ($P < 0.0001$). Both DOTA-CCK-66 and DOTA-CCK-66.2 exhibited distinctly lower human serum albumin binding than DOTA-MGS5, irrespective of the radiometal used (Fig. 2C; Supplemental Table 2). In vitro stability studies in human serum (37°C, 72 h) showed comparable numbers of intact tracer for all 3 ^{177}Lu-labeled CCK-2R ligands (Supplemental Fig. 11, Supplemental Table 3). Because of the overall similar, but slightly more favorable, in vitro properties of DOTA-CCK-66 (independent of the metals used), DOTA-CCK-66.2 was excluded from further experiments.

In Vivo Characterization

In total, 25 animals were used for in vivo stability (2 × 3), biodistribution (3 × 4), imaging (3 × 1), and competition (2 × 2) studies. Intact compound was similar between [^{177}Lu]Lu-DOTA-CCK-66 and [^{177}Lu]Lu-DOTA-MGS5 in murine serum (78.5% ± 3.1% vs. 82.0% ± 0.1%) at 30 min after injection but was higher for [^{177}Lu]Lu-DOTA-CCK-66 than for [^{177}Lu]Lu-DOTA-MGS5 in the urine (77.8% ± 2.3% vs. 23.7% ± 9.2%, $P < 0.001$) (Fig. 3). Biodistribution studies on AR42J tumor–bearing mice revealed high initial tumor uptake (19.4 ± 3.5 percentage injected dose per gram [%ID/g]) for [^{67}Ga]Ga-DOTA-CCK-66, whereas off-target accumulation in all organs was less than 2.6 %ID/g at 1 h after injection (Fig. 4A; Supplemental Table 4). At 24 h after injection, [^{177}Lu]Lu-DOTA-CCK-66 displayed slightly lower activity levels in the tumor than did [^{177}Lu]Lu-DOTA-MGS5 (8.6 ± 1.1 %ID/g vs. 11.0 ± 1.2 %ID/g, $P < 0.02$) but also slightly lower off-target activity retention in most organs (stomach, $P < 0.01$), which resulted in comparable tumor-to-background ratios overall (Supplemental Tables 4 and 5).

Imaging studies (Fig. 4B) corroborated the biodistribution profiles well, revealing high activity levels in the tumor and low levels in all organs for [^{67}Ga]Ga-DOTA-CCK-66 (1 h after injection), as well as for [^{177}Lu]Lu-DOTA-CCK-66 and [^{177}Lu]Lu-DOTA-MGS5 (24 h after injection). Competition studies of both [^{67}Ga]Ga-DOTA-CCK-66 (1 h after injection) and [^{177}Lu]Lu-DOTA-CCK-66 (24 h after injection) using an excess of [^{nat}Ga]Ga-/[^{nat}Lu]Lu-DOTA-MGS5 confirmed specificity of tumor uptake (Supplemental Fig. 12; Supplemental Table 4).

Because of its overall in vitro and in vivo properties [^{68}Ga]Ga-DOTA-CCK-66 was selected for proof-of-concept PET/CT application in 2 MTC patients.

Proof-of-Concept Study in Humans

[^{68}Ga]Ga-DOTA-CCK-66-PET showed a favorable biodistribution, with the highest uptake in tumor lesions and the CCK-2R–expressing stomach. Besides the kidneys, ureters, and bladder

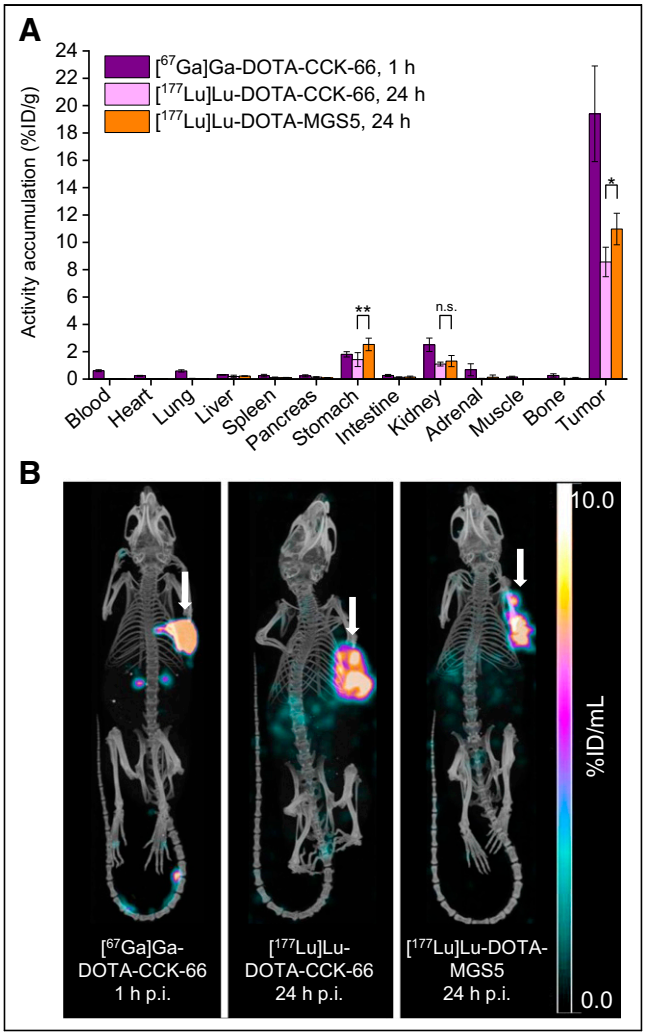

FIGURE 4. (A) Biodistribution of [^{67}Ga]Ga-DOTA-CCK-66 (1 h after injection), as well as [^{177}Lu]Lu-DOTA-CCK-66 and [^{177}Lu]Lu-DOTA-MGS5 (24 h after injection), in selected organs in AR42J tumor–bearing CB17-SCID mice (100 pmol each). Data are %ID/g (mean ± SD, 4 each). (B) Maximum-intensity projection of AR42J tumor (arrows)–bearing CB17-SCID mice (1 each) injected with [^{67}Ga]Ga-DOTA-CCK-66, as well as [^{177}Lu]Lu-DOTA-CCK-66 and [^{177}Lu]Lu-DOTA-MGS5 (100 pmol each). Images were acquired at either 1 or 24 h after injection. n.s. = not significant; p.i. = after injection. *$P < 0.05$. **$P < 0.01$.

(due to excretion), no significant activity levels were found in other organs. [^{68}Ga]Ga-DOTA-CCK-66 was well tolerated, and no side effects or changes in vital signs were observed during the tracer's slow intravenous injection (~2 min) or thereafter (with a follow-up period of 4 h).

A 64-y-old male patient who had initially undergone thyroidectomy and cervical lymph node dissection had a long history of disease, with several local and lymph node recurrences, and presented at the time of PET/CT imaging with a rising calcitonin level of 110 pg/mL and a calcitonin doubling time of 16 mo. On [^{68}Ga]Ga-DOTA-CCK-66 PET/CT, suggestive CCK-2R–expressing lymph nodes were detected in the left retroclavicular region and in the upper mediastinum (Fig. 5). Subsequently, the lymph nodes were surgically resected and histologically confirmed as lymph node metastases of MTC.

A 46-y-old female patient who had undergone thyroidectomy and cervical lymph node dissection, as well as external-beam radiation of the thyroid bed due to local tumor remnants, showed a rising calcitonin level of 380 pg/mL and a calcitonin doubling time of 5 mo at the time of PET/CT imaging. [^{68}Ga]Ga-DOTA-CCK-66 detected several lymph node metastases (bilaterally hilar, right retroclavicular), liver metastases (in both liver lobes), and bone metastases (atlas, right eighth rib, right femur, right os ischii) (Fig. 6). In comparison to the [^{18}F]FDG PET/CT available for this patient, [^{68}Ga]Ga-DOTA-CCK-66 detected additional lymph node, liver, and bone metastases.

DISCUSSION

Because of the ongoing need for novel and improved treatment options for MTC patients, several CCK-2R ligands have been reported over the last few years, particularly compounds addressing the stability issues of minigastrin derivatives by chemical design (*15–18*). In our group, we developed a series of radiohybrid-based minigastrin analogs that revealed a high activity accumulation in the tumor but also suffered from elevated kidney retention due to the presence of a silicon-fluoride acceptor moiety and several negative charges within the linker section (*27,30*). Therefore, we recently focused on shorter CCK-2R ligands and aimed to address metabolic stability by the introduction of PEG linkers, which, however, resulted in a lower stability (*23*). To address this matter in this study, we made some minor modifications within the linker sequence of our minigastrin derivatives and completed in vitro and in vivo evaluations, as well as initiating clinical translation of our most favorable compound.

Synthesis of the precursors was easily accessible via solid-phase peptide synthesis, and complexation proceeded quantitatively, irrespective of the metal or radiometal used. Because of their structural similarity, both novel compounds and the reference peptide, DOTA-MGS5, revealed a comparable CCK-2R affinity and favorable log$D_{7.4}$. On the basis of the similar but slightly more favorable in vitro properties of the DOTA-CCK-66 peptide over the DOTA-CCK-66.2 peptide, we excluded the latter from further evaluation.

In vivo stability at 30 min after injection was comparable for both [^{177}Lu]Lu-DOTA-CCK-66 and [^{177}Lu]Lu-DOTA-MGS5 in murine serum but distinctly different in murine urine, as the former revealed a 3-fold higher amount of intact compound than the reference. This finding suggests that [^{177}Lu]Lu-DOTA-CCK-66 is cleared from the blood mostly intact whereas [^{177}Lu]Lu-DOTA-MGS5 is cleared predominantly metabolized. Because of their structural similarity, this beneficial property can be attributed to the introduction of a γ-glu moiety between the DOTA and the PEG_3 linker, because a previous compound that differed from DOTA-CCK-66 only by the absence of this γ-glu unit exhibited a noticeably lower stability (*23*). The amount of intact peptide in the urine even surpassed that of a recently reported CCK-2R ligand, [^{177}Lu]Lu-DOTA-$(GABOB)_2$-β-Ala-Trp-(*N*-Me)Nle-Asp-1-Nal-NH_2, which also substituted N-terminal amino acids by unnatural moieties and revealed high in vivo stability (77.8% ± 2.3% vs. ~60%) (*16*).

Because of its high metabolic stability, [^{67}Ga]Ga-DOTA-CCK-66 demonstrated a high accumulation of activity in the tumor at 1 h after injection, whereas off-target accumulation was either low or cleared rapidly, resulting in low activity levels in all organs, even in the CCK-2R–expressing stomach. Hence, favorable tumor-to-background ratios were determined and were approximately 2-fold higher in all organs than reported for [^{68}Ga]Ga-DOTA-MGS5 (*21*). The more rapid clearance rates corroborate the distinctly lower human

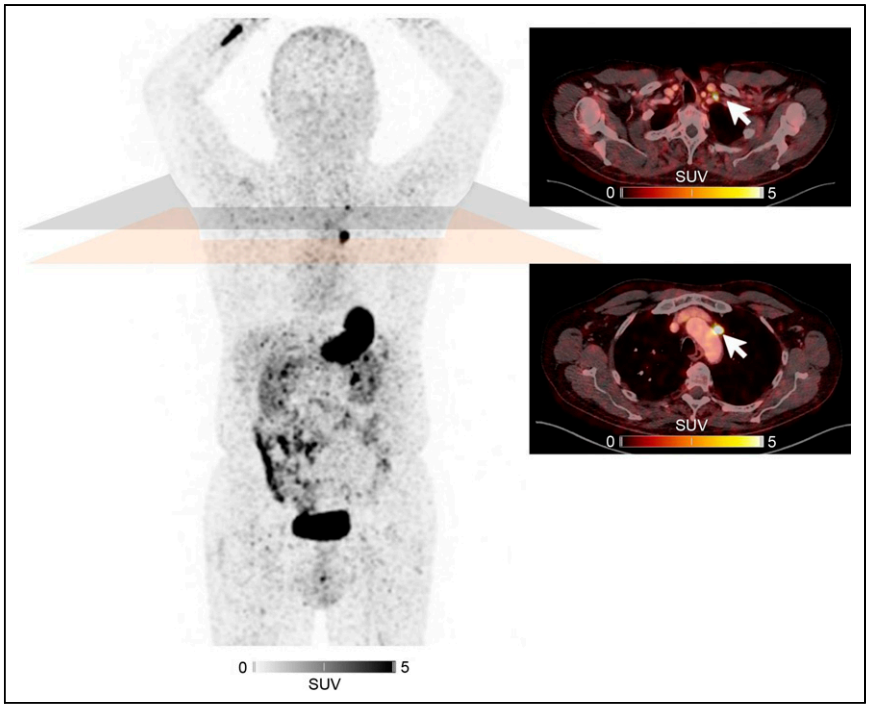

FIGURE 5. Maximum-intensity projection (left) and fused transaxial slices (right) of 64-y-old male MTC patient undergoing PET/CT at 2 h after intravenous injection of 151 MBq of [^{68}Ga]Ga-DOTA-CCK-66. CCK-2R–expressing lymph node metastases could be detected in left retroclavicular region and in upper mediastinum (arrows).

serum albumin binding observed by high-performance affinity chromatography, a finding that might be responsible for the favorably low activity uptake overall (apart from the tumor). The comparison of [^{68}Ga]Ga-DOTA-MGS5 and [^{68}Ga]Ga-DOTA-CCK-66 is a limitation of this study, as biodistribution studies of these compounds have been performed by different groups using different mouse models (BALB/c vs. CB17-SCID) and tumor models (A431-CCK2R vs. AR42J), as well as precursor amounts (20 vs. 100 pmol) (*21*). Comparison of the ^{177}Lu-labeled analogs at 24 h after injection using the same modalities revealed similar tumor-to-background ratios overall, indicating that [^{177}Lu]Lu-DOTA-MGS5 and [^{177}Lu]Lu-DOTA-CCK-66 might be equivalent in the application for radioligand therapy. However, further clinical investigation is needed.

On the basis of the favorable preclinical data of [^{67}Ga]Ga-DOTA-CCK-66, its ^{68}Ga-analog was selected for a clinical proof-of-concept investigation. [^{68}Ga]Ga-DOTA-CCK-66 PET/CT on 2 MTC patients at 120 min after injection revealed high uptake in tumor lesions and the physiologically CCK-2R–expressing stomach. Furthermore, off-target accumulation was low, corroborating the biodistribution profiles in mice well. Hence, several lymph node, bone, and liver metastases could be identified in these 2 MTC patients. Interestingly, we could observe a higher tumor-to-organ contrast at 120 min than at 60 min after injection. A similar trend was also reported for [^{68}Ga]Ga-DOTA-MGS5 (*22*), indicating a slightly decelerated tumor accumulation and a fast off-target clearance of these minigastrin analogs. On the basis of these observations and the similar in vitro properties of [^{nat}Cu]Cu-DOTA-CCK-66, PET/CT examinations using [^{64}Cu]Cu-DOTA-CCK-66 could be a viable alternative in the future, since it would enable later imaging time points.

[^{68}Ga]Ga-DOTA-CCK-66 PET/CT did not show any biosafety issues and allows for radioligand therapy using [^{177}Lu]Lu-DOTA-CCK-66, which might represent an advantage of radiolabeled CCK-2R ligands over [^{18}F]FDG or [^{18}F]F-DOPA. On the basis of the fast renal activity clearance and low activity accumulation observed in the kidneys, we do not expect any issues regarding kidney toxicity using [^{177}Lu]Lu- or even [^{225}Ac]Ac-DOTA-CCK-66 for radioligand therapy. However, activity retention in the human stomach was higher than observed in the murine stomach and has to be monitored carefully during the first treatment cycles to prevent toxicity. Furthermore, the fact that the feasibility of [^{68}Ga]Ga-DOTA-CCK-66 has been shown only for single patients to date is a limitation of this study, thus demanding further clinical evaluation of this compound to verify its clinical value.

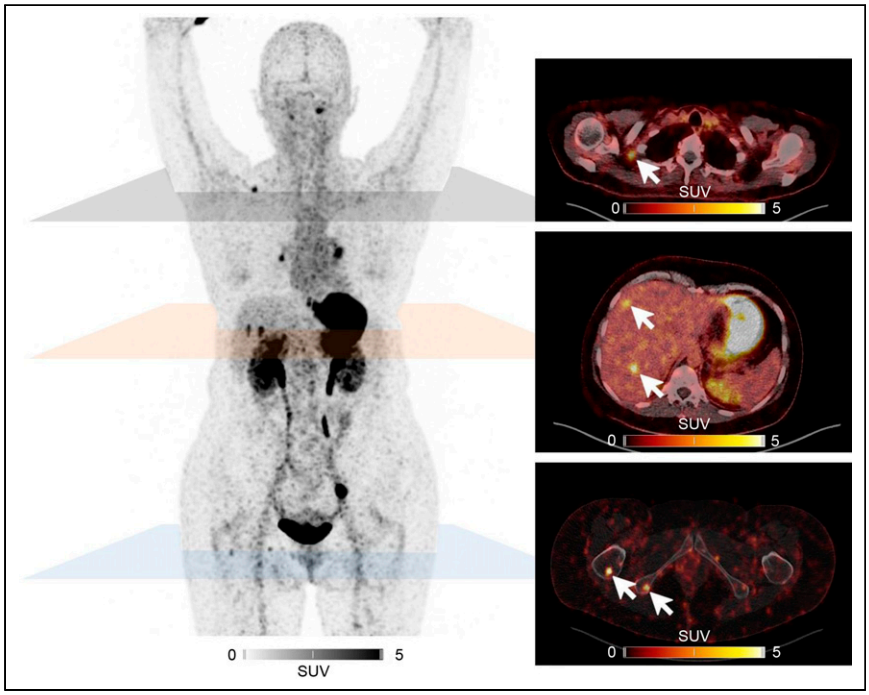

FIGURE 6. Maximum-intensity projections (left) and fused transaxial sections (right) of 46-y-old female MTC patient undergoing PET/CT at 2 h after intravenous injection of 193 MBq of [^{68}Ga]Ga-DOTA-CCK-66. Several lymph node (e.g., right retroclavicular), liver, and bone metastases (e.g., right femur and right ischium) could be detected (arrows).

CONCLUSION

[^{67}Ga]Ga-DOTA-CCK-66 revealed excellent preclinical characteristics, particularly high in vivo stability and rapid activity clearance, thus providing good tumor-to-background ratios. A proof-of-concept investigation on 2 MTC patients using [^{68}Ga]Ga-DOTA-CCK-66 PET/CT showed favorable biodistribution patterns and identified several lesions, which could be histopathologically confirmed as metastases of MTC. One advantage of this compound over the MTC imaging gold standard, [^{18}F]F-DOPA, is the possibility for ^{177}Lu labeling for subsequent radioligand therapy. Therefore, additional patient studies using [^{68}Ga]Ga- or [^{64}Cu]Cu-DOTA-CCK-66, as well as [^{177}Lu]Lu- or even [^{225}Ac]Ac-DOTA-CCK-66, are warranted to elucidate the clinical value of this theranostic tool.

DISCLOSURE

This study was funded by Deutsche Forschungsgemeinschaft (DFG, German Research Foundation—461577150). Thomas Günther received the 2023 Sanjiv Sam Gambhir–Philips and the 2023 Translational Research and Applied Medicine fellowship for support at Stanford University. A patent application on CCK-2R–targeted compounds including DOTA-CCK-66 with Thomas Günther, Nadine Holzleitner, Constantin Lapa, and Hans-Jürgen Wester as inventors has been filed. Hans-Jürgen Wester is founder and shareholder of Scintomics GmbH, Munich, Germany. No other potential conflict of interest relevant to this article was reported.

KEY POINTS

QUESTION: Can a simplistic design modification of the clinically applied CCK-2R ligand [^{68}Ga]Ga-DOTA-MGS5 improve preclinical and clinical characteristics?

PERTINENT FINDINGS: [^{64}Cu]Cu-/[^{67}Ga]Ga-/[^{177}Lu]Lu-DOTA-CCK-66 displayed similar in vitro and in vivo properties to the reference compound but a noticeably improved in vivo stability, which resulted in favorable activity clearance and, thus, tumor-to-organ contrast in animals and proof-of-concept [^{68}Ga]Ga-DOTA-CCK-66 PET/CT applications.

IMPLICATIONS FOR PATIENT CARE: Although further [^{68}Ga]Ga-DOTA-CCK-66 PET/CT (and [^{177}Lu]Lu-/[^{225}Ac]Ac-DOTA-CCK-66 for treatment) applications in MTC patients have to be completed, these preliminary results suggest a promising theranostic candidate for clinical use.

REFERENCES

1. Ganesh K, Massagué J. Targeting metastatic cancer. *Nat Med.* 2021;27:34–44.
2. Thyroid cancer: statistics. Cancer.net website. https://www.cancer.net/cancer-types/thyroid-cancer/statistics#:~:text=In%202023%2C%20an%20estimated%2043%2C720,with%20thyroid%20cancer%20in%202020. Published August 2023. Accessed October 30, 2023.
3. Roman S, Lin R, Sosa JA. Prognosis of medullary thyroid carcinoma: demographic, clinical, and pathologic predictors of survival in 1252 cases. *Cancer.* 2006;107:2134–2142.
4. Stamatakos M, Paraskeva P, Stefanaki C, et al. Medullary thyroid carcinoma: the third most common thyroid cancer reviewed. *Oncol Lett.* 2011;2:49–53.
5. Wells SA Jr, Asa SL, Dralle H, et al. Revised American Thyroid Association guidelines for the management of medullary thyroid carcinoma. *Thyroid.* 2015;25:567–610.
6. Vodopivec DM, Hu MI. RET kinase inhibitors for RET-altered thyroid cancers. *Ther Adv Med Oncol.* 2022;14:17588359221101691.
7. Hadoux J, Schlumberger M. Chemotherapy and tyrosine-kinase inhibitors for medullary thyroid cancer. *Best Pract Res Clin Endocrinol Metab.* 2017;31:335–347.
8. Karges W, Dralle H, Raue F, et al. Calcitonin measurement to detect medullary thyroid carcinoma in nodular goiter: German evidence-based consensus recommendation. *Exp Clin Endocrinol Diabetes.* 2004;112:52–58.
9. Hennessy JF, Wells SAJ, Ontjes DA, Cooper CW. A comparison of pentagastrin injection and calcium infusion as provocative agents for the detection of medullary carcinoma of the thyroid. *J Clin Endocrinol Metab.* 1974;39:487–495.
10. Giovanella L, Treglia G, Iakovou I, Mihailovic J, Verburg FA, Luster M. EANM practice guideline for PET/CT imaging in medullary thyroid carcinoma. *Eur J Nucl Med Mol Imaging.* 2020;47:61–77.
11. Treglia G, Castaldi P, Villani MF, et al. Comparison of ^{18}F-DOPA, ^{18}F-FDG and ^{68}Ga-somatostatin analogue PET/CT in patients with recurrent medullary thyroid carcinoma. *Eur J Nucl Med Mol Imaging.* 2012;39:569–580.
12. Brammen L, Niederle MB, Riss P, et al. Medullary thyroid carcinoma: do ultrasonography and F-DOPA-PET-CT influence the initial surgical strategy? *Ann Surg Oncol.* 2018;25:3919–3927.
13. Terroir M, Caramella C, Borget I, et al. F-18-dopa positron emission tomography/computed tomography is more sensitive than whole-body magnetic resonance imaging for the localization of persistent/recurrent disease of medullary thyroid cancer patients. *Thyroid.* 2019;29:1457–1464.
14. von Guggenberg E, Kolenc P, Rottenburger C, Mikolajczak R, Hubalewska-Dydejczyk A. Update on preclinical development and clinical translation of cholecystokinin-2 receptor targeting radiopharmaceuticals. *Cancers (Basel).* 2021;13:5776.
15. Zavvar TS, Hörmann AA, Klingler M, et al. Effects of side chain and peptide bond modifications on the targeting properties of stabilized minigastrin analogs. *Pharmaceuticals (Basel).* 2023;16:278.
16. Hörmann AA, Klingler M, Rangger C, et al. Effect of N-terminal peptide modifications on in vitro and in vivo properties of ^{177}Lu-labeled peptide analogs targeting CCK2R. *Pharmaceutics.* 2023;15:796.
17. Grob NM, Schibli R, Behe M, Valverde IE, Mindt TL. 1,5-disubstituted 1,2,3-triazoles as amide bond isosteres yield novel tumor-targeting minigastrin analogs. *ACS Med Chem Lett.* 2021;12:585–592.
18. Sauter AW, Mansi R, Hassiepen U, et al. Targeting of the cholecystokinin-2 receptor with the minigastrin analog ^{177}Lu-DOTA-PP-F11N: does the use of protease inhibitors further improve in vivo distribution? *J Nucl Med.* 2019;60:393–399.
19. Braune A, Oehme L, Freudenberg R, et al. Comparison of image quality and spatial resolution between ^{18}F, ^{68}Ga, and ^{64}Cu phantom measurements using a digital Biograph Vision PET/CT. *EJNMMI Phys.* 2022;9:58.
20. Ocak M, Helbok A, Rangger C, et al. Comparison of biological stability and metabolism of CCK2 receptor targeting peptides, a collaborative project under COST BM0607. *Eur J Nucl Med Mol Imaging.* 2011;38:1426–1435.
21. Klingler M, Summer D, Rangger C, et al. DOTA-MGS5, a new cholecystokinin-2 receptor-targeting peptide analog with an optimized targeting profile for theranostic use. *J Nucl Med.* 2019;60:1010–1016.
22. Von Guggenberg E, Uprimny C, Klinger M, et al. Preliminary clinical experience with cholecystokinin-2 receptor PET/CT using the ^{68}Ga-labeled minigastrin analog DOTA-MGS5 in patients with medullary thyroid cancer. *J Nucl Med.* 2023;64:859–862.
23. Holzleitner N, Gunther T, Daoud-Gadieh A, Lapa C, Wester HJ. Investigation of the structure-activity relationship at the N-terminal part of minigastrin analogs. *EJNMMI Res.* 2023;13:65.
24. Khandare J, Minko T. Polymer–drug conjugates: progress in polymeric prodrugs. *Prog Polym Sci.* 2006;31:359–397.
25. Good S, Walter MA, Waser B, et al. Macrocyclic chelator-coupled gastrin-based radiopharmaceuticals for targeting of gastrin receptor-expressing tumours. *Eur J Nucl Med Mol Imaging.* 2008;35:1868–1877.
26. Günther T, Deiser S, Felber V, Beck R, Wester HJ. Substitution of L-tryptophan by a-methyl-L-tryptophan in ^{177}Lu-RM2 results in ^{177}Lu-AMTG, a high-affinity gastrin-releasing peptide receptor ligand with improved in vivo stability. *J Nucl Med.* 2022;63:1364–1370.
27. Holzleitner N, Günther T, Beck R, Lapa C, Wester H-J. Introduction of a SiFA moiety into the D-glutamate chain of DOTA-PP-F11N results in radiohybrid-based CCK-2R-targeted compounds with improved pharmacokinetics in vivo. *Pharmaceuticals (Basel).* 2022;15:1467.
28. Valko K, Nunhuck S, Bevan C, Abraham MH, Reynolds DP. Fast gradient HPLC method to determine compounds binding to human serum albumin. Relationships with octanol/water and immobilized artificial membrane lipophilicity. *J Pharm Sci.* 2003;92:2236–2248.
29. Yamazaki K, Kanaoka M. Computational prediction of the plasma protein-binding percent of diverse pharmaceutical compounds. *J Pharm Sci.* 2004;93:1480–1494.
30. Günther T, Holzleitner N, Di Carlo D, Urtz-Urban N, Lapa C, Wester H-J. Development of the first ^{18}F-labeled radiohybrid-based minigastrin derivative with high target affinity and tumor accumulation by substitution of the chelating moiety. *Pharmaceutics.* 2023;15:826.

Supplemental Data

General information

Analytical and preparative reversed-phase high performance liquid chromatography (RP-HPLC) were performed using Shimadzu gradient systems (Shimadzu Deutschland GmbH, Neufahrn, Germany), each equipped with an SPD-20A UV/Vis detector (220 nm, 254 nm). Different gradients of MeCN (0.1% TFA, 2 or 5% H_2O for analytical or preparative application, respectively) in H_2O (0.1% TFA) were used as eluents for all RP-HPLC operations.

For analytical measurements, a MultoKrom 100-5 C18 (150 mm x 4.6 mm) column (CS Chromatographie Service GmbH, Langerwehe, Germany) was used at a flow rate of 1 mL/min. Both, specific gradients and the corresponding retention times t_R as well as the capacity factor *K*' are cited in the text.

Preparative RP-HPLC purification was performed using a MultoKrom 100-5 C18 (250 mm x 20 mm) column (CS Chromatographie GmbH, Langerwehe, Germany) at a constant flow rate of 10 mL/min.

Lyophilization was accomplished using an Alpha 1-2 LDplus lyophilizer (Martin Christ Gefriertrocknungsanlagen GmbH, Osterode am Harz, Deutschland) combined with a RZ-2 vacuum pump (Vacuubrand GmbH & Co KG, Olching, Germany).

Analytical and preparative radio RP-HPLC was performed using a MultoKrom 100-5 C18 (5 µm, 125×4.6 mm) column (CS Chromatographie GmbH, Langerwehe, Germany). A HERM LB 500 NaI scintillation detector (Berthold Technologies, Bad Wildbad, Germany) was connected to the outlet of the UV photometer for the detection of radioactivity.

Radioactive samples were measured by a WIZARD$^{2®}$ 2480 Automatic γ-Counter (Perkin Elmer Inc., Waltham, MA, USA).

Analytical data of $^{nat/64}$Cu-labeled minigastrin analogs

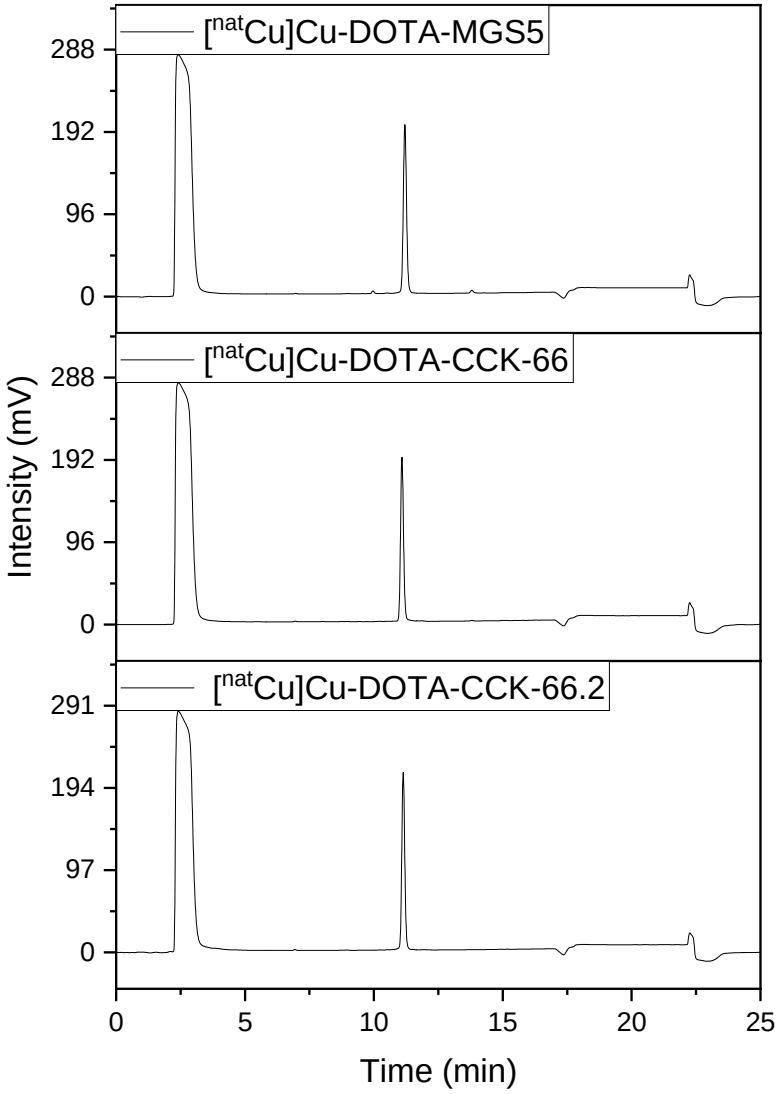

Supplemental Figure 1. Exemplary chromatograms for [^{nat}Cu]Cu-DOTA-MGS5, [^{nat}Cu]Cu-DOTA-CCK-66 and [^{nat}Cu]Cu-DOTA-CCK-66.2, as analyzed by analytical RP-HPLC (10→70% MeCN in H_2O + 0.1% TFA in 15 min).

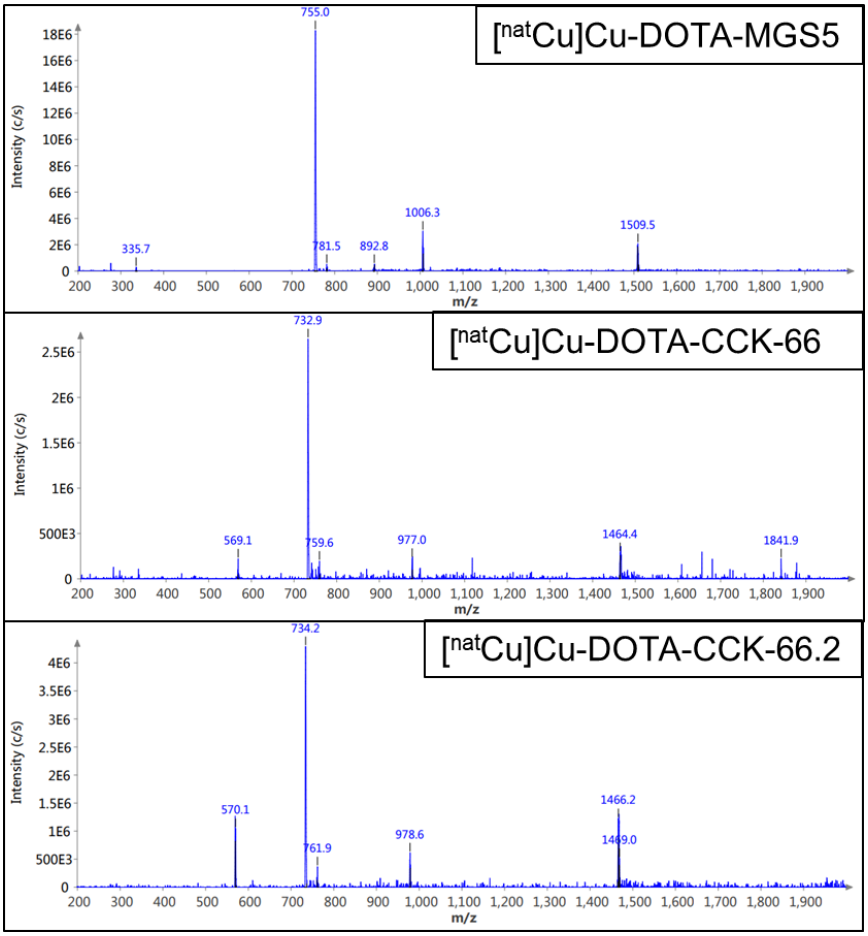

Supplemental Figure 2. Mass spectra of [^{nat}Cu]Cu-DOTA-MGS5, [^{nat}Cu]Cu-DOTA-CCK-66 and [^{nat}Cu]Cu-DOTA-CCK-66.2.

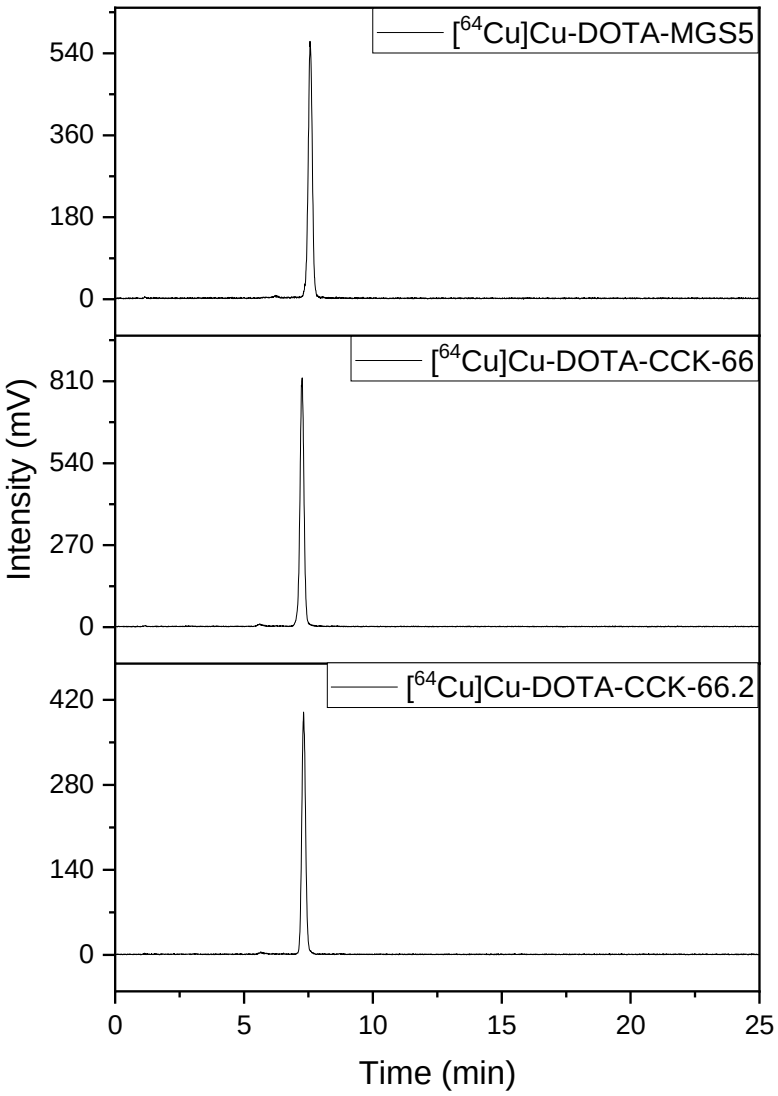

Supplemental Figure 3. Exemplary chromatograms for [^{64}Cu]Cu-DOTA-MGS5, [^{64}Cu]Cu-DOTA-CCK-66 and [^{64}Cu]Cu-DOTA-CCK-66.2, as analyzed by analytical radio-RP-HPLC (30→60% MeCN in H_2O + 0.1% TFA in 15 min).

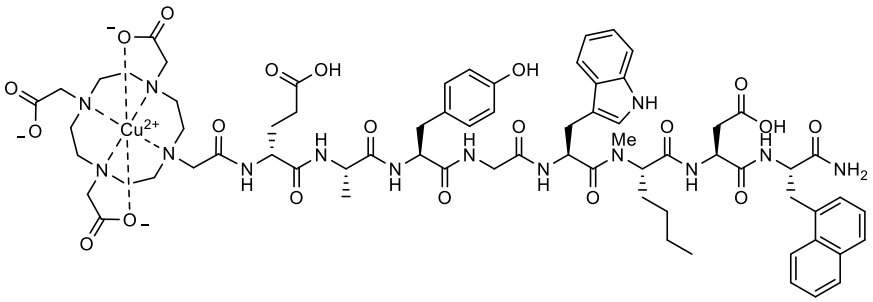

[^{mat}Cu]Cu-DOTA-MGS5. RP-HPLC (10→70% MeCN in H_2O with 0.1% TFA, 15 min, λ = 220 nm): t_R = 11.2 min, *K*' = 5.64; MS (ESI, positive): m/z calculated for $C_{70}H_{90}CuN_{14}O_{20}$: 1509.6, found: m/z = 1509.5 $[M+H]^+$, 755.0 $[M+2H]^{2+}$.

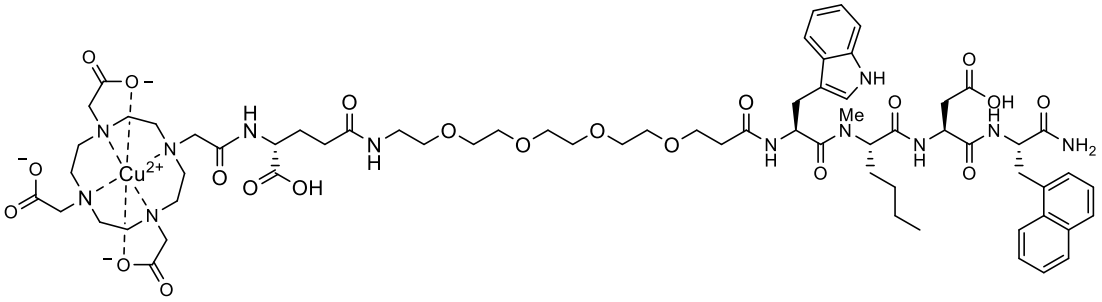

[^{mat}Cu]Cu-DOTA-CCK-66. RP-HPLC (10→70% MeCN in H_2O with 0.1% TFA, 15 min, λ = 220 nm): t_R = 11.1 min, *K*' = 5.58; MS (ESI, positive): m/z calculated for $C_{67}H_{94}CuN_{12}O_{21}$: 1465.0, found: m/z = 1464.4 $[M+H]^+$, 732.9 $[M+2H]^{2+}$.

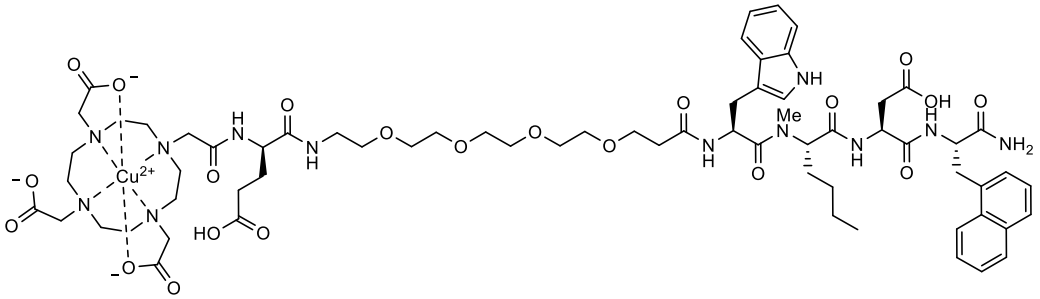

[^{mat}Cu]Cu-DOTA-CCK-66.2. RP-HPLC (10→70% MeCN in H_2O with 0.1% TFA, 15 min, λ = 220 nm): t_R = 11.1 min, *K*' = 5.58; MS (ESI, positive): m/z calculated for $C_{67}H_{94}CuN_{12}O_{21}$: 1465.0, found: m/z = 1466.2 $[M+H]^+$, 734.2 $[M+2H]^{2+}$.

Analytical data of $^{nat/67}$Ga-labeled minigastrin analogs

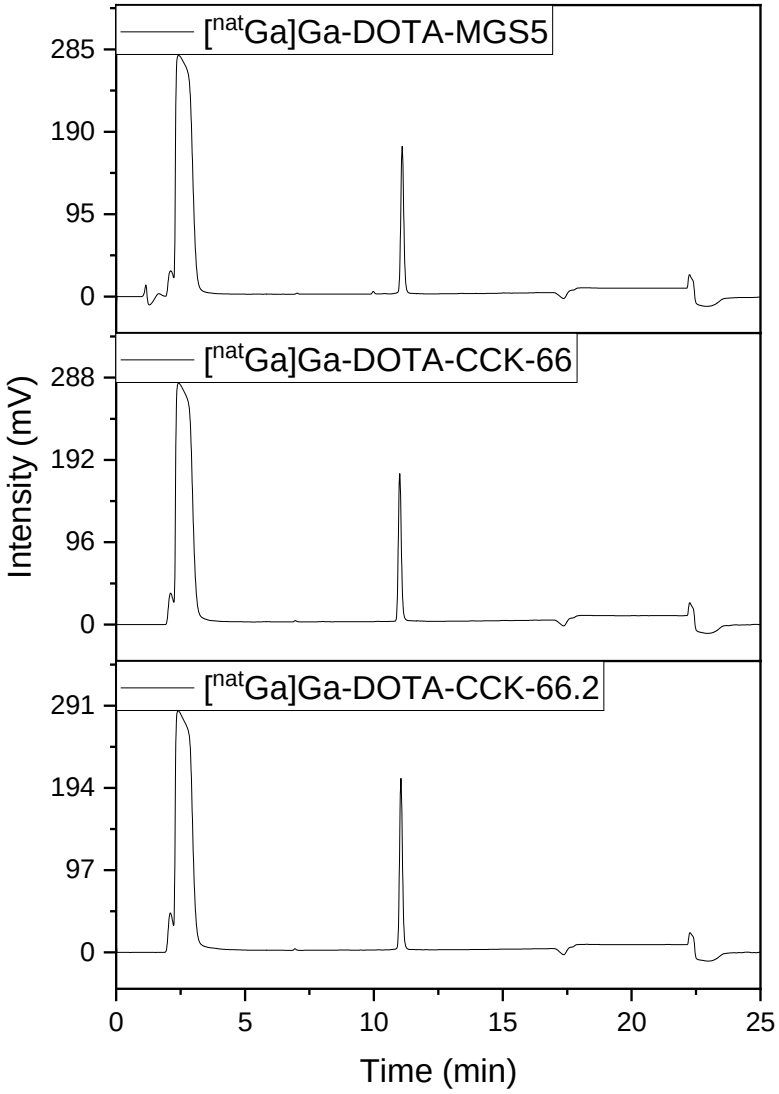

Supplemental Figure 4. Exemplary chromatograms for [^{nat}Ga]Ga-DOTA-MGS5, [^{nat}Ga]Ga-DOTA-CCK-66 and [^{nat}Ga]Ga-DOTA-CCK-66.2, as analyzed by analytical RP-HPLC (10→70% MeCN in H_2O + 0.1% TFA in 15 min).

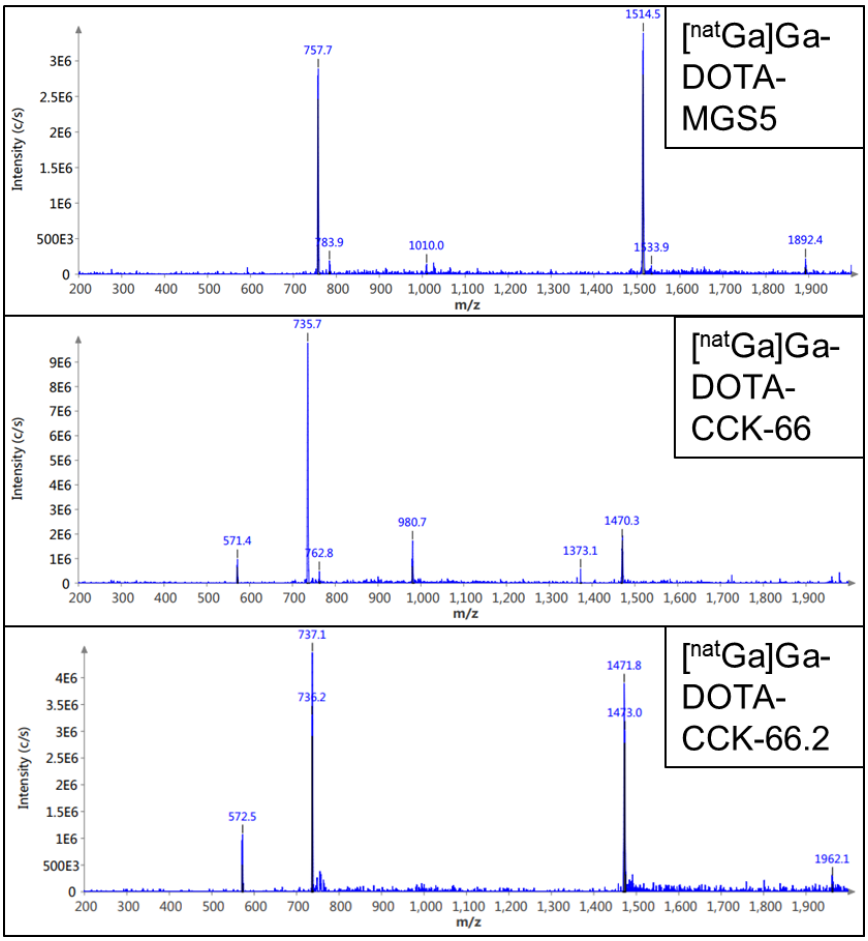

Supplemental Figure 5. Mass spectra of [^{nat}Ga]Ga-DOTA-MGS5, [^{nat}Ga]Ga-DOTA-CCK-66 and [^{nat}Ga]Ga-DOTA-CCK-66.2.

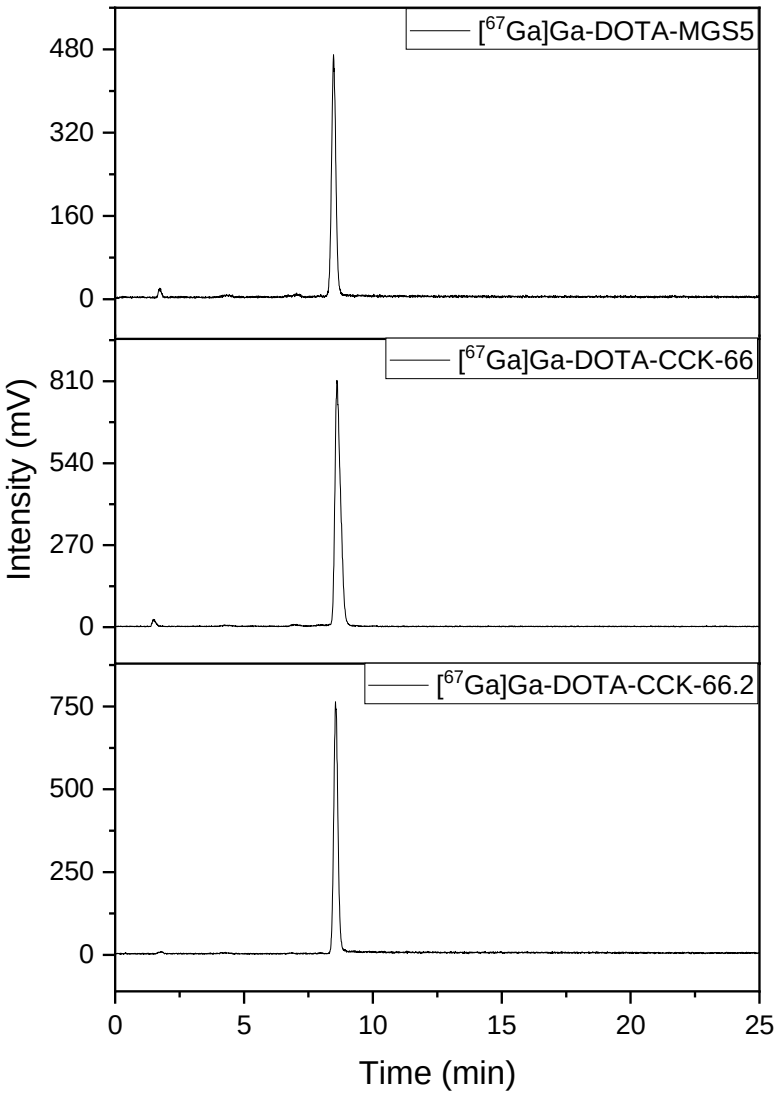

Supplemental Figure 6. Exemplary chromatograms for [^{67}Ga]Ga-DOTA-MGS5, [^{67}Ga]Ga-DOTA-CCK-66 and [^{67}Ga]Ga-DOTA-CCK-66.2, as analyzed by analytical radio-RP-HPLC (30→60% MeCN in H_2O + 0.1% TFA in 15 min).

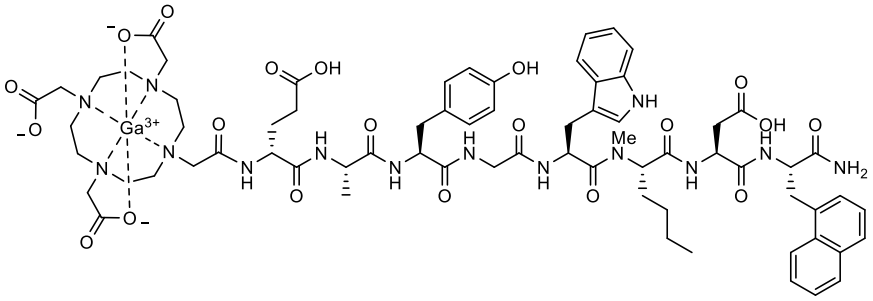

[^{mat}Ga]Ga-DOTA-MGS5. RP-HPLC (10→70% MeCN in H_2O with 0.1% TFA, 15 min, λ = 220 nm): t_R = 11.1 min, *K*' = 5.58; MS (ESI, positive): m/z calculated for $C_{70}H_{90}GaN_{14}O_{20}$: 1516.3, found: m/z = 1514.5 $[M+H]^+$, 757.7 $[M+2H]^{2+}$.

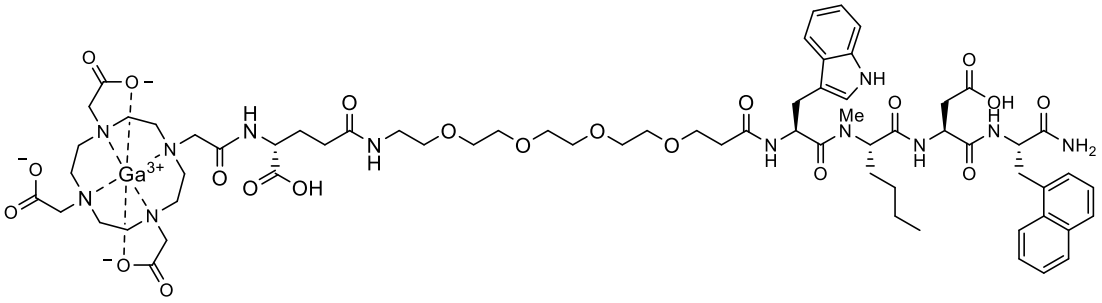

[^{mat}Ga]Ga-DOTA-CCK-66. RP-HPLC (10→70% MeCN in H_2O with 0.1% TFA, 15 min, λ = 220 nm): t_R = 11.0 min, *K*' = 5.52; MS (ESI, positive): m/z calculated for $C_{67}H_{94}GaN_{12}O_{21}$: 1472.3, found: m/z = 1470.3 $[M+H]^+$, 735.7 $[M+2H]^{2+}$.

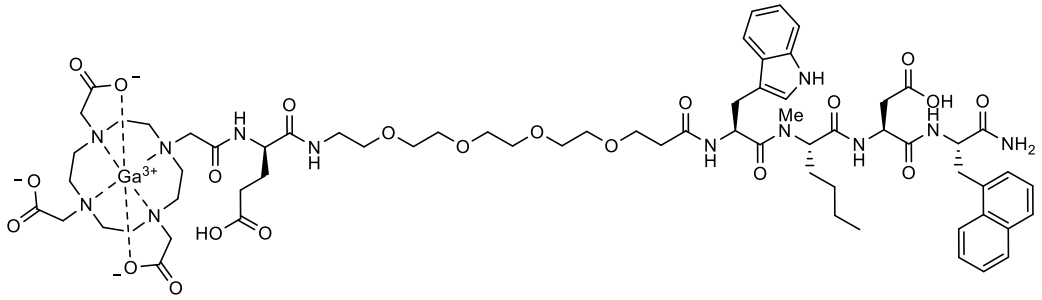

[^{mat}Ga]Ga-DOTA-CCK-66.2. RP-HPLC (10→70% MeCN in H_2O with 0.1% TFA, 15 min, λ = 220 nm): t_R = 11.0 min, *K*' = 5.52; MS (ESI, positive): m/z calculated for $C_{67}H_{94}GaN_{12}O_{21}$: 1472.3, found: m/z = 1471.8 $[M+H]^+$, 737.1 $[M+2H]^{2+}$.

Analytical data of $^{nat/177}$Lu-labeled minigastrin analogs

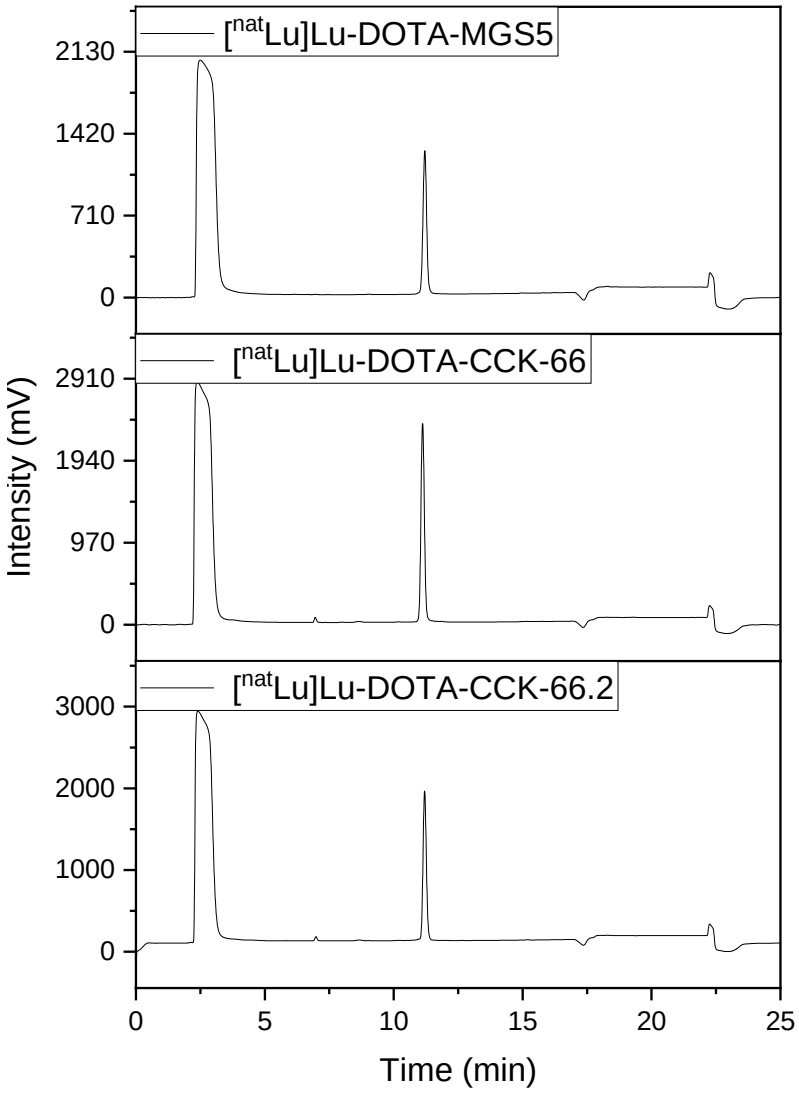

Supplemental Figure 7. Exemplary chromatograms for [^{nat}Lu]Lu-DOTA-MGS5, [^{nat}Lu]Lu-DOTA-CCK-66 and [^{nat}Lu]Lu-DOTA-CCK-66.2, as analyzed by analytical RP-HPLC (10→70% MeCN in H_2O + 0.1% TFA in 15 min).

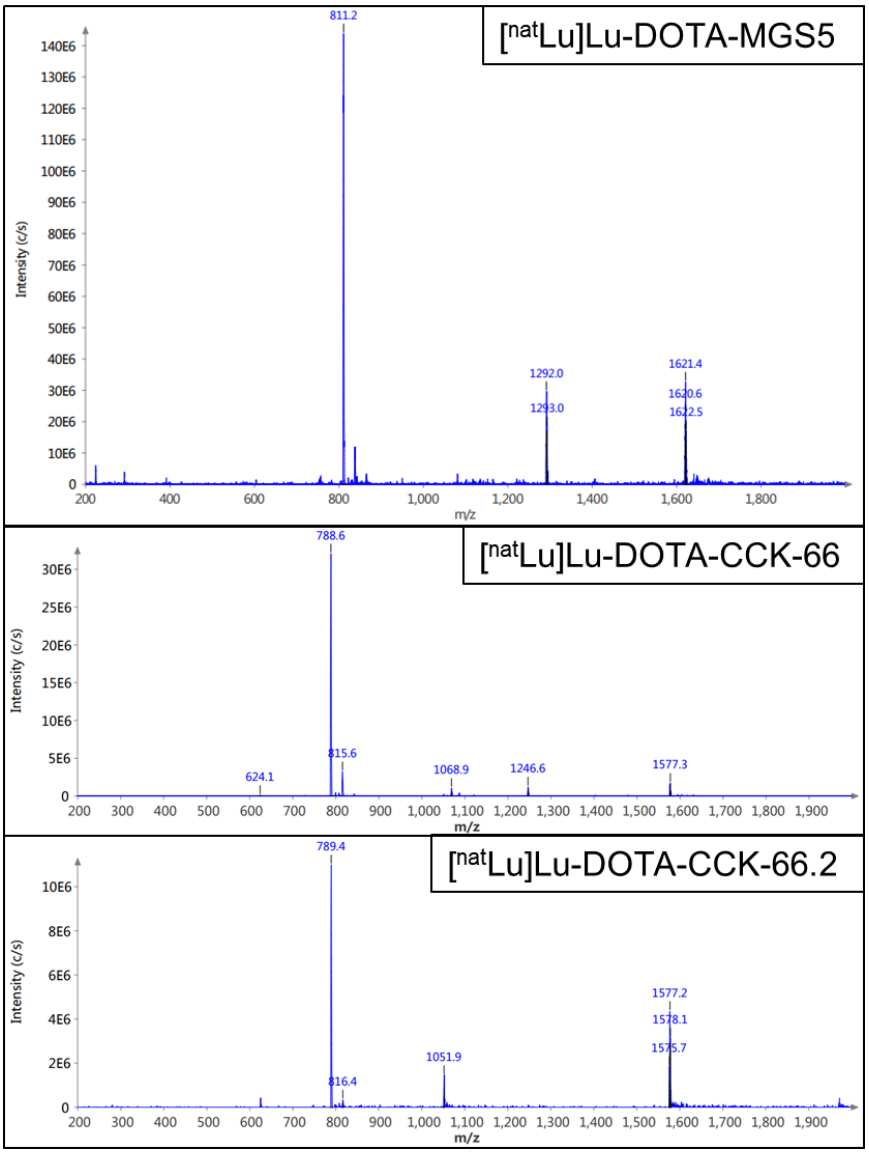

Supplemental Figure 8. Mass spectra of [natLu]Lu-DOTA-MGS5, [natLu]Lu-DOTA-CCK-66 and [natLu]Lu-DOTA-CCK-66.2.

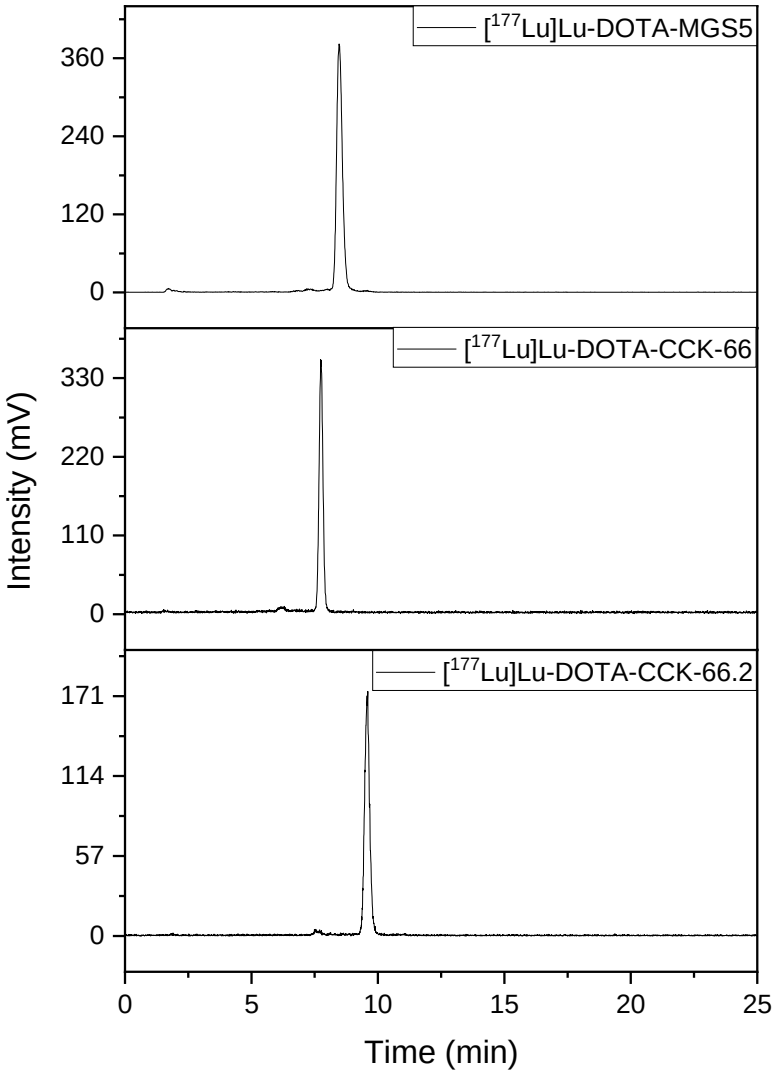

Supplemental Figure 9. Exemplary chromatograms for [^{177}Lu]Lu-DOTA-MGS5, [^{177}Lu]Lu-DOTA-CCK-66 and [^{177}Lu]Lu-DOTA-CCK-66.2, as analyzed by analytical radio-RP-HPLC (30→60% MeCN in H_2O + 0.1% TFA in 15 min).

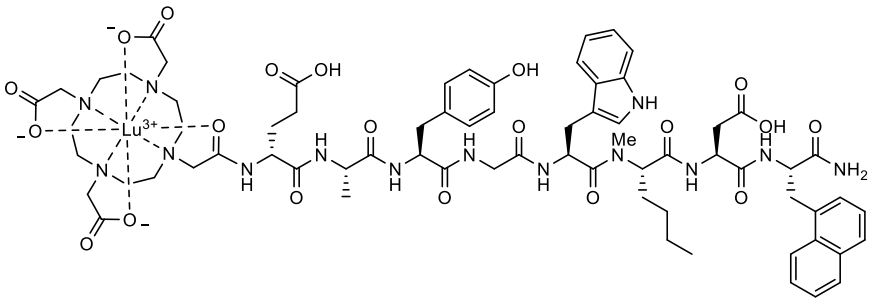

[^{mat}Lu]Lu-DOTA-MGS5. RP-HPLC (10→70% MeCN in H_2O with 0.1% TFA, 15 min, λ = 220 nm): t_R = 11.1 min, *K*' = 5.58; MS (ESI, positive): m/z calculated for $C_{70}H_{90}LuN_{14}O_{20}$: 1621.5, found: m/z = 1621.4 $[M+H]^+$,811.2 $[M+2H]^{2+}$.

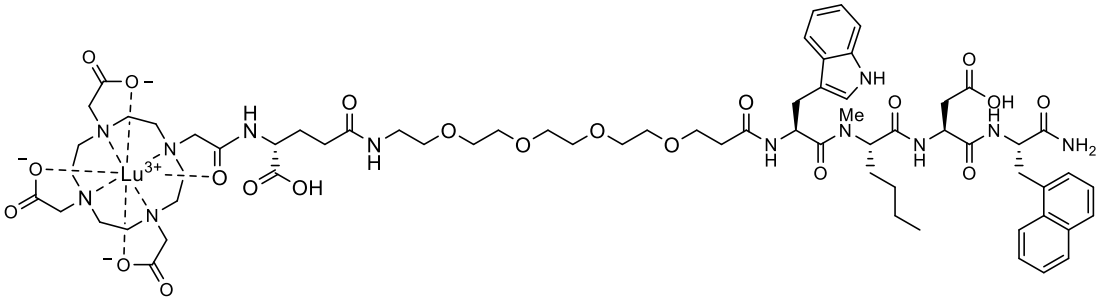

[^{mat}Lu]Lu-DOTA-CCK-66. RP-HPLC (10→70% MeCN in H_2O with 0.1% TFA, 15 min, λ = 220 nm): t_R = 11.1 min, *K*' = 5.58; MS (ESI, positive): m/z calculated for $C_{67}H_{94}LuN_{12}O_{21}$: 1577.5, found: m/z = 1577.3 $[M+H]^+$, 788.6 $[M+2H]^{2+}$.

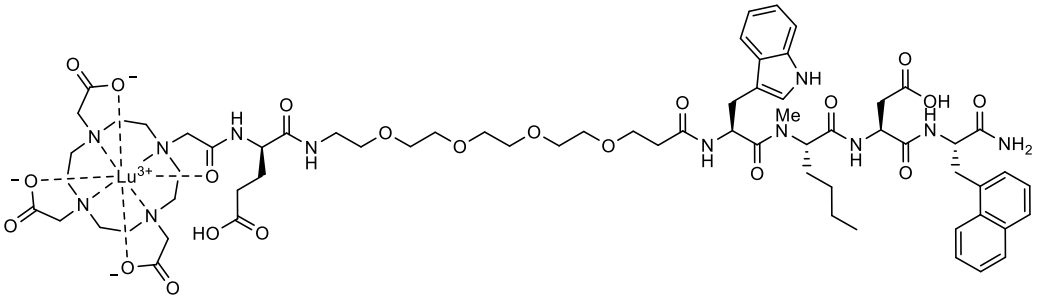

[^{mat}Lu]Lu-DOTA-CCK-66.2. RP-HPLC (10→70% MeCN in H_2O with 0.1% TFA, 15 min, λ = 220 nm): t_R = 11.2 min, *K*' = 5.64; MS (ESI, positive): m/z calculated for $C_{67}H_{94}LuN_{12}O_{21}$: 1577.5, found: m/z = 1577.2 $[M+H]^+$, 789.4 $[M+2H]^{2+}$.

Labeling Procedures

^{nat}Cu-Labeling: The peptide precursors were complexed using a solution of $Cu(OAc)_2$ (24 µL, 10 mM, 3.0 eq.), peptide precursor (80 µL, 1 mM) and Tracepur® H_2O (694 µL) at 80°C for 30 min. Confirmation of peptide integrity was performed via RP-HPLC and ESI-MS.

^{64}Cu-Labeling: A solution of labeling precursor (1 µL, 1 nmol, 1 mM in DMSO), NaOAc buffer (10 µL, 1 M, *pH* = 5.5) and [^{64}Cu]$CuCl_2$ (5-20 MBq, 925 MBq/mL, *DSD Pharma*, Purkersdorf, Austria) was heated to 80°C for 10 min. After the reaction solution was cooled down, sodium ascorbate (10 µL, 1 M) was added. Subsequently, the radiochemical purity was determined using radio-RP-HPLC and radio-TLC (instant thin layer chromatography paper impregnated with silica gel (iTLC-SG), Agilent Technologies Inc., Folsom, United States; sodium citrate×1.5 H_2O (0.1 M)).

^{nat}Ga-Labeling: Complexation of the CCK-2R ligands was accomplished by stirring a solution of [^{nat}Ga]$Ga(NO_3)_3$ (2.5 eq., 10 mM), peptide precursor (1 eq., 1 mM) and Tracepur® H_2O at 70°C for 30 min. Confirmation of peptide integrity was performed via RP-HPLC and ESI-MS.

^{67}Ga-Labeling: To a solution of labeling precursor (1 µL, 1 nmol, 1 mM in DMSO) and 4-(2-hydroxyethyl)-1-piperazineethanesulfonic acid-buffer (2.5 M HEPES, 7 µL), [^{67}Ga]$GaCl_3$ (10-40 MBq, Curium, Petten, The Netherlands) was added and the reaction mixture was heated to 90°C for 15 min. Radiochemical purity was determined using radio-RP-HPLC and radio-TLC.

^{nat}Lu-Labeling: Quantitative ^{nat}Lu-labeling was completed by stirring a solution of [^{nat}Lu]$LuCl_3$ (2.5 eq., 20 mM), peptide precursor (1 eq., 1 mM in DMSO) and Tracepur® H_2O at 90°C for 15 min. Confirmation of peptide integrity was performed via RP-HPLC and ESI-MS.

^{177}Lu-Labeling: Radiolabeling of the peptide precursor (1 nmol) was performed at 90°C for 15 min in a NaOAc-buffered (1 M, *pH* = 5.5) hydrochloric acid (0.04 M) solution using 10-50 MBq of [^{177}Lu]$LuCl_3$ (0.04 M in HCl). Thereafter, sodium ascorbate (1 M in H_2O) was added and radiochemical purity was determined via radio-RP-HPLC and radio-TLC.

In vitro experiments

Cell culture

CCK-2R expressing rat pancreatic cancer cells AR42J (CLS GmbH, Eppelheim, Germany) were cultivated in monolayers in CELLSTAR® cell culture flasks acquired from Greiner Bio-One GmbH (Frickenhausen, Germany) at 37℃ in a humidified atmosphere (5% CO_2) using a HERAcell 150i-Incubator (Thermo Fisher Scientific Inc., Waltham, United States). As nutrient medium RPMI 1640 medium, supplemented with 5 mM L-Gln 5 mL non-essential amino acids (100×) and 10% FCS, was used. Furthermore, a Dulbecco's PBS solution with 0.1% EDTA (*v/v*) was applied to detach the cells for cell passaging. The detached cells were counted using a Neubauer hemocytometer (Paul Marienfeld, Lauda-Königshofen, Germany). In addition, all operations under sterile conditions were accomplished using a MSC-Advantage safety workbench (Thermo Fisher Scientific Inc., Waltham, United States).

Determination of IC_{50}

AR42J cells (2.0×10^5 cells/well) were seeded into 24-well plates 24 ± 2 h prior to testing, using 1 mL of nutrient medium (RPMI 1640, 5 mM L-Gln, 5 mL non-essential amino acids (100×), 10% FCS). Cells were incubated at 37℃ in a humidified atmosphere (5% CO_2).

After removal of the medium, each well was washed with 500 µL PBS. For the cell-based assay, 200 µL of nutrient medium (+5% BSA), [^{177}Lu]Lu-DOTA-PP-F11N (25 µL, 0.3 pmol) as a radiolabeled reference and 25 µL of the peptide of interest in increasing concentrations (10^{-10} to 10^{-4} M) in triplicate were added to the cells. Thereafter, the assay was incubated for 3 h at 37℃ and thereafter, the supernatant was collected. The cells were washed with 300 µL PBS and the collected supernatant fractions were unified. After lysis of the cells with NaOH (300 µL, 1 N) for 15 min, the respective wells were washed with NaOH (300 µL, 1 N) and both fractions were unified. The radioactivity of both, the supernatant and the lysed fractions was quantified using a γ-counter (PerkinElmer Inc., Waltham, United States). The obtained data were evaluated *via* the

GraphPad PRISM software (GraphPad Software Inc., La Jolla, United States), which calculates the half-maximal inhibitory concentration (IC_{50}) of the peptides.

Lipophilicity studies

Lipophilicity (expressed as octanol-phosphate-buffered saline solution (PBS, *pH* = 7.4) distribution coefficient, log$D_{7.4}$) was determined via dissolving the ^{177}Lu-labelled peptide (~1 MBq) in a mixture (1/1, *v*/*v*) of n-octanol and PBS. The suspension was vortexed in a reaction vial (1.5 mL) for 3 min at room temperature and the vial was centrifuged at 9000 rpm for 5 min (Biofuge 15, Heraus Sepatech GmbH, Osterode, Germany). 200 µL aliquots of both layers were measured separately in a γ-counter (Perkin Elmer, Waltham, MA, USA). The experiment was repeated at least five times.

Human serum albumin binding

Human serum albumin (HSA) binding of the minigastrin derivatives was determined using a Chiralpak HSA column (50×3 mm, 5 µm, H13H-2433, Daicel, Tokyo, Japan) at a constant flow rate of 0.5 mL/min at RT. Therefore, an aq. solution of NH_4OAc (*pH* = 6.9, 50 mM) as mobile phase A and isopropanol as mobile phase B were freshly prepared. In order to calibrate the column prior to the experiments, the retention times of nine reference substances with a HSA binding in the range of 13 to 99% were determined using a gradient of 100% A (0 to 3 min), followed by 80% A (3 to 40 min). Furthermore, all substances tested were dissolved in a mixture (1/1, v/v) of A and B reaching a final concentration of 0.5 mg/mL. The HSA binding of all CCK-2R ligands tested was determined using the same gradient as for the calibration probes. The non-linear regression of the calibration experiments and the minigastrin derivatives (**Supplemental Figure 10**) was established using the OriginPro 2016G software (Northampton, United States).

reference	t_R (min)	log(t_R)	lit. HSA (%)	log K HSA
benzyl alcohol	2.32	0.36	13.2	−0.82
aniline	2.49	0.40	14.1	−0.79
phenol	2.93	0.47	20.7	−0.59
benzoic acid	3.32	0.52	34.3	−0.29
carbamazepine	3.87	0.59	75.0	0.46
4-nitrophenol	4.62	0.66	77.7	0.52
estradiol	6.93	0.84	94.8	1.19
probenecid	6.60	0.82	95.0	1.20
glibenclamide	23.2	1.37	99.0	1.69

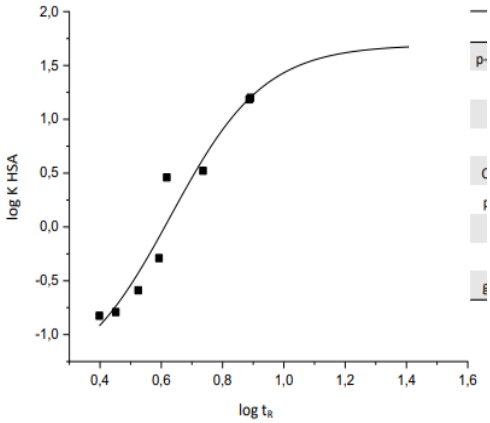

Supplemental Figure 10. Example of a sigmoidal plot, showing the correlation between HSA binding of selected reference substances and their retention time (t_R) on a Chiralpak HSA column. HSA binding values of the reference substances were previously published in the literature (lit. HSA (%)) and the respective logarithmic value of the affinity constant (log K HSA) was calculated. Log(t_R): logarithmic value of experimentally determined retention time

In vitro stability studies in human serum

The ^{177}Lu-labeled CCK-2R ligands (1 nmol, ~5 MBq) were incubated at 37°C for 72 h in human serum (200 µL). After incubation ice-cold EtOH (125 µL) and MeCN (375 µL) were added and the suspension was centrifuged for 5 min at 5000 rpm. Then, the supernatant was transferred into new vials and centrifuged for another 5 min at 5000 rpm. After separating the precipitate from the solution, the stability of the ligands was determined *via* RP-HPLC chromatography (10→30% MeCN in H_2O + 0.1% TFA in 5 min, 30→60% MeCN in H_2O + 0.1% TFA in 15 min).

In vivo experiments

All animal experiments were carried out in accordance with general animal welfare regulations in Germany (German animal protection act, in the edition of the announcement, dated 18 May 2006, as amended by Article 280 of 19 June 2020, approval no. ROB-55.2-1-2532.Vet_02-18-109 by the General Administration of Upper Bavaria) and the institutional guidelines for the care and use of animals. Exclusion criteria for animals from an experiment were either weight loss of more than 20%, a tumor size of more than 1,500 mm^3, ulceration of the tumor, respiratory distress or a change of behavior. None of these criteria applied to any animal from the experiment. Neither randomization nor blinding was applied in the allocation of the experiments. Health status of the animals is specific pathogen free according to Federation of European Laboratory Animal Science Associations recommendation.

Supplemental Table 1. Affinity (*n*=3) and lipophilicity (*n*=6) data of the compounds evaluated. Affinity data were determined on AR42J cells (2.0 x 10^5 cells/well) using [^{177}Lu]Lu-DOTA-PP-F11N (0.3 pmol/well) as radiolabeled reference (3 h, 37°C, RPMI 1640, 5 mM L-Gln, 5 mL non-essential amino acids (100x), 10% FCS + 5% BSA (*v*/*v*)).

	[$^{nat/64}$Cu]Cu-labeled		[$^{nat/67}$Ga]Ga-labeled		[$^{nat/177}$Lu]Lu-labeled	
Peptide	IC_{50} (nM)	log$D_{7.4}$	IC_{50} (nM)	log$D_{7.4}$	IC_{50} (nM)	log$D_{7.4}$
DOTA-MGS5	3.85 ± 0.96	−2.81 ± 0.01	3.56 ± 0.43	−2.44 ± 0.12	5.19 ± 0.79	−2.21 ± 0.08
DOTA-CCK-66	4.21 ± 0.45	−2.64 ± 0.04	4.97 ± 0.53	−3.01 ± 0.07	5.12 ± 0.51	−2.60 ± 0.07
DOTA-CCK-66.2	5.76 ± 0.21	−2.84 ± 0.08	6.04 ± 1.01	−2.55 ± 0.04	4.84 ± 0.94	−2.69 ± 0.09

Supplemental Table 2. HSA binding of the compounds evaluated, determined by high performance affinity chromatography (HPAC).

	HSA binding (%)		
Peptide	[^{nat}Lu]Lu	[^{nat}Ga]Ga	[^{nat}Cu]Cu
DOTA-MGS5	91.9	82.0	87.6
[^{177}Lu]Lu-DOTA-CCK-66	69.1	53.8	61.5
[^{177}Lu]Lu-DOTA-CCK-66.2	72.7	54.2	61.1

Supplemental Table 3. Amount of intact peptide of the compounds evaluated, determined in human serum via incubation at 37°C for 72 h, as analyzed by analytical radio-RP-HPLC (10→30% MeCN in H_2O + 0.1% TFA in 5 min, 30→60% MeCN in H_2O + 0.1% TFA in 15 min).

Peptide	**Intact peptide (%)**
[^{177}Lu]Lu-DOTA-MGS5	93.1 ± 0.8
[^{177}Lu]Lu-DOTA-CCK-66	90.8 ± 0.9
[^{177}Lu]Lu-DOTA-CCK-66.2	87.3 ± 0.1

Supplemental Table 4. Biodistribution data of [^{67}Ga]Ga-DOTA-CCK-66, [^{177}Lu]Lu-DOTA-CCK-66 and [^{177}Lu]Lu-DOTA-MGS5 in selected organs at 1 or 24 h after injection in AR42J tumor-bearing CB17-SCID mice (100 pmol each). Data are expressed as %ID/g, mean±SD (*n*=4). Biodistribution data of [^{67}Ga]Ga-DOTA-CCK-66 (100 pmol, 1 h after injection) and [^{177}Lu]Lu-DOTA-CCK-66 (100 pmol, 24 h after injection) co-injected either with [^{nat}Ga]Ga-DOTA-MGS5 or [^{nat}Lu]Lu-DOTA-MGS5 in selected organs at 24 h after injection in AR42J tumor-bearing CB17-SCID mice. Data are expressed as %ID/g, mean±SD (*n*=2).

Organ	[^{67}Ga]Ga-DOTA-CCK-66 (1 h after injection)	[^{67}Ga]Ga-DOTA-CCK-66 (1 h after injection) competition studies	[^{177}Lu]Lu-DOTA-CCK-66 (24 h after injection)	[^{177}Lu]Lu-DOTA-CCK-66 (24 h after injection) competition studies	[^{177}Lu]Lu-DOTA-MGS5 (24 h after injection)
Blood	0.61 ± 0.07	0.96 ± 0.07	0.00 ± 0.00	0.01 ± 0.00	0.01 ± 0.00
Heart	0.24 ± 0.03	0.35 ± 0.04	0.02 ± 0.01	0.03 ± 0.00	0.03 ± 0.00
Lung	0.60 ± 0.08	0.79 ± 0.02	0.04 ± 0.02	0.15 ± 0.12	0.03 ± 0.01
Liver	0.31 ± 0.02	0.58 ± 0.04	0.19 ± 0.09	0.28 ± 0.07	0.22 ± 0.01
Spleen	0.25 ± 0.09	0.35 ± 0.02	0.11 ± 0.04	0.38 ± 0.21	0.11 ± 0.02
Pancreas	0.23 ± 0.07	0.21 ± 0.01	0.14 ± 0.03	0.06 ± 0.03	0.09 ± 0.03
Stomach	1.81 ± 0.19	0.31 ± 0.01	1.43 ± 0.51	0.10 ± 0.07	2.53 ± 0.46
Intestine	0.27 ± 0.07	0.49 ± 0.06	0.13 ± 0.04	0.09 ± 0.03	0.15 ± 0.07
Kidney	2.51 ± 0.49	3.41 ± 0.01	1.10 ± 0.14	1.65 ± 0.08	1.32 ± 0.41
Adrenal	0.68 ± 0.44	0.30 ± 0.06	0.03 ± 0.03	0.08 ± 0.01	0.13 ± 0.16
Muscle	0.15 ± 0.05	0.13 ± 0.01	0.00 ± 0.00	0.01 ± 0.00	0.01 ± 0.01
Bone	0.27 ± 0.12	0.17 ± 0.03	0.04 ± 0.03	0.05 ± 0.02	0.06 ± 0.06
Tumor	19.4 ± 3.5	0.96 ± 0.07	8.56 ± 0.00	0.19 ± 0.02	11.0 ± 1.2

Supplemental Table 5. Tumor/background ratios of [^{67}Ga]Ga-DOTA-CCK-66, [^{177}Lu]Lu-DOTA-CCK-66 and [^{177}Lu]Lu-DOTA-MGS5 in selected organs at 1 or 24 h after injection in AR42J tumor-bearing CB17-SCID mice (100 pmol each). Data are expressed as %ID/g, mean ± SD (*n*=4).

Tumor/Background	[^{67}Ga]Ga-DOTA-CCK-66 (1 h after injection)	[^{177}Lu]Lu-DOTA-CCK-66 (24 h after injection)	[^{177}Lu]Lu-DOTA-MGS5 (24 h after injection)
Blood	31.0 ± 6.0	2008 ± 469	1480 ± 329
Heart	82.7 ± 6.1	401 ± 123	436 ± 59
Lung	31.3 ± 7.6	277 ± 134	364 ± 67
Liver	60.1 ± 12.6	53.6 ± 21.7	49.6 ± 2.9
Spleen	103 ± 35	88.8 ± 30.2	105 ± 10
Pancreas	82.4 ± 38.9	64.5 ± 23.8	144 ± 57
Stomach	10.8 ± 1.5	6.72 ± 2.47	4.43 ± 0.68
Intestine	64.4 ± 29.4	73.4 ± 24.2	86.4 ± 23.9
Kidney	7.35 ± 1.85	7.82 ± 0.70	9.35 ± 3.28
Adrenal	58.1 ± 18.6	740 ± 741	247 ± 163
Muscle	162 ± 47.7	10291 ± 13421	1205 ± 568
Bone	85.6 ± 35.1	371 ± 279	315 ± 185

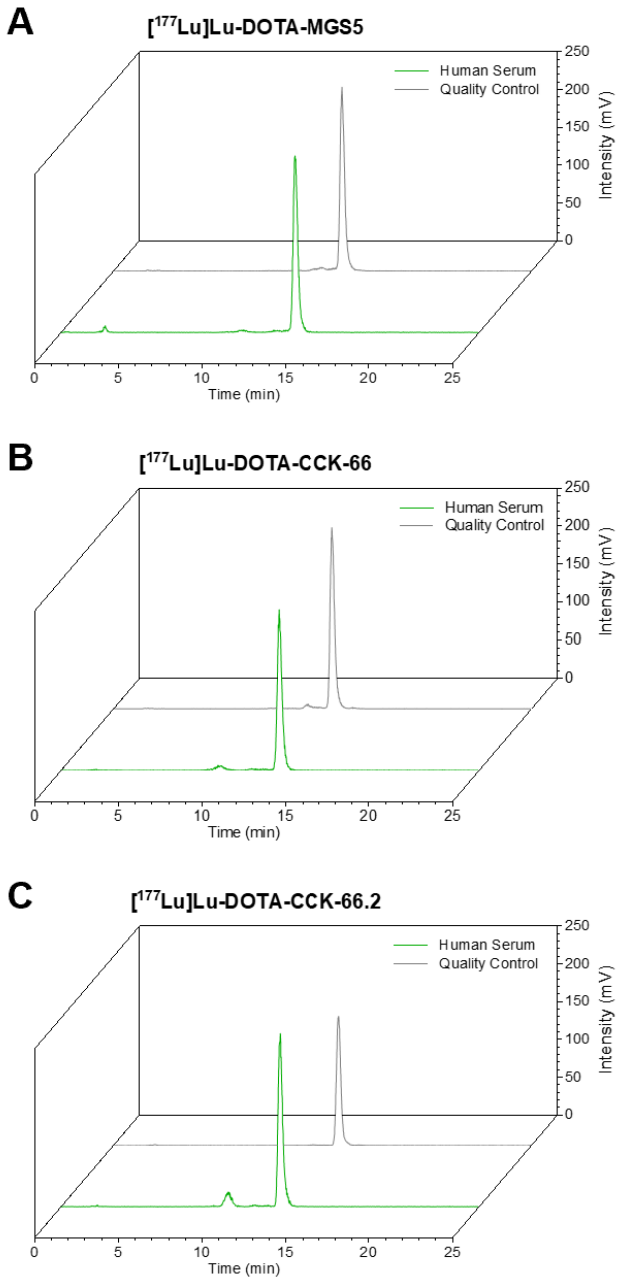

Supplemental Figure 11. In vitro stability of (A) [^{177}Lu]Lu-DOTA-MGS5, (B) [^{177}Lu]Lu-DOTA-CCK-66 and (C) [^{177}Lu]Lu-DOTA-CCK-66.2 in human serum (37° C, 72 h), as analyzed by analytical RP-HPLC (10→30% MeCN in H_2O + 0.1% TFA in 5 min, 30→60% MeCN in H_2O + 0.1% TFA in 15 min). The chromatograms of the respective compounds after incubation in human serum (37° C, 72 h) are depicted in green. Quality controls of the intact compounds are depicted in gray.

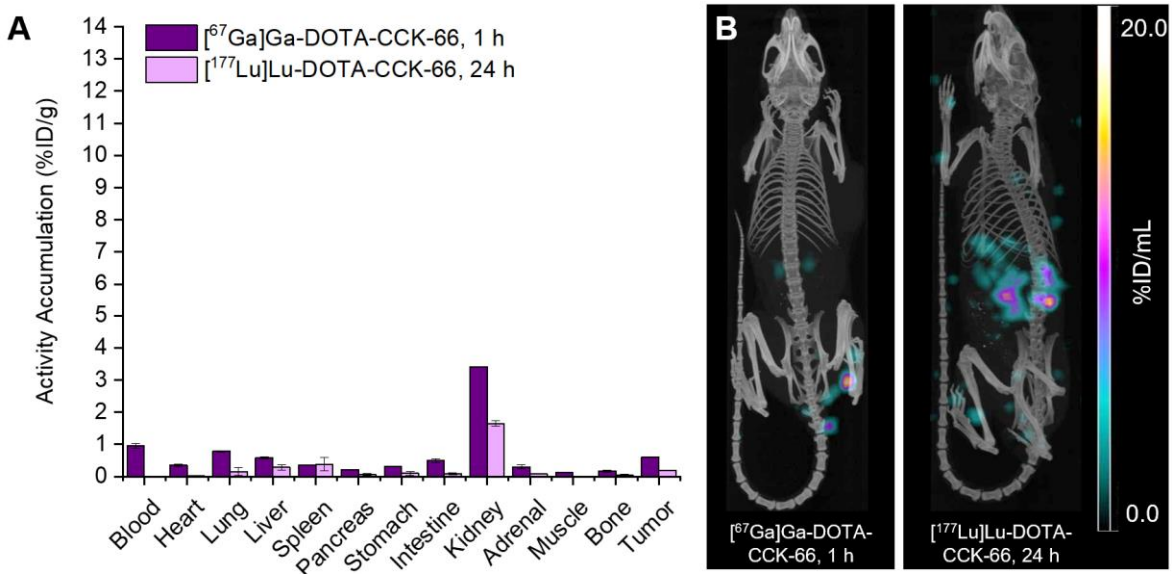

Supplemental Figure 12. (A) Biodistribution and (B) a representative *μ*SPECT/CT image of [^{67}Ga]Ga-DOTA-CCK-66 (100 pmol, 1 h after injection) as well as [^{177}Lu]Lu-DOTA-CCK-66 (100 pmol, 24 h after injection) co-injected either with [^{nat}Ga]Ga-DOTA-MGS5 (40 nmol) or [^{nat}Lu]Lu-DOTA-MGS5 (40 nmol) in selected organs (%ID/g) at 24 h after injection in AR42J tumor-bearing CB17-SCID mice. Data is expressed as mean±SD (*n*=2).

Patient Information

Patient 1. A 64-year-old male patient with familial MEN IIa syndrome. Diagnosis of bilateral phaeochromocytoma and MTC in 1994. Primary treatment for MTC included thyroidectomy and central lymph node dissection. Postoperative TNM-Staging: pT1a (m) pN1 cM0. Lymph node recurrence in 2002 followed by microdissection of the bilateral cervicocentral and cervicolateral lymph node compartments (1 out of 44 lymph nodes affected). Excision of a soft tissue metastasis on the right cervical region in 11/2020. Due to a subsequent increase in calcitonin (110 pg/ml) with a short doubling time (16 months) and repeatedly negative [^{18}F]F-DOPA PET/CT, re-staging with [^{68}Ga]Ga-DOTA-CCK-66 PET/CT was performed in 12/2022.

Patient 2. A 46-year-old female patient with sporadic MTC first diagnosed in 01/2021. Primary therapy included thyroidectomy, resection of the prelaryngeal lymph nodes as well as cercivocentral and cervicolateral lymph node dissection. Postoperative TNM-Staging: pT3a pN1b (20/44) cM0 L0 V0 Pn1 R1. Postoperative [^{18}F]F-DOPA PET/CT could not detect any residual tumor manifestations, so additional [^{18}F]FDG PET/CT was performed in 03/2021. [^{18}F]FDG PET/CT revealed residual tumor tissue in the right thyroid bed and a lymph node metastasis on the left cervical side. In 06/2021, modified radical neck dissection was performed. Histopathologic work-up confirmed 2 lymph node metastases (pN1b (2/19)). Subsequently, the patient underwent external beam radiation of the residual local tumor and the cervical lymphatic regions from 09-10/2021. Follow-up imaging with [^{18}F]FDG PET/CT revealed emergence of new mediastinal lymph node and liver metastases. Due to a rising serum calcitonin level (380 pg/ml) with a short doubling time (5 months), additional re-staging with [^{68}Ga]Ga-DOTA-CCK-66 PET/CT was performed in 03/2023.

2.5 Significant Decrease of Activity Uptake of Radiohybrid-Based Minigastrin Analogs in the Kidneys via Modification of the Charge Distribution Within the Linker Section

This work was submitted to EJNMMI Research and is currently under review.

Article

Significant Decrease of Activity Uptake of Radiohybrid-Based Minigastrin Analogs in the Kidneys via Modification of the Charge Distribution Within the Linker Section

Nadine Holzleitner[1,*], Sebastian Fischer[1], Isabel Maniyankerikalam[1], Roswitha Beck[1], Constantin Lapa[2,3], Hans-Jürgen Wester[1] and Thomas Günther[1,*]

[1] TUM School of Natural Sciences, Department of Chemistry, Chair of Pharmaceutical Radiochemistry, Technical University of Munich, Garching, Germany

[2] Nuclear Medicine, Faculty of Medicine, University of Augsburg, Augsburg, Germany

[3] Bavarian Cancer Research Center (BZKF), Bavaria, Germany

* correspondence: thomas.guenther@tum.de (T.G.) and nadine.holzleitner@tum.de (N.H.)

Abstract: **Background:** We recently introduced radiohybrid (rh)-based minigastrin analogs e.g., DOTA-rhCCK-18 (DOTA-D-Dap(p-SiFA)-(D-γ-Glu)$_8$-Ala-Tyr-Gly-Trp-Nle-Asp-Phe-NH$_2$), that revealed substantially increased activity retention in the tumor. However, one major drawback of these first generation rh-based CCK-2R ligands, is their tremendously elevated activity uptake in the kidneys. Thus, within this study we wanted to reduce kidney accumulation by reduction of negatively charged D-glutamic acid moieties within the linker section via substitution by polyethylene glycol (PEG) linkers of various lengths ((PEG)$_4$ to (PEG)$_{11}$). Furthermore, the influence of differently charged silicon-based fluoride acceptor (SiFA)-moieties (p-SiFA: neutral, SiFA-ipa: negatively charged, and SiFAlin: positively charged) on pharmacokinetic properties of minigastrin analogs were evaluated. **Results:** CCK-2R affinity of most compounds evaluated was found to be in a range of 8-20 nM (by means of IC_{50}), which resulted in slightly increased or comparable IC_{50} values to [^{nat}Lu]Lu-DOTA-rhCCK-18 and [^{nat}Lu]Lu-DOTA-PP-F11N (IC_{50}: 4.7±0.6 and 12.8±2.8 nM), respectively. Ligands containing a SiFA-ipa moiety displayed elevated IC_{50} values. Lipophilicity was noticeably lower for compounds containing a D-γ-glutamate (D-γ-Glu) moiety next to the D-Dap(p-SiFA) unit as compared to their counterparts lacking the additional negative charge. Within this study, combining the most favorable CCK-2R affinity and lipophilicity, [$^{177/nat}$Lu]Lu-DOTA-rhCCK-70 (DOTA-D-Dap(p-SiFA)-D-γ-Glu-(PEG)$_7$-

D-γ-Glu-$(PEG)_3$-Trp-(*N*-Me)Nle-Asp-1-Nal-NH_2; IC_{50}: 12.6±2.0 nM; log$D_{7.4}$: −1.67±0.08) and [$^{177/nat}$Lu]Lu-DOTA-rhCCK-91 (DOTA-D-Dap(SiFAlin)-D-γ-Glu-$(PEG)_4$-D-γ-Glu-$(PEG)_3$-Trp-(*N*-Me)Nle-Asp-1-Nal-NH_2; IC_{50}: 8.6±0.7 nM; log$D_{7.4}$ = −1.66±0.07) were further evaluated *in vivo*. Biodistribution data of both compounds revealed significantly reduced ($p < 0.0001$) activity accumulation in the kidneys compared to [^{177}Lu]Lu-DOTA-rhCCK-18 at 24 h p.i., leading to enhanced tumor-to-kidney ratios despite lower tumor uptake. However, overall tumor-to-background ratios of the novel compounds were lower than those of [^{177}Lu]Lu-DOTA-rhCCK-18. **Conclusion:** We could show that the reduction of negative charges within the linker section of DOTA-rhCCK-18 led to decreased activity levels in the kidneys at 24 h p.i., while maintaining a good tumor uptake. Thus, favorable tumor-to-kidney ratios were accomplished *in vivo*. However, further optimization has to be done in order to improve tumor retention and general pharmacokinetics.

Keywords: cholecystokinin-2 receptor (CCK-2R), cholecystokinin-B receptor (CCK-BR), medullary thyroid carcinoma (MTC), minigastrin, radiohybrid, rhCCK

1. Introduction

Even though medullary thyroid carcinoma (MTC) is a rather rare form of thyroid disease (1), limited 10-year survival rates of less than 40% for patients suffering from locally advanced or progressive disease lead to a growing clinical interest in novel therapeutic approaches (2, 3). Thus, over the past three decades research on peptide-based radiopharmaceuticals targeting the cholecystokinin-2 receptor (CCK-2R), which is overexpressed in over 90% of all MTC patients (4), has been progressing.

Only in 2019, the minigastrin analog DOTA-PP-F11N (DOTA-$(D\text{-}Glu)_6$-Ala-Tyr-Gly-Trp-Nle-Asp-Phe-NH_2), was evaluated ^{177}Lu-labeled in clinical trials as one of the first lead structures for radioligand therapy of MTC (5, 6). However, its moderate metabolic stability and accelerated clearance kinetics limit its therapeutic efficacy (7, 8). One approach to circumvent stability issues *in situ*, is the co-administration of [^{177}Lu]Lu-DOTA-PP-F11N in combination with neutral endopeptidase (NEP)-1 inhibitors, such as sacubitril, which has been evaluated in clinical trials with pending results (NCT03647657), while another theranostic clinical study using [^{177}Lu]Lu-DOTA-PP-F11N (NCT02088645) is currently recruiting (9, 10).

Another approach is stabilization by chemical design, which was done for DOTA-PP-F11N and led to DOTA-MGS5 (DOTA-D-Glu-Ala-Tyr-Gly-Trp-(*N*-Me)Nle-Asp-1-Nal-NH_2), a minigastrin analog comprising 1-Nal instead of Phe and (*N*-Me)Nle instead of Nle, as well as only one D-Glu moiety in the linker section (11). Due to its high CCK-2R affinity accompanied by a favorable biodistribution profile in mice (11), first clinical results of [^{68}Ga]Ga-DOTA-MGS5 looked promising in MTC patients (12, 13). Very

recently, we further modified the DOTA-MGS5 sequence in order to address the Gly-Trp cleavage site, which resulted in DOTA-CCK-66 (DOTA-D-γ-Glu-$(PEG)_3$-Trp-(*N*-Me)Nle-Asp-1-Nal-NH_2), a simplified minigastrin analog displaying higher metabolic stability and thus, improved activity clearance and tumor-to-background ratios in animals, and which has already been successfully translated into the clinic (14, 15).

However, all compounds mentioned above are limited to radiometallation and do not allow for ^{18}F-labeling, lacking the benefits of ^{18}F-based positron emission tomography (^{18}F-PET) (16). Thus, according to the EANM guidelines published in 2020, [^{18}F]F-DOPA, targeting neuroendocrine tumors in general, is still considered the gold standard for MTC imaging (17, 18).

In order to design an ^{18}F-labeled minigastrin analog, we transferred the radiohybrid (rh) concept, which was successfully applied for prostate-specific membrane antigen-targeted compounds, to CCK-2R ligands in a previous study (19), which resulted in DOTA-rhCCK-18 (DOTA-D-Dap(p-SiFA)-$(D\text{-}\gamma\text{-}Glu)_8$-Ala-Tyr-Gly-Trp-Nle-Asp-Phe-NH_2), a rh-based minigastrin analog that enables both ^{177}Lu- and ^{18}F-labeling (20). Compared to earlier generations of minigastrin analogs e.g., DOTA-MGS5 and DOTA-PP-F11N, DOTA-rhCCK-18 displayed 2- to 13-fold increased activity levels in the CCK-2R positive tumor at 24 h p.i. However, this was accompanied by substantially increased activity uptake in the kidneys, most likely due to the charge distribution in proximity to the silicon-based fluoride acceptor (SiFA) moiety (20).

Hence, in this study we wanted to reduce kidney uptake of rh-based minigastrin analogs, while maintaining high activity levels in the tumor. Therefore, we substituted the polyglutamate linker section of DOTA-rhCCK-18 by hydrophilic, uncharged PEG linkers of various length (4 to 11) in combination with or without a D-γ-Glu moiety in proximity to the D-Dap(p-SiFA) building block (Figure 1). In addition, we evaluated the influence of negatively and positively charged SiFA moieties on the pharmacokinetic properties of our compounds. On the one hand the SiFAlin moiety (positively charged), which was already used in somatostatin-based compounds (21), and on the other hand 5-(di-*tert*-butylfluorosilyl)isophthalic acid (SiFA-ipa, negatively charged), which was recently developed in our group (Fischer et al., unpublished data). Furthermore, we used the stabilized peptide sequence of DOTA-CCK-66 (*H*-D-γ-Glu-$(PEG)_3$-Trp-(*N*-Me)Nle-Asp-1-Nal-NH_2) for all compounds evaluated.

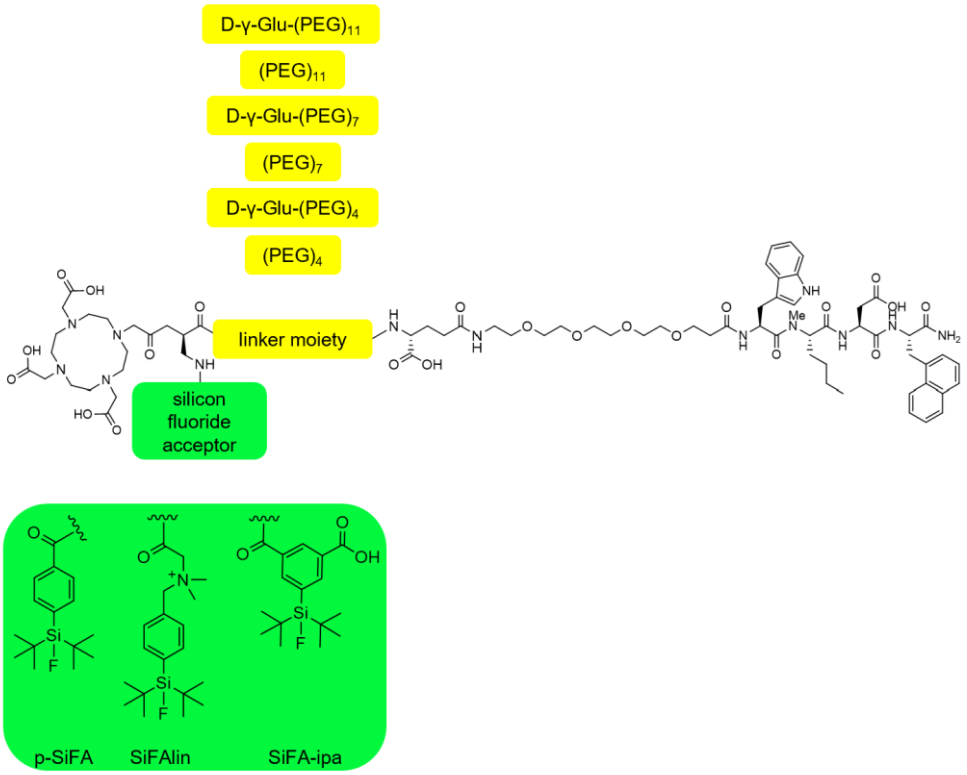

Figure 1. General composition of minigastrin analogs evaluated in this study. Yellow: linker sequences; Green: SiFA moieties.

2. Materials and Methods

Evaluation of peptide identity and integrity is provided in the Supplementary Materials (Figure S1-S12). An expression^{L} CMS mass spectrometer (Advion Ltd., Harlow, UK) was used for characterization of the substances.

2.1. Chemical synthesis and labeling procedures

Synthesis of the compounds was conducted as previously published (7, 20). In brief, peptides were synthesized via standard fluorenylmethoxycarbonyl (Fmoc)-based solid phase peptide synthesis (SPPS) protocols using a *H*-Rink Amide ChemMatrix® resin (35-100 mesh particle size, 0.4-0.6 mmol/g loading, Merck KGaA, Darmstadt, Germany).

(4-(Bromomethyl)phenyl)di-*tert*-butylfluorosilane (SiFA-Br), which was used for generating the SiFAlin building block, was synthesized according to published protocols (22). Synthesis of 4-(di-tert-butylfluorosilyl)benzoic acid (p-SiFA) was completed according to an established protocol (23). Chemical synthesis of the SiFA-ipa moiety is described in the Supplementary Materials (Scheme S1).

Coupling of p-SiFA was conducted in analogy to amino acid couplings to the side chain of a D-2,3-diaminopropionic acid (D-Dap). Conjugation of the SiFA-ipa moiety to the D-Dap side chain was accomplished similarly, yet using a 3-fold excess of SiFA-ipa to prevent dimerization. A 3-fold excess of SiFA-Br dissolved in CH_2Cl_2 was used to conjugate it to the *N*-terminus of *N*,*N*-dimethylglycine under basic conditions, resulting in a SiFAlin moiety.

$^{nat/177}$Lu-Labeling of the peptide precursors was carried out according to literature protocols (20).

2.2 *In vitro experiments*

CCK-2R affinity (by means of half-maximal inhibitory concentrations; IC_{50}) as well as lipophilicity (expressed as n-octanol/phosphate buffered saline (PBS) distribution coefficient; log$D_{7.4}$) were determined as previously published (7, 20). Human serum albumin (HSA) binding was determined via high performance affinity chromatography (HPAC), according to a previously published protocol (14, 24, 25).

2.3 *In vivo experiments*

Animal experiments were carried out according to the general animal welfare regulations in Germany (German animal protection act, in the edition of the announcement, dated 18 May 2006, as amended by Article 280 of 19 June 2020, approval no. ROB-55.2-1-2532.Vet_02-18-109 by the General Administration of Upper Bavaria) and the institutional guidelines for the care and use of animals. Therefore, CB17-SCID mice of both genders and aged 2–4 months (Charles River Laboratories International Inc., Sulzfeld, Germany) were used. After arrival at the in-house facilities, mice were allowed to acclimate for a minimum of one week before inoculation of AR42J cells according to a previously reported protocol (7). Animals were excluded from the study, when reaching one of the following endpoints: a weight loss higher than 20%, a tumor size above 1500 mm^3, an ulceration of the tumor, respiratory distress or change of behavior. None of these criteria applied to any animal from the experiment. Neither randomization nor blinding was applied in the allocation of the experiments. Health status of the animals is specific pathogen free according to Federation of European Laboratory Animal Science Associations recommendation.

Biodistribution studies (n=4) and µSPECT/CT imaging at 24 h p.i. were carried out as previously published (7). For all ^{177}Lu-labeled compounds, approximately 2-3 MBq (100 pmol) were administered.

Acquired data were statistically analyzed by performing a Student's *t*-test via Excel (Microsoft Corporation, Redmond, WA, USA) and OriginPro software (version 9.7) from OriginLab Corporation (Northampton, MA, USA). Acquired *p* values of less than 0.05 were considered statistically significant.

3. Results

3.1. Synthesis and Radiolabeling

Fmoc-based SPPS with concomitant purification via reversed phase high performance liquid chromatography (RP-HPLC) yielded 5-20% peptide precursor (chemical purity >95%, determined by RP-HPLC at λ = 220 nm). Quantitative ^{nat}Lu-labeling was performed at 90°C for 20 min using a 2.5-fold excess of [^{nat}Lu]LuCl$_3$. No further purification step prior usage was required, as the remaining free Lu^{3+} was shown to have no impact on IC_{50} determinations (26). ^{177}Lu-Labeling of all compounds resulted in quantitative radiochemical yields (RCY), radiochemical purities (RCP) higher than 95% as well as molar activities (A_m) of 30±10 GBq/µmol. Confirmation of peptide integrity and quality controls are provided in the Supplementary Materials (Figures S1-12).

3.2. In vitro Characterization

Affinity and lipophilicity data of all compounds evaluated are summarized in Figure 2 and Table S1.

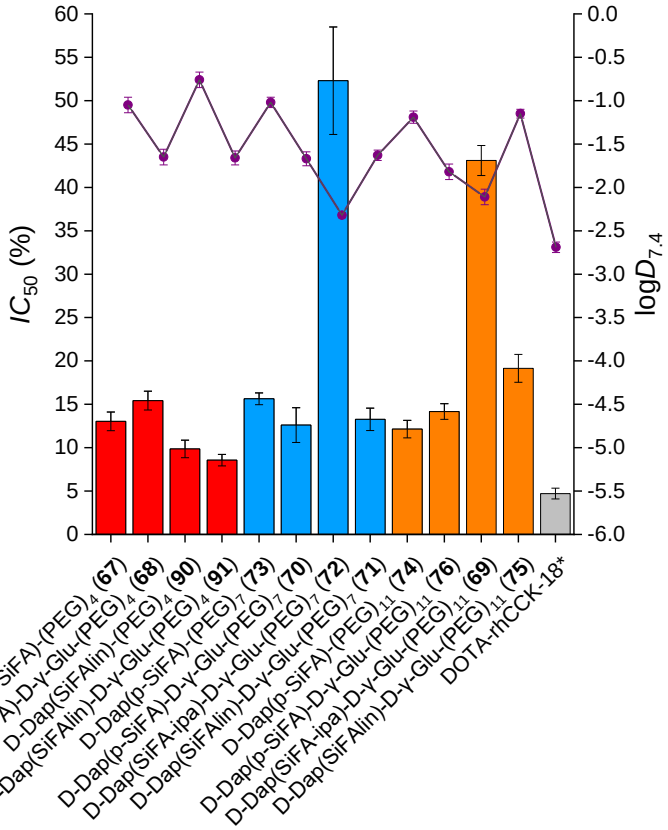

Figure 2. Affinity (IC_{50}) data (depicted in bars) and lipophilicity (log$D_{7.4}$) data (depicted in purple dots) of the PEG_4 containing compounds, [$^{nat/177}$Lu]Lu-DOTA-rhCCK-67 -68, -90 and -91 (red), the PEG_7 containing compounds, [$^{nat/177}$Lu]Lu-DOTA-rhCCK-70 to -73 (blue), as well as the PEG_{11} containing compounds, [$^{nat/177}$Lu]Lu-DOTA-rhCCK-74 to -76 and -69 (orange), compared to the reference [$^{nat/177}$Lu]Lu-DOTA-rhCCK-18 (grey, (20)). All novel compounds comprise a [$^{177/nat}$Lu]-DOTA complex as well as a D-γ-Glu-$(PEG)_3$-Trp-(N-Me)Nle-Asp-1-Nal-NH_2 binding unit linked together by a spacer sequence X (defined on the X-axis). * data taken from Günther et al. (20). These data have been determined in our lab under identical conditions.

IC_{50} values of most rh-based minigastrin analogs evaluated ([^{nat}Lu]Lu-DOTA-rhCCK-67, -68, -70, -71, -73 to -76 and -90) were found to be in a range between 10 to 20 nM. For compounds containing a SiFA-ipa moiety ([^{nat}Lu]Lu-DOTA-rhCCK-69 and -72), noticeably increased IC_{50} values were observed. [^{nat}Lu]Lu-DOTA-rhCCK-91, comprising a PEG_4 linker in combination with a SiFAlin building block, displayed the highest CCK-2R affinity within this study (IC_{50} = 8.56±0.66 nM). However, compared to the reference compound, [^{nat}Lu]Lu-DOTA-rhCCK-18 (IC_{50} = 4.71±0.62 nM, (20)), CCK-2R affinity of **91** was significantly decreased ($p < 0.0014$).

In general, all compounds lacking a D-γ-Glu moiety in proximity to the SiFA building block revealed a significantly higher lipophilicity than their counterparts comprising a D-γ-Glu moiety in said position (log$D_{7.4}$ =–1.2 to –0.8 versus –1.9 to –1.6; p <0.0001). In addition, compounds containing a SiFA-ipa building block displayed the lowest lipophilicity among all compounds (log$D_{7.4}$: –2.4 to –2.1), which was found to be slightly higher than that of [^{177}Lu]Lu-DOTA-rhCCK-18 (log$D_{7.4}$ = –2.71±0.04, (20)).

Data of human serum albumin (HSA) binding experiments are outlined in Figure 3 and Table S1.

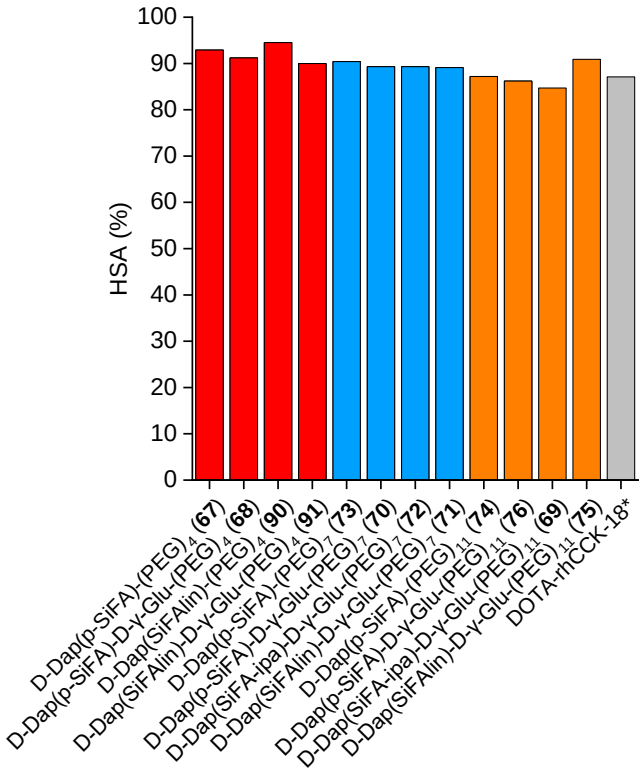

166

167 **Figure 3.** HSA binding of the PEG_4 containing compounds, [^{nat}Lu]Lu-DOTA-rhCCK-67 -68, -90 and -91 (red), the
168 PEG_7 containing compounds, [^{nat}Lu]Lu-DOTA-rhCCK-70 to -73 (blue), as well as the PEG_{11} containing compounds,
169 [^{nat}Lu]Lu-DOTA-rhCCK-74 to -76 and -69 (orange), compared to the reference, [^{nat}Lu]Lu-DOTA-rhCCK-18 (grey),
170 as analyzed by HPAC. All novel compounds comprise a [$^{177/nat}$Lu]-DOTA complex as well as a D-γ-Glu-$(PEG)_3$-Trp-
171 (N-Me)Nle-Asp-1-Nal-NH_2 binding unit linked together by a spacer sequence X (defined on the X-axis). * data taken
172 from Günther et al. (20). These data have been determined in our lab under identical conditions.

173 HSA binding was found to be in a range between 85-95% for all compounds evaluated. Except for
174 [^{nat}Lu]Lu-DOTA-rhCCK-75, an extended PEG linker length led to slightly reduced HSA binding. No
175 trends regarding the influence of different silicon-based fluoride acceptors on HSA interaction were
176 noticed. In comparison, the reference compound, [^{nat}Lu]Lu-DOTA-rhCCK-18 (87.1%), displayed similar
177 HSA binding to the novel rhCCK derivatives.

178 ***3.3. In vivo Characterization***

179 Due to their favorable performance *in vitro*, [^{177}Lu]Lu-DOTA-rhCCK-70 (IC_{50} = 12.6±2.0 nM,
180 log$D_{7.4}$ = −1.67±0.08, HSA = 89.3%), bearing a p-SiFA moiety, and [^{177}Lu]Lu-DOTA-rhCCK-91
181 (IC_{50} = 8.6±0.7 nM, log$D_{7.4}$ = −1.66±0.08, HSA = 90.0%), comprising a SiFAlin moiety, were further
182 evaluated *in vivo* (Figure 4, Table S2 and S3) and compared to [^{177}Lu]Lu-DOTA-rhCCK-18 (20).

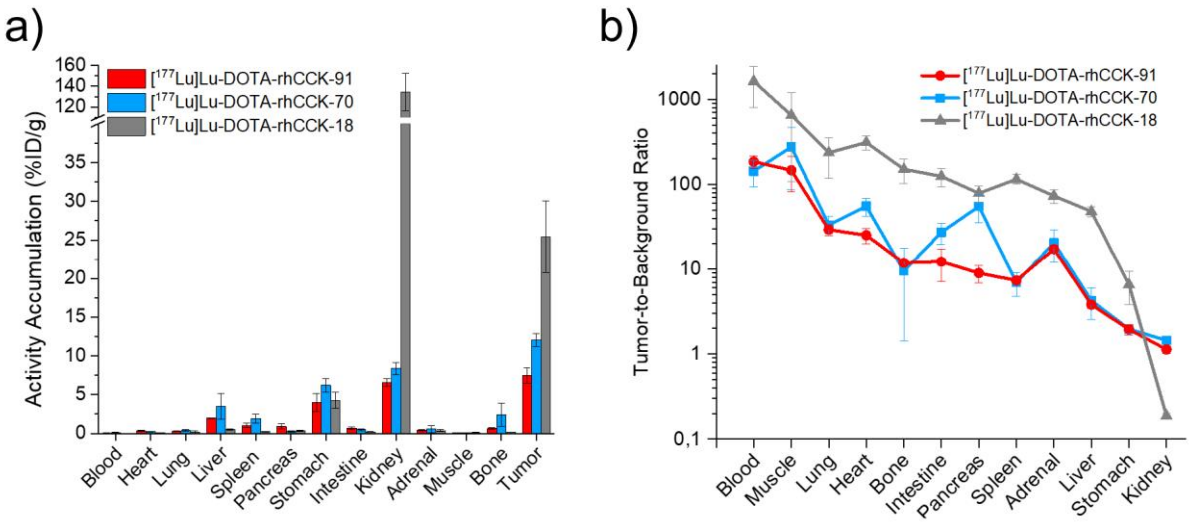

183

184 **Figure 4. a)** Biodistribution data and **b)** tumor-to-background ratios of [^{177}Lu]Lu-DOTA-rhCCK-91 (red) and
185 [^{177}Lu]Lu-DOTA-rhCCK-70 (blue) in selected organs (depicted in percentage injected dose per gram; %ID/g) at 24 h
186 p.i. in comparison to [^{177}Lu]Lu-DOTA-rhCCK-18 (grey, (20)) in AR42J tumor-bearing CB17-SCID mice (100 pmol
187 each). Data of [^{177}Lu]Lu-DOTA-rhCCK-18 taken from Günther et al. (20). These data have been determined in our
188 lab under identical conditions.

189 Activity levels in the AR42J tumor xenograft of 12.0±0.8 %ID/g and 7.5±1.0 %ID/g were found at 24 h
190 p.i. for [^{177}Lu]Lu-DOTA-rhCCK-70 and -91, respectively. Furthermore, activity uptake in the kidneys was
191 observed to be low for both compounds (8.4±0.8 and 6.6±0.5 %ID/g) evaluated. In addition, activity
192 levels in liver (3.5±1.7 and 2.0±0.1 %ID/g) and spleen (1.9±0.6 and 1.0±0.3 %ID/g) were slightly
193 elevated. Activity accumulation in the CCK-2R-expressing stomach was increased (6.2±0.9 and
194 4.0±1.2 %ID/g). Compared to the reference [^{177}Lu]Lu-DOTA-rhCCK-18 (25.4±4.7 %ID/g, (20)), activity
195 levels in the tumor were decreased 2- to 3-fold for [^{177}Lu]Lu-DOTA-rhCCK-70 and -91, respectively.
196 However, kidney accumulation and retention of the novel compounds was reduced 16- to 20-fold,
197 respectively ($p < 0.0001$), thus resulting in enhanced tumor-to-kidney ratios (0.19±0.01 versus 1.44±0.14
198 and 1.14±0.12, respectively).
199 µSPECT/CT imaging studies of [^{177}Lu]Lu-DOTA-rhCCK-70 and [^{177}Lu]Lu-DOTA-rhCCK-91 at 24 h p.i.
200 corroborated the biodistribution data well, revealing high activity levels in the tumor accompanied by
201 reduced activity accumulation in the kidneys (Figure 5).

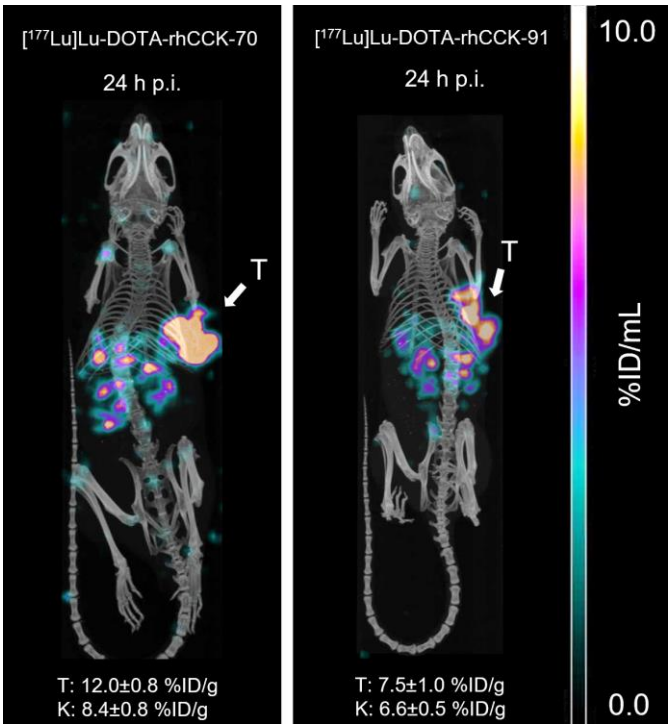

Figure 5. Representative µSPECT/CT images of AR42J tumor-bearing CB17-SCID mice at 24 h p.i. injected either with [^{177}Lu]Lu-DOTA-rhCCK-70 (left) or [^{177}Lu]Lu-DOTA-rhCCK-91 (right) (100 pmol each). Tumors (T) are indicated by white arrows. Mean activity levels in the kidneys (K) and the tumor (T) are shown at the bottom.

4. Discussion

In the past few years, the rh concept was successfully implemented for prostate-specific membrane antigen targeted compounds, enabling the generation of chemically identical ligands that are either ^{18}F- or ^{177}Lu-labeled (19, 27). These so called “true theranostics” allow for the design of chemical identical pairs, such as ^{18}F/^{nat}Lu (PET/CT) and ^{19}F/^{177}Lu (therapy), by combining a chelator as well as a SiFA moiety within the peptide structure. To date, rhPSMA-7.3 (Posluma®) has been approved by the FDA in May 2023 for diagnosis of suspected metastatic as well as recurrent prostate cancer. In addition, clinical trials using rhPSMA-10.1 for therapeutic approaches are ongoing (28, 29, 30, 31).

As currently applied CCK-2R-targeted compounds bear no option for ^{18}F-labeling, we recently transferred the rh concept to minigastrin analogs via introduction of a D-Dap(p-SiFA) moiety into the peptide structure of DOTA-PP-F11N (7, 20). The most promising rh-based minigastrin analog, [$^{18/19}$F]F-[$^{177/nat}$Lu]Lu-DOTA-rhCCK-18, displayed decelerated clearance kinetics accompanied by tremendously elevated activity levels in the tumor at 1 and 24 h p.i., rendering this compound a valuable asset for

PET/CT imaging of MTC. However, elevated renal uptake of DOTA-rhCCK-18 might be a limiting factor for radioligand therapy when ^{177}Lu-labeled (20).

Within this study, we wanted to reduce activity uptake in the kidneys, while maintaining high activity levels in the tumor, to enable both PET/CT imaging and radioligand therapy using chemical identical compounds. We thus modified the charge distribution within the linker section of DOTA-rhCCK-18 by replacement of the poly-D-glutamate chain with PEG linkers of various length. To maintain a suitable hydrophilicity of our compounds, the influence of differently charged SiFA moieties e.g., p-SiFA (neutral), SiFAlin (positively charged) and SiFA-ipa (negatively charged) on *in vitro* and *in vivo* characteristics was evaluated.

Displaying IC_{50} values of 12 to 16 nM, no trend on CCK-2R affinity was observed for peptides comprising different PEG linker length (4 to 11; [^{nat}Lu]Lu-DOTA-rhCCK-67, -68, -70, -73, -74 and -76). Compounds that contain an additional D-γ-Glu moiety in proximity to the SiFA building block ([^{nat}Lu]Lu-**68**, -**70** and -**76**) revealed similar IC_{50} values (12 to 16 nM) than their counterparts lacking said entity ([^{nat}Lu]Lu-**67**, -**73** and -**74**). In contrast, substitution of p-SiFA by SiFA-ipa led to significantly elevated IC_{50} values (p<0.0001, [^{nat}Lu]Lu-DOTA-rhCCK-69: 42.1±1.7 nM and -72: 52.3±6.3 nM), suggesting a low tolerability towards negative charges at the SiFA moiety. Replacing p-SiFA by a positively charged SiFAlin unit had a positive impact on CCK-2R affinity of compounds comprising a $(PEG)_4$ chain ([^{nat}Lu]Lu-DOTA-rhCCK -90 and -91: IC_{50} = 8 to 10 nM), whereas no influence as well as a negative influence on IC_{50} values of peptides additionally containing a $(PEG)_7$ and $(PEG)_{11}$ chain ([^{nat}Lu]Lu-DOTA-rhCCK-71 and -75: IC_{50} = 13 to 19 nM), respectively, was observed.

Compared to the reference [^{nat}Lu]Lu-DOTA-rhCCK-18 (IC_{50} = 4.71±0.62 nM, (20)), all compounds evaluated in this study revealed increased IC_{50} values (8 to 53 nM), suggesting a positive influence of a negatively charged poly-D-γ-glutamate chain on CCK-2R affinity as opposed to PEG linkers. This is supported by Ritler *et al.*, demonstrating a favorable interaction between the negatively charged poly-D-glutamates in the linker section of DOTA-PP-F11N with the positively charged amino acid residues in the CCK-2R binding pocket (32). However, the previously published compound [^{177}Lu]Lu-(*R*)-DOTAGA-rhCCK-16, displaying an IC_{50} value of 20.4±2.73 nM, revealed high activity levels in the tumor (18.0±0.7 %ID/g) at 24 h p.i. in AR42J tumor-bearing CB17-SCID mice (7). We thus consider IC_{50} values below 20 nM as sufficient for rhCCK ligands for high activity levels in the tumor.

As expected, the additional negative charge of a D-γ-Glu moiety in proximity to the SiFA building block resulted in a lower lipophilicity for the respective peptides. Furthermore, peptides comprising a SiFA-ipa moiety displayed the most favorable lipophilicity (log$D_{7.4}$: –2.3 to –2.1). Surprisingly, the additional positive charge of the SiFAlin moiety had no impact on lipophilicity for [^{177}Lu]Lu-DOTA-rhCCK-71, [^{177}Lu]Lu-DOTA-rhCCK-90 and [^{177}Lu]Lu-DOTA-rhCCK-91**,** or even led to increased log$D_{7.4}$ values ([^{177}Lu]Lu-DOTA-rhCCK-75). We assume that this is attributed to the change of the overall charge of the peptides. Namely, introduction of a positive charge via a SiFAlin moiety into the mainly negatively charged minigastrin analog would thus lead to a decreased overall charge and thus, a less beneficial impact on lipophilicity, as observed for our compounds ([^{177}Lu]Lu-DOTA-rhCCK-71, -72, -90 and -91). Except [^{177}Lu]Lu-DOTA-rhCCK-69 and -72, each comprising a SiFA-ipa moiety, no other peptides evaluated within this study displayed log$D_{7.4}$ values within a range of –3 to –2, which we consider ideal due to the favorable pharmacokinetic properties observed for several compounds in the field of nuclear medicine, among those [^{177}Lu]Lu-DOTA-rhCCK-18 (log$D_{7.4}$ = –2.69±0.06 (20)) and [^{177}Lu]Lu-DOTA-MGS5 (log$D_{7.4}$ = –2.21±0.08 (33)) in case of CCK-2R ligands. However, currently clinically applied radiotracers, e.g. [^{177}Lu]Lu-Pentixather (log$D_{7.4}$ = –1.8±0.2 (34)) for C-X-C chemokine receptor type 4 targeting and [^{177}Lu]Lu-NeoBOMB1 (log$D_{7.4}$ = –0.57±0.03 (26)) addressing the gastrin releasing peptide receptor, also display elevated log$D_{7.4}$ values. Therefore, we decided to extend the range of suitable log$D_{7.4}$ values from –2 to –1.5, bearing in mind that enhanced hepatic accumulation and thus, effects on the biodistribution profile could occur.

HSA binding was observed to be high (85-95%) for all rhCCK derivatives tested. In comparison, the reference compound [^{nat}Lu]Lu-DOTA-rhCCK-18 (87%) displayed a similar HSA interaction. All compounds evaluated comprise a SiFA building block within their peptide structure, which was reported to increase HSA binding (28). Elevated HSA binding is usually associated with a decelerated activity clearance and prolonged circulation of the compound in the blood stream, which can result in increased activity accumulation in the tumor (35, 36, 37). This corroborates the observed tumor accumulation and retention for previous rhCCK derivatives, such as [^{177}Lu]Lu-(*R*)-DOTAGA-rhCCK-16 and [^{177}Lu]Lu-DOTA-rhCCK-18. Therefore, we anticipated a similarly beneficial effect on our novel rhCCK ligands.

Hence, we decided to further investigate both [^{177}Lu]Lu-DOTA-rhCCK-70 (IC_{50}: 12.6±2.0 nM, log$D_{7.4}$: –1.67±0.08, HSA binding ~90%) and [^{177}Lu]Lu-DOTA-rhCCK-91 (IC_{50}: 8.7±0.7 nM, log$D_{7.4}$: –1.66±0.08, HSA binding ~90%) *in vivo* at 24 h p.i., as we considered those two ligands the most favorable in this

study. Biodistribution profiles of [^{177}Lu]Lu-DOTA-rhCCK-70 and -91 confirmed our assumption that synergistic effects between the multiple negative charges of the poly-D-γ-glutamate linker section and the D-Dap(p-SiFA) building block led to substantially elevated activity levels in the kidneys for earlier generations of rh-based minigastrin analogs, such as [^{177}Lu]Lu-(*R*)-DOTAGA-rhCCK-16 and [^{177}Lu]Lu-DOTA-rhCCK-18. By the reduction of negative charges within the linker section from eight to two via substitution of D-γ-Glu moieties by PEG_X chains, both [^{177}Lu]Lu-DOTA-rhCCK-70 and [^{177}Lu]Lu-DOTA-rhCCK-91 displayed significantly decreased activity uptakes in the kidneys compared to [^{177}Lu]Lu-DOTA-rhCCK-18 (8.4±0.8 %ID/g and 6.6±0.5 %ID/g vs. 134±18 %ID/g, (20), p<0.0001). Hence, distinctly improved tumor-to-kidney ratios were observed for [^{177}Lu]Lu-DOTA-rhCCK-70 (1.45±0.12) and [^{177}Lu]Lu-DOTA-rhCCK-91 (1.14±0.12) opposed to [^{177}Lu]Lu-DOTA-rhCCK-18 (0.19±0.01, (20)).

However, the increased lipophilicity of [^{177}Lu]Lu-DOTA-rhCCK-70 and [^{177}Lu]Lu-DOTA-rhCCK-91 led to lower overall tumor-to-background ratios, particularly in the liver (3.48±1.66 %ID/g and 1.96±0.08 %ID/g vs. 0.22±0.01 %ID/g) and spleen (1.92±0.60 %ID/g and 1.04±0.26 %ID/g vs. 0.34±0.09 %ID/g). Moreover, tumor accumulation and retention was also reduced noticeably for our novel compounds (12.0±0.8 and7.5±1.0 %ID/g versus 25.4±4.7 %ID/g, (20)). We suggest that this is due to their reduced CCK-2R affinity. However, both compounds revealed a higher CCK-2R affinity compared to [^{177}Lu]Lu-(*R*)-DOTAGA-rhCCK-16, but both exhibited significantly lower activity levels in the tumor, though. Therefore, other properties, such as *in vivo* stability could be responsible, which would have to be confirmed via stability studies. Furthermore, overall charge of the peptide is also an important factor, as [^{177}Lu]Lu-DOTA-rhCCK-91 displayed a higher CCK-2R affinity, yet decreased activity levels in the tumor compared to [^{177}Lu]Lu-DOTA-rhCCK-70. We thus suggest that the positively charged SiFAlin moiety has a negative effect on tumor accumulation, which has to be further elucidated in future studies.

In summary, we could achieve our goal to design a rh-based minigastrin analog with substantially reduced kidney accumulation by modifying the linker section with regard to negatively charged residues. However, these pleasing results were accompanied by a negative impact on overall tumor accumulation compared to our internal benchmarks. Worth mentioning, [^{177}Lu]Lu-DOTA-rhCCK-70 still revealed higher activity levels in the tumor at 24 h p.i. than [^{177}Lu]Lu-DOTA-MGS5 (11.0±1.2 %ID/g, (14)) and [^{177}Lu]Lu-DOTA-PP-F11N (1.9±0.8 %ID/g, (7)), two compounds that are currently evaluated in clinical trials (5, 13). Furthermore, kidney accumulation and retention was observed to be only slightly elevated (8.4±0.8 versus 1.3±0.4 (14) and 3.1±0.6 %ID/g (7)), rendering this peptide a promising lead compound

for further preclinical development in order to pave the way for a clinical translation of rh-based minigastrin analogs.

5. Conclusion

In this study we could demonstrate that a reduction of negative charges within the linker section of rh-based minigastrin analogs via substitution of $(D\text{-}\gamma\text{-}Glu)_8$ by PEG moieties of various length led to a substantially lower activity uptake in the kidneys compared with previous rh-based CCK2R-targeted compounds. However, lower tumor accumulation and thus, overall tumor-to-background ratios in all organs apart from the kidneys were also observed, demanding further optimization of the most promising compound from this study with regard to target affinity, lipophilicity and biodistribution profile.

List of Abbreviations

A_m: molar activities

CCK-2R: cholecystokinin-2 receptor

Dap: 2,3-diaminopropionic acid

DOTA: 1,4,7,10-tetraazacyclododecan-1,4,7,10-tetracetic acid

DOTA-CCK-66: DOTA-D-γ-Glu-$(PEG)_3$-Trp-(*N*-Me)Nle-Asp-1-Nal-NH_2

DOTA-MGS5: DOTA-D-Glu-Ala-Tyr-Gly-Trp-(*N*-Me)Nle-Asp-1-Nal-NH_2

DOTA-PP-F11N: DOTA-$(D\text{-}Glu)_6$-Ala-Tyr-Gly-Trp-Nle-Asp-Phe-NH_2

DOTA-rhCCK-18: (DOTA-D-Dap(p-SiFA)-$(D\text{-}\gamma\text{-}Glu)_8$-Ala-Tyr-Gly-Trp-Nle-Asp-Phe-NH_2)

ESI-MS: electro-spray ionization mass spectrometry

Fmoc: 9-fluorenylmethoxycarbonyl

HSA: human serum albumin

HPAC: high performance affinity chromatography

MTC: medullary thyroid carcinoma

PEG: polyethylene glycol

PET: positron emission tomography

radio-TLC: radio-thin layer chromatography

RCP**:** radiochemical purity

RCY: radiochemical yield

rh: radiohybrid

RP-HPLC: reversed-phase high performance liquid chromatography

SiFA: silicon-based fluoride acceptor

SPPS: solid-phase peptide synthesis

Declarations

Ethics approval and consent to participate

Nothing to declare.

Consent for publication

Nothing to declare.

Availability of data and materials

Data is contained within the article and Supplementary Materials.

Competing interests

H.-J.W. is founder and shareholder of Scintomics GmbH, Munich, Germany. A patent application on CCK-2R-targeted compounds with N.H., C.L., H.-J.W., and T.G. as inventors has been filed. No other potential conflicts of interest relevant to this article exist.

Funding

This study has been funded by Deutsche Forschungsgemeinschaft (DFG, German Research Foundation – 461577150).

Authors' Contribution

N.H. designed the study, carried out the synthesis and evaluation of the peptides and wrote the manuscript. S.F. developed the novel SiFA-ipa building block. I.M. carried out the synthesis and evaluation of the peptides. R.B. acquired funding, revised the manuscript and supervised the animal experiments. C.L. managed the project and revised the manuscript. H.-J.W. managed the project and acquired funding. T.G. wrote the manuscript, designed the study, managed the project and acquired funding. All authors have approved the final version of the manuscript.

Acknowledgements

We would like to acknowledge Denise Dürre for her help with the execution of this project. Furthermore, we acknowledge Markus Fahnauer for providing the SiFA-Br building block as well as Sebastian Fenzl for providing the SiFA-ipa building block.

References

1. Ball DW. Clinical Aspects of Medullary Thyroid Carcinoma. In: Wartofsky L, Van Nostrand D, editors. Thyroid Cancer: A Comprehensive Guide to Clinical Management. Totowa, NJ: Humana Press; 2006. p. 581-9.

2. Araque KA, Gubbi S, Klubo-Gwiezdzinska J. Updates on the Management of Thyroid Cancer. Horm Metab Res. 2020;52(8):562-77.

3. Hundahl SA, Fleming ID, Fremgen AM, Menck HR. A National Cancer Data Base report on 53,856 cases of thyroid carcinoma treated in the U.S., 1985-1995 [see commetns]. Cancer. 1998;83(12):2638-48.

4. Reubi JC, Waser B. Unexpected high incidence of cholecystokinin-B/gastrin receptors in human medullary thyroid carcinomas. Int J Cancer. 1996;67(5):644-7.

5. Rottenburger C, Nicolas GP, McDougall L, Kaul F, Cachovan M, Vija AH, et al. Cholecystokinin 2 Receptor Agonist (177)Lu-PP-F11N for Radionuclide Therapy of Medullary Thyroid Carcinoma: Results of the Lumed Phase 0a Study. J Nucl Med. 2020;61(4):520-6.

6. Sauter AW, Mansi R, Hassiepen U, Muller L, Panigada T, Wiehr S, et al. Targeting of the Cholecystokinin-2 Receptor with the Minigastrin Analog (177)Lu-DOTA-PP-F11N: Does the Use of Protease Inhibitors Further Improve In Vivo Distribution? J Nucl Med. 2019;60(3):393-9.

7. Holzleitner N, Günther T, Beck R, Lapa C, Wester HJ. Introduction of a SiFA Moiety into the D-Glutamate Chain of DOTA-PP-F11N Results in Radiohybrid-Based CCK-2R-Targeted Compounds with Improved Pharmacokinetics In Vivo. Pharmaceuticals (Basel). 2022;15(12).

8. Grob NM, Schibli R, Behe M, Mindt TL. Improved Tumor-Targeting with Peptidomimetic Analogs of Minigastrin (177)Lu-PP-F11N. Cancers (Basel). 2021;13(11).

9. Gubbi S, Koch CA, Klubo-Gwiezdzinska J. Peptide Receptor Radionuclide Therapy in Thyroid Cancer. Frontiers in Endocrinology. 2022;13.

10. Mansi R, Fani M. Radiolabeled Peptides for Cancer Imaging and Therapy: From Bench-to-Bedside. CHIMIA. 2021;75(6):500.

11. Klingler M, Summer D, Rangger C, Haubner R, Foster J, Sosabowski J, et al. DOTA-MGS5, a New Cholecystokinin-2 Receptor-Targeting Peptide Analog with an Optimized Targeting Profile for Theranostic Use. J Nucl Med. 2019;60(7):1010-6.

12. Uprimny C, von Guggenberg E, Svirydenka A, Mikolajczak R, Hubalewska-Dydejczyk A, Virgolini IJ. Comparison of PET/CT imaging with [(18)F]FDOPA and cholecystokinin-2 receptor targeting [(68)Ga]Ga-DOTA-MGS5 in a patient with advanced medullary thyroid carcinoma. Eur J Nucl Med Mol Imaging. 2020.

13. von Guggenberg E, Uprimny C, Klingler M, Warwitz B, Sviridenko A, Bayerschmidt S, et al. Preliminary clinical experience of cholecystokinin-2 receptor PET/CT imaging using the (68)Ga-labeled minigastrin analog DOTA-MGS5 in patients with medullary thyroid cancer. J Nucl Med. 2023.

14. Gunther T, Holzleitner N, Viering O, Beck R, Wienand G, Dierks A, et al. Preclinical Evaluation of Minigastrin Analogs and Proof-of-Concept [(68)Ga]Ga-DOTA-CCK-66 PET/CT in 2 Patients with Medullary Thyroid Cancer. J Nucl Med. 2023.

15. Viering O, Gunther T, Holzleitner N, Dierks A, Wienand G, Pfob CH, et al. CCK(2) Receptor-Targeted PET/CT in Medullary Thyroid Cancer Using [(68)Ga]Ga-DOTA-CCK-66. J Nucl Med. 2023.

16. Alauddin MM. Positron emission tomography (PET) imaging with (18)F-based radiotracers. Am J Nucl Med Mol Imaging. 2012;2(1):55-76.

17. Giovanella L, Treglia G, Iakovou I, Mihailovic J, Verburg FA, Luster M. EANM practice guideline for PET/CT imaging in medullary thyroid carcinoma. European Journal of Nuclear Medicine and Molecular Imaging. 2020;47(1):61-77.

18. Brammen L, Niederle MB, Riss P, Scheuba C, Selberherr A, Karanikas G, et al. Medullary Thyroid Carcinoma: Do Ultrasonography and F-DOPA-PET-CT Influence the Initial Surgical Strategy? Ann Surg Oncol. 2018;25(13):3919-27.

19. Wurzer A, Di Carlo D, Schmidt A, Beck R, Eiber M, Schwaiger M, et al. Radiohybrid Ligands: A Novel Tracer Concept Exemplified by 18F- or 68Ga-Labeled rhPSMA Inhibitors. Journal of Nuclear Medicine. 2020;61(5):735-42.

20. Günther T, Holzleitner N, Di Carlo D, Urtz-Urban N, Lapa C, Wester HJ. Development of the First (18)F-Labeled Radiohybrid-Based Minigastrin Derivative with High Target Affinity and Tumor Accumulation by Substitution of the Chelating Moiety. Pharmaceutics. 2023;15(3).

21. Niedermoser S, Chin J, Wangler C, Kostikov A, Bernard-Gauthier V, Vogler N, et al. In Vivo Evaluation of (1)(8)F-SiFAlin-Modified TATE: A Potential Challenge for (6)(8)Ga-DOTATATE, the Clinical Gold Standard for Somatostatin Receptor Imaging with PET. J Nucl Med. 2015;56(7):1100-5.

22. Niedermoser S, Chin J, Wängler C, Kostikov A, Bernard-Gauthier V, Vogler N, et al. In Vivo Evaluation of ¹⁸F-SiFAlin–Modified TATE: A Potential Challenge for ⁶⁸Ga-DOTATATE, the Clinical Gold Standard for Somatostatin Receptor Imaging with PET. Journal of Nuclear Medicine. 2015;56(7):1100-5.

23. Iovkova L, Wängler B, Schirrmacher E, Schirrmacher R, Quandt G, Boening G, et al. para-Functionalized Aryl-di-tert-butylfluorosilanes as Potential Labeling Synthons for 18F Radiopharmaceuticals. Chemistry – A European Journal. 2009;15(9):2140-7.

24. Valko K, Nunhuck S, Bevan C, Abraham MH, Reynolds DP. Fast gradient HPLC method to determine compounds binding to human serum albumin. Relationships with octanol/water and immobilized artificial membrane lipophilicity. J Pharm Sci. 2003;92(11):2236-48.

25. Yamazaki K, Kanaoka M. Computational prediction of the plasma protein-binding percent of diverse pharmaceutical compounds. Journal of pharmaceutical sciences. 2004;93:1480-94.

26. Guenther T, Deiser S, Felber V, Beck R, Wester HJ. Substitution of L-Tryptophan by a-Methyl-L-Tryptophan in 177Lu-RM2 Results in 177Lu-AMTG, a High-Affinity Gastrin-Releasing Peptide Receptor Ligand with Improved In Vivo Stability. J Nucl Med. 2022;63(63):1364–70.

27. Wurzer A, Parzinger M, Konrad M, Beck R, Gunther T, Felber V, et al. Preclinical comparison of four [(18)F, (nat)Ga]rhPSMA-7 isomers: influence of the stereoconfiguration on pharmacokinetics. EJNMMI Res. 2020;10(1):149.

28. Wurzer A, Kunert J-P, Fischer S, Felber V, Beck R, Rose Fd, et al. Synthesis and Preclinical Evaluation of ¹⁷⁷Lu-Labeled Radiohybrid PSMA Ligands for Endoradiotherapy of Prostate Cancer. Journal of Nuclear Medicine. 2022;63(10):1489-95.

29. Rauscher I, Karimzadeh A, Schiller K, Horn T, D'Alessandria C, Franz C, et al. Detection efficacy of (18)F-rhPSMA-7.3 PET/CT and impact on patient management in patients with biochemical recurrence of prostate cancer after radical prostatectomy and prior to potential salvage treatment. J Nucl Med. 2021;62(12):1719-26.

30. Schuster DM. Detection rate of 18F-rhPSMA-7.3 PET in patients with suspected prostate cancer recurrence: Results from a phase 3, prospective, multicenter study (SPOTLIGHT). Journal of Clinical Oncology. 2022;40(6_suppl):9-.

31. Bundschuh RA, Pfob CH, Wienand G, Dierks A, Kircher M, Lapa C. 177 Lu-rhPSMA-10.1 Induces Tumor Response in a Patient With mCRPC After PSMA-Directed Radioligand Therapy With 177 Lu-PSMA-I&T. Clin Nucl Med. 2023;48(4):337-8.

32. Ritler A, Shoshan MS, Deupi X, Wilhelm P, Schibli R, Wennemers H, et al. Elucidating the Structure–Activity Relationship of the Pentaglutamic Acid Sequence of Minigastrin with Cholecystokinin Receptor Subtype 2. Bioconjugate Chemistry. 2019;30(3):657-66.

33. Holzleitner N, Günther T, Daoud-Gadieh A, Lapa C, Wester H-J. Investigation of the structure-activity relationship at the N-terminal part of minigastrin analogs. EJNMMI Research. 2023;13(1):65.

34. Osl T, Schmidt A, Schwaiger M, Schottelius M, Wester HJ. A new class of PentixaFor- and PentixaTher-based theranostic agents with enhanced CXCR4-targeting efficiency. Theranostics. 2020;10(18):8264-80.

35. Umbricht CA, Benešová M, Schibli R, Müller C. Preclinical Development of Novel PSMA-Targeting Radioligands: Modulation of Albumin-Binding Properties To Improve Prostate Cancer Therapy. Molecular Pharmaceutics. 2018;15(6):2297-306.

36. Kelly JM, Amor-Coarasa A, Ponnala S, Nikolopoulou A, Clarence Williams J, DiMagno SG, et al. Albumin-Binding PSMA Ligands: Implications for Expanding the Therapeutic Window. Journal of Nuclear Medicine. 2019;60(5):656-63.

37. Deberle LM, Benešová M, Umbricht CA, Borgna F, Büchler M, Zhernosekov K, et al. Development of a new class of PSMA radioligands comprising ibuprofen as an albumin-binding entity. Theranostics. 2020;10(4):1678-93.

Significant Decrease of Activity Uptake of Radiohybrid-Based Minigastrin Analogs in the Kidneys via Modification of the Charge Distribution Within the Linker Section

- Supplementary Materials -

Nadine Holzleitner[1,*], Sebastian Fischer[1], Isabel Maniyankerikalam[1], Roswitha Beck[1], Constantin Lapa[2,3], Hans-Jürgen Wester[1] and Thomas Günther[1,*]

[1] TUM School of Natural Sciences, Department of Chemistry, Chair of Pharmaceutical Radiochemistry, Technical University of Munich, Garching, Germany

[2] Nuclear Medicine, Faculty of Medicine, University of Augsburg, Augsburg, Germany

[3] Bavarian Cancer Research Center (BZKF), Bavaria, Germany

* correspondence: thomas.guenther@tum.de (T.G.) and nadine.holzleitner@tum.de (N.H.)

Corresponding co-authors:

Thomas Günther and Nadine Holzleitner

Phone: +49.89.289.12203

Technical University of Munich,

Chair of Pharmaceutical Radiochemistry,

Walther-Meissner-Str. 3

85748 Garching

GERMANY

Fax: +49.89.289.12204

E-Mail: thomas.guenther@tum.de and nadine.holzleitner@tum.de

ORCID-ID: 0000-0002-7412-0297 (TG) and 0000-0001-8258-3526 (NH)

General Information

Analytical and preparative reversed-phase high performance liquid chromatography (RP-HPLC) were performed using Shimadzu gradient systems (Shimadzu Deutschland GmbH, Neufahrn, Germany), each equipped with a SPD-20A UV/Vis detector (λ = 220 and 254 nm). Different gradients of MeCN (0.1% TFA, 2 or 5% H_2O for analytical or preparative application, respectively) in H_2O (0.1% TFA) were used as eluents for all RP-HPLC operations.

For analytical measurements, a MultoKrom 100-5 C18 (150 mm × 4.6 mm) column (CS Chromatographie Service GmbH, Langerwehe, Germany) was used at a flow rate of 1 mL/min. Both, specific gradients and the corresponding retention times t_R as well as the capacity factor K' are cited in the text.

Preparative RP-HPLC purification was performed using a MultoKrom 100-5 C18 (250 mm × 20 mm) column (CS Chromatographie GmbH, Langerwehe, Germany) at a constant flow rate of 10 mL/min.

Lyophilization was accomplished using an Alpha 1-2 LDplus lyophilizer (Martin Christ Gefriertrocknungsanlagen GmbH, Osterode am Harz, Deutschland) combined with a RZ-2 vacuum pump (Vacuubrand GmbH & Co KG, Olching, Germany).

Analytical and preparative radio RP-HPLC was performed using a MultoKrom 100-5 C18 (5 µm, 125 × 4.6 mm) column (CS Chromatographie GmbH, Langerwehe, Germany). A HERM LB 500 NaI scintillation detector (Berthold Technologies, Bad Wildbad, Germany) was connected to the outlet of the UV photometer for the detection of radioactivity.

Radioactive samples were measured by a WIZARD$^{2®}$ 2480 Automatic *γ*-counter (Perkin Elmer Inc., Waltham, MA, USA).

Analytical Data of $^{nat/177}$Lu-labeled Minigastrin Analogs

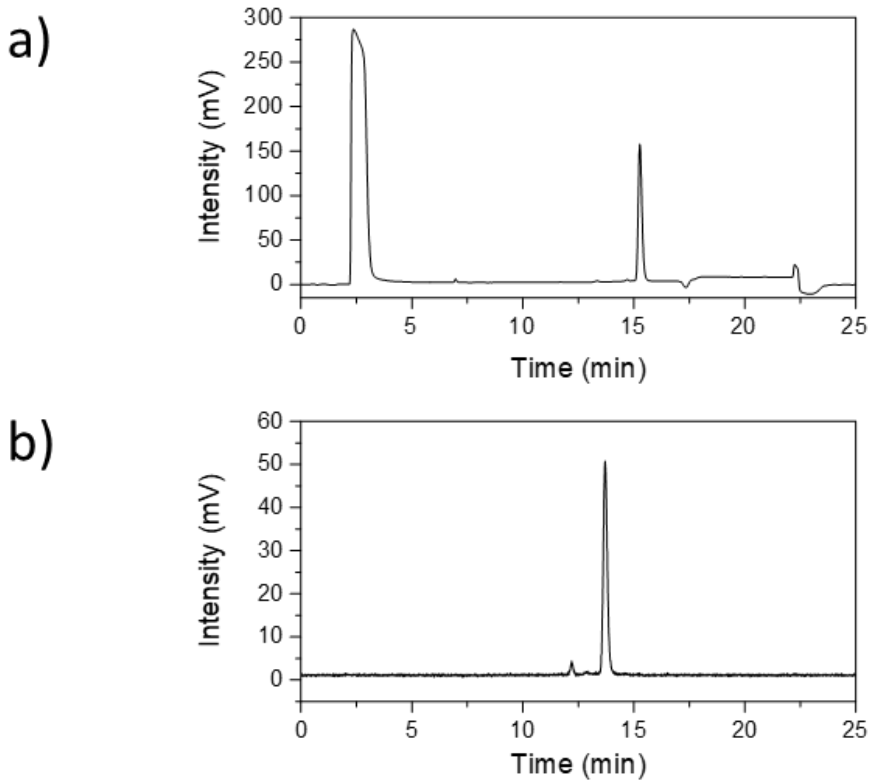

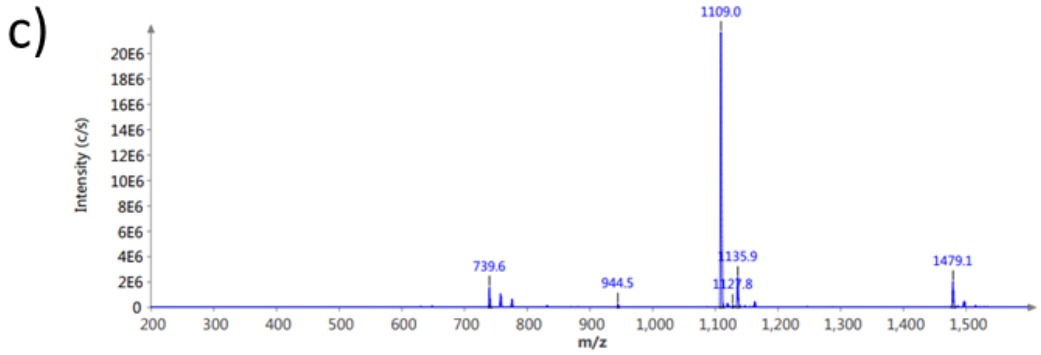

Figure S1. Confirmation of peptide identity and integrity for **a**) [^{nat}Lu]Lu-DOTA-rhCCK-67 and **b**) [^{177}Lu]Lu-DOTA-rhCCK-67 as analyzed by analytical (radio-)RP-HPLC 10→70% MeCN in H_2O + 0.1% TFA in 15 min). **c**) Mass spectrum of [^{nat}Lu]Lu-DOTA-rhCCK-67.

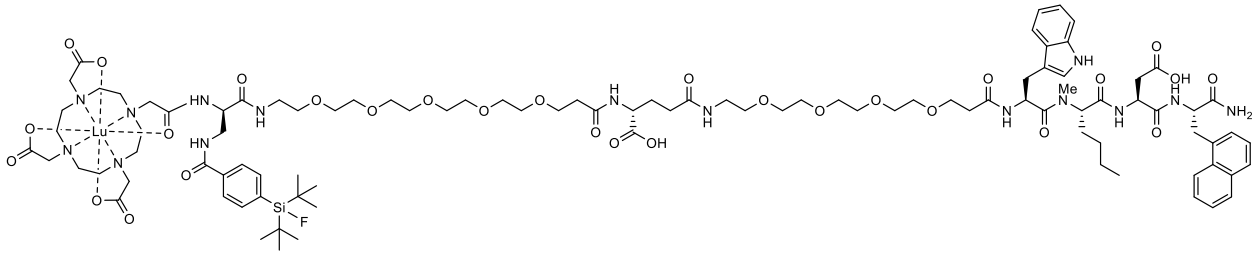

[^{nat}Lu]Lu-DOTA-rhCCK-67: RP-HPLC (10→70% MeCN in H_2O with 0.1% TFA, 15 min, λ = 220 nm): t_R = 15.3 min, K' = 8.07; MS (ESI, positive): m/z calculated for $C_{98}H_{145}FLuN_{15}O_{29}$: 2218.0, found: m/z = 1109.0 $[M+2H]^{2+}$.

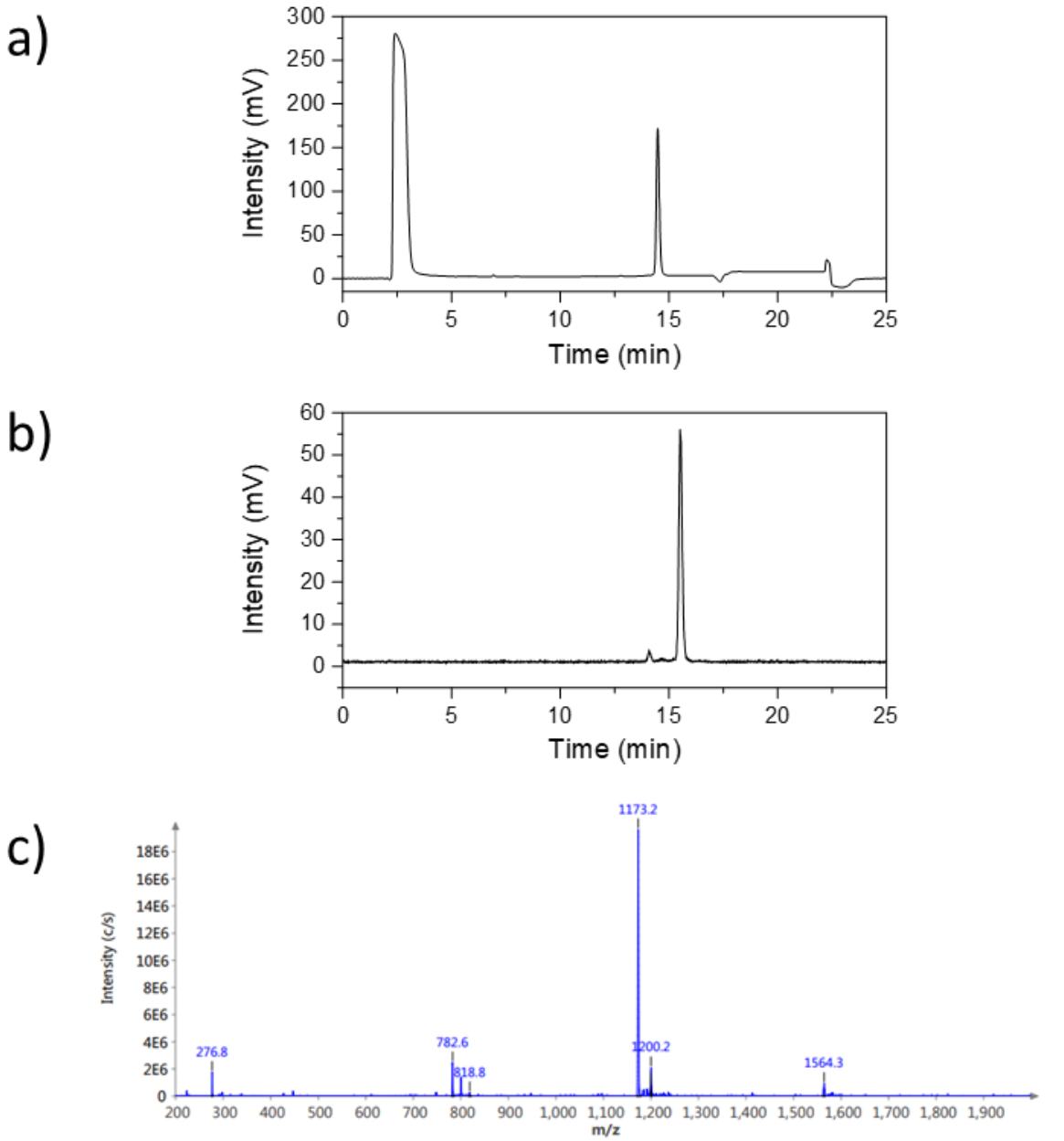

Figure S2. Confirmation of peptide identity and integrity for **a**) [^{nat}Lu]Lu-DOTA-rhCCK-68 and **b**) [^{177}Lu]Lu-DOTA-rhCCK-68 as analyzed by analytical (radio-)RP-HPLC (10→70% MeCN in H_2O + 0.1% TFA in 15 min). **c**) Mass spectrum of [^{nat}Lu]Lu-DOTA-rhCCK-68.

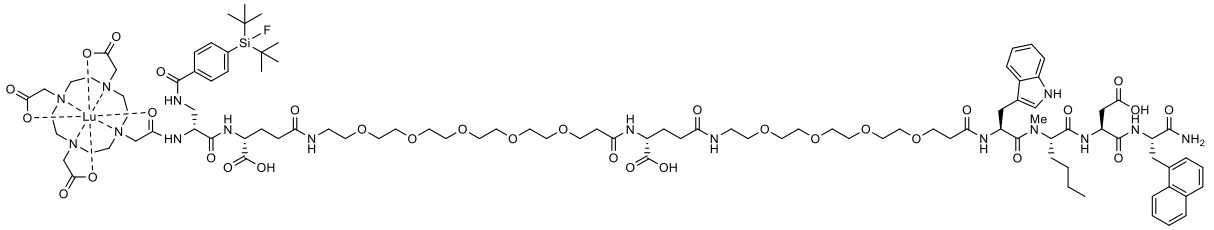

[^{mat}Lu]Lu-DOTA-rhCCK-68: RP-HPLC (10→70% MeCN in H_2O with 0.1% TFA, 15 min, λ = 220 nm) t_R = 14.5 min, K' = 7.60; MS (ESI, positive): m/z calculated for $C_{103}H_{152}FLuN_{16}O_{32}Si$: 2348.5, found: m/z = 1173.2 $[M+2H]^{2+}$.

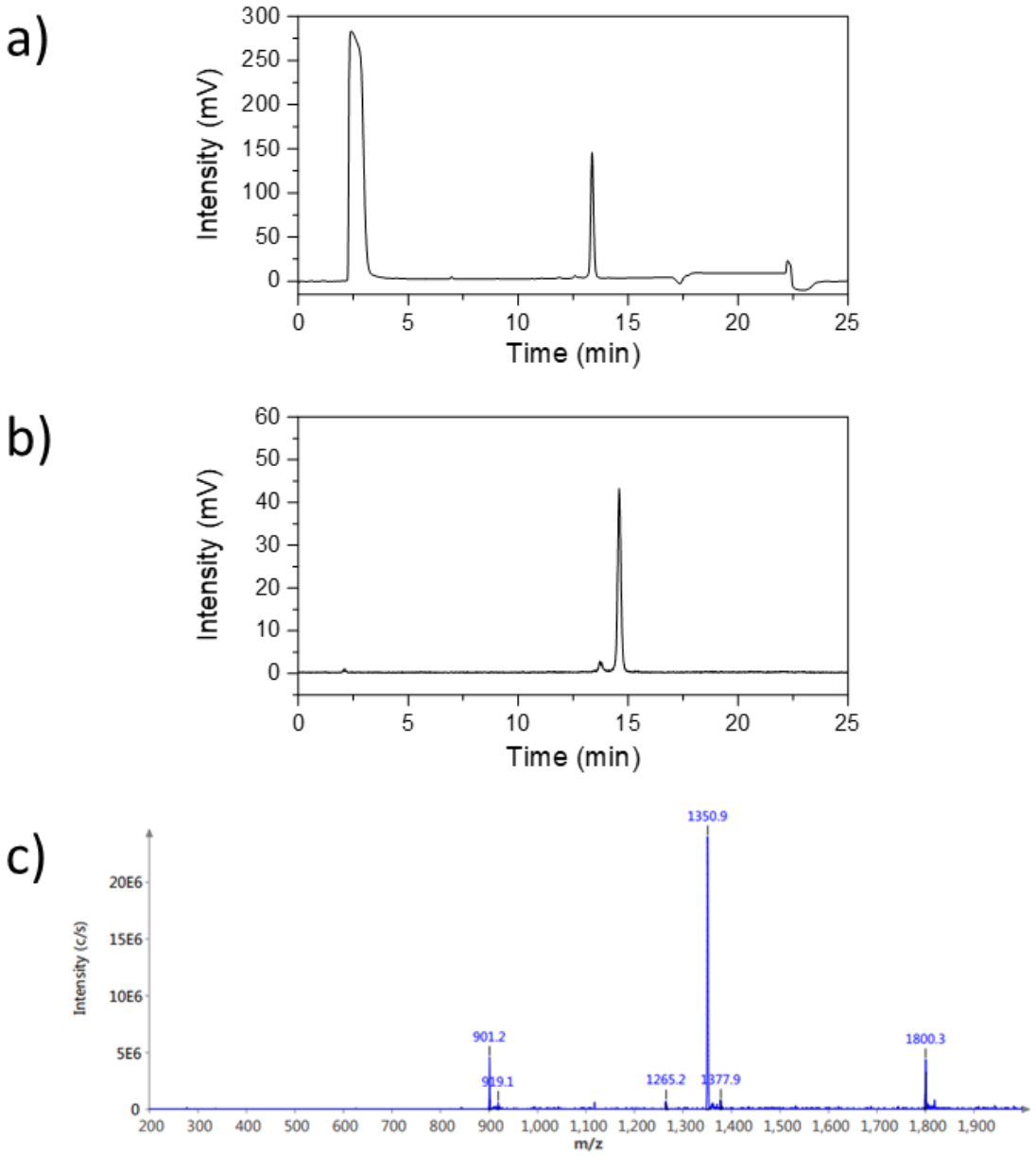

Figure S3. Confirmation of peptide identity and integrity for **a**) [^{nat}Lu]Lu-DOTA-rhCCK-69 and **b**) [^{177}Lu]Lu-DOTA-rhCCK-69 as analyzed by analytical (radio-)RP-HPLC (10→70% MeCN in H_2O + 0.1% TFA in 15 min). **c**) Mass spectrum of [^{nat}Lu]Lu-DOTA-rhCCK-69.

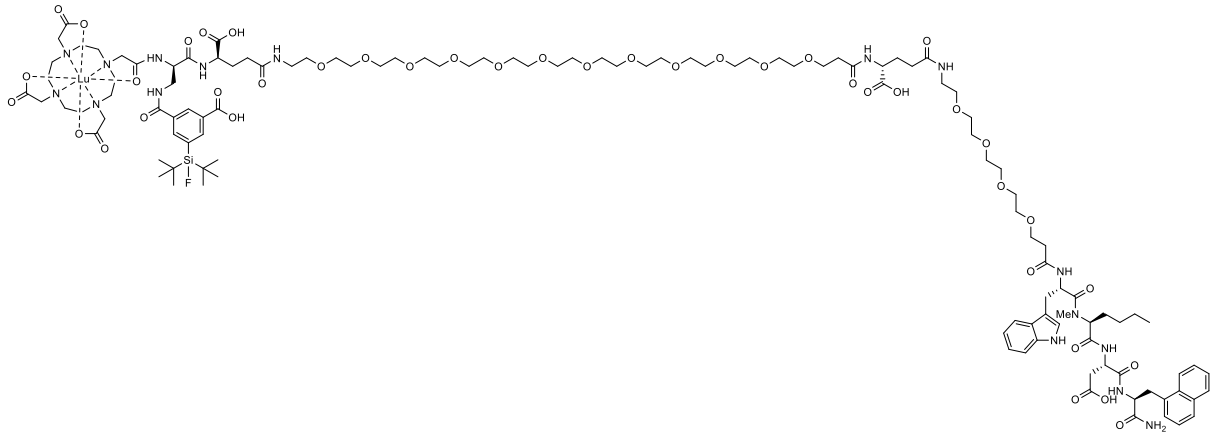

[^{mat}Lu]Lu-DOTA-rhCCK-69: RP-HPLC (10→70% MeCN in H_2O with 0.1% TFA, 15 min, λ = 220 nm) t_R = 13.4 min, K' = 6.94; MS (ESI, positive): m/z calculated for $C_{118}H_{180}FLuN_{16}O_{41}Si$: 2699.17, found: m/z = 1350.9 $[M+2H]^{2+}$, 901.2 $[M+3H]^{3+}$.

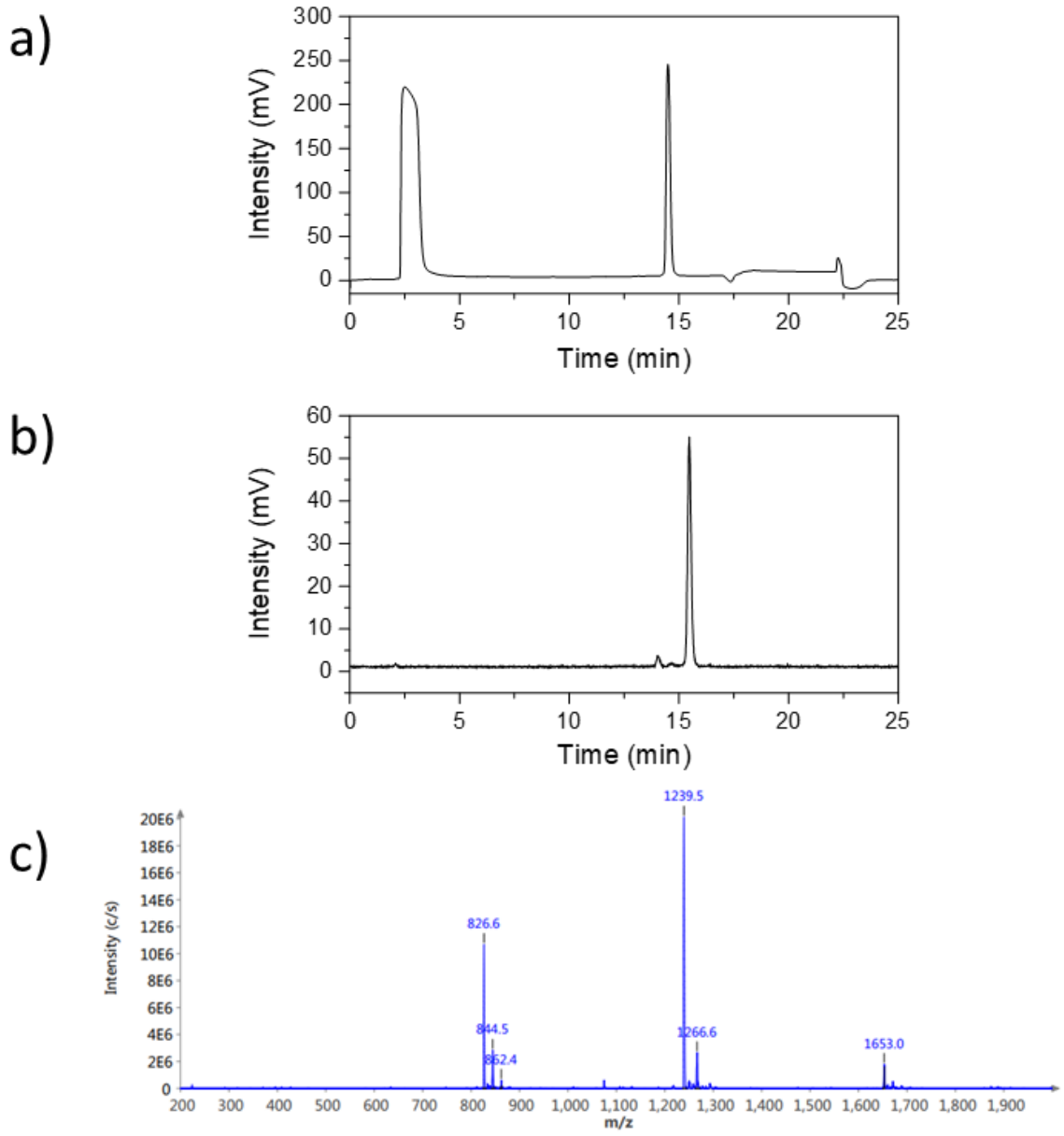

Figure S4. Confirmation of peptide identity and integrity for **a**) [^{nat}Lu]Lu-DOTA-rhCCK-70 and **b**) [^{177}Lu]Lu-DOTA-rhCCK-70 as analyzed by analytical (radio-)RP-HPLC (10→70% MeCN in H_2O + 0.1% TFA in 15 min). **c**) Mass spectrum of [^{nat}Lu]Lu-DOTA-rhCCK-70.

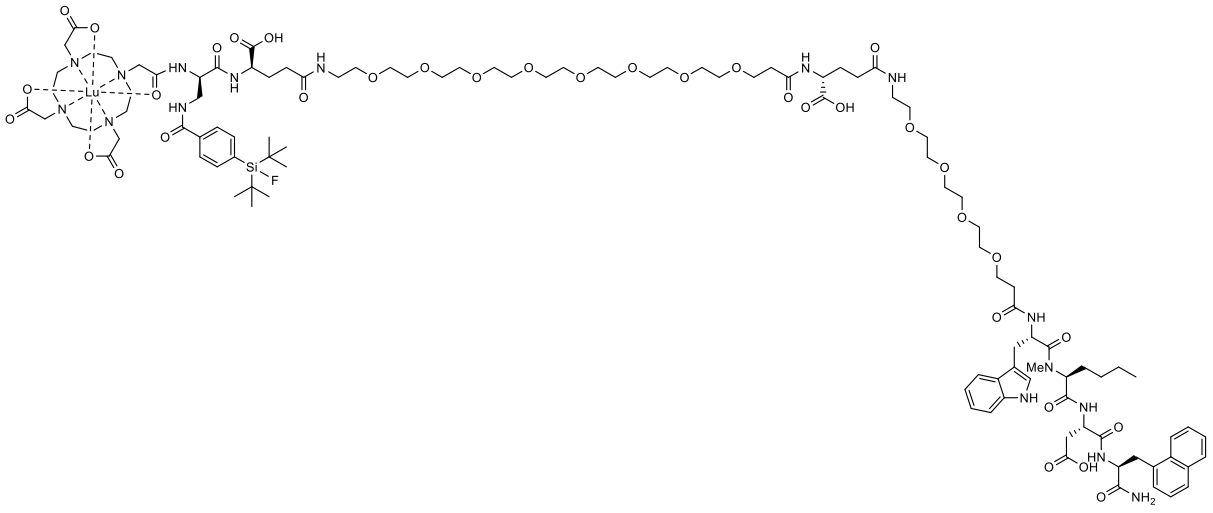

[^{mat}Lu]Lu-DOTA-rhCCK-70: RP-HPLC (10→70% MeCN in H_2O with 0.1% TFA, 15 min, λ = 220 nm) t_R = 14.8 min, K' = 6.40; MS (ESI, positive): m/z calculated for $C_{109}H_{164}FLuN_{16}O_{35}Si$: 2479.1, found: m/z = 1239.5 $[M+2H]^{2+}$, 826.6 $[M+3H]^{3+}$.

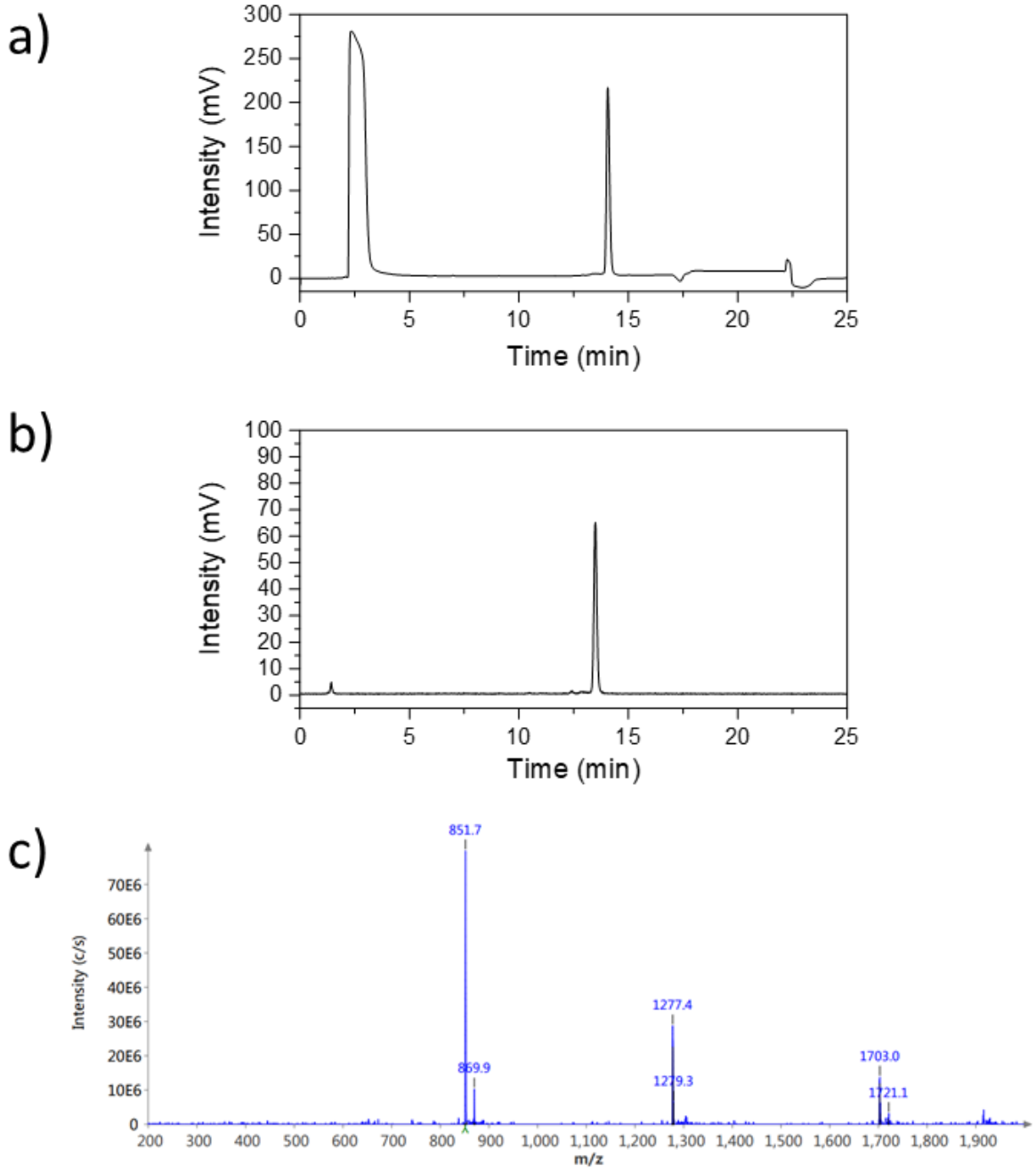

Figure S5. Confirmation of peptide identity and integrity for **a**) [^{nat}Lu]Lu-DOTA-rhCCK-71 and **b**) [^{177}Lu]Lu-DOTA-rhCCK-71 as analyzed by analytical (radio-)RP-HPLC (10→70% MeCN in H_2O + 0.1% TFA in 15 min). **c**) Mass spectrum of [^{nat}Lu]Lu-DOTA-rhCCK-71.

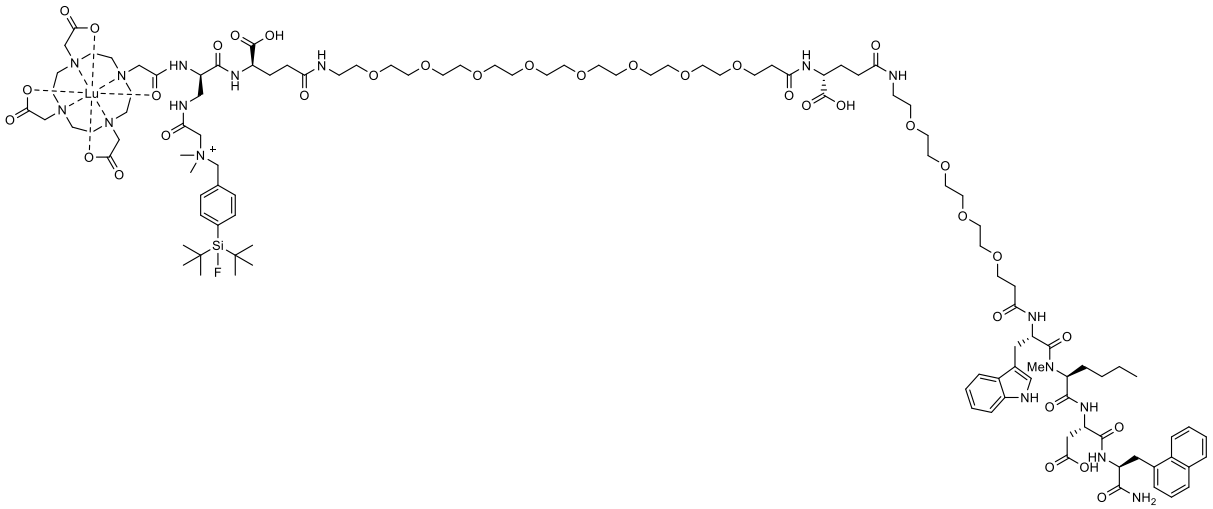

[^{mat}Lu]Lu-DOTA-rhCCK-71: RP-HPLC (10→70% MeCN in H_2O with 0.1% TFA, 15 min, λ = 220 nm) t_R = 14.1 min, K' = 7.36; MS (ESI, positive): m/z calculated for $C_{113}H_{174}FLuN_{17}O_{35}Si^+$: 2551.2, found: m/z = 1277.4 $[M+2H]^{2+}$, 851.7 $[M+3H]^{3+}$.

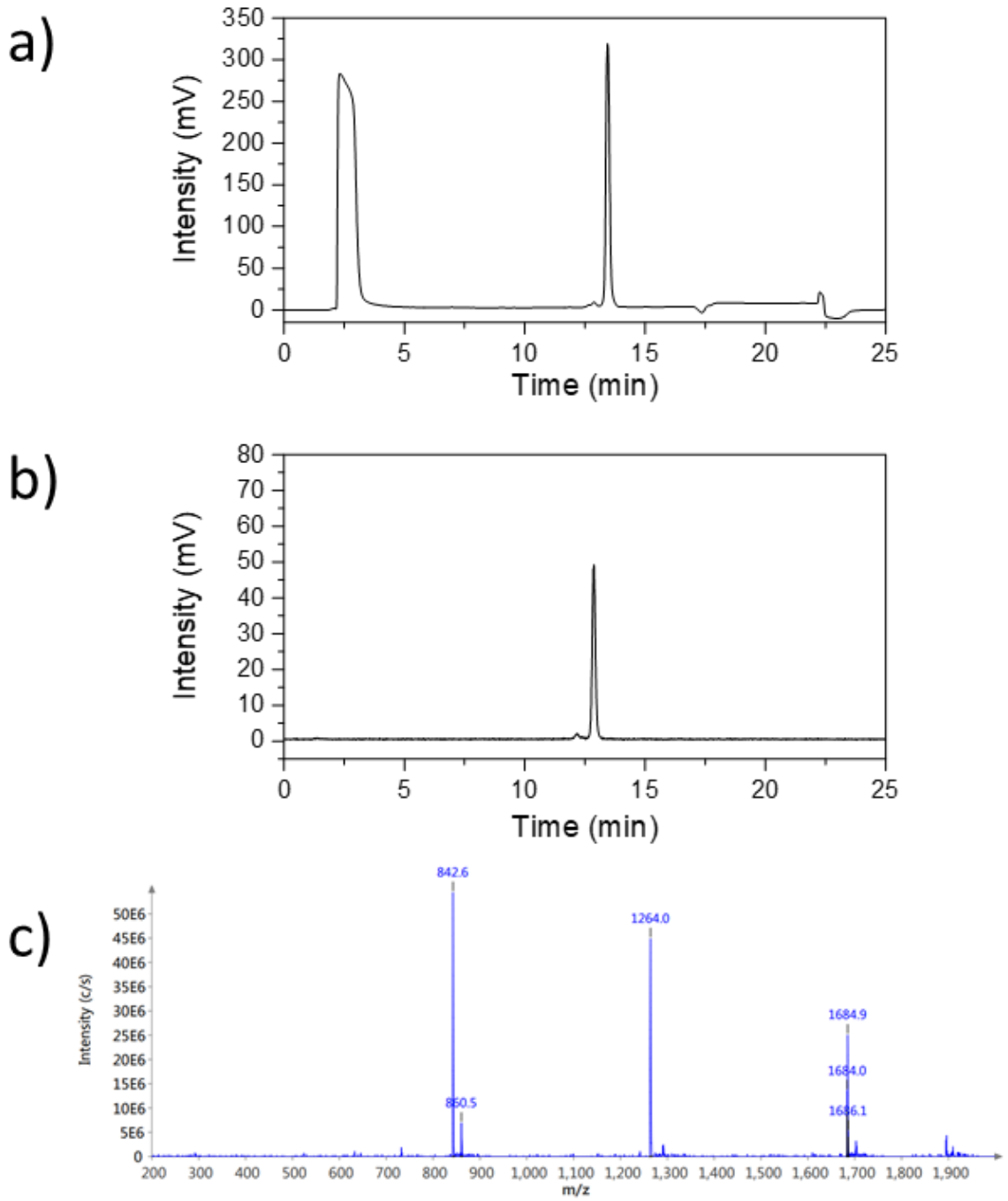

Figure S6. Confirmation of peptide identity and integrity for **a**) [^{nat}Lu]Lu-DOTA-rhCCK-72 and **b**) [^{177}Lu]Lu-DOTA-rhCCK-72 as analyzed by analytical (radio-)RP-HPLC (10→70% MeCN in H_2O + 0.1% TFA in 15 min). **c**) Mass spectrum of [^{nat}Lu]Lu-DOTA-rhCCK-72.

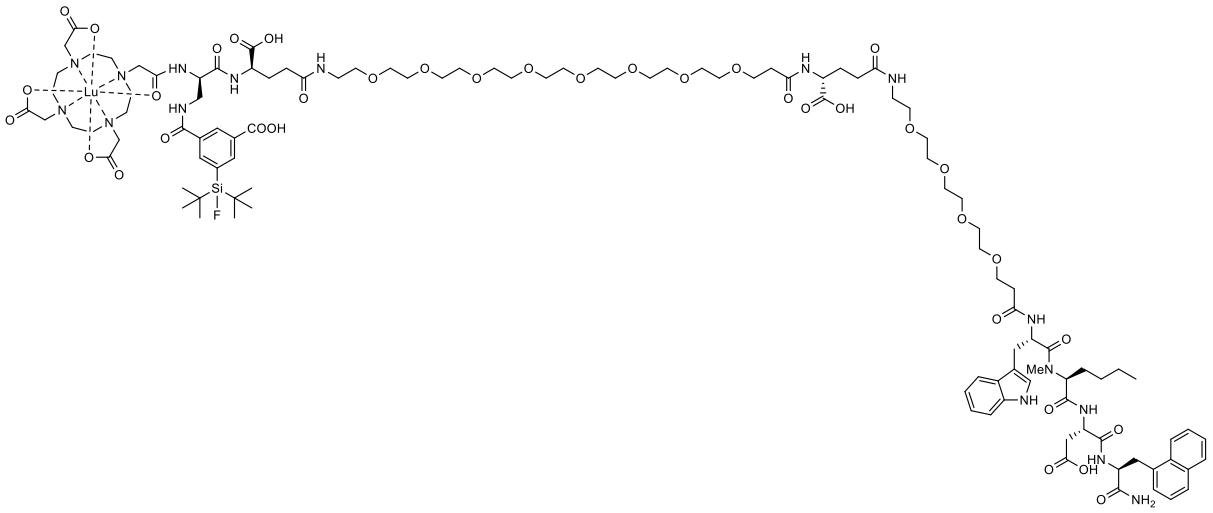

[^{mat}Lu]Lu-DOTA-rhCCK-72: RP-HPLC (10→70% MeCN in H_2O with 0.1% TFA, 15 min, λ = 220 nm) t_R = 13.4 min, K' = 6.94; MS (ESI, positive): m/z calculated for $C_{110}H_{164}FLuN_{16}O_{37}Si$: 2523.1, found: m/z = 1264.0 $[M+2H]^{2+}$, 842.6 $[M+3H]^{3+}$.

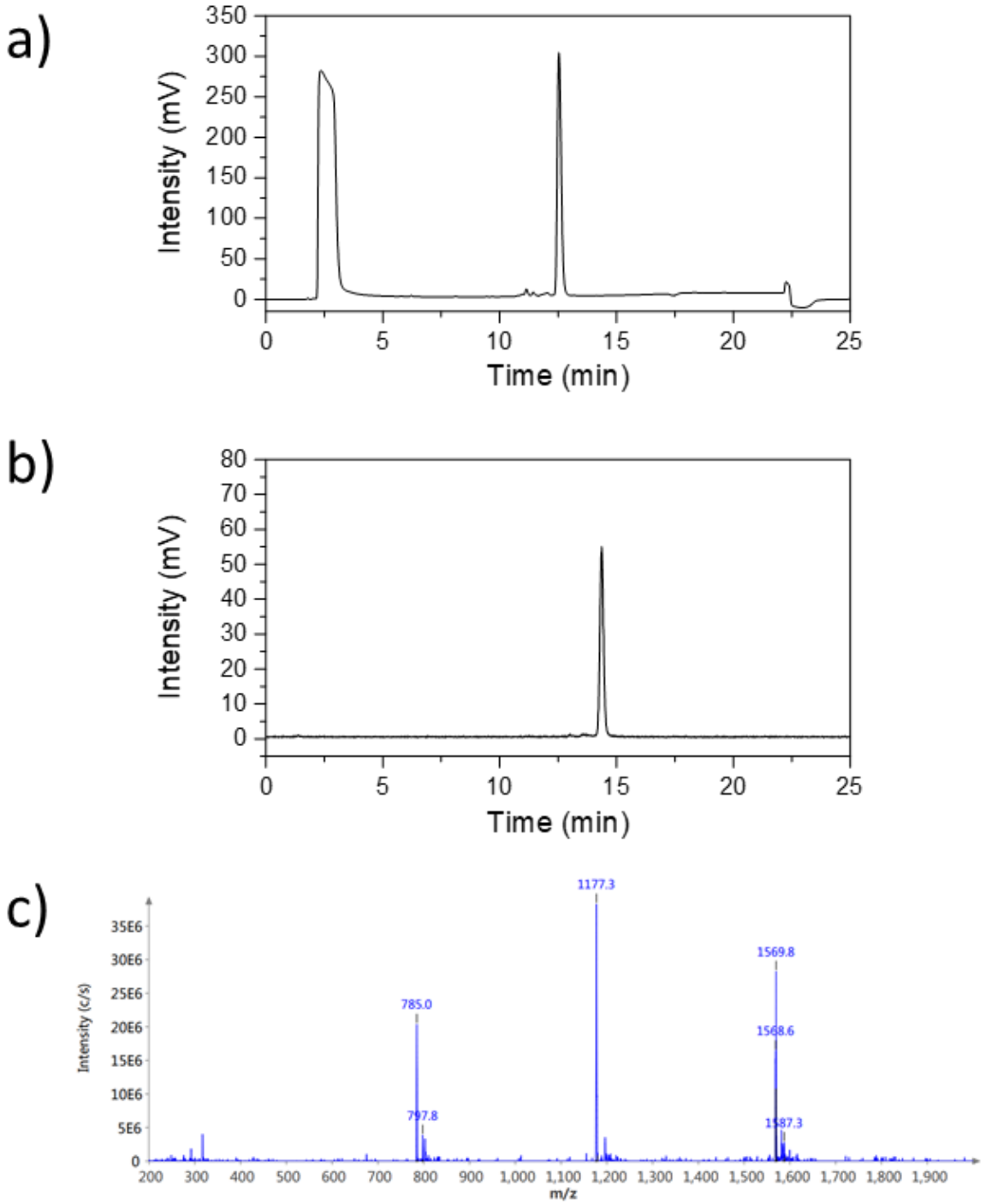

Figure S7. Confirmation of peptide identity and integrity for **a**) [^{nat}Lu]Lu-DOTA-rhCCK-73 and **b**) [^{177}Lu]Lu-DOTA-rhCCK-73 as analyzed by analytical (radio-)RP-HPLC (10→90% MeCN in H_2O + 0.1% TFA in 15 min). **c**) Mass spectrum of [^{nat}Lu]Lu-DOTA-rhCCK-73.

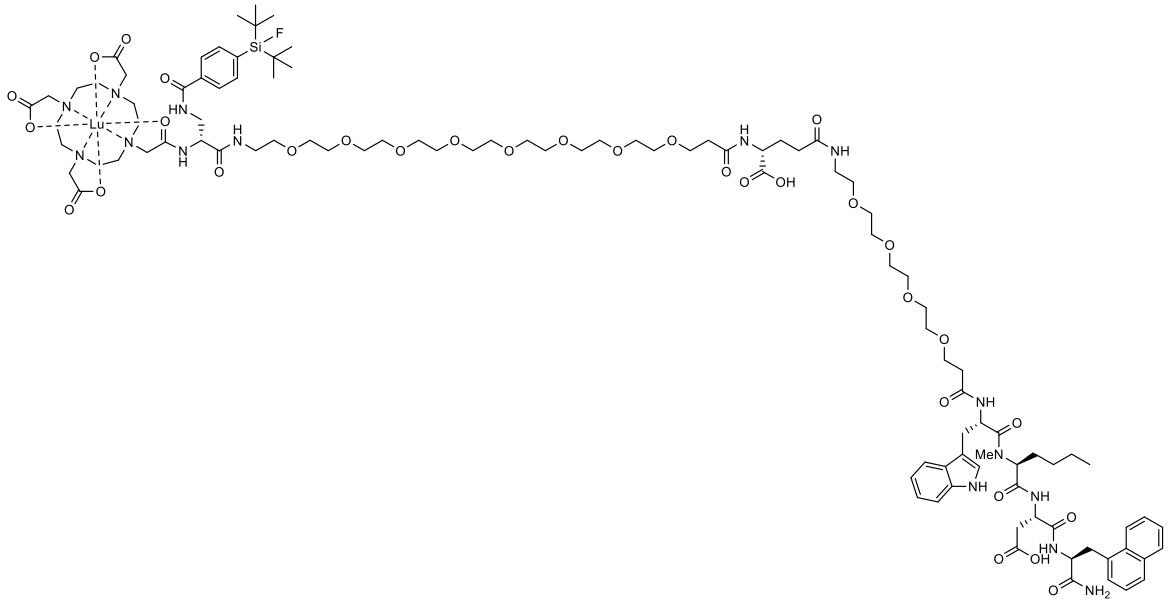

[^{mat}Lu]Lu-DOTA-rhCCK-73: RP-HPLC (10→90% MeCN in H_2O with 0.1% TFA, 15 min, λ = 220 nm) t_R = 12.5 min, K' = 6.41; MS (ESI, positive): m/z calculated for $C_{104}H_{157}FLuN_{15}O_{32}Si$: 2350.0, found: m/z = 1177.3 $[M+2H]^{2+}$, 785.0 $[M+3H]^{3+}$.

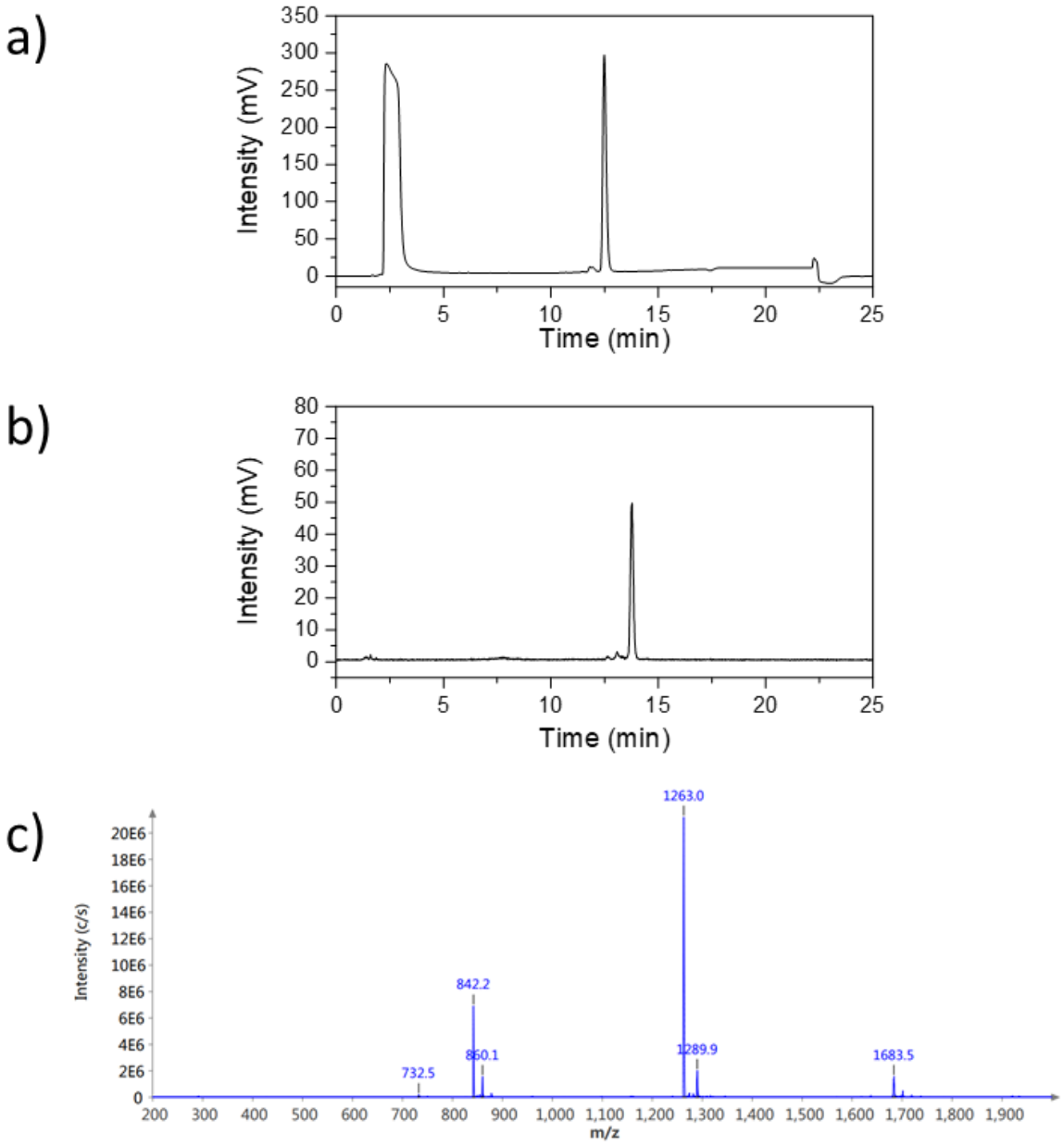

Figure S8. Confirmation of peptide identity and integrity for **a**) [^{nat}Lu]Lu-DOTA-rhCCK-74 and **b**) [^{177}Lu]Lu-DOTA-rhCCK-74 as analyzed by analytical (radio-)RP-HPLC (10→90% MeCN in H_2O + 0.1% TFA in 15 min). **c**) Mass spectrum of [^{nat}Lu]Lu-DOTA-rhCCK-74.

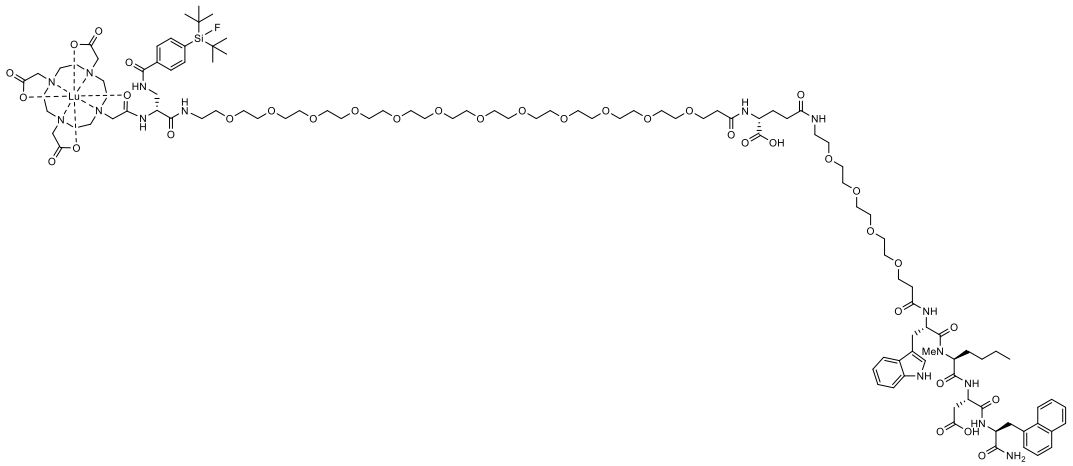

[^{mat}Lu]Lu-DOTA-rhCCK-74: RP-HPLC (10→90% MeCN in H_2O with 0.1% TFA, 15 min, λ = 220 nm) t_R = 12.5 min, K' = 6.41; MS (ESI, positive): m/z calculated for $C_{112}H_{173}FLuN_{15}O_{36}Si$: 2526.1, found: m/z = 1263.0 $[M+2H]^{2+}$, 842.2 $[M+3H]^{3+}$.

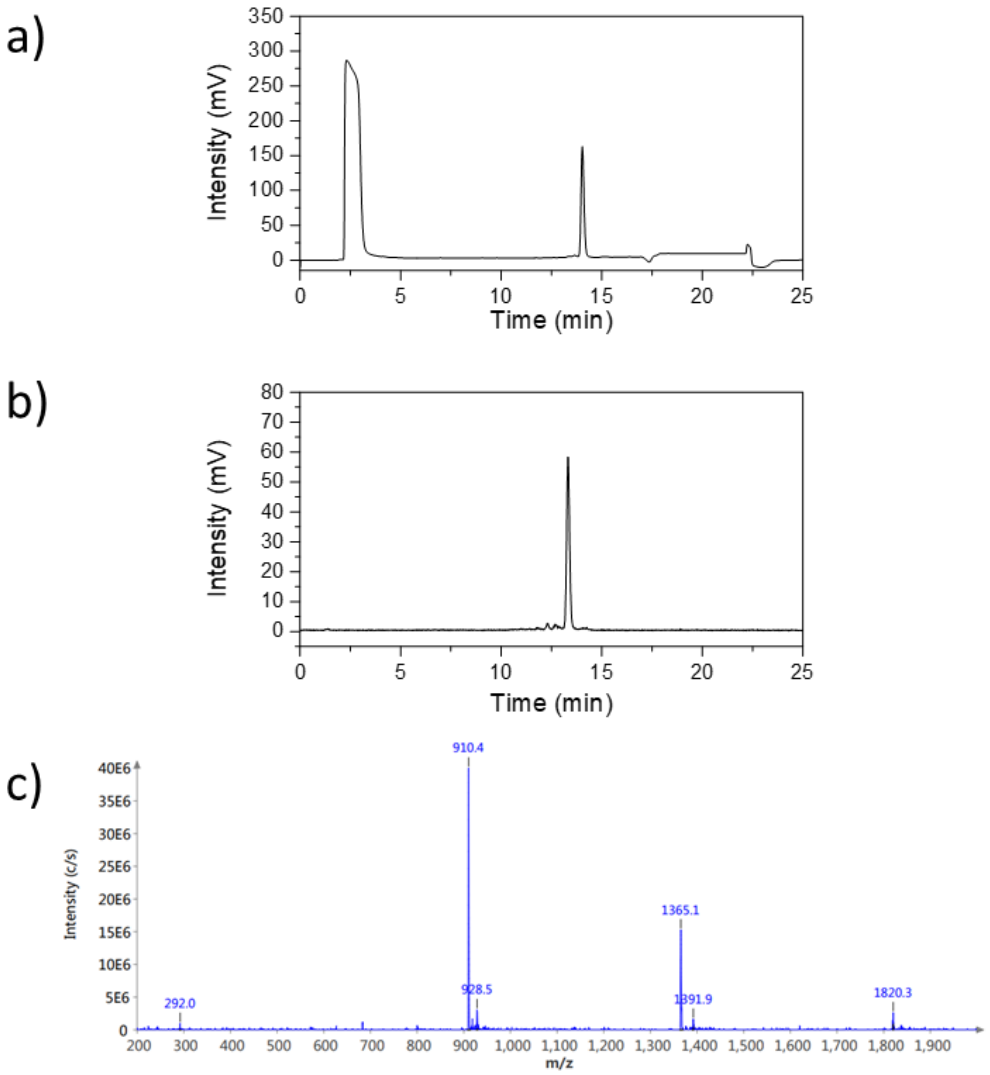

Figure S9. Confirmation of peptide identity and integrity for **a**) [^{nat}Lu]Lu-DOTA-rhCCK-75 and **b**) [^{177}Lu]Lu-DOTA-rhCCK-75 as analyzed by analytical (radio-)RP-HPLC (10→70% MeCN in H_2O + 0.1% TFA in 15 min). **c**) Mass spectrum of [^{nat}Lu]Lu-DOTA-rhCCK-75.

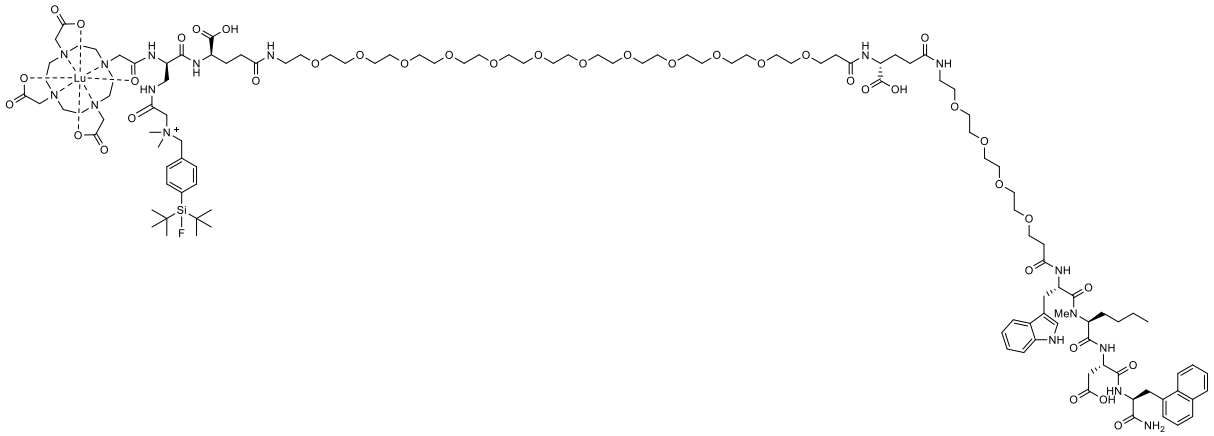

[^{nat}Lu]Lu-DOTA-rhCCK-75: RP-HPLC (10→70% MeCN in H_2O with 0.1% TFA, 15 min, λ = 220 nm) t_R = 14.0 min, K' = 7.30; MS (ESI, positive): m/z calculated for $C_{121}H_{190}FLuN_{17}O_{39}Si^{+}$: 2727.3, found: m/z = 1365.1 $[M+2H]^{2+}$, 910.4 $[M+3H]^{3+}$.

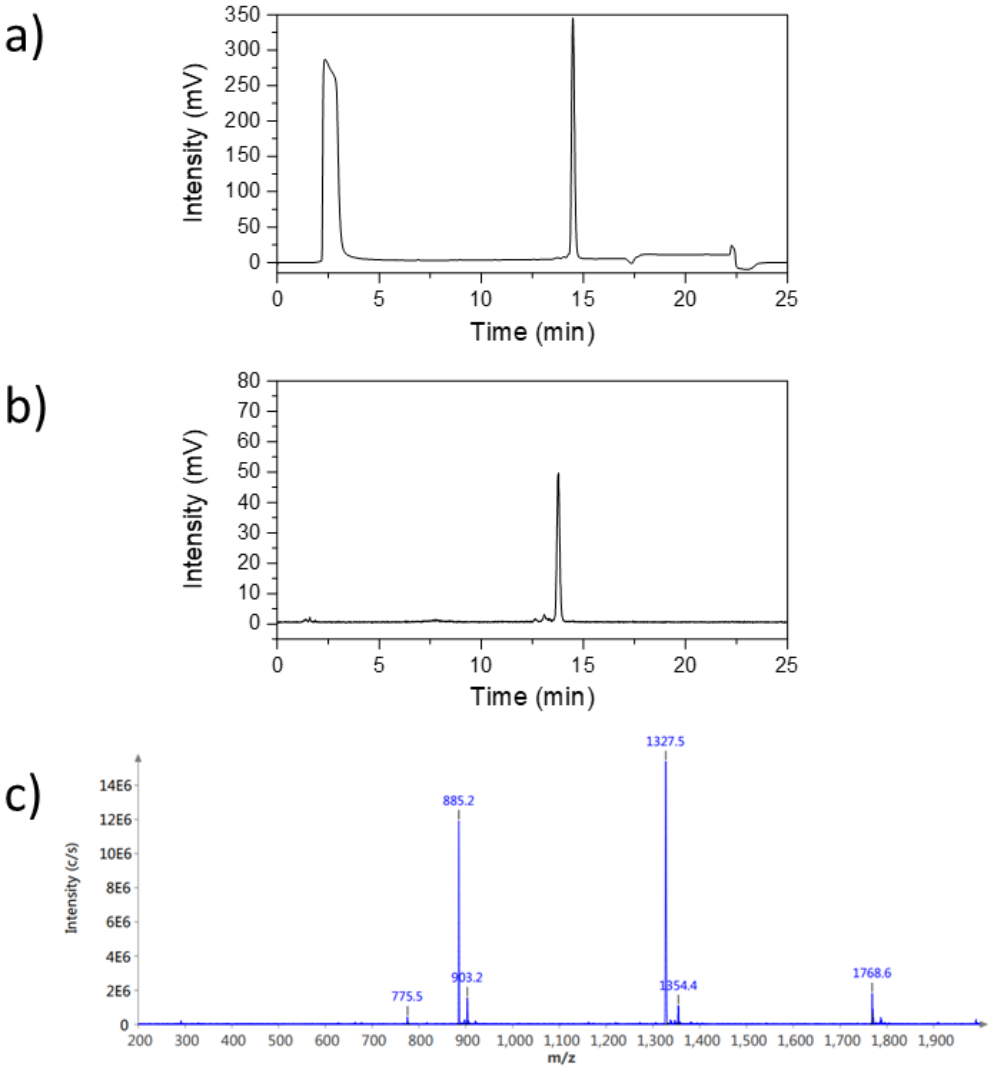

Figure S10. Confirmation of peptide identity and integrity for **a**) [^{nat}Lu]Lu-DOTA-rhCCK-76 and **b**) [^{177}Lu]Lu-DOTA-rhCCK-76 as analyzed by analytical (radio-)RP-HPLC (10→70% MeCN in H_2O + 0.1% TFA in 15 min). **c**) Mass spectrum of [^{nat}Lu]Lu-DOTA-rhCCK-76.

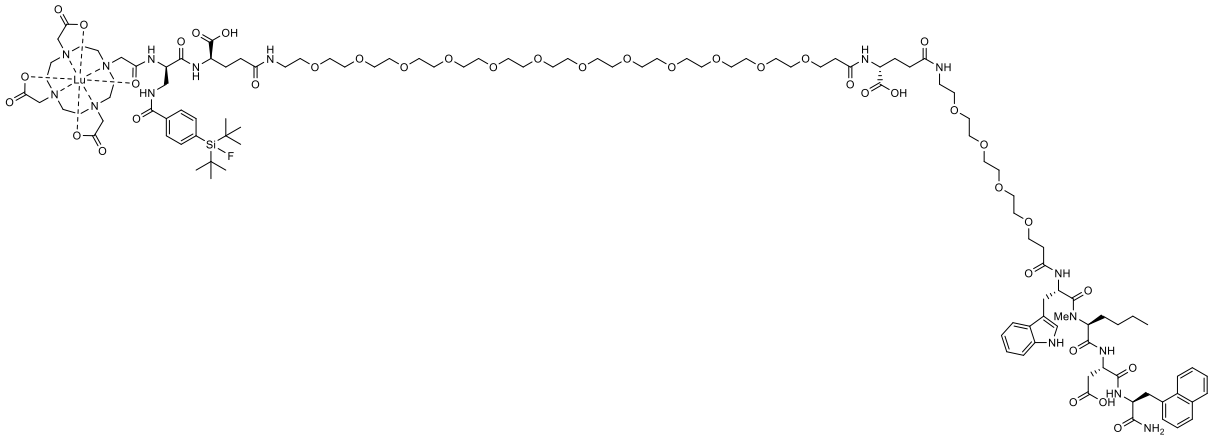

[^{nat}Lu]Lu-DOTA-rhCCK-76: RP-HPLC (10→70% MeCN in H_2O with 0.1% TFA, 15 min, λ = 220 nm) t_R = 14.5 min, K' = 7.60; MS (ESI, positive): m/z calculated for $C_{118}H_{183}FLuN_{16}O_{39}Si$: 2655.2, found: m/z = 1327.5 $[M+2H]^{2+}$, 885.2 $[M+3H]^{3+}$.

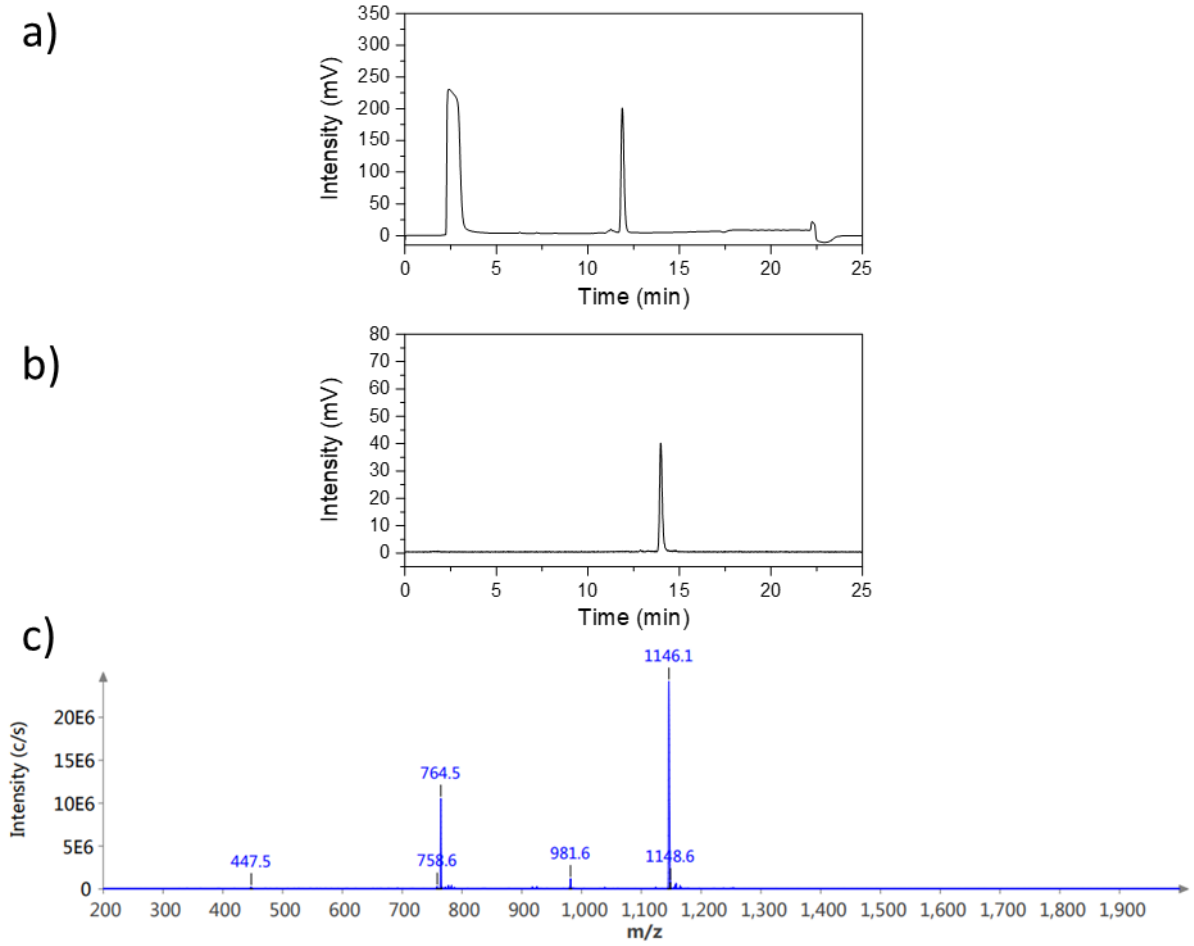

Figure S11. Confirmation of peptide identity and integrity for **a**) [^{nat}Lu]Lu-DOTA-rhCCK-90 and **b**) [^{177}Lu]Lu-DOTA-rhCCK-90 as analyzed by analytical (radio-)RP-HPLC (10→90% MeCN in H_2O + 0.1% TFA in 15 min). **c**) Mass spectrum of [^{nat}Lu]Lu-DOTA-rhCCK-90.

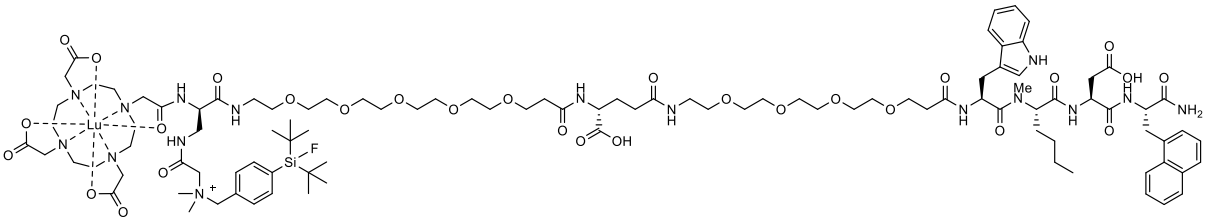

[^{mat}Lu]Lu-DOTA-rhCCK-90: RP-HPLC (10→90% MeCN in H_2O with 0.1% TFA, 15 min, λ = 220 nm) t_R = 11.9 min, K' = 6.05; MS (ESI, positive): m/z calculated for $C_{102}H_{155}FLuN_{16}O_{29}Si^+$: 2290.0, found: m/z = 1146.1 $[M+2H]^{2+}$, 764.5 $[M+3H]^{3+}$.

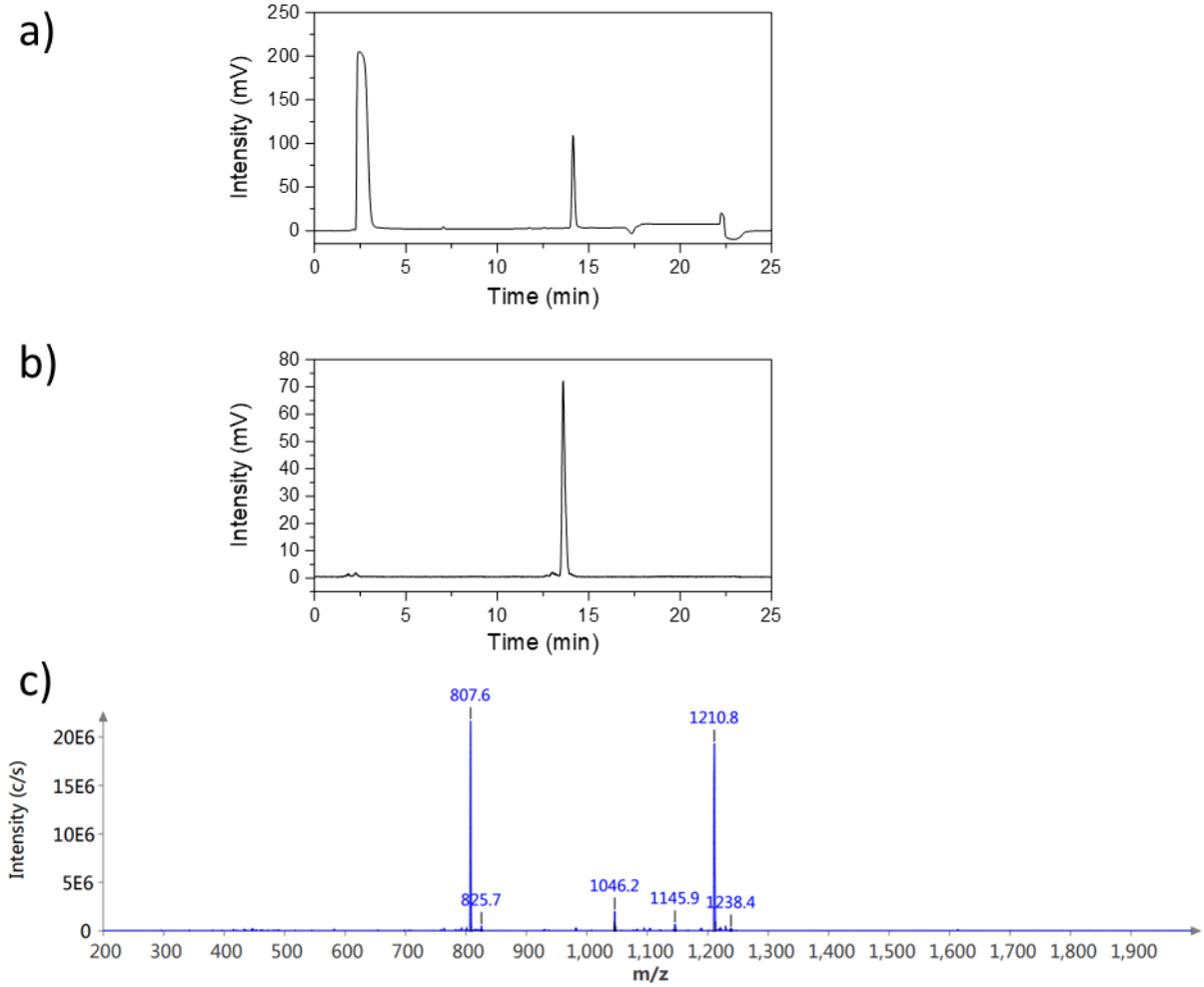

Figure S12. Confirmation of peptide identity and integrity for **a**) [^{nat}Lu]Lu-DOTA-rhCCK-91 and **b**) [^{177}Lu]Lu-DOTA-rhCCK-91 as analyzed by analytical (radio-)RP-HPLC (10→70% MeCN in H_2O + 0.1% TFA in 15 min). **c**) Mass spectrum of [^{nat}Lu]Lu-DOTA-rhCCK-91.

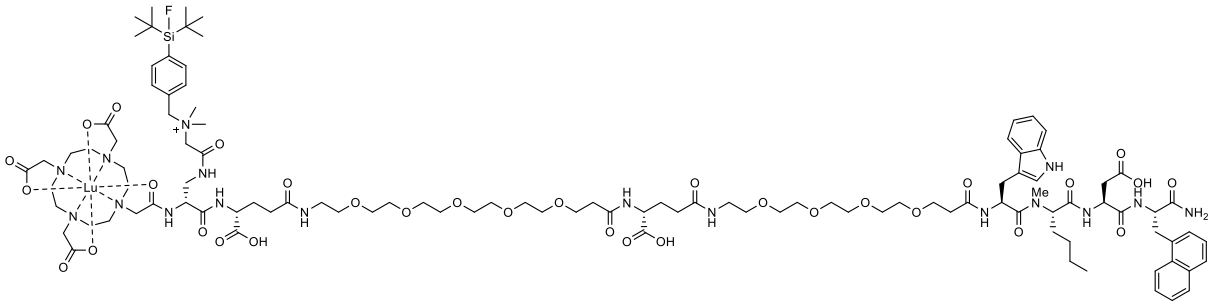

[^{nat}Lu]Lu-DOTA-rhCCK-91: RP-HPLC (10→70% MeCN in H_2O with 0.1% TFA, 15 min, λ = 220 nm) t_R = 14.1 min, K' = 7.36; MS (ESI, positive): m/z calculated for $C_{107}H_{162}FLuN_{17}O_{32}Si^+$: 2419.1, found: m/z = 1210.8 $[M+2H]^{2+}$, 807.6 $[M+3H]^{3+}$.

Synthesis of the SiFA-ipa Building Block

Di-*tert*-butyl(3,5-dimethylphenyl)fluorosilane (i)

1-Bromo-3,5-dimethylbenzene (4.5 g, 25.1 mmol, 1.0 eq.) was dissolved in 73 mL dry THF and cooled to –78°C. Afterwards, ^{t}BuLi (34.7 mL, 55.5 mmol, 1.6 M in pentane, 2.2 eq.) was added dropwise and stirred for 30 min at –78°C. A second solution was prepared by dissolving di-*tert*-butyldifluorosilane (5.0 g, 27.7 mmol, 1.1 eq.) in 49 mL dry THF and cooling it to –78°C. Then, the first solution was added and the reaction mixture was stirred overnight, while slowly warming to room temperature. Addition of 100 mL brine terminated the reaction, aqueous layer was extracted with Et_2O (3×100 mL), combined organic phases were dried using $MgSO_4$ and the solvent was removed under reduced pressure. Di-*tert*-butyl(3,5-dimethylphenyl)fluorosilane (i, 6.6 g, 24.8 mmol, 99 %) was obtained as a colorless solid.

^{1}H NMR (500 MHz, $CDCl_3$): d (ppm) = 7.19 (s, 2H; H_o), 7.04 (s, 1H; H_p), 2.33 (s, 6 H; CH_3), 1.06 (s, 18 H; CCH_3). RP-HPLC (50 to 100% B in 15 min, 100% B for 10 min): t_R = 16.4 min. K' = 8.21.

5-(Di-*tert*-butylfluorosilyl)isophthalic acid (SiFA-ipa, ii)

1.1 g Di-*tert*-butyl(3,5-diemethylphenyl)fluorosilane (i, 1.1 g, 4.0 mmol, 1.0 eq.) were dissolved in 17 mL ^{t}BuOH/CH_2Cl_2 (*v/v* = 3.5/1) and NaH_2PO_4×H_2O (16 mL, 40 mmol, 2.5 M in H_2O, 10 eq.) as well as $KMnO_4$ (7.6 g, 48 mmol, 12 eq.) were added. Afterwards, the reaction mixture was slowly heated to 75°C and stirred for 24 h. Subsequently, the reaction was terminated by addition of 50 mL saturated aqueous $NaSO_3$ solution and residual MnO_2 was dissolved with 10 mL concentrated HCl. The aqueous phase was extracted with Et_2O (3×100 mL), the combined organic phases were dried over $MgSO_4$ and the solvent was removed under reduced pressure. SiFA-ipa (ii, 1.3 g, 4.0 mmol, >99%) was obtained as a colorless solid.

^{1}H NMR (400 MHz, DMSO-D_6): d (ppm) = 8.53 (t, 1 H, $^4J(^1H,^1H)$ = 1.7 Hz; H_{Ar-2}), 8.32 (d, 2 H, $^4J(^1H,^1H)$ = 1.6 Hz; $H_{Ar-4,-6}$), 1.03 (s, 18 H; CH_3).

$^{13}C\{^1H\}$ NMR (101 MHz, DMSO-D_6): d [ppm] = 166.5 (s; COOH), 137.9 (d, $^3J(^{13}C,^{19}F)$ = 4 Hz; $C_{Ar-4,-6}$), 134.0 (d, $^2J(^{13}C,^{19}F)$ = 14 Hz; C_{Ar-5}), 131.4 (s; C_{Ar-2}), 130.8 (s; $C_{Ar-1,-3}$), 26.8 (s; CCH_3), 19.7 (d, $^2J(^{13}C,^{19}F)$ = 12 Hz; CCH_3).

$^{19}F\{^{29}Si\}$ NMR (376 MHz, DMSO-D_6): d (ppm) = –187.1.

$^{29}Si\{^1H\}$INEPT NMR (79 MHz, DMSO-D_6): d (ppm) = 13.8 (d, $^1J(^{19}F,^{29}Si)$ = 299 Hz).

RP-HPLC (50→100% MeCN in H_2O with 0.1% TFA, 15 min, λ = 220 nm) t_R = 5.7 min, K' = 2.20; MS (ESI, positive): m/z calculated for $C_{16}H_{23}FO_4Si$: 326.1, found: m/z = 327.2 $[M+H]^+$, 309.2 $[M–H_2O+H]^+$.

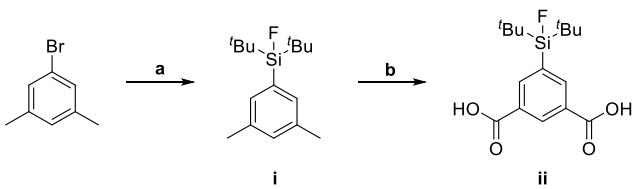

Scheme S1: Synthesis of SiFA-ipa (ii): a) ^{t}Bu$_2$SiF$_2$, ^{t}BuLi, −78°C to rt, overnight (THF) b) $KMnO_4$, 75°C, 24 h (CH_2Cl_2/^{t}BuOH/NaH_2PO_4×H_2O buffer).

Labeling Procedures

^{nat}Lu-Labeling

Quantitative ^{nat}Lu-labeling was conducted by addition of a 2.5-fold excess of [^{nat}Lu]$LuCl_3$ (20 mM in H_2O) to the peptide precursor (1 mM in DMSO), followed by heating the reaction mixture to 90°C for 15 min. Peptide identity and integrity were confirmed using RP-HPLC and ESI-MS.

^{177}Lu-Labeling

^{177}Lu-Labeling of the peptide precursor (1 nmol) was performed at 80°C for 10 min in a NaOAc-buffered (1 M, pH = 5.5) hydrochloric acid (0.04 M) solution using [^{177}Lu]$LuCl_3$ dissolved in hydrochloric acid (0.04 M, 40 GBq/mL) acquired from ITM Isotope Technologies Munich SE (Garching, Germany). After the reaction was finished, sodium ascorbate (1 M in H_2O, 10 vol-%) was added as radiolysis quencher. Radiochemical purity was determined via radio-RP-HPLC and radio-TLC (instant thin layer chromatography paper impregnated with silica gel (iTLC-SG, Agilent Technologies Inc., Folsom, United States); sodium citrate*1.5 H_2O (0.1 M)).

In Vitro Experiments

Cell Culture

CCK-2R positive rat pancreatic cancer cells AR42J (CLS GmbH, Eppelheim, Germany) were cultivated in monolayers in CELLSTAR® cell culture flask (Greiner Bio-One GmbH, Frickenhausen, Germany) at 37°C in a humidified atmosphere (5% CO_2). Therefor, a HERAcell 150i-Incubator (Thermo Fisher Scientific Inc., Waltham, United States) was used. RPMI 1640 medium, supplemented with 5 mM L-Gln 5 mL non-essential amino acids (100×) and 10% FCS, was used for cell nutrition. Detachment of the cells for passaging was conducted with a Dulbecco's PBS solution supplemented with 0.1% EDTA (*v/v*). Cell numbers were determined with a Neubauer hemocytometer (Paul Marienfeld, Lauda-Königshofen, Germany). All operations requiring sterile conditions, were accomplished using a MSC-Advantage safety workbench (Thermo Fisher Scientific Inc., Waltham, United States).

IC_{50} Determination

24 ± 2 h prior to the experiment, AR42J cells (2.0×10^5 cells/well) were seeded into 24-well plates, 1 mL of nutrient medium (RPMI 1640, 5 mM L-Gln, 5 mL non-essential amino acids (100×), 10% FCS) was added and the cells were incubated at 37°C in a humidified atmosphere (5% CO_2). On the next day, medium was removed, cells were washed with PBS (300 µL) and fresh nutrient medium supplemented with 5% BSA (200 µL) was added. The peptide of interest (25 µL in nutrient medium) in increasing concentrations (10^{-10} to 10^{-4} M) in triplicate as well as [^{177}Lu]Lu-DOTA-PP-F11N (25 µL, 0.3 pmol) were added to the cells and the assay was incubated for 3 h at 37°C. Subsequently, the supernatant was collected cells were washed with PBS (300 µL) and both fractions were unified. Cell lysis was conducted by addition of NaOH (300 µL, 1 N) and incubation for at least 20 min at room temperature. Supernatant was collected, the respective wells were washed with NaOH (300 µL, 1 N) and both fractions were unified. Radioactivity of all fractions collected was quantified using a γ-counter (PerkinElmer Inc., Waltham, United States). Half-maximal inhibitory concentration (IC_{50}) was calculated via the GraphPad PRISM software (GraphPad Software Inc., La Jolla, United States).

Log$D_{7.4}$ Determination

^{177}Lu-Labeled peptide precursor (~1 MBq, 10 µL in 0.04 M HCl) was added to a solution of *n*-octanol/PBS (1/1, *v/v*, 1 mL) and vigourously mixed for 3 min at room temperature ($n \geqslant 5$). Afterwards both phases were seperated using a Biofuge 15 centrifuge (Heraus Sepatech GmbH, Osterode, Germany) at 9,000 rpm for 5 min. 200 µL aliquots of both layers were collected separately, measured in a γ-counter (Perkin Elmer, Waltham, MA, USA) and the log$D_{7.4}$ value was obtained.

Human Serum Albumin Binding

Human serum albumin binding was determined via high performance affinity chromatography. Therefore, a Chiralpak HSA column (50 × 3 mm, 5 µm, H13H-2433, Daicel, Tokyo, Japan) was used at a constant flow rate of 0.5 ml/min at room temperature. Mobile phase A consisted of a freshly prepared aqueous solution of NH_4OAc (pH = 6.9, 50 mM) and mobile phase B of isopropanol. Calibration of the column was performed daily prior to experiments, by determining the retention times of nine reference substances displaying a HSA binding from 13 to 99%. HPLC gradient for all compounds tested was 100% A (0 to 3 min), followed by 80% A (3 to 40 min). All substances tested, were dissolved in a mixture of A/B (0.5 mg/mL, 1:1, *v*/*v*). OriginPro 2016G software (Northampton, United States) was used for non-linear regression and data evaluation.

Table S1. Affinity, lipophilicity and human serum albumin binding data of the compounds evaluated. Affinity data were determined on AR42J cells (2.0×10^5 cells/well) and [^{177}Lu]Lu-DOTA-PP-F11N (0.3 pmol/well) as radiolabeled reference (3 h, 37 °C, RPMI 1640, 5 mM L-Gln, 5 mL non-essential amino acids (100×), 10% FCS + 5% BSA (*v*/*v*)).

Peptide	***IC*$_{50}$** (nM)	**log*D*$_{7.4}$**	**HSA** (%)
[$^{nat/177}$Lu]Lu-DOTA-rhCCK-67	13.0 ± 1.1	−1.05 ± 0.09	92.9
[$^{nat/177}$Lu]Lu-DOTA-rhCCK-68	15.4 ± 1.1	−1.65 ± 0.09	91.2
[$^{nat/177}$Lu]Lu-DOTA-rhCCK-69	43.1 ± 1.7	−2.11 ± 0.09	84.7
[$^{nat/177}$Lu]Lu-DOTA-rhCCK-70	12.6 ± 2.0	−1.67 ± 0.08	89.3
[$^{nat/177}$Lu]Lu-DOTA-rhCCK-71	13.3 ± 1.3	−1.63 ± 0.06	89.1
[$^{nat/177}$Lu]Lu-DOTA-rhCCK-72	52.3 ± 6.2	−2.32 ± 0.03	89.3
[$^{nat/177}$Lu]Lu-DOTA-rhCCK-73	15.6 ± 0.7	−1.02 ± 0.06	90.4
[$^{nat/177}$Lu]Lu-DOTA-rhCCK-74	12.1 ± 1.0	−1.19 ± 0.07	87.2
[$^{nat/177}$Lu]Lu-DOTA-rhCCK-75	19.2 ± 1.6	−1.15 ± 0.05	90.9
[$^{nat/177}$Lu]Lu-DOTA-rhCCK-76	14.2 ± 0.9	−1.82 ± 0.09	86.2
[$^{nat/177}$Lu]Lu-DOTA-rhCCK-90	9.9 ± 1.0	−0.76 ± 0.09	94.5
[$^{nat/177}$Lu]Lu-DOTA-rhCCK-91	8.6 ± 0.7	−1.66 ± 0.08	90.0

Table S2. Biodistribution data of [^{177}Lu]Lu-DOTA-rhCCK-70 and [^{177}Lu]Lu-DOTA-rhCCK-91 in selected organs at 24 h p.i. in AR42J tumor-bearing CB17-SCID mice (100 pmol each). Data are expressed as %ID/g, mean ± SD.

organ	**[^{177}Lu]Lu-DOTA-rhCCK-70** *(n=4)*	**[^{177}Lu]Lu-DOTA-rhCCK-91** *(n=4)*
Blood	0.10 ± 0.04	0.04 ± 0.01
Heart	0.23 ± 0.05	0.31 ± 0.07
Lung	0.39 ± 0.12	0.26 ± 0.05
Liver	3.48 ± 1.66	1.96 ± 0.08
Spleen	1.92 ± 0.60	1.04 ± 0.26
Pancreas	0.24 ± 0.08	0.90 ± 0.32
Stomach	6.21 ± 0.85	3.99 ± 1.16
Intestine	0.48 ± 0.13	0.68 ± 0.16
Kidney	8.37 ± 0.78	6.58 ± 0.53
Adrenal	0.55 ± 0.46	0.44 ± 0.09
Muscle	0.06 ± 0.03	0.06 ± 0.01
Bone	2.40 ± 1.51	0.64 ± 0.12
Tumor	12.0 ± 0.8	7.47 ± 1.01

Table S3. Tumor-to-Background ratios of [^{177}Lu]Lu-DOTA-rhCCK-70 and [^{177}Lu]Lu-DOTA-rhCCK-91 in selected organs at 24 h p.i. in AR42J tumor-bearing CB17-SCID mice (100 pmol each). Data are expressed as %ID/g, mean ± SD.

	[^{177}Lu]Lu-DOTA-rhCCK-70 *(n=4)*	**[^{177}Lu]Lu-DOTA-rhCCK-91** *(n=4)*
Blood	143 ± 49	185 ± 32
Heart	55.4 ± 13.4	25.3 ± 5.2
Lung	33.4 ± 8.53	29.3 ± 4.2
Liver	4.26 ± 1.70	3.80 ± 0.37
Spleen	6.95 ± 2.17	7.35 ± 0.75
Pancreas	55.2 ± 19.6	8.98 ± 2.10
Stomach	1.97 ± 0.24	1.95 ± 0.27
Intestine	27.4 ± 7.7	12.3 ± 5.1
Kidney	1.44 ± 0.12	1.14 ± 0.12
Adrenal	20.5 ± 8.5	17.3 ± 1.9
Muscle	276 ± 189	147 ± 65
Bone	9.48 ± 8.05	11.8 ± 0.72